Lecture Notes in Civil Engineering

Krishna R. Reddy
Arvind K. Agnihotri
Yeliz Yukselen-Aksoy
Brajesh K. Dubey
Ajay Bansal *Editors*

Sustainable Environment and Infrastructure

Proceedings of EGRWSE 2019

Springer

Lecture Notes in Civil Engineering

Volume 90

Lecture Notes in Civil Engineering (LNCE) publishes the latest developments in Civil Engineering - quickly, informally and in top quality. Though original research reported in proceedings and post-proceedings represents the core of LNCE, edited volumes of exceptionally high quality and interest may also be considered for publication. Volumes published in LNCE embrace all aspects and subfields of, as well as new challenges in, Civil Engineering. Topics in the series include:

- Construction and Structural Mechanics
- Building Materials
- Concrete, Steel and Timber Structures
- Geotechnical Engineering
- Earthquake Engineering
- Coastal Engineering
- Ocean and Offshore Engineering; Ships and Floating Structures
- Hydraulics, Hydrology and Water Resources Engineering
- Environmental Engineering and Sustainability
- Structural Health and Monitoring
- Surveying and Geographical Information Systems
- Indoor Environments
- Transportation and Traffic
- Risk Analysis
- Safety and Security

To submit a proposal or request further information, please contact the appropriate Springer Editor:

- Mr. Pierpaolo Riva at pierpaolo.riva@springer.com (Europe and Americas);
- Ms. Swati Meherishi at swati.meherishi@springer.com (Asia - except China, and Australia, New Zealand);
- Dr. Mengchu Huang at mengchu.huang@springer.com (China).

All books in the series now indexed by Scopus and EI Compendex database!

More information about this series at http://www.springer.com/series/15087

Krishna R. Reddy · Arvind K. Agnihotri ·
Yeliz Yukselen-Aksoy · Brajesh K. Dubey ·
Ajay Bansal
Editors

Sustainable Environment and Infrastructure

Proceedings of EGRWSE 2019

Springer

Editors
Krishna R. Reddy
Department of Civil, Materials
and Environmental Engineering
University of Illinois
Chicago, IL, USA

Yeliz Yukselen-Aksoy
Department of Civil Engineering
Dokuz Eylül University
İzmir, Turkey

Ajay Bansal
Dr. B. R. Ambedkar National
Institute of Technology
Jalandhar, Punjab, India

Arvind K. Agnihotri
Dr. B. R. Ambedkar National Institute
of Technology
Jalandhar, Punjab, India

Brajesh K. Dubey
Department of Civil Engineering
Indian Institute of Technology Kharagpur
Kharagpur, West Bengal, India

ISSN 2366-2557 ISSN 2366-2565 (electronic)
Lecture Notes in Civil Engineering
ISBN 978-3-030-51353-5 ISBN 978-3-030-51354-2 (eBook)
https://doi.org/10.1007/978-3-030-51354-2

This Springer imprint is published by the registered company Springer Nature Switzerland AG
The registered company address is: Gewerbestrasse 11, 6330 Cham, Switzerland

Preface

Sustainable engineering in a broader sense is the process of utilizing the available resources in a way that does not compromise the need for the same resources for future generations.

Sustainable engineering isn't necessarily restricted to civil engineering and infrastructure projects and can be an integral part of any engineering discipline. All engineering disciplines should incorporate sustainability into their practice in order to improve the quality of life. Furthermore, with the creation of the sustainable development goals, engineers will continue to play a decisive role in their success. The necessity for environment-friendly technologies will require the expertise of engineers across different backgrounds. Therefore, the UNESCO Engineering Initiative (UEI) is working with partners to develop engineering curricula that incorporate sustainability as an overarching theme.

The ever-increasing global population has resulted in a tremendous load on the natural resources. Adding to this, the rapid industrialization and urbanization activities are exacerbating the current situation. All these developments have been at a heavy cost of deteriorated environmental conditions and adverse risk to human health and the environment. This has drawn the attention of technocrats and researchers to look for technologies that are sustainable. As a consequence of a huge domestic and industrial waste generation and deteriorating environmental conditions, in general, statutory regulatory bodies have become more active and the pollution-related norms have become more stringent than ever before. We are running a race against time to look for technologies with sustainable viability. In this regard, the recycling of waste materials is one of the key features of sustainability.

Waste material has been defined as any type of material by-product of human and industrial activities that has no lasting value. The amount of waste material is increasing day by day with an increase in population. It is a general practice to dump these waste materials on lands, which creates environmental and social problems. The reuse of these waste materials is one of the effective ways of minimizing such problems. The bulk use of wastes like pond ash, rice husk ash, fly ash, and tire wastes as admixture is now becoming popular in the construction of

geotechnical structures. Researchers have shown that these materials can be used in the subgrade of roads, embankments of roads, as fill materials in retaining walls, etc. The growing quantities and types of waste materials, shortage of landfill spaces, and lack of natural earth materials highlight the urgency of finding innovative ways of recycling and reusing waste materials. Additionally, recycling and subsequent reuse of waste materials can reduce the demand for natural resources, which can ultimately lead to a more sustainable environment. The construction industry is a massive consumer of natural resources and a huge waste producer as well. The high value of raw material consumption in the construction industry becomes one of the main factors that causes environmental damage and pollution to our Mother Earth and the depletion of natural and mineral resources.

The greatest challenge before the processing and manufacturing industries is the disposal of the residual waste products. Waste products that are generally toxic, ignitable, corrosive, or reactive have detrimental environmental consequences. Thus, the disposal of industrial wastes is equally a major issue for the present generation. This issue requires an effective, economic, and environment-friendly method to tackle with the disposal of the residual industrial waste products. One of the common and feasible ways to utilize these waste products is to go for the construction of roads, highways, and embankments. If these materials can be suitably utilized in the construction of roads, highways, and embankments, then the pollution problem caused by the industrial wastes can be greatly reduced. This book covers a variety of such multidisciplinary articles focused on sustainable environmental and infrastructure systems which will be useful for students, working professionals, practitioners, and researchers. Each article was reviewed by two professionals with relevant technical background. The editors are thankful to the authors and the reviewers for their contributions.

Editors

Chicago, USA — Krishna R. Reddy
Jalandhar, India — Arvind K. Agnihotri
İzmir, Turkey — Yeliz Yukselen-Aksoy
Kharagpur, India — Brajesh K. Dubey
Jalandhar, India — Ajay Bansal

Contents

About the Editors

Dr. Krishna R. Reddy is a Professor of Civil and Environmental Engineering, Director of Sustainable Engineering Research Laboratory, and also the Director of the Geotechnical and Geoenvironmental Engineering Laboratory at the University of Illinois at Chicago. He received his Ph.D. in Civil Engineering from the Illinois Institute of Technology, Chicago. He received gold medals for being first in his class of B.E. (Civil Engineering) at Osmania University and M.E. (Civil Engineering) at the Indian Institute of Technology, Roorkee. Dr. Reddy has over 25 years of teaching, consulting and research experience within the fields of civil engineering, geotechnical engineering, environmental engineering, and sustainable engineering.

Dr. Arvind K. Agnihotri is a Professor in the Department of Civil Engineering NIT Jalandhar. He completed his Ph.D. from IIT Roorkee, M.Tech. from NIT Kurukshetra and B.E. from Panjab University Chandigarh. He has over 29 years' experience in research, teaching and academic administration, with several years spent holding key leadership positions. His areas of interest are Geotechnical and Geoenvironmental Engineering, Reinforced Earth (Geosynthetics and Geofibers), Ground Improvement and Soil-Structure-interaction. He has supervised 9 Ph.D. theses and 40 M.Tech. dissertations. He has 50 publications in international refereed journals, 10 publications in national refereed journals and 34 publications in various national and international conferences/symposia.

Dr. Yeliz Yukselen-Aksoy is a Professor in the Geotechnical Engineering Division of Department of Civil Engineering of Dokuz Eylul University. She received a B.S. from Dokuz Eylül University, and an M.S. from the Dokuz Eylül University. She received her Ph.D. in Geotechnical Engineering from the University of Dokuz Eylül. She was also at the University of Illinois at Chicago in the Department of Civil and Materials Engineering for one year as a visiting professor. Her research efforts have focused on environmental geotechnics, ground improvement, surface properties of

clay minerals, and remediation of contaminated soils. Dr. Yukselen-Aksoy has published over 40 journal papers, 1 book chapter, and 25 conference papers. She was the recipient of the Turkish National and Scientific Research Council Scholarship.

Dr. Brajesh K. Dubey is an Associate Professor in Environmental Engineering at the Department of Civil Engineering at Indian Institute of Technology, Kharagpur, India. Dr. Dubey received his Ph.D. from the University of Florida, USA. He obtained his B.Tech. (Hons.) in Civil Engineering from IIT Kharagpur. He has more than 17 years of research, teaching, training and industrial outreach experience in areas of integrated solid and hazardous waste management, sustainable engineering and application of life cycle assessment techniques, environmental risk assessment, circular economy and environmental nanotechnology. He has published 62 journal papers, 26 conference papers, and 6 book chapters. He has received awards from Government of Australia, International Research Group on Wood Protection – Sweden, Hinkley Center for Solid, and Hazardous Waste Management, Florida. He has also worked as a Waste Management Expert for UN agencies and World Bank.

Dr. Ajay Bansal is a Professor of Chemical Engineering at Dr B R Ambedkar National Institute of Technology, Jalandhar, India. Dr Bansal received his Ph.D. in Chemical Engineering from Panjab University, Chandigarh, M.Tech. from Indian Institute of Technology, Delhi, and B.E. from Government Engineering College, Raipur (now NIT Raipur). Dr. Bansal has over 24 years of teaching, consulting and research experience within the fields of chemical and environmental engineering. His research expertise includes Nano-photocatalysis,) Advanced Oxidation Processes, Waste Water Treatment, Solid Waste Management, Multiphase Reactors, and Rheologically complex fluids. He has supervised 8 Ph.D. dissertations, published 3 books, 3 book chapters, 40 journal papers, and 60 conference papers. He has been an active member of various professional societies and is Fellow of Institution of Engineers (India), Fellow of Indian Institute of Chemical Engineers (IIChE), Kolkata.

Enhancing the Properties of Recycled Aggregate Concrete Using Beneficiation Technique

Ram Lal Riyar, Kanish Kapoor, Mahesh Patel, and S. P. Singh

Abstract The concrete industry is a huge industry that is growing at a faster rate and that leads to the consumption of a plenty of Natural Aggregates (NA) which puts the non-renewable natural resources in danger of extinction and the NA resources are remarkably waning day by day. On the other hand, millions of tons of construction and demolition waste residues are generated. Therefore, the use of recycled concrete aggregate obtained from construction and demolition waste in new concrete is a solution for effective waste utilization. Recently, effective uses of Recycled Concrete Aggregate (RCA) in the concrete industry have attracted a lot of attention resource preservations but the use of recycled coarse aggregate directly does not give the safe result in terms of durability properties and compressive strength. So, it has must improved the properties of RCA for replacing it with NA. To enhance the properties of RCA, adhered mortar has to be removed or strengthened. Removing and strengthening the adhered mortar are the two common methods for improving the properties of RCA. The process of removal of adhered mortar is carrying by chemically and mechanically processed. The current study aimed to evaluate the strength and durability properties of concrete at different replacement levels of natural aggregate and recycled coarse aggregate. This study was also intended to enhance the strength and durability properties of concrete by using chemically and mechanically beneficiated recycled aggregate and thus recommend the most appropriate replacement level and the beneficiation method.

Keywords Beneficiation · Recycled concrete aggregate · Recycled aggregate concrete

R. L. Riyar (✉) · K. Kapoor · M. Patel · S. P. Singh
Department of Civil Engineering, Dr. B R Ambedkar National Institute of Technology, Jalandhar 144011, Punjab, India
e-mail: civilengineer.ramlal@gmail.com

K. R. Reddy et al. (eds.), *Sustainable Environment and Infrastructure*, Lecture Notes in Civil Engineering 90, https://doi.org/10.1007/978-3-030-51354-2_1

1 Introduction

Concrete, being to its availability, easy preparation and sculpture, is the most popular and highly dominated material in the construction industry. After water, concrete is the second highest consumed material. Due to the enormous amount of concrete produced, the demolition waste of concrete is generated in a huge amount. So, sustainability in construction should be increased by using renovation operations of demolition waste to diminish the impact associated with the material used. Construction and demolition waste (CDW) materials are produced in large quantities annually in the world. In the UK alone, the waste produced annually is 110 million tonnes which is 60% of the total waste produced [1]. Only 40% of this waste is recycled and reused. At the same time, a lot of natural aggregates are used. In India, 54 million tons of solid waste is produced every year and CDW makes 25% of it [2]. In developing countries, the construction industry is one of the biggest industries and the usage of a lot of virgin aggregates takes a toll on non-renewable natural resources which can be prevented if construction and demolition waste can be used in much more amounts than it has been used currently. But the use of recycled concrete aggregates decreases the strength of the aggregates and hence its use is limited. The use of Recycled Concrete Aggregate (RCA) can reduce compressive strength by up to 40% [3]. Thus, current standards and specifications limit the usage of recycled concrete aggregates.

Recycling of construction and demolition waste is not the most favorable solution to achieve a greater Sustainability as it is desirable to carry out some specific approach that can diminish the use of natural raw material and restrain the waste production. Thus, most of the CDW is still not recycled because of the reduced final strength of concrete and is deposited as a landfill. Due to this, useful lands are becoming dump yards for construction debris thus increasing the cost of the land. So, the more the CDW is recycled more virgin aggregates are replaced, and hence, less impact is there on the natural resources. But the reason the more CDW is not recycled is the decrease in the strength. So, if the strength of the RCA is somehow increased the replacement percentage can be increased. Also, the more replacement means less use of virgin aggregates which serves another purpose: the crushing to produce virgin aggregates evolves carbon dioxide gas in air which is another environmental hazard. Apart from their problems, certain minor issues are promoting the recycling of C&D waste [4]. Recycled concrete aggregates derived from construction and demolition waste have a lot of adhered mortar and are porous and less dense. The volume of the adhered mortar varies from 25 to 60% depending upon the amount of mortar [5]. This adhered mortar is the reason why the strength of recycled aggregate concrete (RAC) is less. Recycled aggregate can be extracted from demolished waste of concrete and thus it is termed as RCA [6].

The old mortar that is adhered to the aggregate is porous and has cracks and fissures which make it weak. In some researches, for a particle size of 20–30 mm, the adhered mortar was found to be 20% [7, 8]. The loss in strength is because of the additional Interfacial Transition Zone (ITZ). The presence of another (ITZ) in case

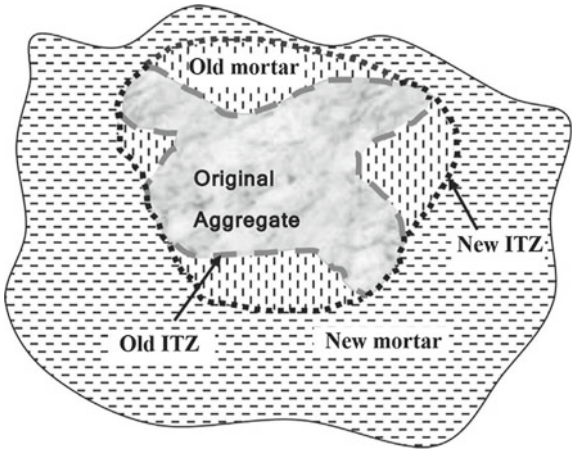

Fig. 1 Schematic of old and new ITZ in RCA concrete [7]

of RAC: one ITZ is between aggregate and old mortar (adhered mortar) and other ITZ is between old mortar and new mortar, which reduces the strength of recycled concrete aggregates. So, there are two planes of weakness in the recycled aggregate concrete. ITZ is highly porous and contains the crystals of calcium hydroxide in it which is a product of hydration of cement (Fig. 1).

There is a certain challenge that may develop in construction due to the deficiency and shortage of sources, limitation on the launch of new sources, and raised the cost of production. By using Recycled Aggregate (RA) it may help to locate some of these challenges. Recycled aggregate can be extracted from the demolished waste of concrete and thus it is termed as RCA [8]. There are many groups of countries like the UK, Germany, the Netherland, etc., which have been aiming to a target of 20–40% recycling rate of its demolition waste since 1995 [9].

2 Experimental Programs

2.1 Materials

Cement: There is Ordinary Portland cement of 43 grades is used with 28 days' compressive strength of 42.6 MPa. The physical properties of cement are given in Table 1.

Aggregates: Medium coarse river sand was used as Natural Fine Aggregate (NFA). The properties like water absorption, specific gravity were determined and are tabulated in Table 2.

Normal crushed stone was used as Natural Coarse Aggregate (NCA) in this investigation. The properties of NCA like flakiness and elongation index, specific gravity,

Table 1 Physical properties of cement

S. No.	Properties		Values obtained	Permissible values	Standard reference
1	Fineness		2.5%	Less than or equal to 10%	IS: 4031-1998(Part-1)
2	Standard consistency		31%	26–33%	IS: 4031-1998(Part-4)
3	Specific gravity		3.155	3.12–3.19	IS: 4031-1998(Part-3)
4	Initial setting time		43 min 50 s	Not less than 30 min	IS: 4031-1998(Part-5)
5	Final setting time		8 h 17 min	Not more than 10 h	IS: 4031-1998(Part-5)
6	Compressive strength	3 days curing	26 MPa	Not less than 23 MPa	IS: 4031-1998(Part-6)
		7 days curing	36 MPa	Not less than 33 MPa	

Table 2 Physical properties of fly ash

S. No	Properties	Values obtained	Permissible values	Standard reference
1	Specific gravity	2.642	2.4–3.0	IS: 2386-1963(Part-3)
2	Water absorption	2.17%	Less than 5%	IS: 2386-1963(Part-3)
3	Zone	II		IS: 2386-1963(Part-1)
4	Fineness modulus	2.81	2–4	IS: 2386-1963(Part-1)

and sieve analysis were found by performing various tests. The results are shown in below Table 3.

RCAs are produced from construction and demolition waste can be used as a replacement of aggregates in concrete. Both RCA and NCA had a maximum size of 20 mm and a minimum size of 4.75 mm. The properties of RCA like flakiness and elongation index, specific gravity, and sieve analysis were found by performing various tests. The results are shown in below Table 4.

Table 3 Properties of natural coarse aggregate

S. No.	Properties	Values obtained	Permissible values	Standard reference
1	Specific gravity	2.71	2.6–2.8	IS: 2386-1963 (Part-3)
2	Water absorption	1.6%	0.1–2%	IS: 2386-1963 (Part-3)
3	Flakiness index	16%	Less than 35%	IS: 2386-1963 (Part-1)
4	Elongation index	12%	Less than 35%	IS: 2386-1963 (Part-1)

Table 4 Properties of soil: fly ash mix

S. No.	Properties	Values obtained
1	Specific gravity	2.316
2	Water absorption	3.39%
3	Flakiness index	17.31%
4	Elongation index	19.41%

2.2 Beneficiation of RCA

RCA differs from NCA mainly because it contains two additional components: adhered mortar and an ITZ between the NCA and the original cement mortar. The original cement mortar attached to RCA is more porous than NCA. RCA has higher porosity and water absorption, and lower strength compared with NCA. To enhance the properties of RCA, adhered mortar has to be removed or strengthened. The process of removal of adhered mortar or strengthen of adhered mortar is called beneficiation of RCA. Removing and strengthening the adhered mortar are the two common methods for improving the properties of RCA. In this current study, the adhered mortar of RCA is removed by three methods named as a mechanical beneficiation, chemical beneficiation and combination of chemical-mechanical beneficiation. The beneficiated RCA is used to make the concrete at different percentage mixes with NCA. The Mechanically Beneficiated RCA (MBR) was treated in an abrasion testing machine for the removal of adhered mortar from RCA.

2.3 Mix Proportions

To investigate the effect of different types of beneficiated RCAs, the current study is aimed to design three concrete mixes with a replacement of 100% beneficiated RCA with NCA. These mixes are designed to produce concrete with a 28-day target strength of 30 MPa. The results are shown in Table 5.

Table 5 Mix proportions

Mix code	Water kg/m^3	OPC kg/m^3	FA kg/m^3	NA kg/m^3	RCA kg/m^3	MB RCA kg/m^3	CB RCA [0.5] kg/m^3	MCB RCA [0.5] kg/m^3	Fly Ash kg/m^3
C-N100	140	270	862	930	0	0	0	0	115
C-N0R100	140	270	862	0	930	0	0	0	115
C-N0MBR100	140	270	862	0	0	930	0	0	115

Fig. 2 Compressive testing machine

3 Testing of Concrete

3.1 Compressive Strength of Concrete

Compressive strength of concrete specimens was performed at the curing age of 7, 28, and 56 days. Concrete samples made with NCA, treated and untreated RCA, are tested at room temperature on digitalized Compression Testing Machine (CTM) with a maximum load limit of 1000 KN in accordance with IS:516 [10]. All specimens were tested straight after extraction from water at the surface dry condition. The size of the specimens used to conduct the compression strength was 150 mm × 150 mm × 150 mm and three specimens were tested in each of the concrete mixes to calculate the average compressive strength of concrete (Fig. 2).

3.2 Initial Surface Absorption Test

This test of concrete is used to determine the flow of water per unit area for a specific time period. The specimen used in this test setup is a cube of the size of 150 mm × 150 mm × 150 mm and the test is performed in reference to BS 1881-208:1996. Concrete specimen of each mix is tested at the curing age of 28 and 56 days. It is performed at the interval of 10, 30, and 60 min, and readings are noted as $I_{10,}$ $I_{30,}$ and I_{60} (Fig. 3).

Fig. 3 Initial surface absorption testing apparatus

3.3 Rapid Chloride Penetration Test

In the RCPT, the specimens were placed between two acrylic cells. One of the cells is filled with a NaOH solution and the other cell is filled with a NaCl solution. The cells were connected to a 60-V power source. The amount of charge that passes through the concrete disc specimen (50 mm × 100 mm slice) is measured for 6 h. The fundamental assumption behind this test is that more permeable concrete will allow more charge to pass through and vice versa. A charge that passes through the concrete sample is estimated and presented in coulombs. This quantified charge is an indirect estimate of the chloride ion penetration and the durability of concrete (Fig. 4).

4 Results and Discussions

4.1 Mechanical Treatment of RCA Results

Mechanical beneficiation of RCAs was done in Los Angeles abrasion apparatus. The results are shown in the graph-1 below (Fig. 5).

The revolution mechanism was repeated for five cycles of aggregates. Test results clearly show that there is a prominent increase in the removal of adhered mortar percentage while increasing the number of revolutions. The first cycle of revolution consists of 100 revolutions in which the removal percentage of the adhered mortar

Fig. 4 Rapid chloride penetration test apparatus

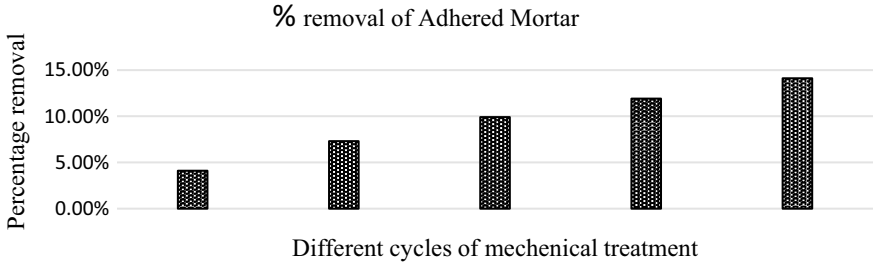

Fig. 5 Mechanical treatment of RCA

was 4.10%. Further, the percentage of removal of adhered mortar from RCA was 7.30%, 9.90%, 11.90%, and 14.10% for the 200, 300, 400, and 500 revolutions, respectively. Thus, it gives a clear understanding that the strength of RCA concrete can be enhanced by incorporating the mechanical beneficiation with higher no of revolutions.

4.2 Compressive Strength Test Results

The compressive strength test was performed at the curing age of 7, 28, and 56 days. This test was performed on three different types of concrete mixes, for example, fully NCA concrete mix (C-N100), fully RCA concrete mix (C-N0R100), and fully MBR concrete mix. The results are shown in the graph-2 below (Fig. 6).

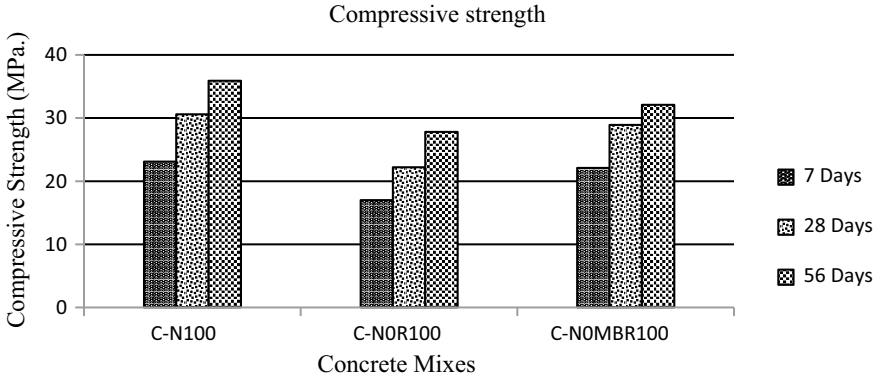

Fig. 6 Compressive strength test result

It was observed from the results that the compressive strength of beneficiated concrete mix (C-N0MBR100) become a little bit lesser equal to the strength of fully NA concrete mix (C-N100) at the curing age of 7 days, as the strength was only 4.34% less than the comparatively of C-N100. Moreover, a decrement of 26.4% was seen in compare to fully replaced recycled aggregate mix (C-N0R100) when compared to C-N100 at the curing age of 7 days. Similarly, the decrease in compressive strength of C-N0R100 and C-N0MBR100 at the curing age of 28 days was 27.4% and 7.8% when compared to the C-N100 concrete mix. Furthermore, only a 9% decrease of compressive strength was observed in the C-N0MBR100 concrete mix at the curing age of 56 days when compared to the C-N100 concrete mix. The results are shown in the graph-2 earlier.

4.3 Initial Surface Absorption Test Results

Cube samples of size 150 mm × 150 mm × 150 mm were made for Initial Surface Absorption (ISA) test and were tested for curing periods of 28 and 56 days for all the mixes. The results are shown in the graph-3 below (Fig. 7).

The ISAT (Initial Surface Absorption Test) results for 10-min period (ISA-10) were tested and it was found that the ISA-10 values were increased when NCA is replaced with RCA completely for a curing period of 28 days. The increase in the ISA-10, ISA-30, and ISA-60 values was of the order of 18.27, 22.86, and 30.08% at fully replacement of NCA with RCA for 28 days curing period. If ISA value is higher, it means there is surface porosity. The higher values of ISA-10 for concrete mixes C-N0R100 and C-N0MBR100 indicate higher porosity of concrete with respect to control C-N100 which can be because of the presence of RCA in the concrete mixes.

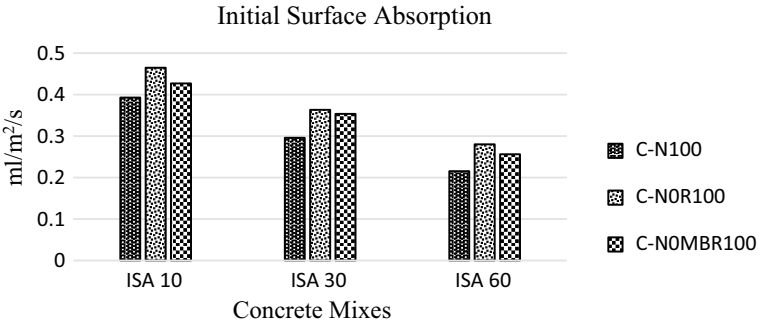

Fig. 7 Initial surface absorption test results

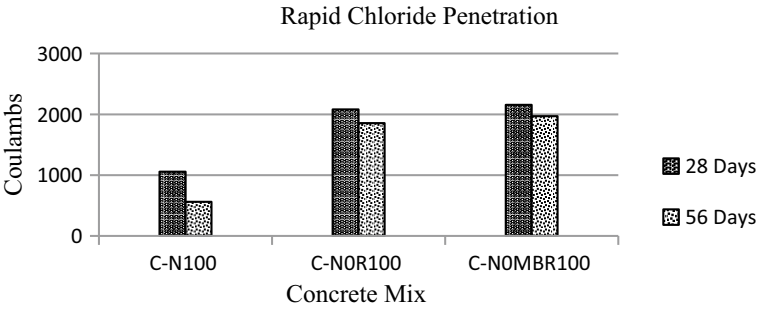

Fig. 8 Rapid chloride penetration test result

4.4 Rapid Chloride Penetration Test Results

In the RCPT, the current passing through the concrete specimens in the first 6 h is measured, and the resistance of the concrete chloride penetration is assessed according to the total charge passed within 6 h. The charge passed obtained from RCPT shows that the NA concrete mix C-N100 has a very low permeability, but the concrete mix made with recycled aggregate shows some less resistance against the chloride ion penetration, although C-N0R100 and C-N0MBR100 also come under the low category. The results are shown in the graph-4 below (Fig. 8).

5 Conclusion

This research aiming to banish fears regarding the use of RCA into fresh concrete, some of the very useful conclusions were obtained. The key conclusion of this research is that the properties of RCA can be enhanced in such a way to be used in some major construction activities. A simple treatment method, in the recycling

process of RCA, is capable to reduce the percentage of adhered mortar at such level that decreases the negative effects and creates a better quality RAC which is competitive to normal concrete.

The gap in compressive strength of concrete made with fully recycled aggregate is 26% at the curing age of 28 days. However, this gap can be reduced by up to 5.6% by removing the adhered mortar and enhancement of recycled aggregate. So, by the use of mechanical treatment on RCA, the compressive strength is increased. The surface absorption of the RCA concrete mix is increased; by the beneficiation method, these gaps are reduced. The chloride penetration in concrete made with RCA is increased; however, these chloride penetration values are under the low category. So, these results conclude that compressive strength and durability properties of concrete made with RCA can be increased by using the beneficiation method on RCA.

References

1. Akbarnezhad A, Ong KCG, Zhang MH, Tam CT, Foo TWJ (2011) Microwave-assisted beneficiation of recycled concrete aggregates. Constr Build Mater 25(8):3469–3479
2. Behera M, Bhattacharyya SK, Minocha AK, Deoliya R, Maiti S (2014) Recycled aggregate from C&D waste & its use in concrete—A breakthrough towards sustainability in construction sector: a review. Constr Build Mater 68:501–516
3. Dilbas H, Şimşek M, Çakir Ö (2014) An investigation on mechanical and physical properties of recycled aggregate concrete (RAC) with and without silica fume. Constr Build Mater 61(March 2006): 50–59
4. Duan ZH, Poon CS (2014) Properties of recycled aggregate concrete made with recycled aggregates with different amounts of old adhered mortars. Mater Des 58:19–29
5. George D, Pericles S, Petrou MF (2018) Enhancing mechanical and durability properties of recycled aggregate concrete. Constr Build Mater 158:228–235
6. Kisku N, Joshi H, Ansari M, Panda SK, Nayak S, Dutta SC (2017) A critical review and assessment for usage of recycled aggregate as sustainable construction material. Constr Build Mater 131:721–740
7. Gholampour A, Ozbakkaloglu T (2018) Time-dependent and long-term mechanical properties of concretes incorporating different grades of coarse recycled concrete aggregates. Eng Struct 157(September 2017):224–234
8. Huang Y, He X, Sun H, Sun Y, Wang Q (2018) Effects of coral, recycled and natural coarse aggregates on the mechanical properties of concrete. Constr Build Mater 192:330–347
9. Kurda R, de Brito J, Silvestre JD (2017) Combined influence of recycled concrete aggregates and high contents of fly ash on concrete properties. Constr Build Mater 157:554–572
10. Pepe M, Toledo Filho RD, Koenders EAB, Martinelli E (2014) Alternative processing procedures for recycled aggregates in structural concrete. Constr Build Mater 69:124–132

Early Introduction of STEM Through Sustainable Engineering

Tyler Klink, Morgan Sanger, Renee Olley, Angela Pakes, Tuncer Edil, and Sydney Klinzing

Abstract To educate the next generation of scientists and engineers, it is important to cultivate critical thinking and problem-solving skills within the context of sustainability. *Eva the Engineer*, an elective course developed by the University of Wisconsin–Madison engineering students, uses sustainability-focused civil engineering lessons to (1) introduce sustainable engineering practices at the middle school level and (2) encourage young women to pursue science, technology, engineering, and mathematics (STEM). *Eva the Engineer* students explore the environmental, social, and economic impacts of the infrastructure around them and practice sustainable engineering decision-making with hands-on activities. The primary topics of discussion are infrastructure design, water resources, and waste management. As civil engineering is a central theme of the course, the primary examples of sustainable engineering involve the energy and water reductions using recycled materials in construction applications. For example, students make concrete stepping-stones with recycled materials and calculate energy, water, and greenhouse gas emission savings achieved when recycled materials replace virgin aggregate in concrete. Later, a field trip to a concrete production facility, a landfill, a recycling facility, and a wastewater treatment facility demonstrate the practical implications of construction and waste generation. By the end of the program, students exhibit an understanding of contemporary environmental challenges, basic engineering principles, and the benefits of recycled materials in engineering applications. Program survey results also illustrate a ubiquitous increase in self-confidence in STEM capabilities among students. Engaging the next generation of engineers and scientists in a discussion of present issues is proving to be beneficial for all involved.

Keywords Recycled materials · Education · Sustainability · Civil engineering

T. Klink (✉) · M. Sanger · R. Olley · A. Pakes · T. Edil · S. Klinzing
University of Wisconsin-Madison, 1415 Engineering Dr., Madison, WI 53706, USA
e-mail: tklink2@wisc.edu

K. R. Reddy et al. (eds.), *Sustainable Environment and Infrastructure*, Lecture Notes in Civil Engineering 90, https://doi.org/10.1007/978-3-030-51354-2_2

1 Introduction

A study published in Science magazine reported children at the age of 5 are equally as likely to assume a person of their own gender when given the description "A person in my office is really, really smart—they solve problems faster and better than anyone else." By the age of 6 and 7, however, girls are 20–30% less likely than as their male counterparts to assume the person being talked about is of their own gender [1]. It is not clearly understood exactly what causes this early and dramatic shift, but this pattern continues into adulthood. According to the 2009 Census, women hold 48% of total jobs in the United States, but only 24% of all science, technology, engineering, and mathematics (STEM) jobs. The lowest percentages of women are found in engineering fields, only 14% of engineers in the United States are female [2]. There are clear obstacles for women to enter STEM fields, and this has a negative impact on those fields.

In learning of the *Science* magazine article and observing the gender discrepancy in the engineering courses at the University of Wisconsin–Madison, the authors were inspired to visit local middle schools and encourage young women to consider pursuing STEM. The authors developed a program called *Eva the Engineer* to teach young women in Madison area middle schools. The title of the program, *Eva the Engineer,* was intended to personify a female engineer of any cultural background such that she is approachable and relatable to all students. Additionally, the alliteration of *Eva the Engineer* continues with the program objectives: to educate, excite, and encourage young women to pursue careers in sustainability and civil engineering. Each lesson has a technical focus and utilizes hands-on activities to inspire critical thinking and problem-solving. The *Eva the Engineer* course curriculum uses hands-on activities to teach lessons on sustainability, the principles of civil engineering, and women in STEM. Life cycle assessments, water use and water treatment, concrete materials, and the use of recycled materials in construction applications are just a few of the sustainability-focused engineering principles developed to engage and inspire young female students. This report illustrates the curriculum development process and presents the results of the *Eva the Engineer* program using pre- and post-program surveys.

2 Program Development and Implementation

2.1 Program Development

All lessons created for the program were original and drew upon fundamental engineering concepts such as force design, product sustainability, and project planning. The mission of the program is to "Educate, Excite and Encourage young women to pursue careers in STEM," with a focus on sustainability and civil engineering.

Learning objectives and lesson materials were developed within the scope of the mission.

2.2 Curriculum Outline

The course content was organized and developed in three units: professionalism, sustainability, and infrastructure. The units were selected to teach the principles of civil engineering, sustainability, and women in STEM. Each unit is described in some detail in this section, and a summary curriculum map is presented in Table 1.

Sustainability Unit. In the sustainability unit, examples and products from civil engineering and from daily life are used to demonstrate the environmental, social, and economic components of sustainability. Students engage with contemporary environmental issues surrounding water usage, municipal solid waste, and construction and demolition waste. Students conduct qualitative and simple quantitative life cycle assessments of a shoe, bottled and tap water, and recycled materials in construction applications. Students learn to define sustainability and critically consider the impacts of personal decisions and the impacts of engineering decision-making in infrastructure. The sustainability unit is identified as Unit 1 in Table 1.

Professionalism Unit. In the professionalism unit, lessons emphasize the historical impact of women on science and engineering, and how that has translated to the workforce today. Practical applications of the engineering and sustainability concepts are enforced with a field trip experience. The field trip includes tours of a ready-mix concrete facility, a recycling facility, and the county landfill. After the field trip, many students noticed that there no women were encountered throughout the day at any of the visited sites. This important observation is addressed in the course with examples of women in STEM history and local women in STEM. Homework for this course involves reading and interacting with the book *Women in Science: 50 Fearless Pioneers Who Changed the World* to illustrate the crucial role of women in STEM history [3]. In the final lesson of the program, a panel of women in STEM careers from the Madison area is assembled to speak with the class and answer questions. In this forum, the students interact with and relate to these women. The professionalism unit is identified as Unit 2 in Table 1.

Infrastructure Unit. In the infrastructure unit, lessons focus on the design and materials of modern infrastructure. Simple structural design is presented using static force balance and force body diagrams. Interactive team projects require students to build small structures with limited materials and time, exercising static force concepts and their problem-solving abilities. Team projects encourage participation and engage the students in a small-group discussion regarding the lesson material. In this unit, the use and composition of concrete are a primary focus because concrete is the most prevalently used material in the construction industry. Students learn the different ingredients of concrete and the purpose of each component using a cookie analogy. The students also have the opportunity to work with concrete in both its

Table 1 Curriculum map

Unit*	Objective	Content	Assessment
2	Introduce the course	Women in STEM statistics, class core concepts [2]	Introductory survey
2	Breadth of STEM fields	Breadth of STEM fields, Responsibilities of engineers [4]	Women in STEM worksheet
1	Waste generation and treatment	Waste sources, Solid waste treatment [5]	Landfill in a bottle activity
3	Concrete uses and components	Concrete history, Concrete impacts, recycled materials	Analogy of concrete mix design and cookies
2	Occupations in civil engineering	Field trip to wastewater treatment plant, concrete production facility, landfill, recycling facility	
1	Global water usage, LCAs	Global water usage, qualitative LCA comparison [6, 7]	Personal water usage sheet
1	Construction waste	Construction waste generation and disposal [8, 9]	Decomposition rate survey
1	Practice LCA	Product sustainability, Triple bottom line [10]	LCA of a Boot worksheet
3	Infrastructure	Infrastructure definition and importance [11, 12]	UCLA water main case study
3	Mechanics, infrastructure	Compressive and tensile forces, static force equilibrium [13]	Popsicle bridge design and creation
3	Mechanics, infrastructure	Engineering decision-making, material use [13]	Newspaper chair design and creation
3	Experience with concrete	Components of concrete, recycled materials	Concrete stepping stones
1	Recycled materials in construction	Recycled concrete, Acid–base chemistry	Water and concrete chemistry experiment
2	Celebrate women in STEM	Accomplishments of women in STEM history [3]	Women in STEM Bingo
2	Interact with professional STEM women	Career panel of local professional women in STEM	Exit survey

*Unit 1: Professionalism; Unit 2: Sustainability; Unit 3: Infrastructure

viscous and solid phases, an opportunity not available to most middle school students. The infrastructure unit is identified as Unit 3 in Table 1.

2.3 Lesson Instruction

Eva the Engineer has been taught three times at three different schools in the Madison area: Badger Rock Middle School, Toki Middle School, and Verona Badger Ridge Middle School. For the first two iterations of the program, the elective class was taught once a week for an hour for one academic quarter. In the third and most recent generation of the program, the curriculum was expanded to 15-hour-long lessons taught weekly as an after-school program.

The lessons are generally structured to include a 10-minute lecture introducing the technical concept followed by a hands-on activity. The instructors maintain student engagement during the lecture by establishing an open discussion of the material, and by posing questions to incite critical thinking, per the Socratic Method. The hands-on activities allow the students to practice problem-solving, communication, teamwork, and understanding of the technical concepts.

3 Results

Eva the Engineer has proven to be beneficial for the middle school students, the instructors, and the partners from industry. The students enrolled in the course are afforded an opportunity to explore engineering in an approachable and engaging environment. While there are local day programs for young women in science and technology, bringing the program directly to the classroom made the opportunity accessible for students of all socioeconomic backgrounds. By providing students with role models they could relate to, it was conveyed that people of all identities and backgrounds are capable of succeeding in STEM fields.

To quantify the impact of the program and to solicit feedback from the students, pre- and post-program surveys are administered. The surveys first ask the students to evaluate their perceptions of their own abilities on a scale of 1–10 (1 = incapable, 10 = very capable) in nine categories pertinent to STEM careers: problem-solving, math, science, writing, confidence, social, leadership, creativity and hard-working. During the first and last sessions of the program, the students are given a survey to evaluate their perceptions of their own abilities in categories pertinent to STEM careers. Most notably, the female students rate themselves higher in all nine categories at the end of the program (Fig. 1). Figure 1 demonstrates that, following the lessons and activities, the students feel more certain in their own STEM capabilities. This observed tendency is consistent for each of the three schools.

A control group of male students was surveyed using the same method in order to compare to the pre-program survey administered to the female students (Fig. 2).

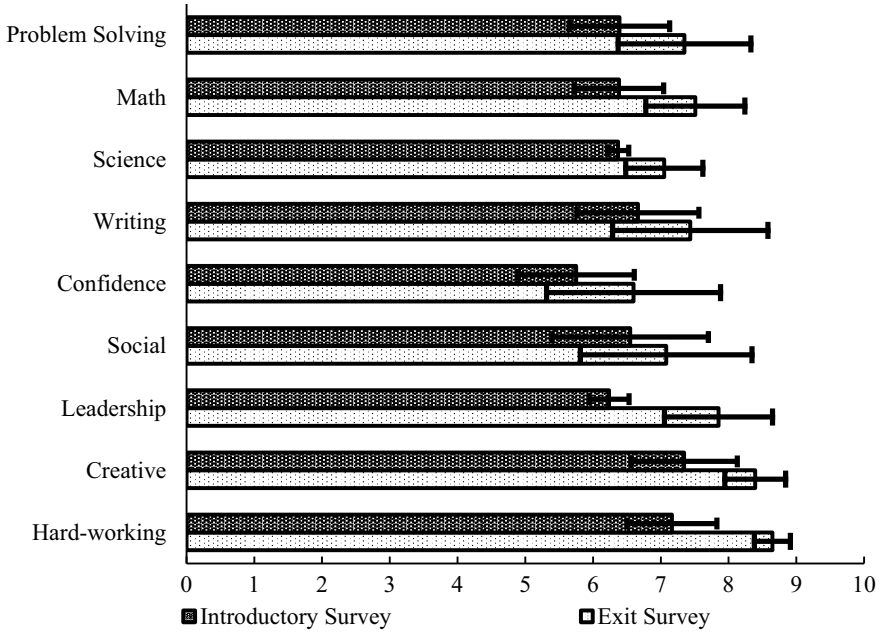

Fig. 1 Average response and standard deviation of 43 female students when asked to rate themselves on a scale of 1–10 in the listed categories

Different sample sizes limit the conclusiveness of this data; however, the present data illustrate some a difference in perception of capabilities dependent upon gender. Female students rate themselves highest in writing capabilities, creativity, and work ethic, and rate themselves lowest in math, science, leadership, and problem-solving (Fig. 2). Male students rate themselves highest in social skills, leadership, problem-solving, confidence, and work ethic, and lowest in writing and creativity (Fig. 2).

In addition to the self-evaluation survey, the end of the program survey includes a feedback questionnaire. The students are asked to recall the most interesting thing they learned in *Eva the Engineer*, and their responses include:

1. "How many different engineering jobs there are."
2. "That engineering is more than one thing."
3. "How big of an impact it is to drink bottled water (social and economic impact)."
4. "There is a degree for exercise."

The responses of the students indicate that the content and activities of the program achieve the mission to educate, excite, and encourage young women in STEM fields. The responses of the first and second students tell communicate that the students are introduced to potential careers that they did not yet know. The third student commented that the most interesting thing that she learned was the relative impacts of drinking bottled water instead of tap water, referring to the social and economic impacts; she is recalling information from the second lesson, demonstrating that the

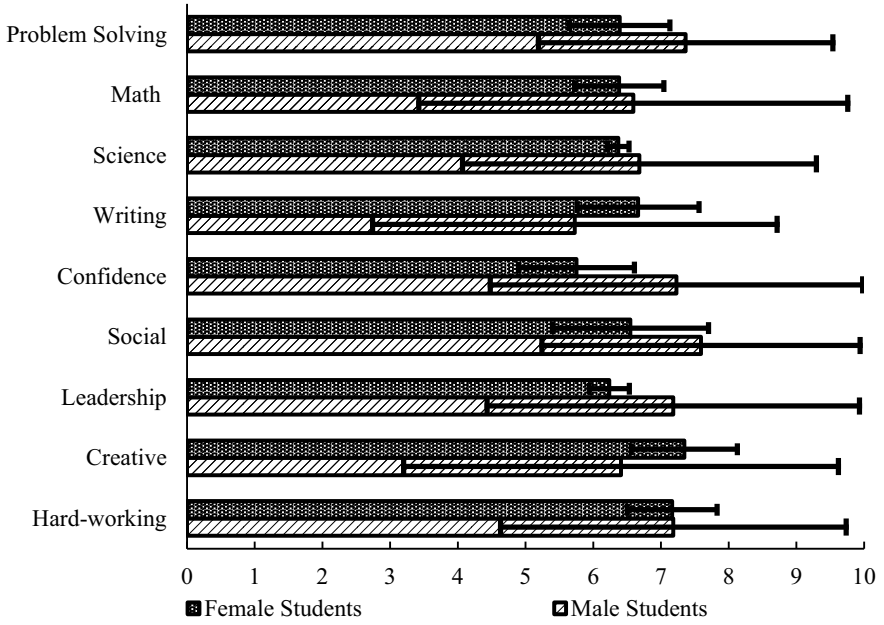

Fig. 2 Average response and standard deviation of student responses when asked to rate themselves on a scale of 1–10 in the listed categories. Note sample sizes: 43 female students, 13 male students

material and activities were impactful and memorable. The fourth student was most interested to learn that there is a college degree for exercise. She is referring to one of the women on the Women in STEM career panel who has a degree in kinesiology. This comment is great feedback because although the student may not have been as interested in civil engineering as a future career, the career panel in the final lesson showed her other STEM opportunities that she found interesting.

4 Conclusions

A program such as *Eva the Engineer* is critical in educating the next generation of female engineers and scientists, engaging them in discussions of contemporary environmental challenges, and instilling fundamental engineering principles. Students leave the STEM program with increased confidence in their abilities related to sustainability and engineering. By presenting examples of successful female engineers of diverse backgrounds and allowing young women to explore the engineering field interactively, students envision themselves succeeding in STEM fields. Having more women in STEM will benefit the industry, as a more diverse workforce will be better equipped to deal with the engineering challenges of the future.

The authors are planning to continue this program in schools within Dane County, Wisconsin and looking to expand the impacts of the program via industry partnerships. Future funding of this program would sponsor the development of a downloadable website package, complete with all program materials, available for university students across the nation to use to teach the program in their communities.

Acknowledgements This research was funded by the Morgridge Center for Public Service at the University of Wisconsin–Madison, the Wisconsin Concrete Pavement Association, and the Portland Cement Association. The authors greatly appreciate and acknowledge their support. The authors would also like to thank Hong Tran and Jamie Ames from Badger Rock Middle School, Nicole Schaefer and Elizabeth Long from Akira Toki Middle School, and Alan Buss, John Bremmer, and Michael Murphy from Badger Ridge Middle School for their partnership, administrative support, and supervision in conducting the program. The authors would also like to thank Kevin McMullen from the Wisconsin Concrete Pavement Association for serving as a community and industry partner. The Recycled Materials Resource Center at the University of Wisconsin–Madison provided financial support, technical content, and guided development of the program.

References

1. Hioslki E (2017) Young girls are less likely to believe their gender is brilliant as they age. Science. https://doi.org/10.1126/science.aal0663
2. Economics and statistics administration: women in STEM: A gender gap to innovation. United States Department of Commerce (2011). https://www.esa.doc.gov/sites/default/files/womeninstemagaptoinnovation8311.pdf
3. Ignotofsky R (2016) Women in science: 50 fearless pioneers who changed the world. Ten Speed Press, Berkeley, California
4. American Society of Civil Engineers: Code of Ethics (1914)
5. Bureau of land management: It's a gas. U.S. Department of the Interior (2018). https://www.blm.gov/wo/st/en/res/Education_in_BLM/Learning_Landscapes/For_Teachers/science_and_children/energy/index/energy8.html
6. Mekkonnen M, Hoekstra A (2011) National water footprint accounts: the green, blue, and grey water footprint of production and consumption. Value of water research support series No. 50, UNIESCO-IHE, Netherlands
7. United State geological survey water school: how much water does the average person use at home per day. United States Geological Survey (2016)
8. Delaney P (2013) How long it takes for everyday items to decompose. https://www.down2earthmaterials.ie/2013/02/14/decompose/
9. Product Stewardship Institute Inc.: Marine debris and plastic source reduction toolkit for colleges and universities. United States Environmental Protection Agency (2015). https://www.epa.gov/sites/production/files/2016-03/documents/marine-debris-toolkit-epar9-2015.pdf
10. Masanet E (2014) How green is that product? An introduction to life cycle environmental assessment. Northwestern University
11. Global Projects Center: What are key infrastructure in our community and in the United States today. Stanford University (2015)
12. Global Projects Center: What does the California water project tell us about public work infrastructures. Stanford University (2015)
13. Costanzo F, Gray G, Plesha M (2009) Engineering mechanics: statics, 2nd edn. McGraw-Hill, New York

Prediction of Moisture Damage in Asphalt Pavements Using a Nanomechanistic Approach

Sumon Roy and Zahid Hossain

Abstract Stripping-related moisture damage in asphalt pavements is a complex phenomenon that deteriorates the durability and performance of the pavements. In recent years, several studies have been conducted at both macro- and micro-levels to find the root causes of the moisture damage. The main goal of this study is to predict the moisture-induced damage using one of the emerging technologies using an Atomic Force Microscopy (AFM) tool. Binder samples originated from two different crude sources have been collected and tested in the laboratory using an advanced mode of nanomechanical mapping, namely the Peak Force Quantitative Nanomechanical Mapping (PFQNM™) mode. In this study, two Performance Grade (PG) base binders and their modified counterparts using polyphosphoric acid (PPA), styrene–butadiene–styrene (SBS), and SBS plus PPA have been evaluated to achieve the goals of this study. To observe the moisture effects, asphalt binder samples were tested under both dry and wet conditions. Test results showed that the surface topography of the asphalt binders and their mechanical properties have had changed notably because of the presence of moisture. It is also evident that the base binders used in this study are highly susceptible to moisture damage, whereas SBS-modified binders have sufficient strength that can be used for the construction of durable pavements. The findings of this study are expected to the State Departments of Transportations (DOTs) and other transportation agencies to gain in-depth knowledge of moisture damage mechanisms in asphalt pavements.

Keywords Moisture damage · Asphalt pavements · Atomic force microscopy (AFM)

S. Roy · Z. Hossain (✉)
Arkansas State University, State University, Jonesboro, AR 72467, USA
e-mail: mhossain@astate.edu

K. R. Reddy et al. (eds.), *Sustainable Environment and Infrastructure*, Lecture Notes in Civil Engineering 90, https://doi.org/10.1007/978-3-030-51354-2_3

1 Introduction

1.1 Background of the Study

Moisture damage due to stripping is a major concern to state highway and transportation agencies. According to some researchers, moisture damage can be defined as the loss of strength/stiffness in the presence of moisture as a result of mechanical loading, which is also known as stripping [1]. It is reported that this phenomenon may occur due to the penetration of water into the asphalt mixtures that lowers their mechanical properties [2]. Moreover, some researchers reported that stripping-related moisture damage has a significant effect in inducing other pavement distresses, including rutting and fatigue cracking, pumping, raveling, and potholes [1, 2]. Similarly, Cho and Kim [3] reported that the presence of moisture can accelerate damage in asphalt pavements as a combined effect of other types of distresses [3]. Therefore, moisture damage is considered as a serious concern in designing and constructing of new asphalt pavements.

Moisture damage in asphalt concrete is a complex mechanism, and it can happen due to the failure of the bond between the asphalt binder and the aggregate (also known as adhesive failure), or due to failure within binder itself (also known as cohesive failure) or a combined effect of adhesive and cohesive failures [4, 5]. Multiple researchers also reported that moisture damage resistance of asphalt mixtures largely depends on the adhesive bond strength of the asphalt binder–aggregate system in dry and wet conditions [6, 7]. To describe the root causes of moisture damage in asphalt mixtures, several studies have been conducted. Mostly, the current moisture sensitivity tests methods, such as tensile strength ration (TSR), are empirical and focused on macro-level test results. Thus, the necessary conclusions are made merely based on the overall strength of the specimens and unable to quantify the moisture-induced damage in the asphalt mixtures [2]. Therefore, a comprehensive knowledge of moisture damage mechanism at the atomic level is expected to be helpful to develop an effective tool or model to quantify the moisture damage of asphalt pavements.

In recent years, the Atomic Force Microscopy (AFM) technique, one of the emerging technologies, has been used to analyze the surface morphology and mechanical properties such as adhesion, deformation, DMT (Derjaguin, Muller, and Toropov) modulus, and energy dissipation of asphalt binders [8–13]. These researchers described the binders' morphology based on three distinct phases, namely the dispersed phase (Catana), the interstitial phase (Peri-phase), and the matrix (Para-phase). The AFM tools were also used by several researchers in the qualitative characterization of the micromechanical properties of the asphalt binders [14–16]. Moreover, AFM technology was found to be useful in evaluating the moisture susceptibility of asphalt binders and mixture samples [2, 17, 18]. This study focuses on mainly two different mechanical properties (modulus and adhesion force values) to predict the moisture damage of asphalt materials using the AFM tests.

1.2 Objectives of the Study

The main goal of this study is to quantify the moisture resistance of asphalt binders. Specific objectives of this study are to (i) analyze the morphological and mechanical properties of the asphalt binders at the atomic level and (ii) predict the moisture susceptibility of asphalt binders based on the AFM tests results.

2 Materials and Test Methods

2.1 Materials

In this study, asphalt binders used were collected from two different sources, namely Source 1 (S1) and Source 2 (S2) Two performance grade (PG) binders, PG 64–22 binders, were evaluated as the base binders because of their suitability in pavement constructions in Arkansas PG 64–22. In addition, Polyphosphoric Acid (PPA)-modified PG 70–22 binders, Styrene–Butadiene–Styrene (SBS)-modified PG 76–22 binders, and the binders modified with both PPA and SBS were also tested in this study. Sample specimens were tested under dry and wet conditions to observe the moisture effects by using the AFM tool.

2.2 Sample Preparation for the AFM Tests

Two sets of specimens were prepared from the asphalt binder samples for conducting the AFM tests by following the heat cast approach (HCA). Several researchers used this approach as it provides a smooth surface of the asphalt binder for the AFM testing [15–17]. A brief description of the sample preparation is stated below:

Dry Sample Preparation

(i) At first, a small amount of asphalt binder is placed on a 2in. x 3in. (50 mm × 75 mm) glass plate.
(ii) The glass plate was then placed in an oven at 160 °C for about 15 min. However, the heating time is extended from 15 to 20 min for stiff binder samples.
(iii) A uniform and smooth surface of the asphalt binder is developed on the glass plate during this time of heating.
(iv) Later, one set of the heat cast samples was stored in a humidity-controlled desiccator.
(v) These specimens were called “Dry” and were tested using the AFM techniques after three days.

Wet-conditioned Sample Preparation

(i) The "Wet-conditioned" specimen was prepared using another set of heat cast samples. These specimens were stored in the desiccator and were removed after an hour of curing time in the air considering that microstructures of the specimens were stabilized within this time period.
(ii) Later, the air-cured specimens were placed in aluminum cans, which were filled with deionized water with a minimum of 1 inch (25 mm) depth of water above the specimens.
(iii) Then the aluminum cans containing the submerged specimens were placed in a vacuum container.
(iv) Later, a vacuum of 20–25-Hg partial pressure (67–84 kPa absolute pressure) was applied for 10 min using a vacuum oven at 104 °F (40 °C).
(v) Afterward, the de-gassed specimens were left submerged in water for another 10 min.
(vi) Then each specimen was placed in a ziplock bag in which 10-ml deionized water was added.
(vii) The specimens were then placed in a freezer at 68 °F (−20 °C) for 24 ± 1 h.
(viii) After 24 h of freezing, the specimens were removed from the freezer and placed in a water bath for another 24 ± 1 h at 140 ± 0.5 °F (60 ± 1 °C).
(ix)) Then the specimens were placed in a water bath for another 2 h ± 10 min at 77 ± 1 °F (25 ± 0.5 °C maintaining a water depth of 1 inch above the specimens.
(x) The specimens were then removed from the water bath and the excess water was dabbed off from the surface of the specimens using paper towels.
(xi) Later, the specimens were placed in the oven for 16 h at 77 ± 2 °F (25 ± 1 °C) to remove the free water from the surface of the asphalt binders.
(xii) Thus, the prepared specimens were called "wet-conditioned" and were then tested using the AFM tool.

2.3 The AFM Tests Parameters

In this study, a Dimension Icon AFM (Bruker Inc.) was used to evaluate the prepared all specimens using the Peak Force Quantitative Nanomechanical Mapping (PFQNM™) mode of AFM at an ambient temperature of 25 °C. A scan size of 10 μm × 10 μm, a scan rate of 0.500 Hz, and the samples/lines of 512 were selected as the scan parameters during the tests. Three replicates were tested for each test condition and the average values were taken to compare the test results. Afterward, the AFM-based maps were analyzed to observe the surface morphology and mechanical properties of asphalt binder were using the NanoScope Analysis 1.5 software.

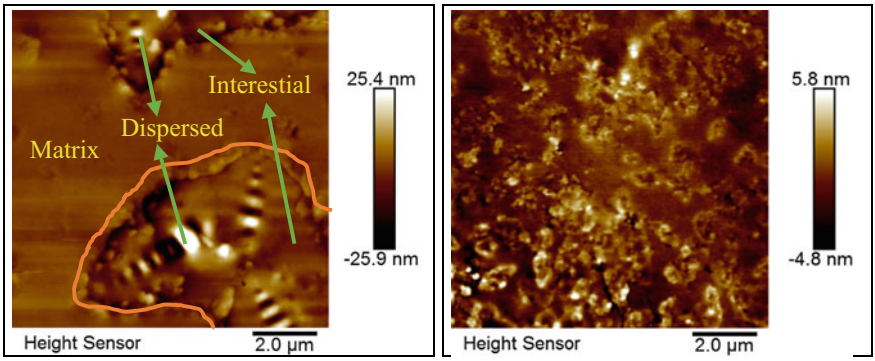

Fig. 1 Typical AFM maps of morphology of PG 70–22 (SBS-modified) binder of S2: dry sample (left side) and wet-conditioned sample (right side)

3 Analysis of Results and Discussions

3.1 Moisture Effects on Morphology

Based on the AFM test results, three distinct phases, namely Dispersed (Catena), Interstitial (Peri), and Matrix (Perpetua) were evident in the binder's surface topography. The "bee structures" were found to be changed significantly in quantity, size, and shape in most of the asphalt binders. Interestingly, these bees are decreased in numbers and sometimes found to be dispersed in the wet-conditioned specimens. The overall average surface roughness values were reduced by nearly 50% (from 4.9 nm to 2.11 nm) for SBS-modified S1 and S2 binders. However, the control and PPA-modified binders from S2 showed an opposite phenomenon where a smaller increment was noticed in the wet-conditioned specimens. Thus, it can be concluded that moisture damage has a significant effect on the degradation of the microstructures of binder samples. Figure 1 shows typical morphological maps of an SBS-modified binder obtained from the AFM scan.

3.2 Moisture Effects on Modulus Values

The moisture effects on the DMT modulus values were also observed from the AFM test results, which are summarized in Table 1. As seen from Table 1, lower modulus values are found for S1 binders in the wet-conditioned specimens than their corresponding binders from S2. Also, the modulus value for PPA-modified binder of S2 reduced from 963 to 491 MPa.

Based on the AFM test results, PG 64–22 binder showed a higher value ranging from 43 to 175 MPa, a lower variation in modulus values was observed in the cases of

Table 1 Moisture Effects on Modulus (MPa) Values using AFM

Binders	Sample condition	Source 1 (S1) Binders			Source 2 (S2) Binders		
		Average value	Dispersed and interstitial phase	Matrix phase	Average Value	Dispersed and interstitial phase	Matrix phase
PG 64–22	Dry	536	250–842	79–324	43	30–114	26–51
	Wet	272	56–630	53–339	175	43–345	39–225
PG 70–22 (PPA)	Dry	462	120–1334	56–278	963	747–1173	444–965
	Wet	198	70–546	57–122	491	195–814	74–494
PG 70–22 (SBS)	Dry	490	188–2028	128–723	591	264–1085	244–473
	Wet	306	65–532	44–353	652	303–2005	231–563
PG 76–22 (SBS + PPA)	Dry	142	36–342	20–132	173	111–359	62–130
	Wet	76	53–133	46–81	189	951–406	64–197

PPA- and SBS-modified binders (e.g., from 173 to 189 MPa) among all S2 binders. Moreover, it can be concluded that PPA plus SBS-modified binders from S1 and S2 had a better moisture resistance among all the asphalt binders tested in this study. Furthermore, it can also be said that the base binders tested in this study were found to be most susceptible to moisture damage.

3.3 Moisture Effects on Adhesion Values

Table 2 presents a comparison of the average adhesion values of tested binder samples due to the presence of moisture. The AFM test results showed that the average

Table 2 Moisture effects on adhesion force (nN) values using AFM

Binders	Sample Condition	Source 1 (S1) Binders			Source 2 (S2) Binders		
		Average Value	Dispersed and interstitial phase	Matrix phase	Average value	Dispersed and interstitial phase	Matrix phase
PG 64–22	Dry	85	18–172	13–94	5	2–16	1–5
	Wet	20	4–52	2–19.4	10	3–29	2.22–10
PG 70–22 (PPA)	Dry	113	50–199	12–125	221	160–278	113–209
	Wet	54	18–112	7–24	130	74–190	34–122
PG 70–22 (SBS)	Dry	16	7–24	3–14.5	13	3–16.2	1–8
	Wet	9	3–11	2–5	11	3–20	2–8
PG 76–22 (SBS+PPA)	Dry	31	17–79	4–14	24	12–39	3–11
	Wet	7	2–20	2–9	33	14–84	5–36

adhesion values were reduced in all S1 binders due to the moisture damage. The PPA plus SBS-modified PG 76–22 binder provided the lowest reduction rate in adhesion values than any binder from S1 varied from 31 to 7 nN. A similar decreasing pattern was also observed for S2 binders except SBS-modified PG 70–22 which varied from 13 nN to 11.50 nN. It is well known that a high adhesion value of asphalt binder is an indicator of high resistance against moisture damage. The AFM test results concluded that SBS-modified binders from both sources (S1 and S2) showed a better resistance to moisture damage as they provided higher adhesion values in the wet condition than the dry specimens.

4 Conclusions

In this study, an AFM tool was used to evaluate morphology and mechanistic properties such as modulus and adhesion values to predict the asphalt binder's moisture damage resistance. Based on the findings of this study, it can be said that an AFM can be a useful tool to investigate the molecular-level properties of asphalt binders. It is observed that SBS or PPA plus SBS-modified PG 70–22 and PG 76–22 binders were found to have a better resistance to moisture damage, while the base binders were more susceptible to moisture damage than any other tested binders were.

References

1. Moraes R, Velasquez R, Bahia HU (2011) Measuring the effect of moisture on asphalt-aggregate bond with the Bitumen bond strength test. Transp Res Rec: J Transp Res Board 2209(1):70–81
2. Yao Z, Zhu H, Gong M, Yang J, Xu G, Zhong Y (2017) Characterization of asphalt materials' moisture susceptibility using multiple methods. J Constr Build Mater 155:286–295
3. Cho D-W, Kim K (2010) The mechanisms of moisture damage in Asphalt pavement by applying chemistry aspects. KSCE J Civ Eng 14(3):333–342
4. Little DN, Jones DR (2003) Chemical and mechanical processes of moisture damage in hot-mix asphalt pavements. In: National seminar on moisture sensitivity of asphalt pavements, TRB Miscellaneous Report, pp 37–70
5. Santucci L (2010) Minimizing moisture damage in Asphalt pavements. In: Pavement technology update, University of California Pavement Research Center, 2(2), pp 1–12
6. Bhasin A, Howson JE, Masad E, Little D, Lytton RL (2007) Effect of modification processes on bond energy of asphalt binders. Transp Res Rec 1988:29–37
7. Masad E, Zollinger C, Bulut R, Little DN, Lytton RL (2006) Characterization of HMA moisture damage using surface energy and fracture properties. Asphalt Paving Technology: Association of Asphalt Paving Technologists 75:713–748
8. Masson JF, Leblond V, Margeson J (2006) Bitumen morphologies by phase-detection atomic force microscopy. J Microsc 221(1):17–29
9. Dourado ER, Simao RA, Leite LFM (2012) Mechanical properties of asphalt binders evaluated by atomic force microscopy. J Microsc 245(2):119–128
10. Fischer H, Stadler H, Erina N (2013) Quantitative temperature-depending mapping of mechanical properties of bitumen at the nanoscale using the AFM operated with PeakForce TappingTM mode. J Microsc 250(3):210–217

11. Nahar SN, Schmets AJM, Schitter G, Scarpas A (2014) Quantitative nanomechanical property mapping of bitumen micro-phases by peak-force atomic force microscopy. In: 12th ISAP conference on asphalt pavements, Raleigh, N.C.
12. Rashid AF, Hossain Z (2016) Morphological and nanomechanical analyses of ground tire rubber-modified asphalts. Innov Infrastruct Solut 1(1):36
13. Rashid F, Hossain Z, Bhasin A (2017) Nanomechanistic properties of reclaimed asphalt pavement modified asphalt binders using an atomic force microscope. Int J Pavem Eng 1–9
14. Hung AM, Fini EH (2015) AFM study of asphalt binder "bee" structures: origin, mechanical fracture, topological evolution, and experimental artifacts. J Royal Soc Chem Adv 5(117):96972–96982
15. Pauli AT, Branthaver JF, Robertson RE, Grimes W (2001) Atomic force microscopy investigation of SHRP asphalts. Am Chem Soc Div Petrol Chem, Petrol Prepr 46(2):110–114
16. Schmets A, Kringos NA, Pauli T, Redelius P, Scarpas T (2010) On the existence of wax-induced phase separation in bitumen. Int J Pavement Eng 11(6):555–563
17. Tarefder RA, Arifuzzaman M (2011) A study of moisture damage in plastomeric polymer modified asphalt binder using functionalized AFM tips. J Syst, Cybern Inf 9(5):1–12
18. Das PK, Kringos N, Wallqvist V, Birgisson B (2013) Micromechanical investigation of phase separation in bitumen by combining atomic force microscopy with differential scanning calorimetry results. Road Mater Pavement Des 14(2):25–37
19. Roy S (2018) Evaluation of moisture susceptibility of asphalt binders using Atomic Force Microscopy (AFM). In: ProQuest, Master's Thesis, Arkansas State University, Jonesboro, AR 72467

Experimental Study of Pervious Concrete and Artificial Clogging

Kanish Kapoor, Mudasir Nazeer, Gowhar Afzal, and S. P. Singh

Abstract Pervious concrete is a form of lightweight porous concrete, obtained by eliminating or by minimizing the content of fines from the normal concrete mix. The special property of pervious concrete is 'adequate permeability' because of its high percentage of porosity (15–40%). However, with the passage of time, pores of pervious concrete get closed or blocked with sediments like sand, clay, or mud, etc. In the present study, to predict the life period in which the pervious concrete works with full efficiency, an artificial method, known as artificial clogging, is performed on pervious concrete to find the critical sediment and effect on the rate of infiltration. An investigation is performed on two mixes (M1 and M2) using sand, clay, and mixture of both as sediment of clog. A total of six cycles were repeated with an increment of 10 g per cycle and the infiltration rate was recorded after each cycle. It was observed that the decrease in infiltration rate was 30%, 50%, and 45% after the sixth cycle where sand, clay, and combination were used, respectively. Furthermore, compressive strength and permeability test were performed on six separate mixes of pervious concrete.

Keywords Pervious concrete · Artificial clogging · Permeability test

1 Introduction

Concrete, the most commonly used composite material composed of fine aggregates, coarse aggregates, cement, and water having relatively high compressive strength but low tensile strength. It is being estimated that the consumption of concrete is approximately 10 billion tons per year throughout the world. Such a tremendous impermeable building material which can be used to mold any shape and perform

K. Kapoor · M. Nazeer (✉) · S. P. Singh
Department of Civil Engineering, Dr. B.R. Ambedkar National Institute of Technology, Jalandhar 144011, Punjab, India
e-mail: mudasir13m@gmail.com

G. Afzal
Department of Civil Engineering, Lovely Professional University, Phagwara, India

K. R. Reddy et al. (eds.), *Sustainable Environment and Infrastructure*, Lecture Notes in Civil Engineering 90, https://doi.org/10.1007/978-3-030-51354-2_4

under all environmental conditions. Concrete is the most durable, fire-resistant, and energy-efficient material having 65–80% of aggregates that acquires the properties of the rock made with constituent particles having a very close bond together [1]. Pervious concrete is relatively a unique kind of concrete, gaining fast prominence in sustainable construction. It allows the flow of water through a concrete matrix, sometimes also referred to as porous concrete. The proportioning of this special concrete is done by gap grading the coarse aggregates and either eliminating or reducing the volume of fine aggregates to form a network of interconnected pores. Pervious concrete contains no or a small percentage of fine aggregates so also known as no-fines, gap-graded, zero-slump concrete. Pervious concrete is primarily used in pedestrian footpaths, car parks, and other low traffic areas [2]. Pervious concrete pavements are designed to minimize the stormwater runoff by allowing it to percolate into the ground instead of making it run over the surface or toward stormwater drains [3]. Pervious concrete has usually high porosity that ranges between 15 and 40%, thus provides good permeability, drainage, and high noise absorption characteristics [4]. The compressive strength of this concrete ranges up to 28 MPa at 28-day testing but can be increased to 46 MPa with the introduction of supplementary cementitious materials like silica fume, metakaolin, etc. [3, 5, 6]. Porous concrete retains suspended solid impurities like phosphorus, nitrogen, copper, and motor oil, improving groundwater quality [7]. It also improves skid resistance and heat island effects in cities [8].

Although porous concrete clearly has many benefits but is inevitably susceptible to clogging that leads to premature degradation and serviceability problems. Physical clogging is caused due to sediments of sand, clay, and debris built upon the surface. Algae, bacteria, and plant root penetration are responsible for biological clogging. This leads to the reduction in permeability which in turn leads to a susceptibility of inland flooding and freeze–thaw damage thus decrease the life span of pervious concrete pavements [9, 10]. The aim of this study was to check the serviceability of the pervious concrete, which was examined by doing artificial clogging due to sediments like sand and clay in different cycles. Compressive strength test and permeability tests were performed and ultimately the age of the pavement is defined.

2 Experimental Programme

2.1 Preparation of Specimens

To make the mix permeable and to maintain both permeable and strength properties, various trials of mixing are performed. A simple hand mixing procedure was adopted to avoid the chances of making slurry inside the pervious concrete. A cylinder of diameter 12 inches and height of 12 inches was cast for checking the infiltration rate of pervious concrete and, at the same time, cubes of size 150 mm were cast in order to check the compressive strength of the pervious concrete. And a total of six mixes

Table 1 Properties of cement

S. No.	Properties	Obtained value	IS Code recommendation
1	Specific gravity	3.15	3.10–3.15
2	Initial setting time(min)	49	30
3	Final setting time(min)	284	600
4	Consistency	27.7%	26–33%

were performed, starting with highly impermeable mix T1 in which cement content was in access and the size of aggregates were too large and, in the case of T2, T3, T4, T5, the cement quantity was reduced also the size of aggregates were changed. In the case of mix T6, aggregate size was reduced and replaced with some amount of fine aggregates as a replacement of coarse aggregates [11]. In the current study, the cement used was Ordinary Portland Cement of 53 Grade [12] (Tables 1, 2, 3 and 4).

Table 2 Aggregate properties

S. No.	Properties	Specified requirements	Result-1 10 mm	Result-2 20 mm
1	Impact value	30 or 45%	12.8	13.3
2	Abrasion value	30 or 50%	15.2	13.4
3	Water absorption	5%	0.58	0.53
4	Specific gravity	2.1–3.2	2.58	2.58
5	Crushing value	30%	13.1	13.2
6	Soundness	12%	6.4	5.1

Table 3 Trial mix of pervious concrete

Mix	Mix proportion	Max size coarse aggregates (mm)	Replacement of coarse aggregate with sand	W/C ratio
T1	1.5:3	20	0%	0.35
T2	1:4	20	0%	0.32
T3	1:4	20	0%	0.35
T4	1:4	10	10% 2.36 mm passing	0.35
T5	1:4	16	0%	0.32
T6	1:4	15	10% 2.36 mm passing and 90 microns retaining	0.35

Table 4 Mix design samples for clogging purpose

S. No.	Material	Mix (M1)	Mix (M2)
1	Aggregate	32.4 kg	33 kg
2	Cement	9 kg	8.25 kg
3	Sand	3.6 kg	0 kg
4	Water	2.88 kg	2.64 kg
5	Water/cement ratio	0.32	0.32
6	Cement/aggregate ratio	1:4 (10% replacement of coarse aggregates by sand)	1:4 (0% replacement of coarse aggregates by sand)

In addition to the above six samples, two separate samples (M1 and M2) were prepared for the artificial clogging system. The procedure and material properties were the same as that of the above-casted samples.

2.2 Testing Mechanism

Compressive Strength Test: Compression test is performed on UTM or CTM and the same cubes are cast as that of normal concrete (150 mm × 150 mm × 150 mm). Testing is done for 7, 14, and 28 days of curing age.

Permeability Test: The procedure of test on the apparatus is in accordance with [13].The apparatus consists of a cylindrical water reservoir with a hemispherical base of same diameter mounted on a moving stand. The cylindrical portion is not provided with covering on the top and to vary the flow from the hemispherical bottom portion, a value is connected to its base. A graduated pipe is attached to the external face of the cylindrical portion from top to bottom. The water reservoir of the apparatus is made of stainless steel and the stand is composed of casted iron.

A special type of stainless-steel cylinder specimen having diameter 12 inches and height 18 inches, having two marked lines at 10 mm and 15 mm at a height of 12 inches above the bottom to maintain the head between the two marked lines. The pervious concrete is filled up to the bottom mark of the cylinder keeping the 10 mm and 15 mm lines visible for head maintenance. The portion above the base marked line acts as the fitted ring for checking permeability instead of having an external ring (Fig. 1).

The time of infiltration is recorded and used in the following formula:

$$I = \frac{KM}{D^2} \times t \text{ In/hr.} \tag{1}$$

K = rate of permeability, M = mass of water, T = time of infiltration, D = diameter of the specimen.

Fig. 1 Infiltrometer and sample in a specimen

2.3 Mechanism Followed for Artificial Clogging

For artificial clogging, cylinder specimens of 12-inch diameter and 12-inch height were cast and the clogging operation was followed after 28 days of curing. Clogging was performed on two mixes M1 and M2 in the laboratory by artificial means where sand and clay were used as sediment material. Before proceeding with the artificial clogging mechanism, the infiltration rate was measured by using laboratory-based apparatus. After getting the initial results of all the samples, the sedimentation effect or clogging effect of all the samples were checked by following three ways: (a) By using sand only: Artificial clogging by using sand is done in consecutive six cycles in each cycle 10 g of sands is rolled over and infiltration rate was measured after every cycle. Overall, 100 g of sand were used and six readings of the infiltration were collected using sand as the sediment material for mix M1. In mix M2, six cycles were performed, and in each cycle, 25 g of sand were used, Overall, 150 g of sand were poured over**.** (b) By using clay only: Artificial clogging by clay is done using the same procedure as in the sandy mechanism. Six cycles with an increment of 10 g in each cycle is performed and a total of 60 g of clay were used in the first specimen. Similarly, six cycles with an increment of 25 g in each cycle were utilized to clog it artificially. (c) Combination of sand and clay: In this combination, 5 g of sand and 5 g of clay were mixed and rolled over the surface. Overall, six cycles were repeated and a total of 60 g of the mixture were used with an increment of 10 g in each cycle. And similarly, six cycles were repeated for the second sample, in which, 25 g of the mixture was rolled and a total of 150 g were utilized to clog the pervious concrete artificially (Fig. 2).

Fig. 2 Sample before infiltration and after infiltration

3 Results and Discussions

3.1 Compressive Strength

The compressive strength of porous concrete is influenced by different factors like cement content, w/c ratio, aggregate characteristics, and compaction extent during placement. The graph below clearly shows the gradual increase in compressive strength from 7 to 28-day curing age in all mixes. It is observed from the graph that mix T1 shows higher strength at all curing ages of 7, 14, and 28 days. The 14- and 28-day curing age compressive strengths were increased by 38% and 54%, respectively, when compared to 7-day strength of the same mix T1. Moreover, not much change in compressive strength was observed from mix T2 to T5 at all ages of 7-, 14-, and 28-day curing. Furthermore, fair values of compressive strength were observed for mix T6, where 7-day curing strength was observed as 13.2 MPa. The increase in compressive strength up to 36% and 54%, respectively, at 14- and 28-day curing ages was observed, which was quite good as compared to other mix proportions (Fig. 3).

3.2 Infiltration

The variation of aggregates size and water–cement ratio is the key factor to maintain the specified value of infiltration. It is clearly observed from the graph that mix T1 have zero permeability because the ratio of cement with respect to aggregate was very high and the size of aggregates was between 4.75 and 20 mm, smaller sized aggregates are responsible for making the mix impermeable. The rate of infiltration shows a gradual increase from T1 to T5 mixes. A prominent decrease in infiltration was

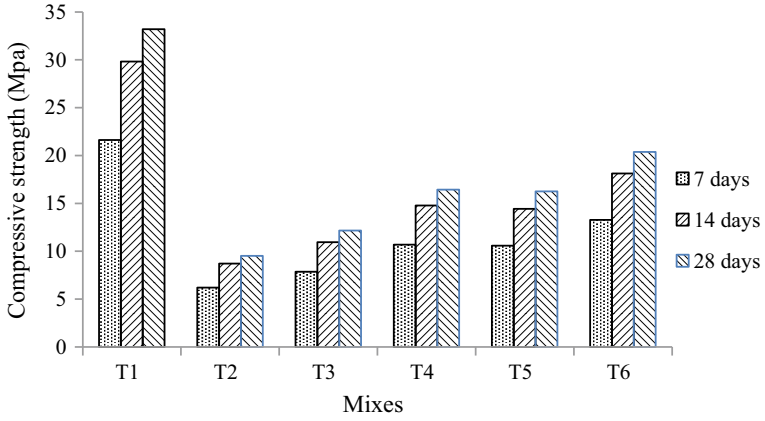

Fig. 3 Compressive strength variation

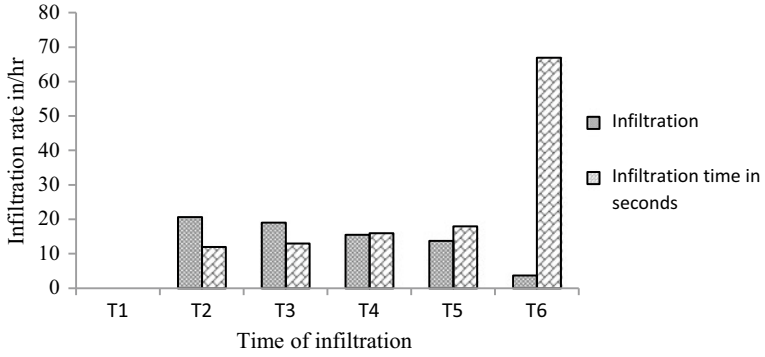

Fig. 4 Infiltration rate (mm/s)

observed in mix T6, this is because a good range of coarse aggregates with a maximum size of 10 mm and 10% of fine aggregates (2.36 mm) were used but the infiltration range was under drainage limits. The time of infiltration was approximately 3 times more and infiltration was 2.7 times less in case of mix T6 when compared to mix T5 (Fig. 4).

3.3 Results of Artificial Clogging of Mix M1

The observations and results of artificial clogging with sand, clay, and combination of both clay and sand, and the variation of infiltration rate under different conditions are discussed for mix M1 (Tables 5, 6 and 7).

Table 5 Clogging with sand for mix M1

S. No.	Cycle No.	Amount of sand (g)	Time of infiltration (s)	Infiltration rate (in/hr.)
1	0	0	67	525.995
2	1	10	69	510.748
3	2	20	73	482.762
4	3	30	77	457.683
5	4	40	85	414.607
6	5	50	95	370.964

Table 6 Clogging with clay for mix M1

S. No.	Cycle No.	Amount of clay (g)	Time of infiltration (s)	Infiltration rate (in/hr.)
1	0	0	67	525.995
2	1	10	75	469.888
3	2	20	85	405.076
4	3	30	100	352.416
5	4	40	115	306.449
6	5	50	133	264.974

Table 7 Clogging with sand and clay for mix M

S. No.	Cycle No.	Sand (g)	Clay (g)	Total sediment (g)	Time of infiltration (s)	Infiltration rate (in/hr.)
1	0	0	0	0	67	525.995
2	1	5	5	10	71	496.361
3	2	10	10	20	81	435.082
4	3	15	15	30	88	400.473
5	4	20	20	40	102	345.506
6	5	25	25	50	116	303.807

It is clearly seen from the above observations that, at initial stages of artificial clogging test, change in the rate of infiltration was very less with an insertion of 10 g of sand, clay, or both combined in mix M1. But there is a gradual decrease in the infiltration rate from cycle one onwards. In the last cycle, when sediment (sand) used for artificial clogging was 50 g and time of infiltration was 95 s, the decrease in infiltration was only 30% when compared with the control cycle (cycle zero). Furthermore, a 50% decrease in infiltration was observed when sediment for artificial clogging was clay as compared with the control cycle. Moreover, a 42% decrease in infiltration was seen in the combined case of artificial clogging where sediment utilized was 50 g (both sand and clay) in mixture state.

3.4 Results for Artificial Clogging for Mix M2

The observations and results of artificial clogging with sand, clay, and combination of both clay and sand, and the variation of infiltration rate under different conditions are discussed for M2 mix (Tables 8, 9 and 10).

The observation table clearly shows that there is a prominent decrease in infiltration from the initial cycle to cycle 4. The decrease in infiltration by artificial clogging when sediment used for clogging is sand is 85% compared to the control cycle (cycle zero). Furthermore, clogging effect by clay is more prominent than by sand. The result shows that there is a 90% decrease in infiltration when the last cycle (cycle 4) was compared to the control cycle. Moreover, the effect of clogging by the combination of both sand and clay was approximately the same as that of clay clogging alone. The decrease in infiltration was approximately 90% on making a comparison with the initial control cycle. Thus, it is observed that the effect of clay on the rate of infiltration was prominent as compared to the effect of sand and combination. But the effect of sand on artificial clogging is more in M2 as compared to mix M1. This is because the void ratio is more in case of M2, as no fines were used unlike in the case of M1.

Table 8 Clogging with sand for mix M2

S. No.	Cycle	Sand (g)	Time of infiltration (s)	Infiltration rate (in/hr.)
1	0	0	13	2710.897
2	1	25	19	1854.824
3	2	50	35	1006.904
4	3	75	57	618.274
5	4	100	86	409.786

Table 9 Clogging with clay for mix M2

S. No.	Cycle	Clay (g)	Time of infiltration (s)	Infiltration rate (in/hr.)
1	0	0	13	2710.897
2	1	25	23	1532.246
3	2	50	48	734.201
4	3	75	82	429.776
5	4	100	130	271.089

Table 10 Clogging with sand and clay for mix M2

S. No.	Cycle	Sand (g)	Clay (g)	Total sediment (g)	Time of infiltration (s)	Infiltration rate (in/hr.)
1	0	0	0	0	13	2710.897
2	1	12.5	12.5	25	21	1678.174
3	2	25	25	50	43	819.573
4	3	32.5	32.5	75	79	446.097
5	4	50	50	100	121	291.253

4 Conclusion

The following conclusions were drawn from the whole study of pervious concrete:

Clogging effect by clay is dominating both mixes (M1 and M2). In mix M1, the clogging effect by clay was 20% more and in case of M2, it was only 5% more than sand. So, it is here clearly concluded that pervious concrete is deteriorated more by clay than sand sediments. While replacing coarse aggregates by 10% of fine aggregates, fair to good strength is achieved without being compromising with the infiltration rate. So, clay sediment is more worrisome than sand sediment. Furthermore, pervious concrete can be used for low to moderate traffic pavements if the proper percentage of fines is used which enhances the strength of concrete.

References

1. Chang JJ, Yeih W, Chung TJ, Huang R (2016) Properties of pervious concrete made with electric arc furnace slag and alkali-activated slag cement. Constr Build Mater 109:34–40
2. Lee M-G, Huang Y-S, Chang T-K, Pao C-H (2011) Experimental study of pervious concrete pavement. 3(Vii), 93–99
3. Chandrappa AK, Biligiri KP (2016) Comprehensive investigation of permeability characteristics of pervious concrete: a hydrodynamic approach. Constr Build Mater 123:627–637
4. Maguesvari MU, Narasimha VL (2013) Studies on characterization of pervious concrete for pavement applications. Procedia - Soc Behav Sci 104:198–207
5. Deo O, Neithalath N (2011) Compressive response of pervious concretes proportioned for desired porosities. Constr Build Mater 25(11):4181–4189
6. Kia A, Wong HS, Cheeseman CR (2018) Defining clogging potential for permeable concrete 220(February):44–53
7. Sriravindrarajah R, Wang NDH, Ervin LJW (2012) Mix design for pervious recycled aggregate concrete. Int J Concr Struct Mater 6(4):239–246
8. Neithalath N, Sumanasooriya MS, Deo O (2010) Characterizing pore volume, sizes, and connectivity in pervious concretes for permeability prediction. Mater Charact 61(8):802–813
9. Kevern JT, Schaefer VR, Wang K, Suleiman MT (2019) Pervious concrete mixture proportions for improved freeze-thaw durability 5(2):1–12
10. Vancura M, MacDonald K, Khazanovich L (2011) Microscopic analysis of paste and aggregate distresses in pervious concrete in a wet, hard freeze climate. Cem Concr Compos 33(10):1080–1085

11. Ramkrishnan R, Abilash B, Trivedi M, Varsha P, Varun P, Vishanth S (2018) Effect of mineral admixtures on pervious concrete. Mater Today Proc 5(11):24014–24023
12. Bureau of Indian Standards (2013) IS 269 : 2013; Ordinary Portland Cement. March
13. Standards O (2010) Standard test method for infiltration rate of in place pervious concrete 1. Annu B ASTM Stand C:9–11

Sustainable Engineering Approaches Used in Electrical Discharge Machining Processes: A Review

Ranjit Singh, Ravi Pratap Singh, and Rajeev Trehan

Abstract Sustainable engineering is the approach in which the process is designed in such a way that there is a balance between the use of energy and resources so that it will not affect the environment and can be conserved for fulfilling the needs of future generations. Sustainable engineering in manufacturing focuses on the enhancement of productivity by controlling process parameters. So, it has become a hot topic in almost every field of manufacturing, aiming to achieve more economical and efficient processes. The key methods of sustainable production mainly include the optimization of energy usage and the innovation of machining techniques, etc. Nowadays, many relevant investigations have been conducted. In this paper, the main study is focused on the sustainable engineering approaches used in the electrical discharge machining processes, various optimization techniques used for better productivity in EDM processes. Effect of different process parameters like pulse-on, pulse-off, peak current, spark gap voltage, tool feed, flushing pressure, electrode polarity, dielectric fluid, etc., in machining operations has been discussed. For better machining time and less energy consumption, the optimization of process parameters, the problem of wire rupture in case of wire electrical discharge machining (WEDM), and the use of different electrode materials in EDM machining operations have been reviewed in this study. Efforts have been made to enhance EDM operations by sustainable engineering approaches with a systematic review of different research articles, industrial catalogs, technical fundamentals, etc. Various conclusions are drawn based on a thorough review of research articles and a list of gaps or future scopes have been provided in this paper.

Keywords EDM · WEDM · PMEDM · MRR · UCM · SEM · TWR · Ra

R. Singh (✉) · R. Pratap Singh · R. Trehan
Dr. B. R. Ambedkar National Institute of Technology, Jalandhar, 144011 Punjab, India
e-mail: ranjitsingh.tmk@gmail.com

K. R. Reddy et al. (eds.), *Sustainable Environment and Infrastructure*, Lecture Notes in Civil Engineering 90, https://doi.org/10.1007/978-3-030-51354-2_5

1 Introduction to Sustainable Engineering

Sustainable engineering is the method of utilizing resources in such a manner that it would not affect the surrounding environment and resources are conserved for future generations. For practicing sustainable engineering in a complete way, it needs an interdisciplinary approach in every phase of engineering and it should not be designated as the sole responsibility of environmental engineering. All engineering fields should incorporate sustainability into their practice to enhance the quality of life for all. Sustainable development is broadly defined as "meeting the needs of the present without compromising the ability of future generations to meet their own needs" [1]. Within this field, sustainable manufacturing is termed as the "Creation of manufactured products that use processes that minimize negative environmental impacts, conserve energy and natural resources, are safe for employees, communities, and consumers and are economically sound" [2].

2 Concept of Sustainability in Manufacturing Environment

In today's scenario, the manufacturing sector is playing quite an essential role in the country's economy. In 2012, the manufacturing area generated a turnover of €7000 billion and engaged over 30 million people directly in employment. The European industry is a world leader in a number of manufacturing sectors with mechanical engineering area having a global market share of 37% [3]. The use of men, machines, and material in a sustainable manner is very much required in the upliftment of this sector and also for conserving our environment and existing resources. The conventional machining processes involve direct contact between the tool and workpiece, which results in a number of losses in terms of energy, power, tool material, workpiece material, etc. The limitation of these processes is machining of hard and fragile components, complex and intricate shape formation. As compare to the conventional machining operations, advanced machining operations overcome these limitations. In non-conventional machining operations, there is no direct contact of tool with the workpiece, which helps in preventing from wear of tool and workpiece. One of the important operations among these is electrical discharge machining (EDM), in which a series of electrical discharge is used in the presence of dielectric fluid for machining of the workpiece. EDM is used for machining of hard and fragile materials with complex shapes without any barrier to their hardness. Still, this process needs some improvement for saving the loss of energy, power, wear of tool and workpiece. The advanced machining operation like EDM is crucial in the manufacturing processes, and sustainable engineering approaches in these machining operations lead to better productivity in terms of energy, material, and process optimization in manufacturing processes.

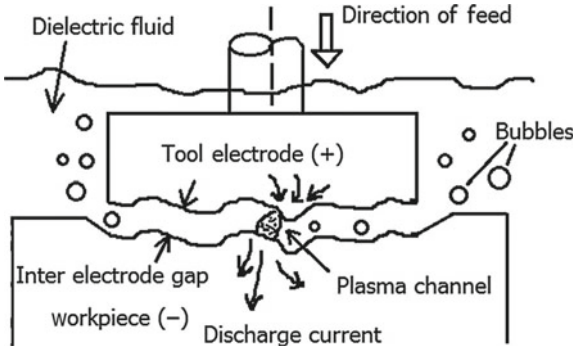

Fig. 1 Schematic view of the concept of EDM process [4]

3 Principle of Electrical Discharge Machining (EDM) Process

EDM is a type of thermo-erosive process in which spatially and temporally controlled separated pulsed discharges are utilized to machine electrically conductive materials irrespective of their chemical, mechanical, and thermophysical properties [4]. The tool used for spark erosion as an electrode is a negative replica of the contour, which the investigators want to produce on the workpiece. Figure 1 shows the schematic view of the EDM process.

Discrete sparks are produced in series between the workpiece and shaped tool electrode, and a complete arrangement is submerged in the dielectric fluid. Dielectric fluids, namely deionized water, EDM oil, kerosene, and paraffin oil among others are used in the EDM process. A very small inter-electrode gap between the workpiece surface and tool electrode must be kept via which the dielectric fluid is passed [5].

4 Review of Literature

EDM is a significant non-conventional machining operation used for the machining of hard and fragile components irrespective of their hardness and depth. The machining of small and microcomponents is a unique application of EDM process as compared to other conventional processes. Complex and intricate shapes with fine accuracy, precision, and surface properties are added advantages of EDM process, which are very hard to obtain with the other conventional machining operations (Fig. 2).

Sustainability in the EDM processes is a need of today's concern, as there are certain losses that can be cured with the application of sustainable approaches. Wear of tool, workpiece, more loss of power, optimization of electrical and non-electrical process parameters, and responses are of important concern in obtaining a sustainable and quality product. The review of literature on sustainable approaches on EDM process has been discussed below.

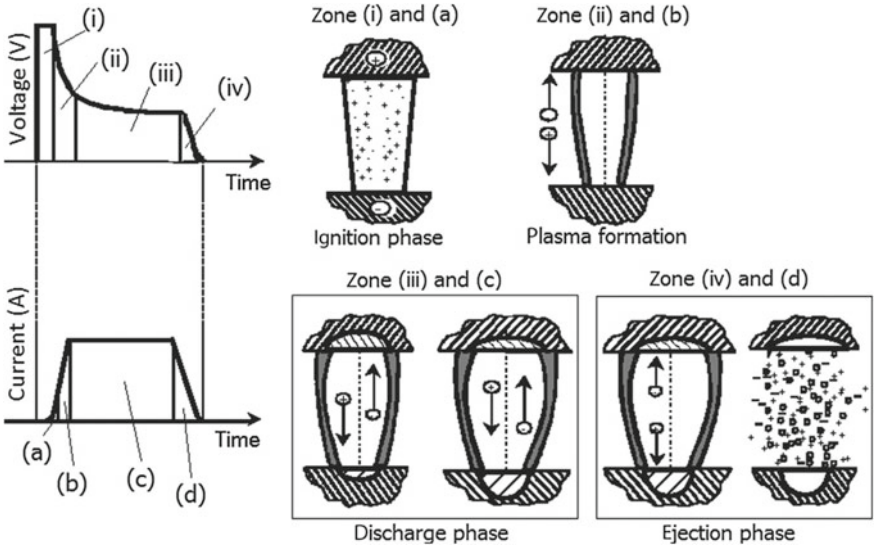

Fig. 2 Schematic view of voltage and current trends of pulse along with the phases of an electrical discharge [4]

Gamage et al. [6] investigated the sustainability of non-conventional machining processes and the evaluation of research needs for optimizing the process. For machining complex, intricate and difficult to cut materials, the unconventional machining practices play a major role in the manufacturing of such products. The product with high precision and fine accuracy can be achieved with the use of non-conventional machines (Fig. 3).

The objective of the present study is to determine the existing state of the art in sustainability evaluation of unconventional machining practices and spot out different gaps in research. An environmental assessment study on EDM revealed a data collection effort to calculate the total environmental impact of three EDM techniques, namely die-sinking EDM, micro-EDM, and WEDM.

This study has revealed that during 1 h of EDM roughing process, the electrical energy for EDM process and the hydrocarbon oil, which is utilized as a dielectric fluid in the process, are the main factors that contribute for the total impact amounting to 47.3% and 23.1%, respectively. It has been observed from the current study that dielectric fluid and energy cause similar amount of burdens on the environment during EDM operation. The operator's health and safety hazards may be reduced with the utilization of non-hydrocarbon-based dielectrics. A thorough review of the utilization of dielectric fluids, which are environmentally friendly in EDM reveals that water-based dielectrics, a substitute to hydrocarbon oil, can be used for die-sinking EDM.

Xiang et al. [7] researched on the sustainable production of micro-gears combining EDM and precise forging of micro-reciprocated wire. This paper presents a hybrid

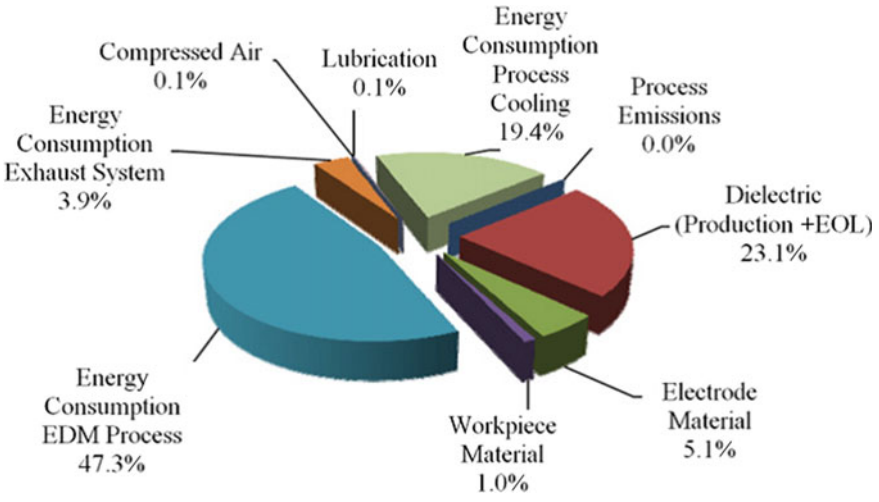

Fig. 3 Distribution of the environmental impact during one hour of EDM roughing operation [6]

process that combines micro-reciprocated wire EDM, which uses reciprocated traveling wire with a diameter of 50 μm as an electrode tool, with accurate forging, achieving economical and efficient sustainable production of micro-gears. The economical and high-precision manufacture of SKD11 micro-gear mold is first carried out by micro-reciprocated wire EDM.

Pramanik et al. [8] investigated the sustainability in machining of titanium alloys in WEDM. The study aims at understanding the wire rupture. The uninterrupted machining is necessary for reducing energy and machining time for making the process sustainable. Understanding the mechanism and factors that will result in wire electrode rupture is important for reducing machining time to preserve resources and improve sustainability of the process. The study aims at studying the wire rupture mechanism while doing machining of Ti–6Al–4V in EDM. To aid the analysis of pulse-on time, wire tension, and electrolyte flushing pressure was varied to understand the effects of these parameters on wire rupture. The occurrence of wire rupture occurs at high wire tension and lower flushing pressure. The effect of pulse-on time on wire rupture depends on the interaction of flushing pressure and wire tension (Fig. 4).

The wire gets deformed in three stages before fracture. At the initial point, the round section of wire converts into oval shape following a gradual decrease in overall cross section, and finally, necking takes place. Chakraborty et al. [9] aim at the study of different dielectric fluids and their effect on EDM. In EDM, material removal occurs in the presence of dielectric fluid; so, this working fluid plays an important role in the material removal phenomenon in EDM (Fig. 5).

The dielectric fluid plays the role of a medium for the production of electrical discharge in EDM, flushes away the debris produced during machining, works as quenching medium to solidify and cool gaseous debris in EDM, and works as a heat

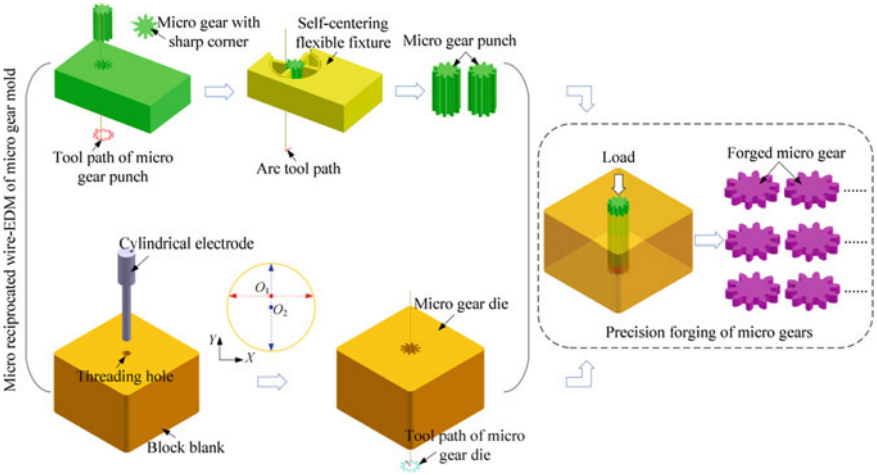

Fig. 4 Machining process of micro-gears combining micro-reciprocated wire EDM and precision forging [7]

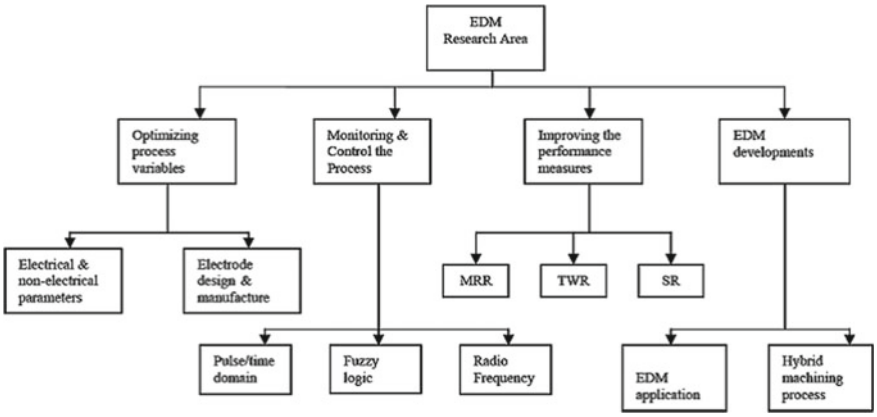

Fig. 5 Classification of major EDM research areas [10]

transfer medium for transferring the heat produced by electrical discharges from both the workpiece and electrode [11]. The dielectric fluids are of different types: mineral oils, kerosene, mineral seal, transformer oil, etc. Water-based dielectric plays an important role in EDM. The use of water as a dielectric fluid is an alternative to the hydrocarbon oil. The approach behind using water as a dielectric is to promote a safe environment and better health while working on EDM. The hydrocarbon oils like kerosene get decomposed and harmful vapors are released, i.e. CO and CH_4 [12]. Powder additives are also one of the new and less explored areas of research in EDM in which fine abrasive powder is mixed with the dielectric fluid. The EDM operation

with powder mixed in the dielectric is known as powder-mixed EDM (PMEDM) [13]. The powder reduces the dielectric insulating strength and results in an increase in spark gap between tool and workpiece. With the use of powder in dielectric, the EDM process becomes more stable, and machining efficiency, material removal rate (MRR), and surface quality get improved. Kou et al. [14] investigated the sustainable manufacturing of titanium alloys by using high-speed electrical discharge milling operation with moving electric arcs while using water-based dielectric. For solving the problem of environmental pollution and low machining efficiency of the conventional EDM process, sustainable manufacturing, a new method of EDM milling, along with water as the dielectric medium has been proposed. The moving electric arc is provided better output energy in case of high-speed EDM milling as compare to the spark in the conventional EDM process. More MRR achieved while machining with high-speed EDM milling operations up to five times of conventional EDM. Urso et al. [15] investigated the sustainability of micro-EDM drilling process by studying the effects of workpiece and electrode materials in EDM process. The three different workpiece materials, i.e., tungsten carbide, stainless steel, and aluminum machined with two electrode materials, brass and tungsten carbide. The machining accuracy is also taken into account for calculating the sustainability index. Tool wear has the maximum impact on the sustainability of the process. From the electrode point of view, the brass electrode is more sustainable than that of the tungsten carbide in terms of electrode wear and energy consumption.

Sarkar et al. [16] investigated the optimization and modeling of WEDM of γ-TiAl in the trim cutting operation. A second-order mathematical model, in prerequisites of machining parameters, was advanced for cutting speed, surface roughness (SR), and dimensional deviation using response surface methodology (RSM). Manjaiah et al. [17] investigated the effect of process parameters on the responses such as MRR and SR of Ti50Ni40Cu10 SMA machined by WEDM using the Taguchi techniques to acquire optimum machining process parameters. Experimental results exhibit that peak current, pulse-on time, and servo voltages are major significant factors affecting the MRR and surface finish during machining. Pulse-off time and wire feed had no significance on the responses (Fig. 6).

Rao et al. [18] studied the effect of WEDM parameters on aluminum alloys as the application of Al is rising in various industries. In this present investigation, the parametric examination of WEDM parameters was performed by using Taguchi techniques on SR and MRR. The rising discharge energy usually increases surface irregularities due to a large amount of melting and resolidification of materials. So, the minimum surface roughness is obtained at lower values of peak current and pulse-on time. Prasad and Krishna [19] presented a model for MRR and SR in terms of input variables using RSM. A non-dominated sorting algorithm was then applied to obtain the pareto-optimal solutions for optimization purposes.

Pilligrin et al. [20] investigated the effects of electrode material and its impact on the performance measures in electrical discharge micro-machining. Miniaturization is one of the important concepts in which commercial products are reduced in their size without affecting their functionality. This results in sustainability in the machining processes, where the components are micro-machined, which in turn

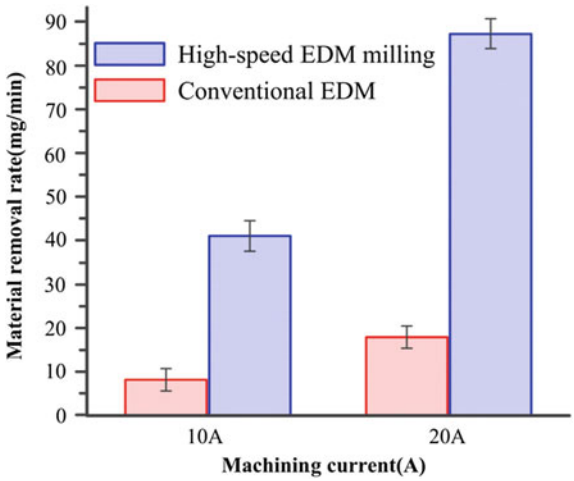

Fig. 6 Comparison of MRR between conventional EDM and high-speed EDM milling [15]

results in the reduction in machining time and conservation of resources. The effect of performance parameters, discharge energy, spindle speed, tools material (Cu, Cu–W, W), and their impact on the response parameters MRR, TWR, Overcut, Taper angle, surface roughness, has been studied. It is found that TWR is low when the thermal conductivity, boiling, and melting point of the electrode is high. It is found from the experimental investigations that TWR and overcut are in the order of Cu>Cu–W>W. This is due to the variations in the thermal properties of electrode material. The surface roughness is found to be low at low spindle speed and low discharge energies. This is due to proper flushing and stable machining conditions. The different sustainable engineering approaches used in EDM processes found from the literature survery are: parametric optimization, heat treatment of electrodes, coating of electrodes and workpieces, use of different tool electrodes at different angles and geometries, heat treatment of workpieces, use of hybrid dielectric fluids, tool feed mechanism, work table movement, surface characterization.

5 Future Scopes

A very less work has been reported on the use of water-based dielectric with an organic compound in the EDM processes. This is a new approach toward sustainability of the EDM process. Compared with the different hydrocarbon oil-based dielectrics, water-based dielectrics are more environmentally friendly and clean. The generation of harmful and airborne particles in the case of water-based dielectrics is quite less as compared to the hydrocarbon oil-based dielectrics. The processing parameters related to the highest material removal rate efficiency have not yet been studied up to a sufficient extent. Very less work has been reported on the optimization of parameters for preventing tool wear in EDM process. In future work, artificial

intelligence (AI) techniques should be considered for optimizing different process parameters in EDM process.

6 Conclusion

The following conclusions can be made by studying and investigating different sustainable approaches applied in EDM processes:

1. The micro-EDM process is highly versatile and therefore has an enormous potential for the manufacture of various microstructures and microsystems and devices in a wide range of hard to machine materials.
2. A straight-through micro-hole can be produced by controlling the important process parameters such as pulse-on time, peak current, and flushing pressure properly. In order to increase the yield of micro-manufacturing, innovative hybrid micro-machining processes can also be developed for micro-EDM to machine alloys like Ti–6Al–4V.
3. The sustainable fabrication of micro-gears with high accuracy, productivity, and low cost is achieved by combining EDM and precise forging with micro-reciprocated wire.
4. The precise forging of micro-gears on ultra-fine grained copper is carried out using the machined micro-gear mold, which achieves the sustainable production of micro-gears with high precision and productivity.
5. The pulse-on time influence depends on the interaction between wire tension and flushing pressure in the wire rupture mechanism. The wire break occurs at an instantaneous high temperature due to the creation of unnecessary arcs when the EDM debris/wastes are not properly flushed away.
6. EDM's energy consumption rate depends on the machine tool and machining variables in which chillers/water coolers and pumps consumed the highest energy consumption.
7. In roughing operations, PMEDM can also improve processing efficiency. Electrically conductive powder reduces the dielectric fluid's insulating strength and thus increases the gap between the tool and the workpiece. The EDM process is stabilized and also improves MRR and SQ.
8. Lower viscosity dielectric oils can increase efficiency during micro-EDM. The dielectric oil of low viscosity has a greater influence on the machining cycle than the hydrocarbon oils.
9. The high-speed EDM milling can achieve a higher MRR on titanium alloy with a moving electric arc. Comparative experiments show that the high-speed EDM milling MRR is nearly five times the conventional EDM.

References

1. The World Commission on Environment and Development. Our Common Future. Oxford University Press (1989)
2. U.S. Department of Commerce. How does commerce define sustainable manufacturing? sustainable manufacturing initiative (2013)
3. European Commission (2014) Advancing manufacturing—Advancing Europe. Report of the task force on advanced manufacturing for clean production. Brussels: European Commission (2014)
4. Kunieda M, Lauwers B, Rajurkar KP, Schumacher BM (2005) Advancing EDM through fundamental insight into the process. CIRP Ann Manuf Technol 54(2):64–87
5. D'Urso G, Merla C (2014) Workpiece and electrode influence on micro-EDM drilling performance. Precis Eng 38(4):903–914
6. Gamage JR, De Silva AKM (2015) Assessment of research needs for sustainability of unconventional machining processes. Procedia CIRP 26:385–390
7. Chen X, Wang Z, Xu J, Wang Y, Li J, Liu H (2018) Sustainable production of micro gears combining micro reciprocated wire electrical discharge machining and precision forging. J Clean Prod 188:1–11
8. Pramanik A, Basak AK (2018) Sustainability in wire electrical discharge machining of titanium alloy: understanding wire rupture. J Clean Prod 198:472–479
9. Chakraborty S, Dey V, Ghosh SK (2015) A review on the use of dielectric fluids and their effects in electrical discharge machining characteristics. Precis Eng 40:1–6
10. Ho KH, Newman ST (2003) State of the art electrical discharge machining. Int J Mach Tools Manuf 43:1287–1300
11. Kern R (2009) Sinker dielectric fundamentals. EDM Today January/February issue
12. Zhang QH, Du R, Zhang JH, Zhang Q (2006) An investigation of ultrasonic-assisted electrical discharge machining in gas. Int J Mach Tools Manuf 46:1582–1588
13. Zhao F-L, Lu Z-Z, Wang H, Qian Z-Q (2005) Research on effecting mechanism of particles in powder-mixed EDM. Dalian Ligong Daxue Xuebao/J Dalian Univ Technol 45:668–671
14. Kou Z, Han Z (2018) On sustainable manufacturing titanium alloy by high-speed EDM milling with moving electric arcs while using water-based dielectric. J Clean Prod 189:78–87
15. Urso GD, Giardini C, Ravasio C (2018) Effects of electrode and workpiece materials on the sustainability of micro-EDM drilling process. Int J Precis Eng Manuf 19(11):1727–1734
16. Sarkar S, Sekh M, Mitra S, Bhattacharyya B (2008) Modeling and optimization of wire electrical discharge machining of γ-TiAl in trim cutting operation. J Mater Process Technol 205:376–387
17. Manjaiah M, Narendranath S, Akbari J (2014) Optimization of wire EDM parameters to achieve better MRR and surface finish. Procedia Mater Sci 5:2635–2644
18. Rao PS, Ramji K, Satyanarayana B (2014) Experimental investigation and optimization of wire EDM parameters for surface roughness, MRR and White layer in machining of Aluminum alloy. Procedia Mater Sci 5:2197–2206
19. Prasad DVSSSV, Gopala Krishna A (2009) Empirical modeling and optimization of wire electrical discharge machining. International J Adv Manuf Technol 43(9–10), 914–925
20. Pilligrin JC, Asokan P, Jerald J, Kanagaraj G (2018) Effects of electrode materials on performance measures of electrical discharge micro-machining. Mater Manuf Process 33(6):606–615

Partial Replacement of Cement with Red Mud in Concrete—A Review

Jaspal Singh and Sanjeev Naval

ABSTRACT Indian aluminium industry generates a significant amount of solid waste such as red mud. Red mud is produced during the refining of alumina by Bayer's process. It is estimated that for production of 1 tonne of alumina, about 1.0–2.5 tonne of red mud is generated. Annually, more than 4 million tonnes of red mud is produced in India. As red mud contains some toxic elements, dumping of red mud contaminates the soil and water and also covers valuable land. By taking cementitious behaviour of the red mud into account, it can be used in mortar and concrete technology for construction practices by partially replacing cement. The use of red mud with partial replacement of cement proves to be economical because red mud, a by-product of alumina industry is available free of cost. The present study recapitulates the research on utilization of red mud as partial replacement of cement and its effect on mechanical and durability properties in mortar and concrete. Based on data given by different researchers, equations have been formulated for compressive, tensile and flexural strengths of mortar and concrete.

Keywords Cement · Sustainable · Red mud · Concrete

1 Introduction

Aluminium plants are being set up rapidly throughout the world due to the increasing demand for aluminium as it is being used as a replacement of steel and other materials [1]. In aluminium industry, red mud is one of the by-products obtained when alumina is extracted from the bauxite ore through the Bayer process. To digest the bauxite ore, high concentration of sodium hydroxide (NaOH) solution is used at high temperature and pressure [2]. India is considered to be the fifth largest producer of bauxite which

J. Singh (✉)
Department of Civil Engineering, Punjab Agricultural University, Ludhiana, India
e-mail: jaspalsingh@pau.edu

S. Naval
Civil Engineering Department, DAVIET, Jalandhar, India
e-mail: sanjeevnaval@gmail.com

K. R. Reddy et al. (eds.), *Sustainable Environment and Infrastructure*, Lecture Notes in Civil Engineering 90, https://doi.org/10.1007/978-3-030-51354-2_6

is the primary ore of aluminium in the world. In our country, the main producers of aluminium being National Aluminium Company (NALCO), Bharat Aluminium Company (BALCO), Hindustan Aluminium Company (HINDALCO) and Sesa Sterlite (now renamed as Vedanta). Mostly, the aluminium industries located closer to the sea dispose of the red mud into the sea thereby having an unfavourable effect on the aquatic plants and animals. In other cases, the residue which is in the form of slurry that is red mud (having a high solid concentration of 30–60% with a high ionic strength) is disposed of and dried in the large disposal area. Depending on the amount of bauxite and the type of process adopted in the aluminium industry, 1.0–2.5 tonnes of red mud are generated for every one tonne of alumina produced [3]. At present, 120 million tonnes of red mud is generated worldwide annually which is not being disposed of or recycled satisfactorily. Moreover, disposing activities are becoming expensive and difficult. India contributes approximately 6.25% of the global red mud production that categorically consists of solid and metallic oxide impurities [3]. Some researchers have found the potential use of red mud in the brick production and ceramic products [4, 5]. Red mud can also be used as a catalyst and as an adsorbent for removal of some valuable metals such as titanium and iron which can be recovered from the red mud [6, 7]. Red mud has a high alkalinity (pH ranging from 9 to 14) due to which it becomes a hazardous waste material creating the problem of surface and groundwater pollution. These environmental concerns have drawn considerable attention to investigating the feasibility of using red mud in various civil engineering fields. Red mud reduces the permeability thereby augmenting increase in the strength of the concrete. Red mud prevents the corrosion of reinforcement and it also acts as a good binding material [3]. Therefore, it can be used as a partial replacement of cement in mortar and concrete. Different researchers utilized the red mud in their studies to increase the strength of concrete and cement-based materials and to improve the durability characteristics besides reduction in the cost of concrete.

1.1 Red Mud Production

The production of aluminium in China is more than 50% whereas India covers about 5% of the world's smelter production. Nowadays, more and more aluminium industries are being set up resulting in more production of alumina which in turn increases the production of red mud. As it is pertinent from the pie chart, China share in total world's production of aluminium is more than 50%, whereas our country's share is about 5% from the total world's production (Fig. 1).

1.2 Use of Red Mud in Cement Production

The practicality of red mud in cement production has been studied by different researches all around the world. In India, around two million tonnes of red mud is

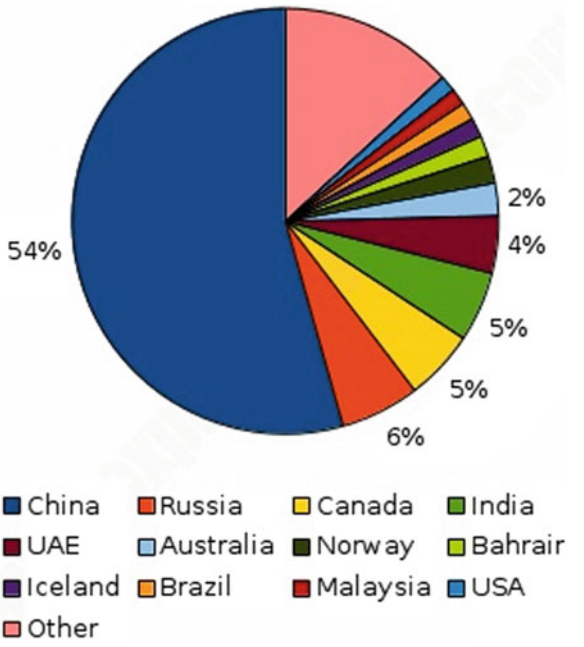

Fig. 1 Percentage of production of aluminium in the world

used in cement production [8]. In Japan, red mud is used as raw material with other raw material such as clay and limestone during the production of cement. The cement developed using red mud also meets with the specification of Standards.

Singh et al. [9] developed the new types of cement using different variations of red mud, lime, bauxite and gypsum. It was found that the compressive strength of these types of cement was comparable to Ordinary Portland Cement. The 28-day compressive strength of cement made with 50% lime, 30% red mud and 20% bauxite was around 10 MPa. The optimum firing temperature and firing time for the production of this cement was 1300 °C and 1.5 h, respectively. In another study, Singh et al. developed the cement using red mud, lime, gypsum and bauxite. The maximum compressive strength of 25 MPa was achieved using 47.5% of lime, 7.5% of gypsum, 40% red mud and 5% bauxite. The optimum firing temperature and firing time for the production of this cement was 1250 °C and 1 h, respectively.

Tsakiridis et al. [10] found that the addition of red mud up to 3.5% with a raw material of clinker in cement production reduces the burning temperature of clinker. The mineralogical composition of red mud-based clinker was similar to Portland clinker. The 90-day compressive strength of red mud-based clinker was around 55 MPa, which was more than the Portland clinker.

Table 1 Physical properties of red mud

Physical properties Research reported by author(s)	Specific gravity	PH
Pujar and Prakash [11]	2.90	10–14
Rathod et al. [12]	2.51	10.5–12.5
Metilda et al. [13]	2.51	10.5–12.5
Shinge et al. [14]	–	11.3
Yamuna [15]	2.90	–
Mahin Sha et al. [16]	–	10–13
Kumar et al. [17]	2.90	–
Kumar and Sagar [18]	–	10–12
Deepika et al. [19]	2.83	10–13
Nikbin et al. [20]	1.96	–
Pateliya and Solanki [21]	2.98	11.8
Syam Sai and Sukesh [22]	2.51	10.5–12.5
Tharani et al. [23]	2.6	12–13
Singh et al. [24]	3.25	11.0
Bayat et al. [2]	2.95	10.3

2 Properties

2.1 Physical Properties

The specific gravity of red mud ranges from 1.96 to 3.25 and fineness ranges from 1000 to 3000 cm^2/gm. The density of red mud is 3.26 gm/cm^3 and the particle size is 14.8 μm. Red mud is basic in nature. The other physical properties of red mud determined by different authors are given in Table 1.

2.2 Chemical Properties

The chemical properties of red mud such as MgO, K_2O and MnO range from 1.13 to 1.7, 0.1 to 0.73 and 0.078 to 0.1, respectively. The other chemical properties of red mud determined by different authors are given in Table 2.

Table 2 Chemical properties of red mud

Oxide composition / Research reported by author(s)	SiO_2	Al_2O_3	Fe_2O_3	CaO	Na_2O	TiO_2	LOI
Pujar and Prakash [11]	9	22	47	3.50	3.5	12.4	19
Rathod et al. [12]	11.4	21.6	38.3	1.47	6.87	–	–
Metilda et al. [13]	11.53	14.14	48.50	3.96	7.50	5.42	–
Shinge and Pendhari [25]	4.6	–	34.3	4.8	4.0	8.35	15
Shinge et al. [14]	19.497	22.522	34.752	0.503	10.684	3.58	–
Mahin Sha et al. [16]	12–15	20–22	40–45	1–2	4–5	1.8–2.0	–
Kumar and Sagar [18]	18	6.31	12.38	35.3	2.71	–	–
Deepika et al. [19]	12–15	20–22	40–45	1–2	4–5	1.8–2.0	–
Nikbin et al. [20]	14.8	17.7	27.6	14.7	5.4	7.2	9.7
Syam Sai and Sukesh [22]	12–15	20–22	40–45	1–2	4–5	1.8–2.0	–
Tharani et al. [23]	17	15	61	1	4	4	7
Singh et al. [24]	9.93	18.1	42.9	–	5.58	9.03	0.35
Tang et al. [26]	–	17.093	61.608	1.076	15.11	3.587	–
Bayat et al. [2]	13.26	15.41	20.54	19.87	5.87	4.97	16.3

2.3 Mechanical and Durability Properties

Pujar and Prakash [11] examined the use of washed and unwashed red mud in concrete for the partial replacement of cement at 0–20% at an interval of 2%. Different tests such as compressive strength, flexural strength, split tensile strength, shear strength, water absorption and workability were conducted to determine the properties of concrete. It was found that the shear strength, compressive strength, flexural strength and split tensile strength increased with the increase of washed red mud up to 8% and unwashed red mud up to 2%, thereafter reduction in strengths was observed. Further, it was observed that water absorption and sorptivity decreased with the increase of washed red mud up to 8% and unwashed red mud up to 2%. The strength, workability and sorptivity of washed red mud were higher than the unwashed red mud.

Rathod et al. [12] replaced 5, 10, 15, 20, 25, 30, 35 and 40% of cement with red mud taking control mix with 0%. It was observed that the compressive strength and tensile strength decreased with the increase in the proportion of red mud. The optimum percentage of red mud to be replaced with cement was recommended as 25%.

Metilda et al. [13] studied the use of red mud in concrete in which the cement was partially replaced by red mud at 0–25% with an interval of 5%. Based on the experimental investigation, it was observed that the compressive strength, tensile strength and flexural strength increased with the increase in the percentage of red mud up to 15%, but beyond 15%, there was a reduction in the strength. Therefore, it was recommended to replace cement with red mud to the extent of 15%.

Shinge and Pendhari [25] partially replaced cement by red mud at different proportions of 0, 5, 10, 15 and 20%. It was found that the compressive strength decreased with the increase in the percentage of red mud. Also, it was observed that the tensile and flexural strength increased with the increase in the percentage of red mud. On the basis of experimental studies, it was suggested that 10% of red mud can be effectively used for partial replacement of cement without compromising the compressive strength.

Shinge et al. [14] encapsulated the use of red mud and rice husk ash in cement-based materials (mortar). Proportions of red mud and rice husk ash used were 5, 10, 15 and 20%. The compressive strength at 0, 5, 10, 15 and 20% of red mud was 36.72 N/mm^2, 36.10 N/mm^2, 34.33 N/mm^2, 30.33 N/mm^2 and 25.25 N/mm^2, whereas tensile strength was 3.00 MPa, 3.19 MPa, 3.43 MPa, 3.51 MPa, 3.66 MPa at 28 days implying that the compressive strength of red mud-based mortar decreased, while tensile strength increased with the increase in red mud proportion.

Yamuna [15] investigated the use of red mud and quarry dust in cement mortar and concrete. Cement and fine aggregates were partially replaced by red mud and quarry dust. Different proportions of red mud such as 0, 5, 10, 15, 20, 25 and 30% in cement mortar were used. From the compressive strength point of view, the optimum percentage of red mud in cement mortar was recommended as 20%. Keeping the red mud as 20% and replacing fine aggregates by quarry dust at proportions of 0, 10, 20, 30, 40, 50 and 60%, tests were conducted to determine the split tensile strength. The split tensile strength increased up to 40% of quarry dust and then decreased.

Mahin Sha et al. [16] studied the effect of red mud concrete on workability, compressive strength and tensile strength. The replacement levels of cement by red mud such as 0–25% at an interval of 5% were used. The experimental study indicated that the compressive strength and the tensile strength decreased with the increase in the percentage of red mud, whereas the workability of concrete increased with the increase in the percentage of red mud. Therefore, the optimum use of red mud as a cement replacement was recommended as 20%.

Kumar et al. [17] investigated the effect of red mud in cement mortar in addition to the effect of red mud and quarry dust for the partial replacement of cement and sand. Firstly, cement was partially replaced by red mud at different levels ranging from 0 to 30% at an interval of 5%. It was found that the compressive strength of cement mortar increased up to 20% followed by a subsequent decrease. Therefore, the optimum percentage of red mud was 20% for the partial replacement of cement. Secondly, this optimized percentage of red mud in combination with variable percentages of quarry dust was employed for the partial replacement of sand (from 0 to 60% with an increment of 10%). It was observed that the compressive strength and split tensile strength increased up to 40% of quarry dust and then reduced. So, it can be concluded that the optimum percentage of red mud was 20% in cement, whereas the optimum percentage of quarry dust was 40% in concrete.

Kumar and Sagar [18] investigated the use of red mud and quarry dust in concrete. Red mud was used at different replacement levels such as 0, 5, 10, 15, 20 and 25% and quarry dust at 0, 10, 15, 20, 25, 30, 35 and 40% for the partial replacement of cement and sand. They witnessed a significant increase in the compressive strength and the

flexural strength with respect to the upsurge in the percentage of red mud. On the contrary, the strengths (compressive and flexural) were reduced with the increase in the percentage of red mud beyond 15%; therefore, it was established as an optimum percentage. Further, at the optimum percentage of red mud (that is 15%), sand was partially replaced by quarry dust at different replacement levels and various tests were conducted to determine the mechanical properties. The compressive strength and the flexural strength increased with the increase in the percentage of quarry dust, but there was a reduction in the strength beyond 30% of quarry dust. Therefore, it can be concluded that the optimum percentage of red mud and quarry dust for the partial replacement of cement and sand was 15% and 30%, respectively.

Liu and Poon [27] studied the mechanical properties of self-compacting concrete using red mud. It was found that the 28 days compressive strength of red mud-based self-compacting concrete was 38 MPa compares to 33 MPa of fly ash based self-compacting concrete. The elastic modulus and tensile strength of red mud-based self-compacting concrete was also better than the fly ash-based self-compacting concrete. Experiments were also done on the drying shrinkage and water permeability of self-compacting concrete based on red mud. Minimum drying shrinkage was observed in the mix with 40% red mud as cement replacement. However, the water absorption of concrete was increased with an increase in red mud content due to high porosity. The internal curing of red mud was attributed to lower drying shrinkage, which consumes the extra water within its porous structure.

Sowmyashree et al. [28] studied the water absorption, acid resistance and carbonation of red mud-based concrete. It was found that the compressive strength of concrete after acid treatment decreased with increase in red mud content while the water absorption of concrete increased with increase in red mud content, which can be observed from Fig. 3. The carbonation resistance of different grades (M20 and M40) of red mud concrete was also investigated. In M20 grade of concrete after carbonation test, the compressive strength of 25% red mud and 30% red mud was decreased by 24% and 20%, respectively. However, for M40 grade of concrete, the reduction of strength was lesser with 14 and 12% for 25% red mud and 30% red mud. High grade of concrete was denser than a lower grade of concrete, which reduces the penetration depth of CO_2 in the concrete. Due to less carbonation in M40 grade of concrete, compressive strength was better than M20 grade of concrete. Based on the study, the optimum percentage replacement of red mud with cement by weight was recommended as 30% both in the case of M20 and M40 grade of concrete (Fig. 2).

Deepika et al. [19] replaced cement by partially replacing with red mud at various proportions such as 0, 10, 15 and 20%. Different tests (such as compressive strength, tensile strength and flexural strength) were conducted to determine the mechanical properties of the red mud concrete. It was investigated that the compressive strength, tensile strength and flexural strength increased with the increase in the percentage of red mud.

Nikbin et al. [20] demonstrated the use of red mud in the concrete mixture. Different tests such as compressive strength, tensile strength, flexural strength, specific gravity and modulus of elasticity were conducted. It was determined that the compressive strength tends to decrease with the increase in red mud showing

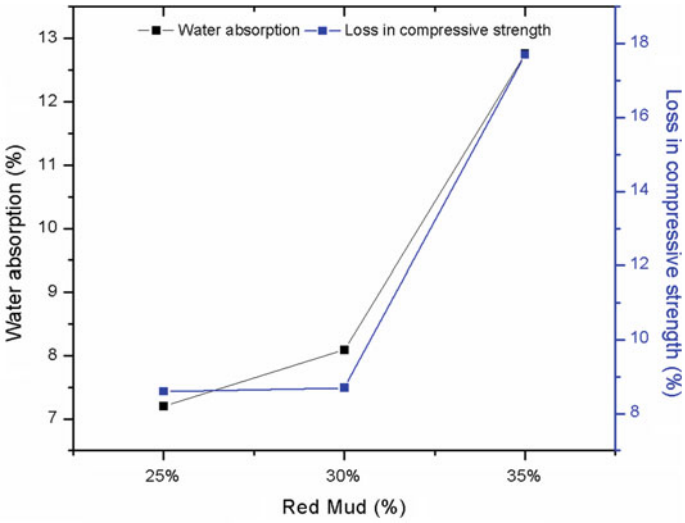

Fig. 2 Effect of red mud addition on the water permeability and loss in compressive strength after acid treatment

the reduction of strength of 3.5, 8.3, 15, 19.7 and 29.5% for specimens containing, respectively, 5, 10, 15, 20 and 25% red mud at the age of 28 days. The reduction in the compressive strength is due to the lower pozzolanic properties of red mud as compared to the cement. Since the particle size of red mud is smaller, therefore, it has a good filling capacity, but this effect is not strong enough to compensate for lower chemical reactivity and hydration of red mud compared to cement and, consequently, the compressive strength of specimens decreased as the red mud content increased. A similar trend was followed for the tensile strength, flexural strength, specific gravity and modulus of elasticity. The reduction in the modulus of elasticity of concrete is due to the fact that the addition of red mud leads to the decrease in aggregate volume in the mixture which results in the lower stiffness of the concrete mixture.

Pateliya and Solanki [21] investigated the use of red mud in mortar and concrete. Cement was partially replaced by red mud at different replacement levels such as 16–24% with an increment of 1%. Different tests were conducted to determine the mechanical (such as compressive strength, flexural strength and split tensile strength) and durability characteristics for three different grades of concrete (M20, M25 and M30). Experimental investigation showed that the compressive strength, flexural strength, split tensile strength and durability characteristics increased up to 18% and then decreased for all the three grades. Therefore, the recommended value of the optimum percentage of red mud was 18% for all the grades.

Syam Sai and Sukesh [22] examined the effect of red mud (ranging from 0% to 20% at an interval of 5%) with 5% or without hydrated lime in concrete. Slump cone and compaction factor tests were used to determine the workability of concrete. It was found that the workability of concrete increased with the increase in percentage

of red mud for M40 and M50 grade. Different tests were conducted to determine the mechanical properties such as compressive strength, flexural strength and split tensile strength for both the grades. Compressive strength and split tensile strength of the red mud concrete increased up to 10%, then decreased for both the grades with or without hydrated lime as shown in Figs. 3, 4, 5 and 6, although the strengths of red mud concrete with hydrated lime was higher than without hydrated lime. Flexural strength of the concrete decreased with the increase in the percentage of red mud as demonstrated in Figs. 7 and 8. Finally, it was concluded to use 10% of red mud for concrete with or without hydrated lime.

Tharani et al. [23] examined the effect of red mud concrete in which the cement was partially replaced by red mud at 0, 5, 10 and 15%. The compressive strength of red mud concrete at replacement levels were 33.43, 34.06, 33.14 and 32.95% at 28 days. Results depict that the compressive strength increased up to 5% replacement level and then decreased. Further, the compressive strength of 10% replacement of cement with red mud was found at par with the conventional concrete. Therefore, the range of the optimum percentage of red mud was recommended as 5–10%.

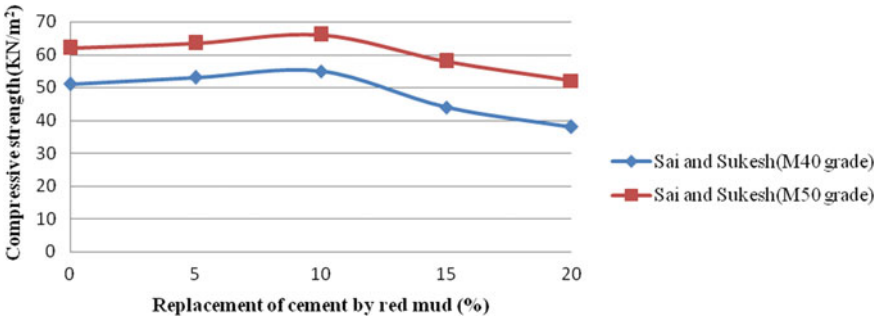

Fig. 3 Compressive strength of concrete for M40 and M50 without hydrated lime

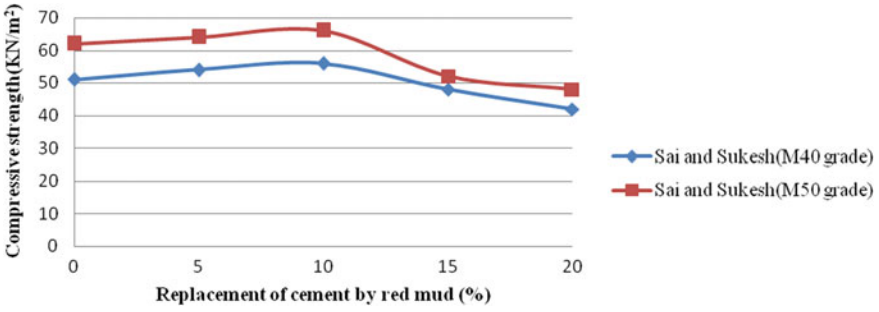

Fig. 4 Compressive strength of concrete for M40 and M50 with 5% hydrated lime

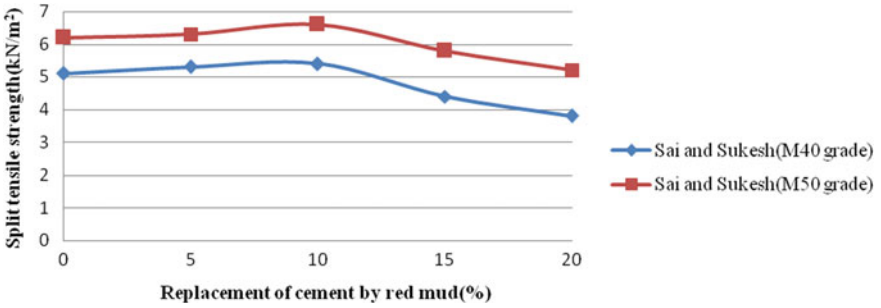

Fig. 5 Split tensile strength of concrete for M40 and M50 without hydrated lime

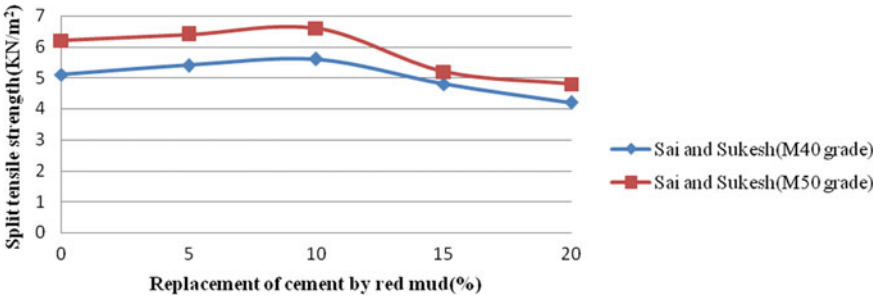

Fig. 6 Split tensile strength of concrete for M40 and M50 with 5% hydrated lime

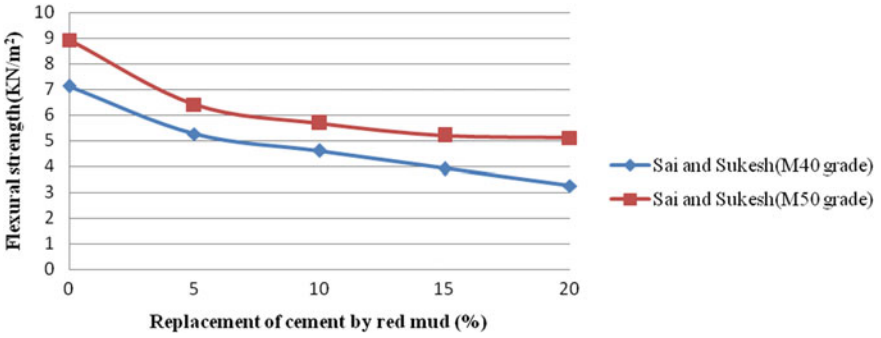

Fig. 7 Flexural strength of concrete for M40 and M50 without hydrated lime

Singh et al. [24] investigated that the red mud-based geopolymer possessed very little compressive strength due to the less amount of silica; hence, silica-based materials such as ground granulated blast furnace slag, microsilica, etc., were added to maintain the Si/Al ratio. The highest strength of red mud-based geopolymer was obtained at 30% for thermally cured samples with SiO_2/Al_2O_3 ratio at 5.1. Ambient cured samples exhibited better compressive strength results than the thermally cured

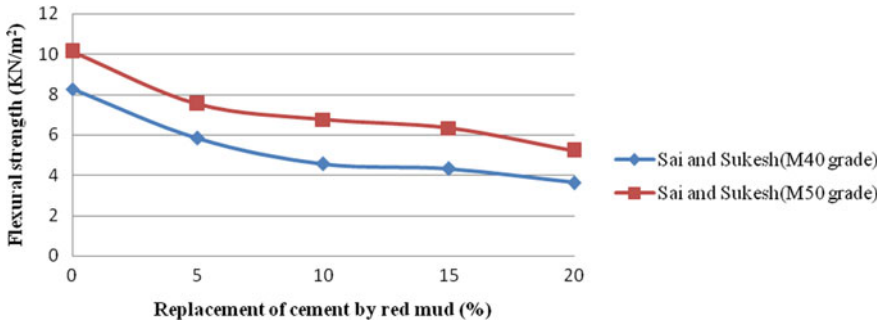

Fig. 8 Flexural strength of concrete for M40 and M50 with 5% hydrated lime

samples. The optimum SiO_2/Al_2O_3 ratio was 4 for ambient cured samples which was lesser than the thermally cured samples. Therefore, the optimum use of red mud for both ambient and thermally cured samples was found to be 30%.

Tang et al. [26] examined the use of red mud on fresh and hardened properties of self-compacting concrete (SCC). Fly ash was partially replaced by red mud at different replacement levels such as 12.5, 25 and 50% by weight. Different tests were conducted to determine the fresh, hardened properties and also the microstructural behaviour of self-compacting concrete. It was depicted that the quantity of superplasticiser required to achieve SCC requirements increased with the increasing of red mud content as the flowability decreased with an increase of red mud. Therefore, the red mud had negative effects on the fresh properties of SCC mixes. Also, it was observed from the experimental investigation that increase in the red mud content increased the compressive strength and elastic modulus but decreased the tensile strength.

Bayat et al. [2] influenced the use of red mud on the fresh and hardened properties of alkali-activated slag (AAS) paste and mortar. It was found that the cohesiveness increased, while the fluidity, consistency and consistency loss rates decreased with the increase in red mud content. The XRD, FTIR, SEM and TG/DTA results showed that after 28 days, the main crystalline minerals in the raw red mud (RM) and the thermally treated RM retained their nature in the gel and were incorporated by the gel structure. The optimum percentage of red mud was recommended as 20% providing the highest compressive strength, while the flexural strength decreased with the increase of red mud content.

3 Twenty-Eight Days Strength of Mortar and Concrete Manifesting Red Mud as a Partial Replacement

3.1 Strength of Mortar Versus Replacement of Cement by Red Mud

Yamuna [15] testified an upsurge up to 20% followed by a subsequent reduction and it is indicated as the optimum percentage of red mud replacement. However, Shinge et al. [14] revealed a significant diminution in the compressive strength corresponding to the increase in the proportion of red mud. Futhermore, Shinge et al. [14] showed that the split tensile strength and flexural strength increased corresponding to the increase in the proportion of red mud. Compressive strength, split tensile strength and flexural strength of mortar incorporating red mud as a partial replacement of cement after 28 days of curing period is given in Figs. 9, 10 and 11.

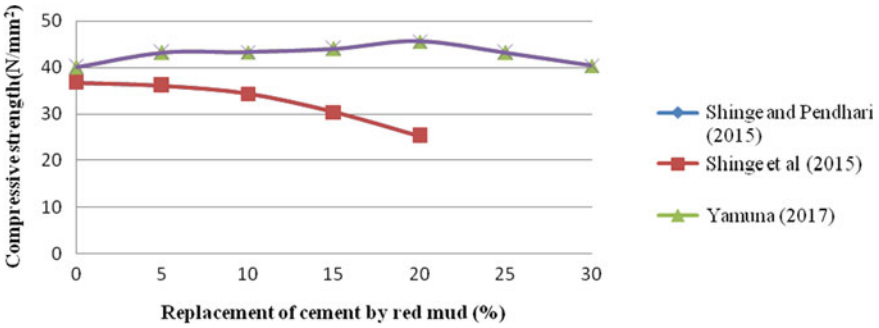

Fig. 9 Compressive strength versus replacement of cement by Red mud

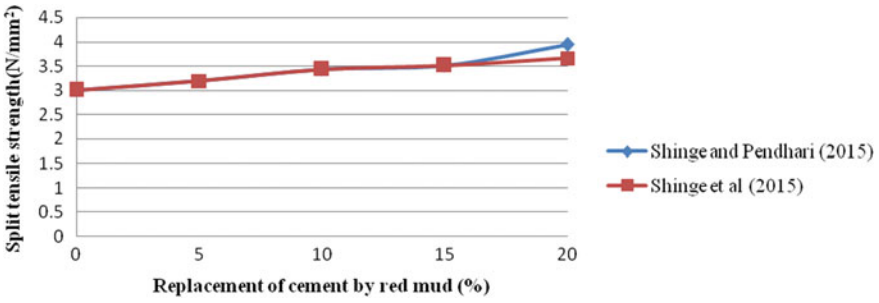

Fig. 10 Split tensile strength of mortar versus replacement of cement by Red mud

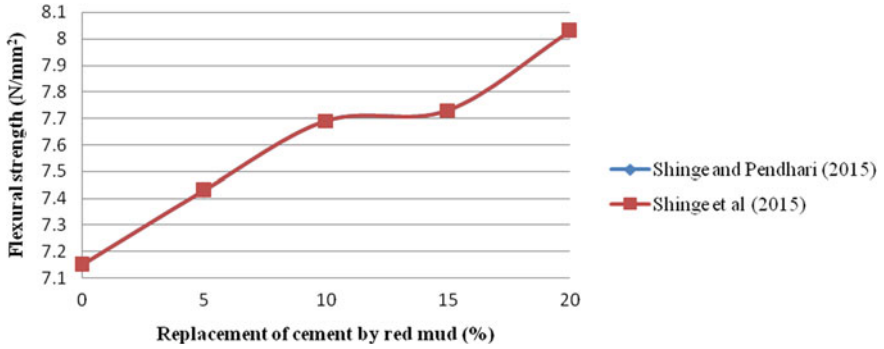

Fig. 11 Flexural Strength of mortar versus replacement of cement by red mud

3.2 Strength of Concrete Versus Replacement of Cement by Red Mud

Tharani et al. reported that the compressive strength was found to be decreased with the increase in red mud content for M 30. Metilda et al. depicted that the compressive strength and split tensile strength increased up to 15% then decreased. However, there was a reduction in the compressive strength and split tensile strength followed by the subsequent increase in red mud content for M25 and M30 grade of concrete as depicted by Mahin Sha et al. and Rathod et al. Compressive strength and split tensile strength of concrete for M 25 and M 30 grade by different researchers is illustrated in Figs. 12 and 13.

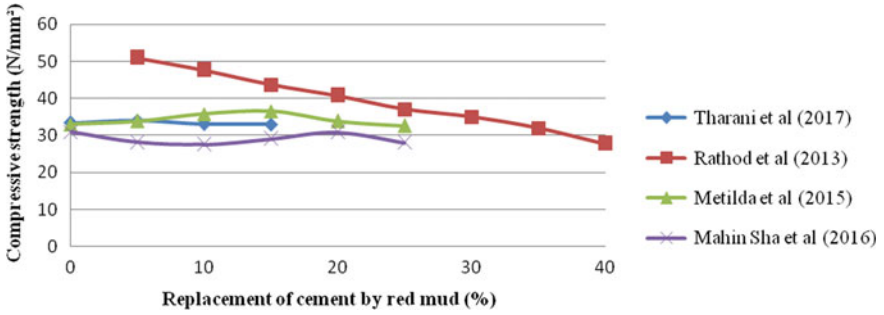

Fig. 12 Compressive strength of concrete versus replacement of cement by red mud

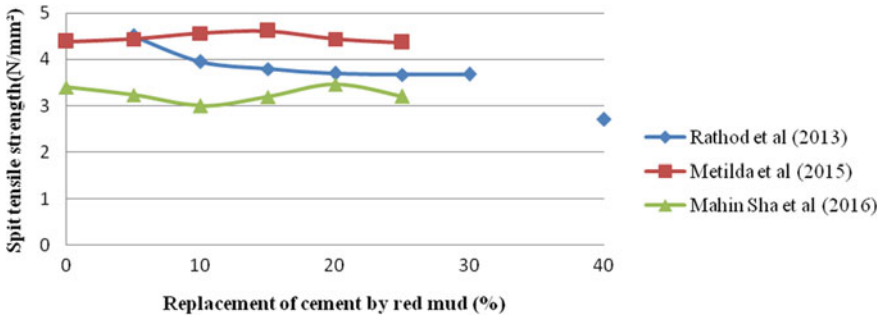

Fig. 13 Split tensile strength of concrete versus replacement of cement by red mud

The research reported on red mud by different research workers has been tabulated in Table 3.

4 Formulation of Equations for Compressive, Tensile and Flexural Strength of Mortar/Concrete Vis-à-Vis Replacement by Red Mud

4.1 Equations Developed for Mortar Manifesting Red Mud as a Partial Replacement

Data given by researchers in various research papers have been used to develop best-fit equation and R^2 value for compressive, tensile and flexural strengths of mortar after 28 days of curing:

	Property	Equation	R^2	Author
Mortar	Compressive strength	−0.5742x +38.288	0.902	Shinge and Pendhari [25]
				Shinge et al. [14]
		0.0243x +42.456	0.0176	Kumar et al. [17]
				Yamuna [15]
	Split tensile strength	0.044x +2.974	0.9533	Shinge and Pendhari [25]
		0.0328x +3.03	0.9749	Shinge et al. [14]
	Flexural strength	0.0412x +7.194	0.962	Shinge and Pendhari [25]
				Shinge et al. [14]

Table 3 Mechanical properties of red mud

Research reported by	% age replacement of cement by red mud	% age replacement of sand along with replacement of cement	Optimum percentage of red mud	Compressive strength results	Tensile strength results	Flexural strength results
Pujar and Prakash [11]	0–20% at an interval of 2%		8% for washed red mud and 2% for unwashed red mud	Increased up to 8% for washed red mud and 2% for unwashed red mud and then decreased	Increased up to 8% for washed red mud and 2% for unwashed red mud and then decreased	Increased up to 8% for washed red mud and 2% for unwashed red mud and then decreased
Rathod et al. [12]	0–40% at an interval of 5%		25%	Decreased with the increase in red mud	Decreased with the increase in red mud	
Metilda et al. [13]	0–25% at an interval of 5%		15%	Increased up to 15% then decreased	Increased up to 15% then decreased	Increased up to 15% then decreased
Shinge and Pendhari [25]	0–20% at an interval of 5%		10%	Decreased with the increase in red mud	Increased with the increase in red mud	Increased with the increase in red mud
Shinge et al. [14]	0–20% at an interval of 5%	Rice husk ash (0–20% at an interval of 5%)	10%	Decreased with the increase in red mud	Increased with the increase in red mud	Increased with the increase in red mud
Yamuna [15]	0–30% at an interval of 5%	Quarry dust (0–60% at an interval 10%)	20%	Increased up to 20% and then decreased	Increased up to 20% and then decreased	
Mahin Sha et al. [16]	0–25% at an interval of 5%		20%	Decreased with the increase in red mud	Decreased with the increase in red mud	

(continued)

Table 3 (continued)

Research reported by	% age replacement of cement by red mud	% age replacement of sand along with replacement of cement	Optimum percentage of red mud	Compressive strength results	Tensile strength results	Flexural strength results
Kumar et al. [17]	0–30% at an interval of 5%.	Quarry dust at 0%–60% with an increment of 10%	20%	Increased up to 20%, then decreased for both mortar and concrete	Increased up to 20% red mud and 40% Quarry dust, then decreased for concrete	
Kumar and Sagar [18]	0–25% at an interval of 5%	Quarry dust (0–40% at an interval of 5%)	15%	Increased up to 15% and then decreased		Increased up to 15% and then decreased
Liu and Poon [27]	With reference to control mix, fly ash was replaced by red mud from 0 to 40% at an interval of 10%			It was better than the fly ash-based self-compacting concrete	It was also better than the fly ash-based self-compacting concrete	
Deepika et al. [19]	0, 10, 15 and 20%.		20%	Increased with the increase in red mud	Increased with the increase in red mud	Increased with the increase in red mud
Nikbin et al. [20]	0–25% at an interval of 5%			Decreased with the increase in red mud	Decreased with the increase in red mud	Decreased with the increase in red mud
Pateliya and Solanki [21]	16–24% at an interval of 1%		18%	Increased up to 18% and then decreased	Increased up to 18% and then decreased	Increased up to 18% and then decreased

(continued)

Table 3 (continued)

Research reported by	% age replacement of cement by red mud	% age replacement of sand along with replacement of cement	Optimum percentage of red mud	Compressive strength results	Tensile strength results	Flexural strength results
Syam Sai and Sukesh [22]	0–20% at an interval of 5%		10%	Increased up to 10%, then decreased	Increased up to 10%, then decreased	Decreased with the increase red mud
Tharani et al. [23]	0–15% at an interval of 5%		5–10%	Increased up to 10% and then decreased		
Singh et al. [24]	0, 10, 30, 50, 70, 90% along with the fly ash		30%	Ambient cured samples exhibited better compressive strength results than the thermally cured samples		
Tang et al. [26]	With reference to control mix, fly ash was partially replaced by red mud at12.5%, 25 and 50%			Increased the compressive strength	Decreased the tensile strength	
Bayat et al. [2]	With reference to control mix, slag was partially replaced by red mud (0–40% at an interval of 10)		20%	Decreased with the increase of red mud content		Decreased with the increase of red mud content

4.2 Equations Developed for Concrete Manifesting Red Mud as a Partial Replacement

Data given by researchers in various research papers have been used to develop best-fit equation and R^2 value for compressive, tensile and flexural strengths of concrete after 28 days of curing:

	Property	Equation	R^2	Author
Concrete	Compressive strength	$-0.6429x + 53.815$	0.9961	Rathod et al. [12]
		$-0.0062x + 34.35$	0.0014	Metilda et al. [13]
		$-0.0303x + 29.462$	0.0356	Mahin Sha et al. [16]
		$-0.0472x + 33.749$	0.3942	Tharani et al. [23]
	Split tensile strength	$-0.040x + 4.558$	0.838	Rathod et al. [12]
		$-0.000x + 4.468$	0.000	Metilda et al. [13]
		$-0.000x + 3.255$	0.001	Mahin Sha et al. [16]

5 Conclusions

1. The red mud generated in the production of alumina is a worldwide problem as it creates a nuisance. The production of red mud in India is more than 4 million tonnes, while in the world, it is 120 million tonnes. By partially replacing cement with red mud, the problem of surface and groundwater pollution can be reduced to a great extent.
2. The properties of red mud are analogous to the properties of cement; hence, it can be effectively used as a partial replacement for cement which in turn decreases the production of cement followed by the subsequent decrease in the CO_2 emissions.
3. Compressive strength, tensile strength and flexural strength of red mud mortar/concrete go on increasing up to 20% of red mud used for the partial replacement of cement and then it is decreased. Hence, we can say that the optimum percentage of red mud may be recommended as about 20%.

References

1. Alam S, Das SK, Rao BH (2017) Characterization of coarse fraction of red mud as a civil engineering construction material. J Clean Prod 168:679–691
2. Bayat A, Hassani A, Yousefi AA (2018) Effects of red mud on the properties of fresh and hardened alkali-activated slag paste and mortar. Constr Build Mater 167:775–790

3. Bavani DA, Karthiga S, Thirumurugan V (2018) Experimental investigation of sulphate resistance on partially replacing fine aggregate with red mud in mortar. Int J Pure Appl Math 119(14):983–988
4. Dodoo-Arhin D, Konadu DS, Annan E, Buabeng FP, Yaya A, Tufflor BA (2013) Fabrication and characterisation of Ghanaian bauxite red mud-clay composite bricks for construction applications. Am J Mater Sci 3(5):110–119
5. Yang J, Zhang D, Hou J, He B, Xiao B (2008) Preparation of glass-ceramics from red mud in the aluminium industries. Ceram Int 34:125–130
6. Kurtoğlu SF, Uzun A (2016) Red mud as an efficient, stable, and cost-free catalyst for COx-free hydrogen production from ammonia. Sci Rep 6(32279):1–8
7. Liu Z, Li H (2015) Metallurgical process for valuable elements recovery from red mud-Areview. Hydrometallurgy 155(Supplement C), 29–43
8. Agrawal A, Sahu KK, Pandy BD (2004) Solid waste management in non-ferrous industries in India. Resour Conserv Recycl 42:99–120
9. Singh M, Upadhayay SN, Prasad PM (1997) Preparation of iron rich cements using red mud. Cem Concr Res 27:1037–1046
10. Tsakiridis PE, Agatzini-Leonardou S, Oustadakis P (2004) Red mud addition in the raw meal for the production of Portland cement clinker. J Hazard Mater 116:103–110
11. Pujar SM, Prakash KB (2014) Effect of replacement of cement by red mud on the properties of concrete. Int J Sci Eng Res 5(9):805–813
12. Rathod RR, Suryawanshi NT, Memade PD (2013) Evaluation of the properties of red mud concrete. J Mech Civil Eng 31–34
13. Metilda DL, Selvamony C, Anandakumar R, Seeni A (2015) Investigations on optimum possibility of replacing cement partially by red mud in concrete. Sci Res Essays 10(4):137–143
14. Shinge KS, Warad BB, Rathod SB, Pendhari SS (2015) Partial replacement of cement in mortar by using red mud and rice husk ash. Int J Sci Eng Res 6(9):1269–1272
15. Yamuna Y (2017) Utilization of quarry dust and red mud in cement mortar and concrete. In: 10th international conference on recent innovations in science, engineering and management, pp 846–852
16. Mahin Sha OB, Remya CP, Salja PA, Shifal KS (2016) Red mud concrete. Int Res J Eng Technol 3(4):2582–2585
17. Kiran Kumar MS, Naik R, Harish KS, Ramesh M (2016) Experimental study on utilization of red mud and quarry dust in cement mortar and concrete. Int J Civil Struct Eng Res 4(1):324–330
18. Kumar RP, Sagar PS (2016) Experimental study on the effect of cement and sand replacement with red mud and quarry dust in cement concrete pavements. Int J Recent Innovat Trends Comput Comput 4(6):636–639
19. Deepika K, Ananthakumar S, Mariadoss R, Nanthagopal J, Saravanakumar V (2017) Experimental investigation of concrete by red mud as replacement of cement using strengthening admixture. Int J Innovat Res Sci Eng Technol 6(3):3928–3933
20. Nikbin IM, Aliaghazadeh M, Charkhtab SH, Fathollahpour A (2015) Environmental impacts and mechanical properties of lightweight concrete containing bauxite residue (red mud). J Clean Prod 1–34
21. Pateliya S, Solanki C (2017) Experimental studies on concrete utilizing red mud as a partial replacement of cement. Int J Adv Res Innnovat Ideas Edu 3(2):5408–5415
22. Sai PS, Sukesh C (2017) Strength properties of concrete by using red mud as a replacement of cement with hydrated lime. Int J Civil Eng Technol 8(3):38–49
23. Tharani P, Adithiya BA, Murali K (2017) Experimental study on concrete with bauxite residue as partial replacement of cement. Int J Chem Tech Res 10(8):35–41
24. Singh S, Aswath MU, Ranganath RV (2018) Effect of mechanical activation of red mud on the strength of geopolymer binder. Constr Build Mater 177:91–101
25. Shinge KS, Pendhari SS (2015) Use of red mud for partial cement replacement. Int J Modern Trends Eng Res 622–626
26. Tang WC, Wang Z, Liu Y, Ciu HZ (2018) Influence of red mud on fresh and hardened properties of self compacting concrete. Constr Build Mater 178:288–300

27. Liu R-X, Poon C-S (2016) Utilization of red mud derived from bauxite in self-compacting concrete. J Clean Prod 112:384–391
28. Sowmyashree A, Manjunath CS, Arpitha DJ, Panditharadhya BJ (2016) Comparison on durability properties of red mud as a partial replacement of cement with hydrated lime for different grades of concrete with and without superplasticiser. Int J Eng Res Technol 5(5):572–577

Parameters Affecting Tufa Precipitation from Recycled Concrete Aggregate

Aiyoub Abbaspour and Burak F. Tanyu

Abstract Aggregate generated from concrete is one of the most considered recycled materials used in the U.S. for construction that requires earthwork. However, recycled concrete aggregate (RCA) is known to produce tufa. This study focuses on understanding the composition of the precipitated tufa material from RCA as well as the factors that affect the precipitation process. The precipitation experiments were conducted using PWP (Plummer–Wigley–Parkhurst) reaction vessel using a synthetic metastable RCA solution. Based on the identified parameters, a parametric study was also conducted to evaluate the effectiveness of the suggested mitigation method in the literature to remove and replace fine particles from RCA. Additionally, as part of this parametric study, the effects of contact time and blending with natural virgin aggregate (V.A.) were investigated as alternative mitigation methods. Minteq A2 and geochemical modeling were utilized to calculate the total solid-phase formation under equilibrium conditions from 100% RCA, 100% V.A., and different blends of the two materials. It is shown that the total ionic strength, availability of carbonate and bicarbonate ions, and saturation conditions of Ca and SO_4 ions control the mineralogy of the tufa precipitation. Depending on the mechanism, it was found that the calcium carbonate or calcium sulfate minerals can be the dominant forms of precipitation in RCA tufa. Other minor elements contributing to RCA tufa formation were found to be Na, K, Cl, and Si. The parametric study showed that the RCA tufa potential is not dependent on the particle size fractions of RCA but can be reduced by blending RCA with V.A. or decreasing the contact time between water and RCA particle by creating a highly permeable layer of RCA.

Keywords RCA · Tufa precipitation · Geochemical modeling · Leach test · Fraction contribution · Blending · Contact time

A. Abbaspour (✉) · B. F. Tanyu
George Mason University, Fairfax, VA 22030, USA
e-mail: aabbaspo@gmu.edu

K. R. Reddy et al. (eds.), *Sustainable Environment and Infrastructure*, Lecture Notes in Civil Engineering 90, https://doi.org/10.1007/978-3-030-51354-2_7

1 Introduction

Evaluating the potential of tufa precipitation from recycled concrete aggregate (RCA) as well as other recycled materials has been an interest to several researchers in the past. Specific studies, mainly in the 1990s, were conducted to evaluate the potential of tufa precipitation from RCA to clog the underdrain drainage systems (particularly the geotextile used in these systems). These studies were conducted both in the laboratory as well as in the field utilizing various test sections [1, 2]. Although the contents of these studies are extensive, in general, these studies were highly fragmented and often failed to provide conclusive results and scientific justifications for the observed behaviors.

For instance, based on case studies by Snyder and Bruinsma [2] and Sadecki [1] on test sections and stockpiles created using different fractions of RCA (fine and coarse fractions), the fine fraction (<4.75 mm) within RCA was held responsible for the high release of calcareous constituents and considered as the main source for tufa precipitation in underdrain systems. Aside from the use of a methodology (i.e., submerging and dissolution in hydrochloric acid as an indication of tufa formation) that would have limitations to differentiate between the tufa and the RCA particles, these past studies have not considered several important parameters during their evaluation of the data. These parameters include (but not limited to) (1) the difference in permeability of fine and course fractionated RCA and change in contact time between water and solid particles, (2) the occurrence of suffosion, and (3) the occurrence of rainfall runoffs that was not percolated through the material, which can affect the measured concentrations of ions. Based on recommendations of these studies, some of the current federal and state highway specifications either restrict or prohibit the use of RCA [3–5] or suggest practices to mitigate tufa precipitation from RCA used in base/subbase layers [6, 7]. These suggested mitigation methods include (i) eliminating fines or reducing the fines to less than 5%, (ii) replacing the fine fraction with fine crushed stone, and (iii) blending RCA with V.A.

Laboratory studies focusing on the leaching behavior of RCA and the role of different fractions on tufa formation have also shown disagreeing results. Name et al. [8] and McCulloch et al. [9] explained a special procedure for collecting RCA tufa precipitation by cycles of bubbling leachate solution from RCA with carbon dioxide (CO_2) and drying and filtering the leachate. The study concluded that the potential of precipitation increases with an increase in fines content of RCA. However, the research did not provide any information on the saturation condition of different ions, pH, or even the mineralogical composition of collected solids. Additionally, the observations noted were often not supported in other parametric studies conducted on RCA leaching characteristics [10, 11]. The overall summary of the previous studies indicates that these studies did not determine the effects of blending and contribution of different fractions on the release of any element that may participate in potential calcareous (and non-calcareous) tufa formations from RCA.

Abbaspour and Tanyu [12] suggested a procedure to induce tufa from RCA over a porous media (nonwoven geotextile) using the Plummer–Wigley–Parkhurst (PWP)

reaction vessel [13] and studied the governing mechanisms on precipitation process and composition of RCA tufa. The focus of this work is to identify the affecting parameters that contribute to the precipitation of tufa from RCA based on induced precipitation tests and to use these parameters in order to evaluate the validity of the mitigation methods previously suggested in the literature (i.e. removal of fine fraction and blending). The paramteric study was conducted using bench-scale leachate extraction and equilibrium geochemistry.

2 Materials and Methods

2.1 Materials

Recycled concrete aggregate used in this study was collected right after it was produced (within a week after being crushed and stockpiled) from a plant in northern Virginia. After collection, it was aged throughout a period of 1 year in the laboratory. The demolished concrete for RCA production in this plant comes from various sources such as curb and gutter, sewage pipes, and buildings and is classified as well-graded silty sand (SW-SM) based on Unified Soil Classification System. Detailed information on sampling procedure, mineralogical makeup, chemical composition, and the physical and index properties, of RCA aterial used in this study are explained in detail by Abbaspour et al. [14].

The V.A. used for this study was collected from a material production quarry in northern Virginia (similar to RCA). Geological composition of the source rock that is used to produce the aggregate is determined to be diabase, which is considered inert in comparison to other carbonic rocks (e.g., dolostone or limestone) with respect to leaching and tufa precipitation. The quarry produces this material to be used for base application and the average gradation of samples collected for the current study is in the range of what is referred by the Virginia Department of Transportation (VDOT) as 21 aggregates (VDOT 2007). Index properties of the V.A. used in this study are listed in Table 1 and the material is classified as SW-SM in accordance with USCS classification. Mineralogical composition and total metal content of the material are also shown in Table 1.

2.2 Methods

Leachate samples for this study were extracted using long-term and short-term batch water leach test procedures as suggested by Hageman [15] and in accordance with ASTM standard D3987. Both methods follow a similar procedure in sample preparation and testing steps except for the agitation time (18 h for long-term test and

Table 1 Physical and mineralogical properties of collected virgin aggregate samples

Physical properties	Mean value	Mineralogical composition	w.t. %
Liquid limit	19%	Plagioclase (calcic)	48.3
Plastic limit	17%	Calcite	0.5
Plasticity index	2%	Diopside	23.5
Particles passing 1 ½" (< 50.8 mm)	100%	Montmorillonite	14.6
Particles passing 1" (< 25.4 mm)	98.1%	Illite-Muscovite	2
Particles passing 3/4" (< 19 mm)	88.7%	Orthoclase	N.D.
Particles passing 3/8" (< 9.5 mm)	66.4%	Actinolite	2.3
Particles passing #4 (< 4.75 mm)	54.3%	Clinochlore	1.8
Particles passing #10 (< 2 mm)	38.5%	Dolomite	2.2
Particles passing #40 (< 0.43 mm)	21.8%	Gypsum	N.D.
Particles passing #200 (< 0.074 m)	10%	Hematite	N.D.
Apparent specific gravity	2.99	Magnetite	0.5
Water absorption	0.85%	Quartz (low)	3.3

Note N.D. = Not detected, w.t. % = Percent by weight

5 min for short-term test). The liquid to solid ratio is 1:20 and ASTM type II deionized (DI) water was used in both methods. Detailed descriptions of the procedures followed for testing, sample preparation, filtration, and preservation can be found in Abbaspour et al. [14]. Liquid and solid samples that were used to generate the leachate were evaluated for their chemical properties and characteristics. The mineralogical composition of solid samples was determined using quantitative X-Ray diffraction method (QXRD) [16]. Liquid samples were evaluated for pH, redox potential (Eh), electric conductivity (EC), and total leached concentrations (TLC) of major, minor, and trace elements using inductive coupled plasma mass spectrometry (ICP-MS). MINTEQA2 software is used for geochemical modeling in this study. MINTEQA2 is a geochemical equilibrium software developed by USEPA in the late 1980s and is an official tool for USEPA to evaluate the equilibrium composition of aqueous solutions in the laboratory and natural waters [17].

Solid and Leachate Sample Preparation. In order to evaluate the RCA tufa characteristics based on thermodynamic equilibrium chemistry and geochemical modeling, RCA samples were obtained with three gradations as listed below:

- *Unfractionated (as-is) samples*: RCA samples with gradation close to the as-is gradation without the oversize fraction (>19 mm)
- *Fine fraction samples*: RCA samples smaller than 4.75 mm
- *Course fraction samples*: RCA samples larger than 4.75 mm and smaller than 19 mm.

For the parametric study on the effect of fraction contribution on RCA tufa potential, leachate samples from these three gradations were extracted using a long-term extraction method, as achieving the solid-liquid equilibrium was necessary for

geochemical analyses. In order to study the effect of blending, two different blends of RCA-V.A. with different proportions (40–60 and 20–80% by weight) were prepared and leachate samples were compared to as-is 100% RCA and 100% V.A. results. The effect of contact time (agitation time) was evaluated by comparing the total leach concentrations between RCA leachate extracted using long-term and short-term methods as explained above.

Induced Precipitation Tests. Two different induced precipitation tests were conducted using PWP reaction vessel and prepared metastable RCA leachate. The reaction vessel included a 1,000-ml beaker, magnetic stirrer, and perforated vinyl coil connected to a commercially prepared CO_2–N_2 (50–50%) gas tank. Details, measurements, applied conditions of both test and procedure followed to prepare the metastable solution is explained in great detail by Abbaspour and Tanyu [12]. The first induced test included continuous stirring and bubbling with CO_2 (as suggested by Nam et al. [8]) and the second test was conducted under pure evaporation conditions (no bubbling-no stirring). Leachate characteristics including ion concentrations, temperature, pH–Eh–EC, and alkalinity by titration were monitored during both tests. Four geotextile samples were submerged with a different time period during each test and were studied using a stereo-microscope with a built-in camera after each test.

3 Results and Discussions

3.1 Characterization of Potential RCA Tufa Based on Induced Precipitation Tests

Figure 1 shows sample images of precipitated crystals from both tests. The mineralogy and morphology of the precipitated crystals reveal that the precipitated tufa is dominated by polymorphs of calcium carbonate (calcite/aragonite) during the first test (Fig. 1a, b), as the leachate was continuously bubbled and stirred. However, during the second test (pure evaporative test), the dominant precipitation was found to be in the form of calcium sulfate polymorphs (gypsum/selenite) as can be seen in Fig. 1c, d.

Measurements of the total alkalinity and pH during the first test showed high activity of bicarbonate ion, which means that bicarbonate ions were readily available to react with Ca and hydronium ions (as suggested by Plummer et al. [13]) to form calcium carbonate crystals. Whereas, in the second test, the bicarbonate and carbonate ion activities were extremely affected and limited by the diffusion rate of atmospheric carbon dioxide into a supersaturated solution. With the initiation of each test, crystal growth was observed over geotextile fibers (which acted only as a platform for nucleation and growth) and continued throughout the entire test. With the increase in immersion time, crystals started to form clusters over geotextile samples. More

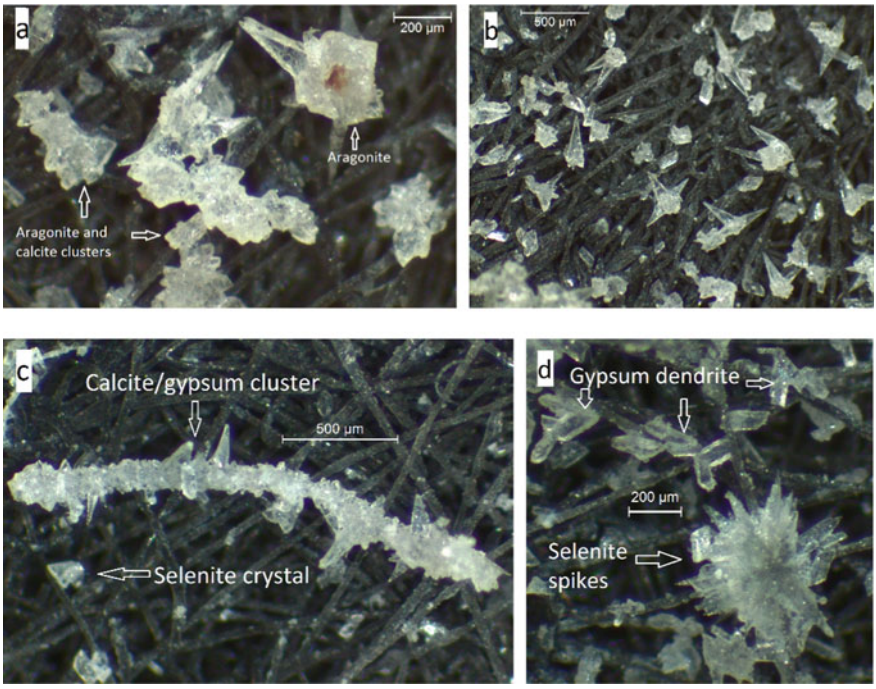

Fig. 1 Crystal growth from metastable RCA leachate with various morphologies under two different conditions, **a** and **b** aragonite and calcite crystal growth under continuous stirring and bubbling with CO_2, **c** and **d** evaporative gypsum and selenite growth (pure evaporation)

details about the use of PWP test setup to precipitate tufa from RCA can be found in Abbaspour and Tanyu [12].

The minor minerals observed from both tests (not shown here) include halite (NaCl), sylvite (KCl), and quartz low (SiO_2) with a total quantity less than 5% by weight of overall precipitation (as collected in the bottom of the vessel). Analyses on the ion activates showed that in addition to precipitation mechanism (abundance of CO_2 vs. pure evaporation), the most important parameters in determining the composition and formation of RCA tufa are total ionic strength of the solution, ionic activities of Ca, S (as SO_4^{2-}), Na, K, Cl, and Si ions [12]. The pH of RCA leachate is only important when the leachate is extracted ($10 < pH < 12$). However, once the solution is equilibrated with atmospheric CO_2, the equilibrium pH value is in the range of 8–8.5, which is in agreement with previous field reports [11].

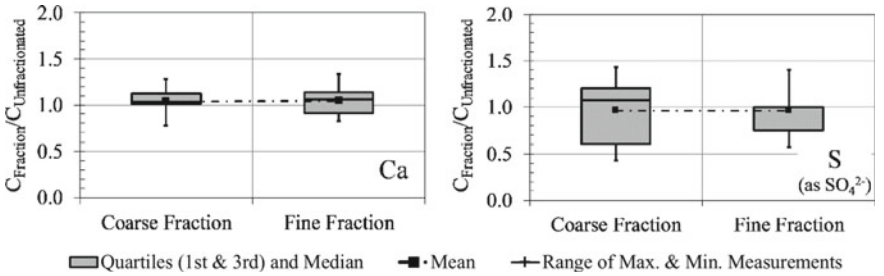

Fig. 2 Statistical analyses for normalized TLC of elements contributing to the major mineral precipitate formation from RCA

3.2 Effect of Particle Size on Potential of Tufa Precipitation

The effect of particle size on release behavior and contribution of each of fine and coarse fractions on the potential of tufa precipitate formation is investigated by measuring and comparing the TLC of several elements, especially elements that participate in RCA tufa formation. Therefore, the TLC of Ca, S (as SO_4^{2-}), Si, K, Na, and Cl were obtained from fine and coarse RCA fractions and normalized by dividing these values by the measured TLC of the same elements from unfractionated samples. The results of the statistical analyses carried out on the normalized data are shown in Fig. 2 in the form of Whisker diagrams for elements that were found to contribute to RCA tufa precipitation. As it is clear from this figure, statistically, data do not show any noticeable effect of particle fraction on the release of major elements or the potential of tufa formation. A similar observation was made for pH and solution ionic strength measured for the leachate samples extracted from different fractions (not shown here). However, other elements with minimal contribution to the tufa precipitation may show some particle size dependency, but it should be kept in mind that the precipitated minerals of K, Na, Cl, and Si only take up less than 5% of the total residue precipitation.

3.3 Effect of Blending RCA with V.A. on Potential of Tufa Precipitation

The TLC of major and minor elements contributing to the tufa formation from 100% V.A. and different blends of RCA/V.A. are depicted in Fig. 3. The release of K, Cl is basically zero from V.A., and Na and Si release is also very low (not shown here). As it was expected, V.A. is not a source of Ca^{2+} nor SO_4^{2-}. The TLC of Ca and S are affected by blending RCA and V.A. and are reduced in comparison to 100% RCA; however, a note should be taken that these reductions in released TLC are not linearly correlated to the TLC of Ca and S from 100% RCA and V.A.

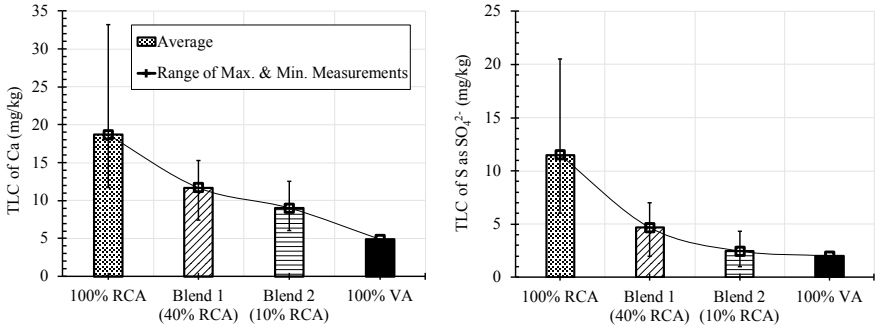

Fig. 3 Total leached concentrations of major elements contributing to tufa precipitation for 100% VA, 100% RCA, and different blends of RCA and V.A

samples. Based on the dominant ion activities, calcium carbonate, and calcium sulfate polymorph are still expected to be the dominant minerals in any potentially formed tufa. Although the formation of tufa from different blends was not simulated in the laboratory, the effect of blending RCA with V.A. at different proportions on potential tufa formation is estimated by calculating the equilibrium amount of any possible solid-phase formation using geochemical analyses and comparing these amounts with the calculated equilibrium amounts for 100% RCA as well as V.A. (Fig. 4).

The geochemical modeling shows that the potential of tufa precipitation reduces with the blending of RCA and V.A. material simply because of the TLC of major elements and consequently, the ionic activities of Ca^{2+} and SO_4^{2-}. The selected V.A. material was diabase in nature, which is considered as inert with respect to releasing calcareous constituents as opposed to calcitic rocks (e.g., limestone and dolostone) which can be a source of Ca release themselves.

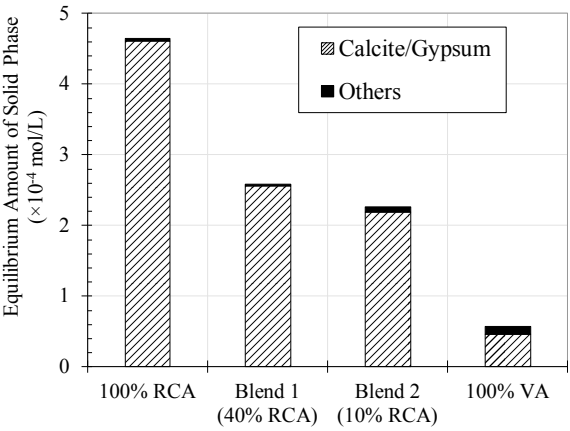

Fig. 4 Effect of blending RCA with V.A. on the potential of forming solid-phase precipitate

Table 2 Calculated ratio between total leached concertation of several elements from USGSLT and WLT batch tests

Element	Average $C_{short\text{-}term}/C_{long\text{-}term}$	Standard deviation
Ca	0.67	0.12
S (as SO_4^{2-})	0.59	0.21
K	0.61	0.25
Na	0.49	0.10
Cl	1.35	1.22
Si	0.19	0.03

3.4 Other Parameters Affecting the Potential of Tufa Precipitation

One of the important parameters that is not addressed in any of the previous studies related to RCA leaching behavior and tufa precipitation potential is the effect of contact time between effluent (percolating water through RCA layer) and the solid matrix (RCA material). Contact time between effluent and solid waste is an important and determinative factor affecting the leaching behavior of any waste and reclaimed substances [18]. The effect of contact time can be different on the release of various elements; however, determining the effect of the contact time on elements contributing to the tufa precipitations (e.g., Ca and S) can be of great importance.

The effect of different contact time on the release concentration of different elements was investigated by comparing the measured TLC of certain elements obtained using long-term and short-term batch tests. Table 2 shows the calculated ratio between the measured TLC of elements contributing to the formation of RCA tufa precipitation. Except for Cl, release concentrations of all other elements are affected by agitation time, especially Ca and S releases decrease by 33% and 44%, respectively. When compared to decrease in total ionic strength in leachate extracted from both procedures (Average $IS_{short\text{-}term}/IS_{long\text{-}term}$ of 0.64 with a standard deviation of 0.12), it can be concluded that the potential for tufa precipitation decreases with a decrease in contact time (about 36% when agitation time decreases from 18 h to 5 min).

Si release shows a major reduction when the agitation time is reduced from 18 h to 5 min (average of 81%) indicating the noticeable effect of transport by diffusion inside the solid pores (kinetics as limiting rate step) on leachability of Si from RCA [14]. However, since Si and Cl have minimal contribution to the tufa formation from RCA, the observed behavior will not affect the solid-phase precipitation from RCA. The effect of contact time between effluent and RCA can be interpreted as the permeability of the RCA layer. The higher the permeability of an RCA layer, the lower the contact time between the effluent and the solid matrix, and consequently, lower potential for tufa formation.

4 Conclusions and Practical Implications

An experimental study is conducted to evaluate the composition and affecting parameters on RCA tufa. In the next step, a parametric study was conducted based on the leaching concentrations of elements contributing to the RCA tufa formation to evaluate the effects of particle size, blending with V.A. and contact time on the potential of leaching out tufaceous constituents from RCA and precipitate formation. Based on the presented results and discussions, the following conclusions may be made:

- Based on induced tufa precipitation tests and depending on the precipitation process, calcite or gypsum (or polymorphs of them) may be the most abundant forms of RCA tufa precipitation. Calcite is dominant when CO_2 is abundant in the system (bubbled) and gypsum is the dominant form in the case of pure evaporation.
- Release of Ca and SO_4^{2-} is not particle size-dependent, and the effect of fine and coarse fractions on the potential of tufa precipitation cannot be concluded based on the statistical analyses.
- Blending RCA with virgin aggregate, in general, reduces the potential for solid-phase formation from leachate samples.
- Contact time was found to have a limited effect on the TLC of elements contributing to the tufa formation and, consequently, to the potential tufa precipitation. Therefore, constructing a base course/subbase layer with higher permeability will lead to a decrease in contact time between effluent and solid matrix and the potential precipitate deposition (for instance, by changing the gradation).

Acknowledgements The financial support for the study described in this manuscript was provided by the National Science Foundation (NSF) and Virginia Department of Transportation (VDOT) and Virginia Center for Transportation Innovation and Research (VCTIR). However, the conclusions and recommendations are those of the authors and do not reflect the opinions or policies of NSF, VDOT, and VCTIR.

References

1. Sadecki RW, Busacker GP, Moxness KL, Faruq KC, Allen LG (1996) An investigation of water quality in runoff from stockpiles of salvaged concrete and bituminous paving. Minnesota Department of Transportation, Saint Paul, Minnesota
2. Snyder M, Bruinsma J (1996) Review of studies concerning effects of unbound crushed concrete bases on PCC pavement drainage. Transp Res Record: J Transp Res Board 1519:51–58
3. VDOT (2007) Road and Bridge Specifications. Virginia Department of Transportation, Richmond, VA
4. MDOT (2012) Standard specifications for construction. Michigan Department of Transportation, Lansing, MI
5. MSHA (2013) Special Provision Inserted-Section 900.03-Recycled Materials. Presented at the
6. FHWA (2004) Transportation applications of recycled concrete aggregate. Federal Highway Administration and U.S. Department of Transportation, Washington D.C.

7. MnDOT (2016) Standard specifications for construction. Minnesota Department of Transportation, Saint Paul, Minnesota, U.S.A
8. Nam BH, Behring Z, Kim J, Chopra M (2014) Evaluate the use of reclaimed concrete aggregate in french drain applications. Florida Department of Transportation, Tallahassee, FL
9. McCulloch T, Kang D, Shamet R, Lee SJ, Nam BH (2017) Long-term performance of recycled concrete aggregate for subsurface drainage. J Perform Constructed Facil 31. In-press
10. Bestgen JO, Cetin B, Tanyu BF (2016) Effects of extraction methods and factors on leaching of metals from recycled concrete aggregates. Environ Sci Pollut Res 23:12983–13002
11. Chen J, Tinjum J, Edil T (2013) Leaching of alkaline substances and heavy metals from recycled concrete aggregate used as unbound base course. Transp Res Record: J Transp Res Board 2349:81–90
12. Abbaspour A, Tanyu BF (2019) Tufa precipitation from Recycled Concrete Aggregate (RCA) over geotextile: mechanism, composition, and affecting parameters. Constr Build Mater 196:317–329
13. Plummer LN, Wigley TML, Parkhurst DL (1978) The kinetics of calcite dissolution in CO_2-water systems at 5–60° C and 0.0–1.0 atm CO_2. Am J Sci 278:179–216
14. Abbaspour A, Tanyu BF, Cetin B (2016) Impact of aging on leaching characteristics of recycled concrete aggregate. Environ Sci Pollut Res 23:20835–20852
15. Hageman PL (2004) Use of short-term (5-Minute) and long-term (18-Hour) leaching tests to characterize, fingerprint, and rank mine-waste material from historical mines in the Deer Creek, Snake River, and Clear Creek Watersheds in and around the Montezuma Mining District, Colorado
16. Raudsepp M, Pani E (2003) Application of Rietveld analysis to environmental mineralogy. In: Environmental aspects of mine wastes. Mineralogical Association of Canada, Québec, Canada, pp 165–180
17. US EPA: MINTEQA2. https://www.epa.gov/exposure-assessment-models/minteqa2
18. Huang K, Inoue K, Harade H, Kawakita H, Ohto K (2011) Leaching behavior of heavy metals with hydrochloric acid from fly ash generated in municipal waste incineration plants. Trans Nonferrous Metals Soc China 21:1422–1427

Synergistic Effect of Hybrid Carbon Nanomaterials as Reinforcing Phase on the Physico-Mechanical Properties and Pore Structure Refinement of Cementitious Nanocomposites

N. C. Kothiyal and Ramanjit Kaur

Abstract In the present study, the enhanced physico-mechanical performance of cement mortar nanocomposites by hybrid graphene oxide-functionalized carbon nanotubes over individual nano additives i.e., graphene oxide and FCNTs as reinforcing phases have been investigated. Graphene oxide (GO) was prepared from ball-milled graphite powder (GP_b) by in-house designed horizontal ball-mill and carbon nanotubes were functionalized by the acid treatment of the pristine multi-walled CNTs. The surface-treated nanofillers were characterized well by FT-IR, SEM-EDX, XRD, AFM, and Raman spectroscopic techniques. The compressive strength of the HCN-CNCs was improved by 43.02% with respect to control sample at the curing age of 90 days for 0.02% HCNs loadings (by weight percentage of cement). This was found to be superior to the strength enhancements of 27.39% by GO and 17.82% by FCNTs at loadings of 0.02 and 0.08%, respectively. SEM images showed compact hydration products in case of cementitious matrices involving hybrid carbon nanomaterial as reinforcing phase. Better hydration of the various phases has also been confirmed by the XRD studies. In addition to the SEM and XRD, the enhancement in the compressive strength has also been interpreted in terms of porosity. Microstructure of the cement mortars was also investigated by Mercury Intrusion Porosimeter to evaluate the effect of HCNs on the porosity and pore size distribution of large capillary pores (>0.1 μm), medium capillary pores (0.01–0.1 μm), and gel pores (<0.01 μm) of the cement matrix. The improvement in the mortar properties using advanced reinforcement at nanoscale can pave a way to better and sustainable construction based infrastructure.

Keywords Hybrid Carbon Nanomaterials (HCNs) · Graphene oxide · Cementitious Nanocomposites (CNCs) · Microstructure · Crystallization behavior · Pore structure

N. C. Kothiyal (✉) · R. Kaur
Department of Chemistry, Dr. B. R. Ambedkar National Institute of Technology, Jalandhar, India
e-mail: kothiyalnc@nitj.ac.in

K. R. Reddy et al. (eds.), *Sustainable Environment and Infrastructure*, Lecture Notes in Civil Engineering 90, https://doi.org/10.1007/978-3-030-51354-2_8

1 Introduction

Ordinary Portland Cement (OPC)-based materials such as mortar and concrete are the most important building materials worldwide. Cement forms a part of most of the civil infrastructures like buildings, bridges, dams, roads, etc. Nevertheless, cement is a versatile construction material, it endures a number of drawbacks such as high brittleness, crack formation and crack propagation, risk of corrosion/erosion, limited mechanical strength, high porosity, disintegration with time and environmental effects, etc. [1–3].

Previously, traditional reinforcing agents such as steel fibers, glass fibers, polymer fibers, and carbon fibers have been utilized to curb all these limitations [4–7]. However, conventional composites are found to be unable to play any significant role at the nanoscale due to the micro-dimensions of the reinforcing components. This leads to the crack initiation at nanoscale and considerably poor mechanical strength at later ages [8]. So, an alternative to this problem can be a reinforcing material, active at nano dimensions. Two reinforcing materials which have extensively been utilized in cementitious matrices due to their outstanding mechanical properties are CNTs (carbon nanotubes) and GO (graphene oxide) [9, 10].

CNTs are the one-dimensional carbon nanomaterial comprising of graphene sheets rolled up in hollow tubular framework [11]. On the other side, graphene oxide (GO), a two-dimensional nanomaterial with hydrophilic characteristics has exceptional mechanical properties [12–14]. Even though, CNTs and GO are excellent materials to be used as nano additives in cementitious matrices, they are coupled with several drawbacks. The key problem associated with the utilization of CNTs is their limited dispersion into the cement matrix as it agglomerates due to high surface energy. Similarly, graphene sheets restack and get agglomerated in the cement matrix due to alkaline environment [15]. This complexity can be alleviated by various methods such as ultrasonication of nanomaterial in aqueous medium in presence of polycarboxylate superplasticizers (PCE-SP), functionalizing the CNTs or by integrating the CNTs with GO to form a 3-D hybrid array owing to the π-π stacking interactions [16] of CNTs over graphene sheets, hence preventing CNTs from agglomeration [17]. Chemical alteration of oxygen functionalities in GO and FCNTs through covalent interaction of–COOH groups of polycarboxylate superplasticizer makes them exhibit highly dispersed features even in alkaline cement pore solution [15, 18].

The focus of the current research is to fabricate cementitious nanocomposites reinforced with sterically stabilized hybrid graphene oxide-functionalized carbon nanotubes nanofiller and to study the effect of hybrid carbon nanomaterials (HCNs) on the physico-mechanical properties. Insight into the hydration behavior as well as nano-mechanical properties of the HCN-CNCs has been made on the basis of microstructural and crystalline studies of various hydrated phases of cement. Moreover, an approach is made to get into the depth of microstructural porosity of HCN-CNCs with the help of Mercury Intrusion Porosimeter at various dosages of HCNs [19, 20].

2 Experimental

2.1 Materials and Chemicals

Multi-walled carbon nanotubes with dimensions 10 nm × 4.5 nm × 3–6 μm (O.D. × I.D. × L) and Graphite powder (GP) with particle size 100 μm were purchased from Sigma Aldrich (India Ltd.). Sodium nitrate ($NaNO_3$), Potassium permanganate ($KMnO_4$), Conc. sulfuric acid (H_2SO_4), Hydrogen peroxide (H_2O_2), and Nitric acid (HNO_3) were procured from Loba Chemie Pvt. Ltd (India).

Ordinary Portland cement (CEM I 42.5) complying to the IS 8112 was purchased from ACC Ltd. (India). The Indian standard sand utilized in the present study complying IS 650:1991 comprising three grades (Grade I, Grade II, and Grade III) was procured from Ennore, Tamilnadu. Polycarboxylate ether-based superplasticizer (PCE-SP) Auramix-300 was procured from Fosroc Chemicals India Ltd.

2.2 Surface Functionalization of Pristine FCNT and GP and Chemical Alteration of GO and FCNT Using SP

Graphite powder was first ball milled with the help of in-house designed ball milled at the rate of 500 rpm for 24 h. GP was taken in the plastic bottle and zirconia balls were taken three times as that of GP for milling process. Graphene Oxide (GO) was prepared from the milled GP, i.e., GP_b using modified Hummer's method [21]. The bright yellow suspension of GO was washed, centrifuged, and then stored for the further use.

Multi-walled CNTs were surface treated by refluxing it with HNO_3 (69%) for 12 h. The functionalized material was then diluted with 1000 ml of water and then centrifuged for further use.

The nanomaterials so prepared were sterically stabilized [15] in order to prevent it from agglomeration in the alkaline environment of cement solution. SP and GO were dispersed in the deionized water in the separate beakers with the help of probe sonicator VCX-750 W operating at 20 kHz for 30 min. Thereafter, the two dispersions were mixed and were heated at around 50–60 °C for 20 min. Similar procedure was followed for FCNTs. Hybrid carbon nanomaterials (HCNs) were then prepared by mixing GO and FCNT dispersions in 1:1 (GO by FCNT).

2.3 Characterization of SP Stabilized Carbon Nanomaterials

The raw materials (GP, GP_b, and CNTs) and the surface-treated counterparts (GO, FCNTs, and HCNs) were characterized with the help of various techniques such as

Field Emission Scanning Electron Microscopy (FESEM), Powder X-ray diffraction (PXRD), Atomic Force Microscopy (AFM), and Raman spectroscopy.

2.4 Mix Designs

In the current study, a total of 13 mixes were prepared as shown in Table 1. Ordinary Portland cement and sand were mixed in the ratio of 1:3 with the help of planetary mixture at the rate of 140 ± 5 rev/min as per IS 10890-1984 [22]. The water to cement ratio (w/c) for each mix was taken to be 0.43. The dispersions of FCNT, GO, and HCNs were prepared by ultrasonication (VCX-750 W) at the ultrasonication amplitude of 80% (20 kHz). The cement mortar paste was then prepared by mixing the nanomaterial dispersions with dry cement–sand mixture with the help of planetary mixture for approximately 5 min. The mortar paste so prepared was then filled into the cubic molds of dimensions 70.6 mm × 70.6 mm × 70.6 mm with the help of vibration tables at the rate of 3600 rpm. The molds were then demolded after the time period of 24 h and the cubes were placed in the water curing tank at 27 °C until different curing ages for further testing.

Table 1 Mix designs

Mix	Cement (g)	Sand (g)	w/c ratio	FCNT (%)	GO (%)	SP (%)
Control mix	100	300	0.43			0.20
0.02%FCNT-CNCs	100	300	0.43	0.02	–	0.20
0.04%FCNT-CNCs				0.04	–	0.25
0.08%FCNT-CNCs				0.08	–	0.30
0.16%FCNT-CNCs				0.16	–	0.35
0.02%GO-CNCs	100	300	0.43	–	0.02	0.20
0.04%GO-CNCs				–	0.04	0.25
0.08%GO-CNCs				–	0.08	0.30
0.16%GO-CNCs				–	0.16	0.35
0.02%HCN-CNCs	100	300	0.43	0.01	0.01	0.20
0.04%HCN-CNCs				0.02	0.02	0.25
0.08%HCN-CNCs				0.04	0.04	0.30
0.16%HCN-CNCs				0.08	0.08	0.35

Percentage of SP, FCNT, GO, and HCNs were taken by weight of cement

2.5 Test Procedures

Compressive and tensile strength of the mortars was tested with the help of Universal testing machine (UTM), Heico (India Ltd.) as per IS 4031 (Part 6)-1988 [23] and IS 5816-1999 [24], respectively.

Microstructure of the hydration products formed inside the cement matrix was visualized with the help of field emission scanning electron microscope (Nova Nano FESEM 450). On the other hand, quantitative as well as qualitative analysis of different crystalline phases was done with the help of X-ray diffractometer (PANalytical XPERT-Pro Diffractometer, Netherlands) operated at 45 kV and 40 mA using CuKα radiation ($\lambda = 1.54$ Å).

Mercury Intrusion Porosimeter (MIP) (Poremaster®, Quantachrome Instruments, USA) was utilized to examine the pore structure refinement and total porosity of the mortar samples. Samples were first dried in the vacuum oven at 100 °C for 24 h before testing.

3 Results and Discussions

3.1 Structural Characterization of Carbon Nanomaterials

SEM images of FCNTs, GO, and HCNs (GO + FCNT in 1:1) where FCNTs are dispersed over the surface of GO by π-π interactions are shown in Fig. 1a–c, respectively. Figure 1d represents the AFM image of GO showing sheet thickness (4.0 nm).

Figure 2 shows the Raman spectra of GP_b, GO, CNT, FCNT, and HCNs and their I_D/I_G values. For GP_b, I_D/I_G ratio was found to be 0.36 which further increased in case of GO due to structural imperfections generated during surface functionalization. For CNTs, I_D/I_G ratio was 1.1 which has increased to 1.4 after surface treatment (functionalization). However, HCNs showed interactions among CNT's and GO's graphitic planes as depicted by further increase in I_D/I_G ratio to 1.5.

3.2 Compressive and Tensile Strength of Cementitious Nanocomposites

Figure 3a represents the comparison of compressive strength values of GO-CNCs and FCNT-CNCs to that of HCN-CNCs at different dispersion dosages at the curing age of 90 days. The compressive strength was found to increase for FCNT-CNCs and GO-CNCs by 17.82 and 27.39% with respect to control sample at the curing age of 90 days for the dosages of 0.08% and 0.02%, respectively. For HCN-CNCs,

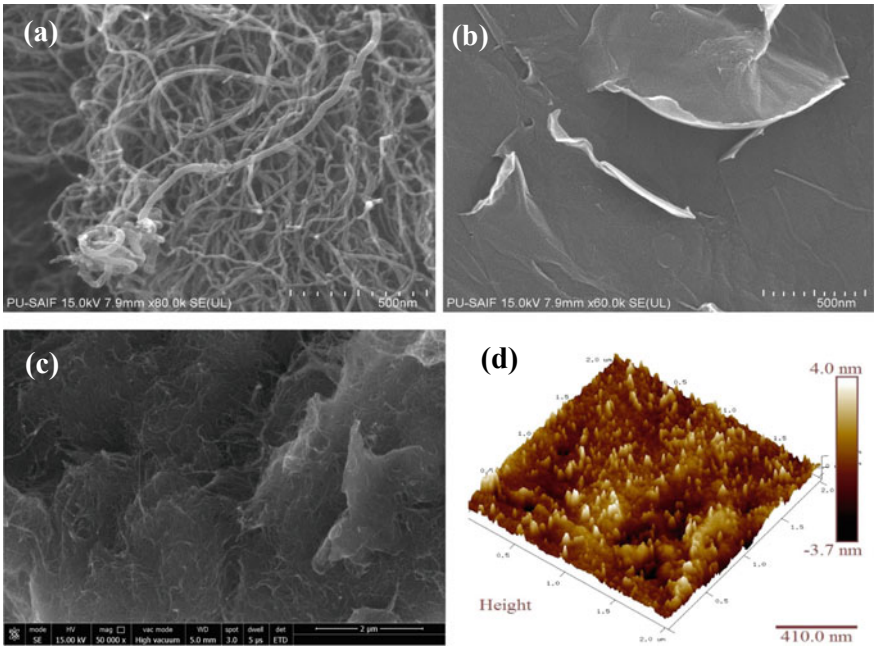

Fig. 1 SEM images of **a** FCNTs **b** GO **c** HCNs and **d** AFM of GO

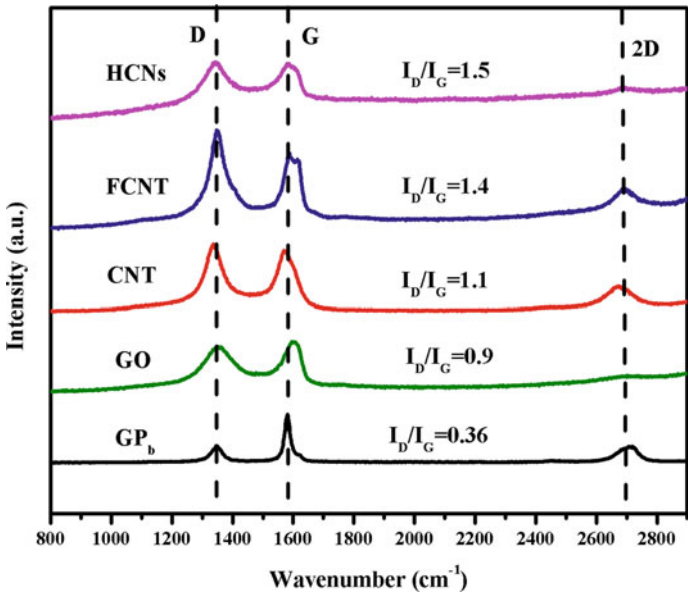

Fig. 2 Raman Spectra of GP_b, GO, CNT, FCNT, and HCNs

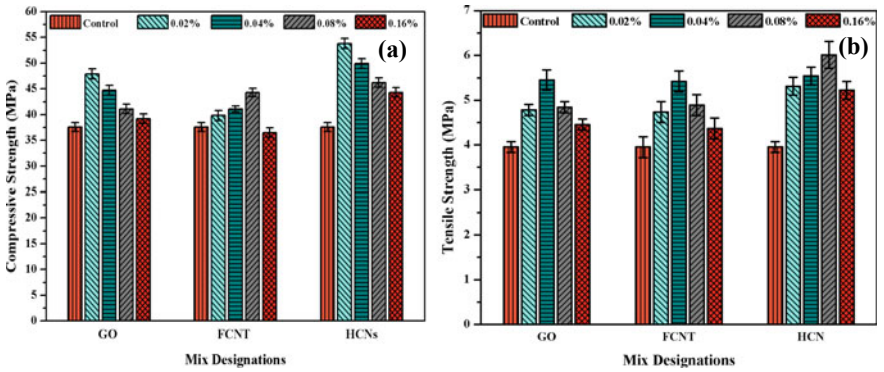

Fig. 3 **a** Compressive strength and **b** split tensile strength values for GO-CNCs, FCNT-CNCs, and HCN-CNCs with respect to control at 90 days of curing

however, the strength improvement was even higher, i.e., 43.02% at the dosage of 0.02%with respect to control.

Figure 3b compares the split tensile strength values of GO-HCNs and FCNT-HCNs to that of HCN-CNCs with respect to control. A maximum tensile strength improvement for GO-CNCs and FCNT-CNCs was found to be 37.97 and 37.21% in comparison to control at the dosage of 0.04%. However, HCN-CNCs showed a maximum boost in the strength at 0.08% of dosage by 52.20% in comparison to control at 90 days of curing. Enhanced tensile strength at higher dosages of HCNs (i.e., 0.08%) as compared to GO and FCNT (i.e., 0.04%) can be attributed to the better dispersion as well as crystallization sites provided by the 3-D HCNs network system in the cement matrix.

3.3 Microstructural and Crystalline Studies of Cementitious Nanocomposites

FESEM images were taken to study the effect of GO, FCNT, and HCNs on the cement hydration process and changes in the surface morphology of the products after 28 days of curing. Figure 4a shows the microstructure of control sample at 28 days curing where thick but fragile structures of C-S-H bars can be visualized. While, in case of GO (Fig. 4b) and FCNT (Fig. 4c) incorporated cement mortar matrix, polyhedral C-S-H gel bars, contributing to the enhanced physico-mechanical strength, can be seen. On the other side, well-dispersed 3-D network of HCNs in the cement matrix produced uniform hydration products in the flower-shaped patterns was responsible for further increase in compressive and tensile strength of the final product (Fig. 4d). This homogeneous growth of hydration patterns filled up the water-packed pores in the cement matrix and hence increasing the strength and reducing the porosity.

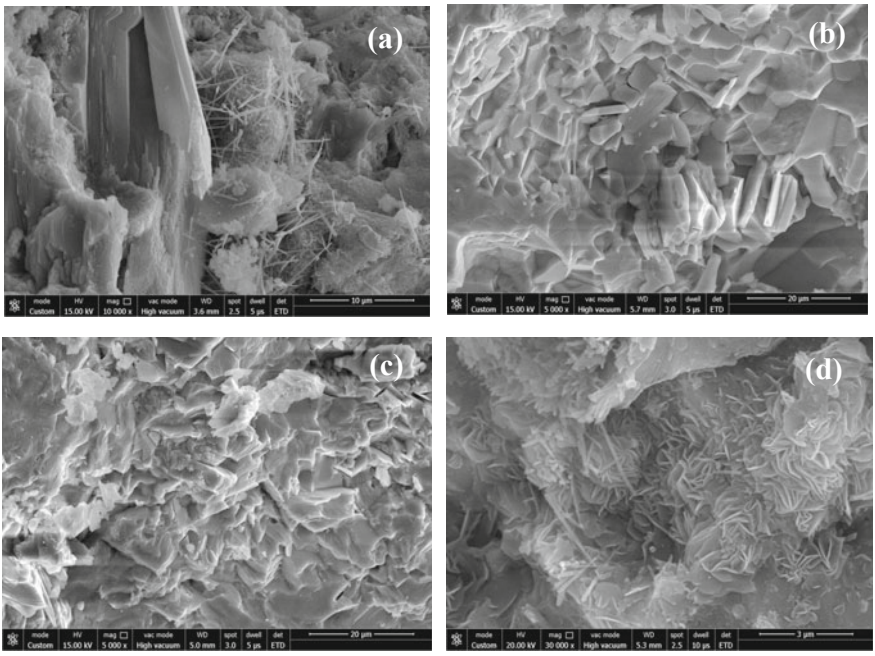

Fig. 4 SEM micrographs for **a** Control **b** GO-CNCs **c** FCNT-CNCs **d** HCN-CNCs at the curing age of 28 days

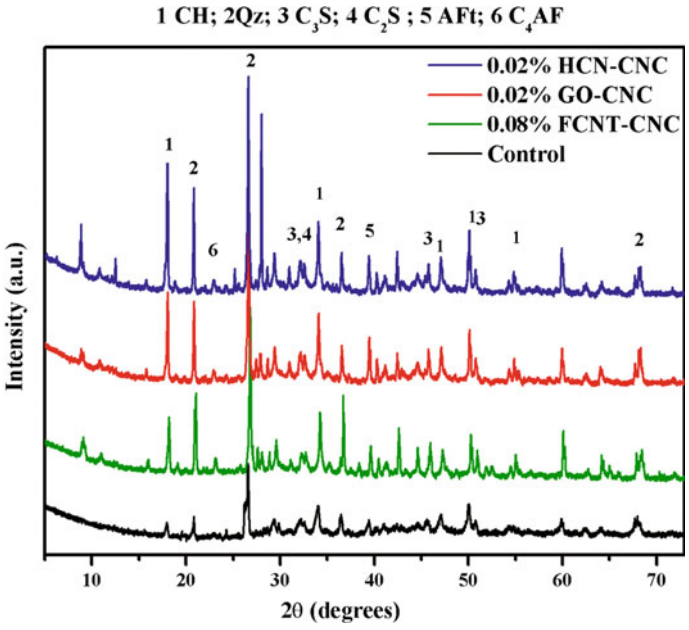

Fig. 5 XRD patterns for various mix at the curing age of 90 days

Figure 5 shows the XRD patterns for various mixes at the curing age of 90 days. The effect of GO, FCNTs, and HCNs on the hydration process was investigated with the help of PXRD. The various peaks appearing in the diffraction patterns correspond to ettringite (Aft), quartz (Qz), calcium silicates (C_2S and C_3S), C_4AF (tetracalcium aluminoferrite), etc.

However, the major crystalline phase calcium hydroxide (C-H) produced during hydration of silicates was taken as the measure of degree of hydration. The peak at $2\theta = 18.1°$ corresponds to the diffraction taking place from (0 0 1) planes of C-H. The higher peak intensity at $2\theta = 18.1°$ for GO and FCNT incorporated mortar samples indicates the better hydration as compared to that of control sample. However, the peak intensity for HCN-CNCs got even greater signifying superior nucleation effect caused by HCNs than that of individual GO and FCNTs [25].

3.4 Porosity of Cementitious Nanocomposites

Mercury Intrusion Porosimeter (MIP) was utilized to find the porosity of the samples at the curing age of 90 days. In MIP measurements, the pore system is imagined to be spherical in shape in order to find the porosity and pore size distribution of the cement matrix system. In addition to this, the pores in the cement matrix can be broadly classified into the three categories, i.e., gel pores (<0.01 μm), medium capillary pores (0.01–0.1 μm), and large capillary pores (>0.1 μm).

The decrease in porosity for FCNT-CNC, GO-CNC, and HCN-CNCs as compared to control was found to be 25.2%, 31.0%, and 46.5%, respectively. The maximum decrease in porosity for HCN-CNCs can be attributed to its ability to act as a 3-D network for crystallization of hydration products in a better way. Thus, the hydration products protrude into voids filled with water and hence refines the cementitious matrix pores. [26, 27] (Fig. 6).

4 Conclusions

In the present investigation, superior reinforcing mechanism of HCNs as compared to individual FCNTs and GO has been discussed and the main points can be summed up as follows:

- For HCN-CNCs at dosages of 0.02% and 0.08%, the compressive and tensile strength were enhanced by 43.02% and 52.20%, respectively. The improvement caused was better than that caused by FCNTs (17.82 and 37.21%) and GO (27.39 and 37.97%) for compressive and tensile strengths.
- The enhanced physico-mechanical properties in case of HCN-CNCs have also been supported by flower-patterned hydration products and more production of hydration products as shown by FESEM and XRD, respectively.

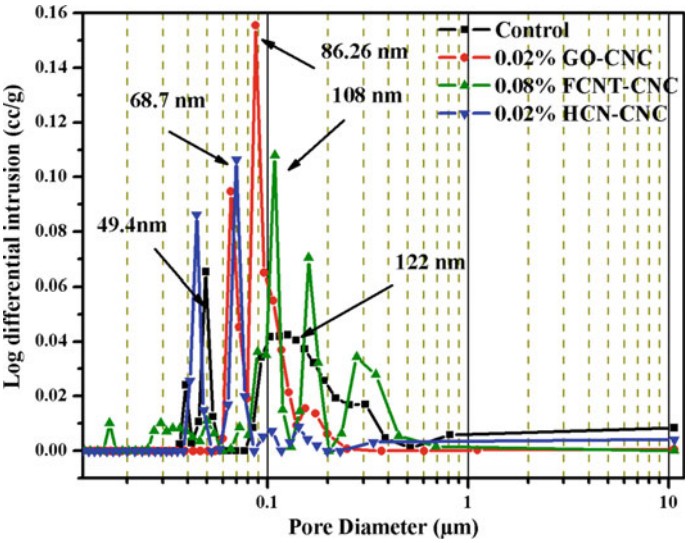

Fig. 6 Log-differential intrusion curve plots for 90 days cured samples

- MIP measurements showed 46.5% reduction in porosity for HCNs incorporated sample at 0.02% dosage as compared to control mix.

The improved microstructure results in the enhanced mechanical strength which further triggers the sustainability of the constructional framework.

Acknowledgments Authors are highly thankful to Dr. B. R. Ambedkar NIT, Jalandhar for providing lab and XRD facilities. Support by Materials Research Center, MNIT (Jaipur) for providing various characterization facilities, is also acknowledged.

References

1. Lu Z, Zhang J, Sun G, Xu B, Li Z, Gong C (2015) Effects of the form-stable expanded perlite/paraffin composite on cement manufactured by extrusion technique. Energy 82:43–53
2. Li X, Korayem AH, Li C, Liu Y, He H, Sanjayan JG, Duan WH (2016) Incorporation of graphene oxide and silica fume into cement paste: a study of dispersion and compressive strength. Constr Build Mater 123:327–335
3. Hoseini M, Bindiganavile V, Banthia N (2009) The effect of mechanical stress on permeability of concrete: a review. Cem Concr Compos 31:213–220
4. Hambach M, Möller H, Neumann T, Volkmer D (2016) Carbon fibre reinforced cement-based composites as smart floor heating materials. Compos Part B 90:465–470
5. Kim H, Kim G, Gucunski N, Nam J, Jeon J (2015) Assessment of flexural toughness and impact resistance of bundle-type polyamide fiber-reinforced concrete. Compos Part B 78:431–446
6. Ates A (2016) Mechanical properties of sandy soils reinforced with cement and randomly distributed glass fibers (GRC). Compos Part B 96:295–304

7. Yoo D, Shin H, Yang J, Yoon Y (2014) Material and bond properties of ultra high performance fiber reinforced concrete with micro steel fibers. Compos Part B 58:122–133
8. Lu Z, Hou D, Meng L, Sun G, Lu C, Li Z (2015) Mechanism of cement paste reinforced by graphene oxide/carbon nanotubes composites with enhanced mechanical properties. RSC Adv 5:100598–100605
9. Sharma S, Kothiyal NC (2016) Comparative effects of pristine and ball-milled graphene oxide on physico-chemical characteristics of cement mortar nanocomposites. Constr Build Mater 115:256–268
10. Mohsen MO, Taha R, Abu Taqa A, Shaat A (2017) Optimum carbon nanotubes' content for improving flexural and compressive strength of cement paste. Constr Build Mater 150:395–403
11. De Volder MFL, Tawfick SH, Baughman RH, Hart AJ (2013) Carbon nanotubes: present and future commercial applications. Science 339:535–539
12. Yu S, Wang X, Ai Y, Liang Y, Ji Y, Li J, Hayat T, Alsaedi A, Wang X (2016) Spectroscopic and theoretical studies on the counterion effect of Cu (II) ion and graphene oxide interaction with titanium dioxide. Environ Sci: Nano 3:1361–1368
13. Wang X, Fan Q, Yu S, Chen Z, Ai Y, Sun Y, Hobiny A, Alsaedi A, Wang X (2016) High sorption of U(VI) on graphene oxides studied by batch experimental and theoretical calculations. Chem Eng J 287:448–455
14. Lambert TN, Chavez CA, Hernandez-Sanchez B, Lu P, Bell NS, Ambrosini A, Friedman T, Boyle TJ, Wheeler DR, Huber DL (2009) Synthesis and characterization of titania-graphene nanocomposites. J Phys Chem C 113:19812–19823
15. Lu Z, Hanif A, Ning C, Shao H, Yin R, Li Z (2017) Steric stabilization of graphene oxide in alkaline cementitious solutions: mechanical enhancement of cement composite. Mater Des 127:154–161
16. Zhang C, Ren L, Wang X, Liu T (2010) Graphene oxide-assisted dispersion of pristine multiwalled carbon nanotubes in aqueous media. J Phys Chem C 114:11435–11440
17. Kharissova OV, Kharisov BI, Gerardo DC, Ortiz E (2013) Dispersion of carbon nanotubes in water and non-aqueous solvents. RSC Adv 3:24812–24852
18. Zhao L, Guo X, Liu Y, Ge C, Guo L, Shu X, Liu J (2017) Synergistic effects of silica nanoparticles/polycarboxylate superplasticizer modified graphene oxide on mechanical behavior and hydration process of cement composites. RSC Adv. 7:16688–16702
19. Nochaiya T, Chaipanich A (2011) Applied Surface Science Behavior of multi-walled carbon nanotubes on the porosity and microstructure of cement-based materials. Appl Surf Sci 257:1941–1945
20. Li X, Li C, Liu Y, Chen SJ, Wang CM, Sanjayan JG, Duan WH (2016) Improvement of mechanical properties by incorporating graphene oxide into cement mortar. Mech Adv Mater Struct 6494
21. Hummers WS, Offeman RE (1958) Preparation of graphitic oxide. J Am Chem Soc 80:1339
22. IS 10890, Specification for planetary mixture used in tests of cement and pozzolana, Bureau of Indian Standards, New Delhi
23. IS 4031 (Part 6), Methods of physical tests for hydraulic cement, Bureau of Indian Standards, New Delhi
24. IS 5816, Splitting tensile strength of concrete-Method of test, Bureau of Indian Standards, New Delhi
25. Chuah S, Pan Z, Sanjayan JG, Wang CM, Duan WH (2014) Nano reinforced cement and concrete composites and new perspective from graphene oxide. Constr Build Mater 73:113–124
26. Sun J, Shi H, Qian B, Xu Z, Li W, Shen X (2017) Effects of synthetic C-S-H/PCE nanocomposites on early cement hydration. Constr Build Mater 140:282–292
27. Shaikh FUA, Supit SWM (2015) Chloride induced corrosion durability of high volume fly ash concretes containing nano particles. Constr Build Mater 99:208–225
28. Choinska M, Khelidj A, Chatzigeorgiou G, Pijaudier-Cabot G (2007) Effects and interactions of temperature and stress-level related damage on permeability of concrete. Cem Concr Res 37:79–88

29. Aldea CM, Shah SP, Karr A (1999) Effect of cracking on water and chloride permeability of concrete. J Mater Civ Eng 11:181–187
30. Kobayashi K, Kojima Y (2017) Effect of fine crack width and water cement ratio of SHCC on chloride ingress and rebar corrosion. Cem Concr Res 80:235–244
31. Kaur R, Kothiyal NC (2019) Comparative effects of sterically stabilized functionalized carbon nanotubes and graphene oxide as reinforcing agent on physicomechanical properties and electrical resistivity of cement nanocomposites. Constr Build Mater 202:121–138

Sustainable Solution for the Disposal of Fiber-Reinforced Plastic Waste

H. B. Rekha, T. Kiran, N. Jayaramappa, and Pooja Tuppad

Abstract Fiber-reinforced plastic (FRP) is one of the gifts to technology that has influenced human life in numerous ways. FRP represents plastic which contains fibers of other materials that add strength, flexibility, durability, and other virtues to the plastic. From the past years, FRP being some composite materials has been used in many industries. But disposal of this FRP waste is becoming a major problem because of increased generation in FRP materials from various industries mainly from windmills. The study deals with use of FRP waste as an additive in concrete, thereby checking the effect of FRP waste on concrete characteristics. Concrete cubes, cylinders, and prisms of M-25 grade concrete were casted with different percentage of FRP waste (0, 1, 2, 3, and 4%) as an additive by the weight of the cement. From the results of compressive strength, flexural strength, and split tensile strength, of the concrete with and without FRP waste, it is observed that the compressive strength, flexural strength, and split tensile strength of the concrete specimens increase when 3% of FRP waste is used as an additive. Hence, 3% of FRP waste can be considered as optimum dosage to be used in concrete.

Keywords FRP waste · Concrete · Compressive strength · Flexural strength · Tensile strength

1 Introduction

The increasing attention about the environment has exceedingly contributed to the issues related with disposal of the generated wastes from the industries. With the shortage of area for landfilling and due to its ever-increasing cost, waste utilization has ends up a captivating choice to disposal [1]. The FRP products are a kind of thermoset plastics commonly made from composites of glass fibers embedded in polyester resin, vinyl ester resin, epoxy resins, etc. [2]. FRPs are many times used in building construction, automobiles, furniture, sports equipment, scientific equipment, and

H. B. Rekha (✉) · T. Kiran · N. Jayaramappa · P. Tuppad
Department of Civil Engineering, Bangalore University, Bengaluru 560056, Karnataka, India
e-mail: rekhahb@gmail.com

K. R. Reddy et al. (eds.), *Sustainable Environment and Infrastructure*, Lecture Notes in Civil Engineering 90, https://doi.org/10.1007/978-3-030-51354-2_9

innumerable other areas. Due to their lightweight and ease of installation FRPs are also the materials of desire in the manufacture of windmills. Hence tones of FRP waste are produced by the windmill blade manufacturing plant per day [3]. Most thermosetting FRP waste is presently sent to landfill, in spite of the significant environmental impact caused by disposing of it in this way. Because more and more waste is being produced throughout the life cycle of FRPs, innovative solutions are needed to manage it [4]. The present study was carried out with an aim to find a way by which FRP waste generated can be gainfully utilized. The main objective of the study is utilization of FRP waste as an additive in concrete, thereby checking the effect of FRP waste on concrete characteristics.

2 Literature Review

Rai et al. [5] studied on fresh and hardened properties of waste virgin plastic mix concrete. A number of concrete mixes were prepared, in which sand was partially replaced by waste plastic flakes in varying percentages by volume, i.e., concrete with four different volume percentages of plastic (0, 5, 10, 15%). Waste plastic mix concrete with and without superplasticizer was tested at room temperature. Forty-eight cube samples were molded for compressive strength tests at three, seven, and twenty-eight days. By increasing the waste plastic ratio, the compressive strength, flexural strength values of waste plastic concrete mixtures decrease at each curing age. The compressive strength increases by about 5% after addition of superplasticizer to the mix. With increasing amount of waste plastic and plastic size, the rate of reduction in strength gets flatter and the maximum reduction is only about 15% for all grades of concrete. This trend can be attributed to the decrease in adhesive strength between the surface of the waste plastic and the cement paste. The literature on FRP waste utilization in concrete is very minimal and the study made an attempt for this.

3 Materials and Methodology

3.1 Cement

In the experimental investigation, JSW Portland slag cement (PSC) was used for concrete mixes, the cement used was fresh and without lumps. The testing for the cement was done as per IS 455: 2015. The specific gravity of the cement was found to be 2.89.

Table 1 Physical and chemical analysis of FRP waste

Sl no.	Parameters	Results
1	Specific gravity	1.15
2	Density	1.04 g/cc
3	Alkali test	0.117%
4	Acid resistant	0.224%

3.2 Water

Potable tap water from the concrete laboratory of the Department of Civil Engineering was used for preparations and curing of specimens.

3.3 Fine Aggregate

As per IS 383:1970, locally obtained manufactured sand was used as the fine aggregate in the concrete mix. The specific gravity of fine aggregate was found to be 2.62.

3.4 Coarse Aggregate

Locally available coarse aggregate passing through 20 mm sieve and conforming IS 383:1970 were used in present work. The specific gravity of coarse aggregate was found to be 2.73.

3.5 Fiber-Reinforced Plastic Waste

Fiber-Reinforced plastic waste belonging to FRP-Polyester resin was used with different percentages (0, 1, 2, 3, and 4%) by the weight of the cement, is added to the concrete in the present experimental work. The properties of FRP waste are shown in Table 1.

3.6 Admixtures

Commercially available La Hypercrete S-20 is used as a superplasticizer to enhance the workability of fresh concrete.

Table 2 Details of number of specimens

Sl no.	Description	Number of concrete cubes//prisms/cylinders casted		
		3 days	7 days	28 days
1	CS: M25	3	3	3
2	M25 + 1% FRP waste	3	3	3
3	M25 + 2% FRP waste	3	3	3
4	M25 + 3% FRP waste	3	3	3
5	M25 + 4% FRP waste	3	3	3

CS = Control specimen

3.7 Mix Design

The concrete mix was designed as per IS 10262: 2009 for M25 grade concrete with 0.48 water–cement ratio. Concrete mixes are prepared by adding different percentages of FPR waste (0, 1, 2, 3, and 4% of weight of cement) as an additive, for every mix of cubes, cylinders, and prisms.

3.8 Test Specimen and Test Procedure

Cement, sand, and aggregate were taken in mix proportion 1:2.57:3.24 which corresponds to M25 grade of concrete, respectively. The 150 mm size concrete cube, cylinder of 150 mm diameter and 300 mm and prisms of size 100 mm × 100 mm × 500 mm were used as test specimens to determine compressive strength, flexural strength, and split tensile strength. The details of the number of specimens casted and days of curing are represented in Table 2. The formulas used to determine compressive strength, flexural strength, and split tensile strength are given in Eqs. 1, 2, and 3.

$$\mathbf{CompresseiveStrength(MPa)} = \frac{\mathbf{Maximumload(N)}}{\mathbf{Areaofthecube}\left(\mathrm{mm}^2\right)} \tag{1}$$

$$\mathbf{FlexuralStrength(MPa)} = \frac{\mathbf{WL}}{\mathbf{bd^2}} \tag{2}$$

where,

b width of prism (mm).
d depth of prism (mm).
L supported length (mm),
W Maximum Load (N),

$$\textbf{Spilt Tensile Strength (MPa)} = \frac{2\mathbf{P}}{\mathbf{dl}} \tag{3}$$

where,

P Maximum Load (N),
d diameter of cylinder (mm),
L Length of cylinder (mm).

4 Results and Discussions

The cubes, cylinders, and prisms of concrete specimens prepared are shown in Fig. 1. The compressive strength, flexural strength, and split tensile strength results of different mixes of (with and without) FRP waste for 28 days of curing are represented in Figs. 2, 3, and 4.

From Fig. 2, it is observed that, after 28 days of curing, the compressive strength of concrete for control specimen was 29.5 N/mm^2 and for control + FRP waste (1, 2, 3, and 4%) is 31.03, 32.72, 32.57, and 31.86 N/mm^2. The Percentage increase in compressive strength varied as 5.18, 10.91, 10.40, and 8.1% when compared to control specimen (cs).

From Fig. 3, it is observed that, after 28 days of curing, the flexural strength of concrete for control specimen was 3.58 N/mm^2 and for control + FRP waste (1, 2, 3, and 4%) is 3.76, 3.86, 3.95, and 3.89 N/mm^2. The Percentage increase in flexural strength varied as 5.02, 7.82, 10.33, and 8.65% when compared to control specimen.

Fig. 1 Concrete specimen

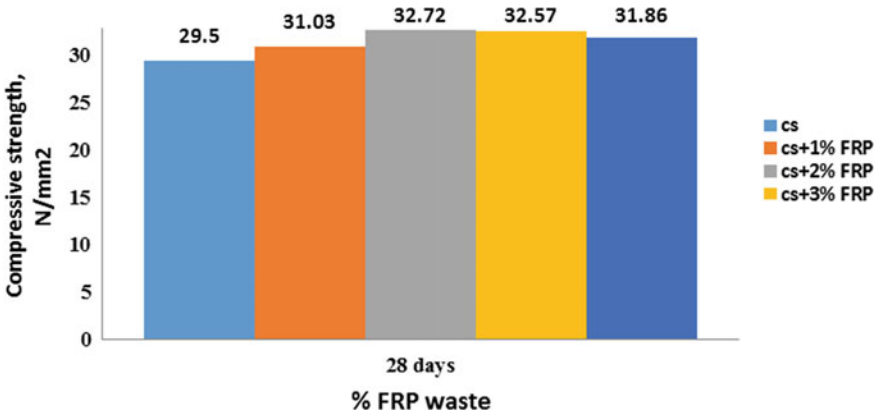

Fig. 2 Percentage increase in compressive strength after 28 days (cs: control specimen)

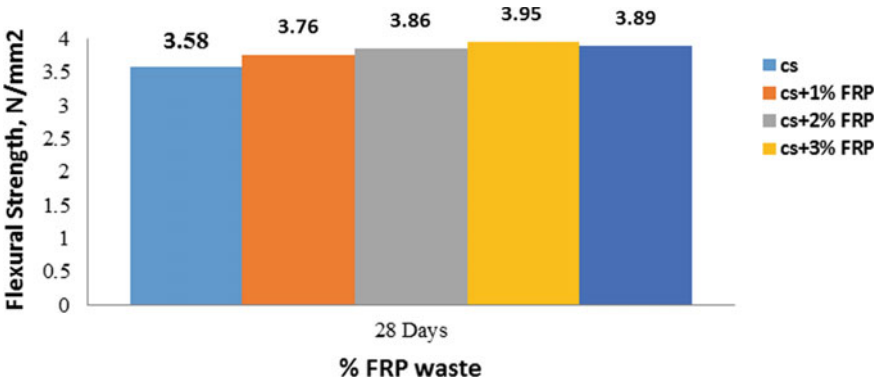

Fig. 3 Percentage increase in flexural strength after 28 days

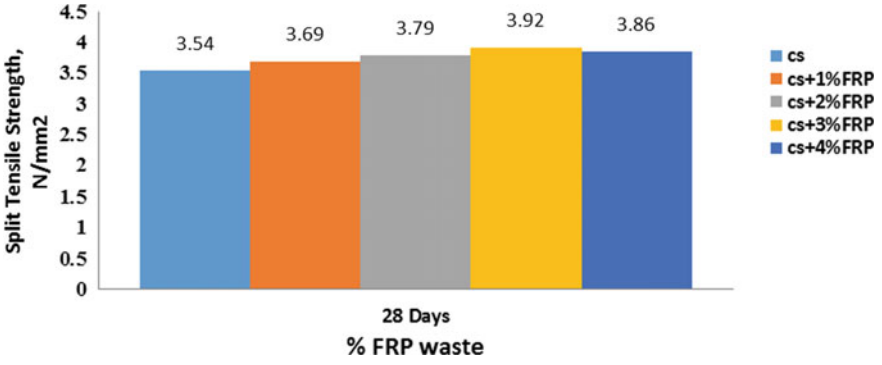

Fig. 4 Percentage increase in split tensile strength after 28 days

From Fig. 4, it is observed that, after 28 days of curing, the split tensile strength of concrete for control specimen was 3.54 N/mm^2 and for control + FRP waste (1, 2, 3, and 4%) is 3.69, 3.79, 3.92, and 3.86 N/mm^2. The Percentage increase in split tensile strength varied as 4.23, 7.06, 10.73, and 9.03% when compared to control specimen.

The results represent that, the strength of concrete with FRP waste is increased when compared with the control specimen. It can be noted that the concrete in which FRP waste is added with 3%, shows a growth in its strength considerably compared to the other percentage of FRP waste which is added to the concrete. Also the study observed that, with 4% of FRP waste, there is a decrease in the strength of the specimens. This decrease in compressive strength, flexural strength, and split tensile strength may be due to, decrease in the adhesive strength between the surface of the FRP waste and the cement paste, as a result of increase in the percentage of FRP waste in concrete specimen.

5 Conclusions

Based on the study carried out, it can be concluded that, the Compressive strength, Flexural strength, and Split tensile strength of concrete specimens after 28 days of curing with FRP waste (3%) increased by 10.91, 10.33, and 10.73% as compared to control specimen. Hence it can be concluded that 3% FRP waste can be used for concrete specimens which is one of the sustainable solutions for the disposal of FRP waste.

References

1. Siddigue R, Kaur I, Kahtib J (2008) Use of recycled plastic in concrete: a review, vol 28, pp 835–185. Elsevier
2. Ministry of Environment, Forests and Climate Chang GOI (2016) Guidelines for disposal of thermoset plastic waste including sheet moulding compound (SMC)/fiber reinforced plastic (FRP), Working Papers id:10822, eSocialSciences
3. Ramesh N, Abbasi T, Tauseef SM, Abbasi SA (2018) Utilization of fiber-reinforced plastic (FRP) waste generated by a wind-turbine manufacturing company. Int J Eng Sci Res 6
4. Ribeiro MC, Fiúza A, Ferreira A, Dinis MD, Meira Castro AC, Meixedo JP, Alvim MR (2016) Recycling approach towards sustainability advance of composite materials industry. J Sci Res 178–193
5. Rai B, Rushad ST, Bhavesh K, Duggal SK (2012) Study of waste plastic mix concrete and plasticizer. Int Sch Res Not Civil Eng 2012:5

Geotechnical Behaviour of Copper Slag Mixed with Different Proportions of Soil, Lime, Fly Ash and Cement—A Review

Kuldeep Sharma and Arvind Kumar

Abstract Many countries perceive a rapid growth in the construction industry, which involves the use of natural resources for the development of infrastructure. This development postures a threat to natural resources that are offered. Copper Slag is an industrial waste material and it can be used as the replacement of fine aggregates and cement in the production of concrete. The possibility of substituting natural fine aggregates with industrial by-products such as copper slag offers technical, economic and environmental advantages which are of great importance in the present context of sustainability in the construction sector. The Copper industries units in India leave thousands of tonnes of copper slag as waste every day. These Large quantities of the accumulated copper slag are directly dumped and left on costly land, causing wastage of good cultivable land. Copper slag can be classified as a non-hazardous material by U.S. environmental protection agency regulations based on the solid waste characteristics. Many researchers have studied the physical and chemical properties of copper slag. Researchers have studied the geotechnical behaviour of copper slag mixed with different proportions of soil, lime, fly ash and cement. Studies have been carried out through unconfined compressive strength tests, direct shear tests and CBR tests in addition to basic tests like sieve analysis and consistency limits, etc. In this paper the outcome of previous research studies has been compared, results summarized and gaps in the study have been highlighted with respect to geotechnical applications.

Keywords Copper slag · Industrial waste · Sustainable material · Basic properties of copper slag · Black cotton soil · Fly ash · Lime

K. Sharma (✉) · A. Kumar
Department Civil Engineering, Dr. B. R. Ambedkar National Institute of Technology, Jalandhar 144011, Punjab, India
e-mail: kuldeepsha333@gmail.com

A. Kumar
e-mail: agnihotriak@nitj.ac.in

K. R. Reddy et al. (eds.), *Sustainable Environment and Infrastructure*, Lecture Notes in Civil Engineering 90, https://doi.org/10.1007/978-3-030-51354-2_10

1 Introduction

In India, there is great demand of aggregates, sand and cement mainly in civil engineering construction work. But nowadays the availability of construction materials is reduced. Due to lack of natural resources, the cost of the materials is much higher. So many researchers are working on the utilization of industrial waste for the development of new construction materials that will lead to the replacement of conventional construction materials. Natural resources are depleting worldwide while at the same time the generated wastes from the industries are increasing substantially. The sustainable development for construction involves the use of non-conventional, innovative and recycled waste materials that in turn will compensate the rising demand of natural resources.

It has been estimated that the production of one tonne of blister copper generates 2.2 tonnes of slag. As of Nov 2010, it was estimated that world smelter copper production was 15,900,000 metric tonnes and its production generated about 34,980,000 metric tonnes of slag (Copper Statistics, U.S. Geological Survey) [1]. Metal industry slag, mine stone and mining waste are generally suitable for recycling or reuse and the use of these inorganic wastes as alternative materials in building, road and geotechnical applications. Copper slag along with binding material or an admixture can be used as an alternative material to that of sand in road construction. If the copper slag is mixed with a calcium-based compound like lime, silica and alumina present in copper slag may react chemically on hydration and it may be used for the improvement of strength parameters in subgrade and subbase. Physical and chemical properties of copper slag are presented in Tables 1 and 2.

Table 1 Chemical properties of copper slag [12, 13]

Property	Range (%)	Average (%)
Fe_2O_3	0.8–68.4	45.4
SiO_2	2.9–71.5	30.4
Al_2O_3	0.22–89.7	5.93
CaO	0.15–25.29	4.77
ZnO	0–8.9	2.32
MgO	0.008–11.92	1.85
SO_3	0.045–3.26	1.06
K_2O	0–3.08	0.821
Na_2O	0–4.12	0.868
CuO	0.16–5.07	0.932
S	0.012–1.5	0.659

Table 2 Physical properties of copper slag [12]

Property	Range (%)
Particle shape	Angular, irregular, Multifaceted
Surface texture	Glassy, Smooth, Granular, Rough
Colour	Blackish grey, Brown with green, red or black tint
Particle size distribution	Gravel (1.00), Sand (98.90), silt + clay (0.05)
Finess modulus	3.47–4.90
Hardness (Moh's Scale)	6–7
Specific gravity	3.30–3.90
Plasticity index	Non-Plasticity
Swelling index	Non-Swelling
Water Absorption	0.15–0.40
Crushing value	10–21
Angle of internal friction	51–53
Impact value	8–26
Conductivity	50 mS/m

2 Review of Results and Discussion

In this paper review of results of many research works on the industrial wastes like Copper Clag (CS), Fly ash (FA), Rice husk ash (RHA) and their combinations with Clay Soiland Black cotton soil (BCS) etc. are presented. Review is focused on some of the useful tests like Liquid Limit (LL), Plastic Limit (PL), Shrinkage Limit (SL), Plasticity Index (PI), Unconfined Compressive Strength(UCS), Direct Shear Test (DST), California Bearing Ratio Test (CBR) and Compaction Test. Researchers have treated soil and/or other materials by adding copper slag in a range of 0–40%.

2.1 Effect of Copper Slag On Atterberg's Limits

Atterberg Limits are generally used for classification of soil and to correlate the engineering behaviour of soil such as compressibility, permeability, compatibility and shear strength [2]. The Atterberg limits tests have been conducted by many researchers after treating different industrial wastes like Rice husk ash, Fly Ash and soil with Copper slag. These test results are shown in Figs. 1, 2, 3 and 4.

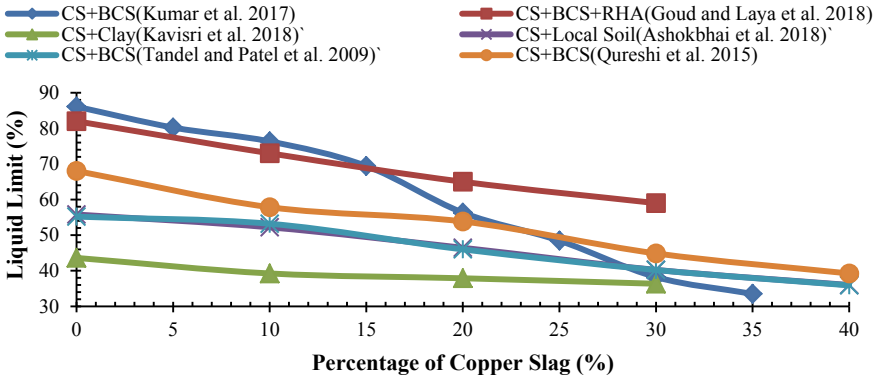

Fig. 1 Variation of liquid limit with copper slag for various combinations of soil/waste

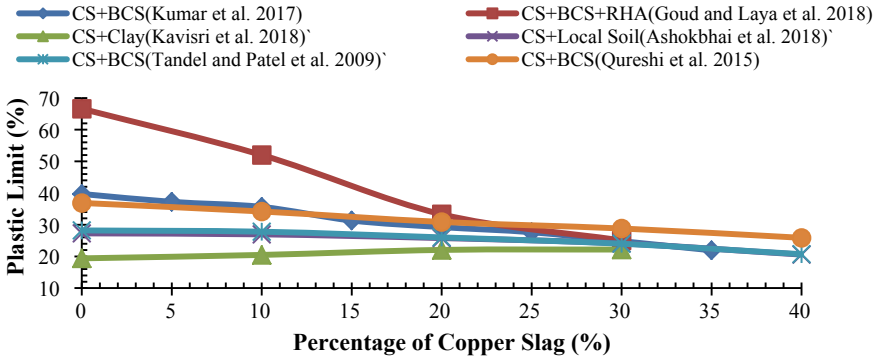

Fig. 2 Variation of plastic limit with copper slag for various combinations of soil/waste

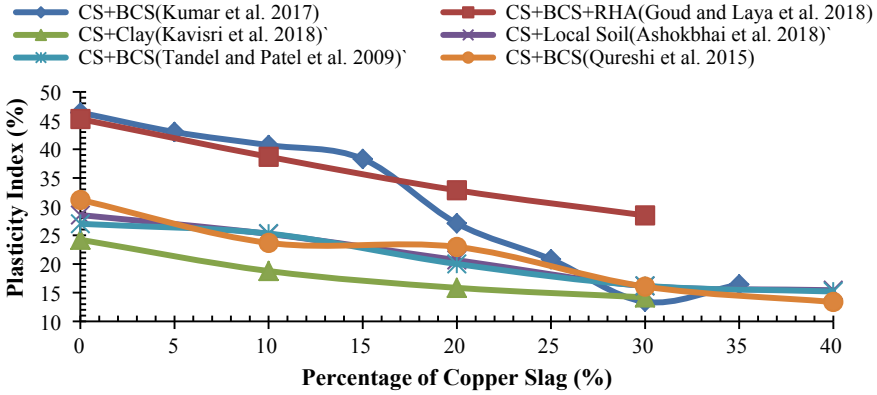

Fig. 3 Variation of plasticity index with copper slag for various combinations of soil/waste

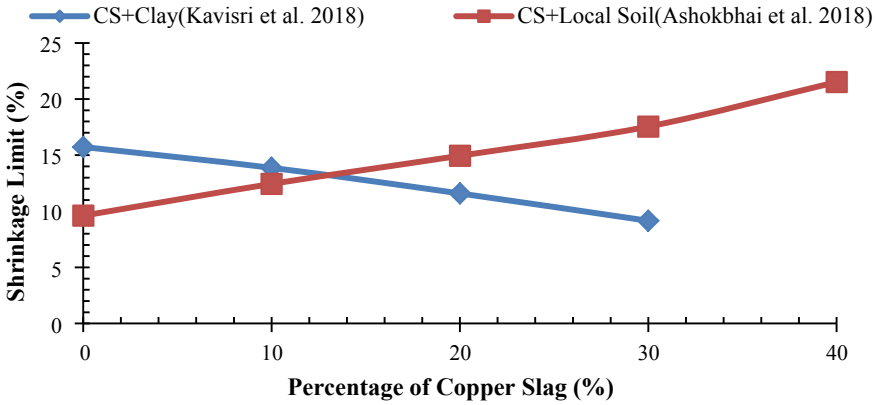

Fig. 4 Variation of Shrinkage limit with copper slag for various combinations of soil/waste

2.1.1 Liquid Limit

The effect of CS on liquid limit based on the outcome of various researchers is presented graphically in Fig. 1.

The LL of BCS decreases with the increase in the percentage of CS. Initially LL of untreated BCS was 86%, but with the addition of 35% of CS, liquid limit decreases to 33.5% [3]. It is happening due to the cohesionless property of CS. There is a 61% reduction with respect to the initial value.

The LL value of BCS decreases with the increase in the percentage of CS + RHA. Generally reduction in LL means reduction in the compressibility and swelling characteristics, which is beneficiary for subgrade [4]. The LL(82%) of untreated BCS, when treated with 30%CS + 6%RHA reduced to 59%. There is a 28% reduction with respect to the initial value.

It is observed that LL of untreated clayey soil reduced from 43.61 to 36.35% after treating with 30%CS [5]. There is 16.65% decrease with respect to the initial value.

The value of LL of untreated Local Soil and BCS is 55.8, 55.2% but after treating with 40%CS, these values reduced to 36% [6, 7]. The increasing addition of copper slag to BCS enhances the content of sand size particles on one hand and reduces the amount of clay mineral on the other hand. In this way the activity of the mix is reduced.

It is observed that LL is lower, if the amount of CS is higher. This is happening due to the cohesionless property of the material [8].

2.1.2 Plastic Limit

The effect of CS on plastic limit based on the outcome of various researchers is presented graphically in Fig. 2.

The PL of BCS decreases with the increase in the percentage of CS. Initially PL of untreated BCS was 39%, but with the addition of 35% of CS, plastic limit decreases to 21.92% [3]. It is happening due to the cohesionless property of CS. There is a 44.80% reduction with respect to the initial value.

The PL (66%) of untreated BCS, when treated with 30%CS + 6%RHA reduced to 25% [4]. There is a 62% reduction with respect to the initial value.

It is observed that PL of untreated clayey soil increases from 19.39 to 22.17% after treating with 30%CS [5]. There is a 14.33% increase with respect to the initial value.

The value of PL of untreated Local Soil and BCS is 27.27, 20.57% but after treating with 40%CS, these values reduced to 20.57 and 20.70% [6, 7]. There is a 25% decrease with respect to the initial value.

Initially PL of untreated BCS was 36.87%, but with the addition of 40% of CS, plastic limit decreases to 25.87% [8]. It is happening due to the cohesionless property of CS. There is a 44.80% reduction with respect to the initial value. It is observed that PL is lower, if the amount of CS is higher. This is happening due to the cohesionless property of the material [8].

2.1.3 Plasticity Index

The effect of CS on the plasticity index based on the outcome of various researchers is presented graphically in Fig. 3.

The PI of BCS decreases with the increase in the percentage of CS. Initially LL of untreated BCS was 46.39%, but with the addition of 30% of CS, Plasticity index decreases to 13.41% [3]. It is happening due to the cohesionless property of CS. There is a 71% reduction with respect to the initial value.

The PI value of BCS decreases with the increase in the percentage of CS + RHA. Generally reduction means reduction in the compressibility and swelling characteristics, which is beneficiary for subgrade [4]. The PI (45.26%) of untreated BCS, when treated with 30%CS + 6%RHA reduced to 28.47%. There is a 37% reduction with respect to the initial value.

It is observed that PI of untreated clayey soil reduced from 24.22 to 14.18% after treating with 30%CS [5]. There is a 41.45% decrease with respect to the initial value.

The value of PI of untreated Local Soil and BCS is 28.53, 27% but after treating with 40%CS, these values reduced to 45.91 and 43.70% [6, 7]. The increasing addition of copper slag to BCS enhances the content of sand size particles on one hand and reduces the amount of clay mineral on the other hand. In this way the activity of the mix is reduced.

Initially PI of untreated BCS was 31.17%, but with the addition of 40%CS, the plastic limit decreases to 13.37% [8]. It is happening due to the cohesionless property of CS. There is a 57% reduction with respect to the initial value. It is observed that PI is lower, if the amount of CS is higher. This is happening due to the cohesionless property of the material [8].

2.1.4 Shrinkage Limit

The effect of CS on the shrinkage limit based on the outcome of various researchers is presented graphically in Fig. 4.

The SL of clayey soil decreases with the increase in the percentage of CS. Initially SL of untreated clayey soil was 15.73%, but with the addition of 30%CS, shrinkage limit decreases to 9.15 [5]. It is happening due to the cohesionless property of CS. There is a 42% reduction with respect to the initial value.

The SL of local soil increases with the increase in the percentage of CS. The value of SL of untreated Local Soil was 9.61% but after treating with 40%CS, this value increases to 21.52% [6].

2.2 *Effect of Copper Slag on Compaction Behaviour for Various Combinations of Soil/Waste*

Compaction is a mechanical process whenever compacting it solidity the soil by the expulsion of voids from the soil. The compaction test has been conducted by many researchers after treating different industrial wastes like Rice husk ash, Fly Ash and soil with Copper slag. These test results are shown in Figs. 5 and 6.

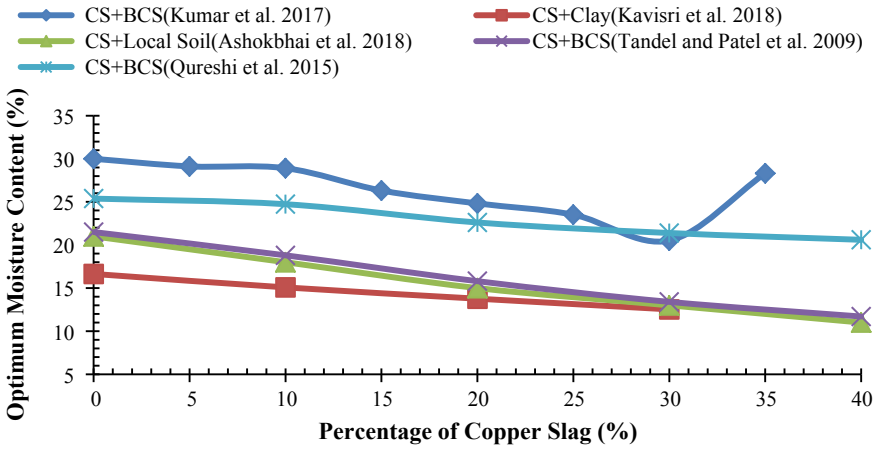

Fig. 5 Variation of optimum moisture content with copper slag for various combinations of soil/waste

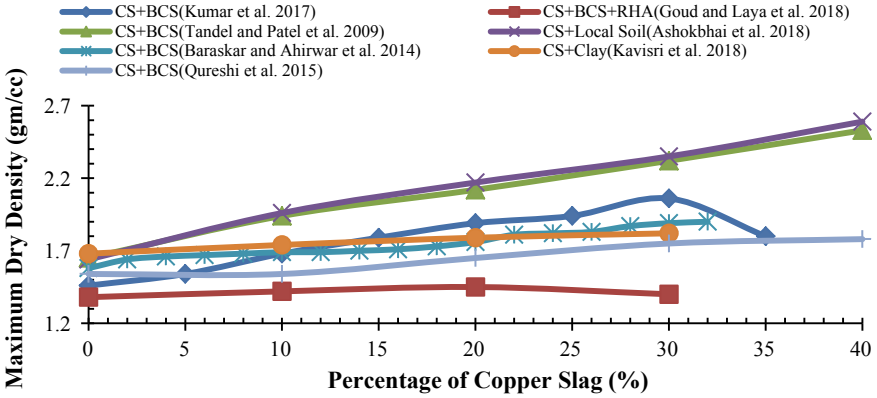

Fig. 6 Variation of maximum dry density with copper slag for various combinations of soil/waste

2.2.1 Optimum Moisture Content and Maximum Dry Density

The OMC of BCS decreases with the increase in the percentage of Copper Slag, vice versa MDD.

Initially OMC of untreated BCS was 30%, but with the addition of 30% of CS, OMC decreases to 20.52% [3]. There is a 31.6% reduction with respect to the initial value. MDD of untreated BCS was 1.46 gm/cc, but with the addition of 30% of CS, MDD increases to 2.06 gm/cc [3]. There is a 31.6% reduction with respect to the initial value.

The MDD value of BCS increases with the increase in the percentage of CS + RHA. The MDD (1.38 gm/cc) of untreated BCS, when treated with 30%CS + 6%RHA increase to 1.40 gm/cc [4]. There is a 2% increase with respect to the initial value.

The OMC (16.64%) of untreated clayey soil, when treated with 30%CS reduced to 12.53%. There is a 25% reduction with respect to the initial value [5]. MDD of untreated clayey soil was 1.68 gm/cc, but with addition of 30% of CS, MDD increases to 1.82 gm/cc [5]. There is a 8% increase with respect to the initial value.

The OMC (21%) of untreated local soil, when treated with 40%CS reduced to 11%. There is a 48% reduction with respect to the initial value [6]. MDD of untreated local soil was 1.64 gm/cc, but with the addition of 40% of CS, MDD increases to 2.59 gm/cc [6]. There is a 58% increase with respect to the initial value.

The OMC (21.5%) of untreated BCS, when treated with 40%CS reduced to 11.7%. There is a 45% reduction with respect to the initial value [7]. MDD of untreated BCS was 1.65 gm/cc, but with addition of 40% of CS, MDD increases to 2.53 gm/cc [7]. There is a 54% increase with respect to the initial value.

The OMC (25.38%) of untreated BCS, when treated with 40%CS reduced to 20.6%. There is a 19% reduction with respect to the initial value [8]. MDD of untreated BCS was 1.54 gm/cc, but with addition of 40% of CS, MDD increases to 1.78 gm/cc [8]. There is a 16% increase with respect to the initial value.

The MDD 1.58 gm/cc of untreated BCS, when treated with 32%CS increases to 1.9 gm/cc. There is a 20% increase with respect to the initial value [9].

Voids of Coarser particles are filled by the finer particles and the unit weight increases as a result causing an increase in the MDD and decrease in the OMC [1].

2.3 *Effect of Copper Slag on CBR Behaviour for Various Combinations of Soil/Waste*

The California Bearing Ratio test has been conducted by many researchers after treating different industrial wastes like Rice husk ash, Fly Ash and soil with Copper slag. These test results are shown in Figs. 7 and 8.

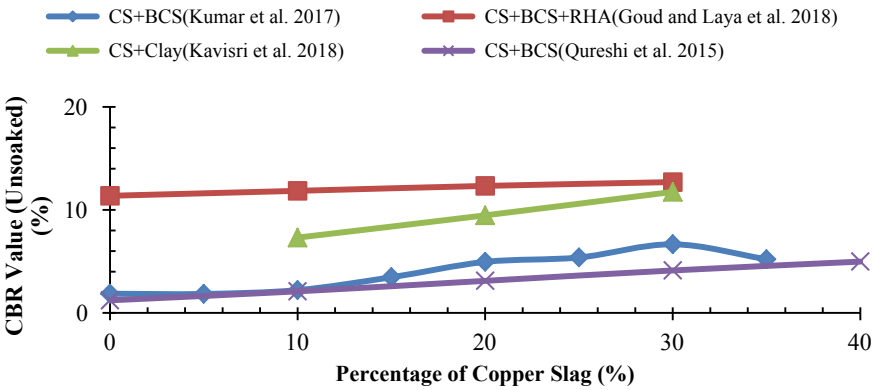

Fig. 7 Variation of CBR (Unsoaked) with copper slag for various combinations of soil/waste

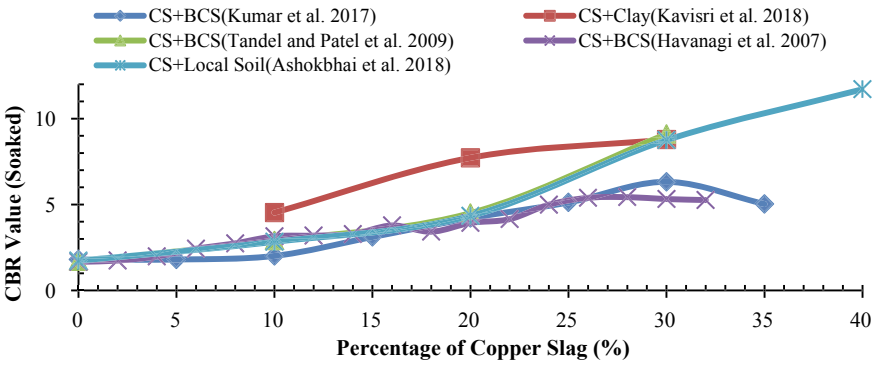

Fig. 8 Variation of Shrinkage limit with copper slag for various combinations of soil/waste

2.3.1 CBR Unsoaked and Soaked Condition Test Results

The CBR (Unsoaked) value of untreated BCS was 1.84%, but with the addition of 30% of CS, CBR (Unsoaked) value increases to 6.66% [3]. There is a 262% increase with respect to the initial value. CBS(soaked) of untreated BCS was 1.8%, but with addition of 30% of CS, CBR (soaked) increases to 6.32% [3]. There is a 251% increase with respect to the initial value.

The CBR value of BCS increases with the increase in the percentage of CS + RHA. The CBR value 11.37% of untreated BCS, when treated with 30%CS + 6%RHA increase to 12.7% [4]. There is a 11.68% increase with respect to the initial value.

The CBR (Unsoaked) value (7.31%) of untreated clayey soil, when treated with 30%CS reduced to 11.75%. There is a 36% increase with respect to the initial value [5]. CBR (soaked) of untreated clayey soil was 4.53%, but with an addition of 30% of CS, MDD increases to 8.78% [5]. There is a 94% increase with respect to the initial value.

The CBR value is increased from 1.22 to 4.98 when we add 40% w/w of CS in [8]. The optimum CBR value has obtained with the addition of 60% BCS and 40% CS. The maximum value of 4.98% satisfied the criteria of soil to be used as subgrade/subbase layer in road pavement.

When CS and BCS is mixed in the ratio 30:70 we obtain a CBR (Unsoaked) value of 9.1% and this value is suitable for a material to be used as subgrade as IRC:37-2001 suggests a minimum value of 2% for subgrade material [7]. The CBR(soaked) value of 12.2% is obtained when CS and BCS are mixed in the ration of 40:60.

It is observed that soaked CBR values of the combination of BCS with CS (2–28%CS) increases and it tend to decrease when we add CS more than 32% [9]. The high value of soaked CBR of 5.43% is obtained when BCS and CS are used in the ration of 72:28. The highest CBR value is a 227% increase from the initial value.

The mixture of CS and local soil in the ratio 40:60 gives the CBR value of 11.71% [6]. This means it increases from 1.73 to 11.71% which is an increase of 576% from the initial value.

2.4 Effect of Copper Slag on Direct Shear Test for Various Combinations of Soil/Waste

The value of C decreases with the increase in the percentage of CS consistent with respect to natural materials. On the other hand the value of an internal angle of friction Ø increase as the percentage of copper slag increases [7]. With the variation of CS from 10 to 40%, the value of Ø increases from 13.8 to 25.6° and cohesion C decreases from 38 to 14.5 kN/m^2.

If we mix CS with BCS the shear strength parameter C and Ø will behave with respect to the local soil [7]. The CS and BCS are mixed in different proportions, the percentage of CS and BCS varies from 0 to 40% and 100 to 60% respectively. The

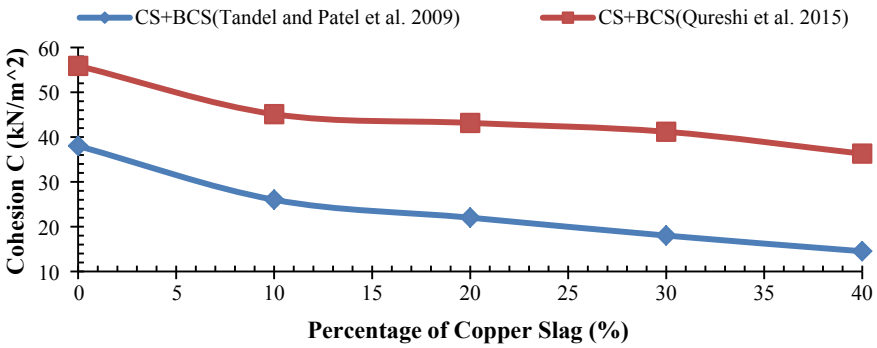

Fig. 9 Variation of Cohesion (C) with copper slag for various combinations of soil/waste [7, 8]

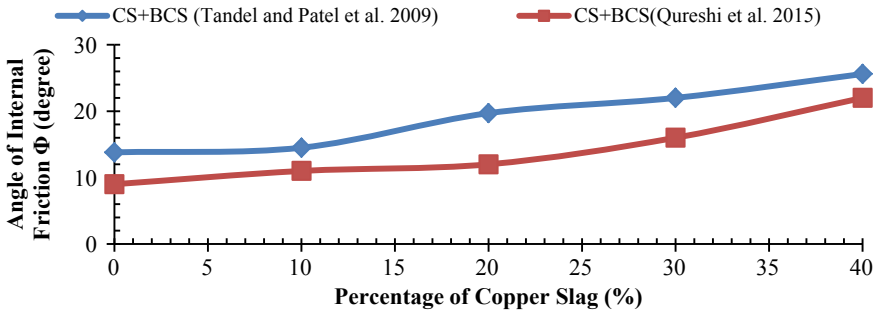

Fig. 10 Variation of Shrinkage limit with copper slag for various combinations of soil/waste [7, 8]

optimum results obtained from the mix of CS and BCS when mixed in the ratio of 40:60 respectively [8]. The value of C decreases from 55.89 to 36.28 kN/m^2 and Ø increases from 9 to 22° (Figs. 9 and 10).

2.5 Effect of Copper Slag on Unconfined Compressive Strength Behaviour for Various Combinations of Soil/Waste

The UCS value increases with the increase in the percentage of CS. The optimum value thus obtained when Cs and FA are mixed in the ratio of 70:30 [10]. The highest value of UCS is 330 kPa (Fig. 11).

The value of UCS increases when we add CS up to 6% and thereafter it starts decreasing. The mix of 6%CS-94%KUTTANAD clay may be considered as optimum [11] because it tends to increase the strength 35% more than that of soil alone.

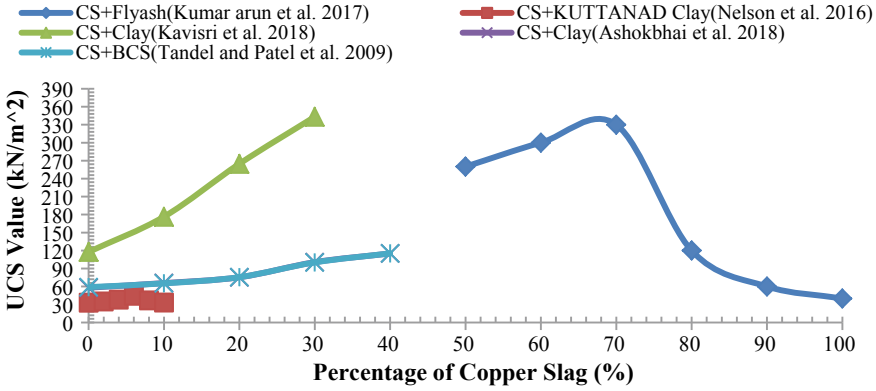

Fig. 11 Variation of UCS value with copper slag of various combinations of soil/waste

The UCS value of clay soil sample with Copper Slag in the ratio of 30:70 mix has high compressive strength value as compare to the mix with 10:90 and 20:80. [5]. The compressive strength increases by 95% from its initial results.

The mix proportion of CS + Clay and CS + BCS give similar results when mixed in the same proportion [6, 7]. The optimum mix proportion is 40%CS + 60% (Clay or BCS). The UCS value increases by 96% of the initial value.

In all cases the UCS value increases with increase in the curing period.

3 Conclusion

- The value of liquid limit comes out to be minimum when we take the mix of CS and BCS in the ratio of 35:65. However the plastic limit and plasticity index comes out to be optimum in case of CS and BCS mix taken in the ratio of 40:60.
- The shrinkage limit is obtained with an optimum percentage of 30%CS + 70%CS. The shrinkage value is outcome 9.15%.
- The highest value of UCS obtained is 343 kN/mˆ2 when we mix CS with clayey soil in the ratio of 30:70.
- The value of C and ϕ is best obtained with a mix of CS and BCS mixed in the ratio of 40:60.
- The CBR value is to be greater than 2% for a material to be used as subbase and subgrade pavement. In this case the CBR value obtained is 12.7% (64%BCS + 30%CS + 6%RHA) under unsoaked conditions and 12.2% (40%CS + 60%BCS) under soaked condition.
- The highest MDD obtained is 2.53 gm/cc when CS and BCS are mixed in the ratio of 40:60.

Table 3 Comparison of result with the relevant IS code (MORT&H & IRC 37) [4, 12]

Properties	Specification of relevant IS code	Results	Optimum mix proportion
Liquid limit (%)	<70%	33.5%	35%CS + 65%BCS
Plastic limit (%)	<45%	20.70%	35%CS + 65%BCS
Plasticity index (%)	<50%	13.37%	40%CS + 60%BCS
MDD (gm/cc)	>1.76 gm/cc	2.53 gm/cc	40%CS + 60%BCS
CBR (%)	> = 2	12.7	30%CS + 6%RHA + 64%BCS

- Use of industrial waste materials as stabilizers gives economic and ecological solutions for stabilization of subgrade of road embankment as well as reducing unnecessary burden on landfills.
- The mixture of copper slag with black cotton soil as subbase and subgrade pavement is an economical and sustainable process because copper slag is a waste which is recycled (Table 3).

References

1. Lavanya C, Rao A, Kumar N (2017) A review on utilization of copper slag in geotechnical applications. Int Res J Eng Technol 4:14–17
2. Rathan Raj R BS & DR (2016) Stabilization of soil using Rice Husk Ash. Int J Comput Eng Res 06:2250–3005
3. Kumar PR, Kumar PSP, Maheswari G (2017) Laboratory study of black cotton soil blended with copper slag and fly-Ash. Int J Innov Res Sci Eng Technol 6:1960–1967. https://doi.org/10.15680/IJIRSET.2017.0602095
4. P. Bharath Goud DSL (2018) Stabilization of black ccotton soil with copper slag and Rice Husk Ash – An environmental approach. Int J Sci Res 7:837–843
5. Kavisri M, Senthilkumar P, Gurukumar MS, Pushparaj KJ (2018) Experimental study on effects of stabilization of clayey soil using copper slag and GGBS. Rasayan J Chem 11:111–117. https://doi.org/10.7324/RJC.2018.1111805
6. Ashokbhai BM, Rajubhai JK, Amarabhai SP, Chavda MM (2018) Utilization of copper slag to improve geotechnical properties of soil. Int Res J Eng Technol 5:666–673
7. Tandel YK, Patel JB (2009) Review of utilisation of copper slag in highway construction. Aust Geomech 44:71–80
8. Mohammed A. Qureshi, Hevin M. Mistry VDP (2015) Improvement of index properties of expansive soil by using copper slag. Int J Adv Res Eng Sci Technol 2:125–130

9. Baraskar T, Ahirwar SK (2014) Study on California bearing ratio of black cotton soil use waste copper slag. Int J Engg Sci Mgmt 4:54–65
10. Kumar KA (2017) Characteristics and utilization of copper slag-fly Ash mix as road construction material. Int J Adv Res Trends Eng Technol 4:38–49
11. Nelson A (2016) A study on the effect of copper slag on lime stabilized clay. Int J Eng Res Technol 5:536–540
12. Dhir OBE RK, de Brito J, Mangabhai R, Lye CQ (2016) Sustainable construction materials: copper slag pp. 1-322
13. Das BM, Tarouin AJ, Jones AD (1982) Geotechnical properties of a copper slag. Transp Res Rec 1–4

A Comparative Study on Using Laterite and Sandstone Aggregates on Mechanical Properties of Concrete

B. C. Gayana, K. Ram Chandar, and Krishna R. Reddy

Abstract Scarcity of natural aggregates in concrete construction is leading to explore the use of alternative materials, especially various industrial waste products. Mining industry is one such major source of waste materials. Sandstone, which is overlying coal seams, is the largest quantity of waste rock being produced by coal mining industry. Laterite is another waste comes from small scale quarries. An attempt is made to assess the use of laterite-GGBS and sandstone as partial replacement for sand in concrete. Sandstone samples were collected from the dumps of a coal mine in south India and laterite samples were collected from different quarries from the southwestern part of India. Various properties of mine waste samples were determined in the laboratory as per IS codes, the properties were found to be very close to that of natural river sand. Mix proportions were prepared for M20 grade concrete. Mechanical properties of concrete with different mixes (0, 25, 50, 75, and 100% replacement with sand) were determined and compared. As a result, the concrete mixes with the replacement of fine aggregates with 100% sandstone increased in strength properties i.e., compressive, splitting tensile, and flexural strength compared to laterite mixes, where the strength properties decreased with increase in replacement levels. This indicates that sandstone can be an effective replacement for the river sand in concrete.

Keywords Aggregates · Mine waste · Compressive strength · Splitting tensile strength · Flexural strength

B. C. Gayana · K. Ram Chandar (✉)
National Institute of Technology Karnataka, Surathkal, Mangalore, India
e-mail: krc_karra@yahoo.com

K. R. Reddy
University of Illinois at Chicago, Chicago, USA

K. R. Reddy et al. (eds.), *Sustainable Environment and Infrastructure*, Lecture Notes in Civil Engineering 90, https://doi.org/10.1007/978-3-030-51354-2_11

1 Introduction

The fine aggregates generally used in concrete is sand from river or sea. Due to the depleting nature of sand and restricted sand mining in many places, researchers are investigating for the best suitable alternative material to replace the river sand partially or fully without compromising the strength and durability characteristics. One of the alternatives could be mine waste. The major concern of waste management in the mining industry is, a large quantity of top layer waste rock to be removed to extract valuable coal or ore. Waste also generated while separating the valuable minerals from the ore, which are called as tailings. Tailings are the processed waste disposed to the tailing ponds. Researchers are investigating the use of these waste materials in the field of construction industry as replacement material for cement, fine and coarse aggregates. This paper is limited to the use of laterite and sandstone in concrete.

Laterite is a semi consolidated rock and is generally rusty red color due to high content of iron oxide. In the investigation on the suitability of laterite-cement mortars, the clay content adversely influenced the strength of the concrete [1]. Laterite has been satisfactorily used as a fill material for foundations and base course for highway construction [2, 3]. Experimental investigations on the properties of laterite in geopolymer concrete were done and the compressive strength obtained was 18 MPa for 28 days curing [4].

Another major waste produced by the mining industry is sandstone. Sandstone disposed in the form of overburden dumps which requires a large amount of area for storage affecting the fertility of the soil [5]. The effects of various parameters on dump stability were investigated. It causes dust pollution and also disturbs the flora and fauna and during the rainy seasons the dumped material may slide into the mine working areas [6]. A study was carried out to use the sandstone for vegetation to improve stability but requires a good amount of additives. So, utilization of it in the field of construction might mitigate the environmental issues of storage and handling of mine waste [7]. The effect of sandstone in brick preparation with incineration bottom ash was observed. With the water–cement ratio of 0.55, the compressive strength of different mix proportion samples was higher than the control mix by 14 MPa [8]. An experimental research was done to examine the suitability of quartz sandstone as a replacement for coarse aggregates. With the increased percentage of replacement of quartz sandstone, the compressive strength, flexural strength, and sulfate attack decrease with reference to control mix [9]. The potential use of sandstone powder as mineral additive to replace cement in concrete was investigated. A decrease in compressive strength by 30% was observed with 50% replacement of sandstone with cement, so 5% silica fume was added to enhance the strength properties and durability properties [10]. Other major mine waste generally used in concrete is iron ore tailings. An extensive survey of the use of mine tailings in the construction industry in the application of concrete pavements [11].

The main aim of the present study is to evaluate the physical and mechanical properties of different marginal materials viz., laterite and sandstone for various applications in the construction industry.

2 Experimental Study

The details of the materials used in the present research work along with the methodology and basic properties are discussed in this section.

2.1 Materials

a. Binder: Cement and Ground-Granulated Blast-furnace Slag (GGBS) are used as binders, the physical properties of the binders used are given in Table 1.
Cement: Commercially available Ordinary Portland Cement (OPC) Grade 43 was used.
GGBS: Ground-Granulated Blast-furnace Slag (GGBS) was collected from the nearby plant and partially replaced OPC by 40%. The specific gravity is 2.9.
b. Water: Potable drinking water was used.
c. Fine aggregates: Three types of fine aggregates are used for the study, river sand, laterite, and sandstone. The physical properties of the same are given in Table 2.
River sand: Locally available river sand was used for the study.
Laterite: The material was collected from different quarries in the southern part of Karnataka state in India.
Sandstone: The sandstone samples were collected by random sampling method from a coal mine in south India.

Table 1 Physical properties of OPC and GGBS

Properties	OPC 43	GGBS	Requirements as per Indian standards
Specific gravity	3.12	2.9	3.10–3.15
Initial setting time (min)	71	–	300 (min)
Final setting time (min)	352	–	600 (max)
Fineness (%)	1.7	–	10 (max)

Table 2 Physical properties of aggregates

Properties	River sand	Laterite	Sandstone	Coarse aggregates
Specific gravity	2.64	2.54	2.56	2.74
Water absorption (%)	1.3	10.86	2.25	0.8
Moisture content (%)	Nil	13.77	2.4	Nil
Maximum size (mm)	4.25	4.25	4.25	20
Liquid limit	–	42	–	–
Plastic limit	–	30	–	–
Plasticity Index (PI) (%)	–	12	–	–
Fineness modulus	2.75	2.25	3.05	–

d. Coarse aggregates: Crushed aggregate is used in the present study.

2.2 Mix Preparation, Casting and Curing of Specimen

The nominal mix ratio was designed for the different materials as replacement for fine aggregates in the present research as discussed below:

Laterite: Mix design was done for M20 grade concrete. Cement was partially replaced by GGBS by 40% and fine aggregates were replaced by laterite at 0, 25, 50, 75, and 100% by volume.

Sandstone: Mix design was done for M20 grade concrete. The fine aggregates were replaced with sandstone at 0, 25, 50, 75, and 100% by volume.

The test blocks were prepared with concrete samples casted in different molds depending upon the test requirements. Four cubes of dimension 150 mm × 150 mm × 150 mm accounting to 12 cubes per mix proportion were casted for the compression test. Four cylinders of 150 mm diameter and 300 mm length were casted for the splitting tensile tests and four beams of dimension 500 mm × 100 mm × 100 mm were prepared for the flexural strength tests. Fresh concrete was used for the slump tests. It should be noted that among the 12 cubes prepared for compression tests, four cubes each were cured for three different curing days (3, 7, and 28 days) prior to testing and for cylinder and beam samples only 28 days of curing was considered prior to testing.

2.3 Results and Discussions

Workability: The workability of concrete at fresh state was tested using a slump cone for different mixes i.e., with partial replacement of sand with laterite and sandstone. Workability of concrete with increased dosage of laterite and sandstone are compared. Figure 1 shows a comparison between the workability of different mixes. Based on the study, workability decreased with increase in laterite-GGBS concrete and increased in case of sandstone. This is due to the water holding capacity of laterite. The increase in slump was observed at 20% mix for laterite-GGBS concrete and incase of sandstone concrete, though there was not much difference after 20% replacement there is a considerable increase in slump value.

Compressive Strength: Concrete cubes of 150 mm × 150 mm × 150 mm were casted with increment replacement percentages of laterite and sandstone. The detailed explanation on the compressive strength of laterite-GGBS concrete and sandstone concrete are reported [12, 13]. The comparison trend of compressive strength for laterite and sandstone concrete is shown in Fig. 2a–c. An increase in trend is observed with increase in sandstone replacement in concrete with respect to laterite-GGBS concrete for 3, 7, and 28 curing days.

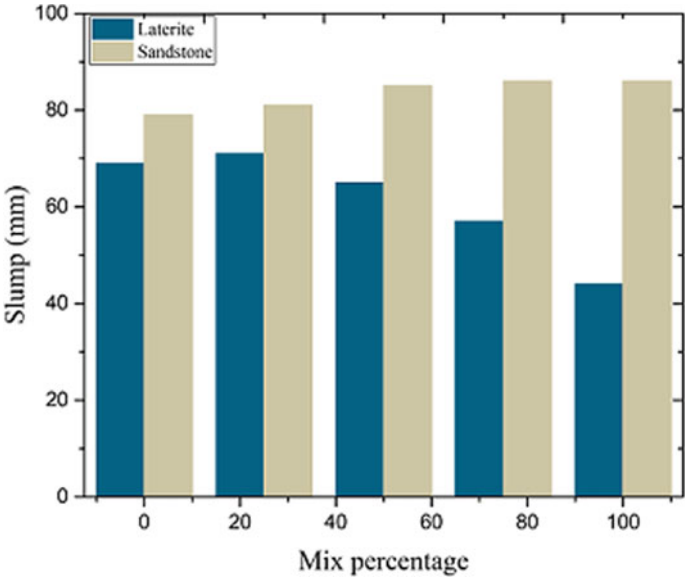

Fig. 1 Workability of laterite and sandstone mixes

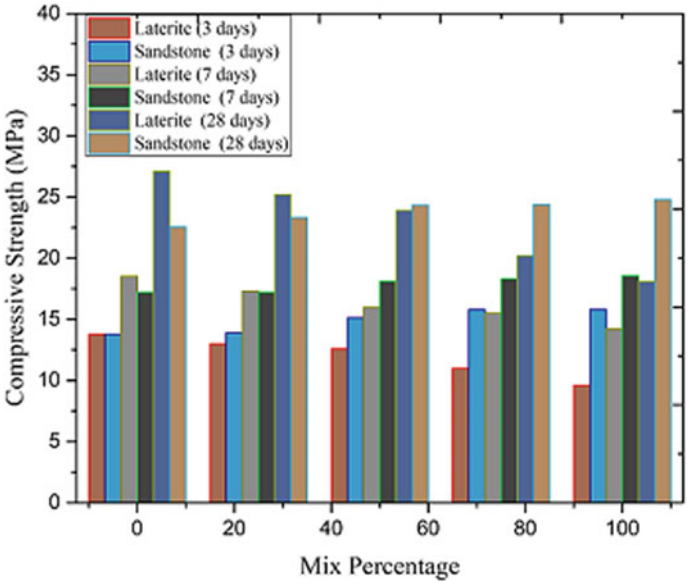

Fig. 2 Comparison of compressive strength of laterite-GGBS and sand stone concrete

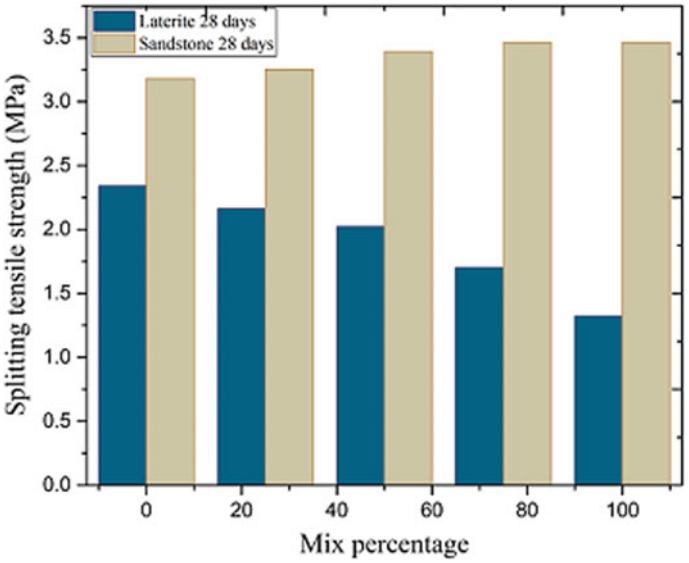

Fig. 3 Comparison of splitting tensile strength

Splitting Tensile Strength: Concrete cylinders of 150 mm × 300 mm were casted with increment percentages of laterite and sandstone. The comparison trend of splitting tensile strength for laterite-GGBS and sandstone concrete is shown in Fig. 3. It is observed that, there is an increasing trend in the splitting tensile strength for sandstone concrete up to 100% replacement and a decreasing trend is observed in laterite-GGBS concrete at 28 curing days. The increase in splitting tensile strength may be due to the bonding between the sandstone aggregates with the binder.

Flexural strength: Concrete prisms of 500 mm × 100 mm × 100 mm were casted with increment replacement percentages of laterite and sandstone. The comparison trend of flexural strength for laterite-GGBS and sandstone concrete is shown in Fig. 4. The flexural strength of sandstone shows an increasing trend compared to the laterite concrete at 28 days curing. The difference is more after 20% replacement.

2.4 Regression Analysis

Statistical model was developed for compressive strength for the different mix percentages and curing days for laterite-GGBS concrete and sandstone concrete.

Prediction Model for Laterite-GGBS Concrete: A regression model was developed to predict the compressive strength of laterite-GGBS concrete. The Eq. 1, was developed considering the mix percentage (Mp), curing days (Cd), and measured compressive strength of laterite-GGBS concrete. The analysis of variance (ANOVA) test summary and parametric estimates are shown in Tables 3 and 4, respectively.

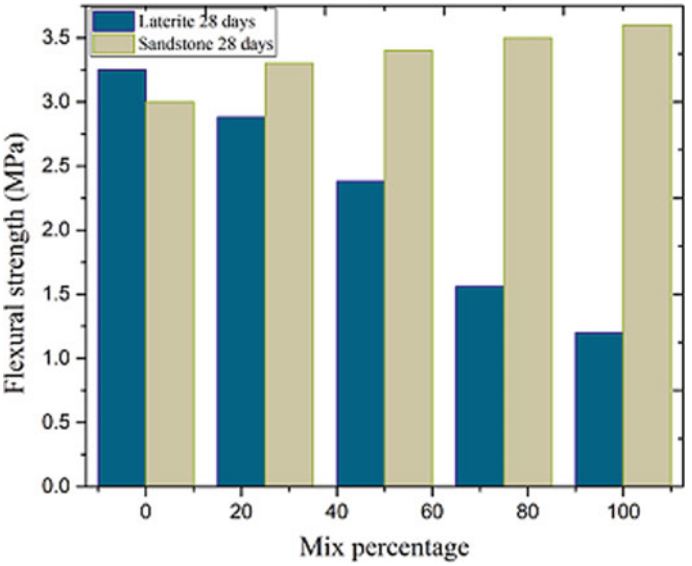

Fig. 4 Comparison of flexural strength

Table 3 ANOVA summary for compressive strength model for laterite

Source	F-value	P-value
Regression	68.99	0.0001
Mp	0.00	0.958
Cd	32.39	0.0001
Mp^2	1.40	0.266
Cd^2	13.55	0.005
Mp * Cd	4.36	0.066

Table 4 Parameter estimates for model for laterite

Variable	Coefficient	Standard error	T-value	P-value
Constant	10.27	1.29	7.95	0.0001
Mp	0.0020	0.0368	0.05	0.958
Cd	1.4200	0.25	5.69	0.0001
Mp^2	−0.0005	0.000438	−1.18	0.266
Cd^2	−0.0279	0.00759	−3.68	0.005
Mp * Cd	−0.0021	0.00102	−2.09	0.066

Notation: Mp = Mix %; Cd = Curing Days

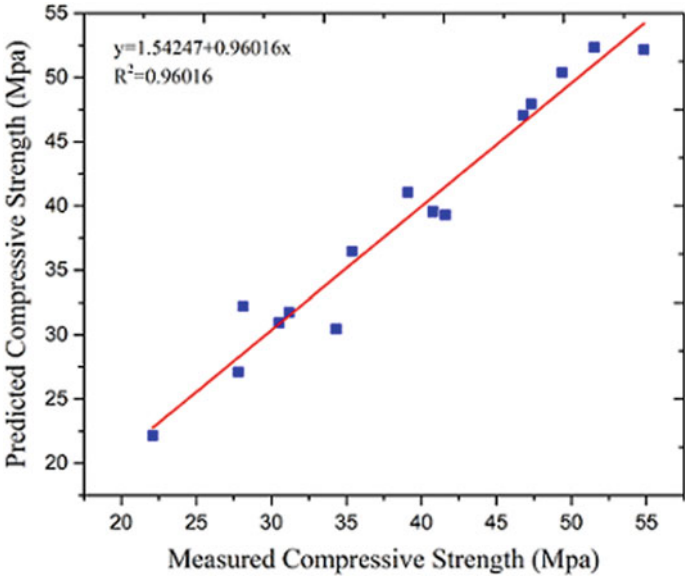

Fig. 5 Predicted versus measured compressive strength

Table 3 indicates that the model is robust and Table 4 shows that all the independent variables except the Mp were significant at a 95% confidence level. The R^2 value obtained is 97.46% and RMSE is 0.8389. The measured versus predicted compressive strength is shown in Fig. 5 and also the error plot is shown in Fig. 6, it is observed that the highest error is 2.09 at sample-12 and lowest error is −1.177 at sample-13.

Regression model for laterite-GGBS concrete:

$$\begin{aligned} \mathrm{CS(MPa)} = {} & 10.27 + 0.0020\ \mathrm{Mp} + 1.420\ \mathrm{Cd} \\ & - 0.000518\ \mathrm{Mp}^2 - 0.02792\ \mathrm{Cd}^2 - 0.00213\ \mathrm{Mp} * \mathrm{Cd} \end{aligned} \quad (1)$$

2.5 *Prediction Model for Sandstone Concrete*

Another model was developed to predict the compressive strength for sandstone concrete. The Eq. 2, was developed considering the mix percentage (Mp), curing days (Cd), and measured compressive strength of sandstone concrete. The analysis of variance (ANOVA) test summary and parametric estimates are shown in Tables 5 and 6, respectively. Table 5 indicates that the model is a good fit and Table 6 shows that all the independent variables except the mix percentage were significant at a 95% confidence level. The R^2 value obtained is 93.59% and RMSE is 0.2458. The measured versus predicted compressive strength is shown in Fig. 7 and also the error

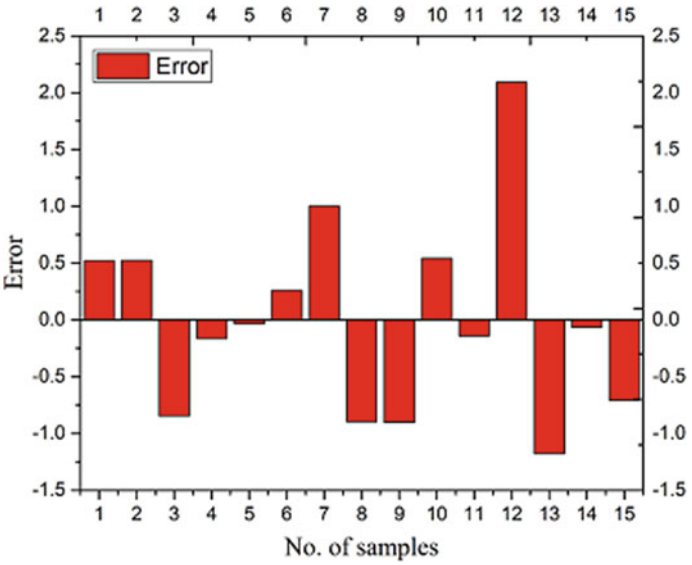

Fig. 6 Error graph for the compressive strength for laterite

Table 5 ANOVA summary for sandstone compressive strength model

Source	F-value	P-value
Regression	433.67	0.0001
Mp	11.80	0.007
Cd	165.65	0.0001
Mp^2	1.67	0.228
Cd^2	71.45	0.0001
Mp * Cd	0.11	0.751

Table 6 Parameter estimates for compressive strength model sandstone

Term	Coefficient	SE coefficient	T-value	P-value
Mp	11.112	0.372	29.87	0.0001
Cd	0.02953	0.0086	3.43	0.007
Mp^2	0.9394	0.0730	12.87	0.0001
Cd^2	−0.000101	0.000078	−1.29	0.228
Mp * Cd	−0.01879	0.00222	−8.45	0.0001
Mp	0.000069	0.000211	0.33	0.751

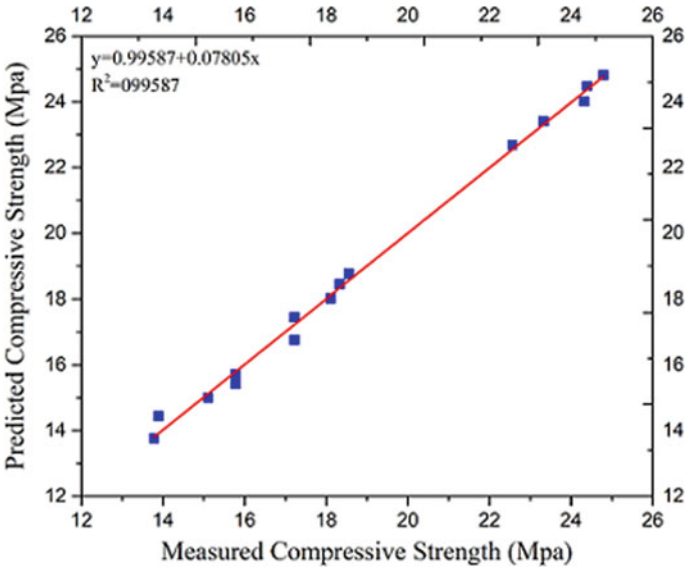

Fig. 7 Predicted versus measured compressive strength for sandstone

plot is shown in Fig. 8, it is observed that the highest error is 0.45 for sample-5 and lowest error is −0.55 fort sample-2.

Regression model for sandstone concrete:

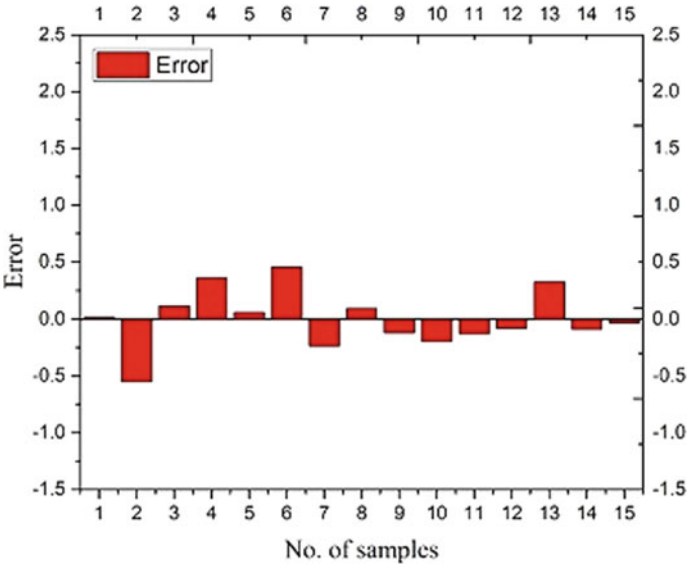

Fig. 8 Error graph for the compressive strength of sandstone

$$\text{CS (MPa)} = 11.112 + 0.02953\,\text{Mp} + 0.9394\,\text{Cd} - 0.000101\,\text{Mp}^2 - 0.01879\,\text{Cd}^2 + 0.000069\,\text{Mp} * \text{Cd} \quad (2)$$

3 Conclusions

An experimental study was done to study the suitability of laterite-GGBS and sandstone in concrete as the replacement for conventional fine aggregates and to compare the effectiveness of the both in concrete. The following conclusions are drawn from the study.

The workability of concrete decreased with increase in laterite-GGBS-blended concrete and in the case of sandstone, it increased with increase in sandstone replacement. The decrease in workability in case of laterite-GGBS mix may be due to the water holding capacity of laterite.

For laterite-GGBS blended concrete, the compressive strength decreased by 33.21% with 100% replacement percentage. This could be due to the high water absorption of the laterite. In case of sandstone concrete, the strength gradually increased with increase in sandstone replacement by 9.09% observed for 100% replacement of fine aggregates with sandstone.

The splitting tensile strength and flexural strength were determined at 28 days curing. The split tensile strength and flexural decreased with increase in replacement levels by laterite-GGBS blended and sandstone aggregate, respectively. In case of sandstone, the maximum splitting tensile strength and flexural strength increase was at 100% replacement by 8.81% and 20%, respectively.

Based on the regression analysis, the R^2 obtained for all the concrete mixes above 95% with the P-value of less than 0.005 and RMSE value between 0.2 and 0.8 which can be considered statistically significant model for the concrete mixes. By comparison between the two marginal materials, sandstone was found to be a better model and can be considered as a replacement for fine aggregates in concrete industry without compromising the strength and durability characteristics and also to mitigate the environmental issues due to dumping of these materials at mine sites.

References

1. Lasisi F, Ajayi EO, Osunade JA (1984) Technical notes: Strength characteristics of laterite-cement mortars. Int J Cement Compos Lightw Concrete 6(3):201–203
2. Ajayi LA (1982) Report of the committee on review of materials testing, control and research. In: Unpublished material, federal ministry of works, Owerri, vol 18
3. Obi-Egbedi RB (1998) Geotechnical properties of laterites—A case study of lateritic soil deposits at Obigbo, Rivers State. A Bachelor of Engineering thesis, Department of Civil Engineering, Federal University of Technology, Owerri, Imo State, Nigeria, vol 78

4. Kazea CR, Djobob JNY, Nanae A, Tchakoutea HK, Kamseub E, Meloa UC, Leonellic C, Rahierd H (2018) Effect of silicate modulus on the setting, mechanical strength and microstructure of iron-rich aluminosilicate (laterite) based-geopolymer cured at room temperature. Ceram Int 44:21442–21450
5. Barapanda P, Singh SK, Pal BK (2001) Utilization of coal mining wastes: an overview. In: Proceedings of the national seminar on environmental issues and waste management in mining and allied industries, Regional Engineering College, Rourkela, Orissa, India
6. Sastry VR, Ram Chandar K (2013) Dump stability analysis of an open cast coal mining project. Min Eng J 15(1):16–23
7. Ram Chandar K, Chaitanya V, Raghunandan ME (2015) Experimental study for the assessment of suitability for vegetation growth on coal over burden. J Mining Miner Eng 6(3):218–233
8. Wu MH, Lin CL, Hang WC, Chen JW (2016) Characteristics of pervious concrete using incineration bottom ash in place of sandstone graded material. J Constr Build Mater 111:618–624
9. Kumar S, Gupta RC, Shrivastava S (2017) Long term studies on the utilisation of quartz sandstone wastes in cement concrete. J Constr Build Mater 143:634–642
10. He Z, Hu L, Li Y, Hu J, Shao Y (2018) Use of sandstone powder as a mineral additive for concrete. J Constr Build Mater 186:276–286
11. Gayana BC, Ram Chandar K (2018) Sustainable use of mine waste and tailings with suitable admixture as aggregates in concrete pavements-a review. Adv Concrete Constr 6(3):221–243
12. Ram Chandar K, Raghunandan ME, Manjunath B (2016) Partial replacement of fine aggregates with laterite in GGBS-blended-concrete. Adv Concrete Constr 4(3):221–230
13. Ram Chandar K, Gayana BC, Sainath V (2016) Experimental investigation for partial replacement of fine aggregates in concrete with sandstone. Adv Concrete Constr 4(4):243–261

Strength Properties of Coffee Waste Based Geopolymers

Tugba Eskisar and Selim Altun

Abstract A considerable amount of coffee waste is disposed in the landfills annually. This study aims to investigate the possible use of coffee waste based geopolymers as a green construction material for landfills. Coffee is an organic and a biodegradable material. In order to use coffee waste as a construction material, the strength development of a coffee-based geopolymer was observed. Fly ash or rice husk ash were used as a precursor. These precursors were preferred because they are silica and alumina rich materials. Alkaline activator formed of sodium silicate and sodium hydroxide (Na_2SiO_3–NaOH) was used to trigger the geopolymerization process. Three variables were tested, the ratio of Na_2SiO_3–NaOH; effect of ash type, and curing time on the strength development of coffee-based geopolymers. By adding 30% of ash into coffee waste, a geopolymer was synthesized with an activator/ash ratio of 1.7 and Na_2SiO_3–NaOH ratio of 90–10%, which provided the highest (up to 1000 kPa) unconfined compressive strengths. This paper denotes that the coffee based-geopolymerization products will further develop the organic material into a nondegradable material, therefore suggesting geopolymers as an option to stabilize highly organic soils.

Keywords Geopolymer · Coffee waste · Unconfined compressive strength

1 Introduction

Recycling the waste products in the construction industry is a popular topic as it provides an alternative way of creating a sustainable environment and contributes to the economy. Environmentally friendly solutions could be achieved with recycled bio-materials. Coffee waste is an insoluble residue that remains after coffee beans are dehydrated, milled, and brewed. The coffee waste comes from two origins, those generated by the soluble coffee industry, which uses almost the half of the global

T. Eskisar (✉) · S. Altun
Ege University, 35100 Bornova, Izmir, Turkey
e-mail: tugba.eskisar@ege.edu.tr

K. R. Reddy et al. (eds.), *Sustainable Environment and Infrastructure*, Lecture Notes in Civil Engineering 90, https://doi.org/10.1007/978-3-030-51354-2_12

coffee harvest each year, and those generated by cafes and the public, constituting the other half [1].

The International Coffee Organization (ICO) estimates that in the years 2018–19, global consumption of coffee is 165.18 million bags leading to a total of 9.9 billion kilograms of coffee in total, the majority of which have been consumed in the EU, the USA, and Japan [2]. The major problem is soluble the producers dump large amounts of coffee waste in landfills, a practice that might affect and harm the local ecology [3].

Coffee waste is a highly organic material, and therefore, when it is planned to be a part of a geotechnical study, it could be regarded as an organic soil and it should be investigated through the soil mechanics concepts. Average coffee waste has 86–89% of organic content; it has low shear strength and high compressibility [4].

Ground improvement methods or geopolymerization process could be different alternatives to treat coffee wastes and use them as fill materials in embankments. Geopolymers, an alternative binder based on fly ash that is activated by an alkaline activator, has a lower carbon footprint compared to cement [5]. According to IPCC data, ordinary Portland Cement is responsible for about 7% of the total CO_2 emissions in the world [6]. Therefore, utilizing geopolymers may be an ecological approach to the solution of the coffee waste problem. Alkaline metals react with alumina-rich and silica-rich materials and produce a three dimensional alumino-silicate complex with a strong bindery network of alumina and silica elements. The initial materials for making geopolymer stabilizer could be any alumina and silica-rich natural minerals such as kaolinite and other clays, and wastes such as fly ash and rice husk ash [7]. Arulrajah et al. [8] recently produced a geopolymer made of coffee waste and fly ash to develop a green engineering fill material.

This study can be divided into two parts: First, traditional improvement techniques were applied to the coffee waste and the success of these methods is discussed. Second, a coffee waste-based geopolymer is synthesized. The aim of this study is to evaluate the strength development in coffee waste with different ash types and a liquid alkaline activator to determine the optimum amount to produce a coffee-based geopolymer to be used in as a fill material in embankments. 7–28–90 days of curing is applied to the specimens in a humidity controlled environment. The optimum liquid alkaline activator content and unconfined compressive strength (UCS) of the composite material are investigated. Test results are examined to see the capability of geopolymer as an alternative stabilizing agent for highly organic coffee waste. Test results contribute to a better understanding of geopolymer stabilization of highly organic waste material and soils.

2 Materials and Testing Methods

Coffee waste was collected from a branch of a USA-based coffee chain store located in Turkey. As the collected waste was moist, it was observed that molds grew within five days. The mold needs air and warmth to grow for this reason, the waste stored in

sealed plastic containers in a cool place, until they were transferred to the laboratory. First, coffee waste was laid flat on a large surface and removed from any other waste like paper cups, coffee filter paper, paper napkins, etc., and air drying was held for a day. Then, the material was placed in a drying oven. Coffee brewing temperature of 90 °C was applied as the oven temperature as higher would burn the organic material. This stage was completed in four days. Grain size distribution analysis was performed on the dry material (see Fig. 1). The particle size distribution of dried coffee waste shows that 85% of the waste was in sand size, and the rest of the material was in silt size. In this way, the grain size distribution of the waste is similar to silty sand, but this material is considered as a highly organic one. Class F fly ash (FAF) and class C fly ash (FAC) were derived from coal plants, and rice husk ash (RHA) was derived from a local producer in Turkey.

Sukmak et al. [9] and Horpibulsuk et al. [10] achieved desired levels of strength when 30% of ash in dry weight was added to the silty clay specimens. The ash content of 30% was kept constant during this study, regardless of the ash type. An alkali activator liquid was used to trigger the geopolymerization process. The activator was composed of two chemicals, NaOH in bead form and Na_2SiO_3 solution, respectively. NaOH with 97% purity and three modules 40 baume Na_2SiO_3 were commercially purchased. WG is also known as water glass, therefore in the text it will be denoted as WG. Different percentages of WG-NaOH were used to see the effects of the chemical compounds forming the geopolymers. The molar concentration of NaOH was eight molars in water solution. Coffee waste and ash was dry mixed and the alkali activator liquid added to this mixture at different percentages relative to the dry weight of the coffee waste and ash. The optimum alkali activator liquid contents were determined for each activator/ash ratios. Standard Proctor testing was performed to achieve the optimum alkali activator contents. After the optimum activator amount was determined, conditions representing wet and dry sides of the optimum were also considered. Specimens with 10 cm height and 5 cm diameter were formed by applying compactive effort. The specimens were wrapped and sealed in stretch film layers to

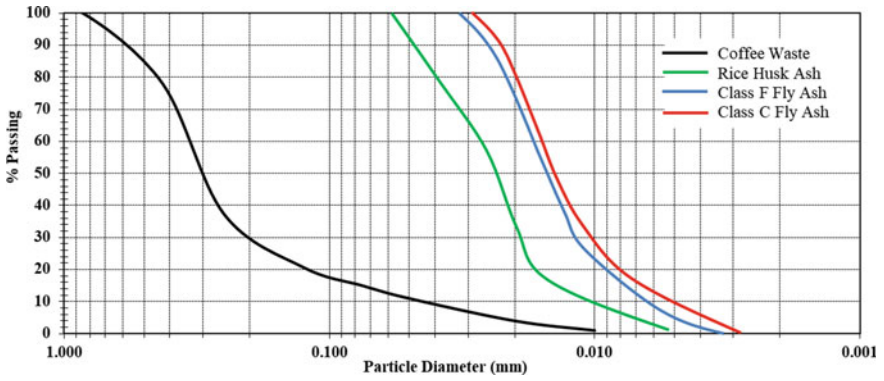

Fig. 1 Grain size distributions of the materials used in this study

avoid moisture content loss and they were cured for 7–28–90 days. Unconfined compressive tests were held on the specimens to observe stress-deformation patterns according to ASTM D2166 [11]. The load was applied so as to produce an axial strain at a rate of 1%/min. The rate of strain was chosen so that the time to failure did not exceed 15 min. The loading continued until the load values decreased with increasing strain, or until 15% strain was reached.

3 Results and Discussion

3.1 Cement Treated Specimens

Before applying the geopolymerization process, the effectiveness of a traditional improvement technique, cement treatment was evaluated. The coffee waste was considered as a weak soil and first its own compressive strength is determined with specimens constituted at the optimum water content of the medium. Similar to a sand specimen, the coffee waste has no cohesion, but it can stand alone in cylindrical form due to the interlocking of irregular porous particles and the suction occurring due to the presence of water between the particles. The coffee waste specimen at the optimum water content resulted in compressive strength of 18 kPa. The additive content is defined as the ratio of the mass of the dry additive to the mass of coffee waste; 3–10% of cement was added into the coffee waste. In a similar manner, some specimens were prepared with cement and FAF. FAF ratio was 10%.

The specimens were cured for 28 days and then subjected to unconfined compression tests (see Fig. 2). Adding 3 or 5% of cement contributed to a rise of the compressive strength. The specimens with 10% of cement had the highest strength of 83 kPa. However, the introduction of 10% fly ash to the mixture reduced the strength of the specimens. This result may be observed because of the insufficient amount of lime content in the composite material. A reduction in the rate of hydration caused lower compressive strength and a similar result was also observed by Saha [12]. As a result of these findings, it is possible to increase the strength of coffee waste with

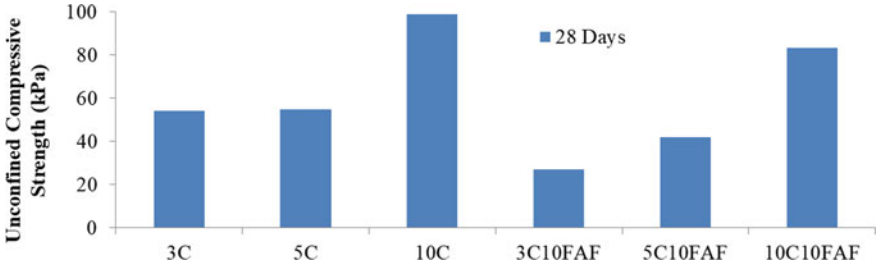

Fig. 2 Unconfined compressive strength of specimens prepared with cement (C), and cement and class F fly ash (FAF)

cement, but there is not enough material—additive interaction to have strength at a desired level. Coffee waste is lack of minerals that are readily available in soils and this condition blocks the development of chemical reactions within the medium. Therefore, an effective solution is necessary to reach high strength values.

3.2 *Liquid Activator Content*

The coffee waste—ash mixtures were treated with three different solutions of WG-NaOH. The percentages of WG-NaOH were 90–10%, 70–30%, and 50–50% by weight, respectively. The compaction curves of the specimens prepared with different WG-NaOH content converged at the same optimum liquid content. As an example, specimens prepared with 70%WG–30%NaOH had a maximum dry density of 8.72kN/m^3 and the corresponding optimum activator content was 51%.

Unconfined compressive testing was performed on seven day specimens to see the effect of liquid activator contents. Three different WG-NaOH contents, activator ratios (dry side, optimum, and wet side) were considered. The ashes are mixed at a ratio of 30% by dry weight into the coffee waste. FAC was the most effective precursor by means of compressive strength, hence, only the unconfined compressive strength (UCS) values of the specimens containing FAC are presented in Fig. 3a.

In Fig. 3a, it is shown that the maximum 7-day UCS is achieved at an activator/ash ratio of 1.7 for 90%WG–10%NaOH for specimens prepared with FAC. 950 kPa of strength was achieved in these specimens. It is seen that FAC caused an early strength development due to its high amount of calcium oxide casing cementing agents in the medium.

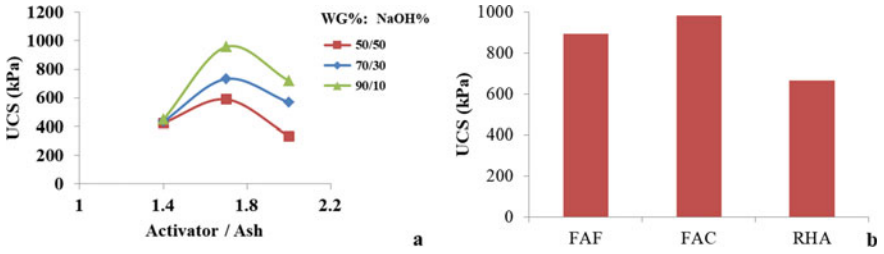

Fig. 3 **a** Unconfined compressive strength of specimens prepared with different activator ratios. Ash type is FAC. **b** Effect of ash type on the specimens prepared with 90%WG–10%NaOH activator content and activator/ash ratio of 1.7

Table 1 Change of UCS with curing time

Specimen	Activator/ash	UCS (kPa) 7 days	UCS (kPa) 28 days	UCS (kPa) 90 days
30%FAC (with 90%WG–10%NaOH)	1.4	448	644	1165
	1.7	957	982	1490
	2.0	720	842	1157

3.3 Precursor Type

The activator content was fixed to with 90%WG–10%NaOH. The optimum amount of activator/ash ratio was 1.7. 28-day specimens were tested to evaluate the effect of ash type (see Fig. 3b). Similar to the 7-day specimens, 28-day specimens containing 30% FAC had the highest UCS. The second highest UCS values were observed in the specimens prepared with 30% FAF. The UCSs were close to each other and this was attributed to the proximity of the grain size distribution of the fly ash materials.

However, RHA was composed of coarser particles in the shape of platelets, this condition may have caused larger voids than the fly ash containing specimens in the macro scale. Another concern is, RHA is a silica-rich component, the presence of NaOH may have leached high amount of SiO_2 and as there was not a high amount of CaO supplied to the medium, less CSH and CASH gels may have formed reducing the strength values. On the contrary, FAC is rich in CaO, and better bonding and geopolymerization was established in the specimens.

3.4 Curing Time

The strength development of the specimens in the long term is given in Table 1. It is evident that geopolymerization is a longer process compared to the well-known methods of stabilization. Kua [13] reported that geopolymerization could be completed from 60 to 90 days. In this study, it was seen that between 28 days and 90 days there is an apparent improvement in UCS values. Curing times longer than 90 days should be checked to see the threshold where the continuous strength development is satisfied.

4 Conclusions

The engineering properties of coffee waste-based geopolymers were evaluated to seek for the possible use of this material as a fill material. Also, geopolymer stabilization effectiveness in improving the mechanical behavior of highly organic waste

material and soils was addressed. The strength developments were observed with unconfined compressive tests.

Coffee waste itself is an organic material and subject to biodegradation. However, in this study, it was stabilized with different types of precursors such as fly ash and rice husk ash, and with alkali activators. This process formed a strengthened medium, thus changing the degradation properties of the waste into a nondegradable state. The strength development was found to be highest in specimens treated with an activator/ash ratio of 1.7 for 90%WG-10%NaOH for specimens prepared with FAC. The strength improvement continued for 28–90 days, showing that geopolymerization is a longer process compared to the traditional stabilization methods.

Recycled coffee waste as well as fly ash/rice husk ash has potential to withdraw the major amount of waste from the landfills if a sustainable stabilization procedure is developed. This paper shows the preliminary research results that geopolymer stabilization is a feasible method for the stabilization of highly organic soils, which can decrease the carbon footprint for future infrastructure projects.

References

1. Scully DS, Jaiswal AK, Abu-Ghannam N (2016) An investigation into spent coffee waste as a renewable source of bioactive compounds and industrially important sugars. Bioengineering 3(4):33
2. International Coffee Organization. Trade statistics. http://www.ico.org/trade_statistics.asp, Accessed on 03 Feb 2019
3. Cruz R, Cardoso MM, Fernandes L, Oliveira M, Mendes E, Baptista P, Morais S, Casal S (2012) Espresso coffee residues: a valuable source of unextracted compounds. J Agric Food Chem 60:7777–7784
4. Arulrajah A, Maghoolpilehrood F, Disfani MM, Horpibulsuk S (2014) Spent coffee grounds as a non-structural embankment fill material: engineering and environmental considerations. J Clean Prod 72(11):181–186
5. Turner LK, Collins FG (2013) Carbon dioxide equivalent (CO_2-e) emissions: a comparison between geopolymer and OPC cement concrete. Constr Build Mater 43:125–130
6. Intergovernmental Panel on Climate Change (IPCC) (2005) Carbon dioxide capture and storage. special report, Cambridge University Press. New York, USA
7. Akbari H, Mensah-Biney R, Simms J (2015) Production of geopolymer binder from coal fly ash to make cement-less concrete. In: World of coal ash conferences WOCA, Nashville, USA, pp 1–8
8. Arulrajah A, Kua TA, Phetchuay C, Horpibulsuk S, Mahghoolpilehrood F, Disfani MM (2016) Spent coffee grounds–fly ash geopolymer used as an embankment structural fill material. J Mater Civ Eng 28(5):04015197
9. Sukmak P, Horpibulsuk S, Chen SL (2013) Strength development in clay-fly ash geopolymer. Constr Build Mater 40(3):566–574
10. Horpibulsuk S, Suksiripattanapong C, Samingthong W, Rachan R, Arulrajah A (2016) Durability against wetting-drying cycles of water treatment sludge-fly ash geopolymer and water treatment sludge-cement and silty clay-cement systems. J Mater Civ Eng 28(1):04015078
11. ASTM D2166 (2016) Standard test method for unconfined compressive strength of cohesive soil. ASTM international, West Conshohocken, PA

12. Saha AK (2018) Effect of class F fly ash on the durability properties of concrete. Sustain Environ Res 28(1):25–31
13. Kua TA (2017) Application of spent coffee ground as a road subgrade construction material. Ph.D. thesis, Swinburne University of Technology

Management and Exploitation of Human Hair "Waste" as an Additive to Building Materials: A Review

Ruhina Anjum, Vaibhav Sharma, Sunil Sharma, and Arvind Kumar

Abstract Recently, biological fibers have become striking topic to researchers, scientists, and engineers as substitute reinforcement, due to their cheap availability, high aspect strength, and appreciable mechanical properties. Human hair fiber (HHF) is one of the unsullied biological fibers. Its accumulation, in the form of waste heaps or in waste stream leads to many environmental problems. All in all, three to four tons of this biological fiber is thrown around like confetti in India annually; posing an environmental challenge. Nowadays, as a commercial application, human hair waste is finding its use in the field of material science. Because of the fact that human hair is strong in tension; it can be used as a fiber reinforcement material. A substantial amount of sulfur is present in human hair because of the presence of "cysteine" amino acid, a major constituent of keratin proteins. Keratin is a primary component of human hair, which is a protein, a polymer of amino acids. Protein "keratin" is incredibly strong, insoluble, and tough. A single strand of HHF can withstand a load of 100–150 gms and on removal of the deforming load, HHF is capable to regain its original position by virtue of its elasticity. This review paper outlines the current scenario of exploitation of HHF as biological composite fiber in various fields of construction. This study shows that HHF is a highly multifaceted material with noteworthy potential in several major areas such as medical applications, cosmetic industry, agriculture, construction material, and pollution control.

Keywords Human hair fiber · Construction material · Environmental challenge · Mechanical properties

R. Anjum · S. Sharma
Department of Civil Engineering, NIT, Hamirpur, India
e-mail: sunils@nith.ac.in

V. Sharma (✉)
Department of Civil Engineering, Dr B R Ambedkar National Institute of Technology Jalandhar, Jalandhar, India
e-mail: civil.vaibhav.sharma@gmail.com

A. Kumar
Department of Civil Engineering, Dr B R Ambedkar National Institute of Technology Jalandhar, Jalandhar, India

K. R. Reddy et al. (eds.), *Sustainable Environment and Infrastructure*, Lecture Notes in Civil Engineering 90, https://doi.org/10.1007/978-3-030-51354-2_13

1 Introduction

To be amazed, use of biological fibers is not new to our generation but they have already been used some 3000 years ago in the ancient Egypt, in composite systems, where clay and straw were mixed in order to build the structures and walls. But recently, biological fibers have become a striking reinforcing material for polymeric composites from an ecological and economical point of view. Though there exists a number of uses of human hair, it is considered as a waste material in almost every part of the world. Its accumulation, in the form of waste heaps or in waste stream leads to many environmental problems [1].

In areas where population density is quite low, especially rural areas, the hair which is thrown away in nature decomposes very slowly taking a very long time, almost over several years, finally returning back the integral elements to their natural cycles. Those elements include carbon, sulfur, oxygen, nitrogen, etc. In highly populated areas, especially urban areas, the hair often accumulates in the solid waste streams in large amounts and as a result chokes the drainage systems, creating a serious problem.

As the degradation process is quite slow, it remains as a part of thr waste stream, engrossing large space for a long time. Eutrophication is one of the unwholesome result due to the increase in the concentration of nitrogen from the leachate of these dumps. Also, it's a widespread practice of burning of waste piles holding human hair which results in the production of toxic gases with foul order such as hydrogen sulfides, ammonia, sulfur dioxide, carbonyl sulfides, phenols, pyrroles, pyridines, and nitriles [2].

Sweat, oils, organic matter, etc., sticking to the waste hair crumble over the passage of time and ultimately become a reason for the malodorous condition, providing a space for pathogens breeding. Even the hair dust generated from the open dumps causes a lot of discomfort to the nearby mortals and can face severe respiratory problems if large amounts of inhalation occurs for a long span of time. In order to solve all the problems discussed above, the finest way is to evolve systems that can utilize the fritter away as a source.

Contribution to the economy will be an additional advantage along with the reduction in waste. Growing cognizance related to the environmental issues in the world has evoked interest of the researchers in the area of utilization of biodegradable materials. The resources of the natural or biological fibers include animals, plants, or minerals.

With the shortfall of energy supplies and ecological risk, the idiosyncratic advantage of using biological fibers include its nontoxicity, abundance in quantity, noncorrosive in nature, no irritation to the eyes, skin, or respiratory system. With all these beneficial properties, polymer composites reinforced with natural fibers have grabbed much interest as an alternative reinforcement in place of synthetic ones [3].

As a possible material resource, the fiber of human hair has a number of advantages, such as it is renewable, completely biodegradable, and most importantly it is available in bulk at a very cheap or nil cost in almost every locality. The property

of lightweight and more volume of natural fibers in comparison with the synthetic fibers helps to improve the efficiency of fuel and also reduces the emissions in the auto applications [4, 5]. Surprisingly, though human hair is thrown as waste in many parts of the world, yet there occurs large scale international trades in the products of and high quality hair.

In 2010, India exported approx. one million kg of hair and human hair products worth US $238 million, and the total global imports were valued at US $1.24 billion [6]. In India, the workers of the hair processing units involved in such trades have reported many number of cases of infections in the respiratory tract and tuberculosis as a result of decaying hair and hair dust [7, 8].

This paper assesses and explores various employment of human hair in different fields, especially as an additive to building materials, from the standpoint of expanding its exploitation as a resource along with addressing the environmental issues related with it as solid waste.

2 Review of Natural Fiber {hhf}

Choudhry and Pandey [9] founded in their studies that composites show a higher flexural modulus, flexural strength, and Izod impact strength with 3–5% by weight of human hair fiber when compared with non reinforced polymer. Also, they found that the flexural strength, Izod impact strength and flexural modulus decreases if the proportion of HHF is increased to 10–15% by weight. Ganiron [10] examined the effects of HHF additives in comp. strength of the mixture of asphalt cement and found that the load-bearing capability of cement asphalt mixture has greatly improved when the percent of HHF is taken in between 6 and 8% by weight of bitumen. Also, he founded that this percentage can be increased if proper gradation is done and the content of bitumen added is also increased simultaneously.

Fueghelman [11] investigated the structure and mechanical properties of alpha keratin fibers like human hair, wool, and others and deduced that HHF possesses the greatest tensile strength when compared to other fibers. He also unclosed the exceptional features of HHF such as low rate of degradation, distinct chemical composition, great tensile strength, elastic recovery, thermal insulation, scaly surface, and unique kind of interactions with oils and water which has made it possible to use this fiber diversely. Figure 1 shows the human hair waste collected from a barber shop.

3 Applications of Human Hair

The uses of human hair depend on many parameters such as length, curliness or straightness, color, contamination, and hair damage. These all variation occurs due to the difference in the culture, hairstyles, ethnicity, and the various practices of hair care in different regions.

Fig. 1 Human hair

3.1 Cosmetic, Theater, and Fashion Industry

Hair Extensions, Wigs, Eyelashes, Beards, Moustaches, and other cosmetic accessories: This is a standout among the oldest and right now the biggest of the human hair based ventures, with an always expanding scale because of worldwide extension of the design business. The ones from 1400 BC Egypt, are the most established wigs known, and some of them are still unblemished today even after 3400 years [12]. This application prevalently utilizes great quality, hair with good length of practically all hues.

Check material for hair care commodity: Human hair samples are utilized as test stuff for new definitions of oils, shampoos, conditioners, colors, etc. These tests utilize hair of various hues, scope of curliness, and distinctive damage levels.

Manufacturing Cosmetic Brushes: Scaly surface of hair can hold the particles of cosmetic powder and apply it consistently on any surface or skin. Hence, hair of mortals has been used for making the brushes [13, 14].

3.2 Cultivation Industry

Vermin Control: Various problems related to vermin as well as issues arising from animals in the farms have been addressed by the use of human hair, although by various mechanisms. In Mauritius [15] human hair has been used to repulse rabbits, in USA [16] for deer and in India [17] for wild boar and rodents.

Also in India [18, 19] human hair is used to dissuade the rhinoceros beetles. Different methods and techniques involving the utilization of human hair in farms/fields help farmers to save their crops from pests and also this is more economical than the usage of pesticides.

As Mulch/Fertilizer: Human hair, a natural fiber, contains noteworthy nitrogen content which is approximately 16% since it is prevalently made up of such proteins which are nitrogen bounded. Likewise, human hair additionally contains carbon, sulfur, and 20 different components basic for plants [20]. In a few networks in India, human hair has been utilized specifically as manure for some products of the soil crops like vegetable and fruits and also in the production of natural manure [21, 22].

3.3 Pollution Check and Indemnification

Water–Oil Separation and Remediation for Oil Spill: Human hair fiber possesses a valuable property of differential affinity toward water and oils. Its surface has a lower affinity for water when compared to oils [23]. This property of hair fibers is very helpful in water–oil separation. Figure 2 shows the usage of hair fibers along with the feathers to fight against the oil spill in Philippines [24].

Removing Pollutants such as heavy metals, Aldehydes, Phenols, and Dyes from Water: Human hair has a tendency to absorb various chemicals from the aqueous solutions. Investigations demonstrate that human hair can assimilate natural toxins, for example, formaldehyde [25], phenol [26], and various heavy metals like copper{Cu}, mercury{Hg}, silver{Ag}, cadmium{Cd} from aqueous solutions [27, 28].

Fig. 2 In Philippines, Human hair and Feathers used to fight the oil spill

3.4 Biomedical Pharmaceuticals and Applications

Medicaments: Protein of human hair ordinarily contain 20 basic amino acids, all of which can be extricated on complete hydrolysis of human hair [29]. A portion of the amino acids acquired in great yield from human hair are, L-leucine, L-cysteine, L-valine, and L-isoleucine. L-cysteine and its synthetic subsidiaries are utilized in numerous beauty care products and pharmaceutical plans.

Ethnomedicinal Applications: A few societies have been utilizing human hair for planning customary medicines. Carbonized fibers of human hair have been utilized in customary Chinese medicine [30] for treating wounds, hemorrhage, scars, and burns.

It is additionally utilized in veterinary drug to quit bleeding and to advance urination [31]. In country networks in Chhattisgarh, India [22], hair fiery debris is applied to open injuries for prompt relief from discomfort just as long haul recuperation.

As a Suture in Surgery: Human hair has adequately high quality for it to be used as suture in many medical surgeries. It is moderately simple to tie hitches with human hair and it is also noninfectious (in light of its moderate decay rate and high similarity with the human body). In Europe, its utilization as suture was known in the medieval times [32]. Due to the flexibility, high strength, and elasticity, it is quite easy to make the stitches on the skin with the fibers of human hair and there is no fear of any kind of infections also.

3.5 Fabrics

In China, cotton, yak hair, and human hair are utilized to make interlining fabric for jackets and coats [33]. Individuals have customarily been making textures by blending human hair with nettle fiber, cotton, and yak hair in Arunachal Pradesh, India [34]. Elasticity, high thermal insulation, and great tensile strength make it possible to use human hair for different variety of fabrics.

3.6 As a Composite Stuff

Framed Objects and furniture: A UK-based business person, Ronald Thompson [35], has built up a technique for making up composite materials which incorporates first meshing human hair fiber into a web or tangle and after that including a basic added substance like sap or adaptable polymer (ideally a biodegradable or recyclable material). This composite possesses high strength and can be utilized for the making of framed or molded structures like mannequins and furniture. A composite comparable with unwoven hair has likewise been utilized for making perishable eyeglasses [36].

Hybrids for Superconducting Systems: Superconducting power types of gear frequently utilize fiber-glass-based amalgams for cryogenic protections. Michael et al. [37] have revealed that composite cover of human hair (and a few other biological fibers) with epoxy pitch shows dielectric breakdown properties reasonable for protection in cryogenic frameworks. A significant decrease in production cost can be seen in cryogenic equipments when these composites are used in place of glass fiber composites used currently.

4 Additive to Construction Materials

Investigation shows that reinforcement of human hair fiber enhances the capacity of thermal insulation as well as the structural strength of the structures made up of clays [38, 39]. Albeit such earth-based developments are presently diminishing in country territories, they are picking up significance in feasible design or sustainable architecture. In hinterlands of Madhya Pradesh and Uttar Pradesh, India [40], Syria [41], European countries [42], and in Bangladesh [43], fibers of human hair and clay mixture together with other binders are employed in lining ovens, plastering walls of the house, making wheels, etc.

Because of high friction coefficient and great tensile strength, human hair fiber has been utilized in reinforcing earth-based constructions. The expansion of hair fundamentally decreases cracking and drags out the life of the hair reinforced structures. Human hair fiber reinforcement even reduces the cracks which are resulted due to the plastic shrinkage in cement mortar composite by approximately 92% [44]. Also this reinforcement boosts up the compressive strength of cement concrete and fly ash concrete by more than three times [45]. The exalted pressure-bearing structures like bridges and petroleum walls utilize the property of improved strength and enhanced fracture resilience of hair reinforced fly ash concrete and cement concrete. The most interesting fact is that any kind of human hair can be utilized in the reinforcement in building material. The versatile property of the Human hair fortified in black-top asphalt may create better remain on traffic stacking by a similar principal component of exchanging the high power forces conferred by the wheel burdens at the surface to bring down dimensions of the subgrade that can suit without misshaping. The investigation by Ganiron [10] demonstrates that on adding human hair and cement to black-top asphalt blend, an extraordinarily increment in the quality of the blend is observed and in this manner making it a decent material for the development of street asphalt. Including of both human hair and cement to black-top asphalt blend enhances the heap bearing limit of the blend.

5 Conclusion

This investigation has shown that fibers of human hair have a substantial number of employments in zones running from farming to drugs to engineering/building industries. Subsisting trade in natural fiber, "human hair," which has advanced around a portion of these utilizations over hundreds of years, gives a few critical lessons. Additionally, numerous new fields are being investigated in scientific research. Huge scale implementation of these utilizations, in any case, requires a few social, environmental, and financial contemplations. This trade has given jobs in numerous parts of the world however has likewise caused worries about the moral accumulation of hair, ecological and well-being security at the human hair processing businesses, and item security for shoppers. The aggregation of human hair fibers can be based on various diverse methods run by both fiscal and nonfiscal factors. In light of a foundational way to deal with the total esteem expansion ties from accumulation to utilization, the vast majority of these worries can be addressed. There is a vast scope for the growing use of human hair fiber as its present percent usage is exceptionally low. Because of its exceptional properties and universal accessibility, human hair fiber can contribute essentially in numerous basic regions of public significance, for example, agriculture, medication, building materials, and contamination control. In order to reduce the human hair waste and to solve the problems due to its accumulation as a waste, there is a need to develop standards and legislations along with building support schemes for several utilizations according to their market scope, entrepreneurial needs, and environmental scope. Alongside, the public must also be informed about its profitable properties and secure practices of aggregation and usage. Because of its high tensile strength, elastic and crack reducing properties, and many more, its exploitation in the field of engineering specifically as an additive to the building material will be very beneficial. Due to its excellent properties and universal availability, human hair fiber can contribute basically in various fundamental areas of open centrality, for instance, horticulture, medicine, building materials, and pollution control. With the help from different stakeholders, it is conceivable to create total use frameworks for human hair fiber, which will lessen solid waste and issues related to environment, generate noteworthy socioeconomic advantages for individuals, and diminish pressure on other fossil fuels and exhaustible materials.

References

1. Kumar S, Bhattacharyya JK, Vaidya AN, Chakrabarti T, Devotta S, Akolkar AB (2009) Assessment of the status of municipal solid waste management in metro cities, state capitals, class I cities, and class II towns in India: an insight. Waste Manag 29(2):883–895
2. Brebu M, Spiridon I (2011) Thermal degradation of keratin waste. J Anal Appl Pyrol 91(2):288–295
3. Khoathane MC, Vosster OC, Sadiku ER (2008) The effect of fiber loading on the mechanical and thermal characteristics of the composites. J Reinf Plast Compos 27:1533–1544

4. Wambua P, Ivens J, Verpoest I (2003) Natural fibre can replace glass in fiber reinforced plastic. J Compos Sci Technol 63:259–264
5. Saheb DN, Jog JP (1999) Natural fiber polymer composites: a review. J Adv Polym Technol 18:351–363
6. UN Comtrade, Import values are based on HS2007 codes 050100, 670300, and 670420 (2012)
7. Vijayalakshmi E (2003) Hair pollution hits Karnataka. Down to Earth. https://www.downtoearth.org.in/node/13180
8. Cohen M (2007) India's export of human hair to China is a booming business but it is also entangled in issues of respiratory diseases and child labor. The Standard. https://www.thestandard.com.hk/newsdetail.asp?ppcat=31&artid=50482&sid=14602467&contype=3
9. Choudhry S, Pandey B (2012) Mechanical behavior of polypropylene and human hair fibers and polypropylene reinforced polymeric composites. Int J Mech Ind Eng 2:118–121
10. Ganiron TU (2013) Influence of human hair fiber on strength of concrete. Int J Adv Sci Technol 55:53–66
11. Fueghelman M (1997) Mechanical properties and structure of alpha-keratin fibers: wool human hair and related fibers. University of New South Wales Press, Sydney
12. Cox JS (1977) The construction of an ancient Egyptian wig (c.1400 B.C.) in the british museum. J Egypt Archaeol 63:67–70 (1977)
13. Malik I (1998) Human hair trade: environmental hazards. Tech Rep. Vatavaran, New Delhi, India
14. Turner J (1992) Brushes: a handbook for artists and artisans. Design Books
15. Facknath S, Lalljee B (2005) Indigenous/traditional knowledge adopted in Mauritius for sustainable agriculture. In: Bandopadhyay A, Sundaram KV, Moni M, Kundu PS, Jha MM (eds) Sustainable agriculture: issues in production, management, agronomy, and ICT applications. Northern Books Center, New Delhi, India, pp 147–164
16. Scott JD, Townsend TW (1985) Methods used by selected Ohio growers to control damage by deer. Wildl Soc Bull 13(3):234–240
17. MOFF (2006) Package of organic practices from Maharashtra for cotton, rice, red gram, sugarcane and wheat, Maharashtra organic farming federation, Pune, India
18. Siddhi H (1997) Hair hinders rhinoceros beetle. Honey Bee 8(2):8
19. Deka MK, Bhuyan M, Hazarika LK (2006) Traditional pest management practices of Assam. Indian J Tradit Knowl 5(1):75–78
20. Zheljazkov VD (2005) Assessment of wool waste and hair waste as soil amendment and nutrient source. J Environ Qual 34(6):2310–2317
21. Subbiah P (1998) Human hair as fertilizer. Velanmai (Tamil Version of Honeybee)
22. Oudhia P (2010) Revised version of selected Botanical.com articles. Part 2. https://pankajoudhia.com/
23. Murthy ZVP, Kaushik G, Suratwala R (2004) Treatment of oily water with human hair as a medium: a preliminary study. Indian J Chem Technol 11(2):220–226
24. Mongabay, News & Inspiration from Nature's Frontline. https://news.mongabay.com/2006/08/feathers-human-hair-used-to-fight-oil-spill-in-philippines/
25. Talaie AR, Bagheri M, Ghotbinasab S, Talaie MR (2011) Evaluation of formaldehyde waste water adsorption on human hair. Health Syst Res 6(4):735–743
26. Banat FA, Al-Asheh S (2001) The use of human hair waste as a phenol biosorbent. Adsorpt Sci Technol 19(7):599–608
27. Tan TC, Chia CK, Teo CK (1985) Uptake of metal ions by chemically treated human hair. Water Res 19(2):157–162
28. Krishnan SS, Cancilla A, Jervis RE (1988) Waste water treatment for heavy metal toxins using plant and hair as adsorbents. Sci Total Environ 68(1):267–273
29. Robbins CR (2012) Chemical and physical behavior of human hair, 5th edn. Springer, Heidelberg, Germany
30. Brand E, Wiseman N (2008) Concise chinese materia medica, paradigm
31. Xie H, Kim MS, Chrisman C (2010) Herbs to stop bleeding. In: Xie H, Preast V (eds) Xie's Chinese veterinary herbology. Wiley-Blackwell, Ames, Iowa, USA

32. Forrest RD (1982) Early history of wound treatment. J R Soc Med 75(3):198–205
33. AnPing JinBoXin Garment Accessories Co. (2004) https://www.horse-hairfabric.com/horse-hair-fabric-horse-tail-lining/hairinterlining-fabric2.htm
34. Ghosh GK, Ghosh S (1995) Indian textiles: past and present. APH, New Delhi, India
35. Thompson RM (2010) Hair-based composite. US Patent 20100178842A1
36. Studio Swine (2012) https://www.studioswine.com/hairglasses
37. Michael DP, Harish S, Bensely A, Lal DM (2010) Insulation characteristics of sisal, human hair, coir, banana fiber composites at cryogenic temperatures. Polym Renew Resour 1(1):47–56
38. Jubran BA, Habali SM, Hamdan MAS, Zaid AIO (1988) Some mechanical and thermal properties of clay bricks for the Jordan valley region. Mater Struct 21(5):364–369
39. Pillai RR, Ramanathan A (2012) An innovative technique of improving the soil using human hair fibers. In: Proceedings of the 3rd international conference on construction in developing countries, pp 4–6, Bangkok, Thailand, July
40. Gupta CS (2008) Clay-traditional material for making handicrafts. Indian J Tradit Knowl 7(1):116–124
41. Heymans NM (2002) Archaeology, experimental archaeology and ethnoarchaeology on bread ovens in Syria. Civilizations 49:197–221
42. Allen P, May N (2003) Clay plasters. https://www.buildingconservation.com/articles/clayplaster/clayplaster.html
43. Abari, Rammed Earth Workshop (2010) https://abari.org/rammed-earth-workshop
44. Al-Darbi MM, Saeed NO, Ajijolaiya LO, Islam MR (2006) A novel oil well cementing technology using natural fibers. Pet Sci Technol 24(11):1267–1282
45. Akhtar JN, Ahmad S (2009) The effect of randomly oriented hair fiber on mechanical properties of fly-ash based hollow block for low height masonry structures. Asian J Civ Eng 10(2):221–228

Compressive and Flexural Behaviour of Glass Fibre Reinforced Blast Furnace Slag Based Material

Daipayan Mandal and B. Ram Rathan Lal

Abstract For sustainable development, conventional fill material required to be replaced by industrial by-products. In this experimental work, Blast Furnace (BF) slag was used as a base material to develop a new material which could replace the use of conventional fill material in civil engineering works. To achieve the aim the BF slag was blended with cement, glass fibre and water. The mix consists 10% cement by dry weight of BF slag and the optimum water content of BF slag. The mixture of slag-cement was reinforced with glass fibres in four different mix ratios of 0.3, 0.6, 0.9 and 1.2%. For each mixing ratio three different aspect ratios (AR) 385, 769 and 1154 of glass fibre were used. The glass fibre reinforced blast furnace slag based material was then moulded into cylinders and beams. The size of cylinder and beam specimen, used in the experimental study was 75 mm diameter 150 mm long and 50 × 50 × 400 mm respectively. The specimens were then cured for 7, 14 and 28 days curing under room temperature. The effect of mix ratios, aspect ratio and curing periods on density, initial tangent modulus, stress–strain relationship, compressive and flexural strength were studied and results were incorporated in the paper. The relationship between the mix ratio and both compressive, flexural strengths was found to be non-linear. The specimens reinforced with AR 1154 glass fibre yield higher compressive strength at 0.6% mix ratio, and flexural strength at 0.9% mix ratio.

Keywords Blast furnace slag · Mix ratio · Glass fibre

1 Introduction

From many past years, humans continuously exploit natural resources to meet their needs without taking much concern about future sustainability. Exploitation of natural resources and the urge for rapid growth in society leads to the scarcity

D. Mandal (✉)
Civil Engineering Department, K.I.T.S Ramtek, Nagpur, India
e-mail: m.daipayan@yahoo.com

B. Ram Rathan Lal
K.I.T.S Ramtek, Nagpur M441106, India

K. R. Reddy et al. (eds.), *Sustainable Environment and Infrastructure*, Lecture Notes in Civil Engineering 90, https://doi.org/10.1007/978-3-030-51354-2_14

of natural resources and increased the cost of raw materials. In the construction sector, the rapid construction growth raises the scarcity of raw material required for the construction. Sand and gravel are the most primary inputs and are most extracted material worldwide causing scarcity of these materials in construction [1]. On the other hand, the rapid industrialization in and around the world generated a huge amount of industrial by-products (e.g. slag, fly ash, bottom ash, marble, etc.). These industrial by-products have a threat to the environment since the industrial by-products were so harmful that they cause a serious health hazard to humans. The past reports of many researchers show that for the sustainable development, the conventional fill material (like sand, mushroom, etc.) used in civil engineering applications can be replaced by the industrial by-product [2]. Using the industrial by-product as a replacement of conventional material found to cut the cost of construction and saves the natural resource [3]. This idea motivated many researchers in the past to replace conventional fill material by industrial by-product such as fly ash, bottom ash, slag.

Blast Furnace Slag (BFS) is a by-product of the manufacture of iron by the reduction in a blast furnace. The slag is formed by the fusion of limestone (and/or dolomite) and other fluxes with the ash from coke and the siliceous and aluminous components of the iron ore burden. The slag floats on the surface of the molten iron and is separated when the furnace is tapped [4]. According to the Indian Bureau of mines reports in India 2.4 million tonnes BF slag was produced annually. It is an inorganic material contains mainly oxide of silicon, calcium, magnesium, iron and aluminium. According to the Indian Bureau of Mines, the BF slag can be divided into air-cooled, granulated and expanded blast furnace slag mainly depending on the method used for cooling the hot molten slag. Most of the BF slag produced in India used by the cement industries. Further consumption of BF slag was a matter of concern [5]. In 1994 Mantel [6] investigated the hydraulic activity of five different blast furnace slags with eight different Portland cement. The author found that the hydraulic activity of slag is mostly predominated by the particle size distribution and percentage of glass in slag.

Fibre reinforcement is an effective and reliable technique of improving the strength and stability of geotechnical materials. The technique is used in a variety of application from retaining structures and embankments to stabilization beneath footings and pavements. The fibre reinforcement technique was found to be effective for improving the mechanical property of cohesive and non-cohesive soil [7]. Randomly distributed fibres in compacted fine-grained soil results in greater strength and toughness. The fibre reinforcement is significant in both engineering practice and nature. A soil reinforced with natural fibres or plant roots contributes to the shear strength of soils and stability of natural slopes.

Commodity or general-purpose fibres are called E-glass. They are characterized by universal applicability, large sales volumes and low unit cost. They represent 99% of the commercial glass fibre market [8]. The alkali-resistant glass fibre in comparison to other types of glass fibre gives better durability with the Portland cement matrix [9]. Since ordinary Portland cement was used for binding the mix in the present study, an alkali-resistant type glass fibre was used for the reinforcement in the present study.

In the present study, blast furnace slag and cement were mixed together. By incorporating the glass fibre in different percentage (mix ratios) and aspect ratios in the mix the mechanical behaviour of mix under compressive and flexural load was studied. The variation in densities, compressive strength and flexural strength with respect to variation in mix ratios and aspect ratios was analyzed and results are incorporated. The pattern of failure, stress–strain curve and load–deflection curve was also studied and discussed.

2 Materials Characterization

2.1 Blast Furnace Slag

Blast furnace slag was procured from Bhilai steel plant (Bhilai, Chhattisgarh, India) and used as the primary material in the present study. The specific gravity of the BF slag used in the experimental study was 2.24. The proctor test result shows that the BF slag had maximum dry unit weight is 13.2 kN/m^3 and Optimum Moisture Content (OMC) 10%. The coefficient of uniformity is 1.56 and coefficient of curvature is 1.00 represents a poorly graded material.

2.2 Glass Fibre

The glass fibre used as reinforcement material in the present study was procured from Danish Doogaji Solution Ltd., Nagpur. Figure 1 shows the photograph of glass fibre. The physical properties were obtained from the manufacturer. It is an alkali-resistant type glass fibre. The specific gravity of fibre is 2.7; the filament diameter is 13 microns. The ratio of length to the diameter of fibre filament is termed as Aspect Ratio (AR) in the present study. Therefore, three different aspect ratios of glass fibre were chosen for the experiments which are 385, 769 and 1154.

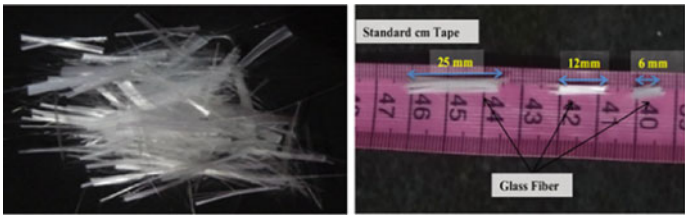

Fig. 1 Photograph of glass fibre

2.3 Cement

Ordinary Portland Cement (OPC) grade 53 was used for binding the BF slag and glass fibre together. The cement was procured from the local vendor at Ramtek, Nagpur. The bulk density of cement is 1429 kg/m^3.

3 Experimental Programme

3.1 Mix Ratios and Specimen Preparation

The ratio between the weight of glass fibre and weight of slag is termed as mix ratio and in the present study they are expressed in terms of percentage. The mix ratios considered were 0.3, 0.6, 0.9 and 1.2%. For each mix ratio three different aspect ratio of glass fibre 385, 769 and 1154 were used. The material calculation for mix ratio was based upon previous research works [10]. After weighing, the mixing of material is done by hand with the help of a trowel. First the slag and cement were blended together and then water was added equal to OMC (10%). Mixing technique was taken from Kaniraj and Gayathri [11]. After, mixing the materials together the mix was filled into metallic cylindrical moulds of 150 mm long and 75 mm diameter in three layers. Each layer is compacted well before filling the next layer. After that the moulds were left for 24 h at room temperature for setting. Thereafter, the 24 h the specimen were removed from the mould and put into the curing tank for 7, 14 and 28 days curing, respectively. For flexural test beams were moulded using the same procedure. The mould used for casting the 400 × 50 × 50 mm beam specimens. All total 78 cylindrical and 78 beam specimens were prepared for the test experiment and cured for 7, 14 and 28 days. Figure 2 shows the specimens and moulds used.

Fig. 2 Photograph of moulds and specimens used in the experiment

3.2 Experimental Procedure

To measure the compressive strength and flexural strength the test was performed after the concerned curing period. Two specimens for each curing period were taken out of curing tank and kept for air drying. Thereafter, the weight of the specimens was taken with the help of a digital weighing machine. Next, the loading frame of 50 kN capacities was prepared to perform the test. A load cell and Linearly Varying Displacement Transducer (LVDT) was calibrated and assembled with the load frame to measure the applied load and respective displacement of the specimen while testing. For compression test the strain rate was set to 0.12 mm/min and for flexural test strain was reduced to 0.012 mm/min since during experimentation it was found that the beam specimen fails quickly initially under higher strain rates. The test data were obtained from the experiment and results were incorporated. To check the reproducibility of specimens for each mix ratio, aspect ratio and curing period, two specimens were prepared and tested. The repeatability of the test results was encouraging with 3–6% deviation.

4 Results and Discussion

4.1 Failure Pattern

The failure pattern under compressive and flexural load was observed and interpreted in this section. Under compressive load it was observed that the specimen with lower fibre content tends to develop vertical cracks parallel to the direction of the applied load. Figure 3a, b show the failure pattern of specimens having low fibre content. When the fibre content was increased in the specimens than it was observed that cracks propagate in a transverse direction in the specimen. Figure 3c, d show the failure of the specimen with high fibre content. This type of failure shows increase in ductility in GFRBFS based material with the inclusion of fibre. Under flexural load

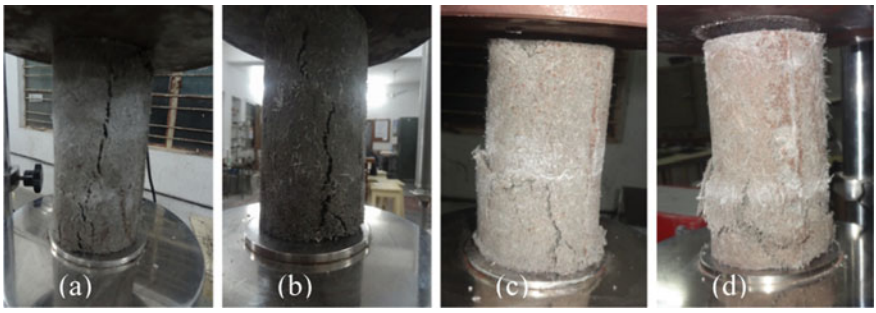

Fig. 3 Failure pattern of specimens under compressive loading

Fig. 4 Failure pattern of specimens of flexural loading

the beam specimen found to develop vertical crack parallel to the direction of the applied load. Figure 4 shows the broken beam specimens failed under flexural load. It was observed that in all specimens cracks develop at bottom of beam first then propagate to the upper side. The failure pattern satisfies the usual failure pattern of a beam under flexural.

4.2 Density Pattern

The density of GFRBFS based material found to affect by the mix ratio and aspect ratio of glass fibre. Figure 5 shows the variation of density with respect to mix ratios. The variation of density with mix ratio found to declining linearly with the increase in the mix ratio. Overall the density found to vary from 1321 to 1328 kg/m^3 depending upon the mix ratio and aspect ratio. The denthesity ranges 1700–1900 kg/m^3 for conventional fill material found by the previous researcher [12]. The density range of the newly developed material was found to be lower than the conventional fill material.

Fig. 5 Density variation with respect to mix ratio

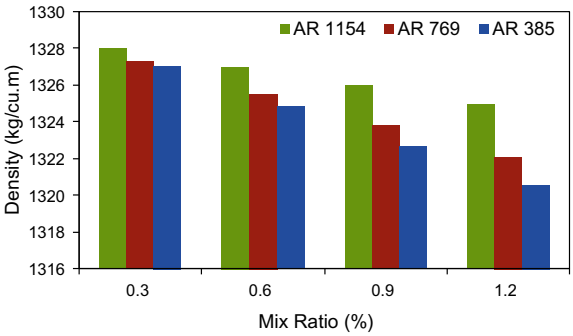

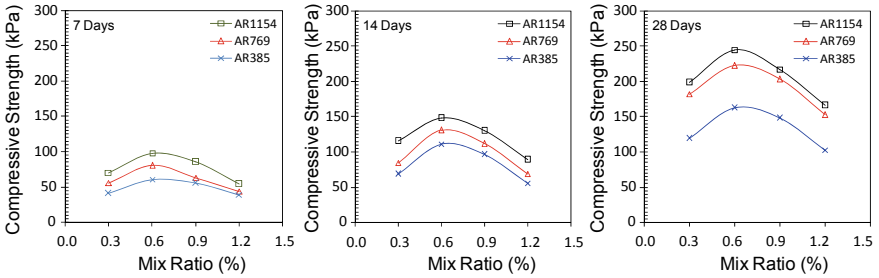

Fig. 6 Variation of compressive strength with respect to mix ratio for three different aspect ratios

4.3 Compressive Strength

The compressive strength was determined from the stress–strain curve. The peak stress from the stress–strain curve was taken as compressive strength. The unreinforced specimen shows failure at lower strain as compared to reinforced blast furnace slag. All the specimens fail in strain varying from 1.07 to 2.53%. Figure 6 shows the variation of compressive strength of GFRBFS based material for different mix ratios, aspect ratios and curing periods. The compressive strength varies non-linearly with respect to mix ratio. The maximum compressive strength was found for 0.6% mix ratios for all aspect ratio and curing periods. The compressive strength found to increase with an increase in aspect ratio. For all mix ratios and curing period the compressive strength found maximum for specimens reinforced with glass fibre aspect ratio AR1154 (15 mm long). Also, the compressive strength found to increase with the curing period for the mix ratios and aspect ratios.

4.4 Flexural Strength

Two specimens for each combination of variables were prepared and cured for 7, 14 and 28 days, respectively. Figure 7 shows the typical variation of flexural strength with mix ratios, aspect ratios and curing periods. The 28 days flexural strength of GFRBFS found to increase by 1.5–2.5 times the flexural strength of unreinforced BFS. The relationship between flexural strength and mix ratio was found to be non-linear. The flexural strength of GFRBFS material found to vary from 28.8 to 96.0 kPa.

4.5 Initial Tangent Modulus

The initial tangent modulus (E_i) was plotted and shown in Fig. 8. The initial tangent modulus is the slope of the line drawn from the origin of the stress–strain curve. The

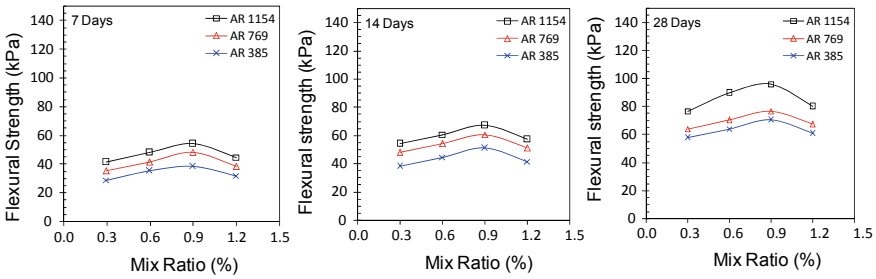

Fig. 7 Variation of flexural strength with respect to mix ratio for three different aspect ratios

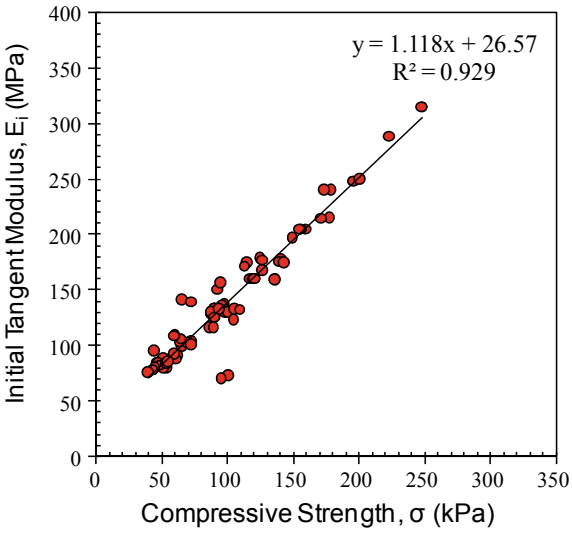

Fig. 8 Initial tangent modulus for compressive strength

initial tangent modulus is useful to determine the behaviour of the material under low stress. The compressive strength of GFRBFS found to increase with the initial tangent modulus. The value of E_i ranges from 67 to 315 MPa. This value is lower than the E_i (79–555 MPa) for lightweight fill material reported by Liu et al. [12].

4.6 Flexural Stiffness

The flexural stiffness (EI) is the measure of deformability under the given set of bending load. It depends on two factors first the elastic modulus (E) of the material and the moment of inertia (I), the function of cross-sectional geometry. The result of EI and the corresponding flexural strength was shown in Fig. 9. The relation between the EI and flexural strength fitted well in the linear trend line. With the

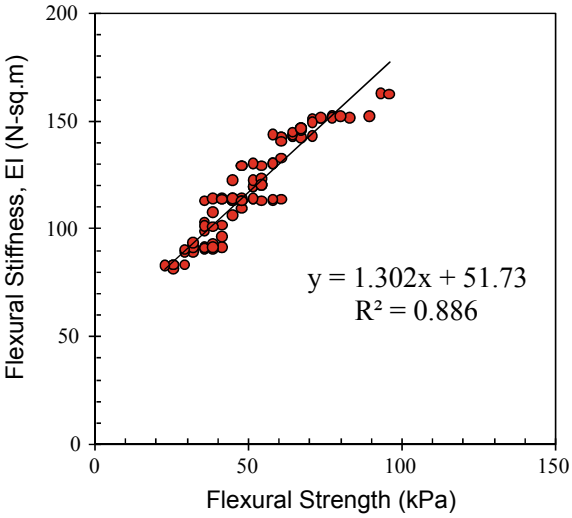

Fig. 9 Flexural stiffness for flexural strength

increase in flexural strength the EI found to increase. Since, the flexural strength and mix ratio vary non-linearly explained in the earlier discussion. The behaviour of EI and mix ratio relation also found to be non-linear. The EI found to vary from 80.73 to 162.5 N-m^2.

5 Conclusion

The density of GFRBFS based material decreases marginally with an increase in mix ratio for both compressive and flexural samples. For all the samples GFRBFS density was found on an average 26.4% less than the density of conventional sand.

The Compressive strength blast furnace slag and cement mix found to increase with glass fibre reinforcement. The compressive strength and mix ratio found to vary non-linearly. The maximum compressive strength found for mix ratio is 0.6%. The strength of unreinforced blast furnace slag increased from 1.14 to 2.72 times with the inclusion of fibre 0.3–1.2% after 28 days curing. Compressive strength found to increase with an increase in aspect ratio and also with curing period.

The flexural strength unreinforced BFS was found to increase by 1.5–2.5 times by inclusion of glass fibre. The relation between flexural strength and mix ratio found is non-linear and the maximum strength found for mix ratio is 0.9%. The relation between the flexural strength and aspect ratio found linear. The initial tangent modulus varies from 65 to 315 MPa. It increases with compressive strength. The flexural stiffness found to vary from 80.73 to 162.5 N-m^2.

References

1. Torres A, Brandt J, Lear K, Liu J (2017) A looming tragedy of the sand commons. J Sci 357(6355):970–971
2. Grober U (1999) The inventor of sustainability. Die Zeit 54(48):98
3. Bijen J (1996) Benefits of slag and fly ash. Constr Build Mater 10(5):309–314
4. Gutt W, Nixon PJ (1979) Use of waste materials in the construction industry. Mater Struct 12(4):255–306
5. IBM page. https://ibm.nic.in/writereaddata/files/08092017094435Slagironsteel2015.pdf. Last Accessed 04 Feb 2019
6. Mantel DG (1994) Investigation into the hydraulic activity of five granulated blast furnace slags with eight different portland cements. ACI Mater 91(5):471–477
7. Gray DH, Ohashi H (1983) Mechanics of fiber reinforcements in sand. ASCE Geotech Eng 109:335–353
8. Gupta PK (1988) Glass fibres for composite materials in Fibre reinforcements for composites materials. Chapter 2, Bunsell AR (Ed) Elsevier, Amsterdam
9. Majumdar AJ, Cottrell AH, Kelly A (1970) Glass fibre reinforced cement and gypsum products. In: Proceedings of the royal society of London. A. Mathematical and physical sciences. Royal Society, London, pp 69–78
10. Ram Rathan Lal B, Nawkhare SS (2016) Experimental study on plastic strips and EPS beads reinforced bottom ash based material. Geosyn Ground Eng 2(3):1–12
11. Kaniraj SR, Gayathri V (2003) Geotechnical behavior of fly ash mixed with randomly oriented fiber inclusions. Geotext Geomembr 21:123–149
12. Liu HL, Deng A, Chu J (2006) Effect of different mixing ratios of polystyrenes pre-puff beads and cement on the mechanical behavior of lightweight fills. Geotext Geomembr 24:331–338

Towards Enhancement of Water Sovereignty by Implementing the 'Constructed Wetland for Reuse' Technology in Gated Community

Rahul S. Sutar, B. Lekshmi, Dilip R. Ranade, Yogen J. Parikh, and Shyam R. Asolekar

Abstract The eco-centric wastewater treatment technology entitled 'CW4Reuse' (Constructed Wetland for Reuse) for treatment of domestic wastewaters employing horizontal subsurface-flow constructed wetland (CW) beds has been developed and demonstrated in India. A case study of treatment of wastewater using CW is presented in this paper based on our current research and demonstration of the developed technology. The CW4Reuse technology has been demonstrated in the Town of Katel, District of Buldhana, State of Maharashtra, India. The CW4Reuse technology has evidently shown the high treatment efficiency for the wastewater treatment in Katel. It is hoped that the CW4Reuse technology will potentially play a significant role to strengthen the country's agricultural economy on one hand and will also improve the rural and peri-urban sanitation on the other hand. Additionally, it will enhance the 'ecosystem restoration and rejuvenation' of urban as well as rural waterfronts in India. Moreover, the CW4Reuse technology is utilizing the skills of rural people—which will ultimately fortify the inclusive growth of the community.

Keywords Constructed wetland · Wastewater treatment · Water reuse

1 Introduction

In India, by and large, the discharge of large volumes of untreated or partially treated sewages into lakes, rivers, ponds, creeks and on the coast has led to their contamination. Additionally, there exists a huge difference between the generation and treatment of wastewaters. Hence, there is a huge potential for the application of natural treatment systems, in particular, constructed wetlands (CWs) in the developing economies such as Asia or Africa in general and India in particular due to their innate strength [1]. For the treatment of sewages and sullages from communities all over the Country, intensive efforts have been made by the Government of India during the past two

R. S. Sutar · B. Lekshmi · D. R. Ranade · Y. J. Parikh · S. R. Asolekar (✉)
Environmental Science and Engineering Department, Indian Institute of Technology Bombay, Powai, Mumbai, India
e-mail: asolekar@gmail.com

K. R. Reddy et al. (eds.), *Sustainable Environment and Infrastructure*, Lecture Notes in Civil Engineering 90, https://doi.org/10.1007/978-3-030-51354-2_15

decades. Therefore, the new recent sewage treatment plants in small rural and peri-urban communities have nominated CW as the 'favoured' technology for treatment of sewages and sullages due to their favourable economics (ecological and economic benefits) or their social acceptability among communities [1–7].

The CWs seem to be a sustainable alternative for the conventional sewage treatment technologies due to several advantages such as low power requirements, higher efficiency for the removal of pollutants, ease of operation and maintenance, simplicity of construction and eco-friendliness [8–12]. Furthermore, wetlands are known for their unique place in urban ecosystems by the virtue of the multiple functions performed by them including storage and purification of wastewater, transformation of nutrients and ecosystem biodiversity. In recent times, CWs are also being employed for treatment of wastewaters from urban and rural communities.

The 'CW4Reuse', an eco-centric wastewater treatment technology using horizontal subsurface-flow CW beds has been developed at Indian Institute of Technology Bombay (IIT Bombay), Mumbai for treatment of domestic wastewaters. CW4Reuse is proved to be eco-friendly, lower in energy consumption, easy to operate and manage. Owing to remarkably lower capital as well as operation and maintenance costs, it is gaining more acceptance in gated communities, academic campuses, peri-urban and rural habitats.

The objective of this paper is to evaluate the CW4Reuse technology for improving sanitation in gated communities as well as in rural and peri-urban settings in India. Furthermore, the performance of CW4Reuse technology for treatment of domestic wastewater in gated pilgrimage community in the Town of Katel has been evaluated.

2 Materials and Method

A horizontal subsurface constructed wetland (HSSF CW), based on CW4Reuse technology, has been employed for the treatment of domestic wastewater generated from a toilet block comprising of 22 toilets and 22 bath units as well as effluent from kitchen of the dining hall at the pilgrimage site (Sant Gulab Baba Sansthan) in the Town of Katel, District of Buldhana, State of Maharashtra, India as shown in Fig. 1 (latitude:21°03′17.2″N; longitude: 76°44′54.6″E). Reportedly, on a daily basis, about 500 devotees use the toilet block. However, this toilet block is used by nearly 6,000 devotees during the designated days for religious services and events.

The main reasons for the establishment of CW4Reuse technology at the Town of Katel were treatment of wastewater at this pilgrimage site and utilize the treated water for beneficial uses such as irrigation, gardening, etc. In septic tanks, the wastewater from toilets is first pre-treated (Fig. 2). Further, the overflow from these septic tanks is carried to the wetland bed having dimensions of 17 m length, 3 m width, 0.7 m depth, porosity of 0.5 and vegetation of *Canna indica* as shown in Fig. 3. The CW bed treats approximately 18 m^3/d wastewater on a daily basis. Furthermore, the additional treated water from the CW bed is deposited into the nearby river—where the untreated

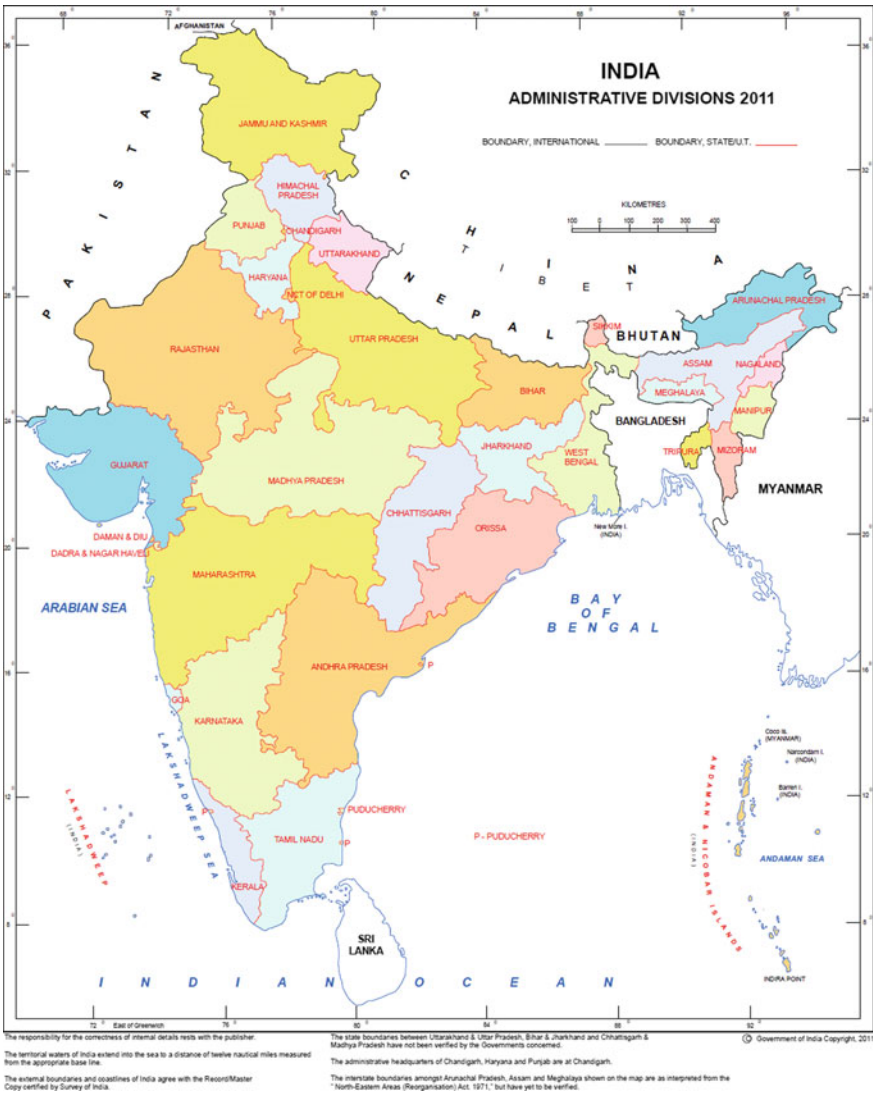

Fig. 1 The location of Katel in the State of Maharashtra in India. *Source* Administrative Atlas—2011, Government of India [13])

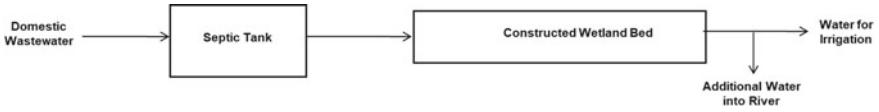

Fig. 2 The flow diagram of wastewater treatment in the Town of Katel, State of Maharashtra

Fig. 3 The CW bed in the Town of Katel, State of Maharashtra

water was discharged earlier in absence of CW-based wastewater treatment at the Town of Katel.

The samples were collected at the inlet as well as outlet of wetland bed. The collected samples were analyzed for chemical oxygen demand (COD), biochemical oxygen demand (BOD_5), pH and total suspended solids (TSS) at IIT Bombay laboratory in Mumbai using the methods and protocols given in the 'Standard Methods' [14].

3 Results and Discussion

This section provides brief information about the treatment performance of the CW bed as well as rural development and improvement in sanitation at the Town of Katel.

Table 1 Removal of pollutants in the CW bed at Katel Village

Sr. No.	Example	Inlet concentration* (mg/L)	Outlet concentration (mg/L)
1	Chemical oxygen demand	131*	45
2	Biochemical oxygen demand	60*	17
3	Total suspended solids	62*	20
4	pH	7.5*	7.9

*Inlet to CW bed was the overflow from septic tank

3.1 Treatment Performance of CW4Ruese Technology at the Town of Katel

The bathroom, toilet and kitchen water generated by the Katel Sansthan is treated in the CW along the nearby riverfront. Figure 3 depicts the CW bed in front of toilet block at the Katel. The treatment performance of the CW4Reuse technology at the Katel is shown in Table 1.

From the results, it can be seen that the removal of COD and BOD were 66% and 72%, respectively—which shows significant treatment efficiency of the CW bed. Furthermore, the first order rate constants for removal of COD and BOD were 0.044 h^{-1} and 0.052 h^{-1}, respectively [2]. The results are excellent in comparison with Indian standards for discharge of treated water into the inland surface water. The prime user of the treated water from the CW-based treatment plant is the agricultural irrigation and garden at the guesthouse of Sansthan.

3.2 Rural Development and Improvement in Sanitation

The CW4Reuse technology (Fig. 4) is playing a very significant role for the improvisation of the sanitation in the rural areas such as Katel. The treated wastewater from CW-based treatment plant is reused by local farmers for agricultural and gardening purposes which is another main aspect of CW4Reuse technology. Additionally, the job opportunities are created for the local people who are easily managing the operation and maintenance of CW-based treatment plant as no highly experienced specialists' or mechanized equipment's are required as compared to the conventional wastewater treatment technologies.

As the wastewater from the Sansthan is treated in CW-based treatment plant, there is no discharge of wastewater into the nearby river which will significantly minimize the river pollution. It is argued that the foul odour and mosquito breeding has been reduced to significant extent at the CW-site in Katel. Thus, treated water can be reused and water quality can be enhanced along with improvement of sanitation with the help of CW4Reuse technology. In addition, for composting and energy, the

Fig. 4 The reuse of treated water in the Town of Katel. *Source* Google Maps, India [15])

vegetative biomass produced from the wetland bed could be gainfully utilized by the rural communities. It is clear that the employment of CW4Reuse technology in Katel can fulfil all social, economic and environmental goals through several above mentioned benefits.

4 Conclusions

For rural and peri-urban communities, the CW-based eco-centric technologies can be employed for the treatment of wastewaters in India. The recyclable and reusable treated water could be utilized for valuable uses in the rural communities for agricultural irrigation and irrigation in urban landscapes. In addition, the inclusive growth of the community has been strengthened owing to the CW4Reuse technology which is utilizing the skill-set of rural people for operation as well as maintenance of CW-based wastewater treatment plant. For the implementation of CW4Reuse technology, there are several opportunities in India where such eco-centric technologies could be executed in real-life by co-operative societies or municipal councils and the recyclable and reusable treated water will be utilized for valuable uses in the respective rural communities. Additionally, this intervention is protecting the drinking water resource for downstream communities by preventing the discharge of untreated wastewater into the river. Thus, for the rural and peri-urban communities

in India, the CW4Reuse technology is of greater importance from the spectacles of community ownership and also, the social benefit through applications of technology.

Acknowledgements The authors acknowledge the co-funding from Rajiv Gandhi Science and Technology Commission, Government of Maharashtra, Earthwatch Institute India Trust and Indian Institute of Technology Bombay for this work.

References

1. Wintgens T, Nattorp A, Elango L, Asolekar SR (2016) Natural water treatment systems for safe and sustainable water supply in the indian context. Saph Pani. IWA Publishing, Alliance House, 12 Caxton Street, London SW1H 0QS, UK
2. Arceivala SJ, Asolekar SR (2006) Wastewater treatment for pollution control and reuse, 3rd edn. McGraw Hill Education India Pvt. Ltd., New Delhi
3. Asolekar SR (2013) Report on experiences with constructed wetlands and techno-economic evaluation. Saph Pani: Enhancement of natural water systems and treatment methods for safe and sustainable water supply in India. Report No. D3.1. Project supported by the European Commission within the seventh framework programme grant agreement No. 282911
4. Kumar D, Asolekar SR, Sharma SK (2015) Post-treatment and reuse of secondary effluents using natural treatment systems: the Indian practices. Environ Monit Assess 187:612
5. Kumar D (2016) Development of strategies for enhancing recycling potential of wastewater through combination of mechanized and natural treatment systems. PhD Thesis, CESE, IIT Bombay
6. Sutar RS, Lekshmi B, Kamble KA, Asolekar SR (2018) Rate constants for the removal of pollutants in wetlands: a mini-review. Desalin Water Treat 122:50–56
7. Sutar RS, Kumar D, Kamble KA, Kumar D, Parikh Y, Asolekar SR (2019) Significance of constructed wetlands for enhancing reuse of treated sewages in rural India. In: GHOSH SK (ed) ICONSWM 2016, waste management and resource efficiency. Springer Nature Singapore Pte Ltd., Singapore, pp 1221–1229
8. Gouriveau F (2009) Constructed farm wetlands (CFWs) designed for remediation of farmyard runoff: an evaluation of their water treatment efficiency, ecological value, costs and benefits. The University of Edinburgh
9. Vymazal J (2008) Constructed wetlands for wastewater treatment: a review. In: Sengupta M, Dalwani R (eds) The 12th world lake conference, proceedings of Taal2007, pp 965–980
10. Vymazal J (2011) Constructed wetlands for wastewater treatment: five decades of experience. Environ Sci Technol 45:61–69
11. Borkar RP, Mahatme PS (2011) Wastewater treatment with vertical flow constructed wetland. Int J Environ Sci 2:590–603
12. Sivaraman C, Arulazhagan P, Walther D, Vasudevan N (2011) Feasibility studies for reuse of constructed wetlands treating simulated nickel containing groundwater. Univers J Environ Res Technol 1:293–300
13. Administrative Atlas, Government of India (2011). https://censusindia.gov.in/2011census/maps/administrative_maps/admmaps2011.html. Last Accessed 15 Feb 2019
14. Standard Methods (for the examination of water and wastewater), 21st edn. American Public Health Association, 800 I Street, NW, Washington, DC 20001–3710 (2005)
15. Google Maps. Last Accessed 15 Feb 2019

Removal of Methylene Blue from Aqueous Solution: An Approach of Environmental Friendly Activated Carbon

M. C. Jayaprakash, M. Chaitra, Prarthana Rai, and D. Venkat Reddy

Abstract Methylene blue (MB) dye was adsorbed on an adsorbent prepared from cashew nut shell. A batch adsorption study was carried out with variable adsorbent amount, initial dye concentration and contact time. Studies showed that as the contact time increases relatively there will be an increase in the removal of methylene blue from the aqueous solution. There was also a comparative increase in the removal of dye with the increase in dosage of adsorbent. As the concentration of MB dye increased the percentage of removal of MB from the aqueous solution decreased for a given particular dosage. The results indicate that cashew nut shell activated carbon could be employed as a low-cost alternative to commercial activated carbon in the removal of dyes from wastewater. This work offers an economic incentive to the industrial practice for waste management and eco-friendly approach for removal of toxic dyes from textile waste water.

Keywords Methylene blue · Cashew nut shell · Activated carbon

1 Introduction

Over the last few decades, society has also become increasingly sensitive towards the protection of the environment. Due to this problem, mankind now-a-days is concerned about the potential adverse effects of the chemical industry on the environment, although the response in some parts of the world has been much faster and more intense than in others. The colour manufacturing industry represents a relatively small part of the overall chemical industry. Dyes and pigments are highly

M. C. Jayaprakash (✉) · M. Chaitra · P. Rai
Department of Civil Engineering, Mangalore Institute of Technology and Engineering, Badaga Mijar, Moodabidri 574225, India
e-mail: jayaprakash@mite.ac.in

D. Venkat Reddy
National Institute of Technology Karnataka (NITK), Mangalore, India

L&T Constructions, Chennai, India

K. R. Reddy et al. (eds.), *Sustainable Environment and Infrastructure*, Lecture Notes in Civil Engineering 90, https://doi.org/10.1007/978-3-030-51354-2_16

visible material. Thus even minor release into the environment may cause the appearance of colour, for example in open waters, which attracts the critical attention of public and local authorities.

There is thus the requirement on industry to minimise environmental release of colour, even in cases where a small but visible release might be considered as toxicologically rather innocuous. A major source of release of colour into the environment is associated with the incomplete exhaustion of dyes onto textile fibre from an aqueous dyeing process and the need to reduce the amount of residual dye in textile effluent has thus become a major concern in recent years. An alternative approach to addressing the problem of colour in textile dyeing effluent has involved the development of effluent treatment methods to remove colour. These methods inevitably add to the cost of the overall process and some present the complication associated with the possible toxicity of degraded products.

To comply with discharge standards, most industries and institutions practice an elaborate effluent and sewage treatment protocol which affects the overall economy of the plant. A conventional continuous flow process requires multiple structures and extensive pumping and piping systems. The need of the hour is a suitable technology for efficient and cost-effective tertiary treatment for recycling or reusing at least a reasonable quantity of the wastewater produced in the plant.

Biological treatment of organic waste using activated sludge is a proven technology used in wastewater treatment facilities. Conventional aerobic and anaerobic treatment processes have been used to reduce the organic carbon concentration of liquid, but these processes have not been successful in reducing both carbon and nitrogen at a reasonable cost. The effluent from primary treatment of wastewater will still have some odour and turbidity and is usually removed by chemical coagulants. However traces of these coagulants will be retained in effluent after coagulation and need to be removed separately. Hence removal of traces of coagulants is an additional cost.

The main advantage of proposed treatment system is the minimization of investment and operational costs as compared to the use of different conventional set ups as followed in tertiary wastewater and colour removal treatments. Using the result of this study, an abundantly available waste by-product of several local industries can be turned into a low-cost activated carbon on large scales efficiently. The carbon can be used for better and more efficient wastewater and colour removal treatment and simultaneously reduce costs. **This work offers an economic incentive to the industrial practice for waste management and eco-friendly approach for removal of toxic dyes from textile waste water in a sustainable manner**.

2 Objectives

- To develop a low-cost activated carbon from the cashew nut shell.
- Removal of methylene blue by adsorbing it onto the prepared cashew nut shell activated carbon.

- Treating the secondary waste water from the cashew nut shell activated carbon by adsorption.

3 Methodology

3.1 Preparation of Activated Carbon

- Preparation of activated carbon from the cashew nut shell.
- Methylene Blue solution was prepared by varying the concentration i.e., 5 ppm, 10 ppm, 20 ppm, 30 ppm, 40 ppm and 50 ppm by using distilled water.
- Conducting the adsorption process by adding cashew nut shell activated carbon in the methylene blue solution.
- Conducting trials by varying the concentration of methylene blue solution, agitation time, sieve size of activated carbon and adsorbent dosage.
- Treating the secondary waste water by the prepared cashew nut shell activated carbon and checking for variation in pH, turbidity, BOD, COD and alkalinity.

The Activated carbon (AC) taken for the experiment are of size 150 microns, 90 microns and 75 microns.

4 Results and Discussion

4.1 SEM Results of Cashew Nut Shell Activated Carbon

To identify the characteristic morphology of samples SEM cashew nut shell charcoal was determined. The SEM images clearly show that pores of different shapes and size are present on the surface of the samples (see Figs. 1, 2 and 3 for 75, 90 and 150

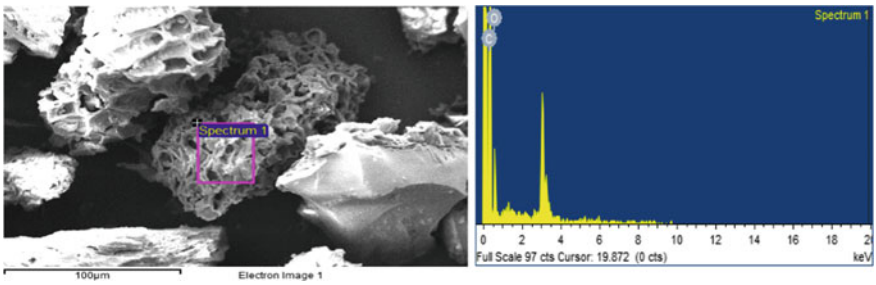

Fig. 1 SEM spectrum of 75 microns sieve sized activated carbon

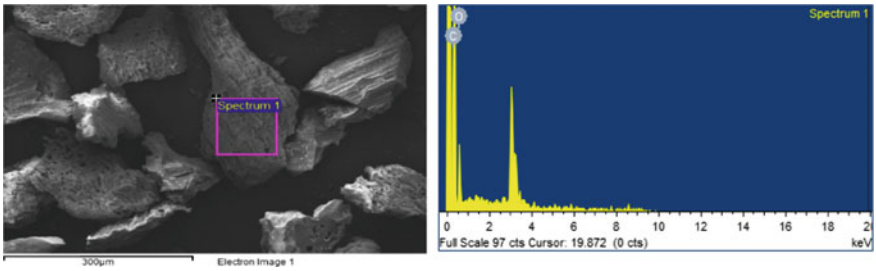

Fig. 2 SEM spectrum of 90 microns sieve sized activated carbon

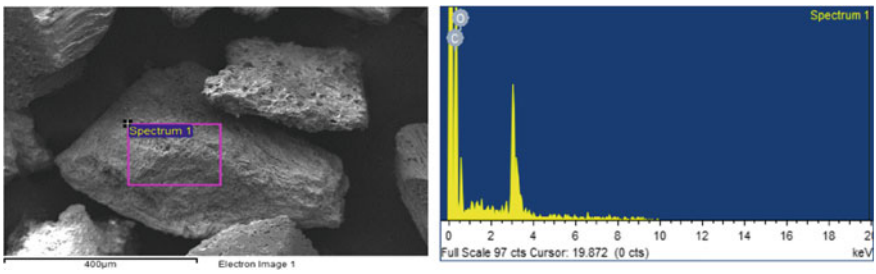

Fig. 3 SEM spectrum of 150 microns sieve sized activated carbon

Table 1 Elemental composition of cashew nut charcoal sample of 75 microns by SEM

Element	Weight %	Atomic %
$CaCO_3$ (C) K	77.63	82.21
SiO_2 (O) K	22.37	17.79

micron size). SEM spectra shows that cashew nut charcoal composed of Calcium, Oxygen and Carbon elements (Tables 1, 2 and 3).

Table 2 Elemental composition of cashew nut charcoal sample of 90 microns by SEM

Element	Weight %	Atomic %
$CaCO_3$ (C) K	77.94	82.47
SiO_2 (O) K	22.06	17.53

Table 3 Elemental Composition of cashew nut charcoal sample of 150 microns by SEM

Element	Weight %	Atomic %
$CaCO_3$ (C) K	76.80	81.51
SiO_2 (O) K	23.20	18.49

4.2 Removal of Methylene Blue from Aqueous Solution

The result shows varying concentration of MB with different particle size of carbon and same concentration of MB with different weight of carbon, the 75 micron particle size of carbon showed 96.20% (Table 4 and Fig. 4 at 5 ppm initial concentration with weight of carbon 0.5 g in 2 h agitation time) of maximum colour recovery, whereas the 75 micron particle size of carbon showed 96.75% (Table 5 and Fig. 5 at 40 ppm

Table 4 Varying concentration of MB with different particle size of carbon

Particle Size of Adsorbent (Microns)	Conc. (ppm)	Wt. of Carbon in grams	Conc. Obtained in (ppm): 1 h Agitation	Conc. Obtained in (ppm): 2 h Agitation	% of recovery (1 h Agitation)	% of recovery (2 h Agitation)
75	5	0.5	0.35	0.19	93	96.20
	10	0.5	1.17	0.85	88.3	91.50
	20	0.5	9.48	7.2	52.6	64
	30	0.5	19.7	19.7	34.33	34.33
	40	0.5	36.1	35.8	9.75	10.50
	50	0.5	47.7	47.7	4.6	4.6
90	5	0.5	0.73	0.34	85.4	93.2
	10	0.5	2.38	1.9	76.2	81
	20	0.5	10.85	9.76	45.75	51.2
	30	0.5	25	23.2	16.67	22.67
	40	0.5	36.6	36	8.5	10
	50	0.5	48	47.8	4	4.4
150	5	0.5	1.4	0.62	72	87.6
	10	0.5	4.67	3.33	53.3	66.7
	20	0.5	13.86	13.39	30.7	33.05
	30	0.5	28.2	26.8	6	10.67
	40	0.5	38.3	37.8	4.25	5.5
	50	0.5	48.2	48	3.6	4

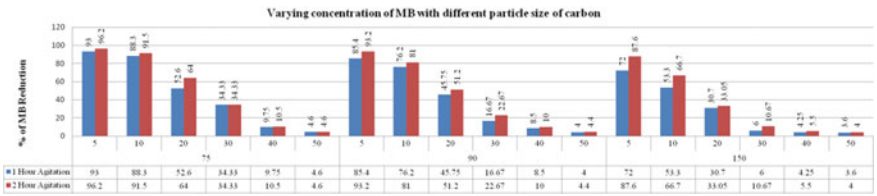

Fig. 4 Graph showing removal percentage of MB with different particle size of 75, 90 and 150 micron and keeping weight of carbon 0.5 g

Table 5 Same concentration of MB with different weight of carbon

Particle Size of Adsorbent (Microns)	Conc. (ppm)	Wt. of Carbon in grams	Conc. Obtained in (ppm): 1 h Agitation	Conc. Obtained in (ppm): 2 h Agitation	% of recovery (1 h. Agitation)	% of recovery (2 h Agitation)
75	40	0.5	36.1	35.8	9.75	10.50
		1	2.1	3.2	94.75	92
		3	1.6	1.8	96	95.50
		5	1.3	1.7	96.75	95.75
90	40	0.5	36.6	36	8.50	10
		1	16.6	15.3	58.50	61.75
		3	2.5	2.2	93.75	94.50
		5	2.1	2.1	94.75	94.75
150	40	0.5	38.3	37.8	4.25	5.50
		1	36.4	33.3	9	16.75
		3	10.7	7.2	73.25	82
		5	4.8	3.3	88	91.75

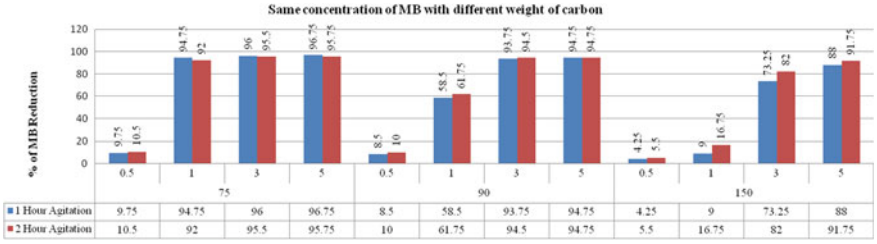

Fig. 5 Graph showing removal percentage of MB with different weight of carbon and keeping concentration 40 ppm of MB

initial concentration with weight of carbon 5 g in 1 h agitation time) compare to 90 and 150 micron size. Hence, the decreasing particle size will increase removal of methylene blue dye from the aqueous solution and decreasing particle size will have more surface area for the effective adsorption with short duration of agitation.

5 Conclusions

The activated carbon prepared by using cashew nut shell charcoal is very efficient to remove methylene blue dye from aqueous solution since the carbon content in the cashew nut activated carbon is high as shown in the SEM results. It is also observed that as the sieve size of the activated carbon decreased and as the agitation time

increased the removal of methylene blue dye from the aqueous solution was more. The quality of the carbon obtained will depend on the quality of the raw material in general, and its residual oil content in particular. This obtained result can show considerable promise of cashew nut shell charcoal as a raw material for activated carbon.

References

1. Lubi MC, Thachil ET (2012) Cashew nut shell liquid (CNSL)- a versatile monomer for polymer synthesis" by (2012)
2. Senthi Kumar P, Ramalingam S, Senthamarai C, Niranjanaa M, Vijayalakshmi P, Sivanesam S (2010) Adsorption of dye from aqueous solution by cashew nut shell: studies on equilibrium isotherm, kinetics and thermodynamics of interactions
3. Senthil Kumar P, Ramalingam S, Sathishkumar K (2010) Removal of methylene blue dye from aqueous solution by activated carbon prepared from cashew nut shell as a new low-cost adsorbent
4. Mane RS, Bhusari VN (2013) Removal of colour (dyes) from textile effluent by adsorption using orange and banana peel. Int J Eng Res Appl Chem 2013. article ID 614083, 9 pages
5. Sanger SH, Mohod AG, Khandetode YP, Shrirame HY, Deshmukh SS (2011) Study of carbonization for cashew nut shell. Res J Chem Sci 1(2):43–55
6. Ramalingam S, Senthil Kumar P (2015) Novel adsorbent from agricultural waste (cashew NUT shell) for methylene blue dye removal: Optimization by response surface methodology
7. Syafalni S et al (2012) Treatment of dye wastewater using granular activated carbon and zeolite filter. Modern Appl Sci 6(2)

An Investigation of Optimal Clay Brick Properties for Evaporative Cooling

Nida Noorani Ikiz and Mehmet Caputcu

Abstract The overuse of electricity, which is an indispensable component of our daily lives, is causing the rapid depletion of fossil fuel resources and emission of greenhouse gasses to the atmosphere. It is known that 40% of the electricity consumption of households and industry is due to the use of cooling systems especially during summer conditions. The aim of this study is to develop a natural refrigeration technique that can save a substantial amount of energy. It is hypothesized that with the use of baked clay structures (referred to as ceramic), a natural evaporative cooling technique can be developed, by which the temperature of the surroundings can be dropped by 6 to 10 °C. This assumption was tested with the help of models. The clay plates with grain sizes 0.700 and 0.250 mm, baked at different temperatures (750, 875, and 1000 °C) were prepared and tested for vertical/horizontal capillarity and falling head permeability. Afterwards, their evaporative cooling effects were compared. Samples baked at 1000 °C and grain size 0.700 mm gave the largest drop in temperature (ΔT ~ 14 °C when the air temperatures were between 30 and 40 °C and humidity percentages were between 35–40%). Based on these results, 0.700 mm particle-sized clay tiles that were baked at 1000 °C, which also demonstrated satisfactory levels of capillarity and permeability, were chosen as the structural material for the future prototype tests.

Keywords Clay · Terra cotta · Natural refrigeration · Renewable energy

N. Noorani Ikiz (✉)
Environmental Engineer, Ph.D., P.E., Suar Engineering and Trade Limited Company, 4. Sanayi Sitesi 129/16 Sokak Bornova, Izmir, Turkey
e-mail: nidanoorani@gmail.com

M. Caputcu
Civil Engineer, Ph.D., Independent Researcher, Turgutreis, Bodrum, Turkey

K. R. Reddy et al. (eds.), *Sustainable Environment and Infrastructure*, Lecture Notes in Civil Engineering 90, https://doi.org/10.1007/978-3-030-51354-2_17

1 Introduction

Earth is warming up due to the adverse effects of technologies introduced in the last century. Excessive use of fossil fuels so far and the subsequent depletion of the available sources create scarcity for future generations. In the same context, environmental degradation and pollution are undeniable threats to humanity. Solution to these problems partly lies in cutting the emission of greenhouse gases.

Air conditioning systems use significant amount of energy to operate, which contributes to the greenhouse gas emissions. It is reported that approximately 50% of annual power demand is due to air conditioning systems [1]. Therefore, the development of energy efficient cooling technologies is of prime importance.

The term passive cooling refers to the cooling of an object or space without the consumption of external power. Evaporative cooling, which is considered as a method of passive cooling, can be achieved by various methods. These methods are classified as direct and indirect techniques based on whether the cooled space is exposed to the engendered humidity during the cooling process [2, 3].

Green roof is an indirect option of evaporative cooling where a layer of vegetation covers the top of a building. A green roof can keep inside of a structure around 25 °C on a warm summer day, whereas a comparable structure with concrete ceiling would measure around 40 °C inside [4]. This kind of a layer can reduce the heat flux into the building through roof slab by 50%, by virtue of a decrease in the surface temperature from about 60 to 30 °C [5]. It also yields an annual energy savings of up to 37% on insulated buildings by means of reduction both in solar heating during the summer and in chilling during the winter [6].

Green roofs (or vegetation) are not the only method applied on roofs for cooling. A roof covering with rock fill material and a waterbed, which is named by Cheikh and Bouchair as "evapo-reflective roof," is aimed to increase the reflection of solar radiation by using a special coating and to cool the building by evaporation [7]. Their study on a model building reports an inside temperature 10 °C cooler than the ambient air on a summer day.

Other applications of passive cooling where water and evaporation are utilized include roof ponds with water flow (1.6 °C temperature drop) [8], a ventilated roof pond with shallow pools and a reflective cover (8–13 °C temperature drop) [9], fan-pad systems (4–5 °C temperature drop) [10], water sprinkling onto roofs (8 °C temperature drop and energy savings of up to 13%) [11], and a closed evaporative cooling unit which utilizes a paraffin core with latent heat storage capability in addition to water sprinklers (13 °C temperature drop) [12].

Effectiveness of evaporative cooling systems depends on a number of factors. These factors include the method of evaporation, the system setup and design of structural elements, method of water supply, properties of construction materials (with special consideration given to capillarity and permeability), the hygrothermal behavior of the structural elements, involvement of electricity consumption, and potential side effects and externalities.

Method of water supply can have a significant role in the effectivity of cooling. Feeding the layer, where evaporation and cooling take place, with water from its bottom or rear surface by capillary attraction is one way, whereas sprinkling water to the evaporation surface is another [13]. Running a water flow cycle [8] and storing static water mass [9] on the roof are some other alternatives. On the other hand, it is not easy to indicate which of these supply methods is superior to others with respect to cooling performance, due to the variation in factors explained below.

Efficiency of evaporative cooling with construction material properties has been evaluated by researchers from different disciplines. As a means of mitigating the heat island effect in urban areas, permeable pavements demonstrate a higher cooling performance with higher void ratio and permeability [13]. Characteristics of mortar used in masonry walls can yield a warmer or cooler wall due to cooling effect of dampness on its surface. Variables like thickness of these walls, water absorption from the foundation, height of rising damp front (capillary rise), and evaporation rate are all interrelated [14].

The trade-off between capillarity and permeability of a construction material must be carefully taken into consideration, and these factors must be optimized for a more effective evaporative cooling behavior [13]. Furthermore, the extent of capillary rise in structural elements can demonstrate a dynamically changing behavior. The leaching of dissolved lime off a structural component, such as mortar and brick, can consequently cause an increase in its permeability [15]. In contrast, clogging of pores due to calcification after repeated exposure to wetting and drying can be expected in some porous materials [16–19]. The distribution of micro-scale pore size in construction materials should also be taken into consideration in the diffusion of fluids with chemical content [20].

In addition to material properties, an understanding of hygrothermal behavior of structural elements is also necessary to maximize the performance of evaporative cooling systems. A study, where moisture content variation on facades of buildings was inspected by means of infrared thermography technique, revealed that evaporative cooling helps with the detection of the surface temperatures [21]. Quantification of superficial moisture was investigated in another infrared thermography study with consideration for the balance between wetting and drying of structural elements. It was seen that superficial evaporation facilitates the recognition of "wet" and "dry" areas and enables the evaluation of a construction material's approximate drying time. The method promises to enhance the development of composite thermal insulation materials for the external surfaces of buildings [22].

Evaporation phenomenon is affected by factors such as ambient temperature, humidity, air movement, and structure's surface condition (e.g., painted or not) [14]. The amount of water that evaporates off the surface of a structural element is strongly tied with the amount of water absorbed into it from a source [15]. Furthermore, the amount of vaporization is also affected by some micro interactions of water and vapor with their surroundings, such as the resistance to the separation of water from the saturated surface (surface resistance) and the resistance to transporting the pore moisture to the ambient air (aerodynamic resistance), which together make up the bulk evaporative resistance [23, 24]. A study of concrete shrinkage due to

rapid evaporation in Arabian Gulf Region reveals that the rate of water loss can be reduced by about 50% (3 kg/m^2/h) when concrete's surface temperature is cooler by 10 °C, while solar radiation and air-concrete interaction are two other variables to be controlled in the process [25].

From an energy savings standpoint, the degree of "passiveness" of an evaporative cooling system, that is whether it requires the consumption of electricity to run [26] and how much, is another critical factor to take into consideration. A system that can be sustained with the least energy supply or none can be considered as the most successful passive evaporative cooling system.

Passive evaporative cooling techniques are promising to mitigate excessive environmental heating in urban areas, and have been recognized as part of eco-efficient design options [26, 27]. On the other hand, the humidity caused by evaporative cooling systems brings along a risk of respiratory illnesses if deployed in the same area where humans live and breathe, such as in the case of direct evaporative coolers [28]. However, this matter can be addressed by positioning the cooling unit outside of living areas and transporting chilled fluid (air) into or through the structure or area to be cooled, as seen in the indirect evaporative cooling systems named bio skin [29, 30]. There are also efforts to combine direct and indirect techniques within one system to overcome the humidity issue of evaporative coolers, by integration of a desiccant-based dehumidifier to the system [31].

In a number of studies, clay-based structural elements of different forms have been utilized for the evaporation and cooling processes. These elements have been experimented with a variety of setups to investigate their effectiveness in evaporative cooling. Baked clay or concrete walls with pores where water is absorbed in or can seep through are considered as means of evaporative cooling [32]. Non-glazed baked clay or ceramic pots and water towers are considered in storage of potable water in hot and humid climates [33]. Porous ceramic pipes vertically placed to soak-up water and evaporate it, for use as a "cooling wall" in a variety of outdoor facilities, yield about 2 °C reduction in ambient temperature [34, 35]. The implementation of evaporative pipes on a modern building demonstrates a 10 °C drop on the surface of evaporative elements [29].

The summary above shows that the performance of an evaporative cooling process can be affected by numerous factors and the properties of the construction materials used is an important one. Being highly available as a natural material option in most parts of the world, clay appears to have an outstanding potential for use in evaporative cooling systems. Furthermore, baked clay containers are well known to have been used for long in cooling of water.

The present research was conducted in a region (Menemen/IZMIR) where clay pottery production is popular. Clay pots have the advantage of keeping its interior cool by enabling evaporation through its permeable structure. This property of clay inspired the researchers of this study to develop a natural refrigeration technique by using baked clay structures. So, in order to obtain a structural element with evaporative cooling property, parametric tests of clay brick samples were conducted for permeability, capillarity, and cooling effectiveness.

2 Methodology

There are three steps in the present study. These are:

a. Permeability Tests
b. Horizontal and Vertical Capillarity Tests
c. Cooling Effect Tests.

These tests were conducted in the Geotechnical Laboratory of the Civil Engineering Department of Gediz University. The tests are explained in detail below.

2.1 Permeability Tests

A permeability test was conducted to measure the ability of the specimen to transfer fluids. Falling Head Permeability Test was performed by following the procedure of ASTM Designation 5856-95. For this test, six different samples were ordered from Menemen Pottery Association, as shown in Table 1.

Table 1 Characteristics of tested clay structures

	Baking temperature (°C)	Sieve size/clay grain size (mm)	Diameter/thickness (mm)
Specimen Type 1	750	0.700	95/10
Specimen Type 2	750	0.250	
Specimen Type 3	875	0.700	
Specimen Type 4	875	0.250	
Specimen Type 5	1000	0.700	
Specimen Type 6	1000	0.250	

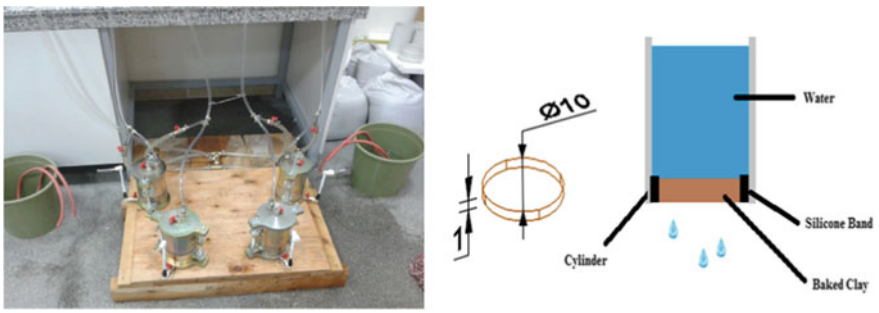

Fig. 1 OCTOPUS experiment set and the schematic diagram of falling head permeability test

For the permeability tests, a system was developed by a professional crew, and the system was named OCTOPUS (Fig. 1). It had four different channels which supply water to four identical permeability devices.

When the falling head permeability test was conducted on the OCTOPUS test set for each and every baking temperature and grain size (1000 °C coarse and fine, 875 °C coarse and fine, and 750 °C coarse and fine). Pore volume was first calculated for each clay sample and then pore volume amount of water was passaged through the samples.

In the first step, the baked clay surfaces were rubbed with emery, and the outer surface of baked clay was covered with silicone band to avoid water leakage. Then the baked clay structures were placed at the bottom of the cylindrical apparatus of the permeability compactors.

Next, the sample was kept in Marshall Water Tank (see Fig. 4) for 24 h. After the completion of saturation process, the cylinder of the permeability device was checked for any leakage. Having confirmed that there was no leakage, the cylinder was placed on the bottom side of the permeability devices and was filled with water, as shown in Figs. 1 and 5.

Then, the valves of OCTOPUS were opened and all air voids were removed to establish the water flow. After ensuring there were no air bubbles in the system, the test was started. During this period, the decrease in the water level on the piezometric glass pipe was recorded every ten minutes. The test was repeated at least three times for each type (baking temperature/particle size) of baked clay in order to reduce the possibility of errors. All data was entered in a spreadsheet software, the graphs (permeability versus time) were drawn, and the permeability constants (k) were calculated. The average value of permeability from the repeated tests was accepted.

2.2 Capillarity Tests

Capillarity test was made to see the ability of clay structure to allow liquid flow through its voids without any external forces. The capillarity was tested using two different methods. First one was the horizontal method, and the second one was the vertical method.

2.2.1 Vertical Capillarity Test

A small water tank was used for this test. The tank was filled with water, and clay plates were placed vertically inside the tank. Thus, water started rising up with capillary action. The bottom periphery upto a height of 2 cm of all samples was insulated with silicone to ensure the water inlet only from the bottom side.

The data was collected every hour and was recorded to be graphed. For this experiment, the baked clay structures with properties listed in Table 1 were used with dimensions 20 × 100 × 200 mm. A photo of the vertical capillarity test is shown in Fig. 6.

2.2.2 Horizontal Capillarity Test

In horizontal method, the baked clay was immersed horizontally into the tank. Thus, water started going to all sides vertically, and the water was not affected by gravity because it was following a horizontal capillary action. Just like the vertical method, in this test, the data was acquired periodically, and was plotted in graphs. Figure 2 summarizes the experiment.

2.3 Cooling Effect Test

Cooling Effect Test was conducted in order to observe the temperature difference between a sample and ambient air temperature as a function of time. In order to accomplish this, clay bottles (of height 30 cm) were ordered from Menemen Pottery Association. Each of the samples was filled with water at 26 °C, and was covered with

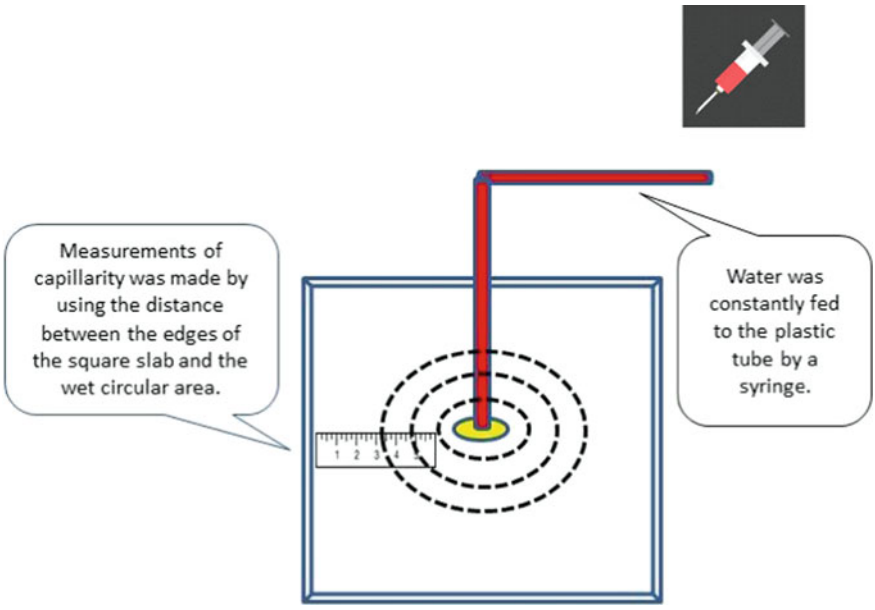

Fig. 2 Schematic diagram of the horizontal capillarity test

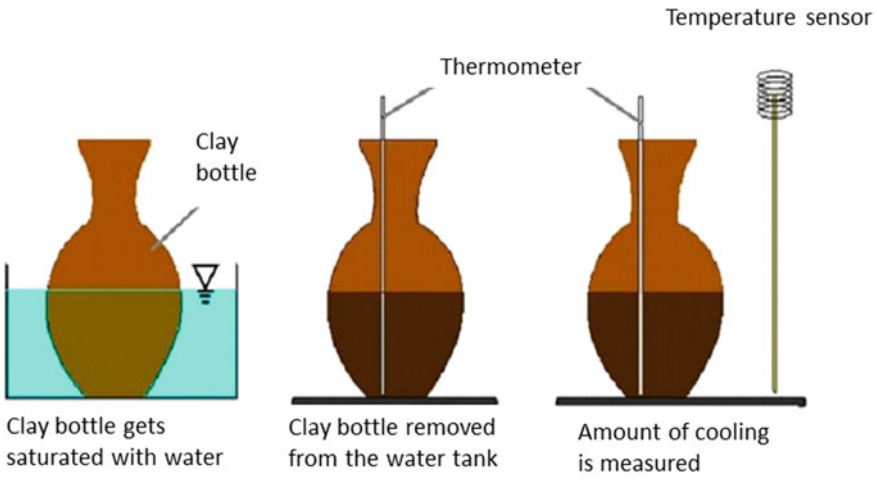

Fig. 3 The testing assembly of clay bottles

styropore covers in order to prevent evaporation from the top. Next, the samples were placed outside, under the sun (around 40 °C) to let the evaporation take place from the sides of the bottles. It was expected that the evaporation would draw heat from the surface of the clay bottles and therefore decrease the temperature of the liquid inside. Figure 3 shows the test assembly. Five samples from each of specimen types 1, 3, and 5 (coarse samples: it was expected that their permeability and capillarity values would be higher compared to the fines) were prepared and used for this test.

3 Results and Discussion

After conducting the tests, the following results were obtained.

3.1 Falling Head Permeability Test

The permeability test was conducted as required by ASTM Designation 5856-95 Falling Head Permeability Testing Procedure. Then, the permeability constant was calculated by the following formula:

$$k = \frac{a}{l} * \frac{t}{A} * ln\frac{h_o}{h_i} \tag{1}$$

where:
k: Permeability constant (cm/s).

a: The area of the cylindrical sample (m^2).

t: Time (s).

h_o: Total head inside the pipette just before starting the permeability test (cm).

h_i: Total head inside the pipette at time t (h).

Even if the total head dropped to zero, the tube was filled again and the testing procedure was repeated till the pore volume was reached (according to ASTM Designation 5856-95). Figures 7, 8, 9, 10, 11, 12 summarize the test results for the 750, 875, and 1000 °C coarse and fine grained clay samples. At least, 2 trials were established on each of the coarse and fine samples.

After the tests were over, the permeability rate constants started to decrease after reaching a certain constant amount as can be seen from Figs. 7, 8, 9 . This is what was expected as written in the literature. The sample averages were obtained for every baking temperature. The average permeability results for 750 °C, 875 °C, and 1000 °C coarse samples were 1.06×10^{-8} cm/s, 2.45×10^{-8} cm/s, and 10×10^{-8} cm/s, respectively. The 1000 °C coarse samples gave the highest permeability results. Higher permeability is desired for better evaporation, hence better cooling effect.

The falling head permeability test results of some of the fine grain samples are presented in Figs. 10, 11, 12 as well. At least 3 trials were established for each fine sample. As can be seen from the fine samples' permeability constant graphs (Figs. 10, 11, 12), the permeability rates reached a certain constant after certain time before the pipettes were refilled again as expected. In this scenario the average permeability rate constants for 750 °C, 875 °C, and 1000 °C fine samples are: 1.2×10^{-8} cm/s, 1.78×10^{-8} cm/s, and 9.43×10^{-8} cm/s respectively.

Coarse grain samples baked at 1000 °C had, on the average, 20% more permeability than the fine samples. Similarly, coarse samples baked at 875 °C had, on the average, 28% more permeability than the 875 °C fine samples. When compared in terms of baking temperature, both grain sizes gave 4X more permeability at 1000 °C than at 875 °C, as can be seen from Table 2. This dramatic increase in permeability is due to syntherization. Syntherization is a process that homogenizes the clay particle shapes at temperatures higher than 900 °C.

Although the effect of baking temperature was the same for the samples baked at 750 °C, fine grain samples had more permeability compared to coarse grain samples (75%). This is thought to be due to the higher particle shape heterogeneity in coarse grain samples, which persists at 750 °C.

Table 2 summarizes the maximum, minimum, and the average values of each sample's permeability test results. It also shows the V_{in}/V_{out} values. ASTM Designation 5856-95 for Falling Head Permeability Test says that only 75–125% of V_{in}/V_{out} values are the acceptable range. Therefore, values out of the range were disregarded (as shown in red color in Table 2) and those test results were not put into consideration.

3.2 Capillarity Tests

The horizontal and vertical capillarity tests were performed for samples at three different baking temperatures and two grain sizes.

3.2.1 Horizontal Capillarity Test Results for 750 °C Coarse and Fine

Figures 13 and 14 summarize the results of horizontal capillarity test baked at 750 °C. The readings were taken from the outer edges of the square blocks. Therefore, they show a decrease in dry zone versus time, instead of increasing wet zone versus time. This decrease fits a linear trendline very precisely, and the R^2 values together with the linear equations are presented.

Horizontal capillarity tests took at least 2 days to complete until the samples became fully saturated. Capillarity increases with time and then the increase slows down.

3.2.2 Horizontal Capillarity Test Results for 875 °C Coarse and Fine

Figures 15 and 16 summarize the results of horizontal capillarity test baked at 875 °C. Researchers observed decrease versus time tor fine grain 875 °C sample as well. Correlation equations were obtained. Then R^2 values were calculated. The R^2 values are close to 1, which proves that the trend is linear.

Researchers observed that the decrease was steeper in 875 fine samples compared to 875 coarse. As the capillary diameter decreases, the capillary height increases which was expected since the capillarity formula states the findings as shown in the formula below.

$$h = \frac{2 * \sigma * \cos Ø}{\rho * g * r} \tag{2}$$

σ: Surface Tension, N/m.
ρ: Density of the liquid, (kg/m^3).
r: radius of the capillary tube (m).
Ø: Contact angle (°).

3.2.3 Horizontal Capillarity Test Results for 1000 °C Coarse and Fine

Researchers did horizontal capillarity test for 1000 °C coarse and 1000 °C fine samples on two consecutive days, and observed a decrease in the water propagation

velocity with time, which is thought to be due to the saturation of the samples. The capillary action in both coarse and fine samples was high compared to the lower baking temperatures (around 2 cm decrease of dry zone in 7.5 h). Figures 17 and 18 summarize the results of horizontal capillarity test baked at 1000 °C.

3.2.4 Vertical Capillarity Test Results for 750 °C Coarse and Fine

The vertical capillarity experiment lasted for 2 days. Measurements were taken every 2 h. Weight and capillarity rise were fast at first but then the rise slowed down and became constant after 24 h. Logarithmic trendline was added to the data.

Figures 19 and 20 summarize the results of vertical capillarity tests for the coarse grain samples baked at 750 °C. As capillary intake increased, the weights of the rectangular blocks increased, showing the progress of the tests (Fig. 19). The capillary climb of the water column (Fig. 20) was measured from the bottom of the rectangular blocks, hence, they show an increase per time. This increase fits a logarithmic trendline very precisely. The measurements, the R^2 values together with the logarithmic equations are presented in Fig. 20.

As for the fine grain samples, weight of the sample increased 36 g in 2 days for 750 Fine A sample (Fig. 21). The reason why 5.88 h capillarity reading was shown as zero is because the reading was impossible due to the $CaCO_3$ leavening caused by hard water on that region. The height of the water column in the fine grain case (Fig. 22) also reached a saturation level, but its onset was a few hours earlier and a few centimeters higher than the coarse grain case.

3.2.5 Vertical Capillarity Test Results for 875 °C Coarse and Fine

Figures 23, 24, 25, 26 summarize the results of vertical capillarity test baked at 875 °C. Researchers used 875 °C baked coarse sample first during the vertical capillarity test, and measured the weights of the samples at different time intervals (every five minutes). For 875 °C coarse particles, the capillary column height could not be determined due to hardness of water (The water was leaving marks on the specimen making the researchers unable to read the capillary column height). 875 °C fine sample test results were obtained in 1.17 day. The increase in weight and capillary column height appears to be quicker in 875 °C compared to 750 °C.

3.2.6 Vertical Capillarity Test Results for 1000 °C Coarse and Fine

Figures 27, 28, 29, 30 summarize the results of vertical capillarity test baked at 1000 °C. 1000 °C coarse sample capillarity test results show weight and capillarity are increasing with time with fine grain displaying a noticeable higher capillary action than 1000 °C baked coarse (due to the formula presented at Eq. 2).

3.3 Results of Cooling Effectivity Test

After getting through with the testing procedure, researchers observed a temperature difference around 14–15 °C between the air and the water inside the clay bottle. The water did not only remain at room temperature but also dropped by around 4 °C within 9.5 h. This proved researchers' assumption. Clay bottles keep and even decrease the inside temperature of the liquid with the help of evaporation (extraction of heat from the surface through evaporation). Figure 31 presents the results of the test.

As can be seen from Fig. 31, the air temperature was 39 °C in average for 21.06.2016. The temperature of water inside the clay bottle stayed the same (around 26 °C) for almost 3 h. An early morning data was also obtained in order to ensure effectiveness. The largest temperature drop occurred for 1000 °C baked coarse sample (around 4°−5 °C) between 12:40 PM and 9 AM of 21st and 22nd of July 2016.

4 Conclusions

In the natural refrigeration systems that utilize evaporation, high capillarity is desired so that water will move quickly and will evaporate more. Consequently, cooler indoor conditions can be achieved. In the present study, it was seen that 750 °C baked clay bricks with fine or coarse grain had very small permeability and capillarity. The samples baked at 875 °C had high permeability but low capillarity. However, 1000 °C baked clays had the highest permeability and capillarity. The same superiority was confirmed in the cooling effect tests, as the drop was approximately 14 °C for the 1000 °C baked samples while it was around 9–10 °C for the others. The elevated performance of the 1000 °C baked clay samples is thought to be due to the synther-ization process that starts at around 900 °C, and makes the clay particles more rigid, durable, and homogenous. Since the coarse grain samples have higher permeability, 1000 °C baked coarse grain clay bricks were determined as the most suitable building material, among all samples in this study.

Acknowledgements This project was funded by The Scientific and Technological Research Council of Turkey (TUBITAK) under the project number **215M162**.

Appendix

Table 2; Figures 4, 5, 6, 7, 8, 9, 10, 11, 12, 13, 14, 15, 16, 17, 18, 19, 20, 21, 22, 23, 24, 25, 26, 27, 28, 29, 30, and 31.

Table 2 Summary of permeability rate constants

			Table 2: Summary of Permeability Rate Constants						
			K (cm/sec)				V in	V out	0.75<% flow<1.25 Vin/Vout
			Min	Max	Av	St.Dv.			
750ºC	Fine	No1	8,2E-09	2,03E-08	1,032E-08	2,19E-09	42,320	34,540	**82%**
		No2	1,14E-08	2,11E-08	1,36E-08	2,23615E-09	35,230	30,840	**88%**
	Coarse	No1	9,78E-09	1,81E-08	1,16E-08	1,53E-09	38,319	37,14	**97%**
		No2	4,21E-09	1,32E-08	9,64E-09	1,28E-09	38,828	34,56	**89%**
875ºC	Fine	No1	1,43E-08	4,01E-09	1,93E-08	4,00E-08	41,818	34,48	**82%**
		No2	1,36E-08	3,19E-09	1,68E-08	4,04E-08	46,32	38,22	**83%**
		No3	5,18E-09	3,33E-08	1,74E-08	4,95E-09			
	Coarse	No1	1,31E-08	7,49E-08	1,81E-08	7,84E-09	**44,567**	**45,96**	**103%**
		No2	2,86E-08	1,23E-07	3,99E-08	1,31E-08	**53,17**	**58,53**	**110%**
		No3	5,10E-09	5,52E-08	1,53E-08	1,10E-08	**39,407**	**30,12**	**76%**
1000ºC	Fine	No1	8,42E-08	2,22E-07	1,00E-07	2,17E-08	**71,887**	**121,74**	**169%**
		No2	4,05E-08	2,23E-06	8,51E-08	2,06E-07	**36,163**	**38,62**	**107%**
		No3	5,13E-08	1,27E-07	6,71E-08	1,44E-08	**52,435**	**57,51**	**110%**
		No4	5,81E-08	2,56E-06	1,23E-07	3,52E-07	**19,361**	**20,57**	**106%**
		No5	7,30E-08	1,62E-07	1,02E-07	2,14E-08	**36,792**	**42,26**	**115%**
		No6	7,98E-08	1,09E-07	8,70E-08	6,78E-09	**14,83**	**24,65**	166%
	Coarse	No1	8,43E-08	1,71E-07	1,09E-07	1,63E-08	**55,955**	**62,72**	**112%**
		No2	1,35E-07	2,10E-07	1,50E-07	1,09E-08	**38,778**	**69,82**	**180%**
		No3	6,71E-08	2,26E-07	9,19E-08	2,74E-08	**45,515**	**49,67**	**109%**
		No4	1,09E-07	1,43E-07	1,17E-07	6,16E-09	**34,9**	60,79	**174%**

Fig. 4 Photo of marshall water tank

Fig. 5 Photo of falling head permeability test

Fig. 6 Photo of the vertical capillarity test

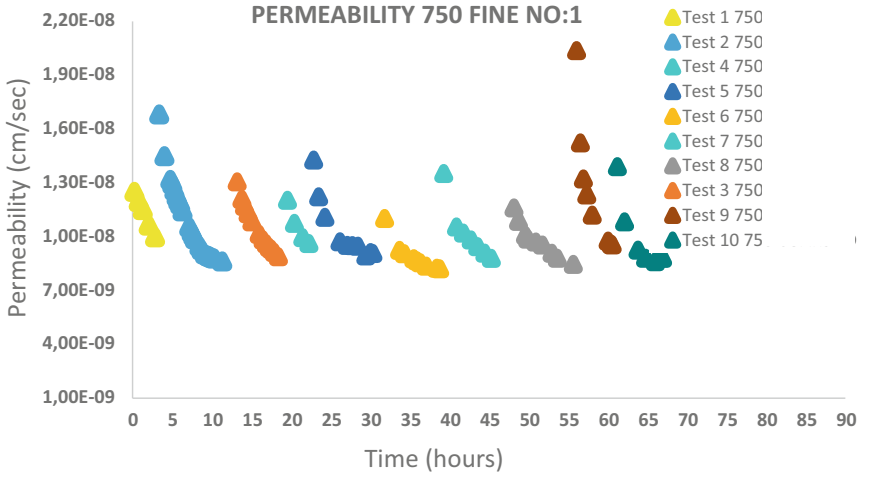

Fig. 7 Falling head permeability test results for 750 °C Fine No:1

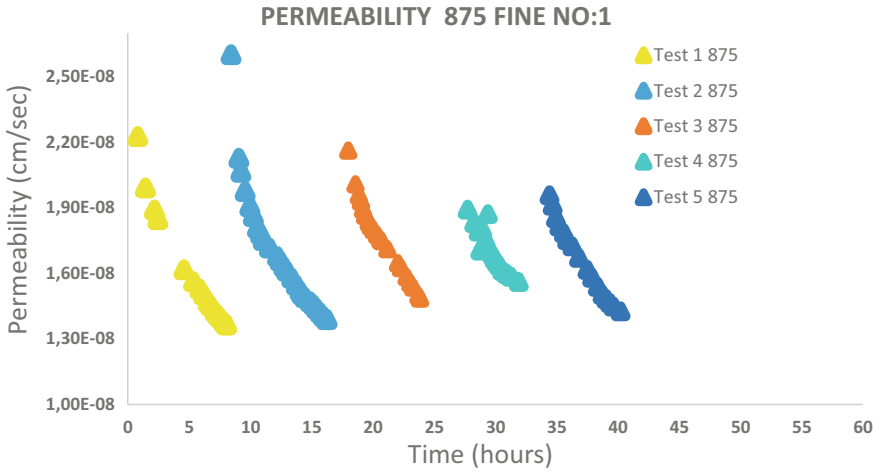

Fig. 8 Falling head permeability test results for 875 °C Fine No:1

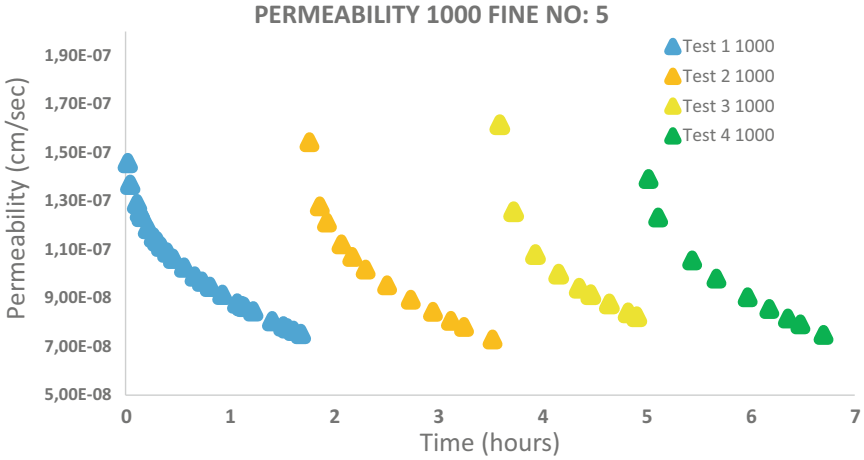

Fig. 9 Falling head permeability test results for 1000 °C Fine No:5

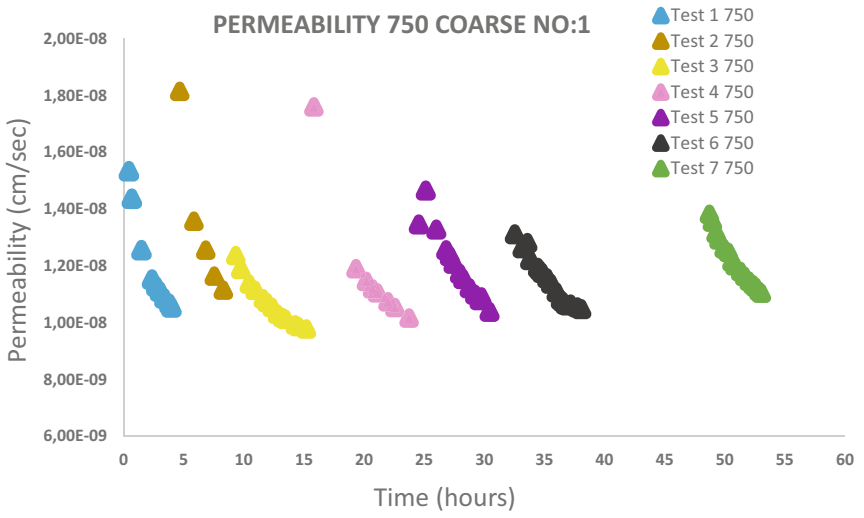

Fig. 10 Falling head permeability test results for 750 °C Coarse No: 1

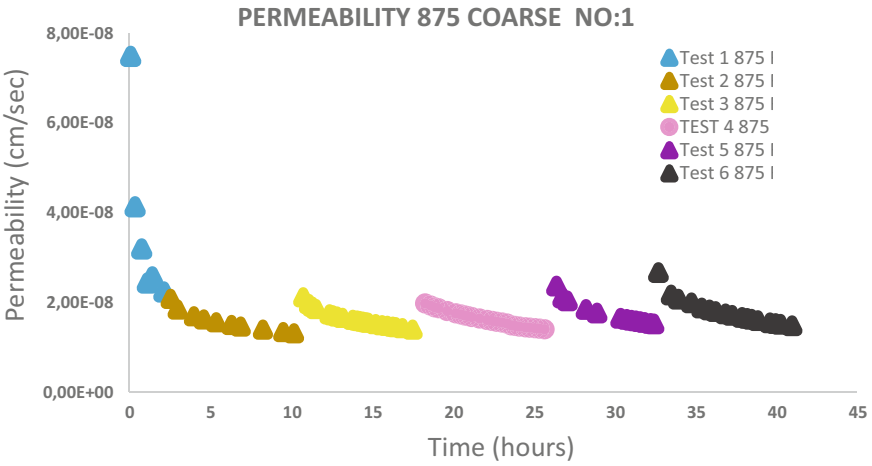

Fig. 11 Falling head permeability test results for 875 °C Coarse No:1

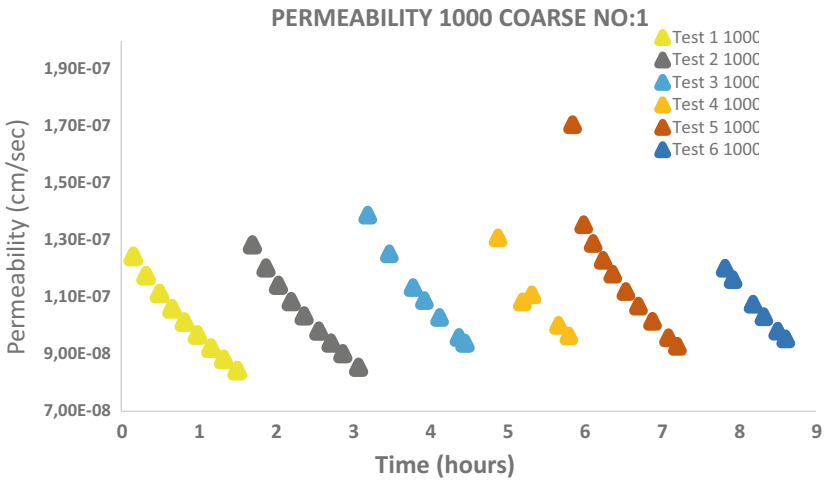

Fig. 12 Falling head permeability test results for 1000 °C Coarse No:1

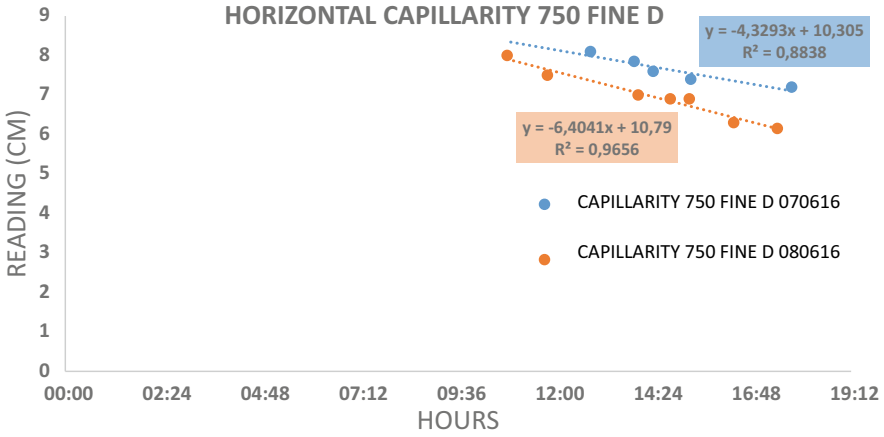

Fig. 13 Horizontal capillarity results for 750 °C Fine D

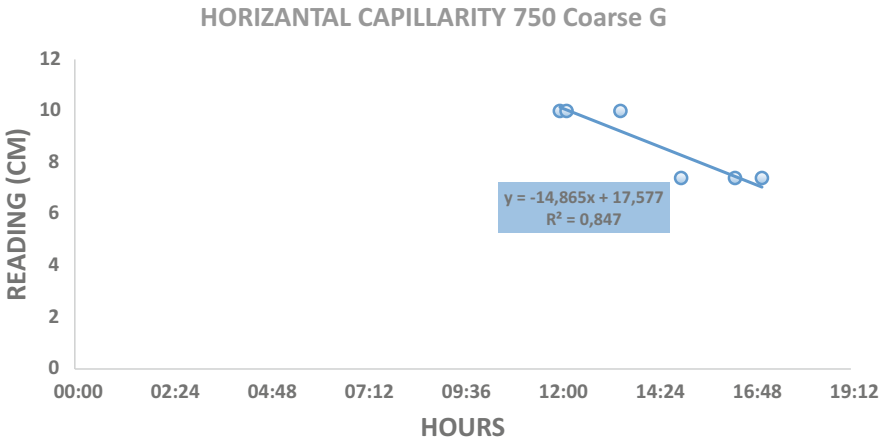

Fig. 14 Horizontal capillarity results for 750 °C Coarse G

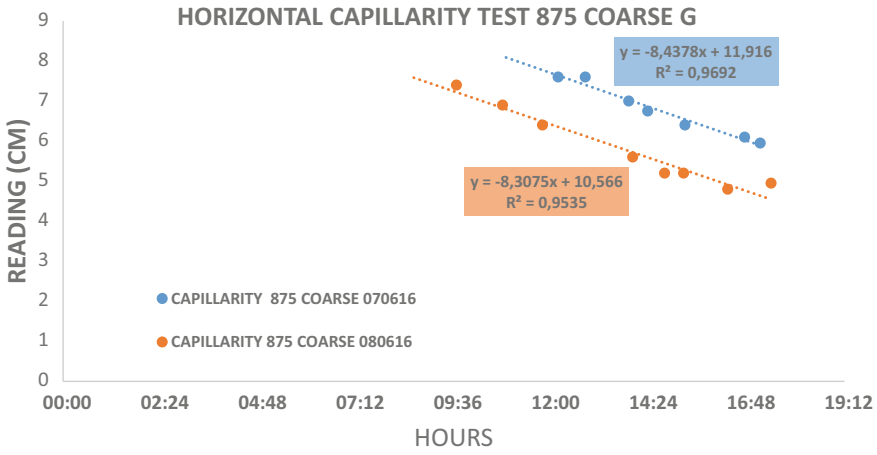

Fig. 15 Horizontal capillarity results for 875 °C Coarse G

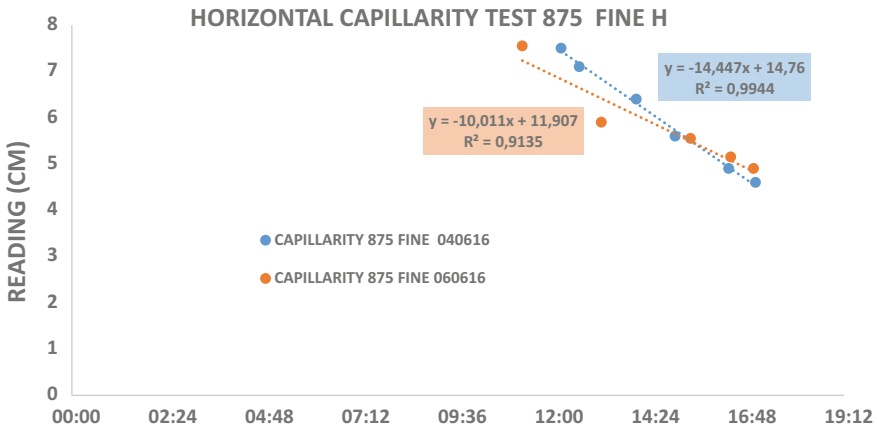

Fig. 16 Horizontal capillarity results for 875 °C Fine H

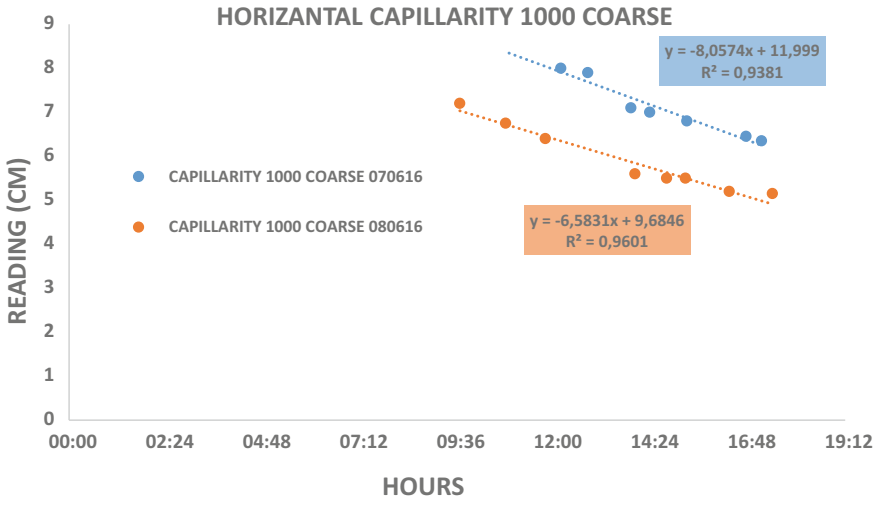

Fig. 17 Horizontal capillarity results for 1000 °C Coarse

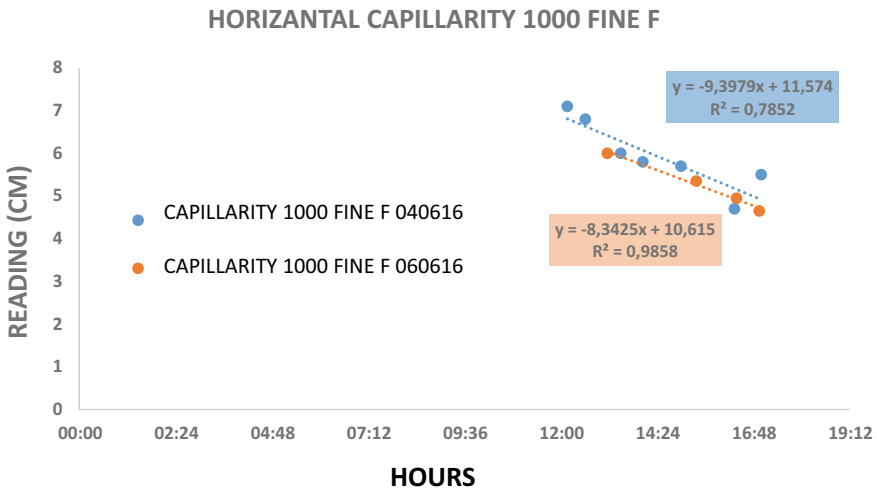

Fig. 18 Horizontal capillarity results for 1000 °C Fine F

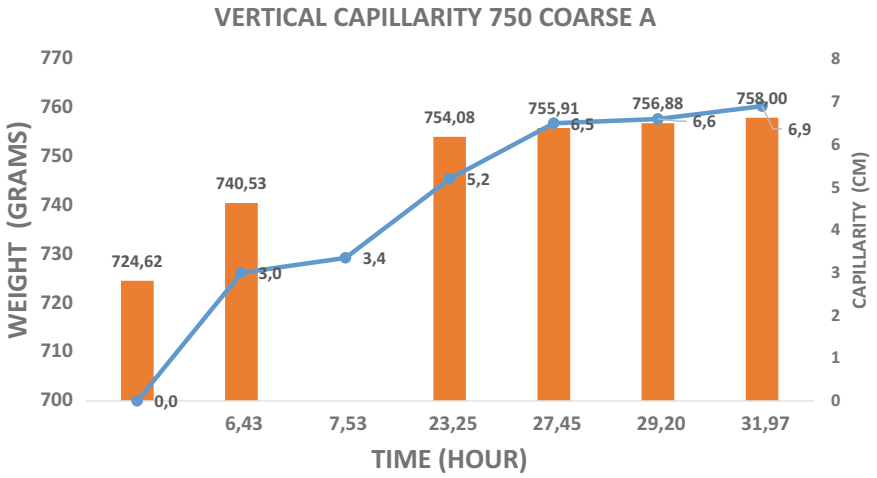

Fig. 19 Vertical capillarity 750 °C Coarse A results

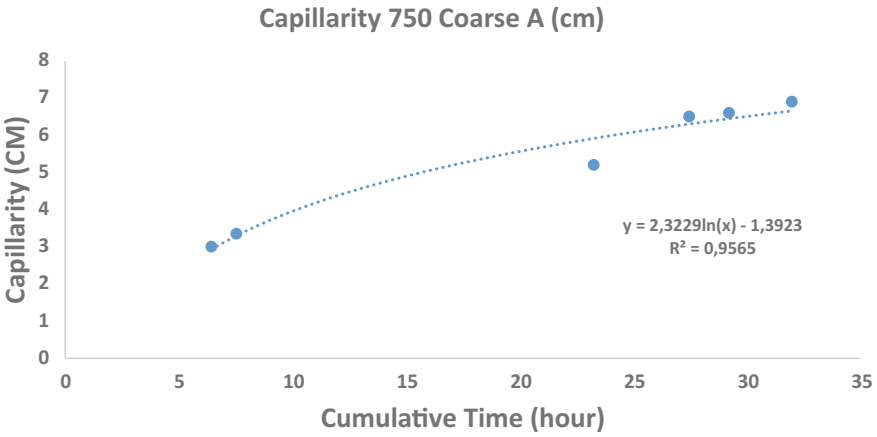

Fig. 20 Vertical capillarity 750 °C Coarse A results

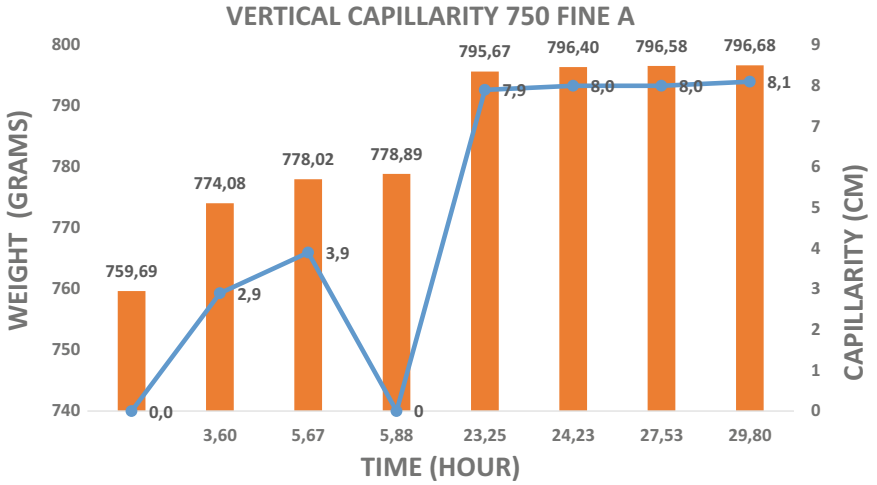

Fig. 21 Vertical capillarity 750 °C Fine A results

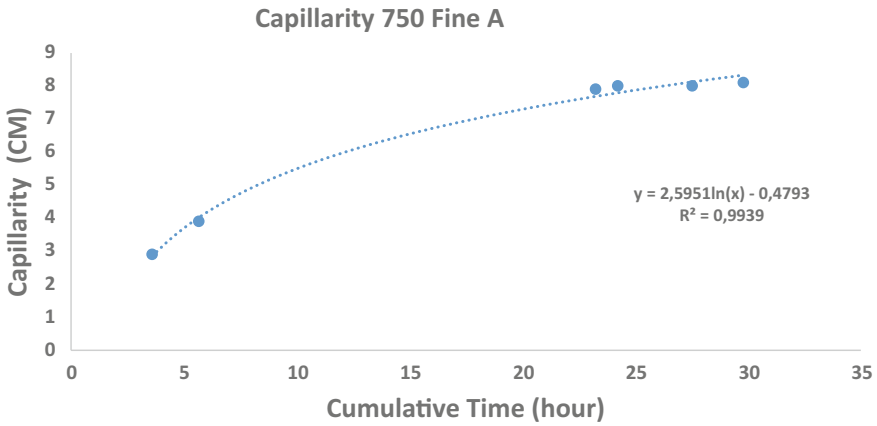

Fig. 22 Vertical capillarity 750 °C Fine A results

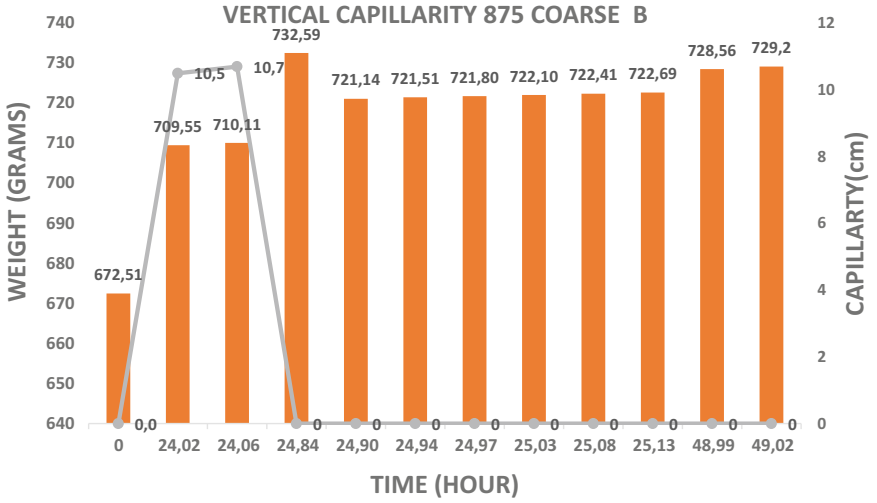

Fig. 23 Vertical capillarity 875 °C Coarse B results

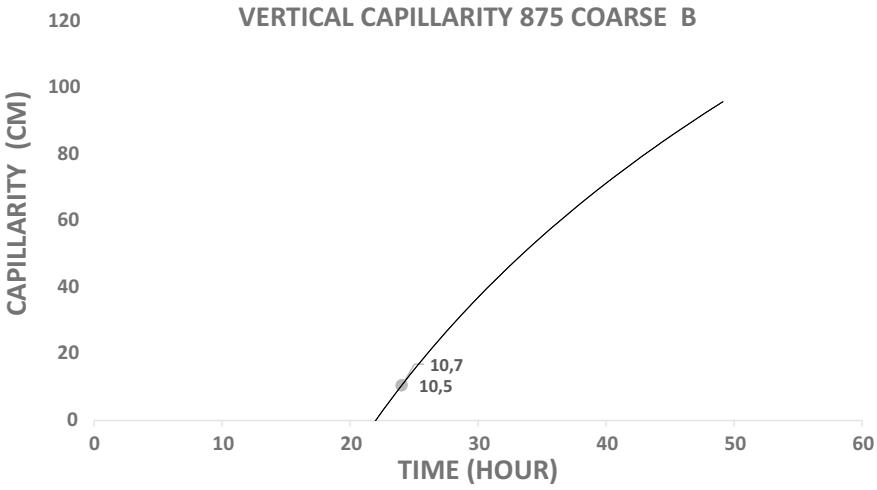

Fig. 24 Vertical capillarity 875 °C Coarse B results

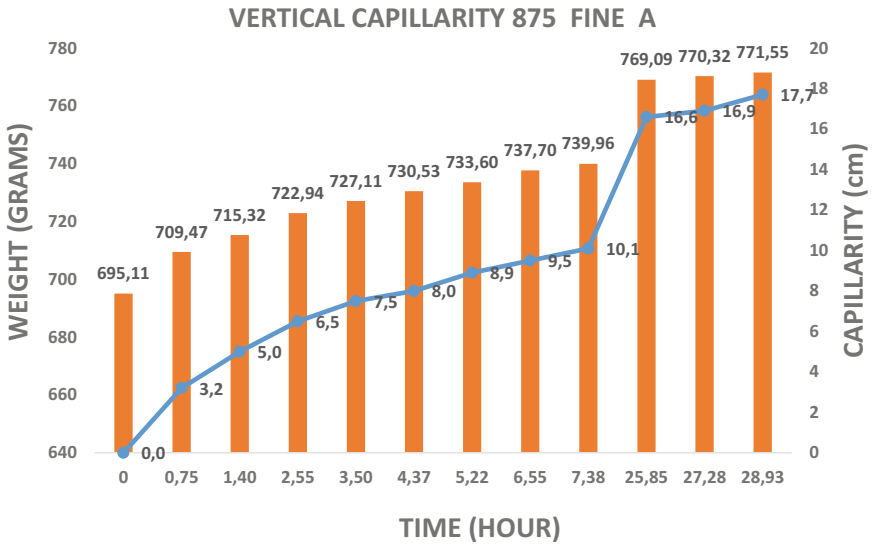

Fig. 25 Vertical capillarity 875 °C Fine A results

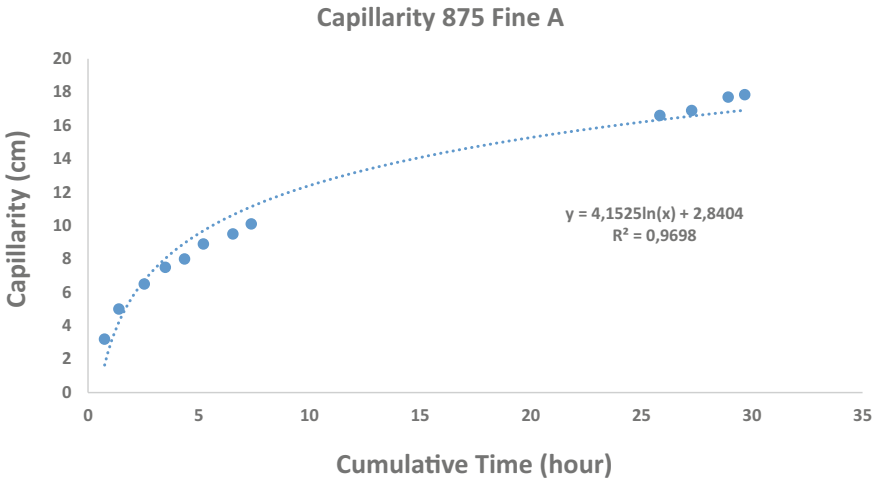

Fig. 26 Vertical capillarity 875 °C Fine A results

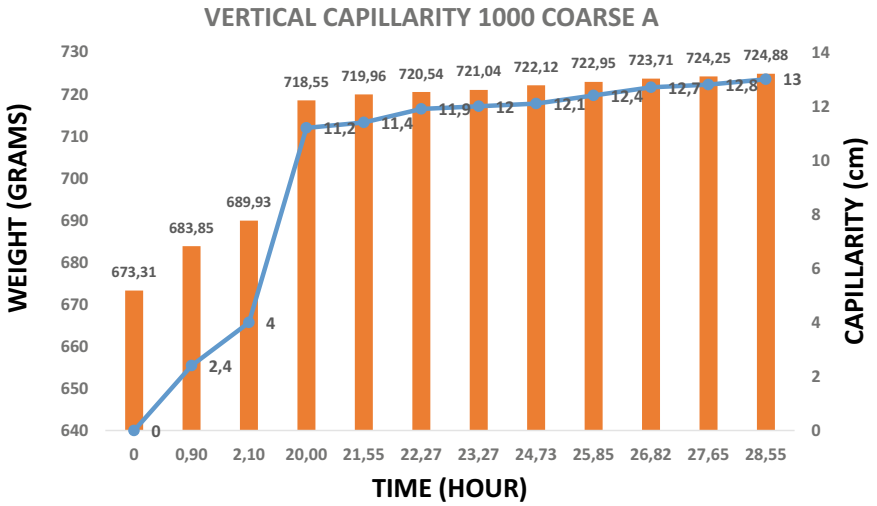

Fig. 27 Vertical capillarity 1000 °C Coarse A results

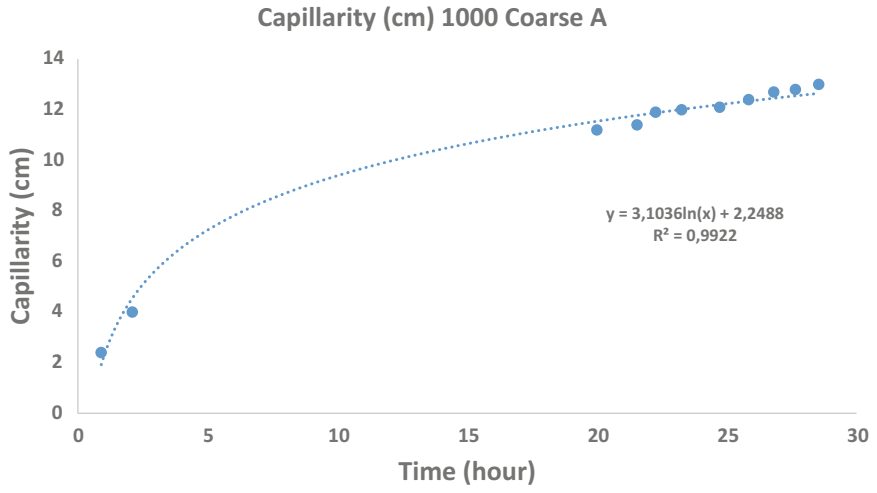

Fig. 28 Vertical capillarity 1000 °C Coarse A results

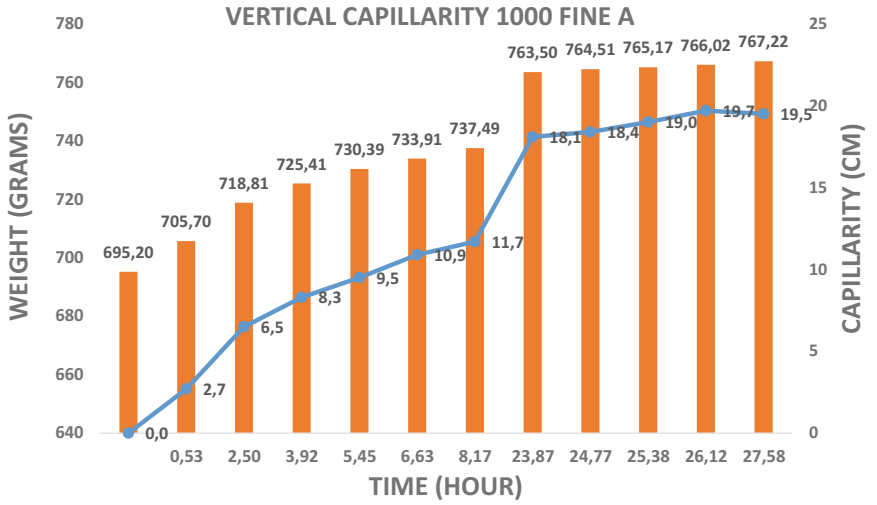

Fig. 29 Vertical capillarity 1000 °C Fine A results

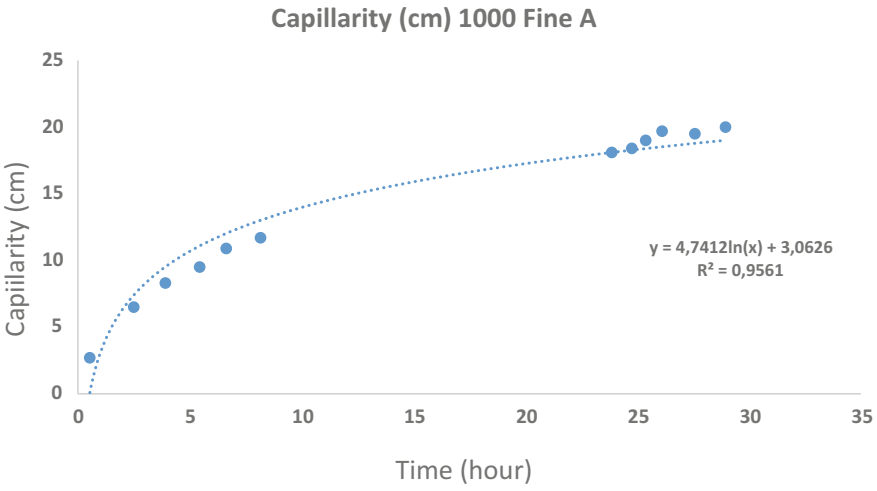

Fig. 30 Vertical capillarity 1000 °C Fine A results

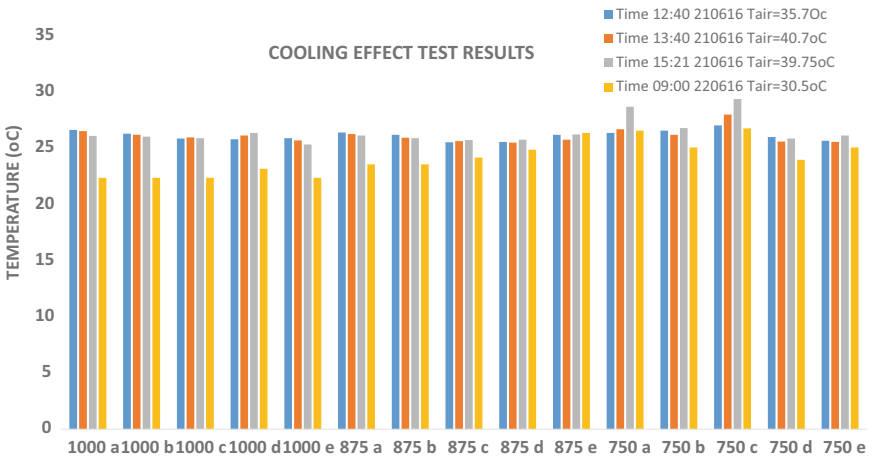

Fig. 31 Temperature of the water inside the clay bottle versus time

References

1. Lombard LP, Ortiz J, Pout C (2008) A review on buildings' energy consumption information. Energy Build 394–398
2. Samuel DL, Nagendra SS, Maiya MP (2013) Passive alternatives to mechanical air conditioning of building: a review. Build Environ 66:54–64
3. Gupta N, Tiwari GN (2016) Review of passive heating/cooling systems of buildings. Energy Sci Eng
4. Takakura T, Kitade S, Goto E (2000) Cooling effect of greenery cover over a building. Energy Build 31(1):1–6
5. Onmura S, Matsumoto M, Hokoi S (2001) Study on evaporative cooling effect of roof lawn gardens. Energy Build 33(7):653–666
6. Niachou A, Papakonstantinou K, Santamouris M, Tsangrassoulis A, Mihalakakou G (2001) Analysis of the green roof thermal properties and investigation of its energy performance. Energy Build 33(7):719–729
7. Cheikh HB, Bouchair A (2008) Experimental studies of a passive cooling roof in hot arid areas. Revue des Energies Renouvelables 11(4):515–522
8. Wongsuwan W, Fongsamootre T, Cole MO (2006) Experimental studies on the roof pond house under tropical climatic conditions. KKU Eng J 33(2):133–139
9. Spanaki A, Kolokotsa D, Tsoutsos T, Zacharopoulos I (2014) Assessing the passive cooling effect of the ventilated pond protected with a reflecting layer. Appl Energy 123:273–280
10. Yağcıoğlu A, Günhan T, Demir V (2006) Tarımsal yapılarda nemli yastıklarla serinletme. Tarım Makinaları Bilimi Dergisi 2(4)
11. Lokapure R, Joshi J (2012) Energy conservation through roof surface evaporative cooling for air conditioning system. Int J Sci Res Publ 2(6):1–5
12. Pires L, Silva PD, Gomes JC (2013) Experimental study of an innovative element for passive cooling of buildings. Sustain Energy Technol Assess 4:29–35
13. Li H, Harvey J, Ge Z (2014) Experimental investigation on evaporation rate for enhancing evaporative cooling effect of permeable pavement materials. Constr Build Mater 65:367–375
14. Rirsch E, Zhang Z (2010) Rising damp in masonry walls and the importance of mortar properties. Constr Build Mater 24(10):1815–1820
15. Mason G (1974) Rising damp. Build Sci 9(3):227–231

16. Lin KL, Chang JC (2013) Feasibility of recycling waste diatomite and fly ash cosintered as porous ceramics. Environ Prog Sustain Energy 32(1):25–34
17. Steefel CI, Lichtner PC (1994) Diffusion and reaction in rock matrix bordering a hyperalkaline fluid-filled fracture. Geochim Cosmochim Acta 58(17):3595–3612
18. Whiffin VS, van Paassen LA, Harkes MP (2007) Microbial carbonate precipitation as a soil improvement technique. Geomicrobiol J 24(5):417–423
19. Dhami NK, Reddy MS, Mukherjee A (2012) Improvement in strength properties of ash bricks by bacterial calcite. Ecol Eng 39:31–35
20. Zhang S, Zong L (2014) Properties of concrete made with recycled coarse aggregate from waste brick. Environ Prog Sustain Energy 33(4):1283–1289
21. Edis E, Flores-Colen I, de Brito J (2014) Passive thermographic detection of moisture problems in façades with adhered ceramic cladding. Constr Build Mater 51:187–197
22. Barreira E, de Freitas VP (2007) Evaluation of building materials using infrared thermography. Constr Build Mater 21(1):218–224
23. Griend AA, Owe M (1994) Bare soil surface resistance to evaporation by vapor diffusion under semiarid conditions. Water Resour Res 30(2):181–188
24. Qin Y, Hiller JE (2016) Water availability near the surface dominates the evaporation of pervious concrete. Constr Build Mater 111:77–84
25. Al-Fadhala M, Hover KC (2001) Rapid evaporation from freshly cast concrete and the Gulf environment. Constr Build Mater 15(1):1–7
26. Pacheco-Torgal F (2014) Eco-efficient construction and building materials research under the EU Framework Programme Horizon 2020. Constr Build Mater 51:151–162
27. Hyde R (2008) Bioclimatic housing: innovative designs for warm climates. Earthscan
28. Aldous MB, Holberg CJ, Wright AL, Martinez FD, Taussig LM (1996) Evaporative cooling and other home factors and lower respiratory tract illness during the first year of life. Am J Epidemiol 143(5):423–430
29. Yamanashi T, Hatori T, Ishihara Y, Kawashima N, Niwa K (2011) Bio skin urban cooling facade. Archit Des 81(6):100–107
30. Loonen RCGM (2015) Bio-inspired adaptive building skins. In: Biotechnologies and biomimetics for civil engineering. Springer International Publishing, pp 115–134
31. Rafique MM, Gandhidasan P, Rehman S, Alhems LM (2016) Performance analysis of a desiccant evaporative cooling system under hot and humid conditions. Environ Prog Sustain Energy 35(5):1476–1484
32. Ahmad I, Khetrish E, Abughres SM (1985) Assessment of ground thermal capacity for space cooling in Libya. Energy 10(9):993–998
33. Faqih ARAKM (2003) U.S. Patent No. 6,574,979. U.S. Patent and Trademark Office, Washington, DC
34. He J, Hoyano A (2010) Experimental study of cooling effects of a passive evaporative cooling wall constructed of porous ceramics with high water soaking-up ability. Build Environ 45(2):461–472
35. He J, Hoyano A (2011) Experimental study of practical applications of a passive evaporative cooling wall with high water soaking-up ability. Build Environ 46(1):98–108

Investigation of Dredged Sediments Reuse as Building Materials

Ahmed Benamar, Laila Mesrar, Frédérique Bourdin, and Sébastien Brasselet

Abstract In order to maintain a required water depth and to allow waterways navigable, dredging operations are of a great importance. So, large volumes of sediments are annually dredged in the ports over the world. In Le Havre harbor the annual dredged volume of sediments is close to 1.5 Mm^3, which are mainly dumped at sea. Because of its perpetual availability and mineralogical characteristics, the sediment is regarded as a suitable raw material for terracotta production. The aim of this work, assessed in laboratory, is to investigate how dredged and deposited sediments from the Seine estuary and port basins can be used as alternative raw material for the heavy clay industry. The chemical and mineralogical composition of dredged sediments were addressed using X-ray fluorescence (XRF) and X-ray diffraction (XRD), respectively. The physical properties, including plasticity index (PI), organic content, and salinity were investigated. The results from all tested sediments in their raw state showed that their chemical and mineralogical compositions are fairly close. However, their low clay minerals content (6.6%) and their high carbonate content (25.2%) constitute a limitation to their use in ceramic industry. The grain size distribution was appraised on a diagram involving three range sizes (clay, silt, sand), and the results indicated that the raw material falls inside the suitable domain of fired-clay products. Additional ceramic tests performed showed that the raw material can be used as bricks making owing to provided interesting properties, such as firing behavior and mechanical resistance. Leaching test was performed on fired bricks in order to assess the environmental suitability of the construction material. In this framework, The SEDIBRIC project is part of the concern of the "sober management of resources" and aims a sustainable remediation with a low impact on the environment and recovery of dredged sediments.

Keywords Dredged sediment · Heavy clay · Geochemical · Bricks · Pollutant

A. Benamar (✉) · L. Mesrar
LOMC UMR 6294 CNRS-Université Le Havre Normandie, 53 rue de Prony, 76600 Le Havre, France
e-mail: ahmed.benamar@univ-lehavre.fr

F. Bourdin · S. Brasselet
GPMH, port authority, service AEM, Terreplein de la Barre, 7600 Le Havre, France

K. R. Reddy et al. (eds.), *Sustainable Environment and Infrastructure*, Lecture Notes in Civil Engineering 90, https://doi.org/10.1007/978-3-030-51354-2_18

1 Introduction

Dredging is essential to maintain waterways in ports, channels, and rivers. Dredging operation impact and sediment disposal effect in open water have been largely investigated. These operations are a huge threat, not only for the marine flora and fauna, but also for human health. Ports authorities have to deal with sediments issue. Dredging operation of these areas is an absolute necessity in order to maintain a nautical depth and to develop new harbor areas. Sediments resulting from dredging operations in major French seaports (Dunckerque, Calais, Boulogne, Le Havre, Rouen, La Rochelle) represent approximately a volume of 6.2 Mm^3/year [1], including 80% of sludge. Dredging operations and damping material have to be managed within international regulations (OSPAR Convention, London Convention, Barcelona Convention). A French order details the chemical threshold values that dredged material must respect before dumping. Various alternative ways to the disposal of dredged material and benefit reuse have been investigated [2–4].

Environmental friendly material recycling and energy saving are important items of concern. As a result of environmental regulations, the demand for clay bricks with higher insulation ability is increasing [5, 6]. Bricks are the most used masonry units. It has the widest used range of products, with its unlimited assortment of patterns, textures, and colors. In 1996, the industry produced 300 million bricks, which were about 55% of the potential production of the available facilities. The export markets included Japan, New Zealand, the Middle East, and other Asian countries. This is equivalent to an annual turnover of 130 million dollars (EPAV, 1998) [7]. In order to supply factories with an available raw material and reduce clay extraction, this investigation was conducted in the framework of SEDIBRIC project supported by Normandy Region and the French environmental agency (Ademe). The study was divided into three parts, consisting of measuring the physical and chemical properties of the sediment, testing the material suitability to be used as raw material for manufacturing bricks and, ultimately, assessing environmental risk through leaching tests on fired bricks.

2 Materials and Methods

2.1 Material Sampling

The dredged sediment was collected from the harbor of Le Havre (Fig. 1a) using a dredging unit (dredger) (Fig. 1b, c) and from a deposit land (2Bis). Selected areas for sediment sampling are located in the basins and the Seine estuary from where large volumes of sediments are often dredged. The deposit land was managed since 2007 and a dense vegetation took place. By collecting several samples, the variability of the deposit over the harbor area can be assessed. Homogenized samples were stored in tanks and maintained at a temperature of 4 °C.

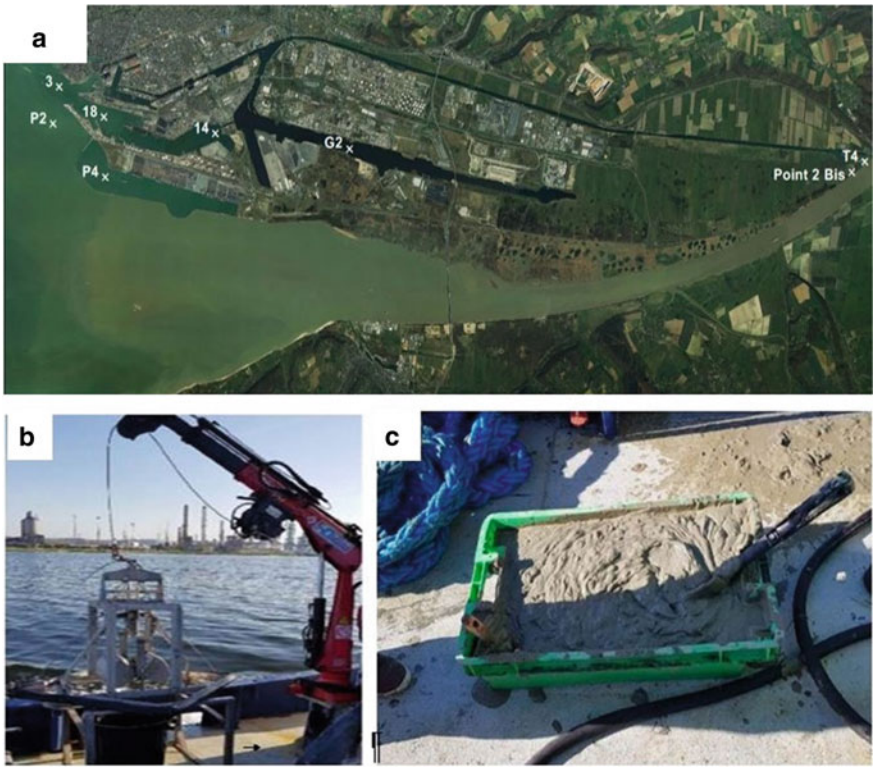

Fig. 1 **a** Map of investigated areas. **b** Dredging operation. **c** Homogenized sample

2.2 Sediments Characteristic and Variability Assessment

The use of dredged sediments required an innovative input compared with the procedures of traditional brickworks. The particle size distribution of the samples was measured by laser scattering (Mastersizer 2000, Malvern Inc). As regard to physical properties, Atterberg plastic limits (NF P 94-052-1) were firstly determined for the assessment of sediment plasticity behavior, since this material is mainly composed by fine particles (as silt and clay) which are strongly influenced by the interaction between grains and their mineralogical composition. Water content (NF P 94 050), pH (ISO 11,265), salinity (ISO10390), organic matter (NF P 94,047), methylene blue value MBV (NF P 094-068), and carbonates content (ISO 10,693) were measured according to standard methods. The geochemical quality of sediment was carried out through chemical and mineralogical properties which were evaluated by means of X-ray fluorescence and XRD devices. Physical properties of the dredged sediment are summarized in Table 1 and compared with physical characteristics of natural clay soil currently used for brick production in France [8]. Table 1 indicates that samples can involve up to 194% of water content.

Table 1 Physical properties of samples

Sediments	3	P2	P4	18	T4	G2	14	2Bis
Water content (%)	136.5	119.9	175.2	194.9	67.73	129.6	183.8	55.47
pH	7.91	8.43	8.39	8.27	8.36	8.2	8.28	8.34
Salinity (ms/cm)	2.86	3.35	2.25	2.13	0.44	2.46	2.31	0.08
Clay% < 2 μm	7.3	5.41	6.48	9.94	4.02	5.15	10.25	9.92
Silt 2–20 μm	47.99	53.71	75.73	60.92	23.65	47.89	64.03	57.86
Sand% > 20 μm	44.7	40.87	31.13	29.14	72.34	46.95	25.72	32.22
Organic matter (%)	4.62	4.06	6.28	5.75	2.96	5.5	4.96	5.06
Methylene blue	2.95	2.61	4.27	3.94	1.85	2.5	3.87	4.1
Carbonates content (%)	23.52	33.6	31.72	20.26	33.6	23.65	32.79	30.01
Plasticity limit (%)	54.36	62.31	65.88	61.84	39.83	38.79	65.88	58.22
Plasticity index	26.02	26.62	24.23	26.02	11.32	25.81	38.79	29.68

Hence, it is obvious to think about drying material before making bricks process. The clay mineral content in the dredged material ranges from 4 to 10% which is quite low than acceptable limits (10–60%) [9]. Silt is considered as a problematic material in brick production because it is non plastic or very slightly plastic. Generally, all sediments have a particle size suitable for use as bricks. However, a grinding is recommended for samples T4 and G2.

The proportion of silty particles is predominant (between 20 and 75%) for all samples collected from deposits. The clay (particles size < 2 μm) content is between 4 and 10% (Fig. 2a, b). The methylene blue values obtained vary between 2.5 and 4.6 for the samples P2, 2Bis, G2, 14, 18, 3, and P4, indicating loamy soils. The plasticity

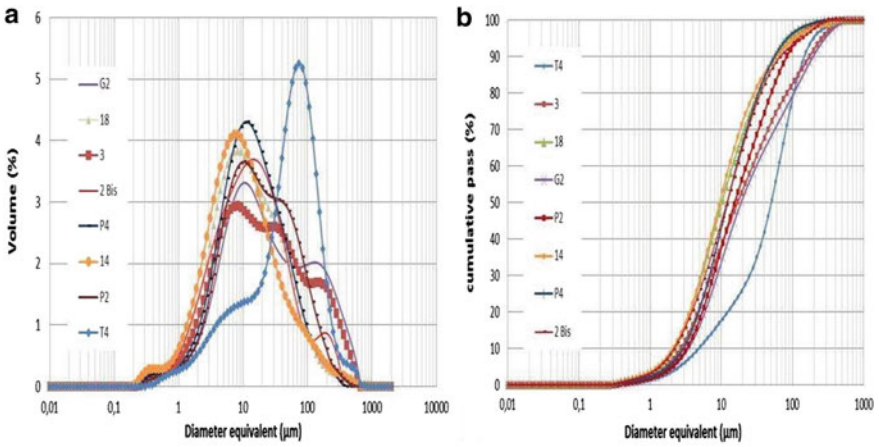

Fig. 2 **a** Particle size distribution curve for all sediment samples, **b** cumulative curve

of sediment is controlled by several factors such as the relative abundances of the fine fraction, and the presence of organic matter. The plasticity limit of all samples was in the range between 38 and 65%, which is the threshold limit under which the raw material is no longer suitable for brick making.

Therefore, plasticity index provides acceptable values (11–29%). It is worth noting that all sediments are rich in carbonates (30%), whose presence impacts the material porosity evolution during firing. The amount of organic matter content of samples ranges from 4.76 to 5.26%. Organic matter and salinity (impacts the ceramic final product because their high value induces micro-cracks in bricks after firing [9]. Hence, organic matter is a factor of fundamental importance but it cannot be used alone. The assessment of the sediment suitability for the production of bricks must also take into account particle size distribution. Figure 2 shows the particle size distribution and cumulative curves of collected sediments. Except sample T4 (collected from the Seine estuary upward), all samples provide a similar grain size distribution, indicating the homogeneity of deposits.

3 Assessment of Material Suitability for Fired Bricks

3.1 Laboratory Bricks Making and Product Characterization

In the first stage, the samples were predried at low temperature (60 °C) for 120 h, and were ground in a porcelain jar grinding media. The samples underwent the following cycle: manufacturing and shaping bricks (22–30% water), drying (90 h at room temperature and 24 h at 105 ± 5 °C). The bricks making obtained with traditional shaping techniques were of dimensions 6 cm long, 3 cm wide, and 1.5 cm thick and were air-dried.

The heating profile used in the sintering experiments consists of preheating (10 °C/min), rapid firing with an electric oven for 1 h (at fixed temperature), and cooling (10 °C/min). The temperature was then increased to the sintering temperature, which ranged between 700 and 1000 °C and held for 60 min. Mechanical properties of all bricks before and after firing investigation were determined by the flexural strength (ISO 10,545). Physical and engineering properties of bricks were compared with the standard French criteria for building bricks. Environmental risk assessment using leaching tests (procedure TCLP, EPA 1312) was performed in order to investigate the leachability of metals from bricks after firing. The heavy metals in leachates were analyzed by using Atomic Absorption Spectrometer ICP-OES.

Table 2 Bulk major oxides in sample 2Bis and values of natural clay used for bricks

Major oxides	SiO_2	Al_2O_3	Fe_2O_3	CaO	MgO	Na_2O	K2O	SO_3	Loss of ignition
Maxi value[a]	80	30	10	18	5	1.5	4.5	0.5	18
Min value[a]	35	8	2	0.5	0	0.5	0.1	0	3
2Bis	41.26	8.88	4.48	17.55	1.75	0.61	0.98	0.38	22.87

[a]Data cited in: [11]

3.2 Mineralogical Properties and Chemical Requirements

The mineralogical composition of dredged sediments was investigated through the XRD analysis which shows that materials involve a small content of clay minerals (11%), whereas non clayey minerals such as quartz (39.8%), carbonates (29.4%), and feldspar (12.6%) are dominant. We also note the presence of salt (1.1%). So, mineralogical analysis agrees with grain size distribution results.

The chemical composition (major elements) of sample 2Bis is shown in Table 2 with respect to the limit values used in bricks manufacturing in France [8]. Results show that this sediment is rich in silica, alumina, and iron oxide, with generally reduced contents of alkaline and alkaline-earth elements. The bulk elementary oxide analysis of the sediment provides a preliminary indication for the material suitability in bricks making. Most oxides of the sediment involve values that are in the upper range of the commercial bricks. However, the loss of ignition shows significant higher values compared with the commercial bricks standards. Consequently, the high content of organic substance can account for the occurrence of micro-cracks in the product. These results are consistent with mineralogical composition [9].

3.3 The Role of Particle Size Distribution in Bricks Building

Previous studies have shown that particle size distribution can have a significant influence on raw materials product [10]. The ternary diagram of McManus [11] assessed the relationship between the particles size fractions (sand, silt, and clay) and their control on porosity and permeability (Fig. 3). The permeability depends largely on the grains size; the inter-particle voids are more and better interconnected in most coarse deposits than in fine sediments (Figs. 3b, 3c). The permeability decreases as the materials become finer (Fig. 3c) due to an increase of the associated capillary pressure that inhibits the passage of fluids. According to McManus, in a well graded aggregate, small particles occupy inter-granular spaces, partly filling voids between larger particles, which reduces porosity and permeability (Fig. 3b).

The permeability facilitates the penetration of water in the clay and allows a fast and important absorption. The water in the ceramic paste must provide enough cohesion to equilibrate workability. However raw materials with high permeability have low cohesion and are difficult to be extruded. In opposite, raw material with

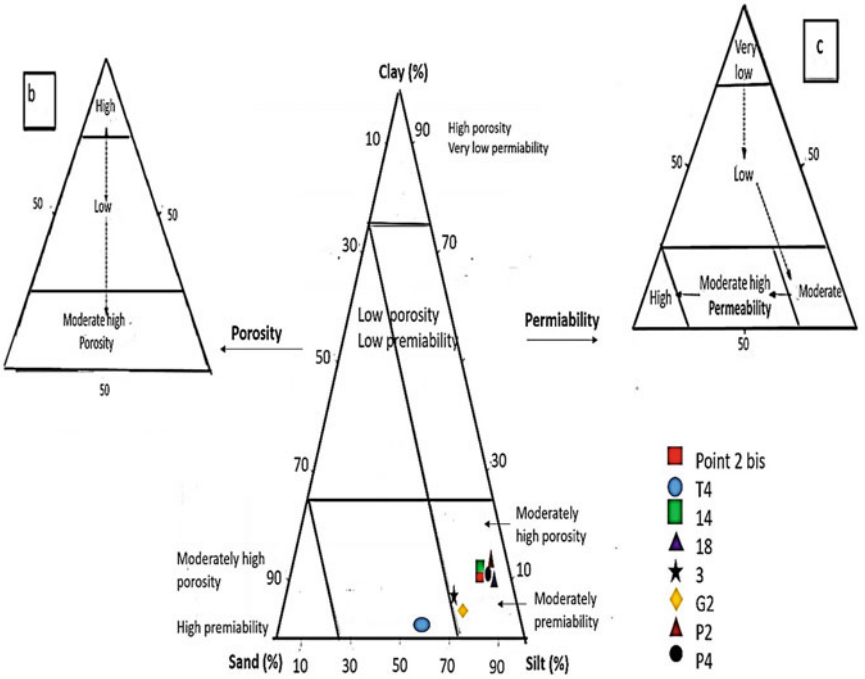

Fig. 3 Ternary diagram of studied samples following, porosity (**b**) and permeability (**c**), WS: well sorted; PS: poorly sorted; MWS: moderately well sorted [11]

low porosity and permeability have desirable properties such as workability and consistency. According to this, most of the studied pastes have a good shaping ability because they fall in the field of low porosity and permeability in the ternary diagram (Fig. 3).

As shown in this diagram, all dredged sediments will provide an acceptable product because they are found to fall in the field of moderate porosity and permeability, except sample T4 which presents high porosity and permeability due to its coarse particle size as discussed previously (Fig. 3). But this inconvenience may be easily overcome by a preliminary mechanical crushing or by mixing with finer material.

3.4 Firing Behavior and Bricks Performance

After firing at each target temperature, bricks bending and compressive strength were measured and results (Fig. 4) show an evolution of the mechanical performance of the bricks. The evolution of mechanical resistance can be explained by the mineralogical and textural changes during firing. The bending strength is an important property

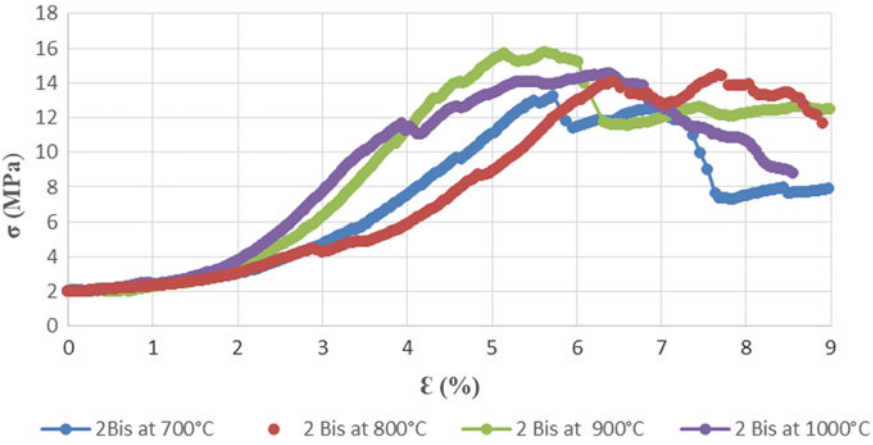

Fig. 4 Stress–strain **c**urves obtained from bending tests on the bricks at different firing temperatures

which restrains the use of this material as bricks. As this study shows, the compressive strength was mainly affected by the sintering temperature (Fig. 4). The bending strength increases linearly with temperature until 900 °C, indicating the solidification process throughout firing in the bricks. The resistance value increases from 12 MPa (at 700 °C) to 16 MPa (at 900 °C). At this range of temperatures, the clay mineral starts its transformation. Nevertheless, different remineralizations occurred which can be attributed to the mineral dynamics invoked by the thermal process [10, 12]. Hence, bricks firing at 900 °C provide a better resistance, which is upper than that required by the industrial guidelines. The value of 16 MPa is classically admitted as the threshold value for industrial materials in laboratory conditions [13]. However, at 1000 °C, the bending strength decreases significantly (14 MPa), remaining in the minimum ASTM C62 limit for the lowest grade (NW) building brick [6]. The main reason is the increase of closed porosity not only due to the decomposition of carbonates (may be also part of clay) but also by presence of the Fe^{3+} (Fe_2O_3 content being higher than > 4%, Table 2) which can lower its valence. In this range of temperatures, the role for formation of closed pores is also for a liquid phase. This consideration is always taken into account for the development of expanded clay material from clay containing illite [10]. This improvement in porosity is appropriate for ceramic products such as for the thermal insulation required for bricks. In addition, the porosity contributes to reduce the weight of the earthenware body, and facilitates portability during the transport of heavy pieces. High porosity contributes also to improve material isolation (acoustic and thermic) performances. The relationship between porosity and bending strength of fired samples highlights high carbonates content and low clay mineral content [14].

3.5 Environmental Suitability

Even though fired bricks from dredged sediments provide interesting mechanical characteristics, because the raw material contains organic and inorganic pollutants [15], a sustainable assessment of the use of fired material must be carried out. For this purpose, leaching tests were performed on shaped bricks before and after firing. During manufacturing and firing, heavy metals behavior in the bricks must be closely monitored. These heavy metals must be tied up to the vitrified structure within the bricks or else they can be released in the environment inducing health and environment risks.

Leaching test of material cubes at acidic pH value according to TCLP, EPA 1312, has been conducted to simulate the leaching process otherwise induced by acid rain, a process which likely occurs when bricks are under extreme environment exposure. We consider a worst case pH value of approximately 4 if the brick is exposed to acid rain. The pH = 4 solutions had a higher Cr leaching ability. Table 3 summarizes metals concentration contained in the raw sediment and leaching values from bricks in different firing conditions. The leachability of chromium increased with the firing temperature. In general, bricks fired at 1000 °C provide higher Cu leachability values than bricks unfired. Leachability of cooper decreases with firing temperature. However, we can notice the influence of heat exposure on the fixation of trace elements in the bricks, Cu presents a value that allows thinking that this element is fixed during thermal treatment as shown in Table 3. Leaching limit values were evaluated according to the guidelines from European Waste Catalogue, based on the soil protection act and pollution of surface waters Act [16]. The leachability of the sediment bricks shows low values only in the acidic range. So, the results of

Table 3 Analysis of leachate from bricks as regard to metals and limit values [16]

Concentration metals (ppm)	Cadmium (Cd)	Chromium (Cr)	Copper (Cu)	Lead (Pb)	Zinc (Zn)
Raw material (2Bis)	4.6	136.34	63.97	63.93	222.8
Leaching metals limit value	10	555	375	1250	1250
Leachate from unfired brick	0.0001	0.0032	0.0635	0.0431	0.0085
Brick fired at 700 °C	0.0002	0.3606	0.0274	0.0338	0.0008
Brick fired at 800 °C	0.0003	0.2224	0.0229	0.0639	0.0132
Brick fired at 900 °C	0.0007	0.3653	0.0116	0.1126	0.0096
Brick fired at 1000 °C	0.0002	0.6232	0.0253	0.0666	0.0034

metals concentration, which are under detection threshold, indicate that the bricks have no hazardous potential exceeding the allowed level.

4 Concluding Remarks

The investigation of beneficial reuse of dredged sediments indicated that overall collected samples the material characteristics indicated the suitability of the raw material to be used in the brick and tile industry. The experience gained with dredged sediments from Le Havre harbor as raw material for making bricks showed that such optimization is feasible.

Grain size distribution, mineralogical, and chemical composition of the dredged sediment were similar to other raw materials used in brickworks in France. Accordingly, the dredged sediments could be a suitable raw material for producing bricks. The brick's physical characteristics also indicated a bending strength of 16 MPa at 900 °C.

Leaching levels of trace metals including Pb, Zn, Cd, Cu, and Cr from bricks samples are less than France regulatory limits. So, the recovery of dredged sediments and their reuse as building materials would contribute to reducing the raw materials consumption, offering a new opportunity for harbors and waterways sediments and lowering their management cost and environmental impact.

Acknowledgments Authors gratefully acknowledge funders of SEDIBRIC project for their support, namely ADEME and Region Normandie.

References

1. Alzieu C (2005) Environmental impacts of port dredging. In: Alzieu C (ed) Dredging and marine environment, Ifremer edn, pp 1–127. ISBN 2-84433-142-4
2. Hamer K, Karius V (2002) Brick production with dredged harbour sediments. An industrial-scale experiment. Waste Manag 22:521–530
3. Kung-Yuh C, Kuang-Li C, Sue-Jean H (2008) Study on the characteristics of building bricks produced from reservoir sediment. Const Build Mater 159:499–504
4. Donald F (2017) Proceedings dredging summit and expo. Western dredging association, pp 26–29
5. Dondi M, Marsighi M, Fabbri B (1997) Recycling of industrial and urban wastes in brick production–a review. Tile@ Brick Int 13(3):302–315
6. Lee CR (2000) Reclamation and beneficial use of contaminated dredged material: implementation guidance for select options. DOER (The Dredging Operations and Environmental Research) Technical Notes Collection (TN DOER C-12). U.S. Army Engineer Research and Development Center, Vicksburg, MS
7. Aeslina AK, Mohajerani A (2011) Bricks: an excellent building material for recycling wastes-a review. In: Proceedings of the IASTED international conference 2011, Calgary, AB, Canada Environmental Management and Engineering, pp 25–45

8. Kornnman M (2009) Matériaux de terre cuite matières de base et fabrication" . Techniques de l'Ingénieur 2:1–35
9. Dondi M, Fabbri B, Guarini G, Marsigli M, Mingazzini C (1997) Soluble salts and efflorescence in structural clay products: a scheme to predict the risk of efflorescence. Bol Soc Esp Ceram 36:619–629
10. Dondi M, Raimondo M, Zanelli C (2014) Clays and bodies for ceramic tiles: reappraisal and technological classification. Appl Clay Sci 96:91–109
11. McManus J (1988) Grain size distribution and interpretation. In: Tucker ME (ed) Techniques in Sedimentology. Blackwell, Oxford, pp 63–85
12. Mesrar L, Akdim M, Akhrif I, Lakrim M, Laaroussi O, Jabrane R (2015) The physico-mechanical characteristics of the clays in and after doping with metal oxide Al_2O_3 in the region of fez (morocco). Present Environ Sustain Dev 9(3):331–341
13. Haurine F, Cojan I, Bruneaux A (2016) Development of an industrial mineralogical framework to evaluate mixtures from reservoir sediments for recovery by the heavy clay industry: application of the durance system (France). Appl Clay Sci 132:508–517
14. Mesrar L, Benamar A, Pantet A, Jabrane R (2017) Investigation of benefit reuse of dredged sediments as eco-geo-materials. In: XVI international clay conference, Granada, Spain, pp 7–23
15. Ammami MT, Portet-Koltalo F, Benamar A, Duclairoir-Poc C, Wang H, Le Derf F (2015) Application of biosurfactants and periodic voltage gradient for enhanced electrokinetic remediation of metals and PAHs in dredged marine sediments. Chemosphere 125(3):1–8
16. JOCE (2003) Council decision of 19 December 2002 establishing criteria and procedures for the acceptance of waste at landfills pursuant to article 16 of and annex II to Directive 1999/31/EC. Reference: 2003/33/EC. Official Journal of European Communities No. L11, pp 27–49

Consolidation Behavior of Compacted Sand–Bentonite–Tire Fiber Mixture for Landfill Application

Krishanu Mukherjee and Anil Kumar Mishra

Abstract Compacted sand–bentonite mixtures have been treated as a good substitute for the barrier material at the landfill. At low stress, desiccation-induced moisture variations may cause a reduction in the plastic deformability of bentonite and shrinkage cracking, which can increase the uncontrolled migration of leachates. According to this fact, a series of consolidation and unconfined compression strength (UC) tests were performed on sand–bentonite mixture mixed in a proportion of 30:70 and added with tire fibers in a proportion of 0, 5, 10, and 15%. Results showed that by increasing the tire fiber content the hydraulic conductivity of the mixture increases. For any given fiber content, a higher value of t_{90} was noticed for the SB30 composite under any range of consolidating pressure. From the shrinkage study, volumetric shrinkage (VS) was reduced as the tire fiber content increased. Surface crack and shrinkage crack developed in the mixture after desiccation and expressed in terms of crack intensity factor (CIF) as well as crack density factor (CDF) both decreased with the inclusion of tire fiber. From UC test, maximum unconfined compressive strength, initial tangent modulus (E_i), secant modulus (E_{sec}), and energy absorption capacity (EAC) of SB30 composite was evaluated and results showed that the improvement of the composite was significant up to 10% tire fiber, thereafter; it starts to reduce sharply with the inclusion of 15% tire fiber.

Keywords Hydraulic conductivity · Desiccation cracking · Tire fiber

1 Introduction

Due to fast development and improvement in standard of living the production of municipal solid waste (MSW) is being accelerated expressively and causing a major environmental issue in many developing countries in recent years. The global urban MSW production has been predicted to increase from 1.3 billion tons in 2010 to 2.2 billion tons in 2025 [1].

K. Mukherjee · A. K. Mishra (✉)
IIT Guwahati, Assam 781039, India
e-mail: anilmishra@iitg.ac.in

K. R. Reddy et al. (eds.), *Sustainable Environment and Infrastructure*, Lecture Notes in Civil Engineering 90, https://doi.org/10.1007/978-3-030-51354-2_19

Landfilling is an appropriate and proposed technique for the discarding of MSW in several countries across the world [2]. Generally, a compacted mixture of sand and bentonite is used as a landfill liner material. Bentonite is used to decrease the movement of contaminants to the adjacent geo-environment and groundwater due to its higher swelling tendency, contaminant adsorption ability, and lower hydraulic conductivity. However, bentonite suffers a large interlayer shrinkage when exposed to chemicals leached due to the formation of crack [3], which leads to an increase in hydraulic conductivity. Desiccation-induced moisture variations on the compacted sand–bentonite mixture at a low stress can affect its plastic deformability [4] and produce shrinkage cracks [5].

A study of the literatures also shows that the waste tire fiber can be used to improve the performance [6, 7] and reduce the shrinkage [8, 9] of soil. Due to rapid rise in the economy, the total number of discarded tires has been projected to grow up to 1.2 billion per year by 2030 [10]. According to this trend, generation of scrap tire causes a serious environmental and health issues for the future, and highlights the importance of innovative reusing methods.

A study of the literature has shown that the bentonite can be mixed with shredded tire to improve its geotechnical properties. Therefore, shredded tire can also be used with mixture of sand–bentonite for landfill application. However, their effect on engineering characteristics such as hydraulic conductivity and time for 90% consolidation, desiccation crack parameter (i.e., CIF and CDF), improvement factor, different elastic modulus (i.e., E_i and E_{sec}) and energy absorption capacity of the sand–bentonite–tire fiber composite need to be ascertained before their application as a landfill liner material. Therefore, various tests were performed to investigate the effect of addition of tire fiber on sand–bentonite mixture mixed in proportion of 70:30, which is generally used as a landfill liner material.

2 Materials and Methods

2.1 Materials

Sand–bentonite mixture mixed in a proportion of 70:30 (SB30) by their dry weight and reinforced with 5, 10, and 15% of tire fiber has been used for this investigation. The tire fiber dosage was selected based on the research conducted by other researchers [11, 12]. The tire fiber used in this study is the by-product of the tire retread process and can be easily used as a waste reinforcement material.

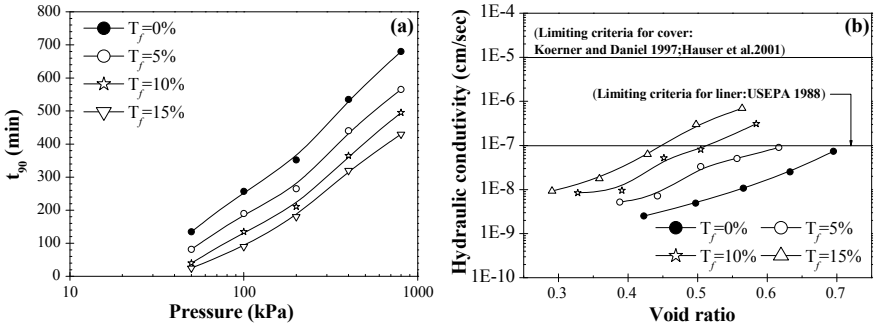

Fig. 1 Consolidation behavior of SB30; **a** t_{90}-pressure; and **b** hydraulic conductivity–void ratio

2.2 *Properties of Sand, Bentonite, and Tire Fiber*

Bentonite with a liquid limit of 286% and plastic limit of 44% was used for this study. The clay content of the bentonite was determined according to ASTM D422 [13] and found to be 46.6%. The specific surface area (SSA) of the bentonite was determined as suggested by Sridharan A, Gurtug [14] and found to be 347 g/m^2.

Locally available Brahmaputra river sand with particles size greater than 2 mm was adopted for this study. The particle-size distribution of sand was performed as per as ASTM D6913 [15].

Waste tire fiber, as shown in Fig. 1, used in this study was passing through 4.75 mm and retained on 2 mm (Fig. 1a). The water absorption capacity of the tire fiber was determined as per as ASTM D6270 [16] and was found to be 3.78%. The specific gravity of the tire fiber was determined to be 1.14.

2.3 *Testing Methodology*

2.3.1 Determination of Hydraulic Conductivity and Time for 90% Consolidation

Consolidation test was performed as per as ASTM D2435 [17] to determine the hydraulic conductivity of a 60 mm diameter and 15 mm thickness sample reinforced with different percentage of tire fiber. The samples were prepared by adding deionized (DI) water to bring its initial water content to its OMC and specimens were compacted it to their respective MDD inside the oedometer ring. Coefficient of consolidation (c_v) for each consolidating pressure was determined by Taylor's square root of time ($\sqrt{T}$) method [18] from the time–settlement curve.

where,

$\Delta\sigma$ = Change in pressure, Δe = Change in void ratio.

Coefficient of consolidation (c_v) evaluated by the square root of time fitting method specified by Taylor [18] as,

$$c_v = \frac{D^2 T_v}{t_{90}} \tag{1}$$

where,

t_{90} = Time for 90% degree of consolidation, T_v = Time factor.

The hydraulic conductivity (k) was calculated by fitting Terzaghi's theory of consolidation [19] for different pressure increments using the c_v and m_v as

$$k = c_v \cdot m_v \cdot \gamma_w \tag{2}$$

Here, γ_w is the unit weight of the DI water.

2.3.2 Determination of Unconfined Compression Strength

Cylindrical samples of 38 mm diameter and 76 mm height were used to estimate the unconfined compressive strength of the unreinforced and reinforced sample. Unconfined compressive strength (σ_c) was performed according to ASTM D2166 [20] under a constant strain rate of 1.25 mm/min to simulate the undrained condition during the testing.

2.3.3 Determination of Volumetric Shrinkage and Desiccation Cracking of Sand–Bentonite–Fiber Composite

Unreinforced and reinforced soil sample had been prepared with a 7.1 cm diameter (i.e., 39.59 cm^2) and 3.01 cm in height. Each specimen had been prepared to their respective MDD and OMC condition under a room condition of 25 °C (±2 °C). The volumetric shrinkage had been defined as the change in volume (ΔV) to the total volume of the soil sample (V) %, stated by

$$Volumetric\ shrinkage\ strain = \frac{\Delta V}{V} \times 100\% \tag{3}$$

The analysis of the image had been done by ImageJ 1.51j8 (Java 1.8.0-112, 64-bit) and fundamental technique of "ImageJ" was described by Burger and Burge [21]. All the areas of compacted specimen (i.e., after desiccation), initial specimen area (I_a), reduced specimen (R_s), cracked area (A_c), shrinkage area (S_a), and combined crack area (C_{ca}) were calculated to get cracked intensity factor (CIF) and cracked density factor (CDF) for analyzing the desiccation crack developed in the soil. CIF and CDF had been defined as:

$$CIF = \frac{A_c \, in \, square \, Pixel}{R_s \, in \, square \, Pixel} \times 100\% \tag{4}$$

$$CDF = \frac{C_{ca}(i.e.\ A_c + S_a) \, in \, square \, Pixel}{I_a \, in \, square \, Pixel} \times 100\% \tag{5}$$

3 Result and Discussion

3.1 Effect of Tire Fiber on Time for 90% Consolidation (t_{90})

It can be seen (i.e., Fig. 1a) that t_{90} increases with increasing the consolidation pressure for all the composite. Upon comparison, a very clear distinction can be observed in the exhibited t_{90} values indicating that tire fiber content in the mixtures plays a major role in consolidation phenomenon. As the fiber content in the mixture is increasing, t_{90} was found to be decreasing. For example, under a consolidating pressure of 100 kPa, t_{90} was reduced from 253 to 191 min, 134 and 91 min with the inclusion of 5%, 10 and 15% tire fiber, respectively (i.e., Fig. 1a). Similarly, at same fiber content, t_{90} was further reduced from 350 to 265 min, 211 and 180 min under the consolidating pressure of 200 kPa. Hence, with the increasing consolidation pressure, the voids and pathways that were available for flow to take place earlier are destroyed leading to a lower hydraulic conductivity and resulting in an increase in the duration needed for 90% consolidation.

3.2 Impact of Tire Fiber on Hydraulic Conductivity

Hydraulic conductivity of the soil is one of the most essential conditions which must be satisfied in order to be used as a liner and cover material at the landfill. Many environmental agencies and researchers [22, 23] have suggested that the landfill liner and cover material should have at least a hydraulic conductivity value of 10^{-7} cm/s and 10^{-5} cm/s or less, respectively. The relationships between hydraulic conductivity and void ratio have been exhibited in Fig. 1b. It seems to clear that void ratio of the mixture was found to be increased as the percentage of the tire fiber increased. For example, hydraulic conductivity was increased from 3.23×10^{-9} cm/s to 9.98×10^{-9} cm/s, 4.35×10^{-8} and 1.05×10^{-7} cm/s due to presence of 5%, 10 and 15% tire fiber at void ratio of 0.45, indicating a pronounced effect of tire fiber on hydraulic conductivity at higher percentage of tire fiber. This trend can be explained in terms of presence of more flow channels for mixture with higher tire fiber contents, which is responsible for a higher value of hydraulic conductivity [9]. However, it is likely to be noticed that SB30 composite was satisfying the suitable construction material for landfill liner.

3.3 *Undrained Behavior of Compacted Sand–Bentonite–Tire Fiber Composite*

Compacted soils used for liner and cover system must have adequate shear strength. Daniel and Wu [24] suggested a minimum unconfined compressive strength of 200 kPa. According to this fact, compressive strength of sand–bentonite–tire fiber composite is an important parameter in estimating its suitability for use as a landfill material. Axial stress–strain behavior has been depicted in Fig. 2. From the figure, it was noticed that unconfined compressive strength (UCS) was found to increase up to 10% tire fiber; thereafter it starts to reduce with the inclusion of 15% tire fiber in to the mixture. For example, UCS was enhanced from 164 to 215 kPa, 249, and 223 kPa with the inclusion of 5%, 10, and 15% tire fiber. The improvement of the composite further defined in terms of improvement factor (I_f), which was calculated as the ratio of peak compressive strength of reinforced soil and peak compressive strength of unreinforced soil (UCS_r/UCS_{ur}). Improvement factor was found to be 1.31, 1.52, and 1.34 at 5%, 10, and 15% tire fiber. This increase can be attributed to the better packing of soil-fiber composite leading to coherent structure, which can sustain higher loading. On the other hand, failure strain of the unreinforced soil was significantly altered in comparison to reinforced soil. The improvement of failure strain was calculated according to displacement ratio (D_r) which is defined as the ratio of failure strain of reinforced soil to failure strain of unreinforced soil (ϵ_r/ϵ_{ur}). The displacement ratio was found to be 1.19, 1.2, and 1.29 with the inclusion of tire fiber, indicating the reinforced specimen gradually becomes ductile in nature.

Typical failure pattern of the composite was exhibited in Fig. 2. From the figure, it has been noticed that unreinforced soil has undergone clear shear failure ($T_f = 0\%$). With the inclusion of 5% tire fiber, specimen shows the well define shear failure, indicating the upper half of the specimen slid over the lower half. With increase the tire fiber from 5 to 10%, composite shows the mild shear failure. However, with

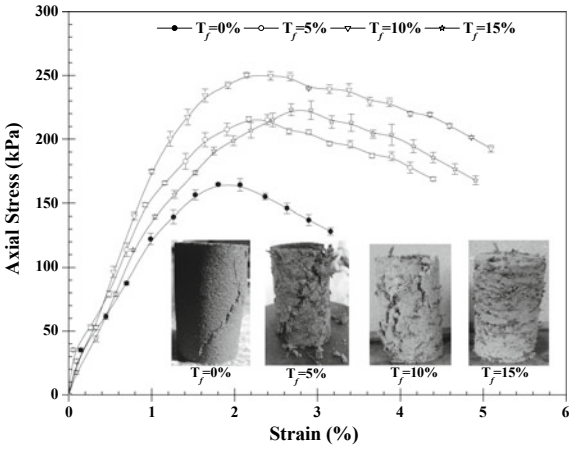

Fig. 2 Axial stress–strain behavior of compacted sand–bentonite–tire fiber

increase the tire fiber from 10 to 15%, the cracks expanded laterally toward central region, indicating that ductile failure was introduced.

Slope of the tangent to the initial section of the curve, a measure of the material's stiffness designated as initial tangent modulus (E_i), was also found out from the stress–strain behavior of the compacted sand–bentonite–tire fiber composite. It was observed that E_i of the composite was significantly increased with tire fiber. For example, initial tangent modulus was enhanced from 13.75 MPa to 16.39 MPa and 17.83 MPa with the inclusion of 5 and 10% tire fiber and then it starts to decrease from 17.83 to 15.66 MPa with increase in tire fiber from 10 to 15%.

According to field condition, the actual stress level can be at any strain level. Therefore, it is more suitable to specify the stiffness modulus at different strain levels. For any point on the stress–strain curve, the stiffness modulus is the ratio of axial stress level to the corresponding strain level. The stiffness modulus (E_{sec}) has been calculated at four different axial strain values (i.e., 0.15%, 0.45, 1.8, and 3.20%) and depicted in Fig. 3a. From the figure, it was noticed that E_{sec} of the composite was reduced with different strain level, but E_{sec} of reinforced composite was always higher in comparison to unreinforced soil. For example, at strain level of 0.15%, E_{sec} of unreinforced soil was found to be 12.74 MPa, but it was continuously enhanced from 12.74 MPa to 17.57 and 20.44 MPa at 5% as well as 10% tire fiber, respectively, however, E_{sec} of the composite was slightly reduced from 20.44 to 15.27 MPa with increase in the tire fiber from 10 to 15%. Hence, it has been observed that increase in elastic modulus indicates that fundamental property of the composite was significantly improved and load carrying capacity of the composite has been increased under a zero confinement.

Additionally, overall improvement of the composite was also emphasized in terms of energy absorption capacity (EAC). The absolute values of energy absorption are achieved by calculating the area under the stress–strain curve up to failure strain and it was shown in Fig. 3b. From the figure, it was found to be observed that energy absorption capacity (EAC) was significantly enhanced with the inclusion of

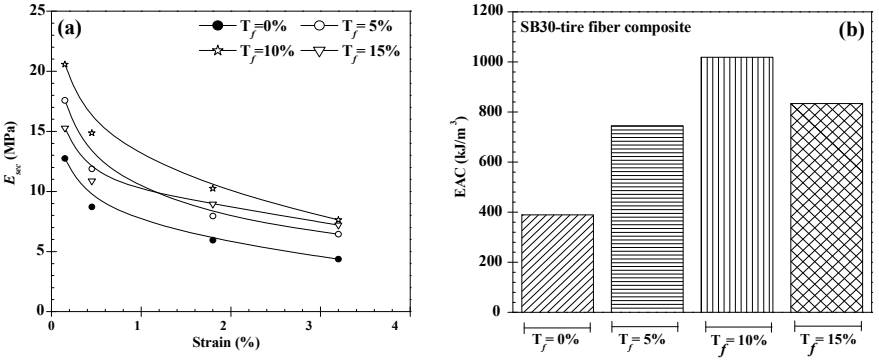

Fig. 3 **a** Secant modulus of SB30-tire fiber composite; **b** Energy absorption capacity of the SB30-tire fiber

tire fiber. For example, EAC of the composite was increased from 387 kJ/m^3 to 744 and 1021 kJ/m^3 with the inclusion of 5 and 10% tire fiber; however, it was reduced from 1021 to 831 kJ/m^3 with the increase in tire fiber from 10 to 15%. Therefore, it is indicating that the composite material becomes more strong and ductile to sustain higher load against failure.

3.4 Impact of Tire Fiber on Volumetric Shrinkage (VS), Crack Density Factor (CDF), and Crack Intensity Factor (CIF)

Daniel and Wu [24] suggested a 4% of VS of the soil as the acceptable limit for the landfill liner and cover material. According to this fact, volumetric shrinkage (VS) was evaluated for the unreinforced as well as reinforced specimen and it was found to decrease with tire fiber content. For example, volumetric shrinkage was reduced from 6.4% to 3.9% 2.3, 1.2% with 5%, 10, and 15% tire fiber and it was presented in Fig. 4. This mechanism could be defined that compressive strength of the composite was enhanced by the reinforcement action, which provided more resistance from the soil–fiber interaction against the shrinkage strain. The CDF of fiber reinforced specimen showed in Fig. 4a and all the CDF was calculated by image analysis; however, output result was presented in the form of the binary image (i.e.4a–4d).

From the figure, it was observed that the CDF was continuously reduced with addition of tire fiber. For example, CDF was decreased from 15.84%, to 10.75%, 3.76%, and 2.64, with inclusion of 5 and 10% tire fiber, respectively, and this trend is indicating to reduce the combined crack area of the composite. Similar trend was also followed by CIF. With the inclusion of tire fiber CIF of the specimen was decreased from 4.49% to 3.87%, 2.34, and 1.22%, indicating that crack area of the compacted

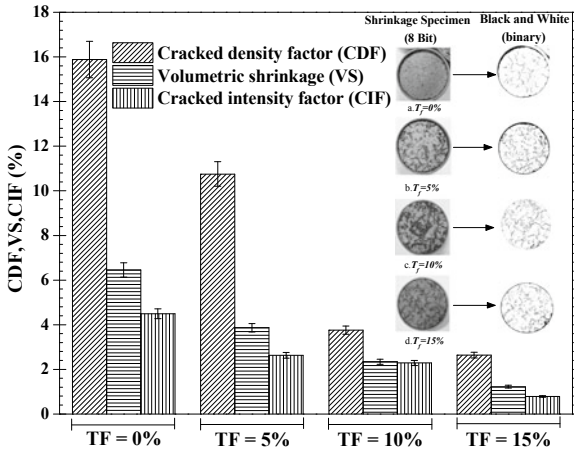

Fig. 4 Volumetric shrinkage and desiccation crack parameter of compacted SB30-tire fiber composite

specimen was reduced by the inclusion of tire fiber. Hence, VS, CDF, and CIF were strongly controlled as the fiber content increased, indicating that fiber additive would minimize the shrinkage crack, surface crack as well as volumetric shrinkage strain of hydraulic barrier when desiccation occurred.

4 Summary

1. Time for 90% consolidation was found to be reduced almost linearly with different consolidating pressure; however, it was also observed that t90 was further reduced with different tire fiber concentration. Hydraulic conductivity of the SB30 composite was found to increase with the addition of tire fiber, However, all the measured hydraulic conductivity was well below from design criteria, which were proposed for landfill liner (10–7 cm/s) and cover (10–5 cm/s).
2. From the UCS test result, it was concluded that the improvement factor, displacement ratio, and energy absorption capacity increased sharply with the inclusion of tire fiber up to 10%; thereafter it starts to decrease with increase the fiber concentration from 10 to 15%. Failure mode of the samples slightly changes from shear failure to ductile failure.
3. Volumetric shrinkage for sand–bentonite reinforced with tire fiber found to be considerably less than those of unreinforced sand–bentonite mixture and this behavior was strongly related to CIF and CDF of the unreinforced as well as the reinforced specimen. CDF was found to be more for unreinforced soil but CDF was sharply reduced as the tire fiber increased and CIF of the composite was maintained the same trend as followed by CDF. However, the decrease in CDF and CIF of the composite indicated that total crack of the composite was strongly controlled by the different percentage of tire fiber.

References

1. Hoornweg D, Bhada-Tata P (2016) What a waste: a global review of solid waste management. World Bank, Urban Development and Local Government Unit, Washington, DC
2. Rowe RK, Quigley RM, Booker JR (1995) Clayey barrier systems for waste disposal facilities. Chapman & Hall, London
3. Quigley RM (1993) Clay minerals against contaminant migration. Geotechn News North Am Geotech Community 11(4):44–46
4. Morris PH, Graham J, Williams DJ (1992) Cracking in drying soils. Can Geotech J 29(2):263–277
5. Rayhani MHT, Yanful EK, Fakher A (2008) Physical modeling of desiccation cracking in plastic soils. Eng Geol 97:25–31
6. Edil TB, Park JK, Kim JY (2004) Effectiveness of scrap tire chips as sorptive drainage material. J Environ Eng 130(7):824–831

7. Mukherjee K, Mishra AK (2018) Hydraulic and mechanical characteristics of compacted sand–bentonite: tyre chips mix for its landfill application. Environ Dev Sustain. 10.1007/s10668-018-0094-2
8. Soltani-Jigheh H, Asadzadeh M, Marefat V (2014) Effects of tire chips on shrinkage and cracking characteristics of cohesive soils. Turk J Eng Environ Sci 37(3):259–271
9. Soltani A, Deng A, Taheri A, Mirzababaei M, Nikraz H (2018) Interfacial shear strength of rubber–reinforced clays: a dimensional analysis perspective. Geosynth Int. https://doi.org/10.1680/jgein.18.00045
10. Thomas BS, Gupta RC (2016) Properties of high strength concrete containing scrap tire rubber. J Clean Prod 113:86–92
11. Ho M, Chan C, Bakar I (2010) One dimensional compressibility characteristics of clay stabilised with cement–rubber chips. Int J Sustain Constr Eng Technol 1(2):91–104
12. Tajdini M, Nabizadeh A, Taherkhani H, Zartaj H (2016) Effect of added waste rubber on the properties and failure mode of kaolinite clay. Int J Civ Eng 15(6):949–958
13. ASTM D422, Standard test method for particle-size analysis of soils. West Conshohoken, PA 6913
14. Sridharan A, Gurtug Y (2004) Swelling behaviour of compacted fine-grained soils. Eng Geol 72(1–2):9–18
15. ASTM D6913 (2009) Standard test methods for particle-size distribution (gradation) of soils using sieve analysis. West Conshohoken, PA
16. ASTM D6270 (1998) Standard practice for use of scrap tires in civil engineering applications. West Conshohocken, PA
17. ASTM D2435 (2011) Standard test method for one-dimensional consolidation properties of soils. West Conshohocken, PA
18. Taylor DW (1948) Fundamentals of soil mechanics. Wiley, New York
19. Terzaghi K (1943) Theoretical soil mechanics. Wiley, New York
20. ASTM D2166 (2016) Standard test method for unconfined compressive strength of cohesive soil. West Conshohocken, PA
21. Burger W, Burge MJ (2016) Digital image processing: an algorithmic introduction using Java. Springer, London
22. United States Environmental Protection Agency (USEPA) (1988) Design, construction and evaluation on of clay liners for waste management facilities. Technical Resource Document, Hazardous Waste engineering Research Laboratory, Office of Research and Development, U. S. Environmental Protection Agency, Cincinnati, Ohio, EPA/530-SW- 86-007F, NTIS PB 86-184496
23. Hauser VL, Weand BL, Gill MD (2001) Natural covers for landfills and buried waste. J Environ Eng 127(9):768–775
24. Daniel DE, Wu YK (1993) Compacted clay liners and covers for arid sites. J Geotech Eng 119(2):223–237

Feasibility Study for Using Waste Tire Rubber in Bituminous Concrete

Raj Kumar Thakur and S. K. Singh

Abstract An experimental programme was undertaken to investigate the performance of rubber modified bituminous mixes by using rubber as an aggregate, bitumen modifier and filler. The research was carried out in three stages. In the first stage, bitumen was modified by blending it with 5, 10, 15 and 20% (by weight of bitumen) crumb rubber (75–150 μ). In the second stage, fine aggregates in bituminous mixes were replaced with 2.5, 5, 7.5 and 10% rubber aggregates (<4.75 mm) whereas coarse aggregates were replaced with 2, 4 and 6% rubber (by weight of aggregates) of similar size (4.75–13.2 mm) by dry process. In the third stage, the mineral filler was replaced with 2, 5 and 8% crumb rubber (by weight of aggregates) passing 75 μ sieve. Marshall mix design was performed for bituminous concrete at different bitumen contents to evaluate the performance of the bituminous mixes having rubber in different proportions. It was observed that penetration and ductility of modified bitumen decreased whereas the softening point, elastic recovery and viscosity increased with the increase in rubber content. When rubber was introduced into the bituminous concrete mix as a fine aggregate mix performance was comparatively better than the mix having coarse rubber aggregates. However, in both cases, stability values showed a declining trend with the increase in rubber content. The optimum bitumen content increased as the percentage of the rubber increased in the bitumen modified and coarse aggregate mixes. Performance of bitumen modified mixes was found to be better as compared to the mixtures where it was used as an aggregate or as a filler.

Keywords Waste tire rubber · Rubber aggregate · Modified bitumen · Bituminous concrete · Wet process and dry process

R. K. Thakur (✉) · S. K. Singh
Punjab Engineering College (Deemed to be University), Chandigarh 160012, India
e-mail: rajkumarthakur.metrn17@pec.edu.in

K. R. Reddy et al. (eds.), *Sustainable Environment and Infrastructure*, Lecture Notes in Civil Engineering 90, https://doi.org/10.1007/978-3-030-51354-2_20

1 Introduction

With the improvement in living standards of the people and construction of new roads for the increasing population, the density of vehicular traffic is increasing day by day. According to the International organization of motor vehicle manufactures, about 1.28 billion vehicles were being used worldwide in 2015 [1]. The numbers are further rising with 94.9 million and 97.3 million cars and commercial vehicles being manufactured in 2016 and 2017, respectively [2]. Due to an increase in the number of vehicles on the roads millions of worn-out tires are generated every year becoming a significant source of waste materials**.** The European tyre and rubber manufacturers association (ETRMA) estimates that about 1.5 billion tires are produced each year and an equal amount can be considered to fall into the category of the end of life tires (ELTs) [3]. India contributes about 6–7% of global waste tire generation. Also, it is estimated that about 60% of waste tires in India are disposed of through illegal dumping [4]. The disposal of waste tires has serious consequences on the environment. Tires are difficult to compact and takes a great deal of space in landfills. Moreover, they are not easily decomposable and float to the top of the landfill because of trapped methane, which can damage the liners of the landfill. Black smoke produced by the burning of tires contains hazardous compounds and toxic gases which leads to air pollution. Utilization of scrapped tire rubber in roads appears to be a promising option as it can conserve natural resources and minimize environmental impact. Before using scrapped tire rubber in bituminous mixes, it is made free from wire and fabric. There are two processes for incorporating rubber into bituminous mixes which are referred to as the wet process and dry process. In the wet process, crumb rubber is blended with bitumen before incorporating the binder into the mixture and in the dry process, rubber is mixed with aggregates before the mixture is charged with bitumen [5].

Heavy axle loads and variations in daily and seasonal temperature of the pavement lead to the development of distresses such as rutting, cracking and potholing which causes deterioration of the surface layer. To minimize pavement degradation, it becomes necessary to modify the materials used in the bituminous surfacing. Studies have revealed that with the incorporation of crumb rubber into bitumen, properties of bitumen and bituminous mixes can be improved. Modified bitumen has a lower susceptibility to temperature variations, and have high rutting and fatigue resistance [6, 7]. Resistance to high temperature susceptibility can be attributed to the decrease in penetration and ductility, and an increase in the softening point of the modified binders. Modification of bitumen is also done to improve the resistance of pavement to the moisture damage as lack of moisture resistance leads to raveling and pothole formation in the surface layer [7, 8].

Polymers, such as rubber absorb bitumen and swell. The absorbed amount depends on the temperature, and viscosity of the bitumen [9]. When the interaction between rubber and bitumen takes place, rubber particles swell in the bitumen due to absorption of lighter fractions of bitumen (maltenes) causing the residual bitumen containing asphaltenes to be stiffer and elastic [10–12]. There are several

factors which affect the performance of crumb rubber bitumen mixtures such as the type of mixing process, size and concentration of the rubber particles and maturation time [8]. Finer size crumb rubber particle tends to react more quickly and produce higher viscosities as compared to larger particle sizes because of increased surface area. Generally, with the increase in the rubber content, the viscosity of the modified bitumen increases [12]. Due to the ease of incorporation of rubber in the dry process, it is possible to consume larger quantities of crumb rubber but inconsistency in the field performance makes the process not used widely [13]. The main concern in the performance of mixes prepared by the dry process is the resilient nature of the rubber particles which causes difficulty in compaction. It can lead to uneven compaction and poor bonding of mix ingredients [14]. High crumb rubber content in the mix causes a rebound effect which increases the percentage of air voids. Due to the increase in the air voids, mixes become more prone to the ingression of moisture which causes stripping and premature surface cracking. So, in contrast to the wet process, mixes prepared by the dry process are more susceptible to moisture than the mixes without rubber [14, 15]. In the dry process, the interaction between rubber and bitumen is kept to a minimum level so that rubber particles do not cause any modification of bitumen, and maintain their properties within the bituminous mixes [13]. However, researchers have found that during mixing crumb rubber does swell and react with bitumen due to which changes in the shape and rigidity of the rubber, and the performance of the bituminous mixture takes place [10, 11]. So, sometimes pre-treatment of crumb rubber is done with additives such as tall oil pitch to prevent it from absorbing the lighter fractions of bitumen during and after mixing [16].

Most of the research works reported in the literature concentrated on the modification of bitumen. Limited research has been done to assess the feasibility for using tire rubber aggregates and filler in bituminous concrete mixes. Moreover, previous researches are done in isolation and comparative behaviour of mixes prepared by using rubber as fine and coarse aggregate, bitumen modifier, and filler has not been studied. The objective of this research is to explore the use of waste tire rubber in bituminous concrete. Shredded tire/crumb rubber can be added in bituminous mixes by three ways that are directly in bitumen, as replacement of fine and coarse aggregate, and filler. Accordingly, the whole of the research is divided into three stages. In the first stage, crumb rubber is used as a blending material to modify the properties of bitumen. Performance of crumb rubber modified bitumen in bituminous concrete is then evaluated. The second stage assesses the possibility of substituting part of the natural aggregates (both fine and coarse aggregates) by scrap tire rubber aggregates and study its effect on the performance of bituminous mixes. The third stage investigates the feasibility of using crumb rubber as a filler in bituminous concrete. Marshall mix design method is used to evaluate the performance of the bituminous concrete mixes by conducting density-voids analysis and stability-flow test on the specimens. To analyse and compare the changes resulting from the use of rubber in conventional mixes, a reference mix without rubber is also prepared. The optimum bitumen contents and rubber percentages for the use of rubber as an aggregate, bitumen modifier and filler are then found out.

2 Materials

2.1 Aggregates

Pavement is subjected to a constant rubbing action which is caused by the movement of traffic. So, to provide good field performance and resist the abrasive action, high-quality aggregates should be used in the surface course. For the purpose of checking the adequacy of aggregates in bituminous mixes characterization of the aggregates was done and the results are shown in Table 1. It was observed that aggregates fulfil the bituminous concrete requirements laid down by the Ministry of Road Transport and Highways (MORTH) and therefore can be used successfully.

The available aggregate stockpiles were sieved into different size fractions and recombined to produce the desired gradation of bituminous concrete. Marshall mix design was conducted for Grading 1 of the MORTH specifications for roads and bridges [17] which is shown in Table 2. In the first and second stage of the research, samples were prepared using grading A (containing 5% filler content). In the third stage where the rubber is used as a filler material, all of the gradings mentioned in Table 2 (corresponding to 2, 5 and 8% filler content) were used to study the effect of filler on the performance of the mix.

Table 1 Properties of aggregates

Test	Results	MORTH specifications [17]	Test procedure
Aggregate impact value (%)	13.63	24	IS 2386 (Part 4):2002
Aggregate crushing value (%)	19.95	–	IS 2386 (Part 4):2002
Los Angeles abrasion (%)	22.42	30	IS 2386 (Part 4):2002
Combined flakiness and elongation index (%)	19.20	35	IS 2386 (Part 1):2002
Apparent specific gravity of coarse aggregate	2.72	–	IS 2386 (Part 3):2002
Bulk specific gravity of coarse aggregate	2.62	–	IS 2386 (Part 3):2002
Water absorption of coarse aggregates (%)	1.37	2	IS 2386 (Part 3):2002
Apparent specific gravity of fine aggregate	2.71	–	IS 2386 (Part 3):2002
Apparent specific gravity of filler (Stone dust)	2.58	–	IS 2386 (Part 3):2002

Table 2 Gradation of aggregates used in the study

Sieve size (Mesh)	Cumulative percent passing			
	Specification limits (Grading 1)	Grading A (5% Filler)	Grading B (2% Filler)	Grading C (8% Filler)
26.5 mm (1.06 in.)	100	100	100	100
19 mm (3/4 in.)	90–100	95	95	95
13.2 mm (0.530 in.)	59–79	69	69	69
9.5 mm (3/8 in.)	52–72	62	62	62
4.75 mm (#4)	35–55	45	45	45
2.36 mm (#8)	28–44	36	36	30
1.18 mm (#16)	20–34	27	27	26
600 μ (#30)	15–27	21	21	23
300 μ (#50)	10–20	15	14	20
150 μ (#100)	5–13	9	8	13
75 μ (#200)	2–8	5	2	8
Pan	0	0	0	0

2.2 Bitumen

The primary role of bitumen is to act as a binder in the bituminous mixes and cohesion provided by it increases with the stiffness of the binder. Addition of additives such as crumb rubber changes the properties of the binder. So, characterization of the binder is essential to understand its behaviour on the performance of the mix. In this study, locally available binder corresponding to 80/100 penetration grade (viscosity grade 10) was used. Properties of bitumen are shown in Table 3.

Table 3 Properties of Bitumen

Test	Results	IS 73:2013 specifications [18]	Test procedure
Penetration at 25 °C	87	80 (Min)	IS 1203:2004
Softening point (°C)	44.5	40 (Min)	IS 1205:2004
Ductility at 25 °C (cm)	93	75 (Min)	IS 1208:2004
Flash point (°C)	265	220(Min)	IS 1209:2004
Fire point (°C)	305	–	IS 1209:2004
Specific gravity at 27 °C	1.02	–	IS 1202:2004

2.3 Rubber

There are two processes for producing crumb rubber namely ambient grinding and cryogenic grinding. Ambient ground rubber is obtained by shredding and grinding the tire rubber at or above room temperature whereas cryogenically ground rubber is obtained by grinding the tire rubber at or below the embrittlement temperature of the rubber using liquid nitrogen as coolant [19–21]. The rubber used in this study was obtained from ambient grinding and supplied by Publix India Incorporation, Ludhiana, India. Different sizes of rubber were separated by sieves. Before using shredded rubber, it was made free from fibres present in it. Properties of shredded rubber are shown in Table 4.

3 Experimental Design and Procedure

Marshall mix design method is generally used in India for designing and controlling of bituminous mixes. This method uses standard test specimens of 63.5 mm height and 101.6 mm in diameter. Each test specimen usually requires approximately 1200 g of aggregate. For each aggregate gradation and rubber content, specimens having different bitumen content were prepared and tested in the laboratory according to AASHTO T245 [22]. The aggregates and bitumen binder were blended at their corresponding mixing temperatures. Samples were compacted by giving 75 blows on each face with a 4.54 kg hammer using a free fall of 457 mm representing heavy traffic conditions. Specimens were then removed from the mold and allowed to cool overnight. Before testing, specimens were immersed in a water bath at 60 °C for 30 min. Determination of optimum bitumen content was done as per Asphalt Institute MS-2 Manual [23]. The Asphalt Institute recommends that when compacted to the design number of blows, the optimum binder content results in 45% air voids and satisfactorily meets all Marshall parameters.

Table 4 Properties of rubber

Apparent specific gravity of rubber	Results	Test procedure
Coarse aggregate (passing 13.2 mm and retained on 4.75 mm sieve)	1.149	
Fine aggregate (passing 4.75 mm and retained on 75 μ sieve)	1.099	IS 2386 (Part 3):2002
Filler	0.958	
Crumb rubber modifier (CRM) passing 150 μ and retained on 75 μ sieve	0.949	

3.1 Wet Process

Laboratory preparation of modified bitumen was done by blending crumb rubber modifier (CRM) and bitumen. To ensure adequate reaction blending was done at a temperature of 160–180 C for 45–60 min. Bitumen was modified with 5, 10, 15 and 20% (by weight of bitumen) crumb rubber passing 150 μ and retained on 75 μ sieve. Marshall test was conducted for each CRM percentage at 4, 5, 6 and 7% bitumen content. Generally, the mixing and compaction temperatures of bituminous mixes are based on the viscosity of bitumen. However, in the case of rubber modified mixes this method estimates unreasonably high mixing and compaction temperatures [24]. So, a mixing temperature of 170–180 °C was selected for this study.

3.2 Dry Process

In the specimens prepared by the dry process, rubber which was the replacement for a specific aggregate fraction was added in the aggregate batch. Before mixing the batch with bitumen, aggregates were heated in the oven. Bitumen was heated to a temperature of 160–170 °C and the mixing was done at 170 °C. During mixing excessive smoking and burning of rubber particles should be avoided as it increases stiffness and fragility of the mix [25]. Moreover, high temperature leads to aging of the bitumen, which affects the performance of the mix [15]. Fine aggregates (passing 4.75 mm and retained on 75 μ sieve) were replaced with 2.5, 5, 7.5 and 10% rubber aggregates (by weight of aggregates).

During experimentation, it was observed that when compacted, rubber aggregates having a size larger than 13.2 mm caused a rebound effect. Due to this high air voids in the specimen occurred and there was a weakening of the bond between aggregates and binder which adversely affected properties of the mix. Hence, rubber aggregates having a size smaller than 13.2 mm were used. Coarse aggregates (passing 13.2 mm and retained on 4.75 mm) were replaced with 2, 4 and 6% rubber aggregates (by weight of aggregates) of similar size. Marshall test were conducted at 4, 5, 6, 7 and 8% bitumen content.

To study the effect of filler on the mix, the conventional filler was replaced with 2, 5 and 8% crumb rubber (by weight of aggregates) passing 75 μ sieve and Marshall tests were conducted at 4, 5, 6 and 7% bitumen content.

4 Results and Discussion

4.1 Crumb Rubber Modified Bitumen

Bitumen was modified by wet process with 5, 10, 15 and 20% (by weight of bitumen) crumb rubber modifier. All the relevant tests were performed to measure the degree of modification of bitumen by crumb rubber (Table 5).

It can be observed that the penetration and ductility of the modified bitumen decreased with the increase in the CRM percentage (see Fig. 1). However, the addition of crumb rubber caused an increase in the viscosity and softening point of bitumen. This behaviour of the modified bitumen can be attributed to the increase in the

Table 5 Consistency tests on modified bitumen

Test	Crumb rubber percentage					IS 15462 specifications [26]	Test procedure
	0	5	10	15	20		
Penetration at 25 °C	87	51	34	23	10	70 (Max)	IS 1203:2004
Softening point (°C)	44.5	49.8	53.2	56.8	60.3	50 (Min)	IS 1205:2004
Ductility at 25 °C (cm)	93	28	19.7	12	10.4	–	IS 1208:2004
Elastic recovery @ 15 °C (%)	18	39	51	65	72	50 (Min)	IS 15462:2004
Industrial viscosity @ 60 °C (seconds)	42	93	178	332	517	–	IS 1206 (Part I):2004

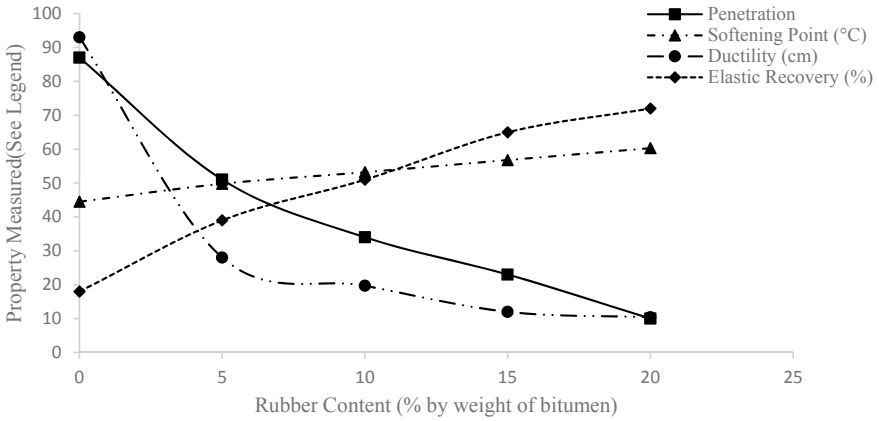

Fig. 1 Variation in the properties of modified bitumen with rubber content

Table 6 Comparison of performance of modified bitumen at OBC

Rubber content (%)	OBC (%)	Marshall stability (kg)	Marshall flow (mm)	Air Voids (%)	VMA (%)	VFB (%)	Bulk density (kg/m^3)
0	5.20	1950	2.30	4	15.70	74.75	2411.5
5	5.60	1215	2.20	4	16.88	75.75	2388.0
10	5.75	1100	2.45	4	17.15	75.25	2382.0
15	6.10	995	2.70	4	17.48	77.25	2379.5
20	6.25	965	2.80	4	18.08	77.75	2369.0
IRC SP53 specifications [29]	5.40 (Min)	1000 (Min)	2.5–4.0	3–5	12 (Min)	65–75	–

stiffness of binder which makes the material less susceptible to high temperatures. Elastic recovery test conducted on the modified bitumen indicated that the ability of bitumen to recover from elastic deformation increased due to an increase in the stiffness of the binder. Results obtained were consistent with the previous studies [6, 27, 28].

Marshall test were conducted on the crumb rubber modified bitumen. It can be observed from Table 6 that as rubber percentage in the mix increases the Marshall stability of the samples decreases. Also, higher rubber quantities produce higher air voids and voids in mineral aggregates (VMA) in the mix due to which bitumen requirement for coating of aggregates increases. Addition of rubber increased the optimum bitumen content (OBC) from 5.20% (without rubber) to 6.25% (20% rubber by weight of bitumen) as shown in Table 6. It was observed that at 15% rubber content, Marshall stability value and voids filled with bitumen (VFB) of the mix do not satisfy the requirements for bituminous concrete. Hence 10% of CRM was selected as optimum for the modification of bitumen.

5 Rubber Aggregates

Replacement of Fine Aggregates

When rubber was used as a replacement for fine aggregates a reduction in the density and air voids of the mix was observed with the increase in rubber content. In contrast to crumb rubber modified bitumen (CRMB) samples, samples made by replacement of fine rubber aggregates showed a decrease in the VMA (Table 7). Crumb rubber mixes containing less than 4% of bitumen binder exhibited poor performance. Olivares et al. [30] also observed similar behaviour and concluded that degradation of the mix occurs in mixes containing less than 4% of bitumen binder. So for 10% rubber content samples, a bitumen content of 4% was taken as optimum. Hence, a compromise in the target air voids (4%) was made. The optimum bitumen content decreased from

Table 7 Comparison of performance of aggregate replacement at OBC

Mix	Rubber content (%)	OBC (%)	Marshall stability (kg)	Marshall flow (mm)	Air Voids (%)	VMA (%)	VFB (%)	Bulk density (kg/m^3)
Control	0	5.20	1950.00	2.30	4.00	15.70	74.75	2411.5
Fine aggregate replacement	2.5	5.65	1350.00	1.75	4.00	16.50	76.25	2318.0
	5.0	5.60	555.00	1.88	4.00	16.28	74.00	2242.0
	7.5	4.45	425.00	2.35	4.00	13.60	70.25	2211.8
	10	4.00	374.00	2.10	3.47	11.84	70.70	2170.8
Coarse aggregate replacement	2.0	6.00	1065.31	2.35	4.90	18.03	72.82	2301.4
	4.0	8.00	319.14	2.79	4.79	21.49	77.72	2198.7
	6.0	8.00	202.15	3.75	7.01	23.03	69.56	2102.1
MORTH specifications [17]		5.20 (Min)	900 (Min)	2–4	3–5	12 (Min)	65–75	–

5.65% at 2.5% rubber content to 4% at 10% rubber content. It was observed that beyond 2.5% rubber content there was a substantial decrease in the stability values. Hence 2.5% replacement of fine rubber aggregates was taken as optimum.

Replacement of Coarse Aggregates

Due to the resilient nature of rubber aggregates, an upward pressure (rebound) occurred within the mix during compaction which made the mix less compact. The rebound effect in the mix increased with the increase in the concentration of rubber aggregates. This caused a significant increase in the air voids and VMA of the mix which was greater than the reference mix but less than the mix having rubber size greater than 13.2 mm. Stability value decreased whereas the flow value increased with the increase in rubber content which was in good agreement with previous researches [14, 15]. The optimum bitumen content (for 4% air voids) at 2% rubber content came out to be 7.2%. However, Marshall stability was not satisfied at this bitumen content. So, OBC was selected at 6% bitumen content which satisfied the stability requirements. At this bitumen content, the air voids were still in the acceptable limits. Corresponding to 6% rubber content and 8% bitumen content, air voids in the mix were 7.01%. Further increase in the bitumen content to reduce voids was not done as the process would not have been economical in the field. Moreover, the mixes were not satisfying stability requirements at this rubber content. So, the percentage of rubber beyond 2% is not feasible in case of coarse aggregates replacement.

5.1 Replacement of Conventional Filler with Crumb Rubber

When crumb rubber was used as a filler in the mix its behaviour was somewhat similar to the replacement of the fine aggregates. Both air voids and VMA decreased with

Table 8 Comparison of performance of filler replacement at OBC

Filler	Filler content (%)	OBC (%)	Marshall stability (kg)	Marshall flow (mm)	Air voids (%)	VMA (%)	VFB (%)	Bulk density (kg/m^3)
Stone dust	2	5.50	1300.00	1.98	4.00	16.63	76.00	2397.5
	5	5.20	1950.00	2.30	4.00	15.70	74.75	2411.5
	8	5.45	1295.00	1.95	4.00	16.30	75.25	2391.0
Crumb rubber	2	5.40	650.00	2.05	4.00	15.90	75.50	2331.3
	5	4.90	962.50	1.90	4.00	14.93	71.50	2228.0
	8	4.00	190.50	3.05	3.75	12.14	69.08	2169.3

the increase in the filler content. OBC decreased from 5.4% at 2% rubber content to 4% at 8% rubber content. However, stability values for 5% rubber content were found to be better than that of 2% and 8% rubber content (Table 8). Increase in the flow values was observed with the increase in the rubber content in the mix.

6 Comparison of Bituminous Mixes Performance at Optimum Bitumen Content

Bituminous mixes prepared by the replacement of fine aggregate, coarse aggregate and filler were compared corresponding to their optimum bitumen content (Tables 7 and 8). It was observed that the inclusion of rubber in the bituminous mix generally yielded lower stabilities and higher flows. Stability of a mix generally depends on the internal friction provided by the aggregate particles [23]. Decrease in the stability values (see Fig. 2a, b) can be attributed to the softening of agglomerate due to an increase of rubber particles in the mix.

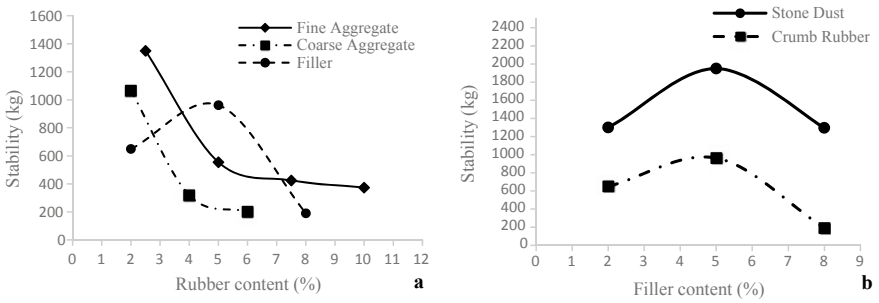

Fig. 2 **a** Variation in the stability of the bituminous mixes with different rubber contents. **b** Variation in the stability of bituminous mixes at different filler contents

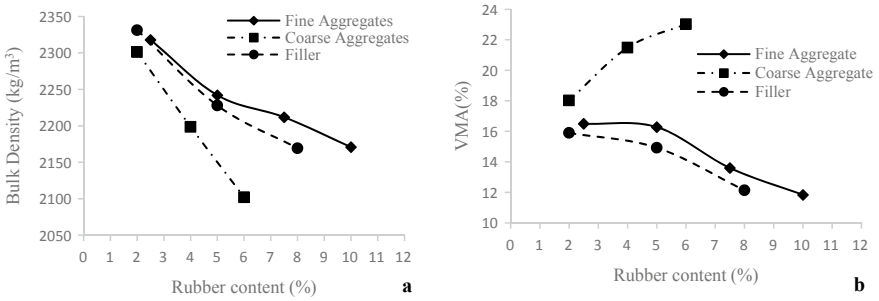

Fig. 3 **a** Variation in the bulk density of bituminous mixes at different filler contents. **b** Variation in the VMA of the bituminous mixes with different rubber contents

Addition of rubber into the mix (by the dry process) decreased the density of the mix (see Fig. 3a). This effect was more pronounced in the replacement of coarse aggregate as compared to the replacement of fine aggregate and filler. Replacement of coarse aggregate with rubber increased the voids in mineral aggregates (VMA) of the mix. However, a decrease in the VMA was observed in the replacement of fine aggregate and filler with the increase in the rubber content (see Fig. 3b). The poor performance of the mixes prepared by the replacement of fine aggregate and filler can be ascribed to the less available space in the mix because of the low density of rubber. The performance of mixes can be enhanced by decreasing the passing percentage of fine aggregate and fillers which will provide space to accommodate rubber particles in the mix [7]. This can be done by following the lower borderline of the fine aggregate gradation mentioned in Table 2.

7 Conclusions

Performance of rubber modified mixes prepared by the wet and dry process was investigated in this experimental study using Marshall mix design method. A sequential laboratory testing procedure was followed to determine the optimum percentages of rubber and bitumen content for using rubber as an aggregate, modifier and filler.

Based on the laboratory test the following conclusions were made:

- Penetration and ductility of the modified bitumen decreased whereas viscosity, softening point and elastic recovery of bitumen increased with the increase in the crumb rubber percentage. This behaviour of the modified bitumen was due to the increase in the stiffness of binder. Addition of rubber in bitumen increased the optimum bitumen content (OBC) from 5.20% (without rubber) to 6.25% (20% rubber by weight of bitumen). 10% (by weight of bitumen) crumb rubber percentage was found as optimum for the modification of bitumen.
- In coarse rubber aggregates, a rebound in the mix occurred during compaction due to the resilient nature of rubber aggregates. Rebound increased with the increase

in the concentration of rubber aggregates. The rebound was more pronounced for rubber aggregates having a size larger than 13.2 mm.

- The density of the mix decreased with the addition of rubber in the mix (by the dry process). The decrease was more in case of coarse aggregates as compared to fine aggregates and filler.
- Air voids and VMA increased with the increase in the rubber content in case of coarse aggregate replacement whereas it decreased in fine aggregate and filler replacement.
- The decrease in the stability values occurred with the increase of the rubber particles in the mix due to the softening of the agglomerate.
- For the addition of rubber into the mix (by the dry process) 2.5% fine aggregate, 2% coarse aggregate and 5% filler (by weight of aggregates) was found to be the optimum percentages for replacement.
- For improving the performance of rubber mixes decreasing the passing percentage of fine aggregate and filler was found to be essential which can be done by following the lower borderline of the fine aggregate gradation.

References

1. International Organization of Motor Vehicle Manufacturers. Vehicle statistics. https://www.oica.net/category/vehicles-in-use/. Last Accessed 14 Feb 2019
2. International Organization of Motor Vehicle Manufacturers. Vehicle production statistics. https://www.oica.net/category/production-statistics/2017-statistics/. Last Accessed 14 Feb 2019
3. ETRMA: End of life tyres: a valuable resource with growing potential. European Tyre and Rubber Manufactures Association, Brussel (2011)
4. Mishra L (2016) Turning waste tyre into green steel. The Hindu, Mumbai. https://www.thehindu.com/business/Turning-waste-tyre-into%E2%80%98green-steel%E2%80%99/article14518524.ece. Last Accessed 14 Feb 2019
5. Heitzman M (1992) Design and construction of asphalt paving materials with crumb rubber modifier. Transp Res Rec 1339:1–8
6. Irfan M, Ali Y, Ahmed S, Hafeez I (2018) Performance evaluation of crumb rubber modified asphalt mixtures based on laboratory and field investigations. Arab J Sci Eng 43(4):1795–1806
7. Dong Y, Tan Y (2011) Mix design and performance of crumb rubber modified asphalt SMA. Geotech Special Pub ASCE 212:78–86
8. Cetin A (2013) Effects of crumb rubber size and concentration on performance of porous asphalt mixtures. Int J Polymer Sci
9. Treloar LRG (1975) The physics of rubber elasticity, 3rd edn. Oxford University Press, Oxford, UK
10. Singleton TM, Airey GD, Collop AC, Widyatmoko I (2000) Residual bitumen characteristics following dry process rubber–bitumen interaction. In: Proceedings of the Asphalt rubber conference, pp 463–482. Vilamoura, Portugal
11. Airey GD, Rahman MM, Collop AC (2003) Absorption of bitumen into crumb rubber using the basket drainage method. Int J Pavement Eng 14(4):344–354
12. Hicks RG, Lundy JR, Leahy RB, Hanson D, Epps J (1995) Crumb rubber modifiers (CRM) in asphalt pavements: summary of practices in Arizona, California, and Florida. Department of Transportation Federal Highway Administration, US

13. Rahman MM, Airey GD, Collop AC (2005) The mechanical properties of the dry process CRM asphalt mixtures following short-term and long-term ageing. In: Proceedings of 7th international conference on the bearing capacity of roads and airfields, Trondheim, Norway
14. Rahman MM, Airey GD, Collop AC (2010) Moisture susceptibility of high and low compaction dry process crumb rubber modified asphalt mixtures. Transp Res Rec 2180:121–129
15. Moreno F, Rubio MC, Martinez-Echevarria MJ (2011) Analysis of digestion time and the crumb rubber percentage in dry-process crumb rubber modified hot bituminous mixes. Constr Build Mater 25(5):2323–2334
16. Kim JR (2001) Characteristics of crumb rubber modified (CRM) asphalt concrete. KSCE J Civ Eng 5(2):157–164
17. Ministry of road transport and highways: specifications for roads and bridge works. Indian Road Congress, New Delhi, India (2013)
18. IS 73: Paving Bitumen – Specifications. Bureau of Indian Standards, New Delhi, India (2013)
19. Pereira SMS, Oliveira JRM, Freitas EF, Machado P (2013) Mechanical performance of asphalt mixtures produced with cork or rubber granulates as aggregate partial substitutes. Constr Build Mater 41:209–215
20. Fontes LP, Triches G, Pais JC, Pereira PA (2010) Evaluating permanent deformation in asphalt rubber mixtures. Constr Build Mater 24(7):1193–1200
21. Presti DL (2013) Recycled tyre rubber modified bitumens for road asphalt mixtures: a literature review. Constr Build Mater 49:863–881
22. AASHTO T245-97: Resistance to plastic flow of bituminous mixtures using Marshall apparatus. American Association of State and Highway Transportation Officials, Washington, DC, USA (2001)
23. Asphalt Institute Manual Series No. 2: Asphalt mix design methods. Asphalt Institute, Lexington, USA (2014)
24. Subhy A, Airey GD, Presti DL (2017) An investigation of the mechanical properties of rubber modified asphalt mixtures using a modified dry process. In: Proceedings of the 10th international conference on the bearing capacity of roads, railways and airfields, Athens, Greece (2017)
25. Aisien FA, Hymore FK, Ebewele RO (2006) Application of ground scrap tyre rubbers in asphalt concrete pavements. Indian J Eng Mater Sci 13:333–338
26. IS 15462: Polymer and rubber modified bitumen–specification. Bureau of Indian Standards, New Delhi, India (2004)
27. Arabani M, Tahami SA, Hamedi GH (2017) Performance evaluation of dry process crumb rubber-modified asphalt mixtures with nanomaterial. Road Mater Pavement Des 17:1–8
28. Liu H, Chen Z, Wang W, Wang H, Hao P (2014) Investigation of the rheological modification mechanism of crumb rubber modified asphalt (CRMA) containing TOR additive. Constr Build Mater 67:225–233
29. IRC: SP 53: Guidelines on use of polymer and rubber modified bitumen in road construction. Indian Road Congress, New Delhi, India (2010)
30. Olivares FH, Schultz BW, Fernández MA, Moro CB (2009) Rubber modified hot-mix asphalt pavement by dry process. Int J Pavement Eng 10(4):277–288

Applicability Evaluation of Mixtures of Steel Slag Aggregate with Lateritic Soil as Base Material for Road Pavements

Nairo D. T. Buitrago, Victor H. S. Oliveira, Luís F. M. Ribeiro, André L. B. Cavalcante, and Fernando F. Monteiro

Abstract Environmental degradation and global warming have become a considerable issue in recent years. The use of more environmentally friendly materials in geotechnical engineering is of preeminent importance. The steel slag aggregate has become an alternative to conventional natural aggregates in road paving works. Therefore, this research aims to evaluate the applicability of the steel slag aggregate as an aggregate for pavement supporting courses (base and subbases). The present research deals with the use of mixtures of steel aggregate and lateritic soil obtained at the site (BR 381/MG) were the subject of the study is located. The experimental program for geotechnical laboratory tests was defined, including the physical and mechanical characterization of the steel slag aggregate, lateritic soil, and three mixtures of these components: 70% steel slag aggregate +30% lateritic soil (M7030), 80% steel slag aggregate +20% lateritic soil (M8020), and 90% steel slag aggregate +10% lateritic soil (M9010). The results of the tests showed that the steel slag aggregate provides satisfactory characteristics to be used as paving material, as long as the expansion of the steel slag aggregate is restrained. The three mixtures of steel slag aggregate and soil, presented satisfactory performance, showing texture compliance, controlled expansion, and high values of California Bearing Ratio (CBR). Therefore, verifying that the steel slag aggregate mixtures can be applied as a base material for road pavements.

Keywords Steel slag aggregate · Lateritic soils · Expansion · CBR

1 Introduction

Road works have high economic and environmental costs and demands for non-renewable natural aggregates. One solution to the costs in question is the development of low cost, environmentally friendly alternatives to building pavements with quality and safety to users. In this scenario, the steel aggregate, steel slag treated at the steel

N. D. T. Buitrago (✉) · V. H. S. Oliveira · L. F. M. Ribeiro · A. L. B. Cavalcante · F. F. Monteiro
University of Brasilia, Brasília 70910-900, Brazil
e-mail: nairodavidtarazona@gmail.com

K. R. Reddy et al. (eds.), *Sustainable Environment and Infrastructure*, Lecture Notes in Civil Engineering 90, https://doi.org/10.1007/978-3-030-51354-2_21

mill with specified characteristics for pavements, has great applicability in Brazil, since the country is the largest Latin American steel producer and one of the largest producers in the world [1].

The relevance of the application of these materials as alternative aggregates in paving works is observed, facing the need to contribute to the planet sustainability, encouraging the reduction of consumption of non-renewable natural resources such as those from rock mining, sand, and other primary materials [2]. Also, there is the possibility of transforming a potential environmental liability of the steel industry into an economic and environmental asset, avoiding the unnecessary disposal of materials in the landfills. Many studies have been performed using steel slag in pavements. In Brazil, steel slag has been used as small and large aggregate in road paving, being particularly suitable for its hardness, durability, free drainage, and high resistance to crushing [3]. Therefore, this research aims to evaluate the applicability of the steel slag aggregate as an aggregate for pavement supporting courses (base and subbases).

Steel slag is formed in electric furnaces or oxygen converters through the conversion of iron and steel scrap; and is composed of various chemical elements that are not utilized in steel production. The slags are compounds formed from additions of CaO (Calcium Oxide), MgO (Magnesium Oxide), and CaF_2 (Fluorite), whose purpose is to absorb the oxides resulting from the reaction of oxygen in the process with the impurities (P, S, M_n, C, etc.). The steel slag is rich in CaO, MgO, and SiO_2 (Silicon Dioxide), making it a material with expansive characteristics [4, 5].

One of the most significant difficulties, however, in the use of steel slag as aggregate in layers of pavements is controlling its swelling potential, because this generates internal stresses that cause cracks in the structural layers of the roads and decrease their strength and durability [6]. Expansive characteristics in the steel slag are mainly due to the hydration of the Calcium oxide (CaO), which is transformed into calcium hydroxide (Ca(OH)) and Magnesium Oxide (MgO). It also influences the swelling processes of change in allotropic forms of calcium silicate (C_2S) and corrosion and oxidation of residual metal iron reported that free calcium oxide and free magnesium oxide in the steel slag, hydrate faster and slower, respectively, and are responsible for the volumetric instability of the slag [7]. The curing process applied to the steel slag by the Brazilian steel industry to generate the steel aggregate has been shown to be effective in controlling swelling potential [8].

2 Materials and Methods

The steel slag aggregate used in this research (Fig. 1a) was generated from steel slag produced in LD type oxygen converter by a steel mill, a member of the Brazilian Steel Institute (IABR). At the plant, all the previous processing of the material was performed. The lateritic soil (Fig. 1b) was collected at the site (BR 381/MG- Brazil) and then, subjected to characterization tests.

The experimental program for geotechnical laboratory tests was defined, including the physical and mechanical characterization of the steel slag aggregate, soil,

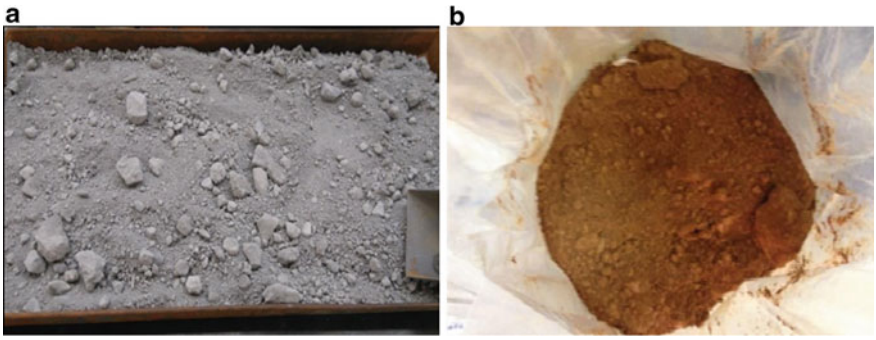

Fig. 1 **a** Treated steel aggregate. **b** Lateritic soil

and three mixtures of these components: 70% steel aggregate +30% lateritic soil (M7030), 80% steel aggregate +20% lateritic soil (M8020), and 90% steel aggregate +10% lateritic soil (M9010). The steel slag was crushed and stabilized in relation to particle size. The reduction of the swelling potential of the material occurred by open-air storage. Compaction and CBR tests were also performed according to ME 164 [9] and ME172 [10].

The soil utilized in the research had a plasticity index of 21.34%, belonging to the MH- OH group, composed of high-plasticity clay-silt soils according to the Unified Soil Classification System. According to the AASHTO Soil Classification System, the soil is classified as A-7: clays and silts (more than 75% of the material passes in the 0.074-mm mesh) with high liquidity index and high-volume changes in dry and wet conditions. Figure 2 presents the particle-size distribution curves with and without chemical breakdown, showing a typical behavior of lateritic soils. The compaction tests for the lateritic soil were carried out manually, without material reuse, with 100% of the modified and standard compaction energy.

Figure 3 presents five particle-size distribution curves of the steel aggregate samples (G1, G2, G3, G4, and G5). Due to the similarity between the particle-size distribution curves, average values were adopted to perform the classification of the material according to the Unified Soil Classification System (SUCS). The steel aggregate was classified as an SP material, that is, a material with characteristics like poorly graded clean sand. The steel aggregate was classified as A-1-a soil in the AASHTO Soil Classification System. From a grain size point of view, the steel aggregate complies with the characteristics required to be employed in the construction of granular pavement layers. The compaction test for the steel aggregate was carried out manually, without material reuse, with 100% of the modified compaction energy.

Table 1 presents the physical properties of the lateritic soil. The steel aggregate was classified as non-plastic (NP). On the compaction test, the steel slag aggregate presented a dry unit weight value equivalent to 23.10 kN/m^3 and an optimum moisture content equivalent to 8.75%. It is worth mentioning that modified compaction energy was applied to the tested sample.

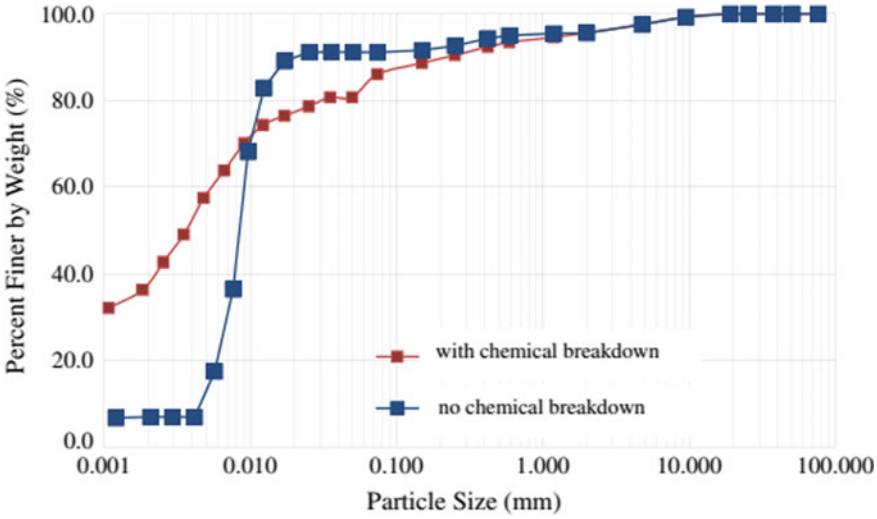

Fig. 2 Soil particle-size distribution curves

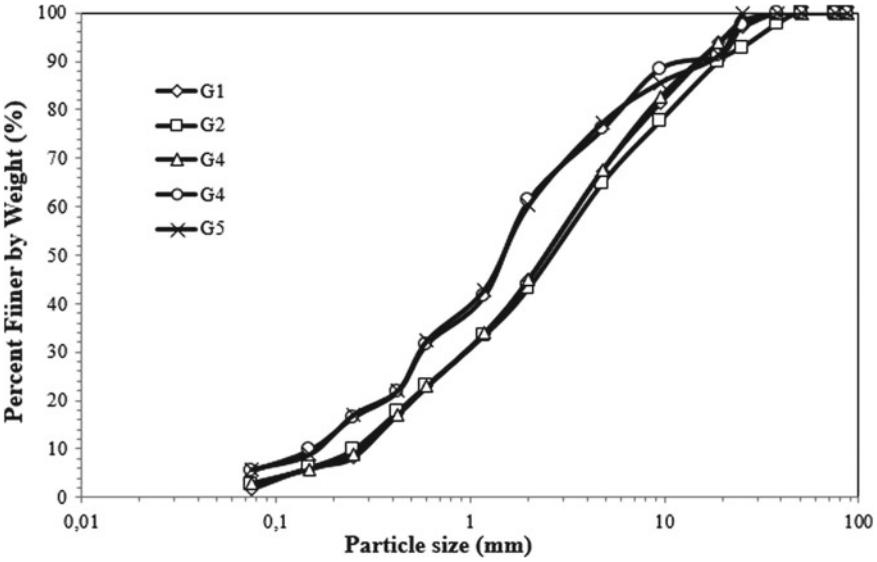

Fig. 3 Steel aggregate particle-size distribution curves

Figure 4 presents particle-size distribution curves of the mixtures of this research (M7030, M8020 and M9010). All three mixtures were classified as non-plastic (NP) materials. The compaction tests for the three mixtures were performed manually,

Table 1 Physical properties of the soil

Property	Value
w_L (%)	68.50
w_P (%)	47.16
Plasticity index (%)	21.34
Unified soil classification system (USCS)	Inorganic silts
γs (kN/m^3)	29.51
wot (%)	31.0 (SCE)
	26.5 (MCE)
γdmax (kN/m^3)	14.0 (SCE)
	15.50 (MCE)

Note MCE = modified compaction energy; and SCE = standard compaction energy

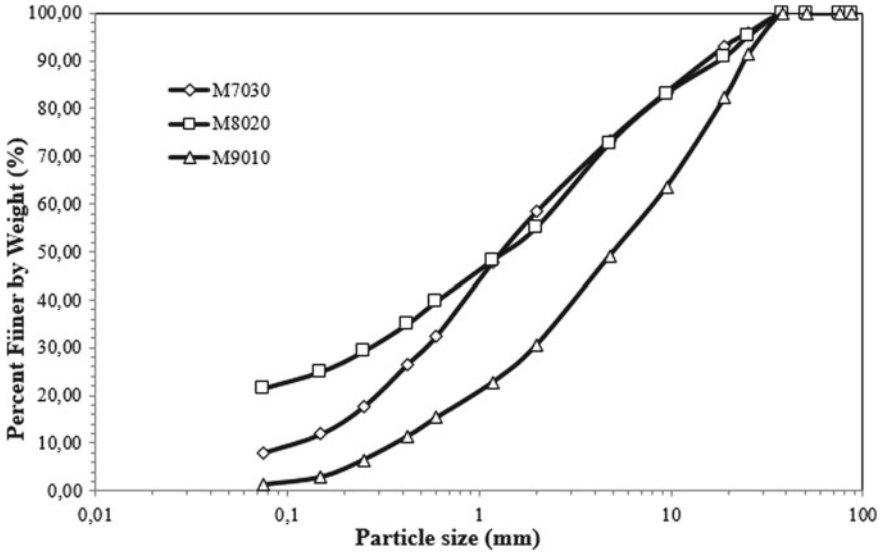

Fig. 4 Mixtures particle-size distribution curves

without material reuse, with 100% of the modified compaction energy. The test specimens molded in the compaction test were immersed in water for five days, to evaluate the sample expansion. After this procedure, the specimens were subjected to CBR tests. It was necessary to present and jointly analyze the results of the compaction and CBR tests for the definition of optimum moisture content and maximum dry unit weight of the mixtures. Therefore, obtaining values that truly represent the point of best mechanical performance for each mixture.

3 Results and Discussions

Two compaction curves were made for the lateritic soil, using manual compaction. One of the curves was made using 100% of the standard compaction energy, with material reuse (due to the availability of material), aiming to obtain an estimate of the optimum moisture content. The other compaction curve was performed with the same methodology applied to the mixtures compaction tests, where modified compaction energy was applied to the samples, without reuse of material, and subsequent determination of CBR. It is worth mentioning that the specimens were immersed in water for expansion determination. The compaction curves are presented in Fig. 5 with the saturation curves of 100% (S = 1) and 90% (S = 0.9). The curves present the typical shape of compaction curves for cohesive soils, presenting a well-defined point of maximum dry density, where the moisture content is optimal for compaction.

The immersion phase of specimens for evaluation of the expansion was only carried out in specimens that were subjected to modified compaction energies since it was performed without reuse of material. In Table 2, the compaction and CBR tests results for standard compaction energy are presented.

This soil presented a maximum CBR value of 26% in the optimum moisture content. It was observed that with the increase in moisture content, the values of CBR decreased to a value of 2.4%. The results of the compaction and CBR tests results for modified compaction energy are presented in Table 3.

A maximum CBR value of 32.5% was obtained for the lateritic soil compacted in the modified energy. The CBR values for soil samples that were compacted in standard energy do not present significantly lower values when compared to the results

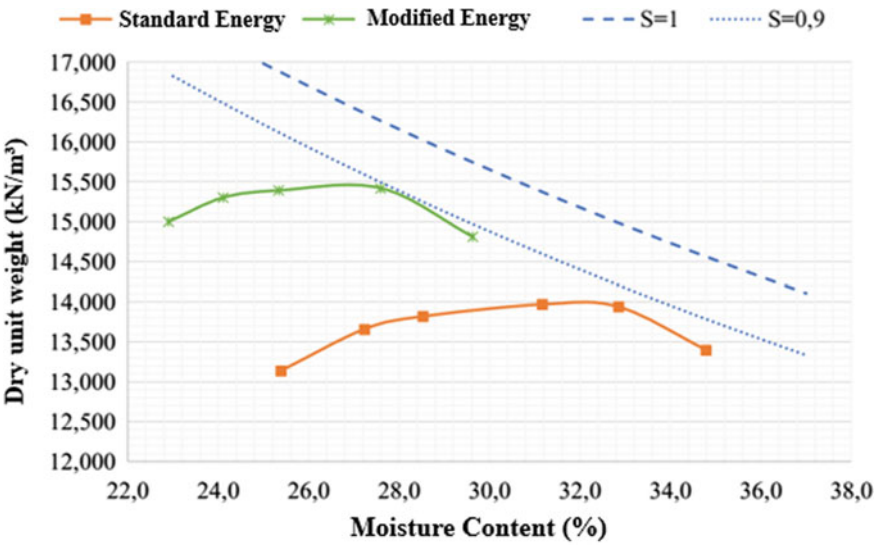

Fig. 5 Lateritic soil compaction curves

Table. 2 Lateritic soil compaction and CBR results—SCE

Point	Maximum dry density (kN/m^3)	Moisture content (%)	CBR (%)
1	13.14	25.4	18.1
2	13.66	27.2	24.5
3	13.82	28.5	25.4
4	14.00	31.0	26.0
5	13.94	32.9	8.7
6	13.40	34.8	2.4

Table. 3 Lateritic soil compaction and CBR results—MCE

Point	Maximum dry density (kN/m^3)	Moisture content (%)	Expansion (%)	CBR (%)
1	15.00	22.9	4.90	7.9
2	15.30	24.1	3.87	19.9
3	15.39	25.3	3.03	32.5
4	15.42	27.6	2.64	22.3
5	14.81	29.6	2.30	9.1

for the samples compacted in the modified energy. The non-immersion of specimens compacted with standard energy in water can explain this phenomenon; since the material was reused. Analyzing the expansion results for the sample compacted in the modified energy, a maximum 4.9% expansion is verified along the dry branch, as for the optimum moisture content, a 3.0% expansion is observed. Thus, verifying that the lateritic soil presents volumetric changes for any moisture content.

The steel aggregate was also subjected to compaction and CBR tests. The steel aggregate sample was compacted with modified energy immersed in water for five days, to evaluate the sample expansion. Table 4 presents the compaction and CBR results for the steel aggregate. Analyzing the expansion results, it is observed that the steel aggregate does not present volumetric variation during the five days of immersion in water at room temperature, which is a satisfactory result for this material. A maximum CBR value of 183% was obtained for the steel aggregate compacted in the modified energy. It was also verified a maximum expansion of 9.1% regarding the

Table. 4 Steel aggregate compaction and CBR results

Point	Maximum dry density (kN/m^3)	Moisture content (%)	Expansion (%)	CBR (%)
1	22.98	5.8	0.00	74.5
2	23.02	7.3	0.00	61.6
3	23.25	8.3	0.00	118.4
4	22.98	9.1	0.00	183.5
5	22.00	10.8	0.00	87.4

optimum moisture content. The compaction tests presented a maximum dry density of 23.10 kN/m^3 and optimum moisture content of 8.75%.

In Fig. 6, the compaction curve for the M7030 mixture is presented, in which only five compaction points are presented, but for its construction, more specimens were cast in function of the variability observed in the results, and the difficulty in obtaining the expected moisture content for each point of the curve. The compaction curve obtained for this mixture clearly shows a point of apparent maximum dry density and that its dry branch is steeper when compared to the wet branch. Table 5 shows the results of the compaction and CBR tests including the expansion results for mixture M7030. From the tests results, it is possible to identify the point of optimum moisture content and maximum dry density, which are, 14.7% and 21.00 kN/m^3, respectively. A CBR value of 213% and an expansion of 0.41% is verified for the M7030 mixture. The saturation curves of 100% (S = 1) and 80% (S = 0.8) presented

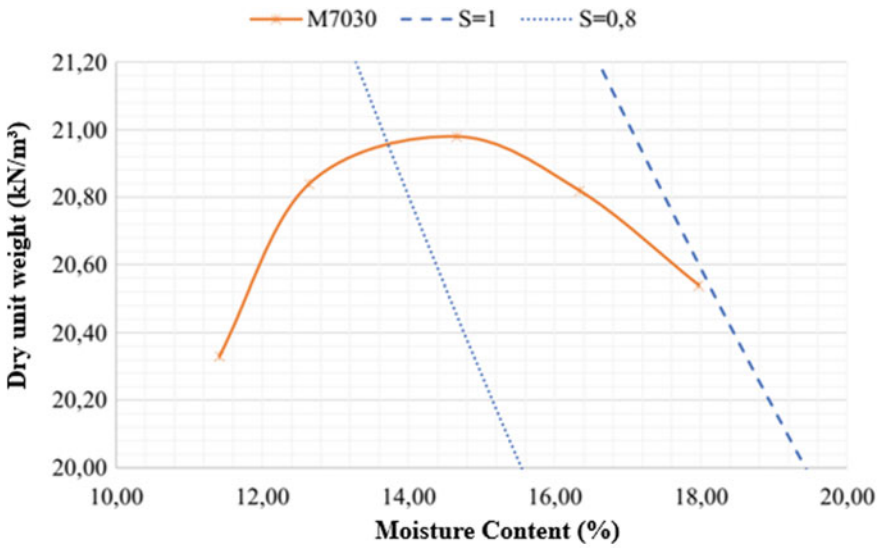

Fig. 6 M7030 mixture compaction curve

Table 5 M7030 compaction and CBR results

Point	Maximum dry density (kN/m^3)	Moisture content (%)	Expansion (%)	CBR (%)
1	20.33	11.41	0.51	142.9
2	20.84	12.64	0.42	170.6
3	20.98	14.66	0.41	213.4
4	20.82	16.34	0.46	151.1
5	20.54	17.97	0.11	143.9

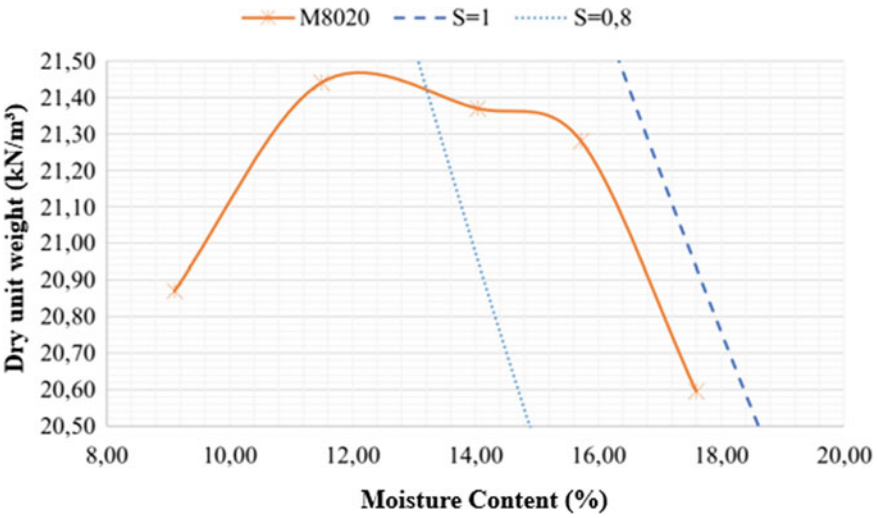

Fig. 7 M8020 mixture compaction curve

with the compaction curve in Fig. 7 were also evaluated, and for the optimum moisture content, the mixture presents a degree of saturation of approximately 85%.

The CBR tests results show that all CBR values are higher than 100%, which means that the material exceeds the specifications proposed by the Brazilian standard NBR 16364 [11], establishing a minimum CBR value of 80% for base and sub-base materials. It is also observed that the lower CBR values were obtained for the lower moisture content values. The mixture presented a 0.41% expansion in the immersion phase. It is verified that the expansion presented in the mixture is attributed to the soil. It is also worth mentioning that the Brazilian standard NBR 16364 [11] reports that acceptable expansion values should be less than 1.0% and 0.5% for sub-bases and bases, respectively. Thus, the mixture attended the specifications for sub-base and base for pavements. The compaction and CBR tests including the expansion results for the M8020 mixture are shown in Table 6.

The compaction curve of the mixture M8020 (Fig. 7) presents a similar curve to the M7030 mixture, presenting an easily identifiable maximum dry density point.

Table. 6 M8020 compaction and CBR results

Point	Maximum dry density (kN/m^3)	Moisture content (%)	Expansion (%)	CBR (%)
1	20.87	9.10	0.43	100.2
2	21.44	11.49	0.38	185.7
3	21.37	14.03	0.18	179.5
4	21.28	15.72	0.15	179.0
5	20.60	17.60	0.08	98.7

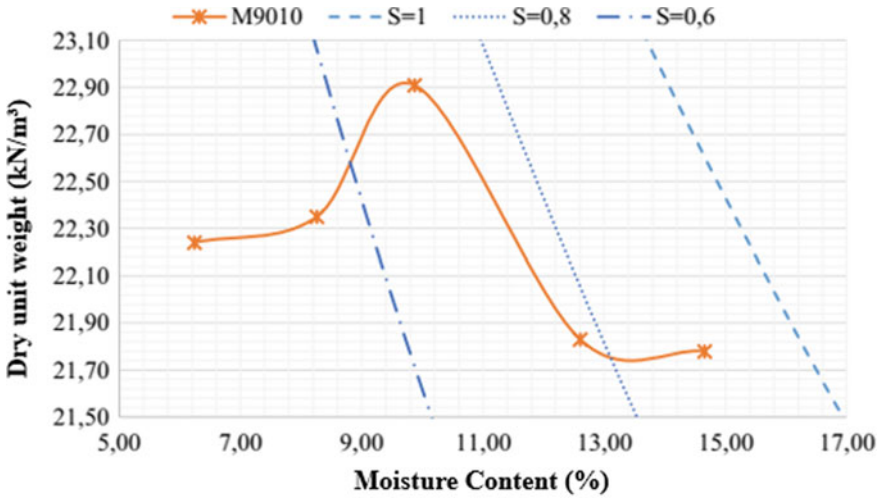

Fig. 8 M9010 mixture compaction curve

In Fig. 8, the compaction curve of the mixture M9010 is presented. From the tests results, it is possible to infer that the maximum dry density presents a value of 21.44 kN/m^3 and optimum moisture content of 11.49%. A maximum CBR value of 185.7% was verified.

The compaction and CBR tests including the expansion results for the M9010 mixture are shown in Table 7. From the tests results, it is possible to infer that the maximum dry density presents a value of 22.91 kN/m^3 and optimum moisture content of 9.87%. A maximum CBR value of 254.87% was verified. This mixture presents the highest CBR values for the optimum moisture content. However, for moisture contents above and below the optimal content, the CBR values are the lowest for the three mixtures, presenting a large variability. As for the expansion results, this mixture presents the lowest values of the three mixtures, consistent with the decrease in lateritic soil content.

In summary, it is observed that the three mixtures broadly comply with the specifications of the standard NBR 16364 [13], which states that the CBR value of the steel aggregate mixtures with lateritic soil to be used as sub-base must be equal to

Table 7 M9010 compaction and CBR results

Point	Maximum dry density (kN/m^3)	Moisture content (%)	Expansion (%)	CBR (%)
1	22.24	6.24	0.22	59.08
2	22.35	8.26	0.10	135.23
3	22.91	9.87	0.05	254.87
4	21.83	12.60	0.03	201.69
5	21.78	14.65	0.00	25.66

or greater than 20% and present an expansion of less than or equal to 1%. It is also verified that the three mixtures attend the Brazilian specifications for application as pavement base. According to the NBR 16364 [11], the CBR value for a pavement base must be 60% or more for an N number less than or equal to 5×10^6 and present an expansion of less than or equal to 0.5%. For N number greater than 5×10^6, CBR values should be equal to or greater than 80% and with an expansion of less than or equal to 0.5%.

4 Conclusions

The steel aggregate presented a maximum CBR value of 183%, well above the 80% specification of the Brazilian standard NBR 16364 for steel aggregate as paving material for road pavements.

The lateritic soil presents a maximum CBR value of 26% for a standard compaction energy, while for a modified compaction energy the maximum observed CBR value is 32%, which are high CBR values for a subgrade material.

The lateritic soil presents volumetric changes for any moisture content, which is undesirable for sub-base and base of pavements.

The three mixtures broadly comply with the specifications of the standard NBR 16364 to be used as sub-base and base material for road pavements.

The expansions determined in the immersion phase before the CBR test execution, presented low expansion values for the three mixtures. The expansion values are under the 1% specification of the NBR 16364. Although; the lateritic soil within the mixture presents high plasticity, these characteristics have little influence on the behavior of the mixtures, as observed in the compaction and CBR tests results.

References

1. Brazilian Steel Institution (IABR) (2018) Sustainability report 2018. IABR, Rio de Janeiro, Brazil
2. Motz H, Geiseler J (2001) Products of steel slags an opportunity to save natural resources. Waste Manag. 21(3):285–293
3. Rodhe L (2002) Electric steel slag in granular layers of pavements: laboratory study. Master's dissertation, Dept. of Civil Engineering, Federal Univ. of Rio Grande do Sul
4. Machado AT (2000) Comparative study of test methods for evaluation of steel slag expandability. Master's dissertation, Dept. of Civil Engineering, Univ. of São Paulo Polytechnic School
5. Castelo Branco VT (2004) Characterization of asphalt mixtures with the use of steel slag as aggregate. Master's dissertation, Dept. of Civil Engineering, Federal Univ. of Rio de Janeiro
6. Raposo C (2005) Experimental study of compaction and expansion of LD slag for paving use. Master's dissertation, Dept. of Civil Engineering, Univ. of Espirito Santo
7. Rubio AR, Carretero J (1991) G: Application of Steel slags in roadways (in Spanish). Civil Engineering, Spain

8. Oliveira V, Buitrago N, Ribeiro L, Cavalcante A (2018) Steel aggregate swelling potential in layers of road pavements. J Environ Eng. **144** (9) (2018)
9. DNIT (National Department of Transport Infrastructure) (2013) Soils—Compaction using unworked samples. ME 164. DNIT, Rio de Janeiro, Brazil
10. DNIT (National Department of Transport Infrastructure) (2016) Soils—Determination of the California support index using unworked samples—test method. ME 172. DNIT, Rio de Janeiro, Brazil
11. ABNT (Brazilian Association of Technical Standards) (2015) Execution of sub-base and base granulometrically stabilized with steel aggregate for road paving - Procedure. NBR 16364. ABNT, Rio de Janeiro, Brazil

Waste Plastic Aggregates as a Replacement of Natural Aggregates

Bhupesh Kumar Gupta, Kanish Kapoor, Mudasir Nazeer, and Mandeep Kaur

Abstract The construction industry is the biggest purchaser of natural aggregates which prompted exhaustion of good quality regular sand (fine aggregates). Stream sand, which is one of the constituents utilized as a part of the creation of ordinary concrete, has turned out to be exceptionally costly and furthermore rare. In the setting of such a depressing climate, plastic aggregates can be used beneficially. In this investigation, the reused plastics were utilized to set up the fine aggregates along these lines furnishing an economical alternative to manage the plastic waste. During this study waste Polythene Terephthalate (PET) heated to make PET agglomerate, then cooled and crushed into aggregates that embrace sort of sizes with definite gradation. The different concrete mixes were created with totally different replacement levels (0, 25, 50, 7, and 100 by volume) of natural fine aggregate (NFA) with plastic fine aggregate (PFA). Compressive strength test, Split tensile strength test, Water absorption test, density, workability, and XRD analysis has been performed in this examination. Decreasing in compressive strength was just around 14% and diminishment in water absorption was around 37% for concrete containing 50% plastic.

Keywords PET · Fine aggregate · Concrete

1 Introduction

Concrete is the most largely utilized man-made construction material which is a mixture of cement, aggregates, and water. The aggregate part in concrete is around 75% of its total volume and in this manner, it assumes a significant part in the general execution of concrete [1, 2]. Stream sand, which is one of the important ingredients utilized as fine aggregate in the formation of ordinary concrete, has turned out to be exceptionally costly and furthermore rare. In order to replace this fine aggregate

B. Kumar Gupta · M. Kaur
Department of Civil Engineering, Lovely Professional University, Phagwara 144402, India

K. Kapoor (✉) · M. Nazeer
Dr. B R, Ambedkar National Institute of Technology, Jalandhar 144011, Punjab, India
e-mail: kapoork@nitj.ac.in

K. R. Reddy et al. (eds.), *Sustainable Environment and Infrastructure*, Lecture Notes in Civil Engineering 90, https://doi.org/10.1007/978-3-030-51354-2_22

as part of concrete and make it economical, there is a substantial interest in elective materials from mechanical waste. Polyethylene terephthalate (PET) is the commonly used plastic material which is used to make blown bottles for soft drink, food packing containers and other consumer goods. These PET bottles are actually an innovation in the field of industrial revolution as they replace the heavy glass container vessels which are not easy to handle and heavy in weight [3]. Besides many advantages and pros of these plastics, waste disposal management has become a challenging task due to the production of waste plastics at large scale. Environmental pollution and detrimental effects on soil are the two main concerns of waste disposal management. Plastics that are thermoplastic in nature are feasible for recycling and regeneration but other non-thermoplastics (which cannot be recycled) are occupying large landfills thus converting fertile land into barren land. Therefore to avoid all the ill effects of these non-recycled waste plastics, these can be utilized in concrete as a replacement of aggregates (fine and coarse) and fibers which also proves a beneficial tool to protect natural mineral aggregate resources [4].

PET as aggregate replacement in concrete may increase the tensile strength of concrete to a good extent. It was investigated by [5, 6] that plasticity of PET-based concrete was 6% more than plane concrete, thus shows better results of tensile strength. [7, 8] studied the effect of PET aggregate on compressive strength, where they found that the compressive strength of PET concrete varies between 16.57 Mpa to 37.2 Mpa at curing age 28 days. Furthermore, the increment in slump value indicates the enhancement in the workability of PET aggregate concrete [5, 6]. [1, 7] conveyed that the fresh density as well as dry density of plastic aggregate concrete diminishes to some extent as compared to conventional concrete.

In this study, fine natural aggregates were replaced by plastic fine aggregates (PET) at a percentage of 25, 50, 75, and 100 by volume. Furthermore, the effect of replacement of NFA with PFA on workability, Density, compressive strength, tensile strength, water absorption, density, and XRD were studied.

2 Properties of Materials Used

In this experiment, ordinary Portland cement (OPC-43) was utilized. The quality of cement was checked by checking different parameters like fineness of cement, consistency of cement, initial and final setting of cement, and compressive strength of cement. The various properties of cement are shown in Table 1.

Normal crushed stone was used as NCA in this investigation. The properties of NCA like crushing value, flakiness and elongation index, specific gravity, and sieve analysis were found by performing various tests. The results are shown in Table 2.

Common river sand was used as natural fine aggregate. The properties like water absorption, specific gravity were determined and are tabulated as shown in Table 3.

Plastic (PET) water bottles and soft drink bottles were collected from nearby garbage shops. After washing PET containers were cut into little pieces (chips) with the help of scissors. The PET flakes are then heated until the fluid state is obtained

Table 1 Physical properties of cement

Property	Result	IS Recommendation [11]
Fineness	9.5%	10% (maximum)
Specific Gravity	3.15	3.15
Consistency	29.75%	26–33%
Initial Setting Time	70 min	30 min (minimum)
Final Setting Time	425 min	600 min (maximum)

Table 2 Properties of NCA

Property	Value	IS Recommendation [12]
Crushing Value	7.35%	30%
Water Absorption	1%	0.1–2%
Specific Gravity	2.7	2.6–2.9
Elongation Index	10.31%	Both flakiness and elongation index should be less than 40%
Flakiness Index	15.39%	

Table 3 Properties of NFA

Property	Value	IS recommendation
Water absorption	2%	3% (maximum)
Specific gravity	2.6	2.4–3

Table 4 Composition of mix

Mix	Mix Composition (vol.%)	Constituents				
		Cement Kg/m^3	Coarse Aggregate Kg/m^3	NFA Kg/m^3	PFA Kg/m^3	Water Kg/m^3
M_0	(NFA) $_{100\ \%}$ + (PFA) $_{0\ \%}$	438	1130	640	–	198
M_1	(NFA) $_{75\ \%}$ + (PFA) $_{25\ \%}$	438	1130	480	85	198
M_2	(NFA) $_{50\ \%}$ + (PFA) $_{50\ \%}$	438	1130	320	170	198
M_3	(NFA) $_{25\ \%}$ + (PFA) $_{75\ \%}$	438	1130	60	255	198
M_4	(NFA) $_{0\ \%}$ + (PFA) $_{100\ \%}$	438	1130	–	340	198

Table 5 Density value of dry and wet specimens

Sl. No.	Mix Notation	Mix Composition	Density (kg/m^3)	
			Dry	Wet
1	M_0	(NFA) $_{100\ \%}$ + (PFA) $_{0\ \%}$	2.54	2.57
2	M_1	(NFA) $_{75\ \%}$ + (PFA) $_{25\ \%}$	2.39	2.44
3	M_2	(NFA) $_{50\ \%}$ + (PFA) $_{50\ \%}$	2.28	2.30
4	M_3	(NFA) $_{25\ \%}$ + (PFA) $_{75\ \%}$	2.24	2.28
5	M_4	(NFA) $_{0\ \%}$ + (PFA) $_{100\ \%}$	2.17	2.20

(a) PFA kept in water (b) Dried under sun (c) Saturated PFA

Fig. 1 **a** PFA kept in water **b** Dried under sun **c** Saturated PFA

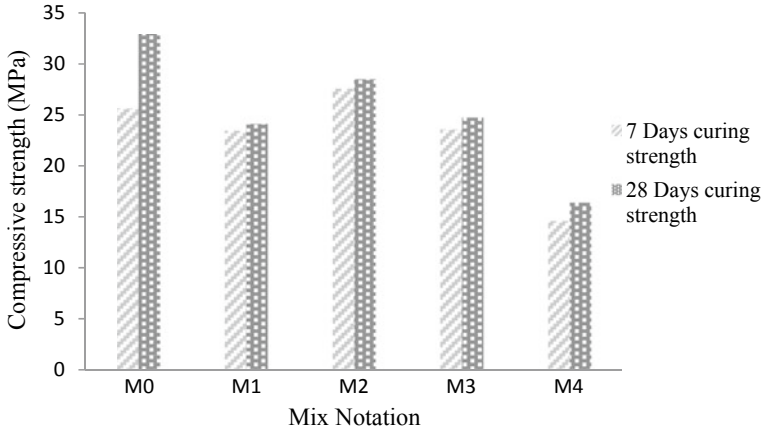

Fig. 2 Compressive strength of concrete

and let to be cooled in a flat plate. Pulverization is done with the help of a hammer to dress it into the shape of aggregates (Fig. 1). After the formation of PFA, they were kept immersed in water for 24 h then dried under open sunlight for 3 h to bring aggregates from dry condition to saturated condition.

3 Preparation of Sample

In this experimental setup, five mixes were prepared with different proportion of fine aggregate replacement. These five mixes are, control mix (M_0), M_1, M_2, M_3 and M_4, control mix is a standard mix having all natural fine aggregate content, whereas mix

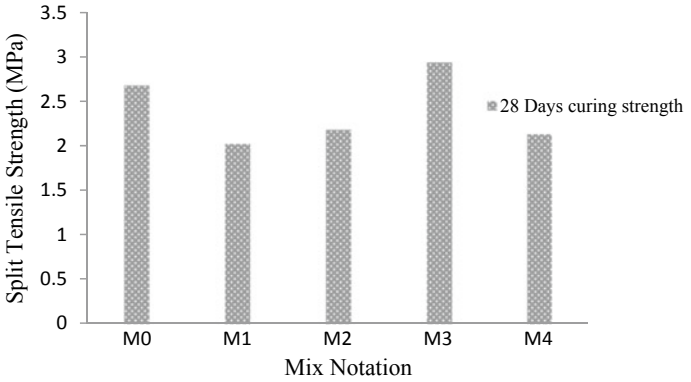

Fig. 3 Split tensile strength

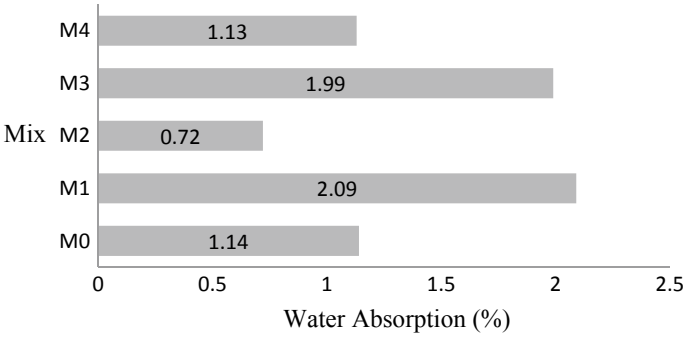

Fig. 4 Water absorption results

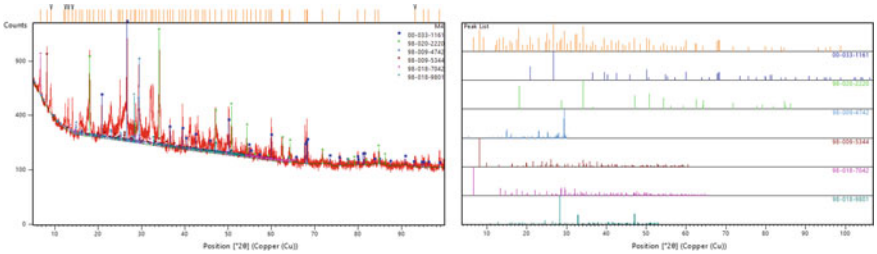

Fig. 5 X-Ray diffraction analysis of concrete with 100% PFA

M_1, M_2, M_3 and M_4, contains 25%, 50%, 75% and 100% of plastic fine aggregate respectively.

3.1 Determination of concrete properties

Density: The density of concrete is determined in both dry condition (before the addition of water) and wet conditions (after the addition of water). It is simply determined by taking the mass of concrete and volume of the same amount of concrete and is expressed in (kg/m^3).

Workability: To check the workability of fresh concrete, a slump test was performed in accordance with [13]. Slump cone was prepared in three layers of tamping and slump values are taken quickly just after the un-jacketing of mold.

Compressive Strength: The compressive strength of concrete specimens is determined with the help of a compression testing machine (CTM) in accordance with IS: 516 [14]. Strength is checked after extraction of samples (100 mm^3) from water in dry surface condition at curing age of 7 and 28 days under CTM having maximum load capacity of 1000 KN. The strength is taken as the average strength of three cubes of each mix.

Split Tensile Strength: Split tensile strength of concrete is determined in a compressive testing machine in accordance with IS: 5816 [15] at the curing age of 28 days. The specimen is cylindrical having diameter 100 mm and height 200 mm, respectively. Specimens are tested in dry surface condition and three specimens of each mix are tested to get the average value of tensile strength.

Water Absorption: Water absorption test is performed on cubic samples of size 100 mm in accordance with ASTM C 642-97 [15]. Two weights of samples W_1 and W_2 are taken to know the water absorption value of sample. W_1 is taken just after the curing age of 28 days then the sample is kept in an oven at 110^0 C $\pm$ 5^0 C for 24 h. It is then again weighed and the difference in weight should not be more than 5% to consider it as dry. Second weight (W_2) is taken after keeping the sample in water for 24 h and water absorption value is determined by Eq. 1.

$$\frac{W_2 - W_1}{W_1} \times 100 \tag{1}$$

Where W_1 and W_2 are weight first and second respectively.

X-Ray Diffraction study: XRD examination is performed to know about the microstructural characterization of concrete. XRD was performed on a sample having a complete 100% plastic fine aggregate content and cured for 28 days. The procedure of this test is that a little amount of powder sample is put into a holder made up of aluminum and the surface is finished smoothly. The holder is then put into the X-Ray diffractometer where samples are filtered with the help of CuKα radiation at 40 kV/20 mA, CPS = 1 k, width 2.5 and speed 2^0/min. In X-Ray diffraction, X-Rays were scattered by particles in a sample that demonstrates grid dispersing of components display in the material investigated. Once the X-Ray examination was finished, the sweeps were investigated utilizing Jade 7—XRD programming. Utilizing Jade, top forces at various points were contrasted and a database of various minerals and mixes. Compounds with similar intensities coordinating those of the

outputs were recognized and the compounds showed in the specimens were found out.

4 Results and Discussion

4.1 Density Measurement

The densities of both wet and dry concrete have been evaluated and a decreasing pattern of this property has been observed in both dry and wet conditions. The dry density decrement was 5.91%, 10.24%, 11.81%, and 14.57% on substitution of NFA by 25%, 50%, 75%, and 100%. respectively. Furthermore the decreasing pattern of wet density was 5.06%, 10.5%, 11.28%, and 14.4% on substitution of NFA by 25%, 50%, 75%, and 100%, respectively. These decreasing results of densities were due to the low specific gravity of plastic aggregates as compared to natural fine aggregates. Moreover, the decreasing percentage of densities in case of wet condition is less than dry condition. It is because the voids in concrete get filled with water, thus a decrease in porosity results in an increase in density. The results of this test are shown in Table 1.

4.2 Workability Measurement

The workability of concrete has been determined by performing a slump test on fresh concrete. Observations show that there is a prominent decrease in slump values of M_1, M_2, M_3, and M_4 as compared to control mix M_0. The decreasing patterns were recorded as 83.75%, 87.5%, 91.25%, and 95% for M_1, M_2, M_3, and M_4, respectively when compared with control mix M_0 the slump values of all mixes were shown in Table 6.

Table 6 Slump value of various mix

Sl. No.	Mix notation	Slump value (mm)
1	M_0	80
2	M_1	13
3	M_2	10
4	M_3	7
5	M_4	4

4.3 Compressive Strength

The graph below shows the compressive strength results of concrete at the curing age of 7 days and 28 days, respectively. The observations show that the compressive strength starts decreasing as we increase the percentage of replacement of natural fine aggregates with plastic fine aggregates. The variation in strength percentage at the curing age of 28 days for various mixes M_1, M_2, M_3 and M_4 are 26.81%, 13.44%, 24.85%, and 50.26%, respectively, as compared to control mix M_0. It is clearly seen that the concrete mix M_2 (50% replacement with PFA) shows the best results of compressive strength as compared to the other three mixes of concrete. Furthermore, the 7-day curing compressive strength of concrete mix also shows good results for mix M_2 (where PFA replacement was 50%), only 7.61% of decrement was seen when compared with control mix M_0. Moreover mix M_1, M_3, and M_4 shows 8.53%, 8.02%, and 42.95% decrease in compressive strength, respectively.

4.4 Split Tensile Strength

The split tensile strength results of various concrete mixes at the curing age of 28 days are shown in graph-2. A significant decrease in tensile strength was observed in concrete mix M_1, M_2, and M_4 having a replacement percentage of PFA, 25%, 50%, and 100%, respectively. The decrease in tensile strength of M_1, M_2, and M_4 was 24.63%, 18.66%, and 20.52% when the comparison is made with control mix M_0. However there is a slight increase of 9.7% in tensile strength of concrete mix M_3 (where replacement of NFA with PFA is 75%). The elastic property of plastic aggregate (PFA) is more than the natural aggregates (NFA) thus the proper combination of PFA and NFA will definitely enhance the split tensile strength.

4.5 Water absorption

It is observed from graph-3 that concrete mix M_1 and M_3 absorbs more water than the control mix of concrete M_0, while mix M_4 has comparatively equal absorption as mix M_0. A different pattern of absorption is seen in the case of mix M_2 having 50% PFA replacement percentage. A significant decrease of approximately 37% was observed when natural fine aggregate was replaced by 50% of plastic fine aggregate. An equal volume of PFA and NFA can produce a homogenous mixture of concrete, resulting in a decrease of void ratio and thus decrease in water absorption rate, which is evident from concrete mix M_2. Furthermore, the percentage of water absorption for mix M_4 is comparatively the same as that of the control mix, which might be due to the presence of equal particle size of PFA and NFA. Previous research [9, 16]

suggests that with an increase in plastic content in concrete, porosity increases and thus water absorption rate increases.

4.6 X-ray Diffraction Analysis

XRD was performed on M_4 concrete mix where 100% plastic fine aggregate was used instead of natural fine aggregates. XRD provides us two types of graphs one is Peak List Graph and the other is Pattern List Graph. Report analysis provides the information that there were six compounds that have maximum intensities at the time of the hydration process. The six compounds are Silicon Oxide, Calcium Hydroxide, Tricalcium Silicate Oxide, Sodium Iron Manganese Octasilicate Hydroxide Hydrate, Dodecacalcium Octasilicate 13-Hydrate, and Neodymium Tungsten Oxide. The occurrence of these might be indicating that PET which contains carbon, oxygen, and hydrogen ($C_{10}H_8O_4$) is also contributing to the reaction of hydration and other reactions. The formation of Dodecacalcium Octasilicate 13-Hydrate in place of Calcium Silicate Hydrate might be another factor responsible for low strength of concrete. The occurrence of an unknown compound like Neodymium Tungsten Oxide might be due to the presence of Neodymium and Tungsten in coarse aggregate. The numeric data furnished by XRD presents the specific element presence in concrete, for example, the data of M_4 mix is like (00-033-1161: Silicon Oxide; 98-020-2220: Calcium Hydroxide; 98-009-4742: Tricalcium Silicate Oxide; 98-009-5344: Sodium Iron Manganese Octasilicate Hydroxide Hydrate; 98-018-7042: Dodecacalcium Octasilicate 13-hydrate; 98-018-9801: Neodymium Tungsten Oxide).

5 Conclusion

In this paper, a series of tests on concrete mix containing PFA have been performed. The use of 25%, 50%, 75%, and 100% PFA replaced concrete mixture results in the following conclusions

- With 100% substitution of plastic fine aggregates, density and workability reduction was 14.4% and 95%, respectively.
- Furthermore, 14% reduction in compressive strength was observed when replacement of NFA with PFA was 50%, which is considered an optimum mix when compared to other concrete mixes. An increase in tensile strength was observed when replacement was 75%.
- Moreover, optimum reduction in water absorption was 37% when replacement was 50%. Microstructure analysis indicates that a plastic aggregate that contains carbon, hydrogen, and oxygen ($C_{10}H_8O_4$) takes an active part in reactions of concrete.

References

1. Silva RV, De Brito J, Saikia N (2013) Influence of curing conditions on the durability-related performance of concrete made with selected plastic waste aggregates. Cem. Concr. Compos. 35(1):23–31
2. Saikia N, De Brito J (2012) Use of plastic waste as aggregate in cement mortar and concrete preparation: A review. Constr Build Mater 34:385–401
3. Frigione M (2010) Recycling of PET bottles as fine aggregate in concrete. Waste Manag 30(6):1101–1106
4. A. A. Mohammed, *Mechanical strength of concrete with PVC aggregates*. Elsevier Ltd, 2019
5. Vali M, Asadi S (2017) Pet Bottle Waste As a Supplement To Concrete Fine Aggregate. Int. J. Civ. Eng. Technol. 8(1):558–568
6. Arivalagan.S, "Experimental Investigation on Partial Replacement of Waste Plastic in Concrete," *Int. J. Eng. Sci. Res. Technol.*, vol. 5, no. 11, pp. 443–449, 2016
7. Choi YW, Moon DJ, Chung JS, Cho SK (2005) Effects of waste PET bottles aggregate on the properties of concrete. Cem Concr Res 35(4):776–781
8. B. K. Gupta, M. Kaur, M. Nazeer, and K. Kapoor, "INFLUENCE OF PLASTIC AGGREGATE ON BEHAVIOUR," pp. 1–10
9. Islam MJ, Meherier MS, Islam AKMR (2016) Effects of waste PET as coarse aggregate on the fresh and harden properties of concrete. Constr Build Mater 125:946–951
10. Foti D (2013) Use of recycled waste pet bottles fibers for the reinforcement of concrete. Compos Struct 96:396–404
11. Bureau of Indian Standard, "IS 8112: 2013, Ordinary Portland Cement, 43 Grade — Specification, Bureau of Indian Standards, New Delhi," no. March, 2013
12. IS: 383, "'Specification for coarse and fine aggreagtes from natural sources for concrete', BIS, New Delhi," 1970
13. IS 1199, "Methods of sampling and analysis of concrete," *Bur. Indian Satandards*, 1959
14. IS-516, "Method of Tests for Strength of Concrete," *Indian Stand.*, pp. 1–30, 1959
15. R. (2004) BIS:5816–1999, "Splitting tensile strength of concrete". Bur. Indian Stand, Dehli, p 2004
16. S. M. Hama and N. N. Hilal, *Fresh properties of concrete containing plastic aggregate*. Elsevier Ltd, 2019

Physical and Mechanical Properties Improvement of Miocene Marls (Morocco) Doped by Iron Oxide Fe_2O_3

Laila Mesrar, Ahmed Benamar, Hamza Mesrar, and Raouf Jabrane

Abstract The Miocene marls or calcareous clay of the southern Rif groove is one of the geological wealth of the region of Taza in Morocco. This study presents a methodology for recycling the waste iron oxide in ceramics bricks, in a cost-effective and environmentally friendly manner, using the tailings produced from iron mines. Due to its iron oxide content, this waste can be used as a raw material in the manufacture of bricks, at the same time reducing the environmental impact. The study was based on the doping process, which is known to conserve energy, we will see how the addition of these quantities can in some cases lead to profound changes in the properties of the basic solid, both at the macroscopic level and at the level of the microstructural evolution of our materials. Physical and chemical characterization of this marl was carried out before and after doping with iron oxide Fe_2O_3 following various analytical techniques such as X-ray fluorescence (XRF), X-ray diffraction (XRD), thermal and ceramics parameters. The doping of the marl was done at different percentages (5, 10, and 15%). The results of the mineralogical analysis of marl after this doping indicate the presence of hematite. Further characterization of the ceramics properties such as linear shrinkage, porosity, and mechanical strength were also investigated by firing doped bricks at a temperature of 900 °C. However, doping with Fe_2O_3 caused a decrease in porosity and an increase in the mechanical resistance of the bricks. Furthermore, the ceramic tests performed on the product show that the doped marl can be used as bricks due provided interesting properties, such as firing behavior and mechanical resistance. Accordingly, the marl doped with 15% Fe_2O_3 gives the best improvements in physic mechanical properties.

Keywords Doping · Marl · Oxide iron · X-ray · Bricks · Ceramics · Mechanical resistance

L. Mesrar · H. Mesrar · R. Jabrane (✉)
Faculty of Science and Technology Fez, University Sidi Mohamed Ben Abdellah, Fes, Morocco
e-mail: raouf.jabrane@usmba.ac.ma

L. Mesrar · A. Benamar
University of Normandie, LOMC, UMR 6294, CNRS, 53 Rue de Prony, 76600 Le Havre, France

K. R. Reddy et al. (eds.), *Sustainable Environment and Infrastructure*, Lecture Notes in Civil Engineering 90, https://doi.org/10.1007/978-3-030-51354-2_23

1 Introduction

One of the great challenges that humanity must face today is to achieve a feasible and viable solution addressing the waste generated by industry. The principles of sustainability and circular economy, as well as respect for the environment, should be a priority in current construction. It is therefore interesting to use different industrial waste in the manufacture of different construction materials, such as ceramic clay bricks. Iron is one of the most abundant elements of the earth's crust (about 5%), in nature, exploitable iron oxide is essentially composed of Fe_2O_3 hematite, Fe_3O_2 magnetite, and FeOOH goethite. Iron is present in clays essentially in the form of oxyhydroxide and/or oxides. Although the most frequently encountered oxyhydroxide is goethite (FeOOH), the main anhydrous oxides contained in clays are hematite [1].

The characterization and incorporation of waste from the iron oxide industry as a raw material in the manufacture of construction materials has been studied by different authors [2]. The use of clay resources by human, mainly in the manufacture of building materials, dates from antiquity.

Morocco is known over North Africa and Europe for its pottery and ceramics and is among the world's top 20 producers and consumers of clayey building materials. Wide varieties of ceramic are produced in the region of Fez (center of Morocco), where clays are well known to be suitable for the manufacture of tiles and bricks for local buildings [3–5]. In this context, the products have also undergone an evolution so that, while some traditional types (i.e., majolica and earthenware) are tending to disappear, others have been introduced into the market are accomplishing a growing success, such as the "single- fired porous tiles." It has become necessary to change the composition of the bodies to suit the new rapid cycles of the clay industry [6]. There has also been a trend toward the use of cheaper raw materials like local marls. One of the major problems encountered by users of these materials is the fragility, low mechanical strength, and non-uniformity color after cooking limits its added value [7]. In order to improve the material performance, the efficiency, and the quality in the manufacture bricks, we opted for doping by dry method, this material by the iron oxide Fe_2O_3, at different percentages of 5, 10, and 15%. The objective of this research is to assess the possibility of using wastes from the iron oxide as reinforcement for marl Miocene for the production of fired bricks. The influence of the waste content in the physical and mechanical properties was studied.

2 Materials and Methods

2.1 Materials

These marls constitute the regional substratum of the whole region and appear locally in the city center and in the surrounding valleys. The quarry is located at the periphery of the urban area in Taza region (Fig. 1).

2.2 Preparation of Composite Marls/Iron Oxide

The implementation of composite consisted first of grinding the marls (Fig. 2a) then made a mixture in the solid-state with the oxide of iron at different percentages of 5, 10, and 15%, and grinding the whole. This method allows obtaining homogeneous powders relatively fine-grained and narrow particle size distribution Laboratory scale brick production and their characterization. The waste used is iron oxide (Fig. 2b).

2.3 Methods

In an aim to study the homogeneity and the degree of Fe_2O_3 incorporation in the clay sheets several analysis techniques were used:

The quantitative chemical analysis of clays was performed by X-ray fluorescence spectrometry (WD-XRF), spectrometer type Axios sequential brand Panalytical. The DRX study was carried with the Philips diffractometer XPERT-PRO" PW 3064, with the Kα1,2 radiation of copper. X-ray diffraction (XRD) data were obtained using unoriented samples prepared on glass slides in the 2θ range of 2–40° at a scanning speed of $2°min^{-1}$ [8]. Thermogravimetric and differential thermal analysis (TGA-DTA) were performed with a SETARAM type 124 apparatus.

The geotechnical tests were conducted as follows: Atterberg limits (NF P 94-052-1), which are conventional water content parameters indicating the soil transition from plastic to a liquid state (WL) and from plastic to solid state (WP);

The ceramics properties for all the bricks after and before doped were evaluated. From a ceramics point of view, the brick was made with traditional shaping techniques were 6 cm long, 3 cm wide, and 1.5 cm thick and were air-dried. The firing cycle consists of preheating (10 °C/min), rapid-firing with an electric kiln for 1 h (at fixed temperature), and cooling (10 °C/min). The temperature was then increased to the sintering temperature, which ranged between 700 and 900 °C and held for 60 min.

In order, to evaluate drying behavior linear shrinkage (100(Lm-Lf)/Lm) was evaluated in accordance with standard (ISO 10545), where Lm is the length of the mold and Lf is the length of the fired specimen, respectively. Porosity was determined

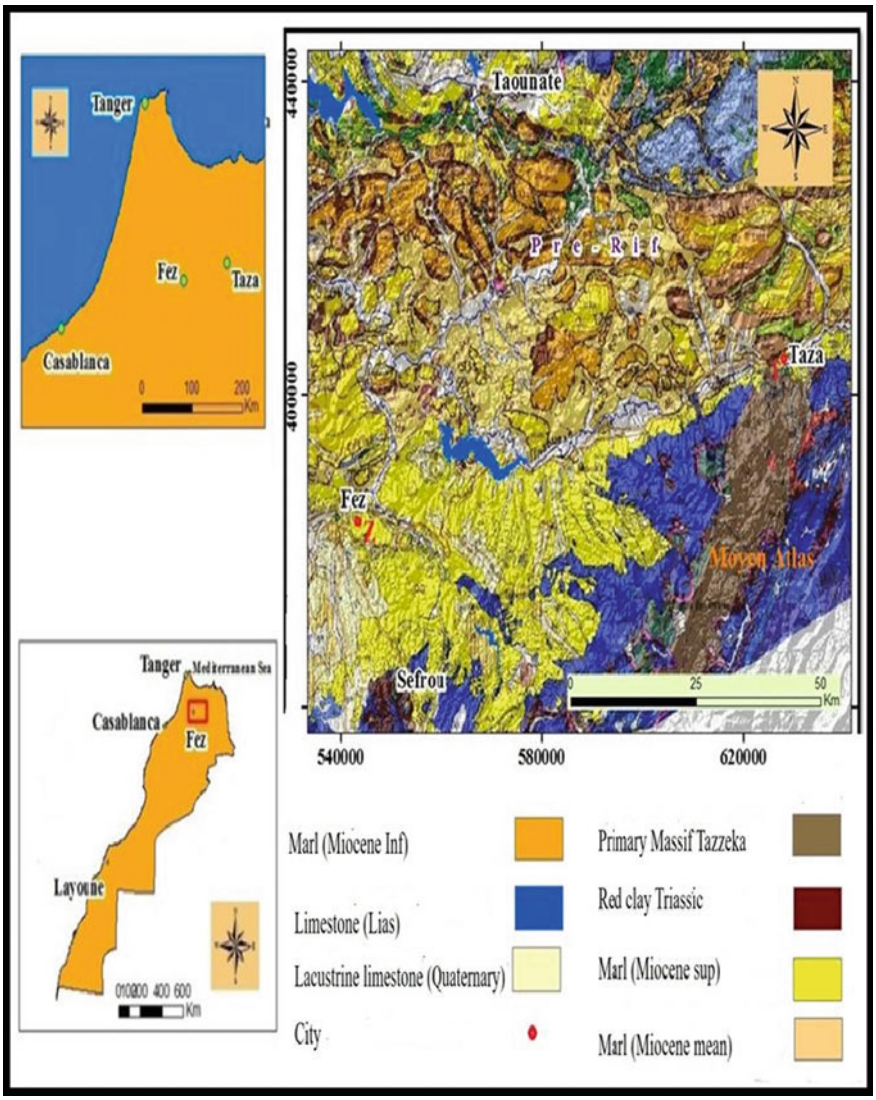

Fig. 1 Map of investigated areas

following the standard procedure (ISO 10545). Each result obtained is the average value of 04 samples tested. Aspect changes (color, texture, etc.), for different drying times, the mass and length values were measured;

Mechanical properties of all bricks before and after firing (at 700–900 °C) investigation were determined by the compressive strength (ISO 10545). The color of the fired specimens was identified using the Munsell soil color charts.

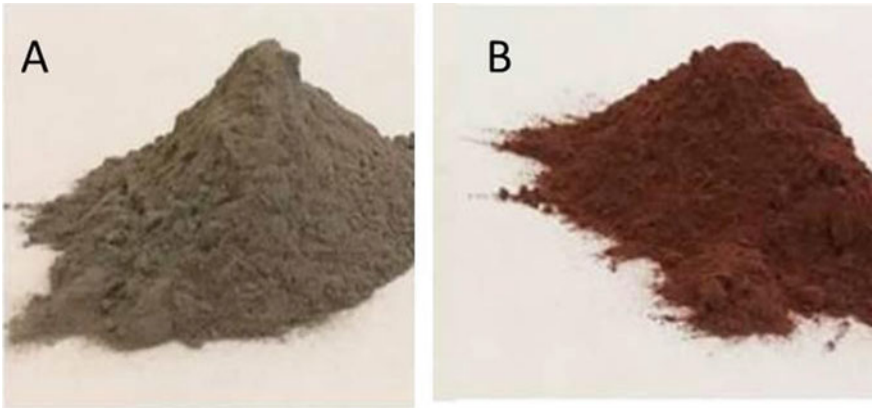

Fig. 2 Photos of **A** the gray marl, **B** and oxide iron

3 Results and Discussion

3.1 Properties chemical

The Easiest way to determine the influence of a doping is to make measurements of the material sample before and after doping. Thus, analysis of the chemical composition by XRF clays doped with Fe_2O_3 reveals a significant enrichment in iron oxide.

Its concentration increases as the doping level is increasing. So doping causes an increase in the content of iron oxide in combination with increasing doping content (5.10 and 15%), it exceed twenty percent (13%).

The slight decrease in the silica, alumina, and calcium content is probably due to an analytical error which is, moreover, less than the admitted error uncertainty (less than 5%) (Table 1). The bulk elemental oxide analysis of the marl provides a preliminary indication of the suitability of product bricks. Most oxide of the marl doped has values that are in the upper range of the commercial bricks in France

Table 1 Percentage major elements of our calcareous clays after and before doping with Fe_2O_3 compared with natural clay used for brick production in France [11]

Major oxides (%)	SiO_2	Al_2O_3	CaO	Fe_2O_3	MgO	K_2O	Na_2O
Max value	80	30	18	10	5	4.5	1.5
Min value	35	8	0.5	2	0	0.5	0.1
T3	47.6	13.8	6.90	5.76	2.89	0.95	0.84
T3 at 5%	45.6	13.5	6.99	9.01	2.75	0.98	0.75
T3 at10%	44.8	12.6	6.74	11.4	2.52	1.02	0.71
T3 at 15%	43.6	12.6	6.64	13.2	2.55	0.91	0.74

(Kornnman 2009). With the exception of marl doped with Fe_2O_3 at 15%, this value exceeds the limit values (13%).

The large amount of flux oxides in the waste could decrease the firing temperature or the time of the ceramic bricks, saving energy in the process (Dondi et al. 1997). Loss on ignition at 1000 °C was 17.7%, probably attributable to a less effective combustion or thermal decomposition of inorganic species. The addition of increasing amounts of iron oxide waste produced a decrease in the loss of ignition (LOI), from 2% with the marl doped at 15%.

3.2 Properties mineralogical

The mineralogical composition of the crude sample (T) shows that the most abundant minerals are quartz, calcite, and dolomite. Concerning clay minerals from the group of layered silicates (kaolinite, smectite, and illite), were detected in low content.

The main associated minerals in the samples are quartz (40–50%), calcite (10–20%), dolomite (5–10%), and clays fraction (10–20%). Hence, the mineralogical composition of iron oxide Fe_2O_3 is Hematite well crystallized.

In general, these minerals are important in the composition of clays for terracotta (bricks, tiles, and pottery), because they promote the sintering at a low temperature [9, 10]. Quartz and calcite have an effect based in relation to other minerals. Indeed, the diffractogram of the marls, respectively, doped with 5.10 to 15%, shows that in all samples, a series of diffraction lines characteristic of the quartz, calcite, kaolinite, smectite, illite, and with the appearance of the hematite pics at all marls doped (Fig. 3). Furthermore, the intensity of hematite peaks increases with increasing proportion of the doping (5, 10, and 15%).

This increase is reflected by the width of the peaks of the curves which corresponds to the increase in crystallinity of the hematite.

3.3 Properties Thermal

The thermal behavior of the marl and doped marl are shown in Fig. 4. Weight loss of 1% at temperatures between 50 and 100 °C was observed, with an endothermic peak centered at approximately 85 °C attributed to the loss of moisture. At temperatures between 150–600 °C, 6% weight loss was observed, associated with the combustion of organic matter, iron oxidation for doped marl and the dehydration of clay minerals, as indicated by the exothermic peaks centered at 200 and 400° C and the endothermic peak centered at 570 °C, respectively. Between 600–800°C, a weight loss of 16% was produced, assigned to the decomposition of the carbonate, as indicated by the endothermic peak centered at 700 °C [12]. Finally, in doped marl, between 800 and 900 °C, two exothermic peaks centered at 825 and 900 °C were observed, associated with the crystallization of phases, such as the silicon, spinel, and fayalite prior to the

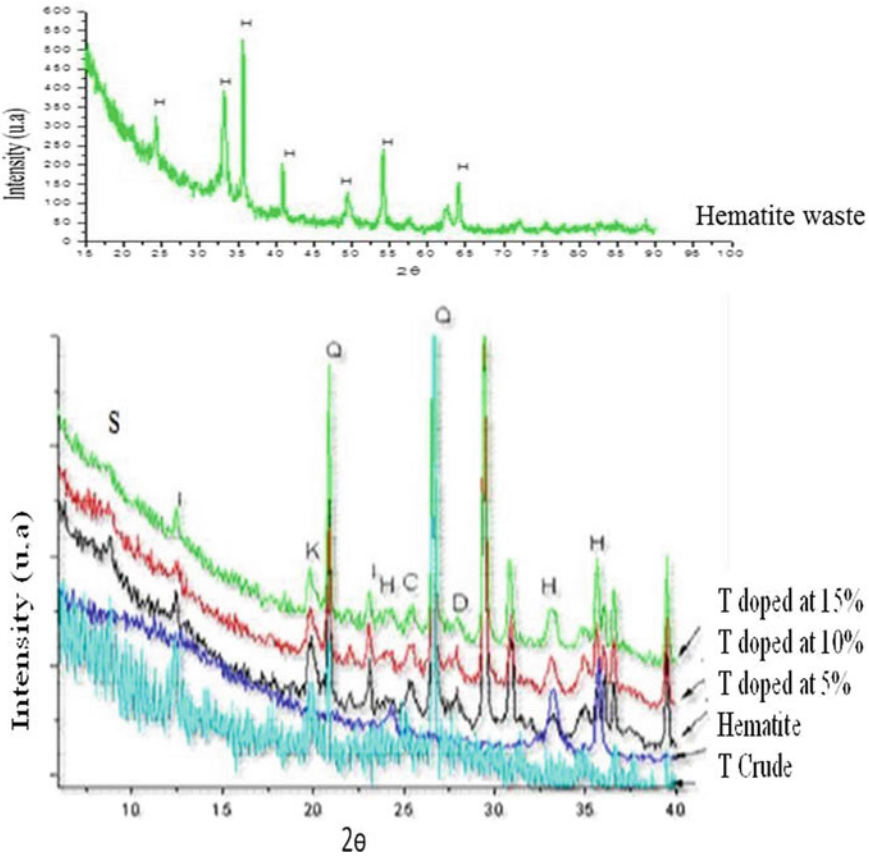

Fig. 3 The spectra of sample crude and samples doped by iron oxide at different percentages (5, 10, and 15%). With; K = Kaolinite, Q = Quartz, I = Illite, C = calcite, D = dolomite and H = hematite marl and doped

mullite phase, as indicated by the exothermic peak at 800 °C. The total weight loss variable of the crude marl was 17% however, it is 16% for the marl doped.

3.4 Ceramic and Technological Properties of Brick Samples

The results of ceramic and technological properties are reported in Fig. 5. Characterization of the Sustainable Fired Bricks Following the firing process, no defects such as fissures, efflorescence, or bloating were observed. The color of the bricks with 100% marl, fired at 900 °C, is a yellowish color (Fig. 5a). As increasing percentages of iron oxide, the bricks become reddish red. This result is confirmed by the reference diagram from Fabbri and Fiori (Fig. 5b).

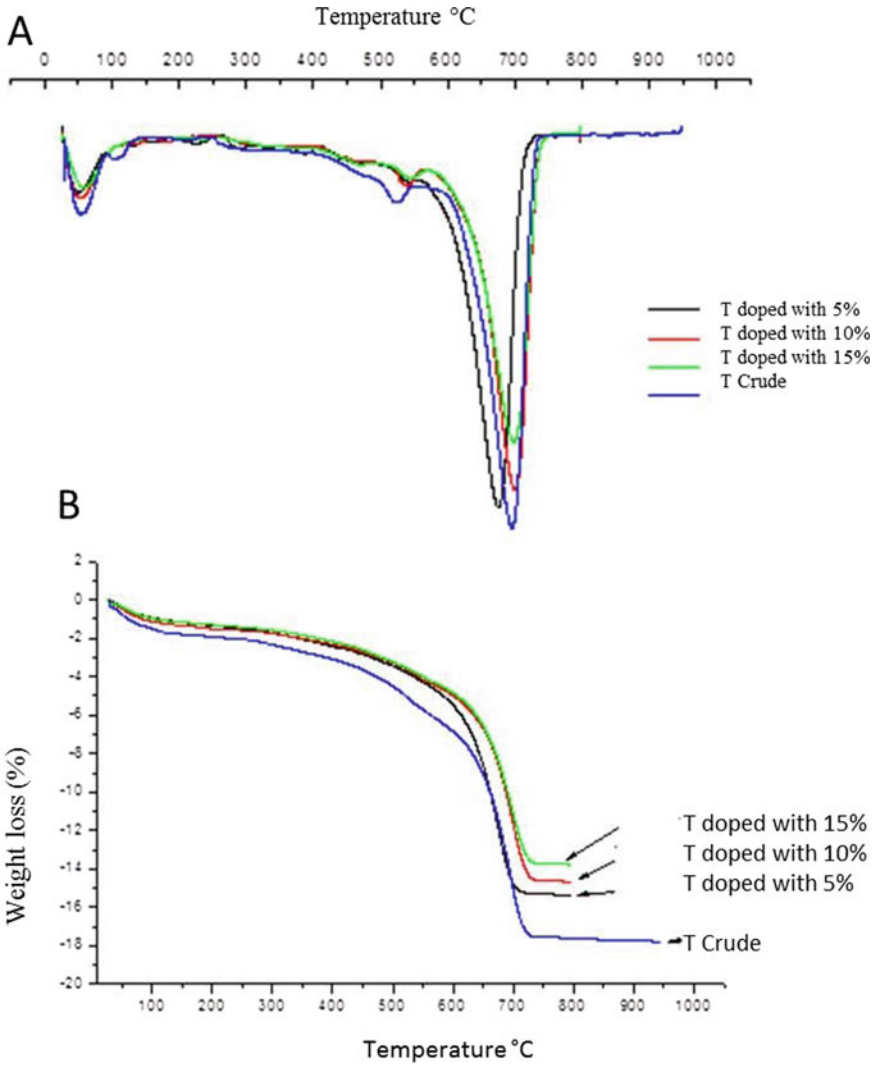

Fig. 4 Thermogravimetric and differential thermal analysis **A** TGA **B** DTA of crude

The linear shrinkage indicates the expansion/contraction behavior during the firing process. Linear shrinkage depends on the quantity of liquid phase produced in the firing process, as well as the decomposition of the gas phases. The linear contraction of crude bricks was—1.42%. The addition of up to 15% of iron oxide waste producing a greater linear expansion value of 5% (Table 2). These data indicate that the release of gases due to the decomposition of organic matter, carbonates, and hematite predominated during the firing process. During the firing process, the melting effect of the waste would produce a liquid phase, which could close the

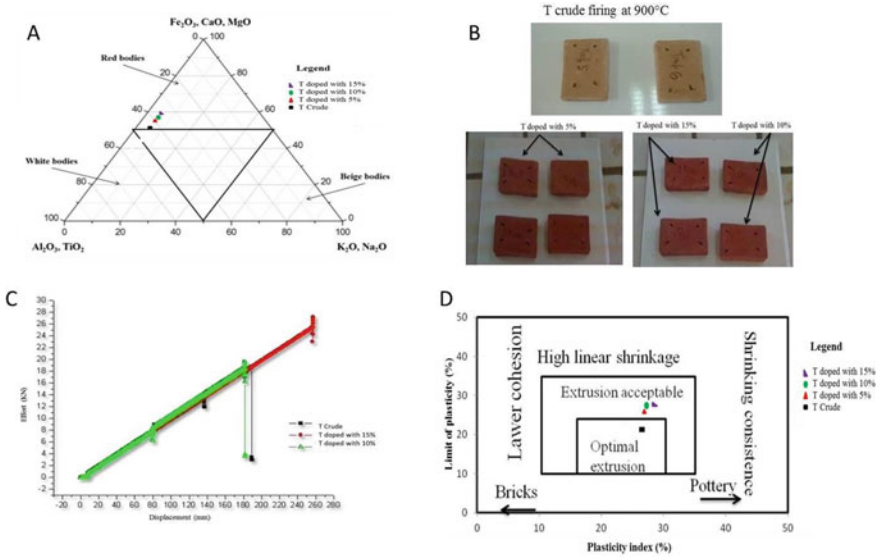

Fig. 5 **A** Colors of bricks T after doping and firing at 900 °C. **B** Ternary diagram applied to our raw materials from Fabbri and Fiori [14]; **C** (mechanical strength of the bricks before and after doping at 900 °C; **D** Evaluation of extrusion behavior according [15]

Table 2 Technological properties of fired and doped bricks

Parameters of bricks fired at 900 °C	T crude	T at 5%	T at 10%	T at 15%
Linear shrinkage (%)	−1.45	2	3.5	5
Porosity (%)	16	14	13	12

internal pores and reduce the number and size of the pores, which would produce a slight densification of the brick (Fig. 5c). Hence, the oxide of iron has filled the free pores with the carbonates and therefore participates in the densification.

The bricks of marls doped at 15% of Fe_2O_3 have a relatively high resistance up to 28 kN compared with crude bricks (Fig. 5e). However, the increase in percentage of iron oxide is definitely correlated positively with mechanical strength. At 900 °C, the bending strength of all the bricks is increased and peaked its maximum (28 kN) in the marls doped with 15%. The increase in resistance is linked to the modification of the crystalline structure of marls [13]. The presence of hematite mineral in bricks induces a stronger resistance. Bain and Highley's (1979) chart shows the relationship between plasticity and suitable molding properties due to their cohesion characteristics. Based on the results of Fig. 5d, we note plasticity has clearly improved with the level of doping. However the greater plasticity is observed in the doped marl with 15% Fe_2O_3. So, doping of this marl with iron oxide increases the plasticity of these materials. This result is more suitable for use in pottery and bricks.

4 Conclusion

The color is a parameter highly sought by ceramics and construction industry and its evaluation is very important (Fig. 5a). Compared to raw bricks color our materials after firing, has been modified. Indeed, in all the doped bricks 5, 10, and 15%, the color changes from beige cream to red bricks in all firing temperatures. This result is confirmed by the reference diagram (Fig. 5b) from Fabbri and Fiori.

The results of chemical analysis showed a higher rate of Fe_2O_3 doping increases, its content increases in the marl. The peak intensity of X-ray hematite increases with an increasing proportion of the doping of 5, 10, and 15% and corresponds to the increase in the crystallinity of the hematite. Technological tests showed suitable industrial properties of these marls; their doping with iron oxide induced an increase in their plasticity. The iron oxide acts as a degreaser and increases shrinkage. The mechanical resistance of the doped bricks marl is also dependent on quantity Fe_2O_3 doping. The marls doped with 15% Fe_2O_3 have a relatively high resistance compared to the others.

Furthermore, the bricks of marls fired at 900 °C and doped with 15% give better mechanical strength of up to 28kN. Finally, the bricks provide nice red color. So, suggesting the use of this composite in ceramics and pottery. In addition to the technical characteristics, the oxide iron in bricks presents economic and environmental benefits that would result from the recovery of this waste by eliminating the amount of waste deposited in landfills.

Acknowledgments This study has benefited from the USMBA Fez and physico-chemical analyses were carried out at CNRST Rabat (Morocco).

References

1. Pauling L, Hendricks SB (1925) The crystal structures of hematite and corundum. Journal American Chemical Society 47:781–90
2. Dondi M, Guarini G, Ligas P, Palomba M, Raimondo M, Uras I (2001) Chemical mineralogical and ceramic properties of kaolinitic materials from the Tresnuraghes mining district (Western Sardinia, Italy). Appl Clay Sci 18:145–155
3. Mesrar L, Akdim M, Akhrif I, Lakrim M, Laaroussi O, Jabrane R (2015) The physico- mechanical characteristics of the clays in and after doping with metal oxide Al_2O_3 in the region of fez (Morocco). Present Environment and Sustainable Development 9(1):1–12
4. Daoudi L, Elboudour EH, Saadi L, Albizane A, Bennazha J, Waqif M, Elouahabi M, Fagel N (2014) Characteristics and ceramic properties of clayey materials from Amezmiz region (Western High Atlas, Morocco). Appl Clay Sci 102:139–147
5. El Ouahabi M, Daoudi L, Fagel N (2014) Preliminary mineralogical and geotechnical characterization of clays from Morocco: application to ceramic industry. Clays Clay Miner 49:35–515
6. Bertolani M, Biondini R, Giliberti T, Loschi AG, Rabitti D (1982) Caratteristiche chimichee mineralogiche di campioni di argille per ceramica dell'area Sassolese. La Ceramica 35(1):16–33

7. Mesrar, L,. El aroussi O., Lakrim M., Lahrach A., Chaouni A., et Jabrane R.: Technological valorisation of the Miocene clay in the region of Fez (Morocco): characterisation and exploitation possibilities. Present Environment and Sustainable Development 7(1),311–317 (2013)
8. Cook HE, Johnson PD, Matti JC, Zemmels I (1975) Methods of sample preparation and X-ray diffraction data analysis, X-ray mineralogy laboratory. In: Hayes DE, Frakes LA et al (eds) Initial ReportDSDP 28. U.S. Govt. Printing Office, Washington, pp 999–1007
9. Dondi M, Raimondo M, Zanelli C (2014) Clays and bodies for ceramic tiles: reappraisal and technological classification. Appl Clay Sci 96:91–109
10. Carretero, M.I., Dondi, M., Fabbri, B., Raimondo, M.: The influence of shaping and firing technology on ceramic properties of calcareous and non-calcareous illitic–chloritic clays. Applied Clay Science 20, 301–306 (2002)
11. Kornnman, M.: Matériaux de terre cuite matières de base et fabrication". Techniques de l'Ingénieur, 1–30 (2009)
12. Farmer, V.C.: The Layers Silicates. The Infrared Spectra of Minerals Monograph Mineralogical Society, London, pp. 331–363 (1974)
13. Jordan M, Boix A, Sanfeliu T, Fuente C (1999) Firing transformations of cretaceous clays used in the manufacturing of ceramic tiles. Appl Clay Sci 14:225–234
14. Fabbri B, Fiori C (1985) Clays and complementary raw materials for stoneware tiles. Mineralogica Petrographica 29A:535–545
15. Strazzera B, Dondi M, Marsigli M (1997) Composition and ceramic properties of tertiary clays from southern Sardinia (Italy). Appl Clay Sci 12:247–266

Fresh and Mechanical Properties of Recycled Steel Fiber Reinforced Self-consolidating Concrete

Ashish Simalti and A. P. Singh

Abstract This paper presents the fresh and mechanical behavior of recycled steel fiber obtained from the end life of scrap tires in self-consolidating concrete. To characterize the fresh and mechanical properties, different fiber volume fractions of 0.5, 1.0, and 1.5% were used. To reduce the cost of concrete, fly ash and silica fume was added which also helps in increasing workability and viscosity, respectively. Fresh properties were characterized by slump flow and J-Ring. Whereas the mechanical properties were investigated in terms of Compressive, split tensile, and flexural strength.

Keywords Recycled steel fiber · Fiber reinforced self-compacting concrete · Fresh properties · Flexural strength

1 Introduction

In the era of rapidly growing technologies, it is a big challenge to preserve the ecology. As technology enhances with urbanization due to an increase in population the demand for automobiles has risen enormously which deteriorates the environment. From the past few decades, disposal of billions of scrap tires into the landfill has paved the way to a serious environmental issue in developed and developing countries [1, 2].

Moving toward sustainability, everyone has to follow the principle of 3 R's i.e., Reducing, reusing and recycling. So, the material recovered from the waste tires and other by-products can also be used in various forms in different fields [3]. Using these recovered/ by-product materials in concrete reduces the cost of new material and save natural resources too [4]. Shredding and pyrolysis are the two different processes to recover the waste from the scrap tires. The former reduces the tire into rubber granules and steel fiber whereas, the latter process reduces the tire into carbon black, steel wire, tire oil, and gases, etc. [5].

A. Simalti (✉) · A. P. Singh
Dr. B. R, Ambedkar National Institute of Technology, Jalandhar, Punjab, India
e-mail: ashusimalti@gmail.com

K. R. Reddy et al. (eds.), *Sustainable Environment and Infrastructure*, Lecture Notes in Civil Engineering 90, https://doi.org/10.1007/978-3-030-51354-2_24

Plain concrete possesses low ductility due to its low tensile and flexural properties. Introducing fiber in concrete has resolved this problem by enhancing its mechanical properties and post cracking behavior through fiber bridging action and bonding between fiber and matrix, [6, 7]. Various type of fibers is used in concrete as single or in hybridized form. Of which, steel fiber is the most popular due to its effectiveness to improve the mechanical properties of concrete [8, 9]. Steel fibers come in the market in various dimensions and forms (hooked end, crimped and undulated, etc.). Every year, 3000 tons of industrial steel fiber are consumed globally with an increment of 20% per year. Manufacturing of new steel fibers requires a large amount of raw material which generates a large amount of CO_2 in the environment. Due to environmental benefits and less cost recycled steel fiber (RSF) it is attracting researchers, construction industries, and planners to use in construction [1, 2]. The experimental work by many researchers concluded that RSF can be used beneficially in concrete [10, 11]. However, RSF can be more or less significantly comparable to industrial fibers but gives an economic sustainable solution.

The addition of the waste materials obtained from the tire in making self-compacting concrete is a solution to reduce the environmental deterioration and attain sustainability [18]. As the name suggests, SCC means the concrete which is able to compact by itself i.e., consolidation takes place due to self—weight, without the help of vibration. SCC is a time and cost-saving solution for construction [19]. Recycled steel fiber (RSF) obtained from the scrap tires can be used in SCC as reinforcing material [2–19]. There are very few works available on the SCC with RSF. In most of the studies, they generally replace steel fiber with RSF [20] or RSF in combination with polypropylene fiber [21]. Younis et al. has explained the effect of length of RSF having a constant diameter on fresh and mechanical properties and concluded that less significant effect on workability due to short fiber. Also, it quoted that the compressive strength was reduced but improvement in flexural strength. Few types of research have done work on SCC with RSF (in different fraction) to make more sustainable by using a ternary blend of the binder as a control mix to omit the demand of viscosity modifying agent (VMA) and reduce the amount of superplasticizer. And then variation of RSF in different fraction to check rheological and mechanical properties of SCC with RSF.

In this study, fresh properties were investigated by slump flow diameter, T500, visual stability Index (VSI), and J-ring. And the mechanical behavior were characterized by measuring compressive, split tensile and flexural strength.

2 Experimental Program

2.1 Material

Ordinary Portland cement (OPC 43 grade) was used [22]. Fly Ash (FA) as per [23] name CI type and silica fume (SF) which were procured from Ropar thermal plant and

Astrra Chemicals, respectively, was used. Three different sizes of coarse aggregate were used of maximum size 12.5 mm was used in three grading proportions i.e., 33% (12.5–10 mm), 42% (10–6.3 mm) and 25% (6.3–4.75 mm) based on packing factor as suggested by Nan su 2001. Fine aggregate of maximum size 4.75 mm was used as per IS 383-2016. A polycarboxylic ether-based superplasticizer (SP) Master Glenium 51 was used in suitable dosages.

Recycled steel fibers have variation in length and diameter due to its tire recycling process i.e., shredding. So, 150 nos. of fiber were randomly taken to study their geometric characterization. The aspect ratio of RSF varied from 20.23 to 360.8 with an average diameter of 0.216, the steel wire obtained from the end life of scrap truck tires. The density of RSF was 3230 kg/m^3, measured by the water replacement method. In the present study, three fiber volume fractions i.e., 0.5, 1, and 1.5% were used of MSF and RSF, respectively. MSF having density 7850 kg/m^3, length 30 mm, and aspect ratio 33.33 was used.

Mix proportioning

The reference mix for SCC was prepared on the basis of [24] and [25]. The fibers were then substituted by coarse aggregate (by weight). The proportion of the mixes are presented in Table 1. 300 L capacity electrical mixer was used to prepare the mixes. First, the coarse and fine aggregate was dry mixed for about 3 min followed by water equal amount to its water absorption so that water in w/c ratio should not alter by the absorption of both the aggregates. The cement, fly ash, and silica fume were added to the mixer and allowed to dry mix for 4 min. Then mix 70–80% required amount of water into the mixer with superplasticizer and mix it for 3 min. Now sprinkle the fiber by hand into mix so that the distribution of the fiber may uniform, after this remaining 20% was added and mix for 3 min. Then after completion of mixing obtained mix poured into the specimens.

3 Methods

Fresh properties

The fresh properties were evaluated as per recommendation of EFNARC 2005 [26], because there is no code for fiber reinforced concrete till date. So, the same code was used to check the fresh properties of SCC with fiber. In this study slump flow spread, T_{500} and J-Ring (T_{500} and spread) were performed. And visual stability index also checks by visual inspection of the mix in the fresh state to evaluate its stability against segregation.

Compressive strength

Compressive test as recommended by [27], cubic specimens (100 × 100 × 100 mm) were used to analyze the capacity of manufactured/recycled steel fibers reinforced SCC in crack behavior during compressive load. The rate of loading was kept

Table 1 Mix proportions in ratio

Mix ID	Binder = 858.75 kg/m^3			Fine Aggregate/Binder	Coarse Aggregate/Binder	SP (% of binder content)	Fiber (%vol.)
	Cement/Binder	Fly Ash/Binder	Silica Fume/Binder				
M0*	0.45	0.44	0.11	0.96	0.58	0.7%	0
M01**	0.45	0.44	0.11	0.96	0.53	0.85%	0.5
M02**	0.45	0.44	0.11	0.96	0.49	0.90%	1.0
M03**	0.45	0.44	0.11	0.96	0.44	0.95%	1.5
M11***	0.45	0.44	0.11	0.96	0.56	0.80%	0.5
M12***	0.45	0.44	0.11	0.96	0.54	0.85%	1.0
M13***	0.45	0.44	0.11	0.96	0.52	0.90%	1.5

*refer to Control Mix without any fiber, ** refer to control mix with MSF, *** refer to mix with RSF

2.5 kN/s, and 2000 kN capacity compression test machine was used. Two cubic specimens were used to investigate the strength of each mix at the age of 7 and 60 days.

Splitting tensile test

This test was done as per the recommendation of [28]. A cylindrical specimens (100 × 200 mm) were used to investigate split tensile strength. The cylinders with a continuous loading rate of 1.3 kN/s, using a compression testing machine capacity of 2000 kN. To perform the test, two specimens were taken from each mix for 7 and 60 days.

Flexural strength test

The test was performed as per method suggested by [27], prism specimen (100 × 100 × 500 mm) were used to investigate flexural testing (MTS- 100 kN servo-controlled) at the loading rate of 0.5 mm/min. From each mix, two specimens were taken after curing age of 60 days to get the flexural strength. The strength was calculated as per Eq. (1) given below:

$$f = \frac{PL}{BD^2} \tag{1}$$

where f = flexural strength (MPa), P = ultimate load, L = span length (450 mm), D = depth of section (100 mm),
B = width of section (100 mm).

4 Result and Discussion

4.1 Fresh Properties

From the Table 2, it can be seen that introducing fiber reduces the workability of the mix as compared to normal SCC. But if SCC with MSF compares with RSF mix

Table 2 Fresh Properties of all the mixes

Workability test	Parameter	Results						
		M0	M01	M02	M03	M11	M12	M13
Slump Flow	Spread (mm)	760	735	725	720	740	730	720
	T_{500}(s)	3.3	4.0	4.4	4.9	3.8	4.1	4.3
J-Ring	flow Spread	750	730	715	705	735	725	710
	T_{500}(s)	3.4	4.7	5.0	5.4	4.2	4.5	4.8
VSI	0-3	0	0	1	1	0	1	0

then it was observed that there is an enhancement in the workability of SCC with RSF mixes. And the requirement of the plasticizer also reduced. So, from the result, it was observed RSF gives better fresh properties as compared to SCC with MSF. But both shows reduction in fresh properties as compared to normal (control) mix with no fiber. And all the mixes were highly stable and stable, having VSI, 0, and 1, respectively. Figures 1 and 2 imply that all the mixes are within the EFNARC range (denoted by two parallel lines).

Mechanical Properties

From the result, as shown in Fig. 3 it can be observed that at 7 days the compressive strength of RSF had no significant change as compared to control mixes. But in the later age, there was a substantial enhancement in the compressive strength of SCC with RSF as compared to control mix but little less than the SCC with MSF. It is relatively equivalent in case of 0.5 and 1% of RSF and MSF in SCC. The RSF was more effective in arresting crack as compared to MSF and delays a smooth failure of samples without much destruction of sample i.e., broken matrix was still stuck to the RSF and not fully detached from the sample, this type of failure was not observed in the control mixes. This may have happened due to the good micro-crack arresting

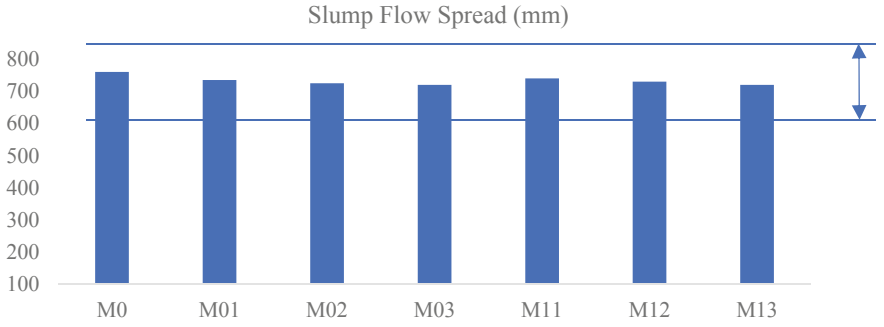

Fig. 1 Slump flow spread for all mix

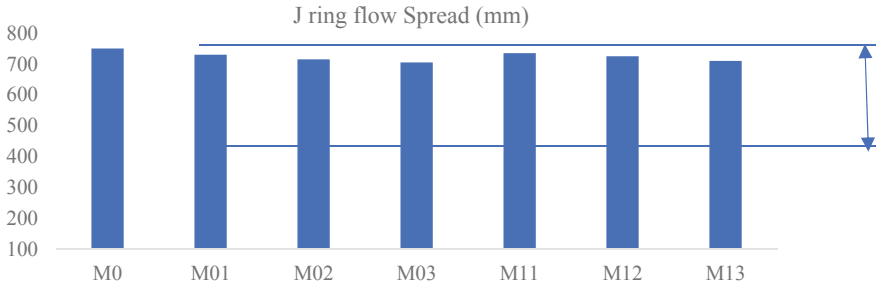

Fig. 2 J- Ring spread for all the mix

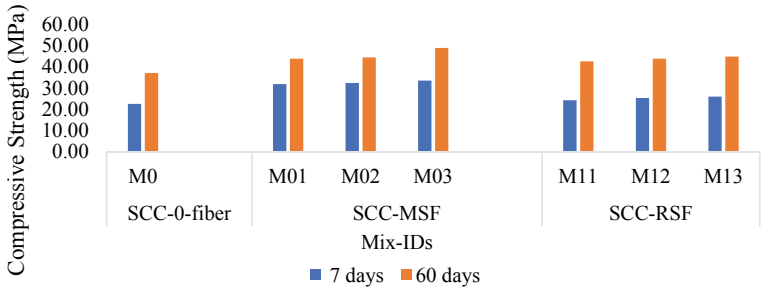

Fig. 3 Compressive Strength at 7 and 60 day for all the mixes

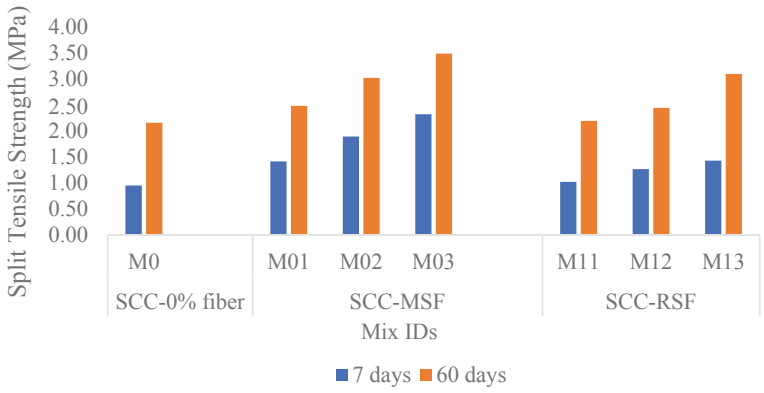

Fig. 4 Split Tensile Strength at 7 day and 60 day for all mixes

property of shot steel fiber and better Matrix and fiber bonding behavior of RSF due to its entangled shape.

Figure 4 shows that there was an increase in split tensile strength as compared to the control mix in SCC with RSF but at 60 days it has been improved significantly. This kind of behavior may be due to high content of pozzolanic content in the binder i.e., around 44% fly ash which slows the hydration process and delays the formation of C-H-S content in the concrete due to which the bonding may not be good during the initial stage of investigation[29]. But as the time of curing reached 60 days there was an improvement in the tensile behavior of mix. RSF and MSF show good tensile behavior at later age i.e., 60 days as compared to SCC with no fiber.

There was no significant improvement in flexural strength of RSF and control mixes except in the case of SCC with MSF 1.5%. And all the specimen was checked for flexure at the age of 60 days.

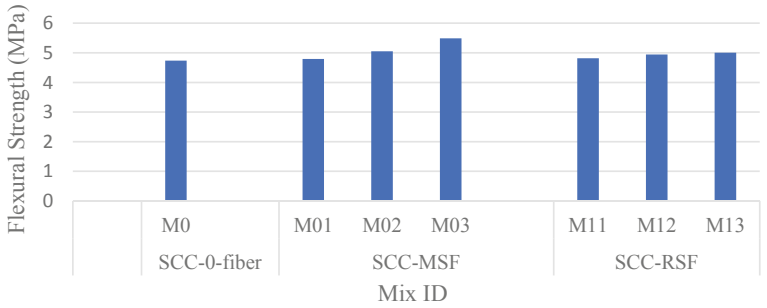

Fig. 5 flexural strength at 60 days for all the mixes

5 Conclusion

On the basis of obtained results, the following statements were drawn-

1. There was an increase in the slump flow and J-ring spread with RSF as compared to ISF. But the overall workability reduced if compared with SCC with no fiber.
2. There was an increase in Compressive and Tensile strength by incorporation of RSF as compared to the Control mix. And comparable with SCC with ISF.
3. There was no significant improvement in flexural strength SCC with RSF as compared to SCC having no fiber. If RSF compared to ISF it shows a reduction in the strength.

From the above, it can be stated that the results of RSF and ISF are comparable. So, RSF can be used over ISF by keeping a view of economic and environmental benefits.

References

1. Mastali M, Dalvand A, Sattarifard AR, Illikainen M (2018) Development of eco-efficient and cost-effective reinforced self-consolidation concretes with hybrid industrial/recycled steel fibers. Constr Build Mater 166:214–226
2. C. Frazão, B. Díaz, J. Barros, J. A. Bogas, and F. Toptan, "An experimental study on the corrosion susceptibility of Recycled Steel Fiber Reinforced Concrete," *Cem. Concr. Compos.*, 2018
3. B. Samiha, "The Importance of the 3R Principle of Municipal Solid Waste Management for Achieving Sustainable Development," *Mediterr. J[1] B. Samiha, "The Importance 3R Princ. Munic. Solid Waste Manag. Achiev. Sustain. Dev. Mediterr. J. Soc. Sci., Sep. 2013.ournal Soc. Sci.*, Sep. 2013
4. Mehta DJMMPK (2006) *Concrete: Microstructure, Properties and Materi- als*, 3rd edn. Third, McGraw Hill Book Company
5. Pilakoutas K, Neocleous K, Tlemat H (2004) Reuse of tyre steel fibres as concrete reinforcement. Proc. ICE-Engineering Sustain. 157(3):131–138
6. Leone M, Centonze G, Colonna D, Micelli F, Aiello MA (2018) Fiber-reinforced concrete with low content of recycled steel fiber: Shear behaviour. Constr Build Mater 161:141–155

7. H. Hu, “Mechanical Properties of Blended Steel Fibre Reinforced Concrete Using Manufactured and Recycled Fibres from Tyres,” vol. 163, no. April, pp. 376–389, 2018
8. Goel S, Singh SP (2014) Fatigue performance of plain and steel fibre reinforced self compacting concrete using S-N relationship. Eng Struct 74:65–73
9. Goel S, Singh SP, Singh P (2012) Flexural fatigue strength and failure probability of Self Compacting Fibre Reinforced Concrete beams. Eng Struct 40:131–140
10. Neocleous K, Tlemat H, Pilakoutas K (2006) Design issues for concrete reinforced with steel fibers, including fibers recovered from used tires. J Mater Civ Eng 18(5):677–685
11. Neocleous K, Angelakopoulos H, Pilakoutas K, Guadagnini M (2011) Fibre-reinforced roller-compacted concrete transport pavements. Proc. Inst. Civ. Eng. - Transp. 164(2):97–109
12. Tlemat H, Pilakoutas K, Neocleous K (2006) Modelling of SFRC using inverse finite element analysis. Mater. Struct. Constr. 39(286):221–233
13. Leone M, Centonze G, Colonna D, Micelli F, Aiello MA (2016) Experimental Study on Bond Behavior in Fiber-Reinforced Concrete with Low Content of Recycled Steel Fiber. J Mater Civ Eng 28(9):04016068
14. Sengul O (2016) Mechanical behavior of concretes containing waste steel fibers recovered from scrap tires. Constr Build Mater 122:649–658
15. O. Onuaguluchi and N. Banthia, “Scrap tire steel fiber as a substitute for commercial steel fiber in cement mortar: Engineering properties and cost-benefit analyses,” *Resour. Conserv. Recycl.*, vol. 134, no. December 2017, pp. 248–256, 2018
16. Al-kamyani Z, Figueiredo FP, Hu H, Guadagnini M, Pilakoutas K (2018) Shrinkage and flexural behaviour of free and restrained hybrid steel fibre reinforced concrete. Constr Build Mater 189:1007–1018
17. Z. Al-Kamyani, M. Guadagnini, and K. Pilakoutas, “Impact of shrinkage on crack width and deflections of reinforced concrete beams with and without steel fibres,” *Eng. Struct.*, vol. 181, no. July 2018, pp. 387–396, 2019
18. Alsaif A, Bernal SA, Guadagnini M, Pilakoutas K (2019) Freeze-thaw resistance of steel fibre reinforced rubberised concrete. Constr Build Mater 195:450–458
19. K. H. Younis, F. Sh. Ahmed, and K. B. Najim, “Self-Compacting Concrete Reinforced with Steel Fibers from Scrap Tires: Rheological and Mechanical Properties,” *IEC2018 Proc. B.*, no. March, 2018
20. Mastali M, Dalvand A, Sattarifard AR, Abdollahnejad Z, Illikainen M (2018) Characterization and optimization of hardened properties of self- consolidating concrete incorporating recycled steel, industrial steel, polypropylene and hybrid fi bers. Compos. Part B 151(March):186–200
21. Mastali M, Dalvand A (2017) Fresh and Hardened Properties of Self-Compacting Concrete Reinforced with Hybrid Recycled Steel-Polypropylene Fiber. J Mater Civ Eng 29(6):04017012
22. Bureau of Indian Standard, “IS 8112: 2013, Ordinary Portland Cement, 43 Grade — Specification, Bureau of Indian Standards, New Delhi,” no. March, 2013
23. “CSA A3000 : Cementitious materials compendium,” 2018
24. S. B. A. V.V. Karjinni, “Mixture proportion procedure for SCC,” pp. 35–41, 2009
25. Su N, Hsu KC, Chai HW (2001) A simple mix design method for self-compacting concrete. Cem Concr Res 31(12):1799–1807
26. The European Project Group, “The European Guidelines for Self-Compacting Concrete: Specification, Production and Use,” *Eur. Guidel. Self Compact. Concr.*, no. May, p. 63, 2005
27. IS-516, “Method of Tests for Strength of Concrete,” *Indian Stand.*, pp. 1–30, 1959
28. Mohamed OA, Syed ZI, Najm OF (2016) Splitting Tensile Strength of Sustainable self-consolidating Concrete. Procedia Eng. 145:1218–1225
29. P.. K.. M. Dan Ravina, “Compressive Strength of Low Cement/ High Fly Ash Concrete,” *Cem. Concr. Res.*, vol. 18, no. 4, pp. 571–583, 1988

Utilization of Waste Lime Sludge and Coal Fly Ash in Construction Industry

Shristi Khosla Kanoungo, Umesh Sharma, and Abhishek Kanoungo

Abstract Large quantities of industrial by-products are produced every year in India and across the globe. These materials have dual problems of disposal and health hazards. By-products such as coal fly ash and sludge from water treatment plants require greater attention since the magnitude of impact on the environment such as land, surface and ground water resources and air is high, if not properly disposed of. One solution to this crisis lies in recycling waste into useful products in the construction activities to replace the natural materials such as soil and conventional products such as cement wherever possible which will lead to reduction in the economic and environmental problem of waste disposal and also conserve the depleting resources. The aim of this paper is to find the reuse potential of water softening sludge and coal fly ash in the construction industry. In this study, a composite material has been formulated using fly ash and lime sludge with replacing cement to make mortar specimen. The compressive strength of the formulated mix was determined by performing an unconfined compressive strength test. The optimum content of cement, fly ash and sludge was found to be 20%, 40%, 40%, respectively, thereby reducing the cement content to a great extent. It was then observed that the strength of the optimum mix invariably increased 31% by proportionately replacing cement with fly ash and sludge which was dependent on the curing technique used. Oven-dried samples had higher strength than lime water cured samples.

Keywords Coal fly ash · Lime sludge · Recycle waste · Composite mix · Compressive strength

S. K. Kanoungo (✉) · U. Sharma
Civil Engineering, Punjab Engineering College (Deemed to Be University), Sector-12, Chandigarh, India
e-mail: shristi24@gmail.com

A. Kanoungo
Civil Engineering, Chitkara University, Baddi, Himachal Pradesh, India

K. R. Reddy et al. (eds.), *Sustainable Environment and Infrastructure*, Lecture Notes in Civil Engineering 90, https://doi.org/10.1007/978-3-030-51354-2_25

1 Introduction

The exponential growth in the world population has lead to the diminution of the conventional resources. The amount of waste generated is also analogous to this increase in the population. The non-decaying waste produced will be buried in the ground for hundreds of thousands of years causing damage to the surroundings resulting in the environmental and economic problem of waste disposal. India generates about 62 million tonnes of waste every year out of which less than 60% is collected and only 15% is processed [1]. Figure 1 depicts the percentage composition of waste generated in India [1]. It is clearly evident that one of the major portions of waste is the recyclables.

The increasing waste generation emphasizes the concern to dispose of the waste in an effective and economic way. Recycling of these waste materials to replace the conventional products wherever possible will not only reduce the problem of waste disposal but will also reduce the dependency on the limited resources.

By-products such as fly ash from thermal power plants and sludge from water treatment plants require our greater attention since the magnitude of impact on the environment such as land, surface and ground water resources and air if not properly disposed of is high. The limitations of the space for landfills and the economic problem created by these materials have driven exploration of new alternative recycled materials. In the following study, an attempt has been made to utilize the coal fly ash from thermal power plants and waste sludge from water treatment plant as a replacement to cement in some civil engineering applications.

Coal fly ash (CFA) is produced as an industrial by-product after the combustion of fuel in thermal power plants. As the population is increasing, similarly is the need for energy. The CFA is recognized as an environmental pollutant and if its disposal is not taken care of it may cause potential harm to living beings. CFA has been nowadays

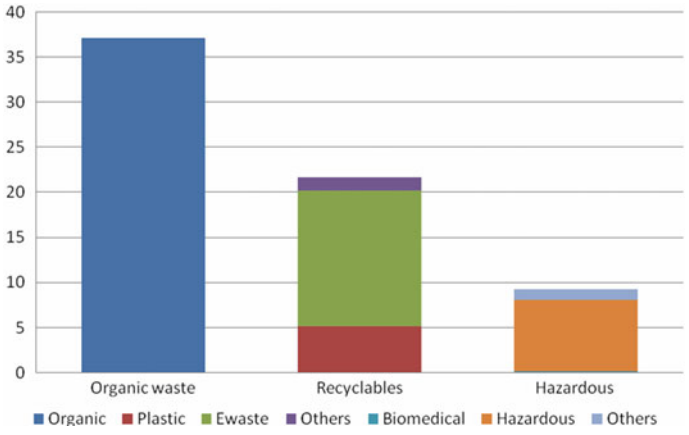

Fig. 1 Waste composition of India, in million metric tonnes per annum

majorly used as a heterogeneous catalyst. As CFA primarily contains metal oxides such as Al_2O_3, SiO_2, it can offer support in thermal stability to be used as catalysts [2]. In 2006, it was estimated that 80% of the CO_2 emissions were produced due to the addition of Portland cement in concrete mixes [3]. The replacement to cement by an optimum amount of CFA is yet to be established by testing so that the properties of concrete are not affected [4]. However, it was observed that replacement up to of 25–30% level can be made to improve the alkali-silica expansion, durability and thermal cracking. This study is intended to evaluate the reuse potential of CFA in replacement to cement and to discover whether CFA can be used as a building material.

Sludge is the solid residue produced after the treatment of water. Usually, this sludge is either dumped directly into the river stream causing hazardous damage to the water body compromising the quality of water and causing concern to public health or dumped as landfills creating space constraints. Measures have now been taken to ensure that the waste from the treatment plants is disposed of in an effective manner. Waste sludge from Water treatment plants (WTP) have a good amount of lime which enables its reuse options. Currently, land-based applications of waterworks sludge are gaining increasing attention as alternative disposal means [5, 6]. The use of waterworks sludge as a filler material and dispersion dye is one another option for the utilization of sludge [7]. It was also reported that lime sludge has high feasibility to be used as landfill liner while some other study showed attempts to use waterworks sludge to cap an inert landfill site and in turf production [8, 9]. The sludge has also been used as a raw material for ceramic products [10]. Lime has been used in mortar for very long because it improves the properties of mortar mix. The study attempts to use this sludge from WTP as a replacement to cement to improve the properties of the mortar mix. Although, sludge has many advantages its use is yet to be accepted in the building materials industry.

The recycling of these waste materials will reduce the problem of their disposal to some extent and prove to be effective in reducing the dependency on conventional resources. This will also increase the life of raw materials available for construction and will reduce the final production costs.

2 Experimental Programme

To assess the effect of replacing cement with CFA and lime sludge, composite specimens were prepared by varying blending lime sludge with CFA and determining the compressive strength of the same by performing Unconfined Compressive Strength Test. Once the optimum value of CFA and lime sludge has been adjudged, mortar cubes were then prepared by varying the percentages of the waste materials so as to obtain a favourable mix. UTM was used to evaluate the mortar strength of each specimen. The flow chart of the experimental study is presented in Fig. 2.

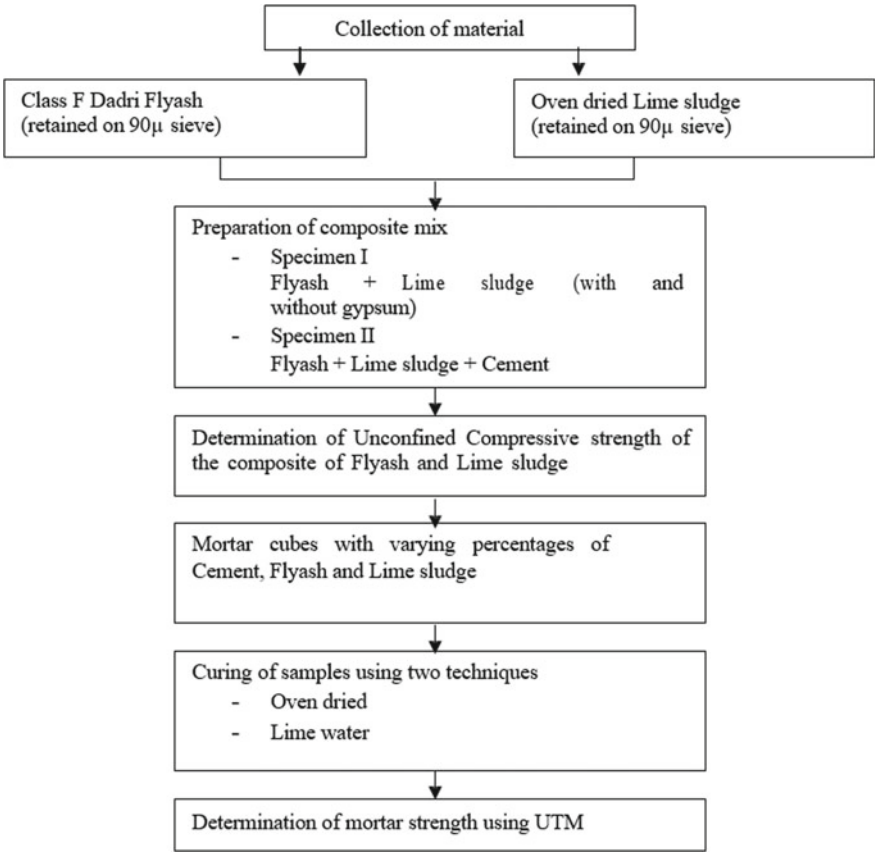

Fig. 2 Flow chart for experimental programme

3 Materials and Methods

This study is focusing on two major waste materials, namely, lime sludge and fly ash that are generated in bulk quantity from water treatment plants and thermal power plants, respectively.

3.1 Lime Sludge

It was collected from Municipal Corporation of Delhi with a treatment capacity of 0.5 MGD and sludge production as 4–5 tonne/day. The sludge after collecting was stored in airtight containers. The scanning electron micrograph (SEM) image is shown in Fig. 3. The sludge particles are asymmetrical in structure.

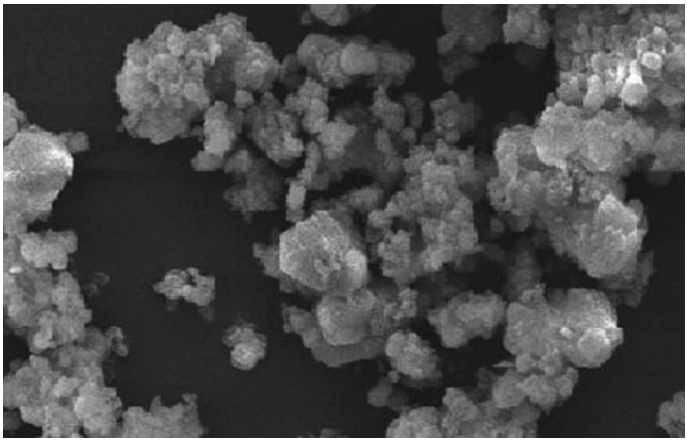

Fig. 3 SEM image of lime sludge

3.1.1 Chemical Characterization

It is necessary to characterize the waste material before it can be put to use. The chemical characteristics of lime sludge are given in Table 1.

Table 1 Chemical characteristics

Properties (% by mass)	Value
Loss on ignition (@900° ± 25°)	61.5
Silica as SiO_2	0.20
Iron as Fe_2O_3	0.04
Alumina as Al_2O_3	0.32
Magnesium as MgO	0.87
Calcium as CaO	35.3
Sodium as Na_2O	0.11
Chloride as Cl	0.006
Sulphate as SO_4	0.2
Phosphate as P_2O_5	0.009
Lead as Pb, ppm	1
Chromium as Cr, ppm	0.3
Cadmium as Cd, ppm	0.1

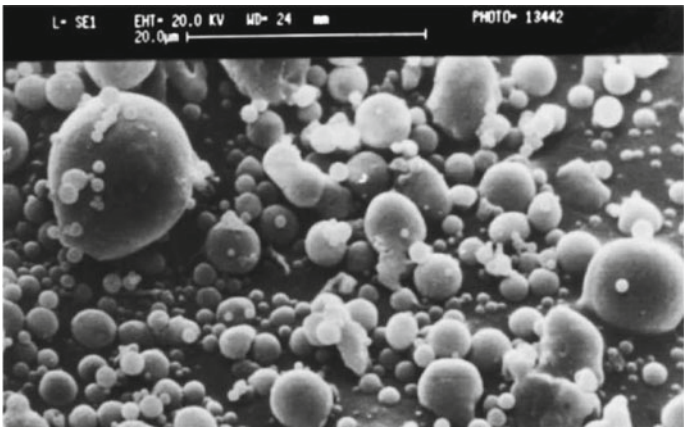

Fig. 4 SEM image of Dadri fly ash

Table 2 Chemical characteristics of Dadri fly ash

Chemical composition (%)	Value
Silica (SiO_2)	60.12
Alumina (Al_2O_3)	30.16

3.2 Fly Ash

The class F Dadri fly ash is used. It was procured from Badarpur thermal power plant. The scanning electron micrograph (SEM) image analysis of the fly ash has been shown in Fig. 4. The particle shape appears to be spherical having a porous structure.

3.2.1 Chemical Characterization

The chemical characteristics of the coal fly ash used are given in Table 2.

3.3 Methods

3.3.1 Unconfined Compressive Strength Test

Unconfined compression strength (UCS) tests were conducted in accordance with IS 4332, Part 5 (BIS 1970). To perform UCS testing, fly ash with MDD (maximum dry density) as 1.25 g/cc was blended with lime sludge and the specimen was prepared for OMC (optimum moisture content) as 24 and 27%. The sludge used is oven-dried

at a temperature of 60–70 °C for about 18 h. Sludge sieved through 150 mm sieve and retained on 90μ sieve is used. The fly ash used was sieved through 150 mm sieve and retained on 90μ sieve. Different proportions of lime sludge were blended with fly ash to get a composite material. The sludge content varied from 10 to 50%, at an interval of 5%.

3.3.2 Mortar Cubes

For testing of mortar cubes, the required composite mix was prepared using cement, fly ash and sludge as binders and cast in cubical moulds. Gypsum was used to increase the strength in the early stages of hydration. Fine cement was taken and portion sieved through 150 mm and retained on 90 microns was used in the test performed. The water content required is determined by the IS: 4031 (Part 4)—1988. The mix prepared was cured using different methods of curing which were—Oven-dried and lime water curing. The specimens were tested on a Universal testing machine.

4 Results and Discussion

The composite mix was prepared and tested by varying the percentage of lime sludge with coal fly ash to determine the optimum percentage of the waste material that can be used to replace cement. The results obtained are elaborated here.

4.1 Optimum Water Content

The 7 and 28-days strength of composite (in various proportions) with 24 and 27% of water content is shown in Figs. 5 and 6, respectively.

Accordingly, the unconfined compressive strength at 24% w/c comes out to be more than that at 27% w/c. Hence, the optimum water content obtained from the interpretation is 24% and the subsequent samples will be prepared taking into account this percentage of water content only.

4.2 Variation of Strength

The variation of strength at different compositions for zero-day, 7 and 28 days has been shown in Fig. 7 and Table 3.

It can be inferred that the 28-day strength is not obtained as expected. In some cases, it is even less than the 7-day strength and hence undesirable for comparison.

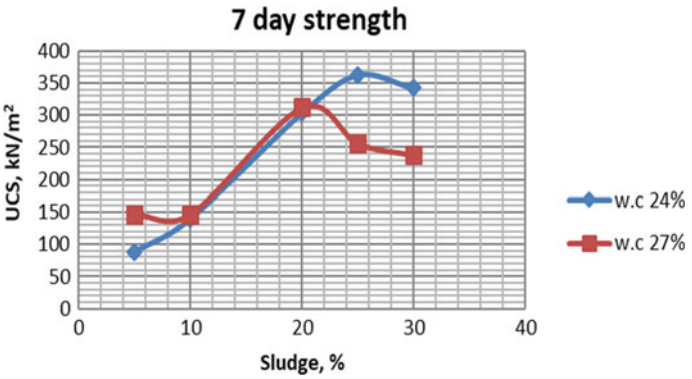

Fig. 5 Variation of 7-day strength at a different water content

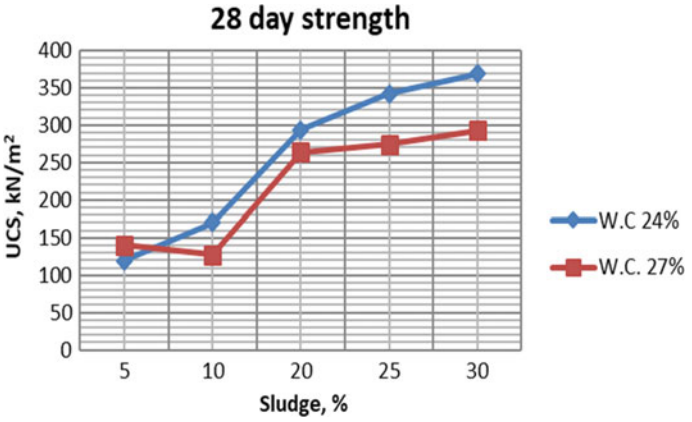

Fig. 6 Variation of 28-day strength at a different water content

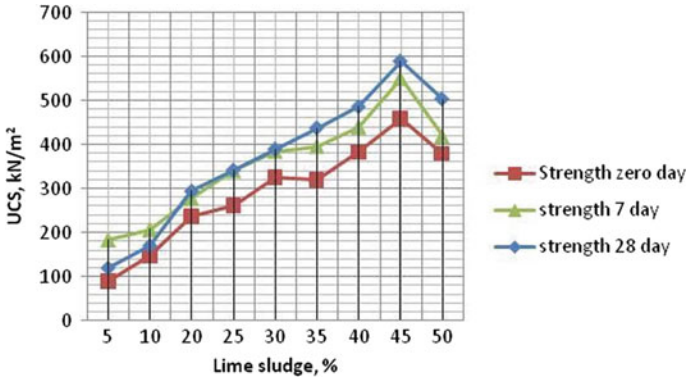

Fig. 7 Variation of strength at different compositions

Table 3 Interpretation of variation of strength

Composite mix (LS:CFA)	Zero day strength (kN/m^2)	7 day strength (kN/m^2)	28 day strength (kN/m^2)
10:90	89	185	119
15:85	147	208	170
20:80	236	279	294
25:75	261	342	342
30:70	325	386	390
35:65	320	397	438
40:60	383	441	486
45:55	460	552	590
50:50	380	420	504

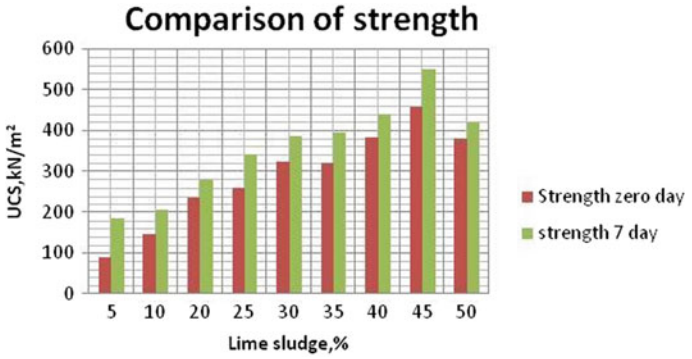

Fig. 8 Comparison of strength with varying percentage of sludge

4.2.1 Optimum LS and CFA Content

Different percentage of lime sludge was blended with fly ash to get a composite material. The sludge content varied from 5 to 50%, at an interval of 5%. The optimum content of LS and CFA is shown in Fig. 8. It is observed that the optimum content of LS: CFA is 45: 55%. As the percentage of sludge increases beyond 45%, the value of strength tends to decrease.

4.3 Mortar Mix

Two samples of mortar mix with varying percentage of LS, FA along with cement was prepared. The strength was measured on UTM and is shown in Fig. 9.

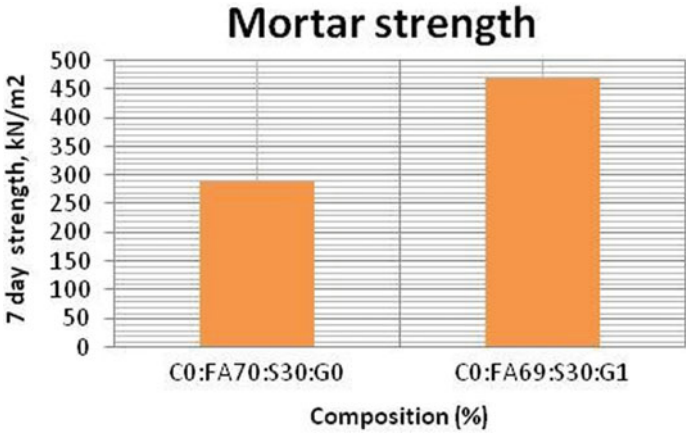

Fig. 9 Mortar strength of oven-dried samples without cement

The mortar strength achieved without using cement is very less and unsuitable for engineering applications. The use of gypsum significantly increases the mortar strength. Therefore, cement should be used for applied strength along with waste material. The optimum content of LS, FA and cement have been achieved as C20: FA40: S40 as depicted in Fig. 10.

It has also been observed that the compressive strength of mortar mould increased with the technique used for curing. Strength with oven-dried curing came out to be more than that of lime water curing. The compressive strength of cement modified composite mix was found to be greater than that of standard cement mortar and the same is depicted in Fig. 11. The strength of the optimum mix increased almost by 31% in comparison to the standard mix.

Hence the use of waste material like LS and FA can be of great importance since it has high reuse potential and thus reduce the problem of disposal as well.

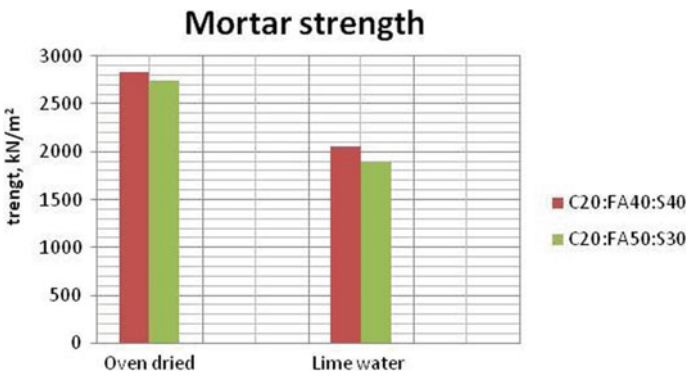

Fig. 10 Variation of strength of mortar mixes with cement

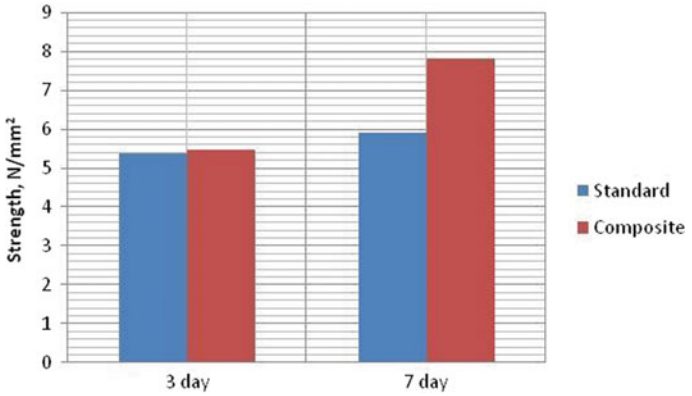

Fig. 11 Comparison of standard and composite mix

5 Conclusions

The successful utilization of fly ash and sludge in the mix to replace cement will promote sustainable development and conservation of natural resources. Based on the experimental results, the following conclusions were drawn. The maximum zero-day strength of 460 kN/m^2 and 7-day strength of 515 kN/m^2 was achieved with combination LS45: FA55 as an optimum ratio. Additionally, it was concluded that a decrease in the compressive strength of cylindrical specimens is accompanied by an increase in the amount of lime sludge beyond 45%. The maximum compressive strength was achieved with a combination of 20% cement, 40% sludge and 40% fly ash (of binder) thereby reducing the cement content by almost 80%. The maximum zero-day strength was 5480 kN/m^2 and 7 days was 7810 kN/m^2. The strength was found to be dependent on the technique of curing that was used. It was observed that the strength of the oven-dried sample was greater than lime water-cured sample. The strength of the composite mix was found to be 31% more than that of the standard cement mortar specimen. It is thus concluded that the composite mortar mix can be made by blending lime sludge with fly ash. The effective utilization of the fly ash and sludge will not only reduce the problem of disposal of these waste materials but will also preserve the non-renewable resources in the construction industry.

References

1. PIB (2016) Solid waste management rules revised after 16 years; rules now extend to urban and industrial areas. Press Information Bureau, Government of India. http://pib.nic.in/newsite/PrintRelease.aspx?relid=138591
2. Wang S, Lu GQ (2007) Effect of chemical treatment on Ni/fly-ash catalysts in methane reforming with carbon dioxide. In: FbioBellot Noronha MS, Eduardo Falabella S-A (eds) Studies in surface science and catalysis, vol 167. Elsevier, pp 275–280

3. Felekoglu B (2006) Utilization of Turkish fly ashes in cost effective HVFA concrete production. Fuel 85(1213):1944–1949
4. Reiner M, Rens K (2006) High-volume fly ash concrete: analysis and application. Pract Period Struct Des Constr 11(1):58–64
5. Basta NT (2000) Examples and case studies of beneficial reuse of municipal by-products. In: Power JF, Dick WA (eds) Land application of agricultural, industrial, and municipal by-products. Book Series No. 6, Soil Science Society of America, Madison, WI
6. Titshall LW, Hughes JC (2005) Characterization of some South African Watertreatment residues and implications for land application. J. Water SA 31(3):299–307
7. Horth H, Gendebien A, Agg R, Cartwright N (1994) Treatment and disposal of waterworks sludge in selected European countries. In: Foundation for water research technical reports No.FR 0428
8. Raghu D, Neilan HH, Yih T (1987) Water treatment plant sludge as landfill line. In: Proceedings of specialty conference on geotechnical practice for waste disposal, USA
9. Flower D, Sanjayan J (2007) Greenhouse gas emissions due to concrete manufacture. Int J Life Cycle Assess 12(5):282–288
10. Vicenzi J, Moura Bernardes A, Bergmann CP (2005) Evaluation of alum sludge asraw material for ceramic products. J Ind Ceram 25(1):7–16

Analysis of Rheological Properties and Moisture Resistance of Nanoclay-Modified Asphalt Binders

M. M. Tariq Morshed and Zahid Hossain

Abstract The primary aim of this study is to improve the rheological properties and moisture resistance of asphalt binder by the modification of a sustainable material named "nanoclay." Rheological properties and moisture resistance of selected nanoclay-modified asphalt binders have been evaluated. Three types of nanoclays (Cloisite 10A, Cloisite 11B, and Cloisite 15A) at 1, 2, and 3% by the weight of asphalt binder were blended with a base binder (PG 64-22) from two sources. A blending protocol consisting of a duration of 2 h, a rotation of 2000 rpm, and a temperature of 1500 C were used to blend the nanoclays with the asphalt binders. Rheological properties of nanoclay-modified asphalt binders were then determined by using a Rotational Viscometer (RV) and a Dynamic Shear Rheometer (DSR). The viscosity of the nanoclay 2% Cloisite 10A-modified binder was about 248% of that of the neat binder. It was found that the consistency of a nanoclay-modified binder was significantly higher than the neat binder. The rutting factor ($G^*/\sin\delta$) also increased significantly for the nanoclay-modified asphalt binders. An Optical Contact Analyzer (OCA) was used to evaluate moisture susceptibility. Binder modified by 3% Cloisite 10A showed the highest surface free energy and cohesiveness. An Atomic Force Microscope (AFM) was used to characterize the nanoclay-modified samples. Surface roughness increased, but no improvement was observed in the DMT (Derjaguin–Muller–Toporov) moduli values. Besides, the adhesion parameter, which indicates the moisture susceptibility, increased significantly.

Keywords Asphalt binder · Nanoclay · Rheology · Moisture resistance · Atomic force microscope

M. M. T. Morshed
Department of Engineering, Arkansas State University, Jonesboro 72467, USA
e-mail: mmtariq.morshed@smail.astate.edu

Z. Hossain (✉)
Department of Civil Engineering, Arkansas State University, Jonesboro PO Box 1740, 72467, USA
e-mail: mhossain@astate.edu

K. R. Reddy et al. (eds.), *Sustainable Environment and Infrastructure*, Lecture Notes in Civil Engineering 90, https://doi.org/10.1007/978-3-030-51354-2_26

1 Introduction

As a viscoelastic material, the general propensity of the asphalt binder is to flow at a higher temperature and turns out to be hard at a lower temperature. Pavement stiffness is depended on the surface chemical properties and temperature susceptibility of asphalt binders. Pavement distresses such as rutting and cracking can happen due to the extreme weather events and the increased amount of wheel loads. As a result, the use of polymer-modified asphalt binders is increased day by day. Among other polymers, styrene-butadiene-styrene (SBS) and styrene-butadiene-rubber (SBR) are commonly being used to modify performance grade (PG) binders so that asphalt can endure increased loads and extreme temperature events. In this study, nanoclay has been used as an alternative asphalt modifier.

Nanoclay is economical and naturally abundant. Moreover, it is expected that the use of nanoclay instead of polymers could significantly reduce the cost of asphalt binders. Nanoclays possess an extraordinary potential for improving the performance of asphalt binders and mixes due to their nanoscale phenomena such as the quantum effects, high surface energy, spatial confinement, and a large fraction of surface atoms. A significant portion of the current usages of polymer-modified binders (PMBs) can potentially be replaced by nanoclay-modified binders.

2 Literature Review

Several publications were explored for gathering the existing research on the nanoclay modified asphalt binders. Publications from different reputed research entity including Transportation Research Records (TRB), Federal Highway Administration (FHWA) records, and projects of Departments of Transportation (DOTs) were considered for the literature review.

A few researchers have effectively used nanoparticles in laboratory studies. Ghile [1] studied Cloisite and stated that nanoclay modification improved mechanical properties such as creep and fatigue resistance. Nanoclay can also be worked as filler reinforcements. Yu et al. [2] reported that montmorillonite modified asphalts had higher viscoelastic properties and rutting resistance. Polacco et al. [3] have examined the effect of clay as the third component in polymer-modified asphalts. Jahromi and Ahmadi [4] tried Cloisite 15A and Nanofill 15 as an asphalt binder modifier and observed increased stiffness, rutting resistance, indirect tensile strength, and resilient modulus, but decreased fatigue performance. You et al. [5] investigated two types of nanoclays (called nanoclay A and B) as modifiers of a PG 58-22 binder in Michigan. The research team stated that a significant increase in rutting resistance was found for nanoclay-modified binders. Hossain et al. [6] evaluated the viscosity and rutting properties of Cloisite 15-modified asphalt binders. Zapién-Castillo et al. [7] investigated the nanocomposite of styrene-ethylene-butylene-styrene (SEBS) and Cloisite 15A modified asphalt binders and reported improved rheological properties.

The surface free energy (SFE) approach was used by some researchers to evaluate moisture susceptibility. The Texas Transportation Institute (TTI) [8, 9] introduced stripping parameters such as cohesive energy, adhesive energy, and "compatibility ratio (CR)" in the surface free energy (SFE) theory. Hossain et al. [10] investigated moisture resistance of nanoclay modified binders using surface free energy (SFE) technique. The research team stated that nanoclay modified binders are expected to have poorer moisture resistance than the base binder. Hossain et al. [11] also suggested that a small amount (about 4%) of nanoclays seemed to be effective in maintaining good wetting ability with different aggregates.

3 Materials and Methodology

Two virgin binders (PG 64-22) were collected from Ergon Inc. One sample originated from a Canadian crude source, and the other binder sample was made from an Arabian crude source. Three types of organically treated nanoclay were used to modify the virgin binders: Cloisite 10A, Cloisite 11B, and Cloisite 15A. The virgin binders were modified using three different percentages of modifiers: 1, 2, and 3%. These nanoclays were collected from Southern Clay Products, Inc. Cloisite 15A and Cloisite 10A had very similar plate dimensions (~13 μ), but they were treated with different types of modifiers. A high shear mixer was used to blend the nanoclay with asphalt binder and a blending protocol (2 h time, 2000 rpm, and 150 °C) was followed for mixing.

The rotational viscosity (RV) tests were conducted to evaluate the viscous behavior of the base binder and nanoclay-modified binders. The RV tests were conducted at 135, 150, 165, and 180 °C based on AASHTO T 316. Dynamic shear rheometer (DSR) test was conducted for determining complex shear modulus (G*) and phase angle (δ) according to AASHTO T 315. Unaged, rolling thin film oven (RTFO) aged and pressure aging vessel (PAV) aged nanoclay-modified binders were used for the evaluation of these parameters. Unaged nanoclay-modified binders were tested at temperatures from 61 to 82 °C.

An optical Contact Analyzer (OCA) was used to evaluate the moisture susceptibility of the nanoclay-modified binders. The Sessile Drop analysis uses the Surface Free Energy (SFE) theory to estimate CR of the modified binder samples. Also, the AFM technology was used for evaluating moisture susceptibility. The PFQNM mode of a Bruker AFM was to estimate molecular level morphological and nanomechanical properties of the nanoclay-modified asphalt binders.

In the naming convention, S1 and S2 indicate the sources of the base binder; PG 64-22 is the PG grade of the base binder, whereas Cloisite 10A, Cloisite 11B, and Cloisite 15A are indicated as 10A, 11B, and 15A, respectively.

4 Results and Discussions

4.1 Rotational Viscosity

The viscosity values were observed to increase after modification (Figs. 1 and 2). For binders with 1% Cloisite 10A, the viscosity values at 135 °C increased by 187%,

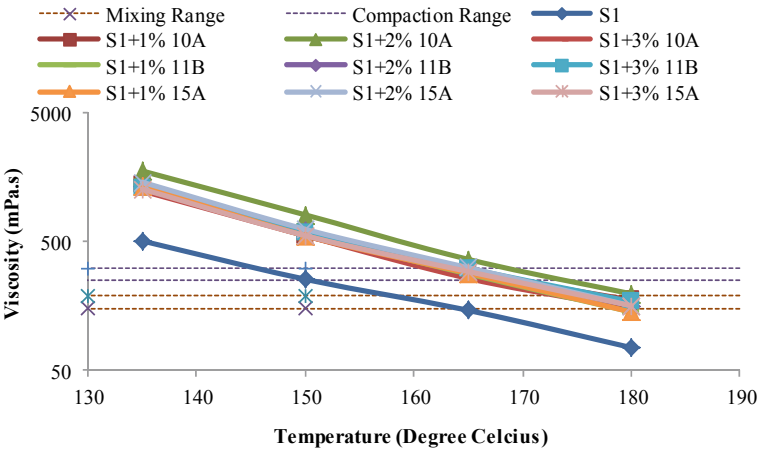

Fig. 1 Viscosity (mPa s) versus temperature (°C) curve for source 1 (S1) modified binder

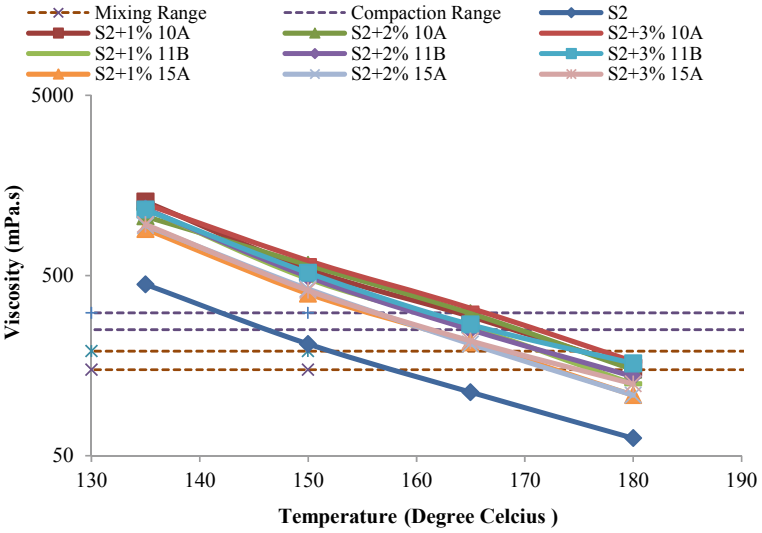

Fig. 2 Viscosity (mPa s) versus temperature (°C) curve for source 2 (S2) modified binder

which is higher than any other nanoclay modified Source 2 binders considered during this study. For 1%, 2%, and 3% Cloisite 10A blended with asphalt binders, the viscosity values at 135 °C increased by 187%, 140%, and 178%, respectively. At the same temperature, there were 162%, 162%, and 159% increase in viscosity when 1%, 2% and 3% Cloisite 11B was mixed with the Source 1 neat binder, respectively. For 1%, 2%, and 3% Cloisite 15A modified binders, viscosity values were increased by 102%, 111% and 114%, respectively at 135 °C.

4.2 Dynamic Shear Rheometer (DSR)

From the DSR results (Figs. 3 and 4), it is observed that the black curves for modified asphalt binders have shifted from the position of the neat binder to left. The G* values for nanoclay-modified asphalt binders increased and δ values decreased with respect to those of the neat asphalt binder. At 64 °C, the maximum G* and the minimum δ are found when the asphalt binder was blended with the 1% Cloisite 11B. Rutting factor (G*/sinδ) was also increased for modified binders and maximum rutting resistance was observed for binder modified with the 1% Cloisite 11B. For Source 2 binder modified with nanoclays, the G* values for nanoclay-modified asphalt binders increased, and δ values decreased with respect to those of the neat asphalt binder. Maximum G* values were found when nanoclay 1% Cloisite 10A mixed with a neat binder.

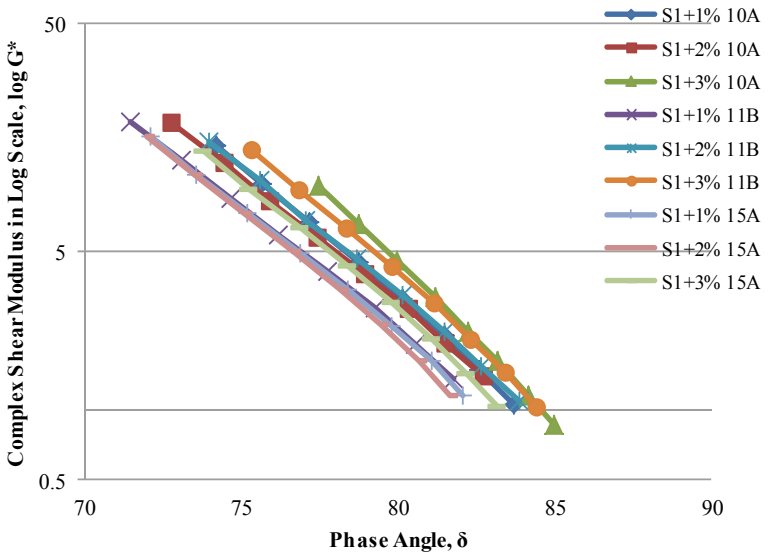

Fig. 3 Complex shear modulus (G*) versus phase angle (δ) curve for Source 1 modified binder

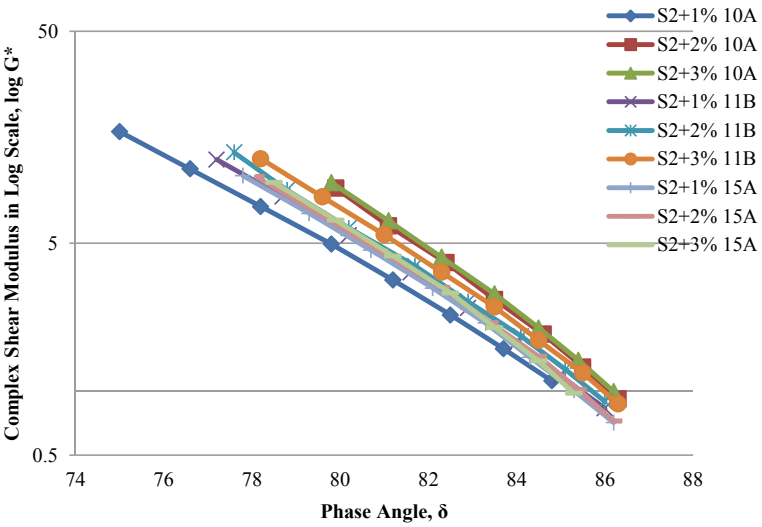

Fig. 4 Complex shear modulus (G*) versus phase angle (δ) curve for source 2 modified binder

4.3 Optical Contact Analyzer (OCA)

The contact angle also increased when the percentages of nanoclays increased. When the contact angle is greater than 900, it is called "poor wetting." The wetting ability is also increased when the contact angle decreased. The SFE of any materials can be divided into the following components: acid component, base component, and Lifshitz-van der Waals component. The maximum SFE was found when a 3% Cloisite 10A was mixed with a base binder, as shown in Fig. 5. The work of cohesion was also found to be the maximum for this composition, and it was greater than that of

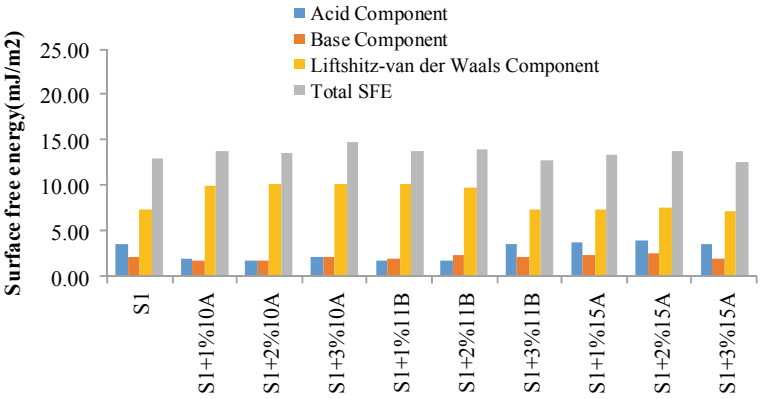

Fig. 5 Surface free energy components for source 1 modified binders

Table 1 Value of the morphological and nanomechanical properties

Sample ID	Average height sensor (nm)	Average DMT modulus (MPa)	Average adhesion (nN)	Average deformation (nm)
S1 (Neat Binder)	7.79	3221	362	5.41
S1 + 1% 10A	7.32	755	73.7	1.94
S1 + 2% 10A	13.5	1768	222	2.8
S1 + 3% 10A	6.52	2937	305	5.37
S1 + 1% 11B	13.7	625	136	4.2
S1 + 2% 11B	8.36	682	102	3.19
S1 + 3% 11B	9.32	2081	196	4.41
S1 + 1% 15A	6.5	694	176	4.21
S1 + 2% 15A	9.46	1522	163	4.05
S1 + 3% 15A	15.8	1234	261	3.55

the neat binder. Higher work of cohesion values indicated better moisture resistance. However, the improved cohesion values were not found when a higher percentage (3%) of Cloisite 11B or 15A was blended with the neat binders.

4.4 Atomic Force Microscope (AFM)

Morphological and nanomechanical properties of nanoclay modified asphalt binders as shown in Table 1. The maximum value of the height sensor was found for the asphalt binder modified by 3% Cloisite 15A and the minimum for asphalt binder modified by 1% Cloisite 15A. The DMT modulus, adhesion and deformation decreased for nanoclay-modified asphalt binders. Asphalt binders from Source 1 with 1% Cloisite 10A showed the minimum adhesion and deformation values.

5 Conclusions

In this study, different amounts of nanoclay-modified asphalt binders were tested in the laboratory. The rheological and mechanical properties of the asphalt binders were found to improve. However, the mixing and compaction temperatures were expected to increase for nanoclay-modified binders. To mitigate it, a rejuvenator can be used to reduce the mixing and compaction temperatures while preserving the beneficial effects of nanoclays. With the addition of nanoclays, the complex shear modulus increased, and the phase angle decreased significantly. Based on the findings of this limited study, rutting resistance was expected to increase significantly due to the addition of nanoclay, but fatigue resistance did not improve. From the

OCA test results, it was found that the nanoclay modified asphalt binders provided a better moisture resistance than the neat binders. Morphological and nanomechanical obtained through an atomic force microscope (AFM) revealed that the surface roughness did not vary significantly, but the adhesion and deformation values were found to decrease. Further laboratory and field performance data are required to establish the uses of nanoclay as an asphalt modifier.

References

1. Ghile DB (2006) Effects of nanoclay modification on rheology of bitumen and on performance of asphalt mixtures. MSc thesis, Department of Civil Engineering, Delft University of Technology
2. Yu J, Zeng X, Wu S, Wang L, Liu G (2007) Preparation and properties of montmorillonite modified asphalts. Mater Sci Eng A 447:233–238
3. Polacco G, Filippi S, Stastna J, Biondi D, Zanzotto L (2008) Rheological properties of asphalt/SBS/clay blends. Eur Polym J 44:3512–3521
4. Jahromi SG, Khodaii A (2009) Effects of nanoclay on rheological properties of bitumen binder. Constr Build Mater 23:2894–2904
5. You Z, Mills-Beale J, Foley JM, Roy S, Odegard GM, Dai Q, Goh SW (2011) Nanoclay-modified asphalt materials: preparation and characterization. Constr Build Mater 25:1072–1078
6. Hossain Z, Zaman M, Saha MC, Hawa T (2014) Evaluation of viscosity and rutting properties of nanoclay-modified asphalt binders. In: Geo-congress 2014 technical papers: geo-characterization and modeling for sustainability, pp 3695–3702
7. Zapién-Castillo S, Rivera-Armenta JL, Chávez-Cinco MY, Salazar-Cruz BA, Mendoza-Martínez AM (2016) Physical and rheological properties of asphalt modified with SEBS/montmorillonite nanocomposite. Constr Build Mater 106:349–356
8. Cheng DX, Little DN, Lytton RL, Holste JC (2002) Surface free energy measurement of asphalt and its application to predicting fatigue and healing in asphalt mixtures. Transp Res Rec, Transp Res Board (Washington, DC) 1810:44–53
9. Bhasin A, Button JW, Chowdhury A (2005) Evaluation of selected laboratory procedures and development of databases for HMA. Rep. No. Federal Highway Administration (FHWA)/Texas (TX)-05/0-4203-3, Texas Transportation Institute, Texas A&M Univ., College Station, TX
10. Hossain Z, Zaman M, Hawa T, Saha MC (2015) Evaluation of moisture susceptibility of nanoclay-modified asphalt binders through the surface science approach. J Mater Civ Eng ASCE 27(10):04014261
11. Hossain Z, Bairagi B, Zaman M, Bulut R (2015) Prediction of the stripping resistance of nanoclay-modified asphalts using their surface chemistries. In: Conference paper, geo-chicago 2016, Chicago, Illinois

A Drainage System for Road Construction on Flat Terrain in New Owerri Nigeria

Ozioma C. Owuama and Kennedy C. Owuama

Abstract Conventional road drainage system commonly adopted in the city of New Owerri Nigeria is grossly ineffective and unsustainable, and this gives rise to prolonged pools of water after cessation of rainfall. The water pools often cause road pavement failure, disruption of free flow of traffic, submergence of residential apartments, disruption of commercial activities and exponential rise in mosquito population due to the occurrence of fertile breeding grounds. Research has shown that the use of a trenchless drainage system in road construction, whereby an engineered open trench is backfilled with relatively permeable material, can be a suitable alternative on the flat terrain. It was observed that a 50 cm depth of water completely drains off in such a system within 30 min of cessation of rainfall, instead of the usual two to three weeks duration. Five conditions were examined in the course of the research. The rate of drawdown recorded for the various conditions are 3.7 cm/min for open trench i.e. without a backfill; 3.3 cm/min for trench backfilled with gravelly sand; 2.8 cm/min with fine sand; 2.0 cm/min with mixed sand and 3.5×10^{-4} cm/min for the open concrete drain. It was observed that materials with higher values of both the diameter at 30% passing and coefficient of uniformity are more effective in the drain ability. The unit construction cost of standard concrete drain was found to be about two (2) to three (3) times higher than that of an equivalent sized trenchless drain filled with gravel.

Keywords Drainage · Road · Flat terrain

O. C. Owuama (✉)
Federal University of Technology Owerri, Owerri, Nigeria
e-mail: chukwunonye.owuama@futo.edu.ng

K. C. Owuama
Odumegwu Oiukwu University of Science and Technology Uli, Uli, Nigeria

K. R. Reddy et al. (eds.), *Sustainable Environment and Infrastructure*, Lecture Notes in Civil Engineering 90, https://doi.org/10.1007/978-3-030-51354-2_27

1 Introduction

Owerri, the capital city of Imo State, is a rapidly growing metropolis in the South Eastern part of Nigeria and is located within latitude 5.433°N and longitude 7.035°E. It links the Oil City of Port Harcourt by the Southern, Commercial City of Aba in the Eastern, Coal City of Enugu in the Northern and Industrial Cities of Onitsha and Lagos in the Western axes. The southward extension of the city is the New Owerri which seats on an apparently flat terrain that covers over 1000 hectares of land. The major natural drainage system in the area is River Otamiri which flows in the South easterly direction, and forms the outer perimeter of the New Owerri along the eastern axis. Owerri is endowed with rain forest climatic system. The average annual rainfall is 2,500 mm with an intensity of 70 mm/h over three to five hours duration in the months of June to September. The geology of the area is typical of Coastal Plain Sand deposited in the Quaternary. However, the sub-areal deposit is lateritic, a sandy clay with permeability coefficients in the order of 0.0001–0.01 cm/s. The static groundwater table occurs at a depth of about 25 m. The topography of the area is generally low with slopes in the range of 0–1.5%, which rapidly changes to 15% by the river banks.

Collector and stormwater drains constructed in the area are mainly the open concrete drainage system and a few underground channels that discharge into River Otamiri through a distance of over 3 km in the extreme. Apparently, the conveyance systems are ineffective and this results in persistent flooding in the area that lingers until the cessation of rainfall by the month of November. The main causes of the flooding scenario have been identified to include the relatively flat nature of the terrain that limits sufficient hydraulic head, siltation of the drain which promotes vegetal growth within it and indiscriminate dumping of solid waste in the drains [1]. As a result of the persistent flooding arising from these factors, engineered and earth road pavements often fail, smooth flow of human and vehicular traffic is disrupted, residential and commercial premises are submerged in most times of the year, and exponential rise in mosquito breeding with its attendant health problems persists. The need therefore arises to evolve a drainage system that can reduce these hazards, hence the trenchless drainage system.

2 Concept of Trenchless Drain

The concept of a trenchless drainage system for road construction is drawn from the classical theory of ‘French drain’ wherein an excavation is backfilled with coarse sand or gravel to serve as a water infiltration system into the subterranean environment. The concept can be adapted to design a system for the control of discharge in a number of different ways and situations. However, a typical infiltration trench design [2] is such that, the design infiltration rate would be at least a half of the in situ soil infiltration rate and a minimum value of 13 mm/h, a backfill material size of 30 mm to 70 mm

clean sand or gravel and a void space of 30–40%. On this note, the trench surface area (A) in m^2, can be determined from,

$$A = V_w/(\mu d_t + f_d T) \tag{1}$$

where V_w = design volume of water entering into the trench, μ = porosity of the backfill, d_t = design depth of trench, f_d = design infiltration rate and T = effective filling time of trench. Further research [3] shows that, for a square drain of unit length wherein the width equals the depth, d_t can be calculated from the expression,

$$d_t = I w_r/\mu(3k - I) \tag{2}$$

where I = rainfall intensity in cm/s, w_r = width of the catchment or road surface, μ = porosity of backfill and k = in situ soil permeability. Equation (2) is simpler to evaluate since the variables are easily determined by common measurement and analysis. The principle is adopted in this study, and particularly to establish the type of materials that could form the backfill which may constitute a most efficient flow disposal system in the reference environment, following the concept of trenchless drainage system.

3 Experimental Study

In order to examine the efficacy of the proposed method, prototype constructions in the form of experimental basins were prepared and various types of backfill were investigated at each setup [4].

3.1 Experimental Basins

Four units of the infiltration basin and one unit of evaporation basin were installed. An infiltration basin comprises the upper and lower units, Fig. 1. The upper basin is a coated steel tank with its top and bottom open. The lower basin is a trench stabilized with watertight concrete tiles on the vertical sides while its base is bare, serving as the infiltration zone. The upper basin was fixed onto the lower unit to form an integral watertight system that receives water from the top and discharges it from the bottom.

Fig. 1 A composite experimental basin

3.2 Experimental Soils

The backfill material used in the investigation was sourced from the alluvial deposit of Otamiri River and then processed into three distinct compositions. The first composition was the unprocessed alluvium referred to as **mixed sand**. A sample of mixed sand was sieved through sieve No 4 and materials retained were referred to as **gravelly sand** while those passing through the sieve size were the **fine sand aggregates**. The properties of these soils were determined and the results are summarized in Table 1. Similarly, the in situ soils at various locations of the infiltration basins were investigated and the average laboratory results are also presented in Table 1 (column 5). The in situ soil is a reddish brown sandy clay often referred to as laterite.

3.3 Drawdown Measurement

The infiltration basins were constructed watertight such that water losses were only through the bottom of the basin. The empty basins were then filled with portable water to mark 'O' and the drawdown was measured as a function of time, in minutes, by means of an electric water level indicator and electronic time watch. Thereafter the lower basins were backfilled with mixed sand, gravelly sand and fine sand in that order. The water level reading was based on the cross-sectional area of the upper basin. The reading was however adjusted to reflect the cross-sectional area of the lower basin through which the water infiltrates into the ground. The drawdown for

Table 1 Properties of experimental soils

Soil	Soil category			
Parameters	Mixed sand	Fine sand	Gravelly sand	In situ soil
Water content, %	13.7	18.2	9.3	32
Void ratio	0.13	0.08	0.23	0.37
Porosity	0.12	0.07	0.19	0.27
Bulk wt, kN/m^3	19.2	18.7	17.9	19.8
Dry unit wt, kN/m^3	16.9	15.8	16.4	15.0
Sat unit wt, kN/m^3	20.4	19.5	19.9	20.7
D_{10}, mm	0.3	0.3	0.6	0.26
D_{30}, mm	0.45	0.52	1.2	0.4
D_{50}, mm	0.75	0.72	2.1	0.57
D_{60}, mm	0.82	0.8	2.6	0.73
Cu	2.43	2.67	4.3	2.81
Cc	0.82	1.13	0.9	0.84
USC Class	SP (cmg)	SP (cmf)	GP (gcm)	Clayey sand

varying soil composition was plotted against time, and typical profiles are shown in Fig. 2, drawdown curve and Fig. 3, the regression line of the drawdown.

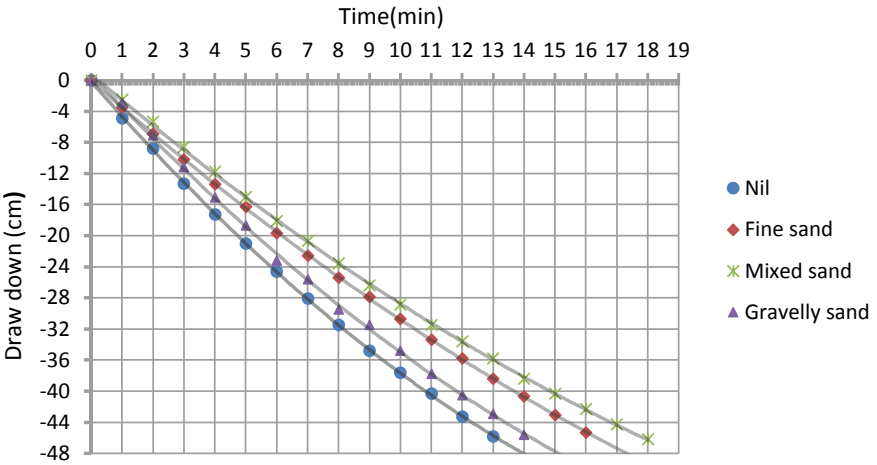

Fig. 2 Drawdown versus time curve with varying backfill

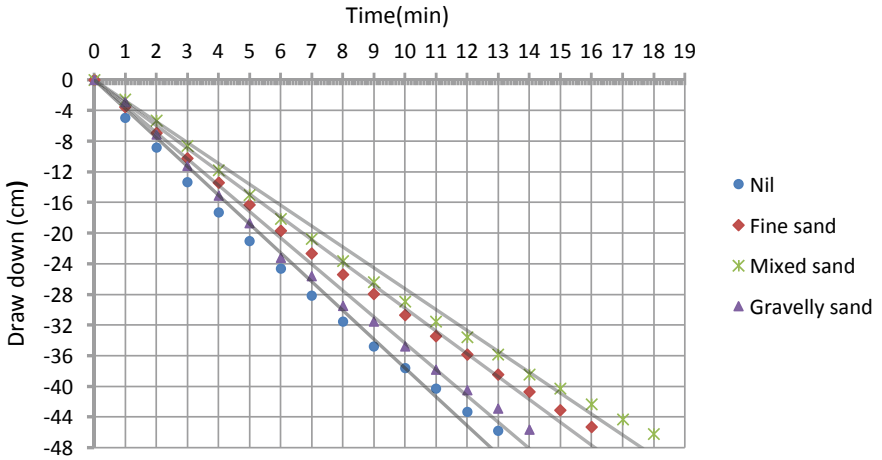

Fig. 3 The regression graph for varying backfill

4 Discussion

The drawdown rate obtained without a backfill best describes the permeability of the in situ soil. It shows a curvilinear graph. By introducing various soil compositions as backfill and measuring the drawdown at each stage, it was observed that the drawdown rate is a function of the type of material introduced. In addition, the rate decreases with decreasing hydraulic head, Fig. 2. This rate of drawdown is higher in gravelly sand compared to fine sand, and lastly mixed sand. The curve can best be described by the equation,

$$h = \mathrm{at}^n \tag{3a}$$

or

$$\log h = \log a + n \log t \tag{3b}$$

where 'log h' is the logarithm of the cumulative infiltration, 'log a' the basic infiltration, 'n' the gradient of the curve and 'log t', the period of the infiltration. However, a regression line provides a simple approximation of the flow rate, Fig. 3. The resulting equation is such that

$$h = \mathrm{at} \tag{4a}$$

or

$$a = h/t \tag{4b}$$

where 'h' is the drawdown, 'a' the drawdown rate and 't' the time, in minutes, taken to achieve 'h'. Introducing a geometric factor, 'c' [5], the equation can be rewritten such that,

$$a = ch/t \tag{5}$$

However results of evaluations of Fig. 3 are such that, for i**n situ soil**: $\Delta h/\Delta t =$ 3.7 cm/min; **gravelly sand**: $\Delta h/\Delta t = 3.3$ cm/min; **fine sand**: $\Delta h/\Delta t = 2.8$ cm/min; and **mixed sand**: $\Delta h/\Delta t = 2.0$ cm/min, while the geometric factor, c, is assumed unity. From these results, it is apparent that the efficiency of a trenchless drain in disposing of impounded water is dependent upon the type of backfill material introduced. Some characteristics of the materials were observed to have a direct relationship with the drawdown rate. For example, from Table 1, it is observed that the higher the values of d_{30} (diameter at 30% passing) and Cu (Coefficient of Uniformity) of the backfill material the higher its infiltration capacity. In the case of the evaporation tank, there was no significant loss of water after a long period of exposure to air temperature. The rate was estimated at 0.00035 cm/min. This typically represents the scenario that occurs in an open concrete drain on flat terrain.

It was estimated that the unit cost of a standard open concrete drain at the time of this research was N7,500.00 (Seven thousand five hundred Naira) compared to N3,000.00 (Three thousand Naira) for gravel- filled trenchless drain of the same geometry.

In general, therefore, the trenchless drainage system, when compared with concrete drain is more economical to construct, more sustainable in practice and more efficient in disposing surface runoff in the New Owerri district of Imo State Nigeria which seats on flat terrain.

However, the philosophy would work best if the runoff to be discharged by the system is sourced from the immediate environment of the construction. To accommodate storm flow or surface runoff from other nearby areas the proposed drainage system would require special design considerations.

5 Conclusion

From the results of the experiment, it is apparent that (i) a trench backfilled with gravelly sand is 1.2 times more effective than fine sand, 1.7 times more effective than mixed sand and 9429 times more effective than an open concrete drain in disposing water from a flooded area; (ii) poor graded backfill with higher values of diameter at 30% passing (d_{30}) and Uniformity coefficient(U) is more efficient as a component in the drainage system; (iii) the concept can be used in conjunction with the design principles developed in [1, 3] on flat terrains. Consequently,

$$d_t = IW_r/\boldsymbol{\mu}(3k - I) \tag{6}$$

where d_t = depth = width of a square drain, I = rainfall intensity in the area, W_r = width of road pavement, μ = Porosity of the backfill and k = in situ drawn down rate/soil permeability.

The method is very effective if the surface runoff to be discharged is mainly sourced from the immediate environment. To ensure that nearby developments do not empty runoff into the system and overwhelm its capacity, an engineered road could be such that the elevations of its pavement and the upper width of the trenchless drain are above the adjoining areas. This may compel every land developer to manage her own consequential runoff and reduce the risk of flooding in the area in focus.

Acknowledgments The authors wish to acknowledge the assistance of TETFUND, a Federal Government of Nigeria sponsored funding agency, for providing the grant that enabled this research. The support received from the academic and non- academic staff of the Institute of Erosion studies in the Federal University of Technology Owerri Nigeria, where this research was carried out, is highly appreciated.

References

1. Owuama CO (2012) Conceptual design of a trenchless drain in a flat terrain. J Environ Sci Eng A (David publishing, USA) 1(12):1301–1307
2. MSMA (2015) Urban storm water Management. Department of Irrigation and Drainage, Malaysia (reproduced by IES), vol l, ll, Kuala Lumper
3. Owuama CO, Uja U Kingsley CO (2014) Sustainable drainage system for road networking. Int J Innov Manag Technol 5(2):83–87 (Singapore)
4. IES (2016) Evaluation of trenchless drainage system for road construction on flat terrain. A research report prepared by Prof Owuama, C.O and presented to TETFUND/FUTO Owerri, 48 p
5. IILRI (1979) Drainage principles and application. Int Inst Land Reclama Improv 16(I–IV) (Wageningen)

The Effect of Tincal Additive on the Consolidation and Shear Strength Behavior of Sand-Bentonite Mixtures Under High Temperature

Sukran Gizem Alpaydin and Yeliz Yukselen-Aksoy

Abstract The importance of thermal behavior of soils has increased considerably in the last decades. The reason for this, soil properties are temperature-dependent and they are significantly affected by high temperatures and thermal cycles. Previous studies indicate that properties of soils such as shear strength, compressibility, and permeability change at high temperatures. High thermal resistance and durable soils are needed for structures where the soil is exposed to heat such as nuclear waste disposal facilities, buried high voltage cables, energy piles, etc. Boron reduces heat expansion of the glasses, protects the glass against acid and scratches, and also is known with its resistance to high temperature. In this study, the settlement and shear strength properties of sand-bentonite mixtures were determined in the presence of boron mineral; namely tincal under high temperature. The sand-bentonite mixtures were prepared with 10 and 20% bentonite and then 10, 20% tincal were added to these mixtures. The direct shear tests were conducted on all mixtures under 80 °C and room temperature. According to the test results, cohesion value increased in the presence of tincal at room temperature. Furthermore, the internal friction angle values at 80 °C are higher than at room temperature in the presence of tincal. The results have shown that the shear strength of sand-bentonite mixtures increased with tincal additive under high temperature.

Keywords High temperature · Tincal · Soil behavior

1 Introduction

Many engineering projects have been related to heat increase in the soil in the last decades. The structures under the soil are directly affected by temperature rise in soil. Energy structures and nuclear waste landfills are examples of this kind of structure. It is necessary to understand the behavior of soil at temperatures up to 100 °C due to the necessity of radioactive disposal [1]. Thus, there is a need for thermally resistive

S. Gizem Alpaydin (✉) · Y. Yukselen-Aksoy
Dokuz Eylül University, Buca İzmir, Turkey
e-mail: gizem.alpaydin@gmail.com

K. R. Reddy et al. (eds.), *Sustainable Environment and Infrastructure*, Lecture Notes in Civil Engineering 90, https://doi.org/10.1007/978-3-030-51354-2_28

and durable soil layers at temperatures up to 100 °C. Heat occurs as a result of the decomposition of organic compounds and biochemical processes of wastes in landfills. Such heat may adversely affect the soil in a hydraulic and mechanical way in terms of long-term behavior in landfills.

Sand-bentonite mixtures are commonly used in landfill liners. Because bentonite is a material with low permeability and high water retention capacity. Bentonite is a highly swelling clay and shrinks when it becomes dry. Therefore, it is used by mixing with sand in landfills.

Many properties of soils are temperature-dependent and change with temperature. Heating soils to higher temperatures can lead to a significant effect on some engineering properties. Previous studies have shown that thermal cycles and high temperatures affect the hydraulic conductivity, volume change (compressibility-swelling), and shear strength parameters of soils [1, 2]. For instance, when bentonite was heated to 100 °C, a decrease in cohesion and an increase in the internal friction angle were observed [3]. The shear strength of the normally consolidated clay increases when the soil temperature increases or subjecting to a temperature history [1]. The resistance of fabric changes against temperature is explained with clay interparticle forces and viscous shear resistance of adsorbed water [4].

Boron is one of the elements commonly found in the earth's crust. Tincal is a boron mineral which is quite rich in terms of sodium minerals ($Na_2B_4O_7.10H_2O$) [5]. Boron is never found free in nature, it occurs as a mineral. It is known that there are hundreds of kinds of boron minerals in nature. Natural borates are used to define concentrated boron ores such as; tincal, colemanite, and ulexite. Boron is used in many application areas like energy, metallurgy, cement, glass, and ceramic. For example, in the production of heat-resistant glassware and high-quality glass for use in electronics and space research. It significantly reduces heat expansion of the glasses, protects the glass against acid and scratches. Moreover, Turkey has the largest reserves in the world. Boron is known for its resistance against high temperatures. For that reason, the tincal added sand-bentonite mixtures may show high resistance against high temperatures and thermal cycles.

The objective of this study is to investigate the shear strength behavior of sand-bentonite mixtures with boron mineral namely; tincal at high temperature. The effect of tincal on the consolidation (at room temperature) and shear strength behavior (at room temperature and 80 °C) were investigated.

2 Material Characterization and Methods

In this study, Na-bentonite, sand, and a boron mineral—tincal were used. The Na-bentonite was supplied from Eczacıbaşı Esan Mining Company. The sand has 20.7% fine content. **The sand sample was sieved through No. 6**. Tincal was gathered from Eti Mining Operations General Directorate of Turkey. The tincal was crushed with jaw crusher and sieved through No.40 for the experiments. The physico-chemical properties of these materials are given in Table 1.

Table 1 The physico-chemical properties of bentonite, sand and tincal samples

	Bentonite	Sand	Tincal
Specific gravity	2.70	2.63	1.67
Liquid limit (%)	476.0	–	60.50
Plastic limit (%)	70.10	–	42.90
pH	9.50	–	9.12

For all experiments, bentonite and sand were used after drying for 24 h in the oven (105 °C). Tincal was used in its natural water content as its structure changes with heat. The water content value of tincal was determined for each test and its initial water content considered at the sample preparation. The test mixtures were prepared in the following order: Firstly 10 or 20% of the total dry weight was weighed as tincal. Then the bentonite was added with 10 or 20% of remaining dry weight and the rest of the mixture was sand. The percentages of the bentonite, sand, tincal in the mixtures, and the test set-up are shown in Table 2. The samples were named as abbreviations of bentonite as "B", sand as "S" and Tincal as "T". For example, 9B-81S-10T sample contains 9% bentonite, 81% sand, and 10% tincal. All tests were carried out with the $w_{opt} + 2\%$ water content value and the dry unit weight value (γ_d) corresponding to the obtained with the Standard Proctor test [6].

The consolidation tests were performed based on the ASTM D-2435 [7]. In the consolidation tests, the materials were mixed in a tray for homogeneity. Then water was added to the mixture (2% wet side of their optimum water content) and mixed with a spatula homogeneously. It was placed into the ring by compaction in 3 layers corresponding to the determined γ_d value. The ring was placed to the cell which was filled with water then 6.9 kPa seating pressure was applied for 24 h. After that, the loading was initiated. When the deformation amounts were negligible, other loading level was started Generally, the loading was completed in approximately 72–96 h. In the consolidation tests the load increment ratio (LIR) was 1.0. When the consolidation completed the sample was unloaded to 196 kPa then to 49 kPa. It was waited until swelling completion at each unloading. At the end of the tests, the samples were dried in the oven (105 °C) to determine the water content.

Table 2 Test set-up

	Test sample	Room temperature		80 °C temperature	
		10% tincal	20% tincal	10% tincal	20% tincal
10% bentonite	10B-90S	–	–	–	–
	9B-81S-10T	✔	–	✔	–
	8B-72S-20T	–	✔	–	✔
20% bentonite	20B-80S	–	–	–	–
	18B-72S-10T	✔	–	✔	–
	16B-64S-20T	–	✔	–	✔

The direct tests were performed in accordance with ASTM D-3080 [8]. In the direct shear tests, the mixtures were prepared in a similar way as in the consolidation tests at the w_{opt} + 2% water content. The soil sample was placed into the square mold (6 cm) in 3 layers by compacting each layer at the dry unit weight value which is obtained from the Standard Proctor test. The mold was waited for 24 h in the submerged condition to get full saturation. During the saturation stage, the required weight was placed on the mold to prevent swelling. Three different normal stresses (49, 98, 196 kPa) were applied in the direct shear tests, the samples were consolidated under these stress levels. Then the samples were sheared with shear rate of 0.5 mm/min [8]. The direct shear tests were performed at room temperature and 80 °C. In the tests, heating was provided by heat rod which was specially produced according to the direct shear test box and the temperature was kept constant by the thermostat through the tests. Heat in the soil samples and the water was controlled and recorded with K-type thermocouples and digital thermometer (UNI-T UT325). At the end of the tests, the soil samples were dried in the oven (105 °C) to determine the final water content.

3 Results and Discussions

In this study, the direct shear and consolidation tests were performed on the 10% sand-bentonite and 20% sand-bentonite mixtures in the presence of tincal. The consolidation tests were performed at only room temperature. Figure 1 shows the relationship between vertical strain and effective stress in the presence of tincal for sand-bentonite mixtures. The total vertical strain values at the compressibility and swelling tests are given in Table 3.

The compressibility test results have shown that the tincal addition to the 10% sand-bentonite mixture increased the vertical strain of the mixture. The vertical strain of 10% sand-bentonite increased from 6.7 to 11.7% by the addition of 10% tincal. The tincal addition increased the total vertical strain values of 20% sand-bentonite mixtures as well. In the presence of 10% tincal the vertical strain value of the 20% sand-bentonite mixture was almost doubled. It should be noted that increment of tincal content from 10 to 20% had no significant effect on the vertical strain especially for 20% bentonite mixture.

The amount of swelling for the 10% sand-bentonite mixture without tincal addition was almost negligible. However, the amount of swelling increased when tincal was added. The amount of swelling increased to 0.87% in the presence of 10% tincal and increased to 1.54% in the presence of 20% tincal. The amount of swelling increased from 1.36 to 3.75% by adding tincal for 20% sand-bentonite mixtures. However, increasing the amount of tincal from 10 to 20% almost had no influence on the amount of swelling. Tincal has sodium (Na^+) molecules in its atomic structure. The Na^+ cations increase the thickness of the diffuse double layer of bentonite. Therefore, the vertical strain increased in the presence of tincal.

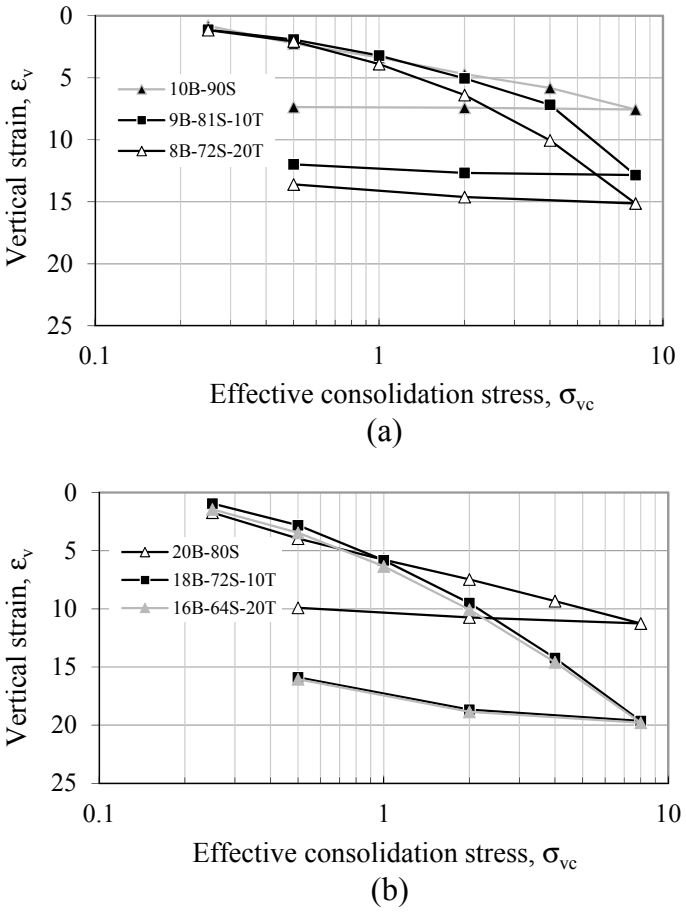

Fig. 1 Vertical strain-effective stress relationships in the presence of tincal **a** 10% sand-bentonite mixtures, **b** 20% sand-bentonite mixtures

Table 3 Total vertical strain of test specimens

Sample	Total vertical strain (%) (compressibility)	Total vertical strain (%) (swelling)
10B-90S	6.74	0.19
9B-81S-10T	11.72	0.87
8B-72S-20T	13.98	1.54
20B-80S	9.53	1.36
18B-72S-10T	18.70	3.75
16B-64S-20T	18.34	3.74

The direct shear tests were performed under room temperature (22 ± 2 °C) and 80 °C and the results were compared. In the presence of tincal, the shear failure envelopes of the 10 and 20% sand-bentonite mixtures are given in Fig. 2. The obtained internal friction angle values and cohesion values are presented in Table 4. The direct shear test of tincal sample at 80 °C could not be performed due to the collapse of tincal during the test. According to the test results for 10% sand-bentonite mixtures, the

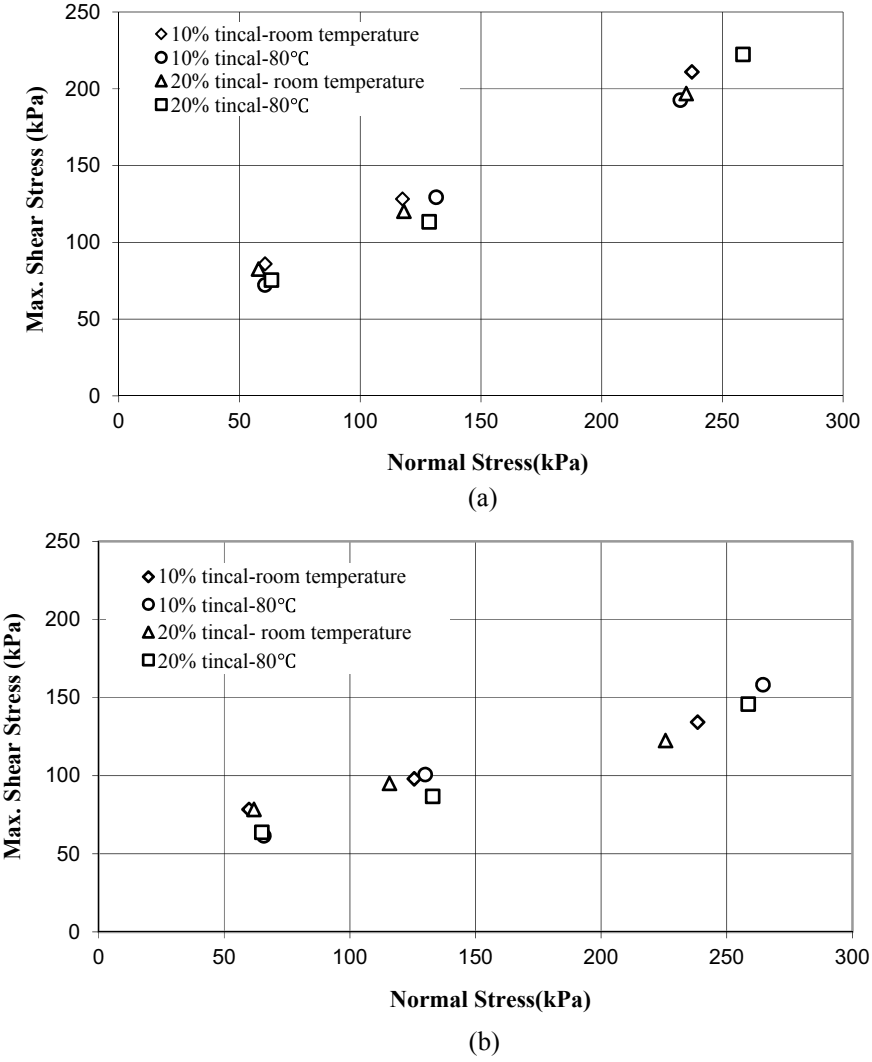

Fig. 2 The shear failure envelopes in the presence of tincal **a** 10% sand-bentonite mixtures, **b** 20% sand-bentonite mixtures

Table 4 The shear strength parameters of the sand-bentonite mixtures in the presence of tincal at room temperature and 80 °C

		Room temperature		80 °C	
		Ø (°)	c (kPa)	Ø (°)	c (kPa)
10% bentonite	0%	33.6	51.7	32	47.3
	10% tincal	35.2	44.2	34.8	33.1
	20% tincal	32.9	44.7	37.4	22.3
20% bentonite	0%	13.6	64.3	6	92.1
	10% tincal	17.2	59.9	25.5	33.5
	20% tincal	14.8	63	23.3	33.3
	100% tincal	15.1	58.7	–	–

maximum shear stress decreased with an increase in tincal content at room temperature. However, at 80 °C temperature, as tincal content increases, generally caused to increase in the maximum shear stress. At room temperature, as tincal content increased, the maximum shear stress decreased by 20% sand-bentonite mixtures as well.

For 10% bentonite samples, at room temperature, as boron (tincal) content increases there were no significant changes in the internal friction angle values. However, the cohesion values decreased as tincal content increased. Similar to 10% bentonite samples, the internal friction angle values did not change while the cohesion values decreased by 20% bentonite mixtures. However, the decrease in cohesion values was lower than 10% bentonite samples. The general test results under high temperature (80 °C) have shown that the angle of internal friction values increased, however; cohesion values decreased as tincal content was increased in the sand-bentonite mixtures.

While the internal friction angle value at 80 °C without tincal additive was 32°, it increased to 37.4° in the presence of 20% tincal and the cohesion value decreased to 22.3 kPa while it was 47.3 kPa. The tincal addition increased the angle of internal friction values of both mixtures at high temperature when compared to the results at room temperature. However, at the same time as tincal content increased the cohesion values decreased under high temperature.

4 Conclusions

Thermally resistant soils are needed around the energy structures. In order to increase thermal resistivity of soils boron minerals may be used because of their wide usage in heat resistant materials production. In this study, the consolidation and shear strength behavior of 10% sand-bentonite and 20% sand-bentonite mixtures were investigated in the presence of 10 and 20% tincal at room temperature and high temperature (80 °C). The consolidation test results showed that the tincal addition

increased the total vertical strain amount of the both mixtures. According to the direct shear tests, the maximum shear stress values decreased at room temperature, however, it increased at 80 °C for both 10 and 20% sand-bentonite mixtures in the presence of tincal. For 10% sand-bentonite samples, at room temperature, as tincal content increases there was no significant changes in the internal friction angle values. However, the cohesion values decreased as tincal content increased. The general test results under high temperature (80 °C) have shown that the angle of internal friction values increased, however; cohesion values decreased as tincal content was increased in the sand-bentonite mixtures. The general results of this study were shown that in the presence of tincal, the shear strength of the sand-bentonite mixtures increases with rising temperature. It can be concluded that the addition of tincal increases the thermal resistance of sand-bentonite mixtures.

Acknowledgments This study is supported by The Scientific and Technological Research Council of Turkey (TÜBİTAK) (Grant no. 217M553). The authors are grateful for this support.

References

1. Abuel-Naga HM (2006) Experimental evaluation of engineering behavior of soft Bangkok clay under elevated temperature. J Geotech Geoenviron Eng 132(7):902–910
2. Pusch R (1990) General microstructural model for qualitative and quantitative studies of smectite clays. SKB Technical Report 90–43, Stockholm, Sweden
3. Wang MC (1990) The effect of heating on engineering properties of clays. In: Physico-chemical aspects of soil and related materials. ASTM STP 1095, Philadelphia, pp 139–158
4. Abuel-Naga HM (2007) Effect of temperature on shear strength and yielding behavior of soft Bangkok clay. Soils Found 47(3):423–436
5. https://www.boren.gov.tr/pages/boron-minerals/102
6. ASTM D4318-98 (1999) Standard test methods for laboratory compaction characteristics of soil using standard effort. ASTM International, West Conshohocken, PA, USA
7. ASTM D2435/D2435M–11 (2011) Standard test methods for one-dimensional consolidation properties of soils using incremental loading. ASTM International, West Conshohocken, PA, USA
8. ASTM D3080/D3080M–11 (2012) Standard test method for direct shear test of soils under consolidated drained conditions. ASTM International, West Conshohocken, PA, USA

Effect of Lime Sludge and Fly Ash on Unconfined Compression and Linear Shrinkage Behavior of Kaolinite Clay

Sandeep G. Burra, Prabir K. Kolay, and Sanjeev Kumar

Abstract The paper investigates the use of lime sludge (LS), fly ash (FA) on unconfined compressive strength, and shrinkage behavior of commercially available kaolinite clay (EPK). The stabilization process was done using lime sludge alone with varying percentages i.e., 2, 4, 6, and 8% by dry weight, as well as a combination with fly ash in varied percentages i.e., 5, 10, 15, and 20% by dry weight. In order to evaluate the strength properties, standard Proctor tests, and unconfined compressive strength (UCS) tests were performed. For estimating the shrinkage, linear shrinkage test was carried out. The UCS samples were prepared based on the optimum moisture content and dry unit weight from standard Proctor tests. The samples were tested after a curing period of 0, 7, and 14 days. In addition, Scanning Electron Microscopy (SEM) tests were performed on UCS samples after shearing. The test results indicated an increase in UCS value with an increase in lime sludge content. Also, the UCS value increased with curing period following a slight decrease. The combination of LS and FA in varied percentages, also had an increase in UCS strength. Also, the UCS value showed an increment in values with the curing period. The reduction in shrinkage behavior of EPK clay was observed with LS and FA. The SEM analysis was conducted to evaluate the reason for strength increase, which was due to the chemical reaction developed between EPK clay, lime sludge, and fly ash.

Keywords Lime sludge · Fly ash · Shrinkage behavior · Compaction · Unconfined compressive strength · SEM

S. G. Burra · P. K. Kolay (✉) · S. Kumar
Department of Civil and Environmental Engineering, Southern Illinois University Carbondale, Carbondale, IL 62901, USA
e-mail: pkolay@siu.edu

S. G. Burra
e-mail: burra@siu.edu

S. Kumar
e-mail: kumars@ce.siu.edu

K. R. Reddy et al. (eds.), *Sustainable Environment and Infrastructure*, Lecture Notes in Civil Engineering 90, https://doi.org/10.1007/978-3-030-51354-2_29

1 Introduction

The process of soil stabilization is common practice to improve soft soil and has been advancing over the years. This process has been challenging with expansive soils, which portray large volume change potential or shrinkage by adsorption or desorption of water and leads to great damage to infrastructures and buildings. The additives commonly used for soil stabilization are commercial products as well as industrial by-products and the latter has been gaining more importance due to various environmental reasons. Yi et al. [1] used ground granulated blast furnace slag (GGBS) and reactive magnesia (MgO) blends for soil stabilization and compared it with GGBS-lime blends and Portland cement (PC). Their results indicated that GGBS-MgO blends were more efficient than GGBS-lime soil stabilization with an optimum range of MgO content varying between 5 and 20%. Also, the unconfined compressive strength (UCS) values for optimum GGBS-MgO mixes were up to 4 times higher when compared to Portland cement mixes. Samaras et al. [2] studied the effect of lime and fly ash addition to stabilize sewage sludge for a period of 35 days. It mainly considered fly ash addition to sewage sludge and compared it with traditional lime treatment. Their method was efficient in combining two solid wastes for soil enhancement. Also, they concluded that low potions of fly ash should be used for stabilizing material in order to have minimal effects with respect to phytotoxic and eco-toxic related properties. Lim et al. [3] studied engineering properties of wastewater treatment sludge altered by hydrated lime, fly ash, and loess. The importance of lime was to sterilize microorganisms in the sludge, the unconfined strength of the altered sludge, fly ash and loess met the requirements for construction materials. Also, extracted hazardous elements from altered sludge were below permissible limits. Chen and Lin [4] investigated the effect of sewage sludge ash and cement for stabilizing soft subgrade soil. Their findings showed that the unconfined compressive strength of the mixes with incinerated sewage sludge ash and cement was 3–7 times more than the untreated sample. A decrease in swell potential from 10 to 60% and enhancement in California Bearing Ratio (CBR) value was 30 times more when compared to the untreated sample. Luo et al. [5] examined the usage of sewage sludge ash/cement and nano aluminum oxide for stabilizing cohesive soil. Proposed mixes replaced 15% of cohesive soil with sewage sludge ash/cement and 1–3% of nano aluminum oxide. CBR and UCS were improved and the optimum value of nano aluminum oxide was reported to be 1%. Smol et al. [6] reviewed the possible usage of sewage sludge ash in the construction industry for creating a circular economy designed by the European system. This system is designed to store, value for the products as long as possible and eliminates waste and to achieve this waste should be converted to a new resource. Sewage sludge has been a very good construction material due to various successful researches on it like producing bricks, raw material for cement production, alternative for sand or cement in stabilized bases, subbases, and embankments in road construction. Seco et al. [7] studied the use of by-products and waste components from industrial processes in stabilizing expansive soils. Their main objective was to reduce swelling capacity and improve mechanical properties. Their findings show a

reduced swelling levels below the Spanish legislation and the compressive strength enhanced between two to four times in lieu with untreated soil. Lime and MgO mix had the highest ability to reduce swelling whereas Lime-Rice Husk Fly-ash (RHFA) and MgO-RHFA mixes yielded effective mechanical properties. Sol-Sanchez et al. [8] studied the stabilization of clayey and marly soils using industrial wastes. The wastes used were dolomitic lime (from residual quarry sludge's), biomass fly ash, steel slag (from electric arc furnace), and conventional lime. The capability of the wastes used was assessed based on the evolution of pH, carbonate content, and particle size at 0, 7, 14, and 28 days. Their findings indicated that the capability of dolomitic lime as a better stabilizer compared to others. Senol [9] investigated the effect of fly ash, multifilament and fibrillated polypropylene fiber on compaction and strength of soft soils. His conclusions revealed the enhancement of strength in fly ash specimens with fiber, and transition of sample behavior from brittle to ductile.

The lime sludge (LS) is obtained as a by-product from water treatment plants, and fly ash (FA) is produced from coal-fired thermal power stations. The continuous production of these wastes, and its disposal to the environment poses a serious concern over the years. Gaining its popularity in construction industry would decrease the risk of disposal and nurture sustainable environment. Hence, the present study uses these two sustainable waste materials for the stabilization of commercially available EPK clay.

2 Materials

2.1 EPK Clay

The EPK clay sample used in the current investigation is a commercially available product provided by Edgar minerals, FL, USA. According to the Unified Soil Classification System (USCS), EPK clay is classified as silt with high plasticity (MH). The specific gravity of the EPK clay was found to be 2.61.

2.2 Lime Sludge

The lime sludge (LS) sample was collected from a water treatment facility in southern Illinois (Saline Valley Conservancy District Water Treatment Plant in Saline County, IL). The Saline Valley Conservancy District Water Treatment Plant treats groundwater and produces softening residue with high concentrations of CaO. Lime sludge sample was dried, crushed, and mixed homogeneously prior to its use in the laboratory. The pH value of lime sludge was 9.10. The percentage of fine sand, silt, and clay size fraction particles present in lime sludge were 12.5, 76.5, and 11%, respectively. The specific gravity of the lime sludge was found to be 2.47.

2.3 Fly Ash

The fly ash (FA) used in the current investigation was collected from Southern Illinois University thermal power plant, Carbondale, IL. The specific gravity (G_s) using a gas pycnometer was found to be 2.76.

3 Methods

In the current investigation, all the tests have been conducted using the respective ASTM standard test methods.

3.1 Physical Properties Test

3.1.1 Linear Shrinkage

To determine shrinkage behavior, one-dimensional linear shrinkage test was carried out on the different mixes of EPK clay, LS, and FA. The mold used was fabricated in SIUC lab, having dimensions of 14 cm in length, 2.54 cm in width, and 1.27 cm in depth. To begin the test, the soil sample must have water content above the liquid limit, also it should be fully saturated. The mold was greased before filling the sample in it, after filling the mold was tapped to remove air bubbles inside the sample. The weight of the sample is recorded at this time and kept in oven for drying for a period of 24 h between 105 °C and 110 °C. After drying, the sample was removed from the oven to cool down and the weight and length of the sample were recorded. In few cases, the sample was crumbled, where the pieces were assembled to take the length. Linear shrinkage was calculated using the following formula.

$$\text{LS}\ (\%) = (\text{L}_\text{S}/\text{L}) * 100$$

where, LS = Linear shrinkage in percent, L_S = Linear shrinkage length after drying in oven, and L = Length of the mold.

3.1.2 Specific Gravity Test

The specific gravity of the samples was performed using a gas pycnometer as per ASTM D 5550 standard. The equipment was calibrated with the respective sleeve size and the spheres (small, medium, and large). Then, the sample was placed in the sleeve and the procedure was followed to get the specific gravity, which is the average of 5 runs. This procedure was efficient and accurate.

3.2 Engineering Properties Test

3.2.1 Standard Proctor Test

Standard Proctor tests were conducted on EPK, EPK with lime sludge, and EPK with lime sludge and fly ash. The mixes used were EPK with different percentages of lime sludge (2, 4, 6, and 8) by weight and EPK with different percentages of lime sludge and fly ash (5, 10, 15, and 20) by weight.

All these tests were performed using a Harvard miniature compaction device. The dimensions of the mold used had a diameter of 33 mm in diameter and 71 mm in height. It had a removable collar and a specimen ejector to remove the sample after compaction. The moisture-density relationships were found using a 20 lb (9.07 kg) hammer with diameter 12.7 mm, compacting the specimen in 5 equal layers and 5 blows per layer.

3.2.2 Unconfined Compressive Strength (UCS)

The optimum moisture content and corresponding dry density, from the standard Proctor test, were chosen to prepare the UCS samples for different mixes. Three samples were prepared for each mix, and an average was taken to get the value for UCS. The samples were prepared by compacting the soil in 3 layers and 25 blows per layer, in a standard UCS mold having a height to diameter ratio as 2:1. The compacted samples were extruded, wrapped in plastic, and placed in a plastic bag. Then, the samples were placed in a water bath having temperature maintained at 25 °C for 7 and 14 days of curing period. The 0 days samples were tested right after preparation without curing. All the cured samples were then loaded under an UCS testing machine with a strain rate of 1.27 mm/min until load reading drops. Load readings were taken at regular intervals of sample deformation. The results are plotted and unconfined compressive strength was taken as the peak value of the stress–strain graph.

3.3 Scanning Electron Microscope (SEM) Test

A scanning electron microscope test was performed by using Quanta^{TM} FEG 450 for EPK clay sample and EPK clay stabilized with lime sludge and fly ash. The soil samples were air-dried to remove moisture from it, before performing the test. The soil sample was sprayed on stubs. After that, the samples were kept in vacuum. The gold coating was applied before performing the test for approximately 10 min and the samples were placed in SEM and were scanned at certain magnification.

Table 1 Linear shrinkage of EPK clay with various percentages of lime sludge

EPK (%)	LS (%)	FA (%)	Linear shrinkage (%)
100	0	0	15.17
98	2	0	10.56
96	4	0	7.20
94	6	0	6.49
92	8	0	4.27
90	5	5	8.55
80	10	10	8.21
70	15	15	7.77
60	20	20	6.29

4 Results and Discussion

4.1 Physical Properties Test

The linear shrinkage tests were performed on EPK and different mixes of EPK and lime sludge, EPK with various percentages of lime sludge and fly ash and the results are presented in Table 1. From Table 1, it can be observed that the linear shrinkage for original clay was 15.17% and it decreased with increase in lime sludge percentage from 10.56 to 4.27%.

From Table 1, it can be inferred that with the addition of fly ash from 5 to 20% and an equal increase in lime sludge from 5 to 20%, the linear shrinkage was decreased from 8.55 and 6.29%.

4.2 Engineering Properties Test

4.2.1 Standard Proctor Test

Results of standard Proctor tests performed on EPK with different percentages of lime sludge, are presented in Fig. 1. From Fig. 1, it can be observed that the dry unit weight and optimum moisture content for EPK clay is 12.98 kN/m^3 and 32.17%. With the increase of lime sludge content from 2 to 6%, the dry unit weight increased from 12.75 to 13.15 kN/m^3. However, for the, 8% lime sludge content the dry unit weight dropped to 13.03 kN/m^3. The overall moisture content decreased from 36 to 31% with the increase in lime sludge content from 2 to 8%. Ai-Sharif and Attom [10] revealed similar results, where burned wastewater sludge ash used for soil stabilization. Their results concluded that a 7.5% of burned sludge by dry weight is the optimum value.

The results of standard Proctor tests performed on EPK with different percentages of lime sludge and fly ash are presented in Fig. 2. From Fig. 2, it can be inferred that

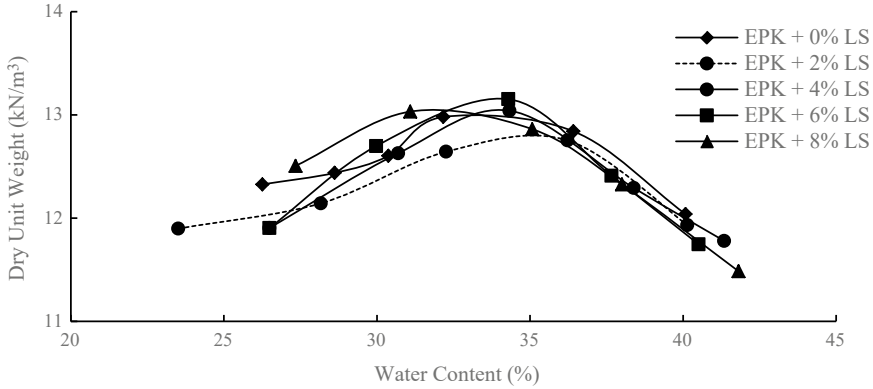

Fig. 1 Compaction curve for EPK clay with different percentages of LS

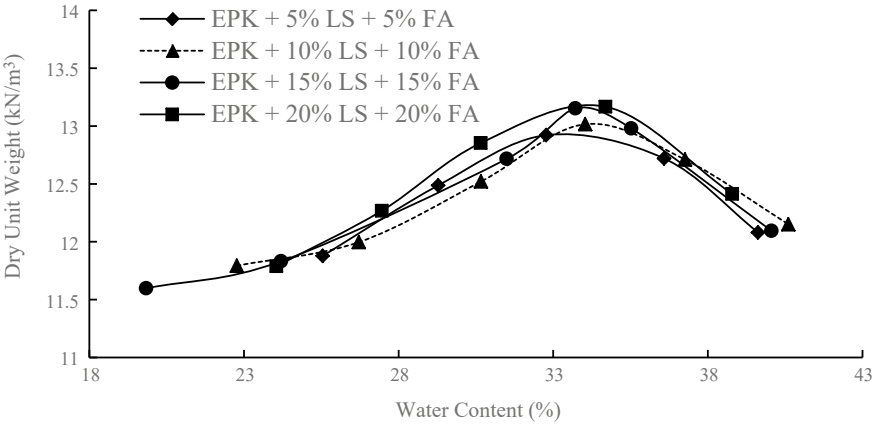

Fig. 2 Compaction curve for EPK clay with different percentages of LS and FA

the dry unit weight increased from 12.92 to 13.16 kN/m^3 with an increase of lime sludge and fly ash content from 5 to 20%.

Also, the optimum water content (OMC) increased from 32.77 to 34.03% for lime sludge and fly ash content of 5–10%, then it decreased to 33.72% for 15% lime sludge and fly ash content and increased to 34.69% for lime sludge and fly ash content of 20%.

4.2.2 Unconfined Compressive Strength (UCS) Test

The results of unconfined compressive strength (UCS) of EPK mixed with different percentages of lime sludge are presented in Fig. 3. From Fig. 3, it can be observed that for 0 days and 14 days, UCS value increased with an increase in lime sludge

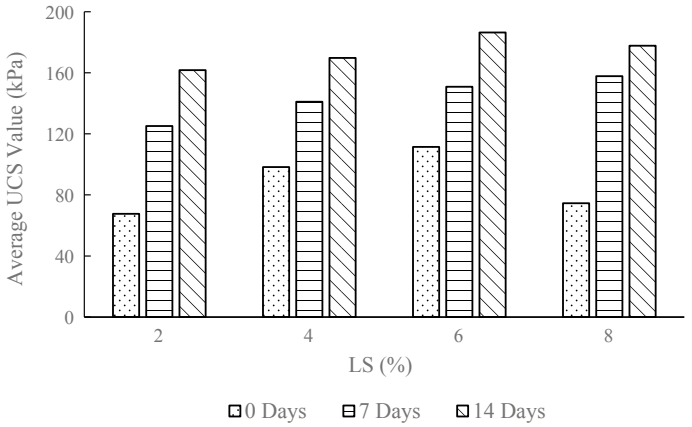

Fig. 3 UCS values of EPK with different percentage of LS at 0, 7, and 14 days curing

content from 2 to 6%. It had a slight decrease for 8% lime sludge for 0 and 14 days. However, UCS value for 7 days increased with an increase in lime sludge content for 2–8%.

Equivalently, the UCS values of EPK mixed with different percentages of lime sludge and fly ash are presented in Fig. 4. From Fig. 4, it can be noticed that the UCS value increased with increase in lime sludge and fly ash content for 7 days and 14 days. For 0 days, the UCS value increased with an increase in lime sludge and fly ash content from 5 to 15% and decreased by 20% lime sludge and fly ash content.

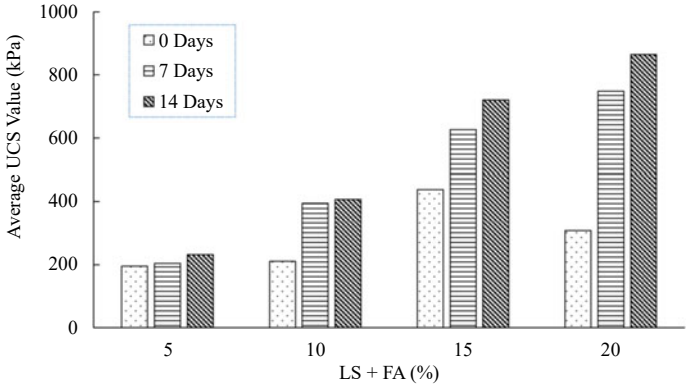

Fig. 4 UCS values of EPK with different percentage of LS and FA at 0, 7 and 14 days curing

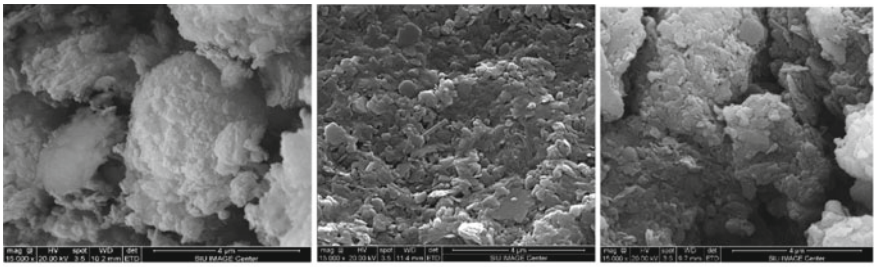

Fig. 5 SEM Micrographs of **a** EPK clay, **b** EPK + 6% LS at 14 days, **c** EPK + 20% LS + 20% FA, 14 days

4.2.3 Scanning Electron Microscope (SEM) Test

Figure 5, shows the SEM micrographs of EPK, EPK + 6% lime sludge at 14 days, and EPK + 20% lime sludge +20% fly ash at 14 days at the same magnification i.e., × 15,000. It can be seen from the micrograph that, the percentage of voids has been reduced for LS and LS + FA mixed sample over a curing period of 14 days. The stabilized samples became dense over time and exhibited high strength as compared to virgin EPK clay sample.

5 Conclusions

The primary purpose of this study was to see the effect of lime sludge alone and a combination of lime sludge and fly ash on physical and geotechnical properties of EPK clay. The following observations were made based on the laboratory study.

- The linear shrinkage of EPK, demonstrated a decrease in value with the addition of lime sludge from 2 to 8%.
- Linear shrinkage of EPK, also had a decrease in value with the addition of both lime sludge and fly ash from 5 to 20%. The decreased value was less when compared to only lime sludge addition.
- Standard Proctor for EPK and different percentages of lime sludge had an increase in dry unit weight from 2 to 6% and a slight drop for 8%. The OMC decreased from 36 to 31% with an increase in lime sludge content from 2 to 8%. It can be concluded that the optimum percentage of lime sludge added to EPK be 6%.
- Standard Proctor for EPK mixed with equal percentages of lime sludge and fly ash had an increase in dry unit weight from 5 to 20%. The OMC had an increase from 5 to 10%, then decreased for 15% and increased for 20%.
- For EPK and lime sludge mixes, the percentage increase in strength for 0 days was 64% from 2 to 6% increase in lime sludge content and decreased to 33% for 8% lime sludge content. For 7 days, the percentage increase in strength was 26%

for an increase in lime sludge content from 2 to 8%. For 14 days, the percentage increase in strength was 15% from 2 to 6% increase in lime sludge content and dropped to 4% for 8% lime sludge content.

- For EPK with lime sludge and fly ash mixes, the percentage increase in strength for 0 days was 58.03%, the percentage increase in strength for 7 days was 266.39% and the percentage increase in strength for 14 days was 272.46%.
- The SEM micrographs for EPK, EPK with lime sludge, and EPK with lime sludge and fly ash show that the voids decreased with curing period and samples became dense. The curing played an effective role in the reactions between EPK, lime sludge, and fly ash and exhibited an increase in strength and thus stabilizing EPK.

References

1. Yi Y, Liska M, Al-Tabbaa A (2013) Properties of two model soils stabilized with different blends and contents of GGBS, MgO, lime, and PC. J Mater Civil Eng 26(2):267–274
2. Samaras P, Papadimitriou CA, Haritou I, Zouboulis AI (2008) Investigation of sewage sludge stabilization potential by the addition of fly ash and lime. J Hazard Mater 154(1–3):1052–1059
3. Lim S, Jeon W, Lee J, Lee K, Kim N (2002) Engineering properties of water/wastewater-treatment sludge modified by hydrated lime, fly ash and loess. Water Res 36(17):4177–4184
4. Chen L, Lin DF (2009) Stabilization treatment of soft subgrade soil by sewage sludge ash and cement. J Hazard Mater 162(1):321–327
5. Luo HL, Hsiao DH, Lin DF, Lin CK (2012) Cohesive soil stabilized using sewage sludge ash/cement and nano aluminum oxide. Int J Transp Sci Technol 1(1):83–99
6. Smol M, Kulczycka J, Henclik A, Gorazda K, Wzorek Z (2015) The possible use of sewage sludge ash (SSA) in the construction industry as a way towards a circular economy. J Clean Product 95:45–54
7. Seco A, Ramírez F, Miqueleiz L, García B (2011) Stabilization of expansive soils for use in construction. Appl Clay Sci 51(3):348–352
8. Sol-Sánchez M, Castro J, Ureña CG, Azañón JM (2016) Stabilisation of clayey and marly soils using industrial wastes: pH and laser granulometry indicators. Eng Geol 200:10–17
9. Şenol A (2012) Effect of fly ash and polypropylene fibers content on the soft soils. Bull Eng Geol Environ 71(2):379–387
10. Ai-sharif MM, Attom MF (2014) A geoenvironmental application of burned wastewater sludge ash in soil stabilization. Environ Earth Sci 71(5):2453–2463

Influence of Fly ash, Lime, Fines Obtained From Demolished Structures Waste On Geotechnical and Strength Characteristics of Soil

Davinder Singh, Tarun Kumar, and Amandeep Kaushal

Abstract Construction and demolished (C&D) waste which produced continuously during the construction work can be used for this purpose. The disposal of such material has become a big issue because this kind of deposit covers huge landfill area. In present study, the effect of fines obtained from construction and demolished (C&D) waste and fly ash in the soil mixture was evaluated. Fly ash content as 5, 10 and 15%, C&D waste as 6, 10 and 14% and lime as 2, 4 and 6%. The study results reveal that due to the addition of admixtures, Specific gravity, Maximum dry density (MDD) increases and plasticity index (PI) and optimum moisture content (OMC) decreases. On the other hand specific gravity, PI, MDD decreases and OMC increases with the addition of FA and lime. But the effect of fly ash on unconfined compressive strength value of soil at 7 and 14 days are least as compared to the lime and construction and demolished (C&D) waste. The result of split tensile strength (STS) value of soil after treatment with different admixtures at variable percentage and at different curing periods of 7 and 14 days shows that the maximum gain in strength is due to the addition of 6% lime.

Keywords Fly ash · Construction and demolished waste · Lime · Soil

1 Introduction

Construction of building or any other engineering project on expansive soil is highly risky due to the tendency of expansive soil to change its behaviour due to the presence of montmorillonite, which leads to shrinkage and swelling of the expansive soil when it comes in contact with moisture. Many of the researchers are working on the improvement of the expansive soil properties by using different types of the admixtures i.e. Construction and demolished (C&D) waste, fly ash, lime, etc. Construction

D. Singh (✉) · T. Kumar
Dr. B. R. Ambedkar National Institute of Technology Jalandhar, Jalandhar, Punjab, India
e-mail: singhdj@nitj.ac.in

A. Kaushal
Rayat Bahra Institute of Engineering and Technology, Hoshairpur, India

K. R. Reddy et al. (eds.), *Sustainable Environment and Infrastructure*, Lecture Notes in Civil Engineering 90, https://doi.org/10.1007/978-3-030-51354-2_30

and demolished (C&D) waste and fly ash are both waste materials and now a day's deposition of these kinds of waste material on land fill is a huge problem because earth surface is already covered with different type of waste material deposits. These kinds of deposits lead to contaminate the underground water, causes environment hazards and ill effects on the health of human as well as animals.

To overcome these kinds of problems due to day by day increment of waste, some alternate methods of using these wastes should be adopted. Usage of these waste materials for civil engineering purpose as a stabilizing material is a viable option. There have been various studies of soil stabilization of the soil by using different admixtures on variable parameters.

2 Literature Reviews

Soil stabilization is the process of improvement of the soil properties by adding different types of stabilizers that can enhance the strength of the soil for long period and make the soil suitable for any civil engineering project. Abhishek et al. [1] show that value of specific gravity and plasticity index shrinkage index and maximum dry density increases observed to be decreases but optimum moisture content of soil increases. Kumar et al. [2] concluded that the expansive soil can be successfully stabilized by the combined action of fibers, lime and fly ash. Chauhan et al. [3] observed that optimum moisture content increases and maximum dry density decreases with increased percentage of fly ash mixed with locally available soil. Sharma et al. [4] concluded that UCS and CBR of soil increase substantially on addition of 20% fly ash and 8.5% lime. Ramlakhan et al. [5] concluded that the optimum moisture content and CBR value increase and maximum dry density decreases with increase in percentage lime and fly ash content. Karthik et al. [6] concluded that plasticity index decreases, specific gravity initially increase up to the addition of 5% fly ash after that it decreases. Jain et al. [7] studied the effect of demolished concrete as stabilizer on the properties of the soil. This study concluded that specific gravity increases and PI gradually decreased and during compaction test it was observed that MDD increases and OMC decreases with the increase in the proportion of admixture. Sharma and Hymavathi [8] concluded that differential free swell and maximum dry density decrease, whereas pH, UCS and soaked CBR value increase with addition of fly ash, C&D waste and lime. Kulkarni et al. [9] used lime and fly ash for the stabilization of soil and observed that plasticity index reduces when fly ash and lime was mixed with the soil and this increment results in reduction of maximum dry density and free swell index on the other hand it increase the optimum moisture content.

3 Materials and Methodology

3.1 Materials

3.1.1 Construction and Demolished waste

The fines obtained from construction and demolished waste after sieve through 75μ was used for the admixture and it was classified as poorly graded sand as per Indian standard soil classification system.

Fly ash
The fly ash used for this project was collected from NIT Jalandhar. The chemical composition is given in Table 2.

Lime
Lime is calcium-containing inorganic mineral which mainly consists of carbonates, Calcium oxide, CaO, Silica, etc. Lime is having cementitious properties that provide long term strength. Lime is in the form of white powder.

Table 1 Properties of Soil and C&D waste

Test conducted	Results	
	Soil	C&D waste
Moisture content (%)	15.13	5.9
Sieve analysis (% finer than 75μ)	21.5	16
Type of soil	CL	–
Specific gravity (G)	2.59	2.78
Liquid limit (%)	32	35
Plastic limit (%)	19.87	–
Plasticity index (%)	12.13	–
Optimum moisture content (%)	19	16

Table 2 Chemical composition of Indian Fly ash

Chemical composition	Range (%)
Silica (SiO_2)	49–67
Alumina (Al_2O_3)	16–29
Iron Oxide (Fe_2O_3)	4–10
Calcium Oxide (CaO)	20–30
Magnesium Oxide (MgO)	0.2–2
Sulphur (SO_3)	0.1–2
Loss on ignition	0.5-3

Methodology Compaction tests

The compaction tests were performed as per [10] to show the clear relationship between the dry density and the moisture content of the soil. After plotting the data from the experiment with water content as the abscissa and dry density as the ordinate, we can obtain the OMC and MDD. The equations used in this experiment are as follows:

Wet density = weight of wet soil in mould gms/Volume of mould in cm^3

Moisture content % = (weight of water gms/Weight of dry soil gms) × 100

Dry density γ_d (gm/cc) = wet density/(1+moisture content/100)

Unconfined compression test

UCS tests were carried out on cylindrical specimens of 38 mm diameter and 76 mm long according to [11] and the mixture was compacted in five layers and each layer was compacted using rammer under a free fall of 450 mm. The average of the three specimens of the result was reported as the UCS.

Split tensile strength test

For conducting this test, samples are prepared same as for unconfined compressive strength test. After curing, the specimens are placed horizontally between bearing blocks of compression test machine adjusted for a strain rate of 1.00 mm/min. The STS is obtained by following equation.

Split tensile strength = $2P/\pi dL$

Where, P = failure load, L = length of specimen, d= diameter of the specimen.

4 Results and Discussion

4.1 Compaction tests

The effect of the stabilizers on OMC shows that with the addition of fly ash and lime, OMC value increases to 24 and 22% from 19%. But the mixing of C&D waste resulted in lowering the value of OMC and it was found to remain constant after addition of 10% C&D waste (Fig.1 and 2). On the other hand, the results of MDD show that with the addition of fly ash, MDD value initially increases but afterward decreases drastically from 1.87 to 1.77 g/cm^3 and addition of lime results in the decrease of the MDD value to 1.82 g/cm^3. On the other hand, mixing of C&D waste showed increase in the value of MDD from 1.87 to 1.92 g/cm^3.

4.1.1 Unconfined Compressive Strength

The gain in the UCS of the soil is maximum with the addition of 6% lime i.e. 931.07 and 1108.82 kN/m^2 at 7 and 14 days curing period while considering C&D waste and

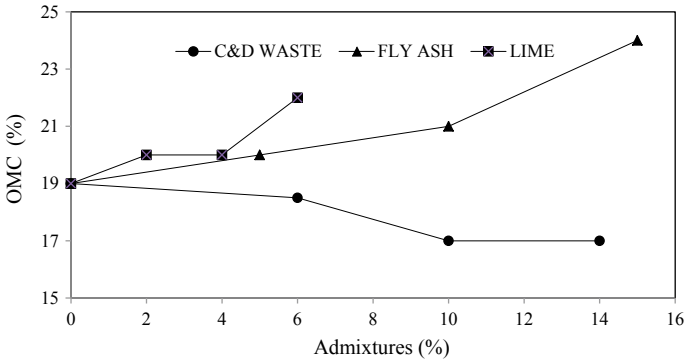

Fig. 1 Effect of variable proportion of C&D waste, fly ash and lime on OMC of soil

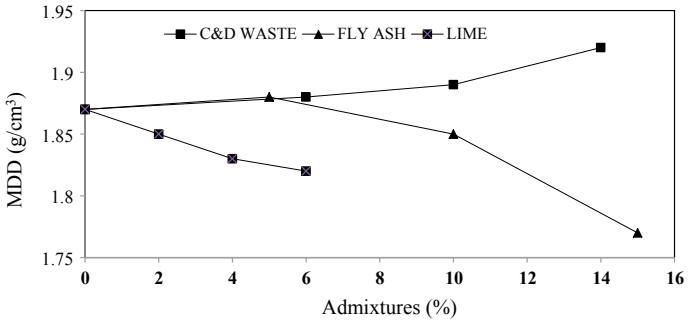

Fig. 2 Effect of variable proportion of C&D waste, fly ash and lime on MDD of soil

fly ash the increase in the UCS is more due to the C&D waste i.e. 874.09 and 1084.20 kN/m^2 at 7 and 14 days curing, respectively (Fig. 3 and 4). The increase is due to the pozzolanic reaction between soil and C&D waste. C&D waste contains cementitious

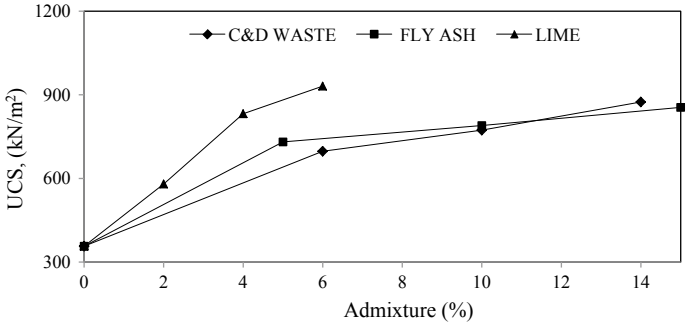

Fig. 3 UCS value of different stabilizers lime, fly ash and C&D waste at curing period of 7 days

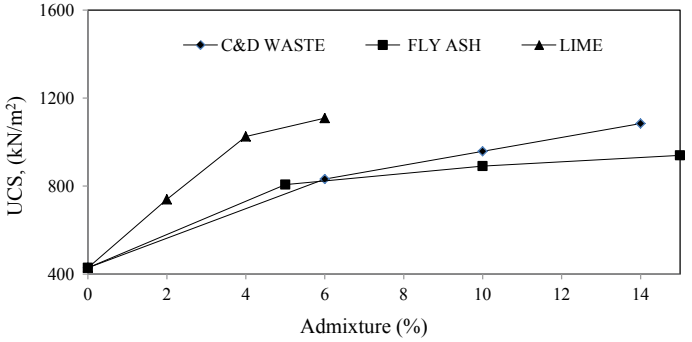

Fig. 4 UCS value of different stabilizers lime, fly ash and C&D waste at curing period of 14 days

materials like fines of cement mortar, concrete bricks, etc. The lime treatment created flocculated structure but the reaction products which were produced through the solution process become less effective because the surface area was too large for the cementitious material to create significant increase in the unconfined compressive strength.

Split Tensile Strength

The results of tensile strength show that the maximum increase in the strength is due to the addition of lime at 7 days and 14 days of curing period i.e. 166.86 and 178.19 kN/m^2, respectively from 126.84 to 141.19 kN/m^2 (Fig. 5 and 6). On the other hand, C&D waste and fly ash as admixtures shows that the gain in tensile strength is only due to the C&D waste i.e. 165.35 and 169.13 kN/m^2. The presence of fly ash was found to reduce the strength. The reason behind increment in strength is due to the time dependency of pozzolanic reaction between soil and C&D waste.

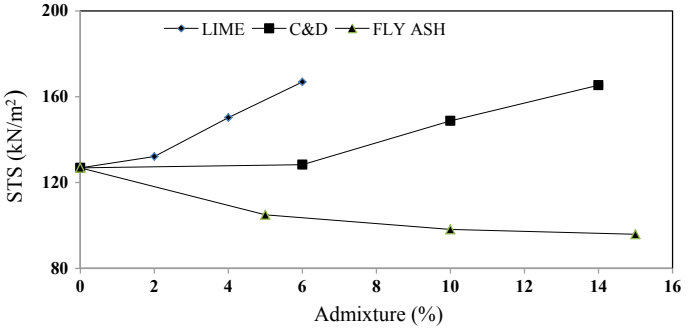

Fig. 5 STS value of different stabilizers lime, fly ash and C&D waste at curing period of 7 days

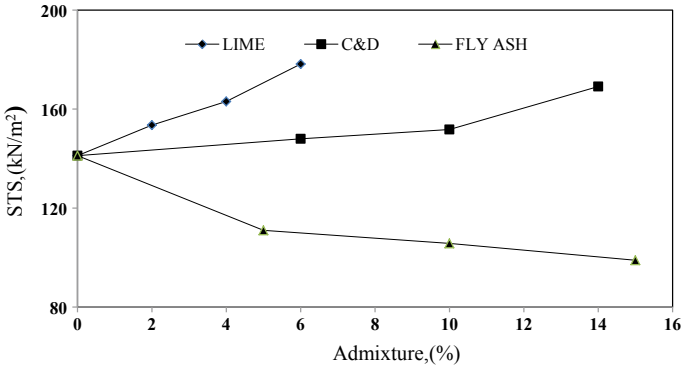

Fig. 6 STS value of different stabilizers lime, fly ash and C&D waste at curing period of 14 days

5 Conclusions

1. Moisture content decreases with the addition of C&D waste and increases with the addition of lime and fly ash while MDD increases with C&D waste and decreases when soil is mixed with fly ash and lime. With the addition of fly ash, MDD value initially increases but afterwards decreases drastically from 1.87 to 1.77 g/cm^3. The addition of lime also resulted in the decrease of MDD value to 1.82.
2. The unconfined compressive strength (UCS) value of soil after treatment with different admixtures at variable percentage and at different curing periods shows that the maximum gain in strength is due to the addition of lime at 14 days curing. While considering fly ash and C&D waste as admixture, C&D waste increases the UCS value of soil more than fly ash at 7 and 14 day.
3. The STS of soil increases with the addition of lime and C&D waste but the effect of lime is high as compared to the C&D waste. On the other hand, fly ash continuously decreases the strength.

References

1. Ansary MA, Noor MA, Islam M (2007) Effect of fly ash stabilization on geotechnical properties of Chittagong coastal soil. Int J Eng Technol Manag Res 3(5):443–454
2. Kumar A, Walia BS, Bajaj A (2007) Influence of fly ash, lime, and polyester fibres on compaction and strength properties of expansive soil. J Mater Civil Eng ASCE 19:242–248
3. Chauhan MS, Mittal S, Mohanty B (2008) Performance evaluation of silty sand sub-grade reinforced with fly ash and fibre. Geotext Geomembr 26:429–435
4. Sharma NK, Swain SK, Sahoo UC (2012) Stabilization of a clayey soil with fly ash and lime: a micro level investigation. Geotech Geol Eng 30:1197–1205
5. Ramlakhan B, Kumar SA, Arora TR (2013) Effect of lime and fly ash on engineering properties of black cotton soil. IJETAE 3(11):535–541

6. Karthik S, Kumar EA, Gowtham P, Elango G, Gokul D, Thangaraj S (2014) Soil stabilization by using fly ash. IOSR J Mech Civil Eng 10(6):2320–334
7. Jain A, Chawda A (2016) Appraisal of demolished concrete coarse and fines for stabilization of clayey soil. Int J Eng Sci Res Technol 1550
8. Sharma RK, Hymavathi J (2016) Effect of fly ash, construction demolition waste and lime on geotechnical characteristics of a clayey soil: a comparative study. Environ Earth Sci 75(5):1–11
9. Kulkarni TA, Padalkar PA, Joshi CG (2017) Stabilization of soil by using fly ash and lime (32):32–38
10. IS 2720 methods of test for soils: determination of water content, 2720, July 1973, BIS (1997)
11. IS 2720 methods of test for soils: Part 10—determination of unconfined compressive strength, 2720, 1–4, BIS, (1991)

Experimental Study on the Influence of Coir and Calcium Chloride on the Strength Characteristics of Expansive Soil

R. Suresh and V. Murugaiyan

Abstract Expansive soils are the problematic soils, this kind of soil is portrayed by its outrageous hardness while drying and with high swelling process on the wetting. This type of soil has been always presented problems for pavements, light loaded structures, by merging under load and by changing volumetrically alongside regular dampness variety. This article illustrates the influence of inclusion of coir in conjunction with Calcium Chloride on expansive soil stabilization is presented. The present study carried out the viability of using the combination of coir and Calcium Chloride in expansive soils. The effect of coir fibre length 10 mm and three percentages (0.3, 0.6, 0.9% by dry weight of soil), coir pith with three percentages (1, 2, 3% by dry weight of soil) and Calcium Chloride with three dosages (0.25, 0.50, 1.0% by dry weight of soil) were considered. Both untreated and chemically treated fibre reinforced with expansive soil samples were prepared. Maximum dry density, optimum moisture content and UCS tests were conducted. Coir consists of pith along with fibre which was separated to study their independent effects of shear strength behaviour. UCS tests were conducted 0, 7, 14 days of curing, it was observed that the combination of 1% coir pith +0.6% coir fiber +1% CaCl exhibited high shear strength. Mix of coir waste and $CaCl_2$ with expansive soil improved the shear strength behaviour of expansive soils. Expansive soil can be successfully stabilized by the coir and Calcium Chloride.

Keywords Coir fibre · Coir pith · Calcium chloride

1 Introduction

Expansive soils are problematic to Civil Engineering by increase and decrease of its volume due to movement of water in and out. Expansive soils are portrayed by its outrageous hardness while drying and with high swelling process on the wetting. They exhibit low shear strength as well as high swell and shrink characteristics.

R. Suresh (✉) · V. Murugaiyan
Department of Civil Engineering, Pondicherry Engineering College, Puducherry, India
e-mail: rangasuresh307@pec.edu

K. R. Reddy et al. (eds.), *Sustainable Environment and Infrastructure*, Lecture Notes in Civil Engineering 90, https://doi.org/10.1007/978-3-030-51354-2_31

Clay soils are found on everywhere in the continuant on the Earth. This type of soil has been always presented problems for pavements, light loaded structures, by merging under load and by changing volumetrically alongside regular dampness variety. Pernicious results caused by this type of soils have been reported in many countries. In India, substantial tracks are secured by expansive soils known as black cotton soils. To tackle the problems due to volume change in soils, stabilization techniques have emerged as a good solution. Recently, there is growing attraction to soil reinforcement using different types of fibers and waste materials. There are high accumulations of waste materials such as fly ash, stone dust, lime, etc. In all over the world a disposal of the waste material causes many environmental issues. To understand the influence of different types of fibers and chemical materials on index and engineering properties of expansive soils have been determined by different researches [1–8] Reinforcement of clay soil with locally available waste materials improved the index and engineering properties of soils. A number of researchers work also concentrated on the effect of reinforcement using fibers on the strength behavior of expansive soils.

Authors [9–13] showing that adding waste materials and chemical materials like marble dust and reinforcing the mix with natural and synthetic fibers improves the strength of expansive soils. Recently, the tendency of substituting the natural material with synthetic material as a part of sustainable development has made the researchers think about using natural fibers for reinforcing expansive soils. Coir fiber has been considered as a attractive choice by many researchers [14–17] during the extraction processes of the coir fiber from the coconut husk, fleshy coir pith is generated. This waste has traditionally been disposed by burning, which results in various environmental problems, including carbon deposits and warming of the atmosphere. Therefore, finding an alternative way for the disposal of coir is for soil stabilization, coir is mixed with $CaCl_2$ considered in this study to improve the shear strength behaviour of expansive soil.

2 Materials and Experimental Study

2.1 Materials

Expansive Soil: The expansive clay soil is collected from nasal in villupuram district is located in Tamil Nadu. The soil is collected in a dry condition at a depth of 1 m and preserved in the laboratory. Identified the index and engineering properties of expansive soils as shown in Table 1.

Calcium Chloride: The chemical composition of Calcium Chloride is $CaCl_2$. It absorbs water from the air and releases heat when it is dissolved in water.

Table 1 Effects of fibres and chemical admixtures in expansive soils

Si. no	Author names	Year	Fibers	Chemical admixtures	Geotechnical properties			DC	MSP
					IP	Swelling	UCS		
1	B.V.S. Viswanadham	2009	v		v	v		v	v
2	N.M. Al Akhras	2008	v		v	v		v	v
3	Anand Puppala	2010	v	v	v		v		v
4	Eedalcokca	2015		v	v		v		v
5	K. Suresh	2009	v	v	v	v	v		
6	B.R. Phani Kumar	2004		v	v	v	v		
7	J.M. Kate	2005		v	v	v	v		v
8	Sayedhessam Bahmani	2016		v	v		v		v

Note: IP-Index properties; DC-Desiccation cracking; UCS-Unconfined compressive strength; MSP-Micro structural properties

Table 2 Physical properties of expansive soils

Si no	Properties of soils	Soil
Physical properties		
1	Liquid limit %	76%
2	Plastic limit %	16.88%
3	Shrinkage limit %	10.25%
4	Specific gravity	2.57
5	Maximum dry density (kN/m^3)	15.39
6	Optimum moisture content (OMC)	22.95%
7	Clay %	52
8	Silt %	18
9	Sand %	30
10	Free swell index %	69
11	Unconfined compression test (kPa)	214.15
Chemical properties		
1	SiO_2	85.83%
2	Al_2O_3	9.13%
3	Fe	2.71%
4	MgO	1.18%
5	Au	1.15%

Coir fiber: The coir fibers used in this study are matured coir fibers consisting of 45% lignin and 43% cellulose. Fiber with length is 10 mm and a diameter with 0.25 mm was investigated in this study.

Coir pith: The air-dried coir waste that passed through the 4.75 mm sieve (Table 2).

2.2 Modification of Coir Fiber

The precipitation method was used for loading of $FeCl_3$ and NaOH. The reaction was carried out at ambient condition, temperature and pressure. For this purpose, in the first step, 50 g of coir fibers were soaked in 500 ml aqueous solution, 0.5 molarity $FeCl_3$ for 24 h to uniformly fill the fiber pores and surfaces by the $FeCl_3$ solution. In the second step, the soaked coir fibers were separated from the $FeCl_3$ aqueous solution and were incubated in another beaker, and 500 mL of sodium hydroxide, 0.5 molarity aqueous solution was then added to it and was kept for 24 h. During this treatment, $Fecl_3$ quickly precipitates as nanoparticles on the fiber surfaces and in the pores. Finally, the coir fibers were separated from the sodium hydroxide solution

and were washed by distilled water to remove the undesired residue of the reaction, such as NaOH. Fibers were then dried at ambient room temperature (Figs. 1 and 2).

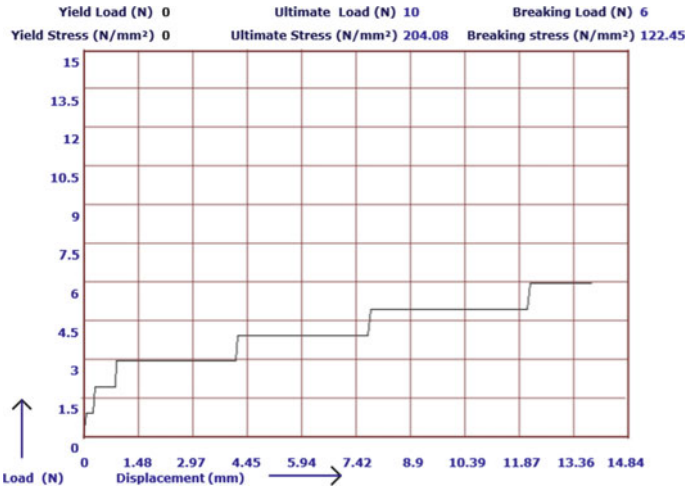

Fig. 1 Tensile strength of untreated coir fiber

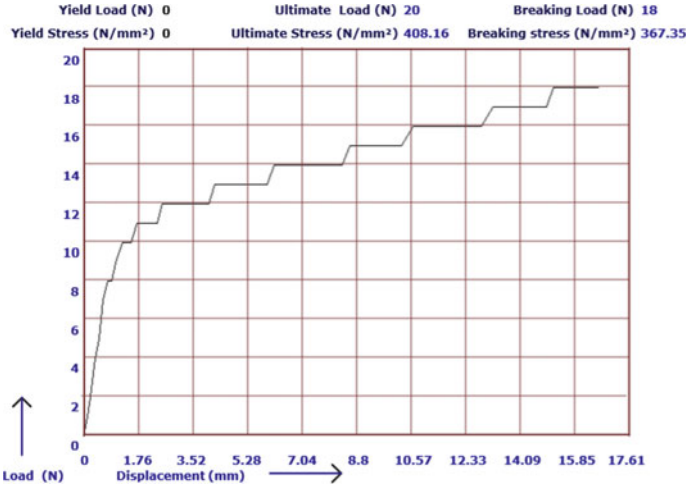

Fig. 2 Tensile strength of treated coir fiber

Table 3 MDD & OMC obtained for various soil sample mixes

Soil sample mixes	MDD ($Kg/m^{3)}$	OMC (%)
Plain soil	15.39	22.95
Soil + coir pith 1%	16.54	21.35
Soil + coir pith 2%	15.29	23.48
Soil + coir pith 3%	15.12	24.1
Soil + coir fiber 0.3%	15.61	22.56
Soil + coir fiber 0.6%	15.87	22.24
Soil + coir fiber 0.9%	15.98	22.51
Soil + $CaCl_2$ 0.25%	15.51	22.3
Soil + $CaCl_2$ 0.5%	15.49	21.6
Soil + $CaCl_2$ 1%	15.31	24.7
S + CP 1% + CF 0.3% + $CaCl_2$ 0.25%	15.11	22.9
S + CP 1% + CF 0.3% + $CaCl_2$ 0.5%	15.46	22.78
S + CP 1% + CF 0.3% + $CaCl_2$ 1%	15.58	22.54
S + CP 1% + CF 0.6% + $CaCl_2$ 0.25%	15.48	22.54
S + CP 1% + CF 0.6% + $CaCl_2$ 0.5%	15.65	22.32
S + CP 1% + CF 0.6% + $CaCl_2$ 1%	16.10	21.87
S + CP 1% + CF 0.9% + $CaCl_2$ 0.25%	15.45	22.78
S + CP 1% + CF 0.9% + $CaCl_2$ 0.5%	15.55	22.74
S + CP 1% + CF 0.9% + $CaCl_2$ 1%	16.30	24.70

2.3 Preparation of Soil Samples

After conducting preliminary experiments, three different percentages of $CaCl_2$ (0.25, 0.5, 1.0%), three different percentages of coir pith (1, 2, 3%) and three different percentages of coir fiber (0.3, 0.6, 0.9%) were selected for this study (Table 3).

2.4 Laboratory Testing Program

The compaction and plasticity characteristics of $CaCl_2$ and coir consists of pith along with fiber are mixed with soil were studied initially. These results are showed in Table 2 and Fig. 3.

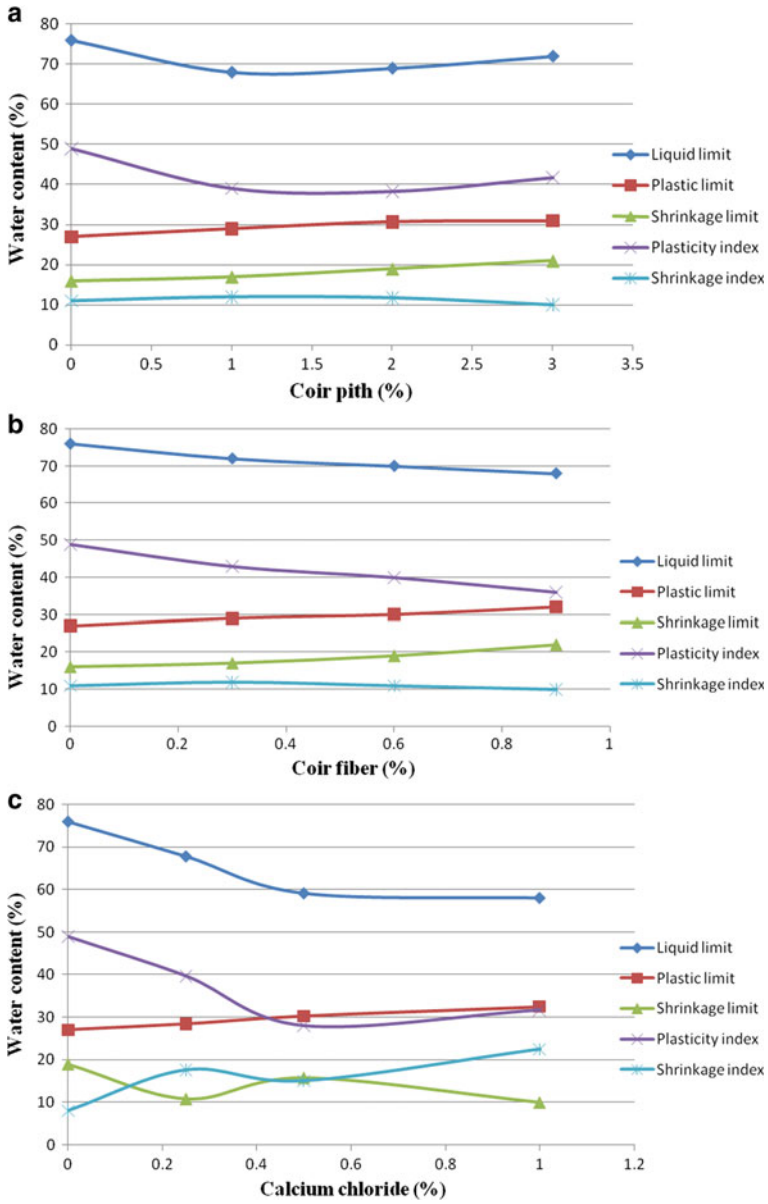

Fig. 3 **a** Variations of atterberg limits, plasticity index and shrinkage index for coir pith, **b** Variations of atterberg limits, plasticity index and shrinkage index for coir fiber, **c** Variations of atterberg limits, plasticity index and shrinkage index for $CaCl_2$

2.5 Unconfined Compression Strength Test

Unconfined Compressive Strength tests were conducted 0, 7, 14 days of curing for untreated and treated samples. UCS tests were performed on both untreated and treated soils. The untreated UCS value for highly sensitive clay soil was 103.96 kPa. The percentages of fibers used were 0.3, 0.6 and 0.9% by dry weight of the untreated soil whereas the fiber length is 10 mm, coir pith (1, 2 and 3% by dry weight of soil) and (0.25, 0.50 and 1.0%) of $CaCl_2$. In addition, the effect of curing time on strength improvement was examined considering curing periods. The shear strength (Table 4) coir pith, coir fiber and $CaCl_2$ admixtures increased the unconfined compression strength (UCS) of clay soil. The increase in unconfined compressive strength is attributed to the tensile strength in the soil due to presence of fibers. Optimum increase was noticed at 0.6% coir fiber dosage with 1% of coir pith and 1% of $CaCl_2$ for 14 days. UCS strength will increase 4.41 times more than initial strength of soil. Beyond 0.6%, the increase in fiber dosage for 10 mm length resulted in a slight decrease in UCS values (Fig. 4).

Table 4 List of bonds recognized by FTIR

Bond	Si–H	Si–H	C–C	Si–O-Si	C = C	C = O	Si–OH
Clay soil	720	790	1010	–	1632	–	3405
soil + CP 1% + CF 0.6% + $CaCl_2$ 1%	688	–	810	1080	–	1650	3403

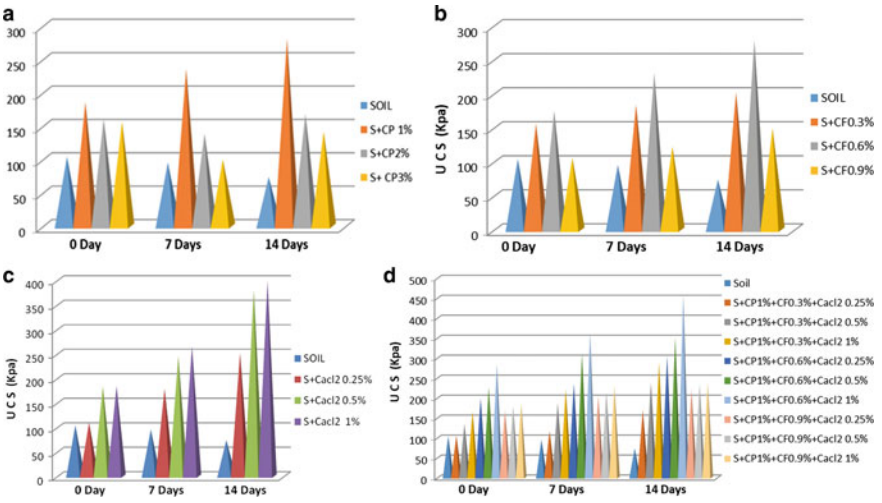

Fig. 4 **a** UCS for soil with coir pith, **b** UCS for soil with coir fiber, **c** UCS for soil with $CaCl_2$, **d** UCS values for untreated and treated soil

3 Microstructural Properties

3.1 SEM Analysis

Two specimens, namely, untreated soil and treated soil with clay soil + CP 1% + CF 0.6% + $CaCl_2$ 1%, where lumens were boarded with spherical particles with the size ranging from 220.4 to 270.4 nm which may indicate the formation of nanosized crystals in the fiber structure. The extended tensile strength in chemically treated fibers may be well explained by nano modification of coir fiber structure resulting from the filling and cross linking effects of crystallized $FeCl_3$ and NaOH contributing to the load sharing phenomenon during the tensile loading (Fig. 5). Figure 6a, b shows EDAX spectrum of SEM analysis for clay soil and clay soil + CP%CF 0.6% + $CaCl_2$ 1%. Eminent peaks Fe, Au, Al are observed in 7(a) and Ca, Al, Ci are observed in clay soil + CP 1% + CF 0.6% + $CaCl_2$ 1%.

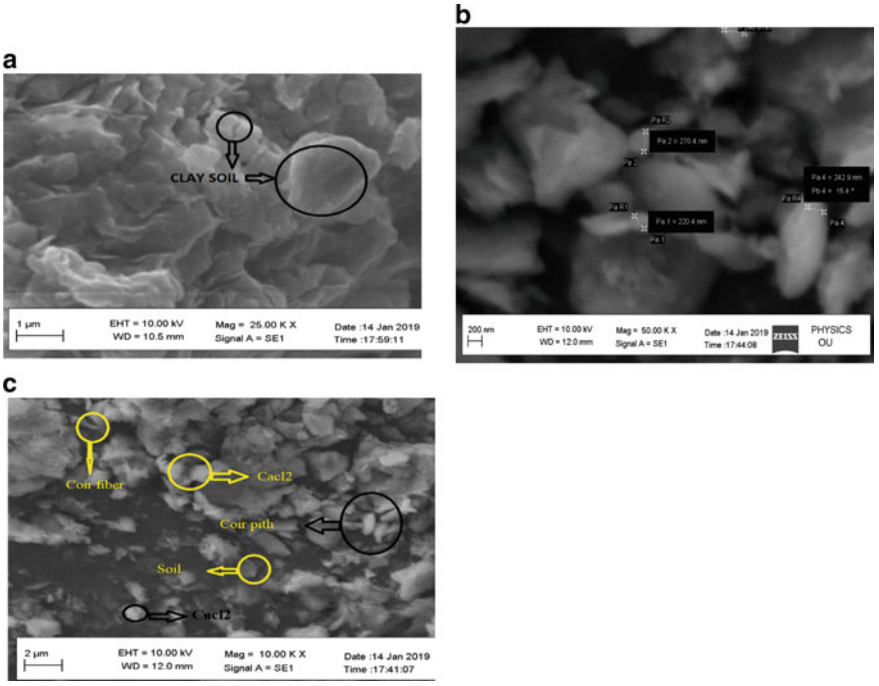

Fig. 5 **a** SEM analysis for untreated clay soil, **b** SEM analysis for treated soil with CP 1% + CF 0.6% + $CaCl_2$ 1% after 28 days of curing, **c** SEM analysis for treated soil with CP 1% + CF 0.6% + $CaCl_2$ 1% after 28 days of curing

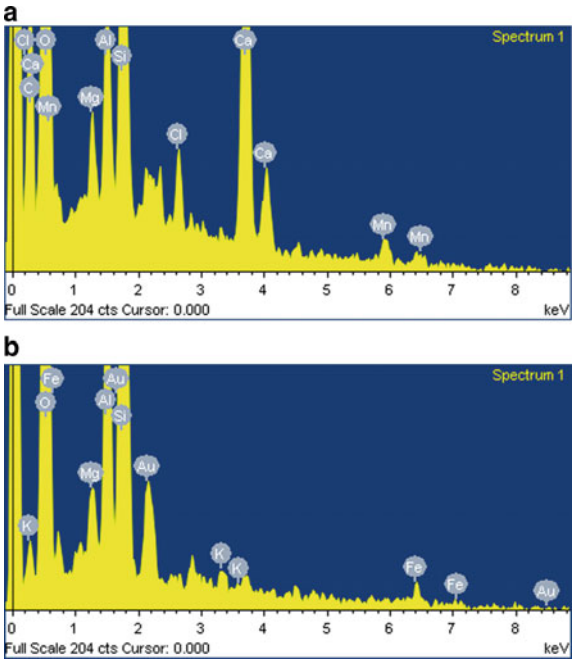

Fig. 6 **a** SEM with EDAX for untreated clay soil, **b** SEM with EDAX for treated clay soil

3.2 XRD

X-ray diffraction peaks identify for clay soil, clay soil + coir pith 1% + coir fiber 0.6% + $CaCl_2$ 1% at 28 days. The most important peak traced were related to CH which were identified at $2\Theta = 26°$ to 36° as seen from the Fig. 7, the addition of coir and $CaCl_2$ in the soil causes CH related peaks to be appeared at the aforementioned 2Θ. It has been carried out to confirm the formation of new minerals which can play a significant role in strength improvement behavior Calcium stabilized with curing period. The intensity has increased for Calcium Chloride treated when compared with the clay soil, which is all evident from X-ray data (Fig. 7).

3.3 FTIR

Using the results of FTIR, it was possible to recognize the important chemical bonds in the materials (as shown in Fig. 8). For clay soil, the week peak at 720 cm^{-1} indicates stretching vibration of Si–H bond. The peak at 790 cm^{-1} indicates stretching vibration of Si–H bond. The broad peak at 1010 cm^{-1} indicates stretching vibration of C–C bond. The peak at 1632 cm^{-1} likely to indicate bending vibration of C = C,

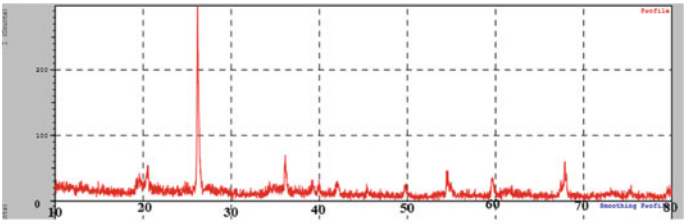

(b) Position (2 theta)

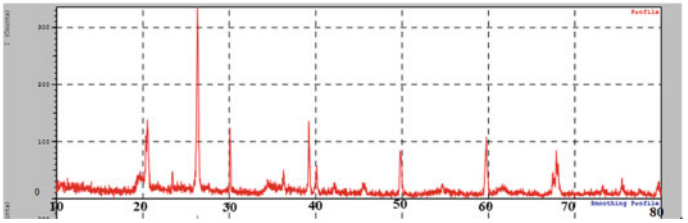

(a) Position (2 theta)

Fig. 7 XRD analysis for **a** untreated soil; **b** treated soil

and the peak at 3405 cm^{-1} present the stretching vibration of Si–OH. For clay soil + coir pith 1% + coir fiber 0.6 % + $CaCl_2$ 1%, the week peak at 688 cm^{-1} presents stretching vibration of Si–H, the peak at 810 cm^{-1} indicates stretching vibration of C–C, the broad peak at 1080 cm^{-1} indicates stretching vibration of Si–O–Si bond [18]. The peak at 1650 cm^{-1} likely to indicate bending vibration of C = O, and the peak at 3403 cm^{-1} present the stretching vibration of Si–OH. A summary of the results for clay soil, clay soil + CP 1% + CF 0.6% + $CaCl_2$ 1% and the mixture of these two components are present in table. Comparing the results shows that the FTIR spectrum of the two-claysoil, clay soil + CP 1% + CF 0.6% + $CaCl_2$ 1% composits includes all the characteristics bands of each of two components. FTIR spectra also confirm that in general the traced Si–O–Si bands were larger in sample with clay soil + CP 1% + CF 0.6% + $CaCl_2$ 1% particles which is consistent with results from the compression test (Table 5).

4 Conclusion

A series of test were performed to study the effect of coir pith, $CaCl_2$ with coir fiber reinforcement on the strength behavior of untreated and chemically treated soils. The effect of coir pith, $CaCl_2$, coir fiber inclusion on index properties, OMC, MDD, UCS of soil specimens was determined. A microstructural property was investigated for untreated soil and chemically treated soil by using SEM analysis, XRD, FTIR analysis. The following are the conclusions from these tests. Modified coir fiber

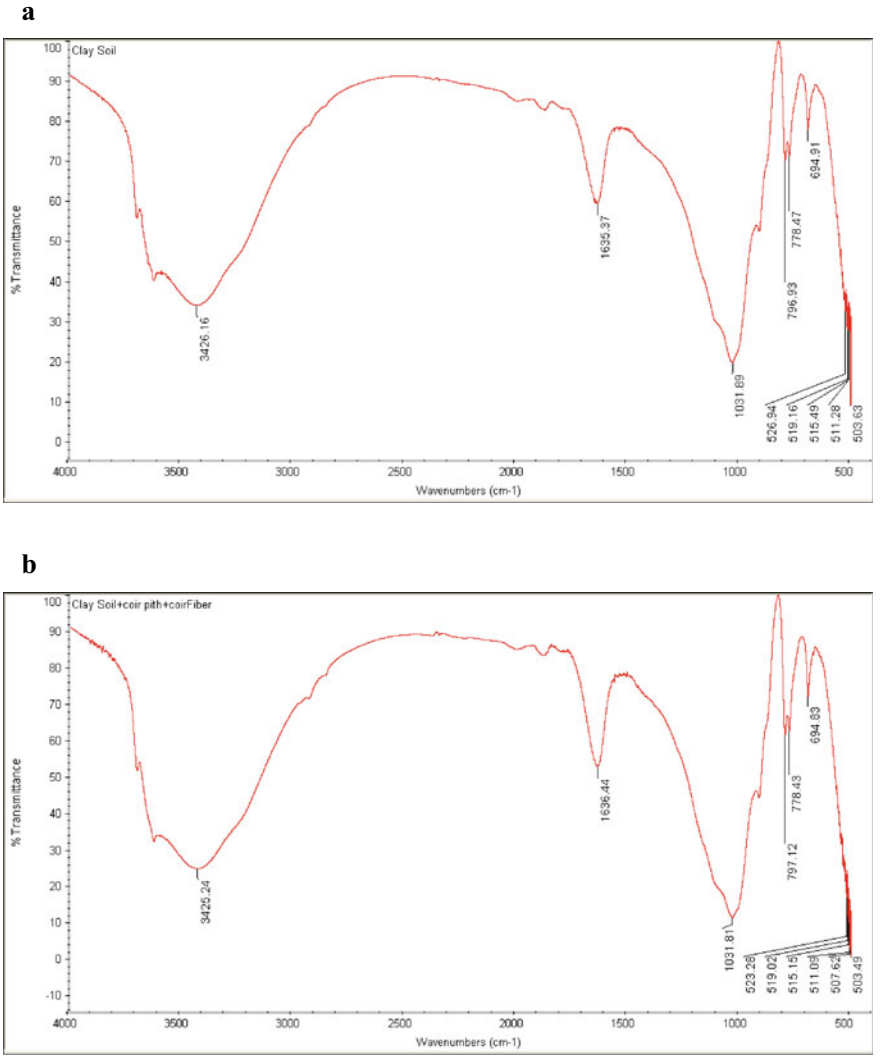

Fig. 8 **a** FTIR analysis for untreated soil, **b** FTIR Analysis for treated soil with CP 1% + CF 0.6% + $CaCl_2$

increases the breaking stress by 122.4535 N/mm^2 to 367.35 N/mm^2 with $Fecl_3$ 0.5 m and NaOH 0.5 M, respectively. The inclusion of Calcium Chloride with coir waste causes an increase in the UCS. The increase in strength of combination of (soil + coir poith 1% + coir fiber 0.6% + $CaCl_2$ 1%) is much more than the sum of the increase caused by them individually. Based on the favorable results obtained, it can be concluded that the expansive soil with coir waste and $CaCl_2$ can be considered as an efficient method for ground improvement.

Table 5 Properties obtained for optimum soil-Coir Pith-Coir Fiber-$CaCl_2$ Mix

Si no	Properties	Plain soil	99% soil + 1% coir pith	99.4% soil + 0.6% coir fiber	99% soil + 1% $CaCl_2$	97.4% soil + 1% coir pith + 0.6% coir fiber + 1% $CaCl_2$
1	Liquid limit (%)	76	69	67.4	58.5	56.35
2	Plastic limit (%)	16.88	19.5	20.25	26.94	29.45
3	Shrinkage limit (%)	10.25	15	17	17	20.25
4	Plasticity index (%)	55.12	49.5	40	31.56	26.9
5	Shrinkage index (%)	6.63	4.5	3.25	9.44	9.2
6	MDD (kg/m^3)	15.39	16.54	15.87	15.31	16.1
7	OMC (%)	22.95	21.35	22.24	24.7	21.87
8	UCS (kPa)	103.96	280.83	278.85	398.16	459.09

References

1. Viswanadham BVS, Phanikumar BR, Mukherjee RV (2009) Swelling behaviour of a geofiber reinforced expansive soil. Geotex Geomembranes:73–76
2. Al Akhras NM, Attom MF, Al-Akhra KM, Malkawi AIH (2008) Influence of fiber on swelling properties of clayey soils. Geosynth Int:306–309
3. Puppala A, Hoyos L, Viyanant C, Musenda C. Fiber and fly ash stabilization methods to treat soft expansive soils. Soft Ground Technol:136–145
4. Cokca E (2001) Use of class C fly ashes for the stabilization of an expansive soil. J Geotech Environ Eng:568–573
5. Suresh K, Padmavathi V, Sultana A (2009) Experimental study on stabilization of black cotton soil with stone dust and fibers. IGC 2009, Guntur, India, pp 502–505
6. Phani Kumar BR, Sharma RS, M.ASCE (2004) Effect of fly ash on engineering properties of expansive soils. ASCE J Geotech Geo Environ Eng:764–767
7. Kate JM (2005) Strength and volume change behavior of expansive soils treated with fly ash. ASCE GSP 136 innovations in grouting and soil improvements
8. Leite R, Cardoso R, Cardoso C, Cavalcante E, de Freitas O (2016) Lime stabilization of expansive soil from Sergipe Brazil. In: E3S Web of Conferences 9, E-UNSAT
9. Puppala AJ, Wattanasanticharoen E, Punthutaecha K (2003) Experimental evaluations of stabilisation methods for sulphate rich expansive soils. Ground Improv:25–35
10. . RamanaMurty V, Hari Krishna P (2007) Amelioration of expansive clay slopes using calcium chloride. J Mater Civ Eng, ASCE:19–25
11. Aldaood A, Bouasker M, Al-Mukhtar M (2014) Free swell potential of lime-treated gypseous soil. Appl Clay Sci:93–103
12. Ragab Azzam W (2014) Durability of expansive soil using advanced nanocomposite stabilization. Int J Geomate:927–937

13. Hessam Bahmani S, Farzadnia N, Asadi A, Huat BBK (2016) The effect of size and replacement content of nanosilica on strength development of cement treated residual soil. Constr Build Mater: 294–306
14. Sivakumar Babu GL, Vasudevan AK, Saida MK (2008) Use of coir fibers for improving the engineering properties of expansive soils. J Nat Fibers 5(1):61–75
15. Vinod P, Bhaskar AB (2009) Effective use of coir products in ground improvement. In: IGC 2009 Guntur India, pp 443–445
16. Rajan A, Emilia Abraham T (2006) Coir fiber–process and opportunities. J Nat Fibres 3:29–41
17. Prasanna S et al (2017) Soil reinforcement using coconut shell ash: a case study of indian soil. J Civ Eng Constr 6(2):73–78
18. Bahmani S et al (2016) The effect of size and replacement content of nanosilica on strength development of cement treated residual soil. Constr Build Mater 118:294–306

Mitigation of Alkali Induced Heave in Transformed Kaolinitic Clays Using Fly Ash and GGBS

P. Lakshmi Sruthi and P. Hari Prasad Reddy

Abstract The paper aims to focus on the possibility of using industrial by-products like fly ash (FA) and ground granulated blast furnace slag (GGBS) for stabilizing the induced heave in alkali transformed kaolinitic clays i.e., red earth (ATRE) and kaolin (ATK). Effective usage of industrial by-products such as FA and GGBS for reducing the alkali induced heave in clays can be best solution for reducing the carbon footprint resulting from other stabilizers such as lime. Furthermore, proceeding toward incorporating by-products for stabilization purposes will also reduce the depletion of natural resources. Studies on transformed clays showed unexpected changes in swelling behavior when inundated with water and alkali solution. Samples that exhibited high swelling (i.e., ATRE with 0.1 N, 1 N NaOH, and ATK with 0.1 N NaOH) were selected for carrying out stabilization studies. Decrease in swelling was noticed with the addition of FA and GGBS. Alkali transformed red earth (ATRE) treated with 20% fly ash showed an overall decrease in swelling of about 86% in 0.1 N and 1 N NaOH, whereas 20% GGBS showed a reduction of about 75% in both solution. Furthermore, alkali transformed kaolin (ATK) inundated with 0.1 N NaOH solution showed a reduction in swelling of about 63% and 77% with addition of 10% FA and 10% GGBS, respectively. The reduction in swelling with FA and GGBS is attributed to the formation of sodium and calcium-based mineral polymers, respectively. These polymers bind the partially reacted and unreacted particles restricting the alkali induced swell. XRD and SEM studies highlighted the micro level alterations.

Keywords Swelling · Fly ash · GGBS · NaOH · XRD · SEM

P. Lakshmi Sruthi (✉) · P. Hari Prasad Reddy
Department of Civil Engineering, NIT Warangal, Warangal 506004, India
e-mail: plakshmisruthi@gmail.com

P. Hari Prasad Reddy
e-mail: ponnapuhari@gmail.com

K. R. Reddy et al. (eds.), *Sustainable Environment and Infrastructure*, Lecture Notes in Civil Engineering 90, https://doi.org/10.1007/978-3-030-51354-2_32

1 Introduction

Chemically contaminated soil often experiences direct or indirect effects, which even leads to substructure failures. Several case studies related to leakage of chemical contaminants like acids [1–5] and alkalis [6–9] due to accidental spillage from industries were widely documented. Further, number of studies on abnormal volume change behavior of alkali-contaminated clays was reported [10–12]. From the observed results of induced swelling by alkali, efforts were made by researchers to control alkali induced heave using salt solutions. Rao and Rao [10] suggested $FeCl_3$ treatment to control alkali effect in red earth. However, studies carried out by Sivapullaiah and Manju [13] showed that $FeCl_3$ treatment becomes ineffective under continuous alkali exposure. Further studies on usage of KCl and $MgCl_2$ salts to control alkali induced volume changes in black cotton soil showed that mineralogical alterations leading to swelling cannot be inhibited [14]. From the abovementioned studies, it is clear that the role of chemical stabilization using salt solutions to control alkali induced heave is insignificant. Moreover, looking for alternate materials to control alkali induced volume changes, studies were carried out using lime, fly ash, and GGBS [15–17]. In recent years, successful application of FA and GGBS to control alkali induced swelling in kaolinitic clays was reported [18, 19]. However, the effectiveness of FA and GGBS to control the alkali induced heave in alkali transformed kaolinitic clays (ATKC's) is unrevealed. Thus, the focus of this research is to investigate the efficacy of the stabilizing material in controlling the alkali induced heave in transformed clays.

2 Materials

2.1 Materials Used

Two kaolinitic clays, namely, red earth (RE) and kaolin (K), were selected for the present investigation. Red earth, naturally available clay was collected from Warangal, India at a depth of 1.5 m from ground level. Commercially available kaolin was collected from Godavari mines and minerals, Visakhapatnam, India.

Fly ash (class F) collected from National Thermal Power Corporation, Telangana and Ground granulated blast furnace slag (GGBS), the by-product of steel industry were selected as heave controlling agents in this study. 10% and 20% of fly ash and GGBS were considered as the quantities of stabilizing agents used.

2.2 Contaminant Used

Sodium hydroxide solution of 0.1 N and 1 N concentration was considered as a contaminant.

2.3 One-Dimensional Free Swell Test

One-dimensional Oedometer tests were undertaken to evaluate the swell potential of stabilized clays and the results were compared with those of unstabilized samples. One-dimensional consolidation test was performed according to Puppala [20]. Studies carried out on swelling behavior of alkali transformed red earth samples (ATRE-0.1N, ATRE-1N and ATRE-4N) and alkali transformed kaolin samples (ATK-0.1N, ATK-1N and ATK-4N) inundated with respective (0.1, 1 and 4 N) concentrations of alkali solution revealed that the percentages of swell observed in ATRE's are 17% (ATRE-0.1N-0.1N), 14% (ATRE-1N-1N) and 7% (ATRE-4N-4N) whereas ATK's are 16% (ATK-0.1N-0.1N), 8% (ATK-1N-1N) and 7% (ATK-4N-4N). Among the above-mentioned samples, those samples that have exhibited higher percentages of swell (ATRE-0.1N-0.1N, ATRE-1N-1N and ATKC-0.1N-0.1N) were only selected for carrying out stabilization studies with fly ash and GGBS.

2.4 Microscopic Techniques

X-ray diffraction (XRD): Samples were analyzed from 6° to 70°, at a step size of 0.01, using copper k-alpha radiation, PANalytical X-ray Diffractometer.

Scanning electron microscopy (SEM): SEM–TESCAN model microscopy equipment was used for finding out the morphological alterations in the clay samples.

3 Results and Discussions

3.1 Effect of FA and GGBS on Swelling Behavior of ATRE Inundated with 0.1 N NaOH Solution

Figure 1a illustrates the effect of FA and GGBS on the swell behavior of RE and ATRE inundated with 0.1 N NaOH solution. Red earth becomes aggressive and exhibited swelling of 27% when inundated with 0.1 N NaOH solutions (RE-0.1N). NaOH solution releases OH^- ions, which gets adsorbed on the edges that make the particles negative in charge. This increase in negative charge leads to dispersion of soil particles (Face-to-Face association), which results in an increase in swelling

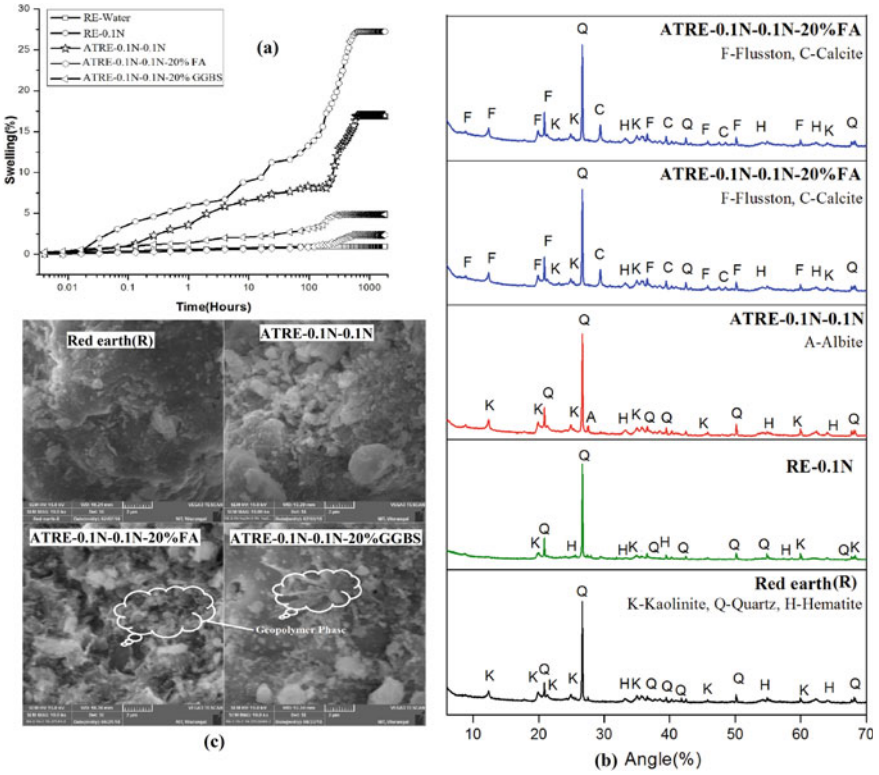

Fig. 1 **a** Swelling behavior **b** XRD patterns **c** SEM images of RE and ATRE-0.1N-0.1N stabilized with 20% FA and 20% GGBS

[21]. Red earth transformed with 0.1 N alkali (represented as ATRE-0.1N) exhibited swelling of about 17% when inundated with 0.1 N solution as pore fluid (ATRE-0.1N-0.1N). The decrease in swelling of ATRE-0.1N-0.1N compare to RE-0.1N is explained as follows: During the transformation process (before sample subjected to swelling) partial dispersion of soil particles i.e., Face-to-Face association takes place [21], which is not reflected during swelling. To effectively reduce the observed swell, 10 and 20% quantities of fly ash and GGBS were considered. But, it was noticed that 10% fly ash and GGBS were not effective in reducing the swell to a greater extent. So, 20% fly ash and GGBS are selected for ATRE samples and the same are presented in Fig. 1a.

From Fig. 1a it is observed that ATRE-0.1N showed a decrease in swelling of about 88% and 75% with the addition of 20% fly ash (ATRE-0.1N-0.1N-20% FA) and GGBS (ATRE-0.1N-0.1N-20% GGBS), respectively, upon inundated with 0.1 N NaOH solution. The reduction in swelling in transformed clay (ATRE-0.1N-0.1N) with the addition of FA and GGBS is due to the replacement of clay with fly ash/GGBS and initiation of mineral polymerization. But high percentage reduction, which is

more than the proportional addition of fly ash/GGBS, indicates that it is majorly due to mineral polymerization. With addition of fly ash, OH^- ions released from NaOH show more inclination towards the dissolution of silica and alumina present in fly ash rather than red earth. The dissolved silica and alumina combines with Na^+ ions to form the cementitious gels, which bind the partially reacted and unreacted particles, ultimately controlling the swelling. In case of GGBS, formation of calcium-based aluminium silicate hydrate gels subsequently resulted in less swelling due to its cementitious properties. The obtained results are well supported by XRD (Fig. 1b) and SEM (Fig. 1c) studies.

XRD patterns of RE and ATRE-0.1N-0.1N stabilized with 20% FA and 20% GGBS were shown in Fig. 1b. RE predominantly contains quartz along with kaolinite and hematite. ATRE-0.1N-0.1N exhibited new mineral peak pertaining to albite. New peaks pertaining to flusston along with quartz and kaolinite were observed in ATRE-0.1N-0.1N-20%FA. Though new mineral is formed, the reduction in swelling is mainly due to the presence of binder phase formed in mineral polymerization. Addition of 20% GGBS to ATRE-0.1N-0.1N, resulted in the formation of garronite (N-C-A-S-H: sodium calcium aluminate silicate hydrate). Presence of garronite peaks indicates the reaction between aluminosilicates and calcium in GGBS that completely binds the particles, thus arresting swell. Thus 20% addition of FA and GGBS controlled the swelling to a greater extent in ATRE-0.1N-0.1N.

Micrograph of red earth (RE) exhibited a compacted and aggregated form of morphology (Fig. 1c). Weathering was observed in the micrograph of ATRE-0.1N-0.1N. SEM image of ATRE-0.1N-0.1N-20% FA revealed the compacted form where voids became close with the formation of binder phases. ATRE-0.1N-0.1N-20% GGBS projected the transformation of morphology into well compacted stable form along with binder phase with almost no voids on its texture and thus represents the arresting of swelling.

3.2 Effect of FA and GGBS on Swelling Behavior of ATRE Inundated with 1 N NaOH Solution

Figure 2a illustrates the effect of FA and GGBS on the swell behavior of RE and ATRE inundated with 1 N NaOH solution. RE exhibits a swelling of about 25% when inundated with 1 N NaOH (RE-1N). In case of RE-1N it is observed from XRD that dissolution of iron oxide coatings is initiated. During this process, OH− ions from NaOH react and leach the iron oxide coating which slightly disperses the particle. Subsequently, the remaining OH^- ions get adsorbed on the edges and make the particles negative in charge. This increase in negative charge leads to dispersion of soil particles (Face-to-Face association), which results in an increase in swelling. However, the marginal decrease in swelling compare to RE-0.1N is due to the accumulation of excess sodium ions.

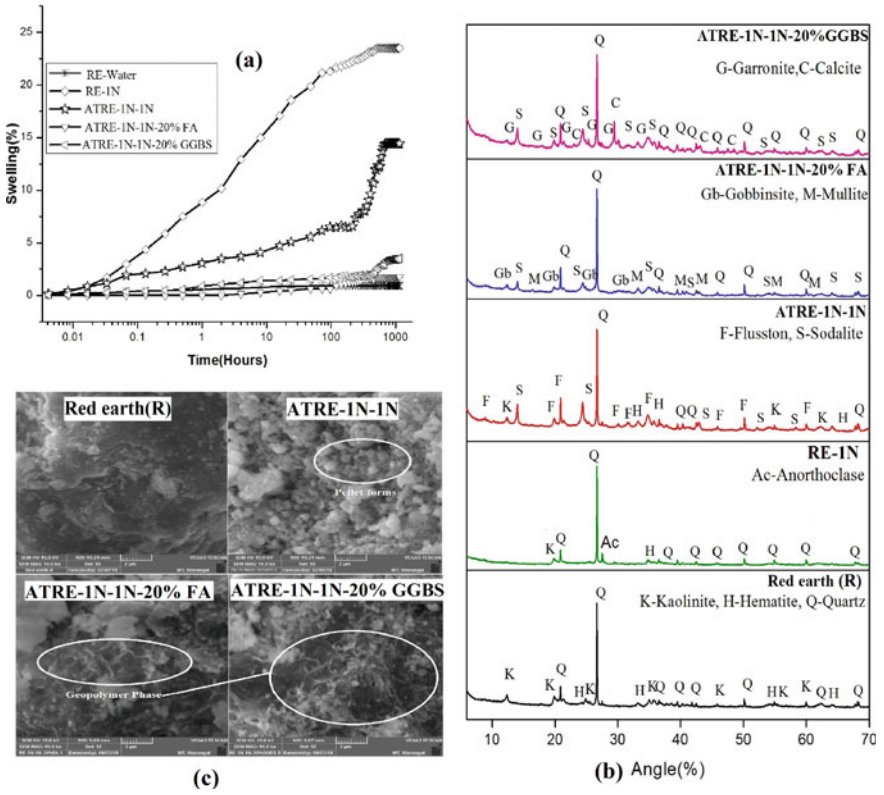

Fig. 2 **a** Swelling behavior **b** XRD patterns **c** SEM images of RE and ATRE-1N-1N stabilized with 20% FA and 20% GGBS

Red earth transformed with 1 N alkali (represented as ATRE-1N) exhibited a swelling of about 14.5% when inundated with 1 N solution (ATRE-1N-1N) as pore fluid. The reduction in swelling in ATRE-1N-1N compared to RE-1N is due to dispersion of particles and dissolution of iron oxide coatings during the transformation period itself, which didn't reflect when subjected to swelling. ATRE-1N exhibited decrease in swelling of about 86% and 76% with the addition of 20% fly ash (ATRE-1N-1N-20% FA) and 20% GGBS (ATRE-1N-1N-20% GGBS), respectively, upon inundated with 1 N NaOH solution. The reduction in swelling is almost same as the percentage reduction in ATRE-0.1N-0.1N-20% FA (88%) and ATRE-0.1N-0.1N-20% GGBS (75%). This indicates that effect of concentration of inundating solution on the swelling behavior has been dominated by the mineral polymerization. The reduction in swelling behavior with that addition of fly ash and GGBS is mainly due to the mineral polymerization over replacement with fly ash/GGBS as explained in Sect. 3.1.

XRD patterns of RE, ATRE-1N-1N stabilized with 20% FA and 20% GGBS were shown in Fig. 2b. XRD pattern of ATRE-1N-1N showed the new peaks pertaining to

flusston and sodalite. Formation of zeolitic minerals (i.e., sodalite) is responsible for the enhanced swelling in ATRE-1N-1N (Fig. 2a). Interesting traces of cementitious compounds were observed ATRE-1N-1N-20% FA and ATRE-1N-1N-20% GGBS. This evidences the reaction between, silicates present in the ATRE; silica in FA; calcium in GGBS under alkali conditions. Formation of gobbinsite and mullite; garronite and calcite were evidenced ATRE-1N-1N-20% FA and ATRE-1N-1N-20% GGBS, respectively. Mullite remains in ATRE-1N-1N-20% FA which indicates the unreacted particles in clay and fly ash mix matrix. Addition of 20% fly ash controlled the swelling significantly where most of the sodalites are well arrested in ATRE-1N-1N-20%FA. This indicates that, large reduction in swelling is due to the formation of significant component of the binder phase. Formation of calcium-based garronite (N-C-A-S-H: sodium calcium aluminate silicate hydrate) is primly responsible for the reduction in swell in ATRE-1N-1N with the addition of 20% GGBS (ATRE-1N-1N-20% GGBS).

Micrograph of RE, ATRE-1N-1N stabilized with 20% FA and 20% GGBS have been presented in Fig. 2c. SEM image of ATRE-1N-1N has been observed with weathering and also highlights the zeolite mineral i.e., sodalite formations with clear pellet morphology. The mineral polymerization phases were well identified with web- or net- formations in both ATRE-1N-1N-20% FA and ATRE-1N-1N-20% GGBS, respectively. These web/net formations clearly bind the particles thus arresting swell.

3.3 Effect of FA and GGBS on Swelling Behavior of ATK Inundated with 0.1 N NaOH Solution

Figure 3a illustrates the effect of fly ash and GGBS on the swell behavior of K and ATK inundated with 0.1 N NaOH solution. Kaolin exhibited swelling of 16% when inundated with 0.1 N NaOH (K-0.1N) solution. The adsorption of OH^- ions on the edges of the particles is responsible for dispersion of particles, which enhanced swelling. Kaolin transformed with 0.1 N alkali solution (represented as ATK-0.1N) exhibited swelling of about 11% upon inundated with 0.1 N NaOH (ATK-0.1N-0.1N), which is less than the swelling exhibited by K-0.1N. This decrease in swelling is mainly due to (i) particle orientation which enhances swelling initiated during transformations (ii) Non-leaching of calcite coatings, which induces swelling is completely absent as the calcite coatings remained unleached (Fig. 3b). ATK-0.1N exhibited decrease in swelling of about 63% and 77% with the addition of 10% fly ash (ATK-0.1N-0.1N-10% FA) and 10% GGBS (ATK-0.1N-01.N-10% GGBS), respectively. The percentage reduction (about 63%) in ATK-0.1N-0.1N-10% FA is more than the proportional increase in the fly ash content, reveals that it is more due to cementation of reaction products due to mineralogical changes, by pozzolanic fly ash. Also significant reduction in swelling (77%) in ATK-0.1N-0.1N-10% GGBS is predominantly due to reaction between alumina silicates from the source of ATK-0.1N and calcium from GGBS under alkali conditions, which leads to formation of

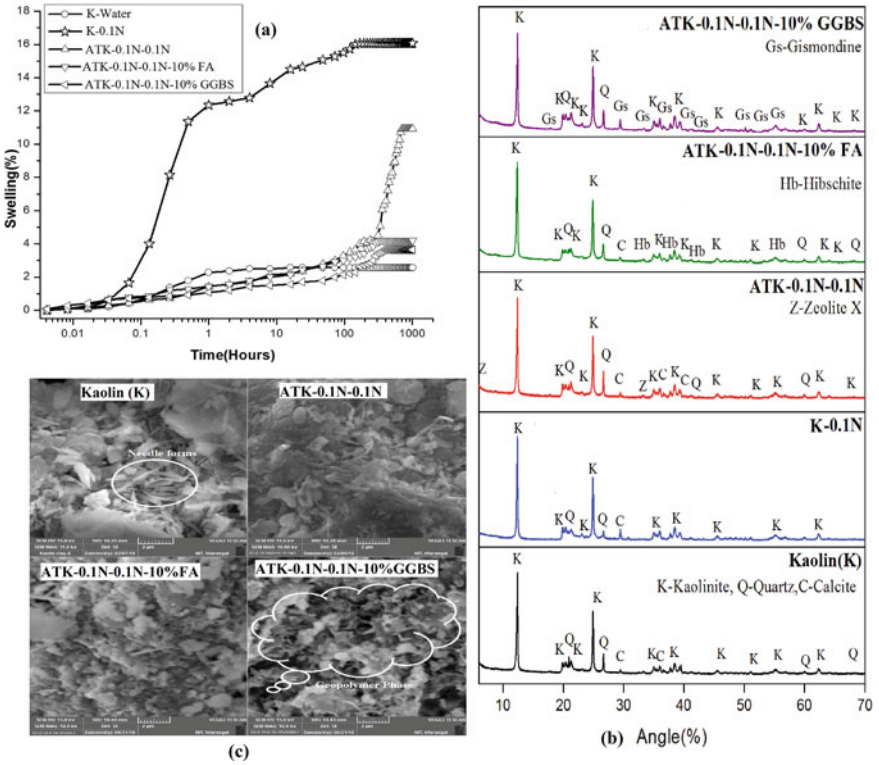

Fig. 3 **a** Swelling behavior **b** XRD patterns **c** SEM images of Kaolin (K) and ATK-0.1N-0.1N stabilized with 10% FA and 10% GGBS

cementitious mineral polymers. Partially reacted particles along with unreacted particles get binded by the cementitious compounds, which ultimately controlled swelling. Samples collected after the swell tests were analyzed to identify the mineralogical and morphological alterations using XRD and SEM, respectively.

XRD patterns of samples K and ATK-0.1N-0.1N NaOH mixed with 10% FA and 10% GGBS were shown in Fig. 3b. Kaolin (K) predominantly consists of kaolinite peaks along with less intense peaks of quartz and calcite. Formation of new mineral zeolite X was observed in XRD pattern of ATK-0.1N-0.1N. Zeolite X is a sodium aluminum silicate mineral formed due to dissolution of silica and alumina from kaolinite mineral which enhanced swelling. Mixing with 10% FA and 10% GGBS to ATK-0.1N-0.1N resulted in the formation of hibschite (C-A-S-H: Calcium Aluminum Silicate Hydroxide) and gismondine (C-A-S-H: Calcium Aluminum Silicate Hydrate) respectively. These calcium-based minerals are responsible for presence of binder phase formed in mineral polymerization. These mineralogical changes were corroborated with SEM images.

Micrograph of kaolin (K) exhibited highly loose fibrous structure with needle morphology (Fig. 3c). Micrograph of ATK-0.1N-0.1N showed dispersed morphology

along with needle formations. Geopolymer phase was clearly noticed in ATK-0.1N-0.1N mixed with 10% GGBS whereas no clear identification of binder phase was noticed in ATK-0.1N-0.1N mixed with 10% FA.

From the above results and discussion it is observed that the amount of binding material required for ATK is relatively less than that of ATRE. Kaolin, commercially available clay, possessing high amount of crystalline kaolinite mineral doesn't easily get attack by alkali compare to red earth, naturally available clay, containing less kaolinite mineral with other impurities. Thus, red earth exhibits high-induced swell compare to kaolin. Furthermore, kaolin requires lesser amount of FA/GGBS due to direct attack of alkali on binding materials leading to mineral polymerization. In red earth, alkali attacks both clay and FA/GGBS demanding higher amounts of binding materials for mineral polymerization.

4 Conclusions

Addition of FA/GGBS to ATKC's effectively reduced the swelling under alkaline conditions: 20% FA/GGBS in ATRE-0.1N-0.1N/ATRE-1N-1N and 10% FA/ GGBS in ATK-0.1N-0.1N.

XRD studies revealed that sodium and calcium-based geo polymers formed are responsible for the effective reduction of induced swelling in ATKC's.

SEM studies revealed web or net formations highlighting the mineral polymerization in ATKC's.

Research highlights that kaolin possessing higher amount of crystalline material requires lesser amount of binding material to mitigate alkali-induce swell compare to red earth with less crystalline material.

References

1. Lukas RG, Gnaedonger Jr RJ (1972) Settlement due to chemical attack of soils. In: Proceedings of ASCE specialty conference on performance of earth and earth supported structures 1. ASCE, Purdue University, Lafayette, Lundiana, pp 1087–1104
2. Sridharan A, Nagaraj TS, Sivapullaiah PV(1981) Heaving of soil due to acid contamination. In: Proceedings of 10th international conference on SM and FE 6. Stockholm, pp 383–386
3. Joshi RC, Pan X, Lohita RP (1994) Volume change in calcareous soils due to phosphoric acid contamination. In: Proceedings of 13th international conference on SM and FE, 4. New Delhi, pp 1569–1574
4. Assa'ad A (1998) Differential upheaval of phosphoric acid storage tanks in Aqaba Jordan. J Perform Constr Facil 12:71–76
5. Schuiling RD, Van Gaans PFM (1997) The waste sulfuric acid lake of the TiO2-plant at Armyansk, Crimea, Ukraine. Part I. Self-sealing as an environmental protection mechanism. Appl Geochem 12:181–186

6. Volkov FE (1977) Variation in the composition and physico-mechanical properties of clayey soils resulting from interaction with alkali solutions. Author's Abstract of Dissertation for Candidate of Geologic and Mineralogical Sciences Moscow
7. Sivapullaiah PV, Allam MM, Sankara G (2004) Structural distortion due to heaving of foundation soil induced by Alkali contamination. In: Proceedings of the international conference on structural and foundation failures 1. Singapore, pp 601–611
8. Sibley MH, Vadgama NJ (1986) Investigation of ground heave at ICI Mond division, Castner-Keller Works, Runcorn. Geol Soc London, Eng Geol Spec Pub 2:367–373
9. Chunikhin VG, Mavrodi VKh, Kramarenko OA, Dobromil'skaya NG (1988) Effect of leakage of industrial alkali solutions on the construction properties of soils. Soil Mech Found Eng 25(6):559–561
10. Rao SM, Rao KSS (1994) Ground heave from caustic soda solution spillage- A case study. Soils Found 34(2):13–18
11. Sivapullaiah PV, Manju (2007) Induced swelling of kaolinitic soil in alkali solution. Soils Found 47:59–66
12. Sivapullaiah PV, Reddy PHP (2009) Fly ash to control alkali induced volume changes in soils. Proc Inst Civil Eng – Ground Improv 162:167–173
13. Sivapullaiah PV, Manju (2006a) Ferric chloride treatment to control alkali induced heave in weathered red earth. Geotech Geol Eng 23(5):1115–1130
14. Sivapullaiah PV, Reddy PHP (2010) Potassium chloride treatment to control alkali induced heave in black cotton soil. Geotech Geol Eng 28(1):27–36
15. Sivapullaiah PV, Manju (2006b) Lime treatment to control alkali induced heave in soils. Proc Inst Civ Eng, Ground Improv 10(1):31–37
16. Sivapullaiah PV, Reddy PHP, Ramesh HN (2008) Mitigation of alkali induced heave in rectorite soil with fly ash. Geotech Waste Manag Remediat, Geotech Spec Pub 177:700–707
17. Ghosh P, Kumar H, Biswas K (2016) Fly ash and kaolinite-based geopolymers: processing and assessment of some geotechnical properties. Int J Geotech Eng 10(4):377–386
18. Vindula SK, Chavali RVP (2018) Role of fly ash in control of alkali induced swelling in kaolinitic soils: a micro-level investigation. Int J Geotech Eng 12(1):46–52
19. Vindula SK, Chavali RVP, Reddy PHP, Srinivas T (2017) Ground granulated blast furnace slag to control alkali induced swell in kaolinitic soils. Int J Geotech Eng:1–8
20. Puppala AJ, Napat I, Rajan KV (2005) Experimental studies on ettringite-induced heaving in soils. J Geotec Geoenviron Eng 131(3): 325–337
21. Mitchell JK (1993) Fundamentals of soil behavior, 2nd edn. Wiley, New York, NY

Using Neural Model for Mimicking the Behavior of Hybrid Foundation

Vikas Kumar and Arvind Kumar

Abstract The main goal of Sustainable foundation is in term of cost and less use of natural resources as this field involves intensive consumption of energy and huge amount of natural resources. Hybrid foundations are complex foundation in terms of design and have significance in modern infrastructure development. These are used in situation where structures to support heavy load and the resulting settlement should remain within the acceptable limit. The analysis of this hybrid system of foundation is complex because there are elements such as pile, raft, and soil that affect the resultant settlement. This is because of inevitable interaction between soil and other elements and hybrid foundation. To understand this complex behavior neural models have been constructed to figure out the relative importance of different parameters with reference to load applied under various conditions. These models mimic the experimental setup and predict the resultant settlement in different conditions. The designing of neural models is based on the extent to incorporate experimental set up in their architecture design. The final optimized model predicts the settlements under various conditions and shows the relative effect of changeable (varied) parameters on settlement.

Keywords Hybrid foundation · Neural model · Settlement

1 Introduction

With rapid development in fast growing and expanding country like India, construction industry is in need of high rise buildings in short period of time, and therefore concept of hybrid foundation is found suitable for development. With parallel vision of smart cities and affordable housing, the use of piled-raft foundation has been done

V. Kumar (✉)
Civil Engineering Department, MMMUT, Gorakhpur, India
e-mail: vikaskumarnitk@gmail.com

A. Kumar
Civil Engineering Department, NIT, Jalandhar, India
e-mail: agnihotriak@nitj.ac.in

K. R. Reddy et al. (eds.), *Sustainable Environment and Infrastructure*, Lecture Notes in Civil Engineering 90, https://doi.org/10.1007/978-3-030-51354-2_33

aggressively by construction industry. The economical aspect is captured effectively in the process of optimizing the number of piles. Soil conditions at many instances in place of construction are not feasible and proper; hence soil improvement methods like piled-raft is used. Piled-raft is an interesting method to provide effective and economical section where large size buildings are required in less area and also the cost needs to be lowered significantly. For any construction, the foundation system is the most important aspect to ensure safety and life of structure. Sustainability in geotechnical engineering is described by the resources used in a project. Limiting the number of pile by optimum performance of piles in piled-raft foundation reduces the quantity and cost of materials used for constructing the pile.

Foundation design of structure depends on the behavior of soil i.e., nature of soil strata. Shallow foundation on those sites where ground improvement is done shows mixed performance as they cannot be designed for heavy load. Various available ground improvement techniques like; use of geosynthetic material, use of stone column, addition of admixture to improve the bearing capacity of loose soil is also gaining popularity but still axial capacity of foundation cannot be increased for high rise buildings like skyscrapers by such methods. Also there is a chance of differential settlement or tilting when raft is provided below the structure. Structure rested on deep foundation like pile, performed better when piles are penetrated to adequate depth. Also group of pile is provided where all the load of the structure is very high and piles are designed considering the high factor of safety. However the cost of construction increases significantly due to large number of piles requires improving the bearing capacity of liquefy soil.

The concept of hybrid foundation comes into play when the foundation provided should be sufficient to carry the axial load with safety and the settlement should be within permissible limit. Piled-raft foundation is a type of hybrid foundation where the total load coming from superstructure partly shared by raft through contact with soil and reaming load shared by piles through skin friction. Piled-raft foundation is different than the traditional foundation design where the load is carried by either raft only or by pile considering the factor of safety. The main objective of introducing these piles is to reduce the differential settlement where bearing capacity of piled-raft is governed by raft only. In conventional piled-raft design the number of piles required is generally high and load carried by each pile is minimum. When the settlement reducing piles are designed as structural component, a low factor of safety can be applied to the geotechnical capacity of the piles and the raft alone is adequate to bear the load. A piled-raft foundation can be applied to situation when soil profile consists of relatively stiff clay or soil profile consists of dense soil.

Piled-raft foundation is a complex foundation consist of three element of pile raft and soil and for the adequate design of piled-raft system a geotechnical engineer should know the interaction of all these elements with respect to each other. A number of parameter of soil, raft, and piles are to be considered for the effective design of such hybrid system. The evolution of advance computational methods like Artificial Intelligence (AI) based models such as artificial neural networks (ANN) can be used to understand the complex dynamics of foundation system and its behavior under different instances. Use of neural models has been done at large scale in construction

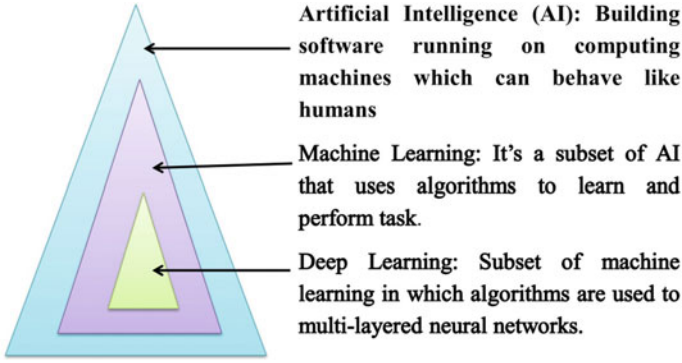

Fig. 1 Umbrella of AI and the terminologies used

and structural engineering over last decade. In past, ANNs have been used in many geotechnical engineering problems such as prediction of settlement, liquefaction, and slope stability prediction, predicting settlements for shallow foundations [1] but there are limited studies done on prediction of settlement in piled-raft foundation system. Therefore, in this study for understanding the dynamics and influence of different parameters used in experimental set up for raft and pile raft were taken [2] and neural model was developed. The AI based models is a wide umbrella which covers machine learning and deep learning. The artificial neural models are basically deep learning models which are used to address many real life problems. The terminology used nowadays under AI can be understood by Fig. 1.

2 Experiments and Data Collection

To study the performance of piled raft foundation series of model tests were conducted in geotechnical lab of NIT Jalandhar. The experimental tests were divided into two categories. In series 1 the tests were conducted on raft foundation whereas in series 2 the test performed on hybrid foundation at 40 and 70% relative density. The experimental set up used for conducting tests on hybrid foundation consists of steel tank of 1.0 m depth. The model raft consist of two square steel plates of 300 × 300 × 25 mm bolted with nine column of 16 mm diameter served as model raft. The modulus of elasticity and Poisson's ratio of steel plates are 2.1×10^8 kPa and 0.20, respectively. The model raft was made with holes threaded internally so that the piles could be put in vertical position at the required spacing of the piles. The model piles used in the experiment are mild steel rod of length 200 mm, 400 mm, and 600 mm and diameter of pile varied as 10 mm, and 20 mm. The modulus of elasticity and Poisson's ratio of the steel pile are kept as 2.1×10^8 kPa and 0.20, respectively, as determined from the data sheet of the technical department of the manufactured company and

also discussed in detail by Kumar and Kumar [2]. Schematic diagram of the model foundation is presented in Fig. 2 and actual experimental set up is shown in Fig. 3.

As can be seen from the schematic that maximum number of piles in series D and E were kept 9 and test are conducted at relative density of 70%. All the experiments conducted under other different scenarios as shown in Table 1 were taken into data preparation process for neural model making.

As can be seen from Table 1, all possible combinations were considered for piled raft foundation under the application of vertical load. The resultant settlement corresponding to load applied was observed.

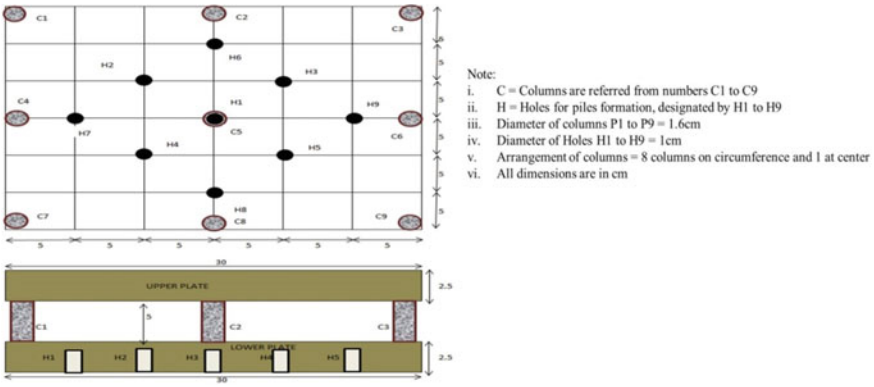

Fig. 2 Schematic for hybrid foundation

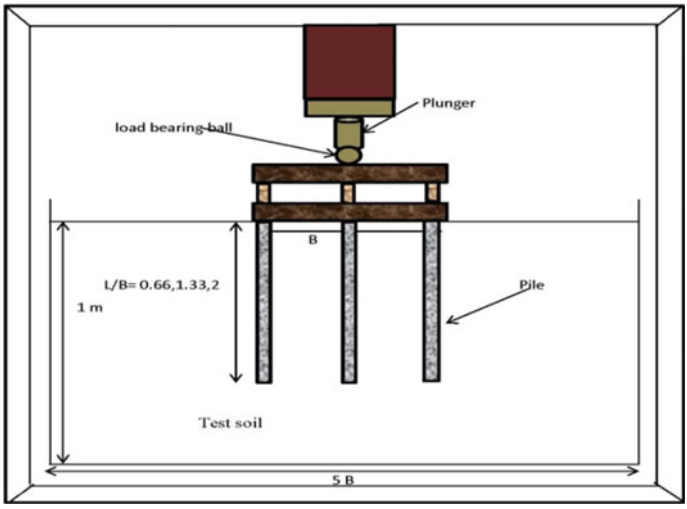

Fig. 3 Actual experimental setup for hybrid foundation

Table 1 Detail of tests on Raft and Piled Raft foundation system

Test series	Foundation	Pattern of piles	Relative density (RD) (%)	Length of pile (L) (mm)	Diameter of pile (ϕ) (mm)	Number of Piles (NP)
A	Raft	–	70	–	–	–
B	Piled-Raft	P1	70	200, 400, 600	10, 20	1
C	Piled-Raft	P2	70	200, 400, 600	10, 20	5
D	Piled-Raft	P3	70	200, 400, 600	10, 20	9
E	Piled-Raft	P4	70	200, 400, 600	10, 20	9

3 Methodology

Based on experimental setup and capturing of results from the proposed set up, the next step was to develop neural models. The neural models were developed for RD 70%. As shown in Table 2, the input and output matrix was prepared for making neural models so that supervised learning and predictions can be done.

3.1 Development of ANN

For modeling the hybrid foundation using neural models feed forward neural network was constructed for predicting the settlement in different cases at RD of 70%. The neural model is developed by first finalizing the data set, then optimizing the number of neurons in hidden layer and then finally training the optimized network. The Levenberg-Marquardt algorithm was used to train the network, input and output matrix as shown in Fig. 4.

As it is very clear from the figure that how different combinations were taken and input matrix of size [283,5] and output matrix of size [283,1] was used and out of that 70% data was used for training and 30% for testing. The topology for neural model was fixed at that instance where the least root mean square error (RMSE)

Table 2 Variables selected as input and output for piled-raft foundation

Inputs	Load (kN), Number of piles L/B Diameter of pile (ϕ)	Total inputs-4
Output	Settlement (mm)	Total output-1

Input Matrix					Output Matrix
Load (kN)	RD (%)	No. of piles	L/B	Diameter of pile (mm)	Settlement (mm)
3	70	1	0.66	10	13.76
15	70	5	2	10	26.78
21	70	9	1.33	20	34.89
23	70	1	0.66	20	88.04

Fig. 4 Some combinations of input and output matrix used in neural model

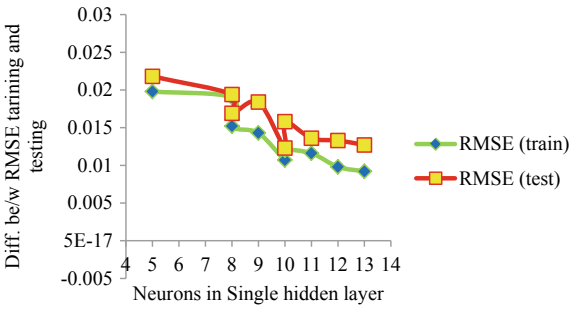

Fig. 5 Behavior of neurons in hidden layer

during testing phase as well as training phase was observed. The behavior of hidden layer for different neurons is shown in Fig. 5.

From Fig. 5, it is very evident that number of neurons in single hidden layer should be kept at 10. Thus final topology obtained was 5-10-1 for predicting settlement in case of hybrid foundation.

3.2 ANN Related Tricks and Points

For ANN models data representation play a crucial role in successful design of neural network [3]. The data points can be discrete, continuous, or both. In this study the values of settlement and loads were continuous while other parameters had discrete values. The data set in this study was normalized between 0.1 and 0.9 using min-max normalization technique. The values were chosen to avoid saturation in the data set [4]. The training is used to optimize the connections i.e., weights and biases with inputs while testing is done on unseen data to predict results and it thus gives the ability of model to accurately predict results. After training, the obtained neural architecture is used to find results for data sets which were not part of training data

set i.e., unseen data. The RMSE is used to assess the performance of neural model and can be calculated using formula given in Eq. (1).

$$\text{RMSE} = \left[\frac{\sum_{i=1}^{N} (\text{Output}_{\text{mesured}} - \text{Output}_{\text{predicted}})^2}{N} \right]^{1/2} \tag{1}$$

4 Results and Discussion

In this study, neural model was developed for predicting settlement in hybrid foundation by optimizing the topology. The predicted results show that neural model constructed good results both during training and testing. The results for training are shown in Figs. 6 and 7.

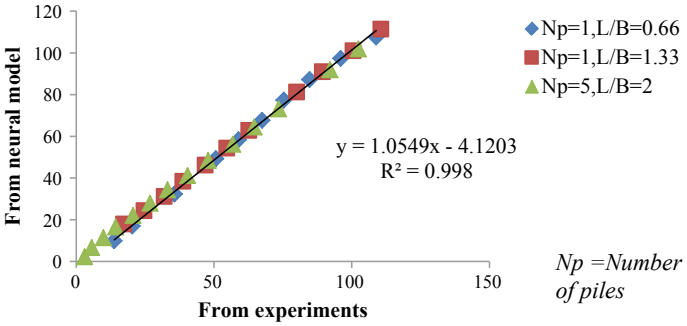

Fig. 6 Predicted settlements versus measured settlements at RD = 70, diameter of pile = 10 mm

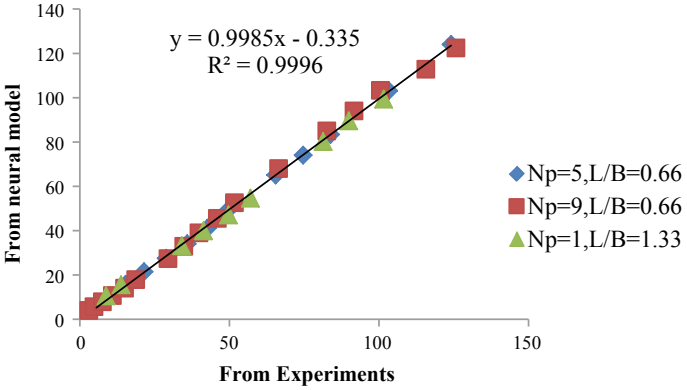

Fig. 7 Predicted settlements versus measured settlements at RD = 70, diameter of pile = 20 mm

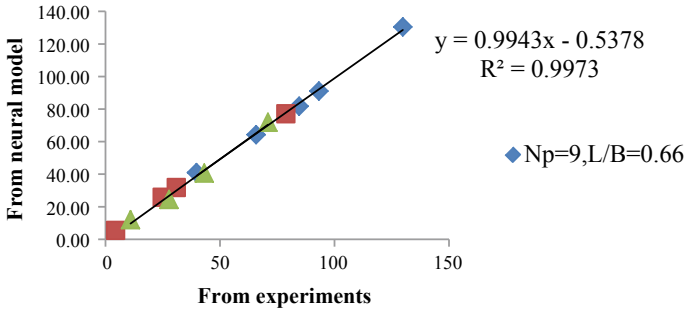

Fig. 8 Predicted settlements during testing at RD = 70, diameter of pile = 10 mm

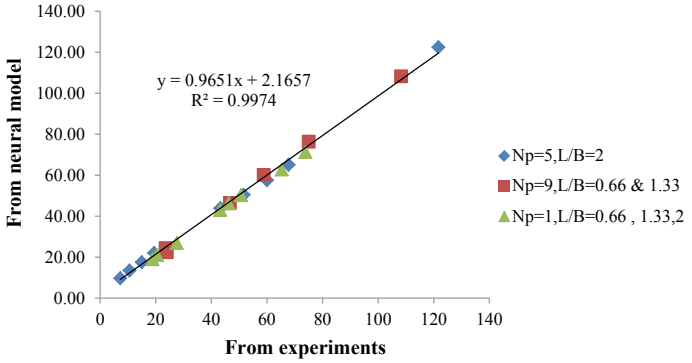

Fig. 9 Predicted settlements during testing at RD = 70, diameter of pile = 20 mm

As can be seen from Figs. 6 and 7 neural model developed is performed well during training phase for all instances with high value of R^2 as shown in graphs.

From Figs. 8 and 9, it can be seen that values predicted by neural model which model has not seen earlier is also very close to experimental values and hence this model can be used for predicting settlement for hybrid foundation in different scenarios.

After getting good predicted results from neural model it is important to understand the effect of individual parameter on settlement that occurs in case of hybrid foundation. By doing sensitivity analysis using the methodology suggested by Garson in 1991 [5] effect of different parameters on settlement can be calculated. The broad categorization for RD and other parameters has been shown in Fig. 10.

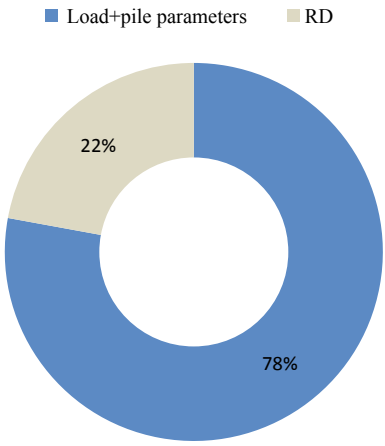

Fig. 10 Effect on settlement by RD and other parameters

5 Conclusions

From this study on hybrid foundation it can be concluded that neural models can be used to predict settlement occurring in such foundation system. For neural models to yield good results, the tuning of parameters and optimization of topology is very important. It is also concluded that relative density alone affects settlement by 22% which means for foundation system the first step is to look for soil strata which coincides with the basic principle of working in geotechnical engineering. Thus, neural model for hybrid foundation can be used successfully in assessing the performance of hybrid foundation system.

References

1. Shahin MA, Maier HR, Jaksa MB (2001) Artificial neural network applications in geotechnical engineering. Aust Geomech 36(1):49–62
2. Kumar V, Kumar A (2018) An experimental study to analyse the behaviour of piled-raft foundation model under the application of vertical load. Innov Infrastruct Solut 3:35
3. Masters T (1994) Practical neural network recipes in C++. Academic Press, Boston, MA
4. Basheera IA, Hajmeerb M (2000) Artificial neural networks: fundamentals, computing, design, and application. J Microbiol Methods 43(1):3–31
5. Garson GD (1991) Interpreting neural-network connection weights. AI Expert 6(7):47–51

Modeling of Degradation and Failure of Earthen Structural Units

Craig D. Foster

Abstract Soil is one of the oldest materials humans have used to build their dwellings and other structures. Almost universally available, easily shaped, highly sustainable, possessing high thermal mass, and easily recyclable, earthen materials are highly sustainable and often a natural choice. Improperly designed, however, earthen structures are subject to erosion, earthquakes, and other types of extreme loading. They may fail in a sudden and brittle manner as well if not properly detailed. We examine the behavior of modern earthen structural elements under shear loading. Cement-stabilized soil block, or compressed earth block, and stabilized rammed earth are used in the number of locations worldwide. In addition to their sustainability, they are cost-effective in many locations. These materials are often stabilized with a small amount of cement for strength and durability. We analyze wall units using a finite element model with embedded strong discontinuities. The bulk material model is a plasticity model that includes both tension and compression caps, a pressure-dependent shear yield surface, differences in triaxial extension and compression strength, isotropic cap hardening, and kinematic shear hardening/softening. The tensile and shear cohesion degradation under large deformation can be modeled. In addition, on detection of localization, an interface may be inserted or activated at the critical orientation. The elements have been extended to include preexisting weak interfaces, such as those between layers of rammed earth, or brick and mortar joints. However, interfaces can also be extended through the bulk material if that path is more critical for a given stress state.

Keywords Rammed earth · Stabilized soil block · Enhanced finite elements

C. D. Foster (✉)
University of Illinois at Chicago, Chicago, IL, USA
e-mail: foster@uic.edu

K. R. Reddy et al. (eds.), *Sustainable Environment and Infrastructure*, Lecture Notes in Civil Engineering 90, https://doi.org/10.1007/978-3-030-51354-2_34

1 Introduction

Soil is one of the oldest materials used by humans have used to build their dwellings and other structures. Even today, nearly one in three individuals live in some form of earthen structure [1]. Almost universally available, easily shaped, highly sustainable, possessing high thermal mass, and easily recyclable, earthen materials are a natural choice for many applications. Improperly designed, however, earthen structures are subject to erosion, earthquakes, and other types of extreme loading. They may fail in a sudden and brittle manner as well if not properly detailed.

Earthen walls can either be constructed in forms, such as rammed earth, or be compressed into bricks, such as in adobe or cement-stabilized soil block (CSSB). The latter types of materials are often joined with standard of soil-cement mortars.

Earthen structural materials exhibit complex behaviors, including differences in shear, tensile, and compressive strength, and both diffuse and localized softening. In addition, these materials possess weak interfaces. Joints between brick and mortar in masonry materials are the most obvious example, but rammed earth also has weak interfaces between compacted layers (Fig. 1).

In this paper, we model earthen structural walls under shear loading. We focus on masonry materials here, which generally have more interfaces, both horizontal and vertical. The bulk material model is adapted from a complex model for geomaterials, accounting for many of the behaviors described above. It also includes localized deformation on surfaces within the material. The same model is used for both preexisting weak interfaces and for interfaces that may propagate through the bulk material, though the material properties may be different. These models are input into an enhanced finite element code that tracks propagating discontinuities. Finally, an example of an earthen masonry wall is run to examine the performance of the model and the response of such a wall to shear loading.

Fig. 1 The interior of a stabilized soil block building on the campus of Indian Institure of Science, Bangalore

2 Material Model

This section details model of the bulk earthen material, along with the surface model for both existing and new interfaces.

2.1 Bulk Material Model

The bulk material model is adapted from the Sandia Geomodel [2, 3]. The model has been modified with a tension cap [4] to better fit tension behavior. We review the essential ingredients of the model here, but the reader is referred to the above references for more details on the model.

The backbone of the model is a nonlinear shear failure surface F_f of the form

$$F_f(I_1) = A - C\exp(BI_1) - \theta I_1$$

where I_1 is the first invariant of the stress tensor and A, B, C, and θ are material parameters. The initial yield is offset by a material parameter N. The surface is also modified by tension and compression cap functions F_c

$$F_c = 1 - H(\kappa - I_1)\left(\frac{I_1 - \kappa}{X - \kappa}\right)^2 - H\left(I_1 - I_1^t\right)\left(\frac{I_1 - \kappa_t}{X_t - I_1}\right)^2$$

Here, H is the Heaviside function, κ and κ_T are material parameters, and X and X_T are related to κ and κ_T, respectively, by

$$X(\kappa) = \kappa - RF_f(\kappa)$$

$$X_T(\kappa_T) = \kappa_T - SF_f(\kappa_T)$$

where R and S are material parameters defining the aspect ratio of the ellipse. The yield surface is also adjusted by a third-invariant modifying function of the Gudehus type [5]

$$\Gamma = \frac{1}{2}\left[1 + \sin\,3\theta + \frac{1}{\psi}(\pi 1 - \sin\,3\theta)\right]$$

where ψ is the ratio of triaxial extension strength to triaxial compression strength, and θ is the Lode angle. The final form of the yield surface, then, is given by

$$f = \left(\Gamma^{\xi}\right)^2 J_2^{\xi} - F_c\left(F_f - N\right)^2$$

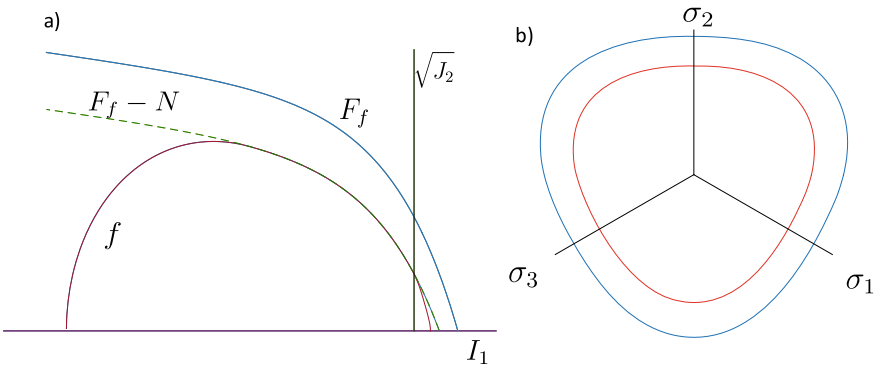

Fig. 2 **a** Yield surface in meridional stress space, showing the pressure-dependent yield surface **b** Yield and failure surface the pi-plane

The yield surface is shown in Fig. 2. The plastic potential follows a similar form, but with different material parameters to more accurately model volumetric deformation.

The model also has kinematic hardening of the yield surface and isotropic hardening on the cap surface. For details see [4].

2.2 Fracture Model

The onset of localization in the bulk material is measured by the standard bifurcation condition as outlined by Rundnicki and Rice [6] and discussed for the GeoModel in [7]. Once localized, a traction–displacement relationship, described below, governs the motion on the bands. Preexisting weak interfaces are considered to have already localized, and motion on interfaces is governed by the same relationship, though with different material properties (Fig. 3).

A combined damage plasticity law governs the opening and sliding on the fracture surface. In tension, an elliptical law between the normal and shear stress governs the displacement. Any motion on the yield surface degrades the cohesion until it reaches zero. Unloading is toward the origin while any cohesion remains. The slip follows a similar elliptical relationship, with different stiffness. Stiffness also degrades with cohesion.

A linear friction law is used in compression, and this follows a more plastic-like formulation. Those interested in the details of the surface model are referred to [8, 9].

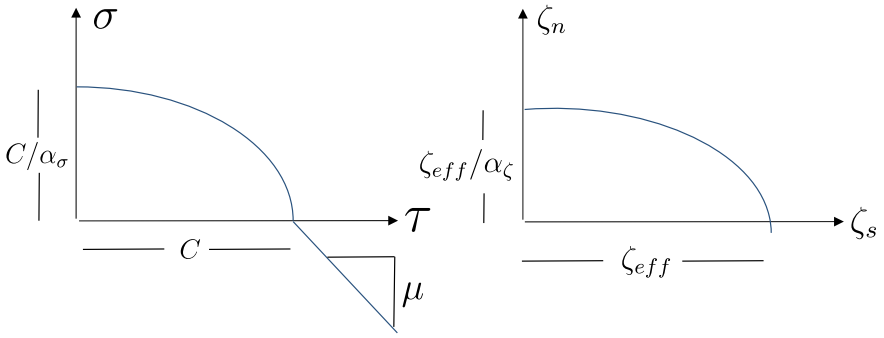

Fig. 3 Yield law in on the surface in traction space (left) and displacement space (right)

3 Finite Element Model

The bulk plasticity model is embedded in the finite element model at the Gauss points in the standard method. Localized deformation is handled using an enhanced strain finite element [10–15, among others]. The element has extra degrees of freedom that correspond to the opening and sliding of the beam, as shown in Fig. 4.

The displacement can be written as continuous part plus the jump across the discontinuity surface

$$u^h = u_{cts} + H_s \zeta$$

Here H_s is Heaviside function across the surface. If we introduce a smooth function f^h that is 0 at nodes on one side of the band (termed the "inactive" side) and 1 at the nodes on the other side (the "active" side), we can reparameterized the displacement field as

$$\begin{aligned} u^h &= \left(u_{cts} - f^h \zeta\right) + \left(H_s - f^h\right)\zeta \\ &= u_{conf} + M_s \zeta \end{aligned}$$

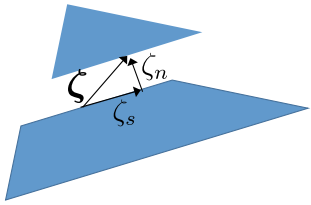

Fig. 4 Enhanced finite element with an opening and sliding jump

If f^h is made to be the sum of the shape functions for the nodes on the active side, then the conforming displacement u_{conf} can be found by the standard finite element shape functions. The corresponding bulk strain, and then stress, can also be found. More details of the implementation may be found in [8].

The fracture may open or slide along a preexisting interface, if one passes through the element, or through the bulk if localization has been detected. Details of the relationship between preexisting and bulk localization are discussed in [10]. Local tracking is employed [11] in this work.

4 Example

We model a wall unit with a window and door opening, shown in Fig. 5, under shear loading. The wall is sheared to the left in this example. The finite element mesh is shown in blue, while the black lines show the interfaces between the bricks. In this problem, the interface is simplified with a single line, although in most materials there are two interfaces with mortar between. Even though the mesh is unstructured, the interfaces are still easily inserted into the problem.

The bulk material properties for the wall are shown in Table 1, while the interface parameters are shown in Table 2. The geometry and material properties are similar to the example shown in [12], but that example was rammed earth structure with only a few interfaces.

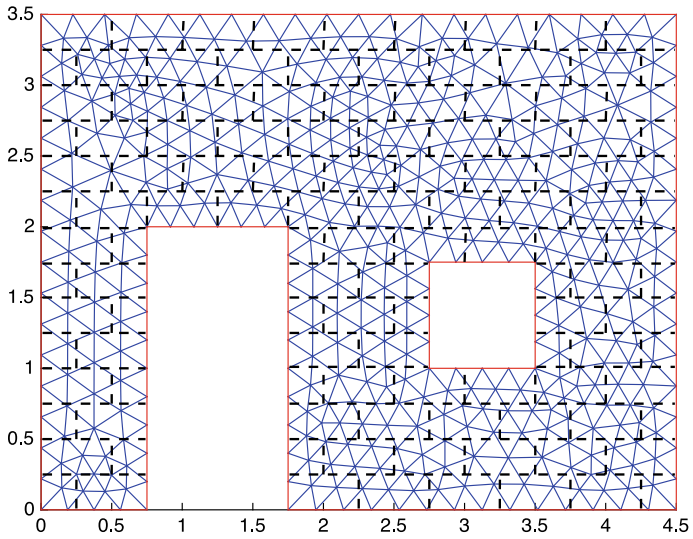

Fig. 5 Geometry and mesh for example problem. Mesh is shown in blue lines. Preinserted interfaces are shown in black lines. Distances in meters

Table 1 Material parameters for bulk material

Young's modulus (E)	2800 (MPa)
Poisson's ratio (ν)	0.14
Isotropic tensile strength (T) tension cap	24.0 (MPa)
Parameter (I_{1T}) compression cap	1.5
Parameter (κ_T) shear yield surface	0.0 (MPa)
Parameter (A) shear yield surface	1.05 (MPa)
Parameter (B) shear yield surface	0.0 (1/MPa)
Parameter (L) shear plastic potential	0.0 (1/MPa)
Parameter (C) shear yield surface	0 (MPa)
Parameter (θ, ϕ)	0.36, 0.18
Aspect ratios (R, Q)	10.0, 10.0
Isotropic hardening parameter (W)	0.8
Isotropic hardening parameter (D_1)	1.47e–3 (1/MPa)
Isotropic hardening parameter (D_2)	0.0
Kinematic hardening parameter (C_α)	1000 (MPa)
Kinematic hardening parameter (N)	0.3 (MPa)
Stress triaxiality parameter ψ	0.85

Table 2 Material parameters for bulk and preexisting interfaces

Bulk interfaces	
Friction angle (degrees)	44.3
Characteristic slip distance	0.5 mm
Normal strength ratio α_σ	2.0
Normal slip ratio α_ζ	2.0
Preexisting Interfaces	
Initial cohesion	5 MPa
Friction angle (degrees)	30.0
Characteristic slip distance	0.5 mm
Normal strength ratio α_σ	2.0
Normal slip ratio α_ζ	2.0

The fracture patterns and horizontal displacement are shown in Fig. 6. They show one major band from the top right to the window, and a second from the window to the door. Some diffuse cracking also occurs, both along the existing interface and in the bulk, before major bands are formed that take to majority of the deformation. In this example, few of the head joints are active. While in traditional fired bricks, the joints are much weaker than the bulk material, this is not always the case in earthen materials.

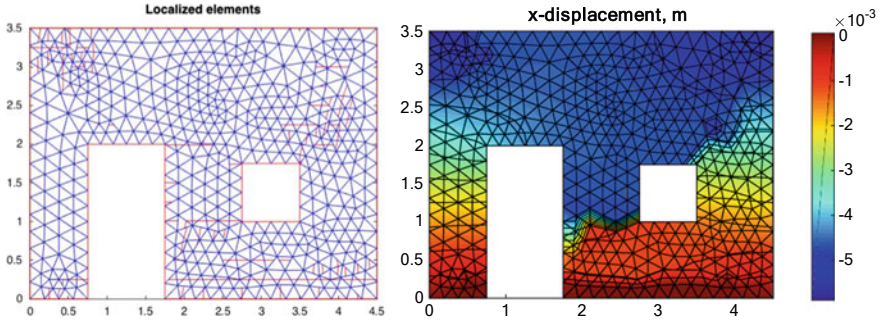

Fig. 6 Left. Fractured elements at the conclusion of simulation. Right, horizontal displacement, showing localized displacement around the windows

The force-displacement curve is shown in Fig. 7. It shows some bulk plasticity, followed by two rapid softening phases, likely corresponding to the propagation of the two major bands.

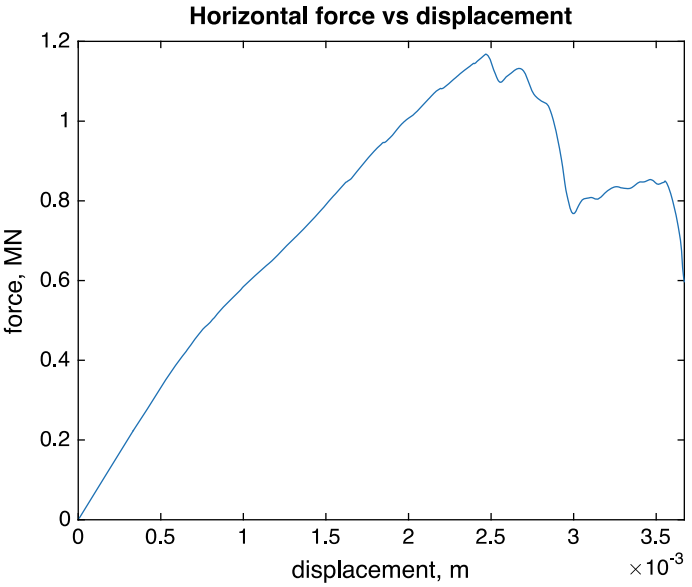

Fig. 7 Force-displacement curve for the simulation

5 Conclusions

In this paper, we apply an enhanced finite element model to examine mechanisms of shear failure in earthen masonry structures. We apply an advanced plasticity model for GeoMaterials to model the bulk behavior of the compressed, cement-stabilized soil blocks, and traction–displacement relationship to govern localized failure both in the bulk and along existing interfaces. These laws are placed in an enhanced finite element framework to analyze wall units with holes for openings.

As anticipated, many of the fractures proceed along the bed joints of the blocks. Between the layers, however, fractures often propagated through the blocks. Unlike traditional masonry, the bond between the blocks is often comparable in strength to the block itself, and so under certain stress states this may occur. The fracture pattern is fairly diffuse in this example, giving hope that fairly large energy dissipation may occur in some events prior to final failure. Future work will compare to experiments.

References

1. Houben H, Guillaud H (1994) Earth construction: a comprehensive guide. Practical Action
2. Fossum AF, Brannon RM (2004) The sandia geomodel: theory and user's guide. SAND report August, Sandia National Laboratories
3. Foster CD, Regueiro RA, Fossum AF, Borja RI (2005) Implicit numerical integration of a three-invariant, isotropic/kinematic hardening cap plasticity model for geomaterials. Comput Methods Appl Mech Eng 194(50–52):5109–5138
4. Motamedi MH, Foster CD (2015) An improved implicit numerical integration of a non-associated, three-invariant cap plasticity model with mixed isotropic kinematic hardening for geomaterials. Int J Numer Anal Methods Geomech 39:1853–1883
5. Gudehus G (1973) Elastoplastiche Stoffgleichungen Guer Trockenen Sand. lngenieur-Archiv 42(3):151–169
6. Rudnicki JW, Rice JR (1975) Conditions for the localization of deformation in pressure-sensitive dilatant materials. J Mech Phys Solids 23(6):371–394
7. Regueiro RA, Foster CD (2011) Bifurcation analysis for a rate-sensitive, non-associative, three-invariant, isotropic/kinematic hardening cap plasticity model for geomaterials: Part I. Small strain. Int J Numer Anal Methods Geomech 25(2):201–225
8. Weed DA, Motamedi MH, Foster CD (2017) A robust numerical framework for simulating localized failure and fracture propagation in frictional materials. Acta Geotech 12(2):253–275
9. Motamedi MH, Weed DA, Foster CD (2016) Numerical simulation of mixed mode (I and II) fracture behavior of pre-cracked rock using the strong discontinuity approach. Int J Solids Struct 85–86:44–56
10. Foster CD, Weed DA, A new method for embedding predefined interfaces in finite elements. Finite Elements Anal Des, in press
11. Parvaneh SM, Foster CD (2016) On numerical aspects of different updating schedules for tracking fracture path in strain localization modeling. Eng Fracture Mech 152:26–57
12. Foster CD, Weed, DA, Motamedi, MH, Tennant AG (2016) Mechanical behavior of Earthen materials in structural applications. GeoChicago
13. Armero F, Garikipati K (1996) An analysis of strong discontinuities in multiplicative finite strain plasticity and their relation with the numerical simulation of strain localization in solids. Int J Solids Struct 33(20/22):2863–2885

14. Borja RI, Regueiro RA (2001) Strain localization in frictional materials exhibiting displacement jumps. Comput Methods Appl Mech Eng 190(2021):2555–2580
15. Foster CD, Borja RI, Regueiro RA (2007) Modeling the effects of variable friction in fractured geomaterials in an embedded strong discontinuity finite element setting. Int J Numer Methods Eng 72:549–581

Numerical Studies on Safeguarding of Cantilever Retaining Structures by Sustainable Backfilling Materials

K. Senthil, Ankush Thakur, and A. P. Singh

Abstract Three-dimensional finite element investigations have been carried out to study the response of retaining structures against lateral earth pressure due to various backfilling materials in order to understand the efficiency of backfilling materials. The behavior of reinforced concrete wall against different backfill soil materials such as sandy soil, clay soil, varying percentage of copper slag along with clay soil and shredded tyre were studied. The elastic behavior of concrete, steel reinforcement bar, sandy soil, clay soil, copper slag, and shredded tyre has been incorporated through elastic model. The behaviors of concrete and backfill material were modeled using suitable material parameters available in literature and identified through detailed literature. The behavior of each element of the wall, i.e., stem, heel, toe, and the shear key against varying sustainable backfill was studied in detail. The lateral displacement, vertical settlement, and stresses developed in each component of the retaining wall were studied and finally the suitable backfill material was identified.

Keywords Sustainable backfill material · Retaining structures · Numerical studies · Choice of backfilling materials

1 Introduction

Several tons of waste material are generated every year globally is due to the unsustainable manufacture of new products from new materials. The waste is ending up in landfill and therefore it has a huge impact on the natural and built environment. It is therefore very important that any waste in the future is minimized by implementing new strategies for reuse of waste material. Hence in the present study, an attempt has been made through finite element investigations to study the structural integrity of retaining structures when it is utilized as backfill. Finite element methods have been widely used in order to study the behavior of retaining wall against lateral earth pressure. Matsuo et al. [1] were conducted an experiment and finite element analysis

K. Senthil (✉) · A. Thakur · A. P. Singh
Department of Civil Engineering, National Institute of Technology Jalandhar, Jalandhar 144011, India
e-mail: urssenthil85@yahoo.co.in; urssenthil85@gmail.com; kasilingams@nitj.ac.in

K. R. Reddy et al. (eds.), *Sustainable Environment and Infrastructure*, Lecture Notes in Civil Engineering 90, https://doi.org/10.1007/978-3-030-51354-2_35

on 10 m height wall and found that density and young's modulus were insensitive whereas it is very sensitive to the Poisson's ratio. Bhatia and Bakeer [2] found that the predicted earth pressure was significantly affected by the size of the element as well as the boundary conditions employed in the study. Chugh [3] found that the discretization of the wall into finite-difference grid affected the natural frequency of free vibrations. Liu et al. [4] found that wall friction angle on deformed profile was found insignificant. Few authors have performed three-dimensional numerical simulations in order to predicted the ultimate load-carrying capacity and allowable bearing pressure [5–12]. The studies available in the literature describe the effect of the lateral earth pressure on the conventional backfilling and soil. However, the studies on the utilization of waste material as backfill are rather few. The influence of waste material as backfill in the retaining wall is rarely studied through numerical simulations and authors not seen any relevant literature in this regard.

The present study focused on the behavior of the cantilever reinforced concrete walls against different backfill soil materials such as sandy soil, clay soil, varying percentage of copper slag along with clay soil and shredded tyre and supported on dense soils. The three-dimensional numerical simulations were carried out using ABAQUS/Standard commercial tool. The elastic behavior of concrete, steel reinforcement bar, and backfill material has been incorporated through elastic model. The behavior of each element of the wall and the shear key was studied in detail in terms of vertical, horizontal displacement, and stresses in steel and concrete and influence thereon the overall behavior of the wall was presented.

2 Numerical Modeling

The design of the 6.35 m height retaining walls has been carried out using Working Stress Method. The grade of concrete considered is 30 MPa and that of steel 500 MPa. The clear cover to stem and the base slab was kept 40 and 60 mm, respectively. The factor of safety against all the stability criteria was considered 1.5. The dimensions of each component of the retaining walls adopted as per the design are shown in [9]. The finite element model of the retaining walls was made using ABAQUS/CAE and isometric view of the model is shown in Fig. 1. The dimensions of the retaining walls and reinforcement were modeled identical to that obtained from the design [9]. The length of the wall considered was 15 m, almost three times its width. The depth of soil below the base slab was calculated based on the stress distribution beneath the base slab obtained from the Boussinesq equation. Based on which the width of the soil mass was also assumed equivalent to 10 m from the edge of the toe as well as heel. In the present study, different backfill soil materials such as sandy soil, clay soil, varying percentage of copper slag along with clay soil and shredded tyre were placed over the heel (shaded area) having width of 1.5 m and total height of 6.06 m and the wall is supported on dense soils, see Fig. 1. The backfill material in the retaining wall for sandy soil, clay soil, clay soil with varying percentage of copper slag as 4, 6, and 8% and shredded tyre, was identified as Case 1, Case 2, Case 3, Case 4, Case 5, Case 6,

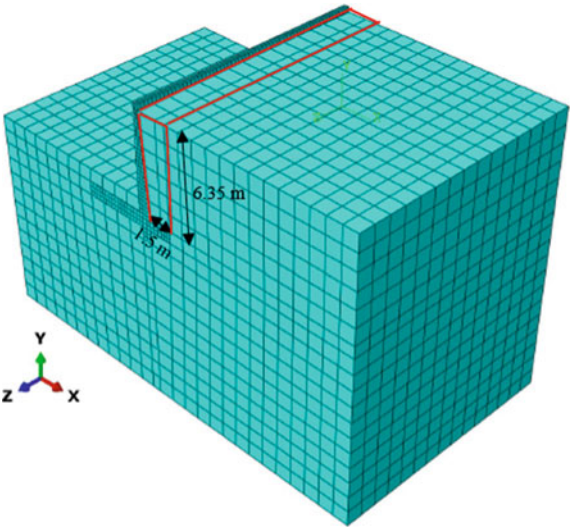

Fig. 1 Finite element model of soil-wall system of earth pressure

respectively. The concrete was modeled as three-dimensional deformable body and the reinforcement as three-dimensional truss. The interaction between concrete and steel was modeled using embedded constraint available in ABAQUS/CAE and the concrete was assumed as host region and the steel as embedded region. The degree of freedom of the steel was governed by the nearest concrete node. The contact between the concrete and the adjoining soil was defined using General contact algorithm considering the concrete as first and the soil as second surface. A coefficient of friction of 0.4 was defined between the concrete and the soil. The soil boundary was restrained with respect to all the degrees of freedom. The concrete was meshed using 8-node linear hexahedral reduced integration brick elements (C3D8R) while the reinforcement with 2-node linear beam element. The size of element was chosen based on the mesh convergence study for both concrete and the reinforcement.

3 Material Parameters

The material behavior of steel, concrete, and soil was treated as linear elastic in the present study. For M30 grade concrete the elastic modulus ($E = 4700\sqrt{f_c'}$) was obtained according to the guideline [13], density was considered 2400 kg/m^3 and poison's ratio 0.17, see Table 1. The reinforcing steel was also assigned the modulus of elasticity (2×10^{11} N/m^2), density (7850 kg/m^3), and poison's ratio (0.3). For sandy soil properties the modulus of elasticity (0.3×10^8 N/m^2), density (1835 kg/m^3), and poison's ratio (0.34) were also defined. In addition to that, the properties of the clay soil density (1420 kg/m^3) were used in the present study is shown in Table 1. The modulus of elasticity of clay soil as well as clay soil combination of 4, 6, and

Table 1 Material parameters for the finite element model

Identity	Description	Density Kg/m^3	Elastic constant	
			Young's modulus N/m^2	Poisson's ratio
Concrete		2400	0.24×10^{11}	0.17
Steel reinforcement		7850	2.0×10^{11}	0.30
Case 1	Sandy soil	1835	0.30×10^{8}	0.34
Case 2	Clay soil	1420	0.73×10^{8}	0.33
Case 3	4% copper slag +clay	1420	0.545×10^{8}	0.33
Case 4	6% copper slag + clay	1420	0.46×10^{8}	0.33
Case 5	8% copper slag + clay	1420	0.35×10^{8}	0.33
Case 6	Shredded tyre	731	1.8×10^{6}	0.29

8% copper slag was calculated based on the stress–strain curve available in literature [14]. However, the density of clay soil as well as clay soil combination of 4, 6, and 8% copper slag was considered same as 1420 kg/m^3, since the addition of effect of copper slag up to 10% in the soil leads to increase the density only 2.5%, which were indicated in [15]. Therefore, the density as well as Poisson's ratio of the clay soil was kept constant for all four cases [clay soil as well as clay soil combination of 4, 6, and 8% copper slag]. The elastic properties of the Shredded tyre are followed as per the literature [16]. The angle of friction for sandy soil, clay soil along with copper slag and clay 30, 34, and 30 degrees, respectively were considered in the present study.

4 Application of Loads

The active and the passive pressures assigned to the retaining wall along with the body force. The numerical values of the active and passive pressures were computed using the simple mathematical expressions which are the function of the height of the wall, see Table 2. The self-weight of soil and concrete was assigned as gravitational body force. The Public Work Research Institute of Ministry of Construction of Japan (1975) studied the pressure distribution of cohesive and sandy soils. The distribution of the earth pressure caused by cohesive soil was found to be triangular while that

Table 2 Analytical expressions for active and passive pressure distribution on wall

Type of backfill	Active pressure		Passive pressure	
	Wall	Shear key	Wall	Shear key
Conventional Soil	$-6116y + 38837$	– 6116y –4893	– 55050y +46793	– 55050y –46793
Clay soil	$-4174y + 26509$			
Copper slag	$-4007y + 25446$			
Shredded tyres	$-3358y + 21726$			

of the sandy soil and gravel, nearly trapezoid. Therefore, in the present study also a triangular pressure distribution has been considered with its resultant at H/3 from the base.

5 Mesh Convergence Study

The size of concrete element was varied as 0.4 m × 0.4 m × 0.4 m, 0.35 m × 0.35 m × 0.35 m, and 0.25 m × 0.25 m × 0.25 m and that of the corresponding reinforcing steel element as 0.4 m, 0.35 m, and 0.25 m. The results thus obtained in terms of displacement and stresses were found to converge at element size 0.25 m × 0.25 m × 0.25 m, giving a total number of 9360 elements of concrete and 22194 elements of reinforcement, see Tables 3 and 4. Thus the size of element adopted was 0.25 m × 0.25 m × 0.25 m for concrete and 0.25 m for reinforcement for all the simulations of cantilever wall. The soil was also discretized into 8-node linear hexahedral reduced integration brick elements (C3D8R) of 1 m × 1 m × 1 m uniform size throughout its volume excluding backfill, see Fig. 1.

However, the mesh size was considered 0.4 m × 0.4 m × 0.4 m over the shaded area shown in Fig. 1. The results of the mesh convergence study for the retaining walls in terms of maximum displacement, normal, and shear stress were shown in Tables 3 and 4 and the maximum displacement developed in the wall corresponding to the varying the mesh size, see Fig. 2. The displacement and stresses were found to be almost same, with the reduction in the size of element. It was observed that the sensitivity of mesh seems insignificant, however, the displacement and stresses

Table 3 Mesh convergence study on retaining wall (Case 4) with 8% Copper Slag along with clay as backfill

Description		Case 1	Case 2	Case 3
Steel	Element size (m)	0.4	0.35	0.25
	No. of elements (B21)	13952	16203	22194
Concrete	Element size (m)	0.4 × 0.4 × 0.4	0.35 × 0.35 × 0.35	0.25 × 0.25 × 0.25
	No. of elements (C3D8R)	2584	3268	9360
Total elements in Wall		16536	19471	31554
U1 (mm)		1.841	1.836	1.856
U2 (mm)		51.5	51.16	51.05
S11 (N/mm^2)		2.42	2.34	2.7
S22 (N/mm^2)		2.12	2.18	2.56
S12 (N/mm^2)		0.91	1.10	1.27
S13 (N/mm^2)		0.24	0.24	0.27

Table 4 Mesh convergence study on retaining wall (Case 5) with shredded tyres as backfill

Description		Case 1	Case 2	Case 3
Steel	Element size (m)	0.4	0.35	0.25
	No. of elements (B21)	13952	16203	22194
Concrete	Element size (m)	0.4 × 0.4 × 0.4	0.35 × 0.35 × 0.35	0.25 × 0.25 × 0.25
	No. of elements (C3D8R)	2584	3268	9360
Total elements in wall		16536	16536	19471
U1 (mm)		4.19	4.21	4.87
U2 (mm)		50.5	50.5	50.5
S11 (N/mm^2)		1.45	1.39	1.62
S22 (N/mm^2)		2.02	2.04	2.36
S12 (N/mm^2)		0.67	0.91	1.06
S13 (N/mm^2)		0.23	0.23	0.26

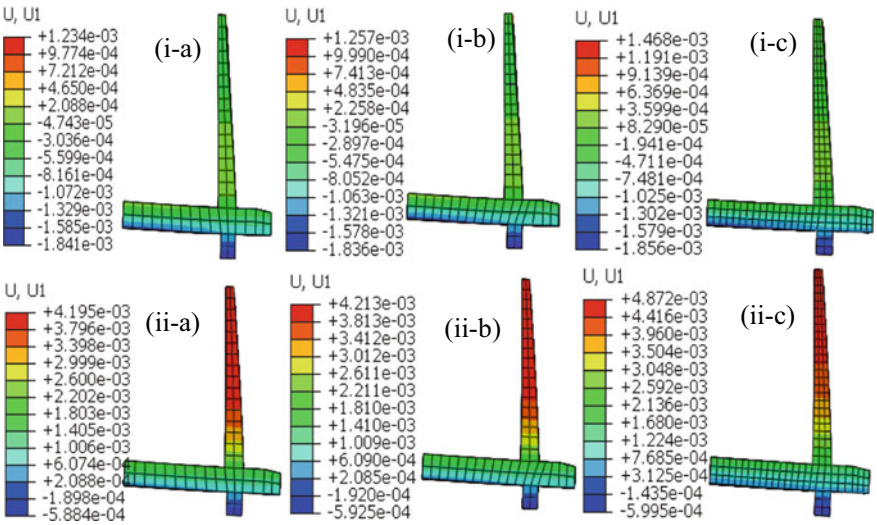

Fig. 2 Displacement (U1) in retaining wall (meter) (i) case 5 and (ii) case 6 with **a** 0.4 **b** 0.35, and **c** 0.25 m mesh size

were changing marginally with decrease of mesh size. In light of computational cost, 0.25 m mesh size was considered in the present study.

6 Results and Discussion

Three-dimensional finite element analysis has been carried out in order to study the effect of lateral earth pressure on the solid retaining walls. The deformation behavior of the different components of the retaining wall such as base slab, stem, and shear key was studied. The results thus obtained in terms of displacement in different components of the wall, and stresses developed therein were presented and discussed. The unit of the displacement contours was "meter" while that of the stress contours, "N/m^2" and the results due to all six cases were presented in Table 5.

The horizontal as well as vertical displacement of the stem has been found to decrease with an increase in the percentage of copper slag in the clay soil. Also, it was observed that the displacement for the wall with Shredded tyres was found to be higher compared to other cases, see Fig. 3. The maximum horizontal displacement at the stem top was found to be 0.022, 2.13, 1.97, 1.78, 1.46, and 4.87 mm for case 1, case 2, case 3, case 4, case 5, and case 6, respectively. It was observed that addition of copper on the clay soil is significantly decreases the lateral displacement of wall, see Fig. 3c–e. It was also observed that the horizontal displacement at the bottom of the wall was significantly low in case of case 6 as shredded tyres backfilling however, the case 6 was experienced maximum displacement at top of stem among the chosen cases. It may be due to the fact that the passive pressure due to soil filling over the toe slab is more than the active pressure resulting of shredded tyre. It was concluded that the use of copper slag and shredded tyre as backfill material improves the structural integrity of the retaining structures.

The vertical displacement of the base slab for all the given cases has been found to be almost the same, see Fig. 4. Also, it was observed that the displacement for the wall with Shredded tyres was found to be less compared to other cases. The maximum vertical displacement at the heel slab was found to be 52.2, 51.08, 51.08, 51.07, 51.05, and 50.5 mm for case 1, case 2, case 3, case 4, case 5, and case 6, respectively. The vertical displacement in the heel slab was found to be higher due to lack of sufficient width of slab. However, the vertical displacement was found to be lesser in case of toe slab of the wall due to sufficient toe width.

Table 5 Results of all six cases and their influence on the behavior of retaining wall

Description		Results	Case 1	Case 2	Case 3	Case 4	Case5	Case 6
Displacement (mm) in concrete		U1	0.022	2.13	1.97	1.78	1.46	4.87
		U2	52.2	51.08	51.08	51.07	51.05	50.5
Stress (MPa)	Concrete	S11	2.95 (+) 3.92 (–)	2.77 (+) 3.77 (–)	2.74 (+) 3.71 (–)	2.7 (+) 3.69 (–)	2.7 (+) 3.64 (–)	1.6 (+) 2.30 (–)
		S22	2.88 (+) 4.25 (–)	2.35 (+) 3.80 (–)	2.43 (+) 3.84 (–)	2.4 (+) 3.87 (–)	2.5 (+) 3.90 (–)	2.3 (+) 3.09 (–)
	Steel	S11	32 (+) 44 (–)	30 (+) 40 (–)	30 (+) 40 (–)	30 (+) 41 (–)	29 (+) 41 (–)	26 (+) 31 (–)

Note Positive and negative sign describes Tension and Compression, respectively

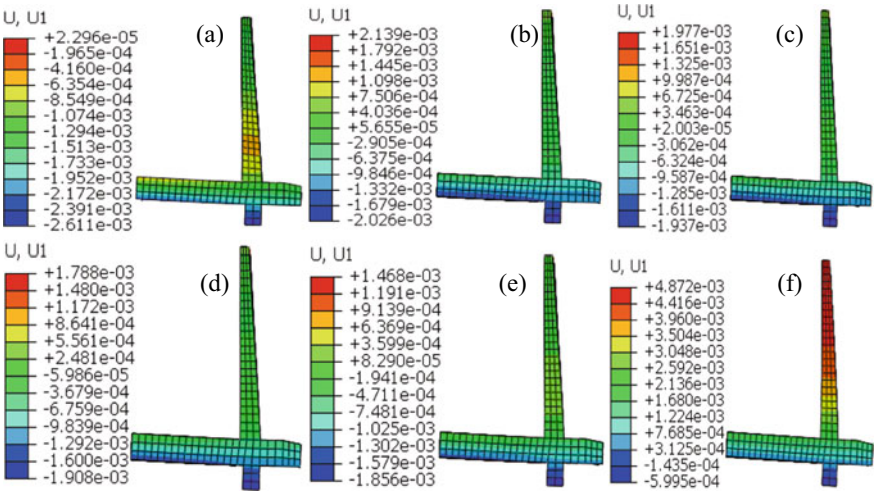

Fig. 3 Horizontal displacement contour of cantilever retaining wall (meter) by **a** Case 1-Sandy soil **b** case 2−clay soil **c** Case 3−clay + 4% copper slag **d** Case 4−clay + 6% copper slag **e** Case 5−clay + 8% copper slag and **f** Case 6−shredded tyres

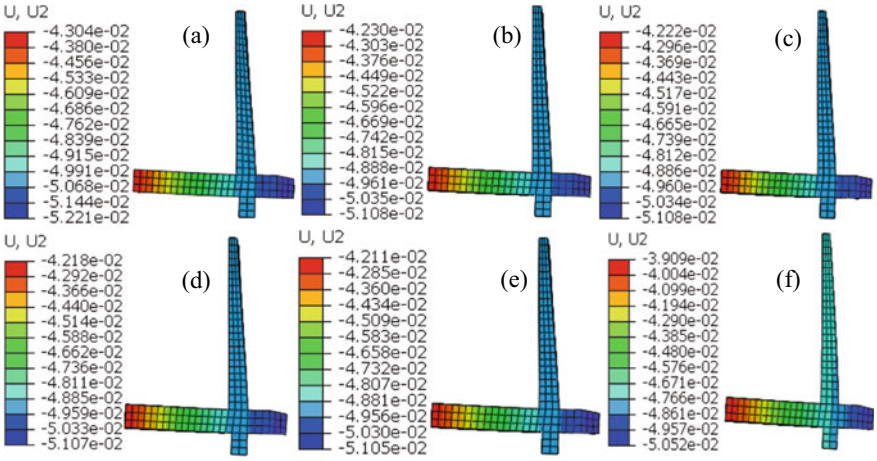

Fig. 4 Vertical displacement contour of cantilever retaining wall (meter) by **a** Case 1, **b** Case 2, **c** Case 3, **d** Case 4, **e** Case 5, and **f** Case 6

The stresses developed in concrete (normal to stem surface) of the retaining walls have been shown in Fig. 5. The maximum compression has been found to develop near the joint of stem and toe slab while maximum tension near the joint of shear key and toe slab; in order to avoid the toppling of the stem. In general, both the compressive and tensile stresses were found to almost the same. It was observed that addition of copper slag on the clay soil, is marginally decreases the stresses in the

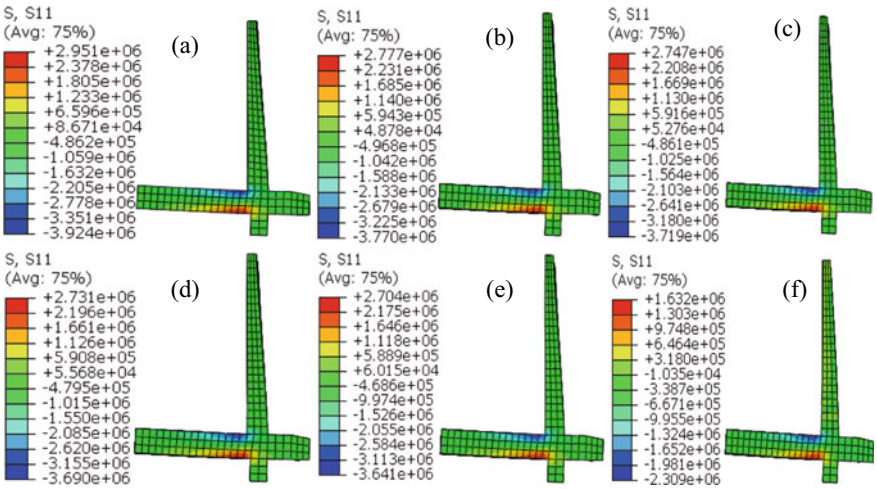

Fig. 5 Normal stresses in horizontal direction of the cantilever retaining wall (N/m^2) by **a** Case 1 **b** Case 2 **c** Case 3 **d** Case 4 **e** Case 5, and **f** Case 6

wall, see Fig. 5c–e. However, both the tensile and compressive stresses were found to be minimum in case of case 6. It was also observed that the tensile stresses were significantly low in case of case 6 as shredded tyres backfilling. It was concluded that the shredded tyres as efficient backfilling material among the selected cases.

The compressive and tensile stresses in vertical direction were found maximum at the base of the stem, see Fig. 6. The tensile stresses in vertical direction were found maximum at the heel face of stem while compressive stresses at the toe face of the

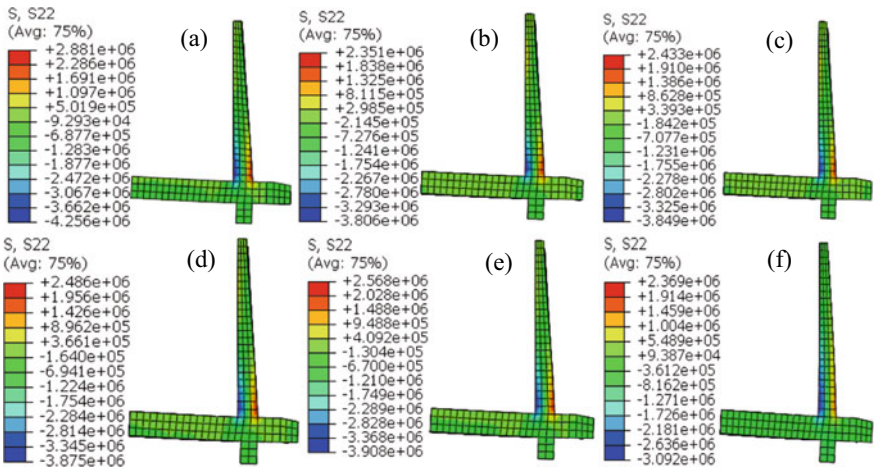

Fig. 6 Normal stress in vertical direction of the cantilever retaining wall (N/m^2) by **a** Case 1 **b** Case 2 **c** Case 3 **d** Case 4 **e** Case 5, and **f** Case 6

stem. The induced compressive stresses on the stem were 4.25, 3.80, 3.85, 3.87, 3.90, and 3.02 MPa against case 1, case 2, case 3, case 4, case 5, and case 6, respectively. Similarly, induced tensile stresses on the stem were 2.88, 2.35, 2.43, 2.48, 2.56, and 2.36 MPa against case 1, case 2, case 3, case 4, case 5 and case 6, respectively. It was observed that the influence of copper slag found to be insignificant in both tensile and compressive stresses. It was also observed that the tensile and compressive stresses were low for the case 6 as compared to remaining all cases. It was concluded that the shredded tyres as efficient backfilling material among the selected cases.

The tensile stresses were found maximum at the joint of toe and shear key as well as joint of stem and heel. The compressive stresses on the other hand were found maximum at the joint of stem and toe. The tension and compression behavior was therefore in agreement with that of the concrete, Fig. 7. The induced compressive stresses on the stem were 44, 40, 40, 41, 41, and 30.9 MPa against case 1, case 2, case 3, case 4, case 5, and case 6, respectively. However, the tensile stresses developed on the stem were almost same as in the range of 26–30 MPa for the selected case. It was also observed that the influence of copper slag found to be insignificant in both tensile and compressive stresses, as like stresses in the concrete. It was also observed that the tensile and compressive stresses were low for the case 6 as compared to remaining all cases. It was concluded that the shredded tyres as efficient backfilling material among the selected cases.

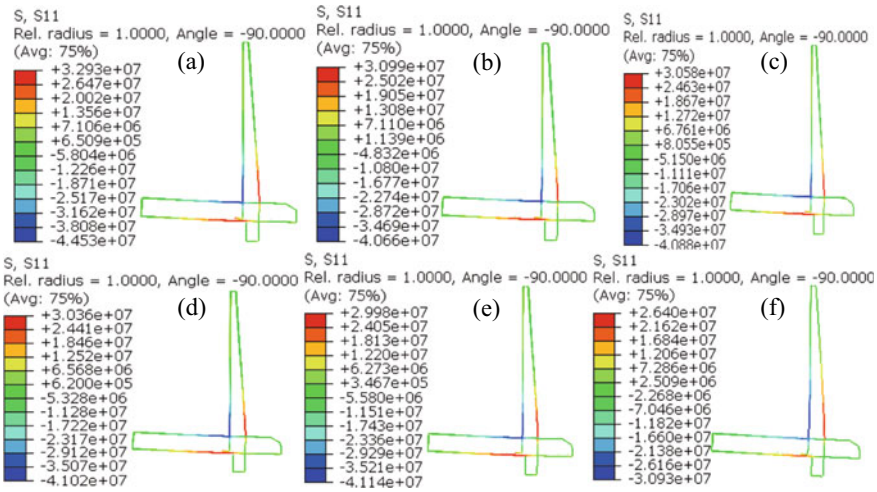

Fig. 7 Stresses in the reinforcement of cantilever retaining wall (N/m^2) by **a** Sandy soil **b** clay soil **c** 4% copper slag **d** 6% copper slag **e** 8% copper slag and **f** Shredded tyres

7 Conclusions

The present numerical study describes the behavior of the cantilever walls subjected to lateral earth pressure. The influence of various backfill materials such as sandy soil, clay soil, copper slag, and Shredded tyres on the behavior of retaining wall was studied. The results thus obtained led to the following conclusions;

- It was observed that the horizontal displacement at the bottom of the wall was significantly low in case of case 6 as shredded tyres backfilling however, the case 6 was experienced maximum displacement at top of stem among the chosen cases. It was concluded that the use of copper slag and shredded tyre as backfill material improves the structural integrity of the retaining structures.
- The vertical displacement in the heel slab was found to be higher due to the lack of sufficient width of slab. However, the vertical displacement was found to be lesser in case of toe slab of the wall due to sufficient toe width.
- It was observed that the influence of copper slag found to be insignificant in light of both tensile and compressive stresses, as like stresses in the concrete. It was also observed that the tensile and compressive stresses were low for the case 6 as compared to remaining all cases. Based on the results, it was concluded that the shredded tyres as efficient backfilling material among the selected cases.

References

1. Matsuo M, Kenmochi S, Yagi H (1978) Experimental study on earth pressure of retaining wall by field test. Jpn Soc Soil Mech Found Eng 18(3):27–41
2. Bhatia SK, Bakeer RM (1989) Use of the finite element method in modeling a static earth pressure problem. Int J Numer Anal Geomech 13:207–213
3. Chugh AK (2005) A counterfort versus a cantilever retaining wall—a seismic equivalence. Int J Numer Anal Geomech 29:897–917
4. Liu NH, Chen JW, Liou JY (2006) The deformed profile of the horizontal backfill in active state. In: International symposium geohazards mitigation. Tainan, Taiwan, pp 174–179
5. Yoo C, Kim S-B (2008) Performance of a two-tier geosynthetic reinforced segmental retaining wall under a surcharge load: Full-scale load test and 3D finite element analysis. Geotex Geomem 26:460–472
6. Nisha S, Shivashankar R, Ravi Shankar AU (2011) Role of shear keys in cantilever retaining wall. In: Proceedings of Indian geotechnical conference. Kochi, pp 627–630
7. Public Work Research Institute of Ministry of Construction of Japan (1975) Large scale model tests of a retaining wall. Research Data, No. 994
8. Salman FA, Fattah MY, Shirazi SM, Mahrez A (2011) Comparative study on earth pressure distribution behind retaining wall subjected to line loads. Sci Res Essays 6(11):2251–2267
9. Senthil K, Iqbal MA, Kumar A (2014) Behavior of cantilever and counterfort retaining walls subjected to lateral earth pressure. Int J Geo Engg 8(2):167–181
10. Senthil K, Rupali S, Iqbal MA (2017) Performance of retaining walls with various configurations against lateral earth pressure. In: International conference on sustainable civil engineering practices. NITTTR Chandigarh, India

11. Rahmouni O, Mabrouki D, Benmeddour D, Mellas M (2016) A numerical investigation into the behavior of geosynthetic-reinforced soil segmental retaining walls. Int J Geotech Eng 10(5):435–444
12. Hosseininiaa ES, Ashjaee A (2018) Numerical simulation of two-tier geosynthetic-reinforced-soil walls using two-phase approach. Comput Geotech 100:15–29
13. ACI Committee 318. Building code requirements for structural concrete (ACI 318 M-11) and commentary. American Concrete Institute, Detroit
14. Parvathy S, Nelson A (2016) A Study on the effect of copper slag on lime stabilized clay. Int J Eng Res Technol 5(9):536–540
15. Sivapriya SV, Vinoth Kumar S, Nagarajan V (2016) Utilization of copper slag as a reinforcing material. Int J Sci Technol Eng 2(12):149–153
16. Shrestha S, Ravichandran N, Raveendra M, Attenhofer JA (2016) Design and analysis of retaining wall backfilled with shredded tire and subjected to earthquake shaking. Soil Dyn Earthq Eng 90:227–239

Behavior of Model Strip Footing Resting on Sand Bed Reinforced with 3D Inserts

Prince Karandeep Singh and Arvind Kumar

Abstract A series of laboratory model test was conducted on strip footing resting on sand bed reinforced with 2D reinforcement, single sided 3D reinforcement and double sided 3D reinforcement. The various parameters were studied include the depth of variation of 2D and 3D reinforcement and height of variation of vertical members of 3D reinforcement. The experimental study showed a 120% increase in bearing capacity was observed when 2D reinforcement was placed at the optimum depth of 0.5B. In the case of single sided 3D reinforcement, as the height of vertical member of 3D reinforcement was increased, load settlement response and bearing capacity of the soil also increased up to certain limits, further increasing the height beyond that limit drop in the load settlement response is observed. In the case of double sided 3D reinforcement A1 was fixed at 2 cm and height of A2 was varied from 1 to 3 cm. An increase in the bearing capacity was observed more than 300% in the case of single sided 3D reinforcement and more than 350% in the case of double sided 3D reinforcement. Double sided 3D reinforcement can provide additional confinement and passive resistance to the soil, as compared to 2D and single sided 3D reinforcement for the same area.

Keywords Unreinforced sand bed · 2D reinforcement · Single sided 3D reinforcement · And double sided 3D reinforcement

1 Introduction

India is going through a rapid urbanization era, and due to the scarcity of land, vertical growth of structures replacing horizontal growth of buildings. This needs a very sound earth to bear such a heavy load. A lot of research is being carrying out to increase the load carrying capacity of earth by modifying its engineering property. The concept of reinforcing the soil by means of Geosynthetics, metal strips has been widely used in highways, under foundations and embankment, etc. Reinforcement

P. K. Singh (✉) · A. Kumar
Dr. B. R. Ambedkar National Institute of Technology, Jalandhar, India
e-mail: princekss.ce.18@nitj.ac.in

K. R. Reddy et al. (eds.), *Sustainable Environment and Infrastructure*, Lecture Notes in Civil Engineering 90, https://doi.org/10.1007/978-3-030-51354-2_36

of soil not only increases the load carrying capacity of the soil but also reduces the settlement significantly. A lot of work has already done on the reinforcement of soil with Geosynthetics and metal strips. Azam [1], Chen [2], Ciceka [3], Kumar [4], Tarfeshi [5], Wakil [6] are some the name of some researcher who focused their research toward the use of soil reinforcement to improve the bearing capacity of soil. These studies show that the load settlement behavior of the soil depends upon the type of reinforcement, soil, and footing. A concept of multi direction reinforcement has developed. It was first developed by Lawton et al. [7], conducted the laboratory investigation of soil reinforced with Geo jack. A series of traixial test was conducted by Zhang et al. [8] using 3D reinforcement and concluded the 3D reinforcement give a better result to improve the load carrying capacity of soil than that of any other type of reinforcement. Hou et al. [9] also performed a series of laboratory plate load tests using single sided horizontal–vertical reinforcement. Hou et al. [10] calculated the ultimate bearing capacity of horizontal–vertical reinforcement based on the failure mode and mechanism of sand bed reinforced with horizontal–vertical reinforcement Harikumar et al. [11] performed as laboratory plate load test on strip footing resting on sand bed reinforced with plastic multidirectional reinforcement. In most of the studies, it has been concluded that using multi directional reinforcement has a more advantage over single directional reinforcement as multi direction reinforcement increases the passive resistance and confinement of the soil significantly as compared to conventional reinforcement. The present study aims to found the effectiveness of multi directional reinforcement with respect to its shape and size. The optimum depth of placement of reinforcement was also aimed to be determined for different types of reinforcement. To achieve these objectives, a series of laboratory tests have been performed on strip footing resting on sand bed reinforced with 2D, single sided 3D and double sided 3D reinforcement. Effects of depth variation of reinforcement layer, variation of height of vertical members of single sided and double 3D reinforcement on the load settlement behavior and load carrying capacity of soil have been studied. Overall, 23 tests were performed, one on unreinforced soil and rest on reinforced soil with different types of reinforcement, Galvanized iron metal strips were used as reinforcement. Each test was performed two times, in order to ensure validity of results.

2 Test Materials

2.1 Sand

The soil used in the current study was sundry sand with a coefficient of uniformity (C_u) as 3 and coefficient of curvature as 0.8. Soil is classified as poorly graded (SP) according to Indian Soil Classification system. The minimum and maximum dry unit weight of the soil was also found to be 16.75 kN/m^3 and 19.20 kN/m^3 in geotechnical lab as per Indian standard. The specific gravity of soil was found to be 2.63. From

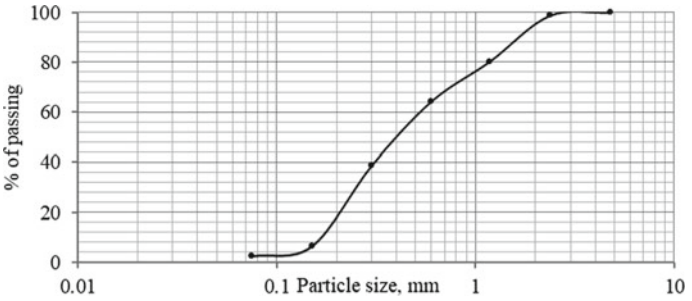

Fig. 1 Particle size distribution of soil

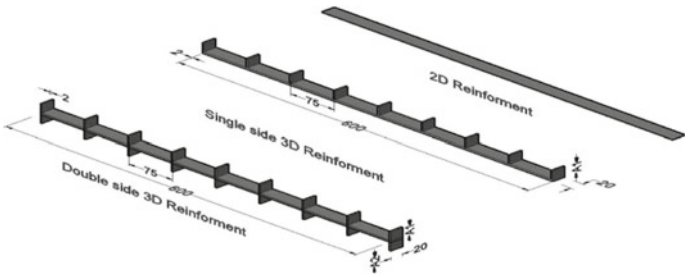

Fig. 2 3D diagram of horizontal, single sided and double sided 3D reinforcements

the direct shear test angle of internal friction was found to be 36°. The grain size distribution of sand is shown in Fig. 1.

Reinforcement

A 2 mm thick, 20 mm wide, and 600 mm long metal strips are used as a 2D reinforcement, single sided 3D reinforcement and double sided 3D reinforcement are shown in Fig. 2. Horizontal c/c spacing between the reinforcement is kept constant at 0.45B where B is the width of strip footing. Spacing between the vertical members of the 3D reinforcement was kept at 7.5 cm.

3 Experimental Setup

Model test is to be conducted on a steel tank of 1500 mm length, 600 mm wide, and 800 mm high. To strengthen the tank walls, vertical Stiffeners were provided on the walls of tank as shown in Fig. 3. In order to eliminate the friction between walls and soil, a polyvinyl sheet of 75μ was fixed inside on the walls of tank. The length of the tank was so decided, that the clear space between the boundary of the tank and footing must be more than five times of the width of footing either side of the footing. Load was applied with a hydraulic jack of 350kN capacity. A 25 mm thick

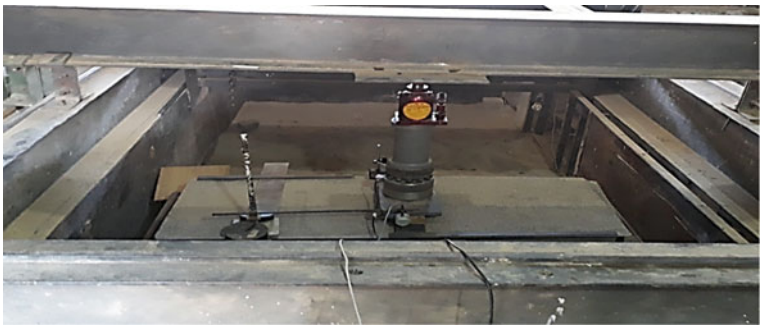

Fig. 3 Actual test setup

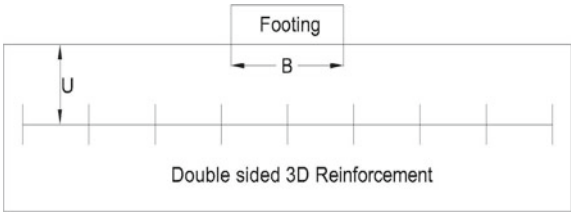

Fig. 4 Diagrammatic view of setup

steel plate of 100 mm width (B) and 600 mm long (equal to the width of the tank in order to meet the condition of plain strain) was taken as a strip footing. The base of footing was roughened by fixing the sand at the bottom of the footing using epoxy glue. Two LVDTs at opposite corners were fixed to record the settlements as shown in Fig. 4.

4 Test Procedure

Before starting the model testing, sand was dried and mix properly in order to avoid discrepancies in test results. The sand was poured into the tank using raining technique method. The unit weight of sand was recorded by falling the sand into a known volume mould from different height. A graph was generated between height of fall and unit weight of sand. The height of fall was decided based on the desired density of sand bed. All tests were carried out on sand with relative density and average unit weight of soil as 63% and 18.22 kN/m^3, respectively. This unit weight can be achieved by filling the soil tank by falling it from a height of 40 cm into different layers, each of 5 cm thick. The density was checked continuously by inserting a known volume container. If the density differs by 5% from the desired density, the sand layers were scarified and sand bed was prepared again. Parameters such as

length of reinforcement, horizontal c/c spacing of reinforcement was kept equal to 0.45 time the width of footing (B). The c/c spacing between the vertical members of 3D reinforcement was kept constant as 7.5 cm for each case taken in the study. Depth of reinforcement, height of vertical member of 3D reinforcement were kept variables. A vertical load was applied slowly and Load and settlements were recorded up to a settlement of 40 mm.

5 Results and Discussion

The load settlement data was further processed and a curve between load applied and corresponding settlement was plotted. The load settlement curves for unreinforced soil as shown in Fig. 5. Using the double tenement method the maximum load carried by the footing was found to be 4.4kN. The load bearing capacity was determined by dividing the load by area of footing and found to be 66.65 kN/m^2.

5.1 Soil Reinforced with 2D Metal Strips

Three tests were conducted with reinforcement as plain metal strips. In each tests, the depth of 2D metal strips was taken as 0.2B, 0.5B, and 0.8B from top of soil. The other parameters as c/c spacing between metal strips and its width kept constant to get the effect of depth of reinforcement may. The maximum load carried by the footing was calculated and it was observed that maximum load was carried by the footing when the reinforcement was placed at a depth of 0.5B from the top of sand. If the depth of reinforcement was increased further, the load carried by the footing was decreased. It may be due to fact that over burden pressure beyond 0.5B sufficiently increased, which may cause the higher settlement. The load settlement curves for all three cases by varying u/B for 2D reinforcement were shown in Fig. 6a.

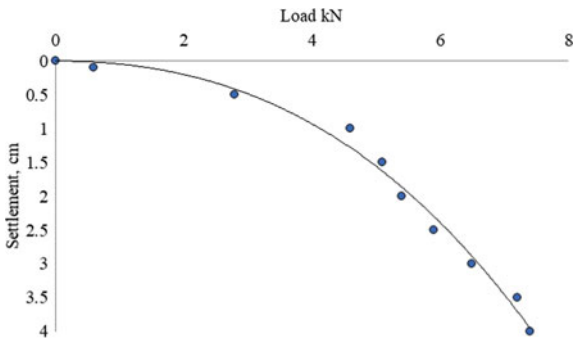

Fig. 5 Load settlement behavior of unreinforced sand

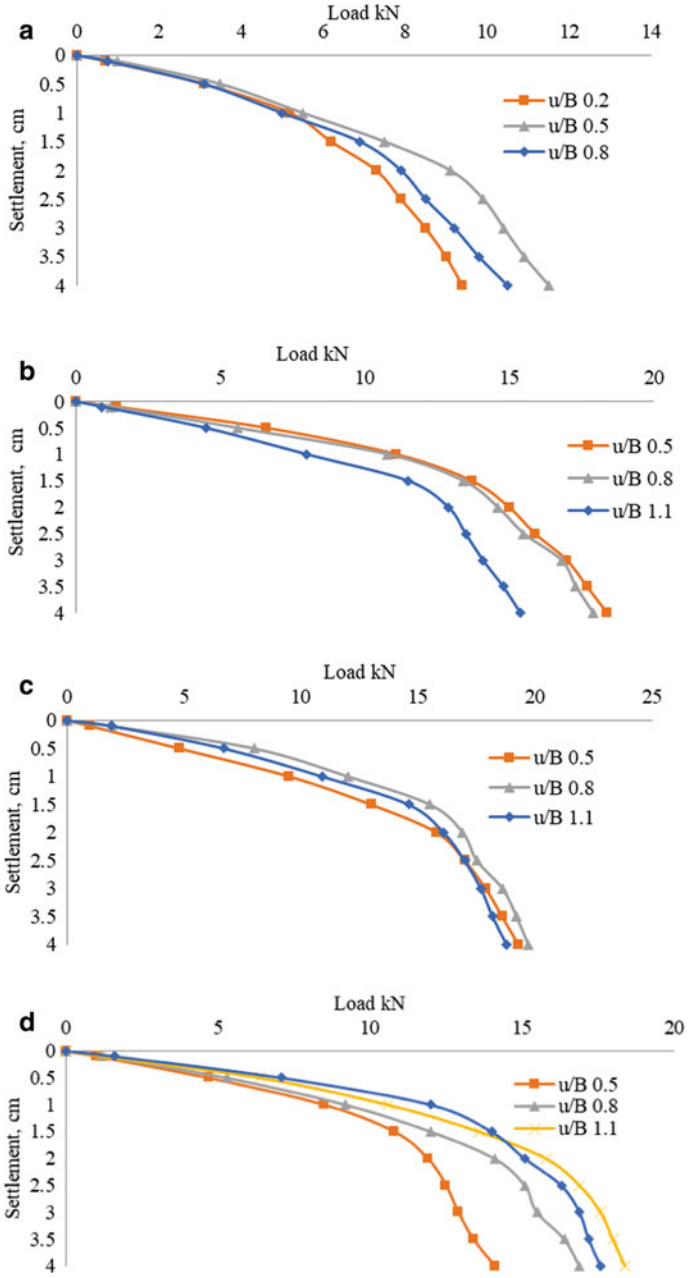

Fig. 6 **a** Load versus settlement for 2D reinforcement. **b** Load versus settlement for single sided 3D reinforcement A1–1 cm. **c** Load versus settlement for single sided 3D reinforcement A1–3 cm. **d** Load versus settlement for single sided 3D reinforcement A1–2 cm. **e** Load versus settlement for double sided 3D reinforcement A1–2 cm A2–1 cm. **f** Load versus settlement for double sides 3D reinforcement A1–2 cm A2–2 cm. **g** Load versus settlement for double sided 3D reinforcement A1–2 cm A2–3 cm

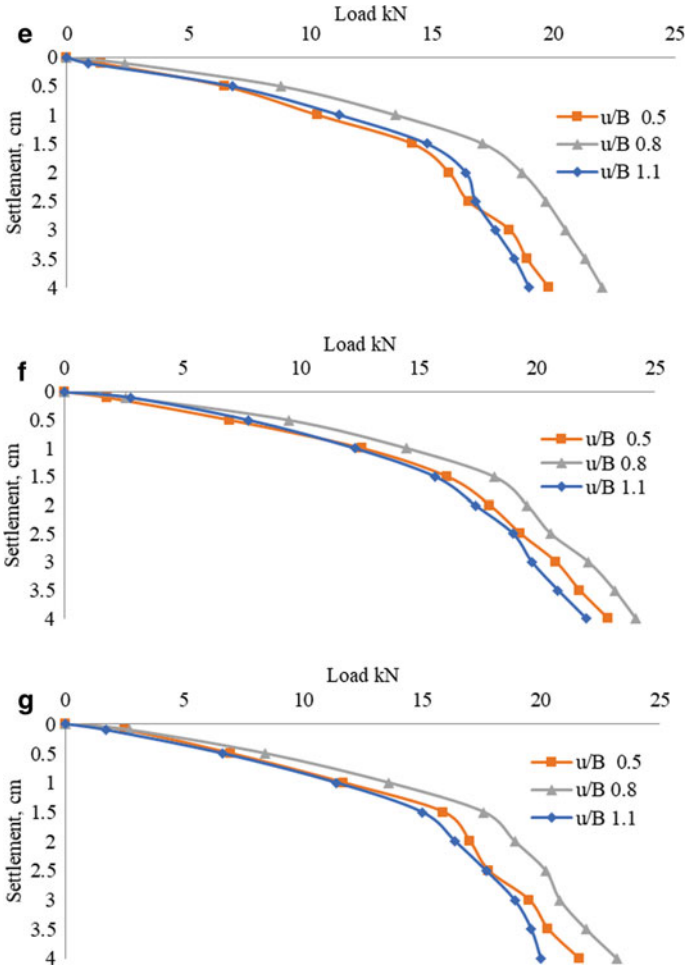

Fig. 6 (continued)

Soil reinforced with single sided 3D reinforcement

Soil was reinforced with single sided 3D reinforcement with variation of height A1 from 1 to 3 cm. The depth of single sided 3D metal strips was also varied as 0.5, 0.8, and 1.1B from top. As the height of vertical blade was varied 1–3 cm, and $1 \geq 0.5B$ it was not possible to place the reinforcement above depth 0.5B, due to the difficulties in positioning the reinforcement. A significant increase in the bearing capacity was observed, when single sided 3D reinforcement with 1 cm high upper blade was used as reinforcement. This may be due to fact as 3D reinforcement can provide the passive resistance to the lateral displacement of the foundation soil and distribute the load to the wider area, thus minimizing the stresses. The vertical blade of reinforcement acts as the retaining wall resulting in the increases of passive resistance of soil

against shearing. When the height of the upper blade was increased to 2 cm, a further significant increase in bearing capacity was observed due to increase in the passive resistance and confinement of soil with increase in the height of the vertical blades. When the height of blade was further increased to 3 cm, a drop in load carrying capacity was observed. With the height of blade (A1) increased to 3 cm, the blade deflected under the lateral earth pressure and hence reduced the passive resistance of soil against shearing. Figure 6b–d shows load settlement behavior of footing with different u/B for single sided 3D reinforcement.

Soil reinforced with double sided 3D reinforcement

In this case, A1 is fixed at 2 cm, as maximum load carrying capacity was observed when height of upper blade (A1) is 2 cm. The height of lower blade (A2) was varied from 1 to 3 cm. The level of placement of double sided 3D metal strips was varied as 0.5, 0.8 and 1.1 B from top. When soil was reinforced with double sided 3D reinforcement having 1 cm high lower blade (A2), load settlement response was found similar to that for single sided 3D reinforcement with 2 cm high upper blade (A1) at a depth 0.5B and 1.1 B. The trend of load settlement response similar but a higher load bearing capacity was observed in case of double sided 3D reinforcement with 1 cm high lower blade (A2), placed at 0.8B as compared to that of single sided 3D reinforcements placed at the same depth. When the height of lower blade (A2) was increased to 2 cm keeping the height of upper blade as 2 cm, a significant increase in the load carrying capacity of footing was observed. It may be due to the fact that it not only provides the passive resistance on the upper side of reinforcement, but also on the lower side of the reinforcement. The movement of soil particle laterally was restricted by the lower blade and hence increases the confinement of soil below the footing also. When the height of lower blade (A2) was further increased to 3 cm, a drop in the load carrying capacity was observed. This may be due to lower blade started deflecting under lateral pressure and passive resistance of soil was reduced below the footing. Figure 6e–g show load settlement response curves with different u/B for double sided 3D reinforcement.

6 Effect of Reinforcement Shape and Dimensions on Bearing Capacity Ratio (BCR)

Figure 7a, b, c clearly indicates that by placing a double sided 3D reinforcement with 2 cm A1 and 2 cm A2 under the footing, highest load was carried by the footing. Figures also depicts that a significant higher load can be carried by the footing if double sided 3D reinforcement was used as compared to any other types of reinforcement irrespective of depth of reinforcement. The maximum load carrying capacity of footing was observed when double sided 3D reinforcement was placed at a depth of 0.8B below the footing.

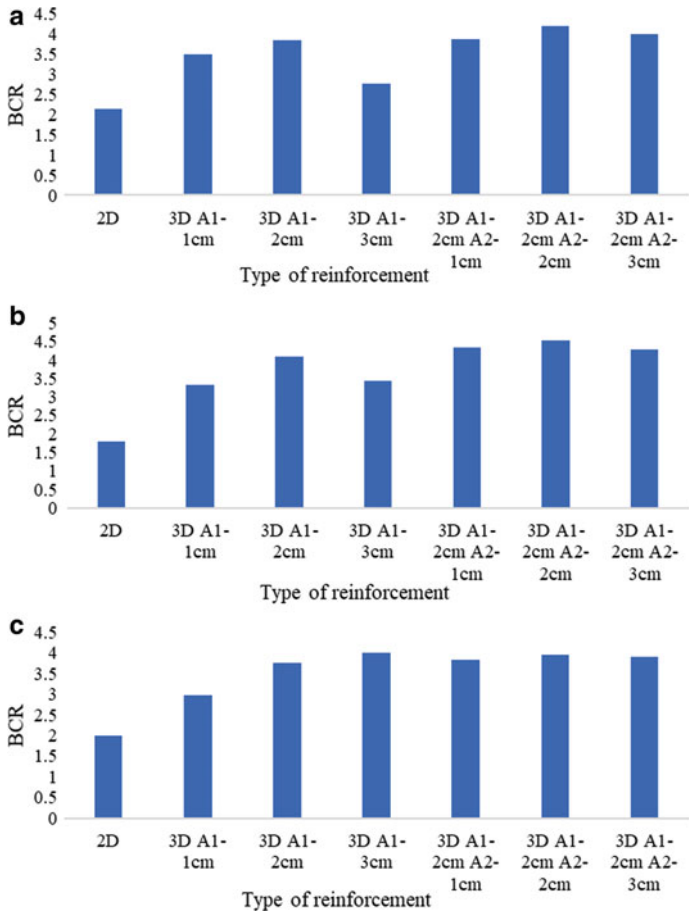

Fig. 7 **a** BCR versus type of reinforcement at u/B 0.5. **b** BCR versus type of reinforcement at u/B **0**.8. **c** BCR versus type of reinforcement at u/B 1.1

7 Conclusion

In the present study, plate load tests were carried out on the strip footing in the lab. The effect of the 2D and 3D reinforcement (one side blade and two side blade) with respect to its level of placement from the top and the height of blades were observed to get the optimum depth of metal strip of different shape and size. From the above study, the following facts may be concluded. The maximum increase of about 111% was observed when 2D reinforcement was placed at a depth of 0.5 times the width of footing from the bottom of footing. In the case of 3D reinforcement, the maximum increase in load carrying capacity about 270% was observed when the height of vertical blade was 2 cm.

This increase was observed when the reinforcement was placed at a depth of 0.8 times the width of footing.

When double sided 3D reinforcement was used, an increase of 353% in load carrying capacity of footing was achieved when it was placed at a depth of 0.8B and the height of upper and lower blades was equal to 2 cm.

References

1. Azzam WR, Nasr AM (2015) Bearing capacity of shell strip footing on reinforced sand. J Adv Res 6:727–737
2. Chen Q, Abu-Farsakh M (2015) Ultimate bearing capacity analysis of strip footings on reinforced soil foundation. Soils Found 55:74–85
3. Ciceka E, Gulerb E, YetimogluaT (2015) Effect of reinforcement length for different geosynthetic reinforcements on strip footing on sand soil. Soils Found 55:661–677
4. Kumar J, Chakrabort M (2015) Bearing capacity of circular foundation on layered sand clay material. Soil Found 55:1058–1068
5. Tafreshi SN, Moghaddas Dawson AR (2010) Comparision of bearing capacity of a strip footing on strip footing on sand with geocell and with planar forms of geotextile reinforcement. Geotext Geomembr 28:72–84
6. Das BM (2013) Principals of foundation engineering. Cengage Learning
7. Lawton EC, Khire MV, Fox NS (1993) Reinforcement of soils by multioriented geosynthetic inclusions. J Geotech Eng 119(2):257–275
8. Zhang MX, Javadi AA, Min X (2006) Triaxial tests of sand reinforced with 3D inclusions. Geotext Geomembr 24:201–209
9. Hou J, Zhang M-X, Dai Z-H, Li J-Z, Zeng F-F (2010) Bearing capacity and mechanism of soil bed reinforced with horizontal vertical inclusions on strip shallow foundation. Doctor of sciences thesis (2010)
10. Hou J, Zhang M, Dai Z, Li J, Zeng F (2016) Bearing capacity of strip foundations in horizontal-vertical reinforced soils. Geotext Geomembr 45(1):29–34
11. Harikumar M, Sankar N, Chandrakaran S (2016) Behaviour of model footing resting on sand bed reinforced with multidirectional reinforcing elements. Geotext Geomemb 44:568–578

Environmental Impact Assessment of Soil Stabilization Materials

Ilyas Bhat, S. Rupali, and Arvind Kumar

Abstract During the past few decades lot of emphasis has been laid upon utilization of waste materials to improve the sustainability in environment. Even though we have been able to successfully utilize the primary waste product but its environmental impact remains the cause of concern. Without determining the toxicity characteristics of compounds formed during the reactions and their potential hazardous characteristics we cannot claim that the added compound has proven to be environment friendly on mere eradication of primary pollutants or waste products. The study has been carried out to determine the formation of compounds on addition of Fly Ash (FA) in soil. X-ray diffraction technique was incorporated in the study to characterize the compounds formed during the analysis. During the course of investigation calcium, aluminum and sulfur-containing compounds were observed. In addition to compounds, a variety of mono-valent, Di-valent ions were also traced. The ecological toxicity level of compounds was determined and compared with the toxicity potential of primary additive compounds.

Keywords Ecological toxicity · X-ray diffraction · Fly ash

1 Introduction

Soil stabilization is generally accomplished using mechanical and chemical methods. Among chemical methods of soil stabilization, the use of calcium-based stabilizers is most prominent. Fly ash is a fine powder consisting of inorganic mineral constituents in the coal and the organic matter which is not fully burnt during the combustion of coal. Due to cementitious properties of fly ash, its use in stabilization has increased from the last few decades. The principle constituents in fly ash are silicon dioxide (SiO_2), aluminum oxide (Al_2O_3) iron oxide (Fe_2O_3) calcium oxide (CaO), and carbon content. Ash also contains smaller amounts of MgO, TiO_2, Na_2O, and K_2O and very small quantities of 20–50 elements [1]. The addition of fly ash is

I. Bhat (✉) · S. Rupali · A. Kumar
Department of Civil Engineering, Dr. B. R. Ambedkar National Institute of Technology, Jalandhar 144011, Punjab, India
e-mail: ilyasab.ce.18@nitj.ac.in

K. R. Reddy et al. (eds.), *Sustainable Environment and Infrastructure*, Lecture Notes in Civil Engineering 90, https://doi.org/10.1007/978-3-030-51354-2_37

primarily incorporated to impart the strength and control expansive characteristics of soil and sustainably eradicate the waste product of various industrial plants which is obtained in the form of Fly ash. It has been reported by various studies that on treatment of soil with fly ash several chemical reactions occur which in turn lead to the formation of compounds like Ettringite ($Ca_6Al_2(SO_4)_3(OH)_{12}\cdot 26H2O$), Thaumisite ($Ca_6Si_2(SO_4)_2(CO_3)_2(OH)_{12}\cdot 24H_2O$), Sulphates ($SO_4^-$), and other heavy metal ions as well [2, 3].

Due to formation of such compounds primarily Ettringite and Thaumisite, the desired engineering properties are affected adversely that include swelling and strength characteristics of soil. Even though it has primarily proven to impart strength, it cannot be called a sustainable means of utilization of fly ash since, disposing of the waste from the sight or primary process treatment of waste does not guarantee its sustainability. Numerous studies have been conducted in the past to determine the post-treatment effects of fly ash or lime-based utilization of stabilization materials. Apart from the studies of engineering behavior one of the important characteristics of this paper is to study the ecological effects of the compounds formed and proportionately study their leaching out chances [4]. XRD analysis was used to determine the chemical composition of the mix. X-Ray Diffraction (XRD) is a technique that is used for characterization of different compounds. Powdered XRD technique was employed as per the method suggested by Moore and Reynolds [5]. Cu-kα radiations were used to obtain the diffraction patterns of the sample. The recorded diffraction patterns were categorized on the basis of data provided by International Centre for Diffraction Data (ICDD).

2 Properties of Materials Used

Kaolin is a type of soil which mainly constitutes kaolinite or hydrated Aluminum silicate as its chief component. These types of soils are generally soft and plastic in nature thus categorized as weak soils for construction purpose [6]. Fly ash on the other hand is in good possession of cementitious properties and is generally used to enhance the strength parameters of weak soils. This study primarily involves in determination of fly ash as a sustainable additive for stabilization of Kaolin clay. Different tests were performed on these materials for determination of their properties. Table 1 describes the physical properties of the soil used during the study.

Fly ash used in the study was locally acquired from a geo-thermal plant. Tables 2 and 3 list out the physical and chemical properties of fly ash used during the course of study. The physical and chemical properties of fly ash are attractive for many civil engineering applications, such as usage in concrete production or soil stabilization. Many construction materials—such as lightweight concrete or low heated concrete products, controlled low strength aggregate material, and fly ash stabilized soils use Fly ash as the chief component. Fly ash is one such pozzolanic material, which mainly consists of silica and alumina. These compounds will form a cementitious material when combined with cement in the presence of water.

Table 1 Properties of Kaolin clay

Properties	Calculated value	Unit
Soil classification	CL	–
Liquid limit (LL)%	42.9	–
Plastic limit (PL)%	18.9	–
Specific gravity (G)	2.68	–
OMC%	19.2	–
Maximum dry density (MDD)	16.75	kN/m^3
Unconfined compressive strength (UCS)	104.2	kPa
Split tensile strength (STS)	23.24	kPa

Table 2 Physical properties of fly ash

Fly ash	Properties
Color	Dark grey
OMC%	30.8
MDD	13.8 kN/m^3
Specific gravity (G)	2.2
pH	12.5

Table 3 Chemical composition of fly ash

Chemical composition (%)	Fly ash
CaO	20
SiO_2	30
Al_2O_3	19
Fe_2O_3	7.0
MgO	5.0
AsO	3.9
HgO	2.9
PbO	4.0
SO_3	6.0
LOI (Loss of Ignition)	1.9

Soil and fly ash were mixed in proportions of (85:15), (80:20), and (75:25), respectively. Different tests were performed on the mixed proportions and strength parameters were determined. It was found that 20% addition by weight of fly ash produced maximum strength in the sample [7]. Table 4 describes the properties of proportionate mixes.

Table 4 Properties of soil: fly ash mix

Mixing ratio (soil:fly ash)	OMC (%)	MDD (kN/m^3)	pH	UCS (Kpa)
85:15	17.9	17.1	8.51	163.6
80:20	17.3	17.2	9.0	175.6
75:25	16.9	17.5	9.1	160.5

2.1 Kinetics of Reaction

Chemical interactions involved in Ettringite formation during lime (CaO or $Ca(OH)_2$) stabilization of soil are given in summary as follows [8, 9]:

$$CaO + H_2O \longrightarrow Ca(OH)_2 \quad \text{(Hydration of quicklime)} \tag{1}$$

$$Ca(OH)_2 \longrightarrow Ca^{2+} + 2(OH)^- \quad \text{(Ionization of calcium hydroxide pH rises } > 12.3) \tag{2}$$

$$Al_2Si_4O_{10}(OH)_2 \cdot nH_2O + 2(OH)^- + 10H_2O \longrightarrow 2\{2Al(OH)^-4H_4SiO_4\} + nH_2O \quad \text{(dissolution of clay mineral, at pH } > 10.5) \tag{3}$$

$$M_xSO_4 \cdot nH_2O \longrightarrow XM^Y + SO_4^{2-} + n \cdot H_2O \tag{4}$$

Dissolution of sulfate minerals; $x = 1$, $y = 2$ or $x = 2$, $y = 1$.

Sulfate (from soil or groundwater) + Aluminum compounds (released from the clay) + Calcium (from hydrate lime or quicklime) → calcium–aluminum sulfate (Ettringite).

$$6Ca^{2+} + 2Al(OH)_4^- + 4OH^- + 3(SO_4)^{2-} + 26H_2O \longrightarrow Ca_6Al_2(SO_4)_3(OH)_{12}, 26H_2O \quad \text{(Formation of Ettringite)} \tag{5}$$

Several investigators have tried to derive and establish equations for the rate of Ettringite formation [1]. The equation suggested by Jander [10] is the most frequently used. This equation is as follows:

$$\left[1 - (1 - \alpha)^{1/3}\right]^N = Pt \tag{6}$$

where α is the reaction ratio (fraction which has reacted), t is time of hydration, and P is a rate constant. This equation is based on the assumption that Ettringite forms when substance A reacts with substance B to form product AB. While Jander [10] reported that the N value was equal to 2.

3 Characterization of Compounds by XRD Data

On pursuance of XRD analysis of soil mixed with fly ash in different proportions even though formation of Ettringite and Thaumisite were not detected on primary levels, the presence of every element of the compound depicts that if feasible conditions are provided by environment it may lead to the formation of Ettringite and Thaumisite. The feasibility of reaction is governed by various factors which include pH, thermodynamic factors, etc. in case of a sulfur attack which can occur from the soil by groundwater capillarity or composition of soil or open environment the chances of formation of Ettringite are gruesome. Heaving of about 30–60 cm has been reported within two years of construction [9]. Figure 1 depicts the XRD patterns obtained on the analysis of sample, while Fig. 2 represents the XRD pattern of the compounds found in major concentrations.

Apart from the Ettringite formation an appreciable content of heavy elements like Palladium, Ytterbium, Arsenic, Lead, and Mercury were determined. The presence of these elements even in traces can prove very harmful and hazardous to aquatic life, crops, and human life. Numerous case studies have reported in the past about the deaths of lead poisoning and raise of cancer and other neurological diseases due to the presence of Arsenic and mercury. Figure 3 represents the elemental data acquired from the sample on XRD analysis.

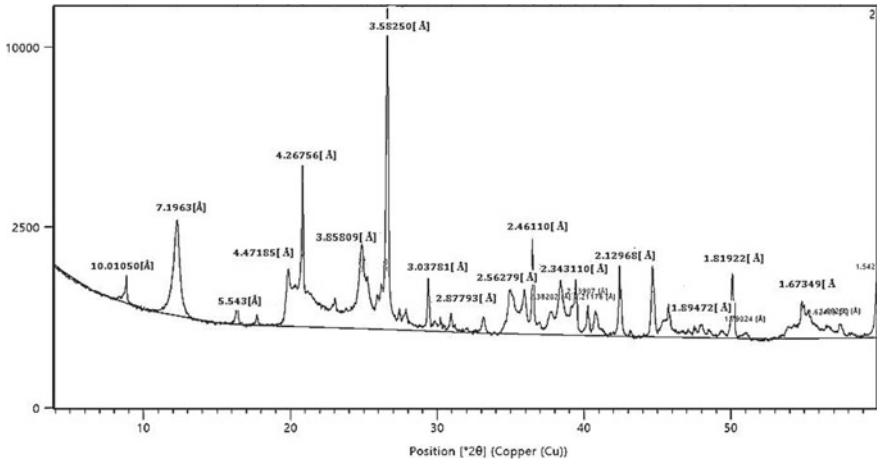

Fig. 1 XRD patterns obtained on the analysis of sample

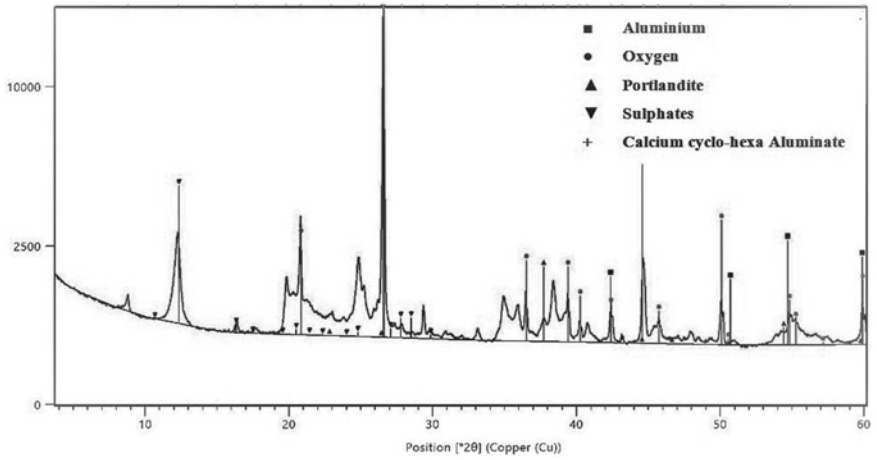

Fig. 2 XRD pattern of the compounds found in major concentrations

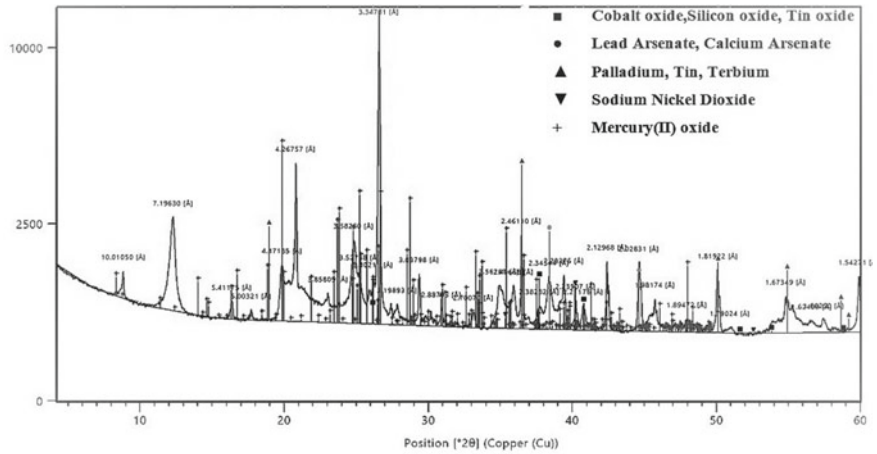

Fig. 3 Elemental data acquired from the sample on XRD analysis

4 Conclusion

Formation of compounds like Ettringite and Thaumiste are highly governed by the feasibility of chemical reaction even if the compounds are present in elemental form can be inhibited to form the compounds. Fly ash a huge waste product has to be used sustainably. Mere dumping or addition to open atmospheric conditions may prove to be hazardous in several means especially in terms of environmental aspects. Leachate characteristics of soil mixed with fly ash can determine the effects of leaching out compounds on environmental conditions.

References

1. Kumar SM (2011) Cementitious compounds formation using pozzolans and their effect on stabilization of soils of varying engineering properties. In: International conference on environment science and engineering IPCBEE Singapore, vol 8, pp 212–220
2. Ouhadi VR, Yong RN (2008) Ettringite formation and behaviour in clayey soils. Appl Clay Sci 42:258–265
3. Grier DG, Jarabek EL, Peterson RB, Mergen LE, McCarthy GJ (2002) Riveted structure refinement of carbonate and sulfite ettringite. In: JCPDS-international centre for diffraction data, advances in X-ray analysis, vol 45, pp194–199
4. Leelarungroj K, Likitlersuang S, Chompoorat T, Dao J (2018) Leaching mechanisms of heavy metals from fly ash stabilised soils. Waste Manag Res (Sage Publication) 1:1–8. https://doi.org/10.1177/0734242X18775494
5. Moore DM, Reynolds RC (1989) X-ray diffraction and identification and analysis of clay minerals. Oxford University Press, New York, p 332
6. Alrubaye AJ, Hasan M, Fattah MY (2016) Stabilization of soft kaolin clay with silica fume and lime. Int J Geotech Eng 1–7. https://doi.org/10.1080/19386362.2016.1187884
7. Shahu JT, Patel S, Senapati A (2013) Engineering properties of copper slag-fly ash–dolime mix and its utilization in the base course of flexible pavements. J Mater Civ Eng 25(12):1871–1879
8. Ouhadi VR (1997) The role of marl components and ettringite on the stability of stablized marl. PhD thesis, McGill University, Canada, p 236
9. Hunter D (1988) Lime induced heave in sulfate-bearing clay soils. J Geotech Eng Am Soc Civ Eng 114:150–167
10. Jander W (1927) Solid state reactions at high temperature in German . Zeitschrift Für Anorganische Und Allgemeine Chemie 163:1–30

The Role of Environmental Geotechnics in Building Earth Dike Made from Side Energy Products

Petr Cernoch and Jiri Kostal

Abstract Brownfields are nowadays frequently being used for storing side energy products from the rear fuel cycle at classic power plants. These products are deposited in liquid form by pipeline need a certain space bounded by an earth dike. The use of traditional soil in the dike can be costly and therefore the construction of dikes from local material—coal slag—is proposed. The earth dike was built on the sediments in former sludge lagoon. Shortly after the first flooding of slag there was a breach of the dike. Geotechnical solution followed the incident: field tests were carried out and laboratory analyzes were performed. Mathematical analysis based on the results from field and laboratory tests was simulated. The numerical calculations were used to determine the most probable causes of the breach and the proposed solution—redevelopment of the dike.

Keywords Energy products · Ponded ash · Earth dike · Mathematical analysis

1 Introduction

The rear fuel cycle at coal-fired power plants is the operation area of removal of side energy products (SEP). Continuing brown coal mining leads to a tight balance situation where a significant problem with free space for the deposition of excavated soil and SEP begins. So-called brownfields (previously claimed to be unfit for buildings and constructions) are nowadays frequently being used. SEP has to be stored somewhere and brownfields are perfectly suited for this purpose. That is why Environmental geotechnics are dealing with non-standard buildings (including their establishment) more and more often [1].

P. Cernoch (✉)
CEZ Energy products, Komenskeho 534, 253 01 Hostivice, Czech Republic
e-mail: cernoch.petr@inset.com

J. Kostal
INSET, Lucemburska 1170/7, 130 00 Prague, Czech Republic

Czech Technical University in Prague Faculty of CE, Thakurova 7/2077, 166 29 Prague, Czech Republic

K. R. Reddy et al. (eds.), *Sustainable Environment and Infrastructure*, Lecture Notes in Civil Engineering 90, https://doi.org/10.1007/978-3-030-51354-2_38

In the case that SEP is deposited in liquid form for storage, a certain space bounded by an earth dike must be built. The resulting structure—redepositing cassette—serves as a repository for liquid SEP. A mixture of coal ash, slag, and water called ponded ash is pumped into this space by pipeline. During the flooding process coarse particles settle down. This results in a decrease in the content of suspended solids in residual water left at the surface which can be further utilized and discharged into natural watercourse [2].

The use of high quality soil in the earth dike can be costly and therefore the construction made from local material is proposed. In our case, there were 5 redepositing cassettes. A new one No. 6 was built in order to increase the capacity for SEP. This cassette was linked to former one (No. 4) and used its main dike (see Fig. 1). Just like the others in the area of interest, this new earth dike was made of solid slag—material produced by granulating boilers composed mainly of coal ash ($SiO_2 + Al_2O_3$) and water. It was 3 m high and 190 m long.

The east side is located in the spoil heap body the north side is located nearby residual mere of former storage lagoon (SEP pond). In the west and in the south passes the boundary of the surface brown coal mine. The foundation and operation of the construction in such an unbearable anthropogenic surrounding faces certain environmental and geotechnical hazards [3].

Fig. 1 Situation of the redepositing cassette No. 6—former storage lagoon in the middle, edge of the coal mine bellow

2 Start State

2.1 Geological Environment

The subsoil of the newly built earth dike was formed by sediments of a former storage lagoon for sludge; coal slag and ash. The SEP material was flooded in this area and consisted of dry ash and coal slag from power plant and coal sludge from coal mine. The pipeline has been shifted several times. All probes of exploratory works carried out in the past showed thick coal sludge positions mixed with ponded ash sediments. The coal sludge was predominantly fine-grained sand like and was about 3–5 times more compressible than the slag-ash sediment. Also coal sludge permeability was 10–100 lower than material composed of ponded ash. However, the effective shear strength values of sludge and ash practically did not differ.

Previously collected sediment samples showed grain fluctuations ranging from predominantly clayey, silty sand to medium-grained sand. This phenomenon is related to the relocation of the pipelines in the past. Close to the pipeline outlet, the coarsest fractions of the suspension are deposited, average grain size decreases with increasing distance. Fine grains are usually carried away for a long time and distance. During the relocation of the pipeline sediment with cross-layer structure is created. In this sediment are subsequently forming coarser and finer positions. The same phenomenon can be observed on coastal sediments of river flows [4].

Before the construction of the dike begun, the area of interest had been covered by overwhelmingly dense, high reeds. The surface had low bearing capacity, and the level of groundwater was almost on the terrain.

2.2 Solution of the Event

After the dike was completed, the earth dike was stable. No significant cracks have been documented, respectively. It is important to say that no geotechnical monitoring has been established and performed during the construction and operation of the redepositing cassette No. 6. Damage of the cassette's earth dike occurred during the first filling (see Figs. 2, 3).

Geotechnical solution followed the incident: first of all it was necessary to carry out field tests and laboratory analyzes. Due to poor accessibility of the structure, low bearing capacity of the surface, and time pressure it was impossible to drill boreholes. Therefore only dynamic probing and dynamic plate load tests with light weight deflectometer were realized.

Field and laboratory tests performed. Dynamic probing (DP)—execution of dynamic penetration probes—involves driving a steel cone vertically into the ground using a sliding hammer and recording the number of blows for each 100 mm of penetration. The test provides a continuous profile of ground resistance with depth, rather

Fig. 2 Filling the cassette

Fig. 3 Damaged earth dike

than at the discrete depths of a conventional standard penetration test. A specific dynamic resistance Q_{dyn} is gathered from recorded values. Dynamic plate load tests with the light weight deflectometer are used to control the soil compaction. Appropriate subsoil deformation measurements are carried out. Sufficient compaction of

the tested subsoil can be determined immediately after the measurement. Geodetic measurements were also carried out.

Two samples of coal slag were collected for following laboratory tests to obtain the oedometric module and shear strength. With oedometer tests are measured the one-dimensional compression and swelling characteristics of a soil. From the changes in thickness of the sample at the end of each load stage the compressibility of the soil may be observed, and parameters measured such as compression index and coefficient of volume compressibility. From the changes in thickness of the sample recorded against time during a load stage the rate of consolidation may be observed and the coefficient of consolidation measured. Laboratory tests on both samples showed for the loading step from 4 to 10 kPa oedometric module 0.4 MPa, for the next step 10 to 20 kPa was resulted 0.8 MPa and for 20 to 30 kPa $E_{oed} = 1.5$ MPa.

Direct shear test or box shear test is used to determine the shear strength of the soil. Shear strength of a soil is its maximum resistance to shearing stresses. Using direct shear test it is possible to find out the cohesion and angle of internal friction.

The shear test of the coal sludge showed an angle of effective internal friction angle of 35.8° and cohesion of 12 kPa. These values are very close to the average coal ash statistics, which are 36° and 7 kPa. We note that the application of these values requires dispersion of the pressure-induced pore pressure, which in the case of coal sludge will be significantly slower than that of the ponded ash sediment.

Results of the tests. Achieved values from performed field and laboratory tests showed presence of a mixture of coal sludge and coal ash or slag at different depths under the surface.

On the basis of the results obtained and the comparison with previous works, it can be stated that the abrupt reduction of the penetration resistance in the DP is associated with a higher admixture of coal sludge in the sediments. The sludge significantly reduces sediment permeability, thanks to their saturation, are soft to mash consistency and low penetration resistance.

Another characteristic of the results of the DP is the marked fluctuation of the penetrating resistance with the depth which was recorded in all probes. It can be assumed to be related to changes in the sediment grain size. In finer positions, it can be affected by induced pore pressure rather than in coarser positions. At the same time, the incidence of coal sludge is very likely to occur. The results of the probes showed that the sediment was in a very loose state and showed the appearance of alternating layers of coal sludge and ponded ash in the area of interest.

In the profile of the dike were locally documented significant decreases in the values of the dynamic penetration resistance, both at the base of the dike and in the entire dike. It is therefore possible to consider the insufficient compaction of the dike in place of DP (see Fig. 4). On the basis of the penetration results it can be expected that the values of the oedometric modulus of the ponded ash are low, about 1 MPa, for the coal sludge the modules will be even lower.

The gathered results from dynamic plate load tests supported the conclusions described above. The tests showed an insufficient density of the earth dike. The calculated value of deformation module $E_{def,\,2}$ was in all cases lower than 5 MPa.

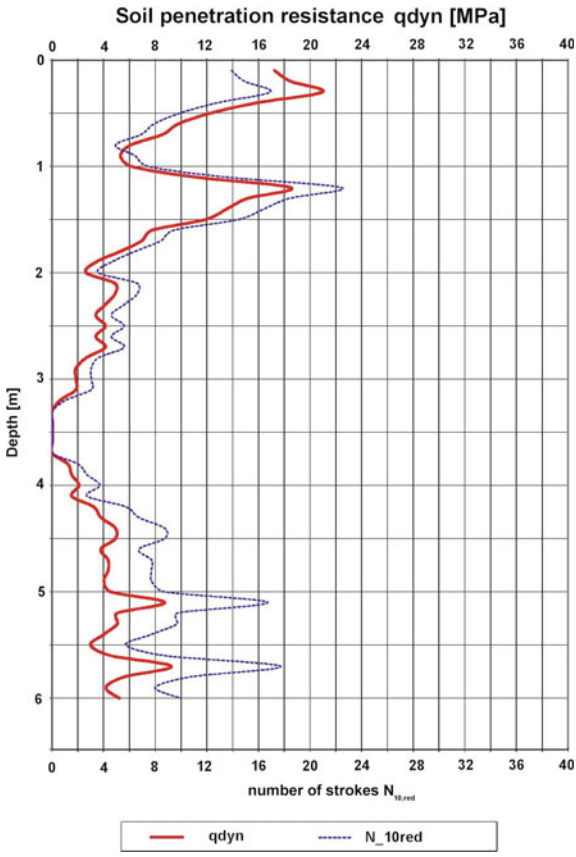

Fig. 4 Penetration curve in the DP6 probe

Geodetic measuring of the height of the dike revealed its uneven settlement—in some places, the altitude of the top of the earth dike settled down by 400 mm in contrast to the blueprint.

2.3 Mathematical Modeling

To determine the probable cause of the occurrence of an extraordinary event and to propose a further course of work and to design a new earth dike, mathematical modeling was performed (see Fig. 5). After determining the input data—results from field and laboratory tests and the geometry of the area including initial and boundary conditions numerical analysis was simulated.

Calculations of stability and deformations made in software PLAXIS used the finite element method. Most of these processes are described using partial differential equations. The variational method is used for solving these equations. Variational

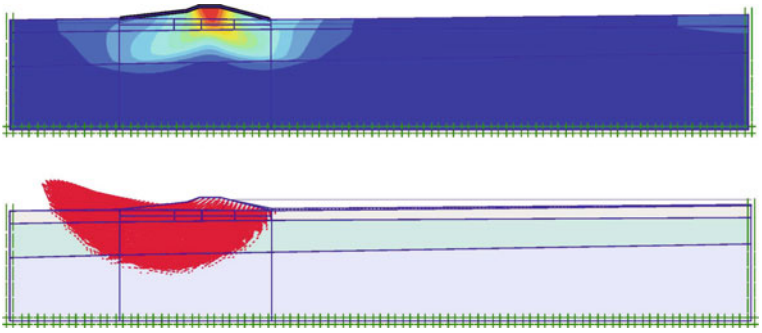

Fig. 5 Mathematical modeling—deformations of the earth dike (influence of the sludge layer) and shear deformation (due to flooding of the cassette)

approaches are primarily based on the philosophy of energy minimization. Slope failure in the finite element model occurs naturally through the zones in which the shear strength of the soil is insufficient to resist the shear stresses. For stability evaluations the Mohr–Coulomb failure envelope was used and thus the effective shear strength parameters were obtained.

The local deformation of the structure was mainly due to the inhomogeneity of the subsoil where the soil with lower shear parameters was stored. At the same time, due to high level of saturation, local loss of stability could occur due to changes in the proportions of active and passive forces but also due to the decrease of soil cohesion, especially in the unconsolidated zone by soil softening.

Furthermore, insufficient compaction of the earth dike at different altitude levels was documented. As a result of it other deformations of the dike could occur. The water could also leak into the dike body through the cracks. Consequently, the integrity of the earth dike was ruptured.

3 Evaluation of Results

From the above, the complexity and non-homogeneity of the environment are significant. The most important factors can be considered: (1) the material composition of the surroundings and (2) the high level of underground water which varies significantly over time.

From a geotechnical point of view, the redepositing cassettes environment is very complicated. It is not well suited for building an earth dike using standard method and classical approach without any technological modifications or subsoil improvements [5, 6].

Despite the inappropriately foundation conditions (former sludge lagoon) geological survey was not carried out, neither field or laboratory tests were performed. There was no archive data for evaluation local soil properties. Further, no monitoring of the construction was established during the construction nor afterwards. Technological failures and poor quality of the project played an important role too.

The subsoil of the earth dike was made of coal ash and slag. These sediments were very loose and their behavior was influenced by the presence of coal sludge located deeper and by the high level of groundwater that was directly related to the level of free water in the residual mere nearby.

An additional survey showed frequent alternation of the ponded ash sediments with coal sludge in the subsoil of the earth dike.

The most probable cause of the break of the dike is the combination of several factors: uneven settlement of the dike body and especially its subsoil; increase in groundwater level in the area of interest; possible dynamic effects from filling of the cassette, which could have led to the loss of bearing capacity underlying soil due to liquefaction and insufficient safety space for the free water level in the cassette (height only of 0.40 m) resulting in possible overflow.

The saturation of coal sludge results in a decrease in its density, up to a third of the original value. This is the cause of a significant reduction in their bearing capacity. It is highly probable that uneven settlement of the earth dike, which was in some places greater than 0.40 m, has occurred. This has resulted also in the overflow of the top of the dike. Subsequently, the dike was already unstable and deformed. The rupture happened in the weakest place, where the coal sludge was closest to the surface.

4 Technical Recommendations

In the earth dike body, transverse and longitudinal cracks were documented. Realized DP probes proved non-homogeneous profile of the dike. Therefore, it was not recommended to carry out the remediation or redevelopment of the dike, but the construction of a new one.

The proposal for redevelopment or remediation of the earth dike as in traditional approach could have been financial and time-consuming. The construction was in such a bad condition that we designed the better and faster solution that was absolutely necessary—building a completely new earth dike from solid slag with an overloading bench that will respect the conclusions from the survey conducted.

It was recommended to drain the area of interest (especially coal sludge) before the construction of a new dike. As with the construction of adjacent redepositing cassettes previously built, the most demanding operation is the storage and compaction of the first layer of the earth dike.

As an improvement of the subsoil, it can be taken to partially homogenize the subsoil at the site of the newly built earth dike and to form the surface spacer layer. It was therefore recommended to use a mixture of slag and gravel (fraction from 9 to 163 mm) with a thickness of 0.50 m. At the same time it was proposed to reinforce the base of foundation of newly constructed earth dike body with assistance of geotextile (tensile strength approx. 30 kN/m). Another option was to use a combination of geosynthetics—geogrid, supplemented with lighter geotextile (grammage approx. 300 g/m^2).

It is not possible to use a roller machine with vibration during compaction of layers of slag. It could result in the liquefaction of loose, saturated sediments forming the immediate subsoil of the earth dike. When rolling and compacting the first slag layer of the earth dike body, contact with groundwater must not occur. Therefore, drainage grooves in the bottom of the cassette have been designed to draw water away from the base of the dike (see Fig. 6).

Compared with previously projected earth dike, it was recommended to reduce its height to 2.50 m (from the original 3.00 m) and reduce the position of overflowing objects so that their axis was 0.80 m (originally 0.40 m) from the top of the earth dike. Total settlement of the subsoil induced by the weight of the earth dike with reduced height to 2.50 m was expected between 0.20 and 0.60 m based on numerical calculations.

Within the structure of the earth dike, it was recommended to connect the geosynthetics so that they could not slip after their contact. Simultaneously it was proposed to create a sealing element from the soil (from the surroundings) on the upstream

Fig. 6 Construction of a new earth dike

slope of the dike. The slopes of the downstream and upstream face were designed in incline 1:3.

It was also recommended to build an overloading bench in downstream face of the earth dike, built from slag.

Last but not least, it was recommended to carry out basic monitoring of the structure both during its construction (control tests) and during subsequent operation (especially geodetic measurement and inspection of the area of interest with emphasis on deformation and leakage).

5 Conclusion

The subsoil of the redepositing cassette for side energy products was formed by coal ash, slag, and coal sludge previously flooded into the former sludge lagoon. It was near the level of water in the residual mere so almost on the surface. It also had a very poor bearing capacity. From the view of Environmental geotechnics this is non-standard and very complicated environment with its specifics, problems, and hazards.

The earth dike of the newly built cassette No. 6 was made of slag. It was closer to the residual mere beside the other older cassettes. During the first filling of the cassette a damage of the earth dike occurred.

This was followed by the solution of the event; field and laboratory tests were performed in no time. Poor geotechnical conditions have allowed only basic survey to be done. After determination of the input parameters a mathematical analysis was executed. Subsequently after field, laboratory tests and numerical modeling, the most probable causes of the accident were identified and a further work has been proposed.

We found that a several mistakes were made both during projection and construction phase. The top of the earth dike suffered of settlement up to 0.40 m. Such values cannot be expected in usual conditions of green fields. But when building earth dike made from side energy products nearby former sludge lagoon with high level of underground water is this common.

It was not recommended to redevelop or remediate the earth dike due to bad compactness and frequent cracks in the body of the dike. We proposed to build a new one that respects the conclusions identified. Technical and building recommendations included implementation of monitoring of the structure during and after construction.

Thorough inspection and strict control of other cassettes in the area of interest followed. At the present the new earth dike is stable even after the test operation period. It is without visible signs of any deformations or cracks (see Fig. 7).

Fig. 7 New earth dike and flooded cassette—a coal power plant in the background

References

1. Cernoch P, Kostal J (2017) Multi-layer population of boreholes with pore pressure probes. In: Proceedings of the 19th international conference on soil mechanics and geotechnical engineering, Seoul, South Korea
2. Cernoch P, Kostal J (2014) Storage solution of secondary energy products into the sludge area (only in Czech). In: Proceedings of 14th congress of hydrogeology and 2nd congress of engineering geology. CAH, Liberec, Czech Republic
3. Cernoch P, Kostal J (2018) Geotechnical risks of foundation of warehouses built on brownfields. Ernst & Sohn, Verlag für Architektur und technische Wissenschaften GmbH & Co. KG, Berlin, Germany
4. Cernoch P, Kostal J (2015) Proof of the minimum amount of residual water from the float energy by-product. In: Proceedings of the XVI ECSMGE geotechnical engineering for infrastructure and development, Edinburgh, United Kingdom
5. Cernoch P, Kostal J (2018) Prediction of the development of groundwater quality in a finished sludge lagoon. In: Acta polytechnica CTU Proceedings, Prague, Czech Republic
6. Cernoch P, Kostal J (2017) Determination of residual water from the float energy by-products on the spoil heap (only in Czech). Engineering structures, Prague, Czech Republic, 1st edn., vol 05/2017

Enhancement in Shear Strength Characteristics of Soft Soil by Using Nanomaterials

B. A. Mir and S. Hariprasad Reddy

Abstract Soil being particulate system, encompasses a wide variety of particles, which has made it one of the most complicated natural materials to be modeled. Among soils, soft soil deposits pose challenging problems to geotechnical engineers for the assessment of reliable behavior of these soils to be used either as a foundation medium or construction material**.** For chemical stabilization of soils, there are numerous chemical additives such as polymers, cement, and other compounds available for treatment of soft soils, however, nanomaterials, including Nano-Alumina and Nano-Silica have attracted great interest among researchers. Unlike other traditional and non-traditional additives, nano additives are used directly with the soil or being an additive for the stabilization of marginal soil deposits. In this study, nanometric additives have been chosen to investigate their influence on strength behavior of clayey soil. Soil samples from three locations were collected and characterized in the laboratory. Also, SEM and XRD tests were carried out to identify the underlying mechanisms of Nanomaterials. Based on basic geotechnical investigations, the soil samples from two locations were selected for treatment using Nanometric additives of Al_2O_3 and SiO_2 at varying percentages of 0.5, 1.0, 1.5, and 2.0%. The test results revealed that the unconfined compressive strength increased significantly with increasing Nano additives. The addition of these nanoparticles increases sample's reactivity even at an early age and subsequently, compressive strength is increased. Therefore, the main goal of this study was to stabilize soft soil deposits for its bulk utilization in various geotechnical applications for sustainable environment.

Keywords Soil stabilization · Soft soil · Nanomaterials · Unconfined compressive strength · SEM · Sustainable engineering

B. A. Mir (✉) · S. Hariprasad Reddy
Deptartment of Civil Engineering, National Institute of Technology, Srinagar 190006, Jammu and Kashmir, India
e-mail: p7mir@nitsri.net; bashiriisc@yahoo.com; bamiriitb@gmail.com

S. Hariprasad Reddy
e-mail: hariprasad.skit@gmail.com

K. R. Reddy et al. (eds.), *Sustainable Environment and Infrastructure*, Lecture Notes in Civil Engineering 90, https://doi.org/10.1007/978-3-030-51354-2_39

1 Introduction

Soft soils are identified as problematic soils due to their low shear strength, high compressibility, low permeability, high swelling, and shrinkage potential. However, due to scarcity of stable construction sites, there is tremendous pressure on Geotechnical engineers for characterization of marginal/weal soil deposits to be used as either as construction material or as foundation medium. Among various ground improvement techniques, soil stabilization can be achieved by means of mechanical stabilization, soil reinforcement, chemical stabilization, etc. However, in the case of clayey soils, chemical improvement is commonly most effective since it can be used to change the nature of the material and to enhance the mechanical properties of the marginal/soft soils. For chemical stabilization of soils, there are numerous chemical additives such as polymers, cement, and other compounds available for treatment of soft soils, however, nanomaterials, including Nano-Alumina and Nano-Silica have attracted great interest among researchers. Nanotechnology is the study of modeling the materials and devices at microscopic scale [1]. The use of Nanotechnology has been previously dominated by Physicists and Chemists at the atomic level for the human benefit [2, 3]. However, with the help of advanced technology, geotechnical engineers, and researchers are also making use of nanotechnology in the field of ground improvement for sustainable and eco-friendly environment.

Many researchers reported that nanomaterials have emerged as a promising research field to improve mechanical properties of marginal/weal soils [4]. Advanced tools capable for characterization of materials of smallest size of picoNwtons (pN = 10^{-12} N) have provided unprecedented opportunities to researchers for analyzing the structure mechanical properties of materials on nanoscale [5, 6]. Alsharef et al. [7] reported that the nano-alumina–soil mixtures significantly enhanced the engineering properties including volumetric shrinkage strain, volumetric expansive strain, compaction characteristics, the crack intensity factor, etc., of the marginal soils due to the displacement and rearrangement of soil particles by the addition of nano-alumina. Similar results have also been reported by other researchers [8–10]. Zhang [11] reported that the composite mixture of nanomaterials-soils exhibited higher consistency limits compared to natural soils and the presence of fibrous nanoparticles significantly improved the shear strength of marginal soils. Similar results have also been reported by Ghazi et al. [12] and Alireza et al. [13] that with addition of Montmorillonite Nano-clay into the soil increased the liquid limit and plasticity index and improved the unconfined compressive strength of the soil. However, Bahmani et al. [14] reported that SiO_2 nanoparticles had no apparent changes in the liquid limit (LL) of the treated soil and the plastic limit initially increased, but decreased with increasing SiO_2 content. Zaid et al. [15] also investigated the influence of different nanomaterials (i.e., Nano MgO, Nano CuO, and Nano-clay) on geotechnical properties of marginal/weal soils and reported that consistency limits (liquid limit, plastic limit, and linear shrinkage) were decreased and dry unit weight increased with increasing Nanomaterial content. However, it was also observed that addition of nanomaterials beyond optimum content decreased engineering properties

of the soil. Norazlan et al. [16] investigated the effect of nano-kaolin on properties of kaolin clay and concluded that about 3% of nano-kaolin was the optimum content to enhance the geotechnical properties of kaolin clay. Beyond the optimum content of nano-kaolin, the engineering properties of kaolin clay decreased. Neethu and Remya [17] investigated effect of nano-clay on the behavior of lateritic soil and kaolinite clay and concluded that nano-clay increased index properties and unconfined compressive strength, however, maximum dry unit weight and coefficient of permeability decreased. Further, it was demonstrated that about 1% concentration of Nano-clay was the optimum content for stabilization of these soils. Shahin et al. [18] reported that nanoparticles exhibit very high surface and react actively in the composite soil matrix to enhance the mechanical response of marginal soils. Changizi and Haddad [19] investigated effect of nanomaterials on geotechnical properties of clayey soil and concluded that the shear strength parameters were improved on the addition of varying percentages of Nano-Silica and Nano-Zeolite. Many other researchers concluded that Nano additives greatly influence the strength, permeability, compressibility, density of soil [20–22]. Thus, it is seen that unlike other traditional and non-traditional additives, nano additives are used directly with the soil or as an additive for the stabilization of marginal soil deposits. Nanomaterials are among the most eco-friendly and noval materials, which can be use for stabilization of marginal soils for development of sustainable environment. Therefore, in this study, Nanometric additives (Al_2O_3 and SiO_2) have been chosen to investigate their influence on strength behavior of clayey soil at varying percentages of 0.5%, 1.0%, 1.5%, and 2.0 and subjected to unconfined compressive strength (UCS) tests as per standard codal procedures. Scanning electron microscopic (SEM) and XRD tests were also carried out on tested samples to identify the underlying mechanisms of Nanomaterials (Nano-Alumina-Al_2O_3 and Nano-Silica-SiO_2) on the engineering properties of stabilized soils. The test results revealed that the unconfined compressive strength increased significantly with increasing Nano additives. The addition of these nanoparticles increased sample's reactivity even at an early age and subsequently compressive strength is increased. Thus, the main goal of this study was to stabilize soft soil deposits for its bulk utilization in various geotechnical applications for sustainable environment.

2 Materials

2.1 Soil Samples

In the present study, undisturbed and disturbed soil samples were collected from two sites (Site-1: S1-Ganderbal district and Site-2: S2-Pulwama district) in J&K State. These samples were collected at a depth of 1.0 m from the ground surface. At each site, undisturbed soil samples were collected, sealed in polythene bags, and transported for determining their insitu properties.

Table 1 Chemical properties of alumina oxide (Al_2O_3) and nano-silica (SiO_2)

Nano-alumina (Al_2O_3)		Nano-silica (SiO_2)	
Property	Value	Property	Value
Purity (%)	99.9%	Purity (%)	99.9%
Molecular formula	Al_2O_3	Molecular formula	SiO_2
Al_2O_3	>99.9%	SiO_2	99.9%
CaO	<0.017%	Al	0.02%
Fe_2O_3	<0.035%	Fe	0.05%
MgO	<0.001%	Mg	0.1%
SiO_2	<0.055	Ca	0.08%
Average particle size	30–50 nm	Average particle size	30–50 nm
Specific surface area (SSA)	120–140 m^2/g	Specific surface area (SSA)	200–600 m^2/g
Bulk density	1.5 g/cm^3	Bulk density	0.10 g/cm^3
True density	3.97 g/cm^3	True density	2.5 g/cm^3
Color	White	Color	White
Morphology	Spherical	Morphology	Porous
Melting point	2055 °C	Melting point	1600 °C

2.2 Nanomaterials

Two nanomaterials, i.e., Nano-Alumina, (Al_2O_3), Nano-Silica (SiO_2) were used in this present study. The Nano-Alumina and the Nano-Silica materials used in this study were in the form of powder with purity equal to 99.99% supplied by Nano Research Lab, Jharkhand. Alumina particle size range between 30–50 nm. The chemical composition and other allied properties of these nanomaterials are given in Table 1. The nanomaterials were also examined under SEM analysis and SEM images of Nano-Alumina taken by SEM machine Model: HITACHI S-3600 N are shown in Figs. 1 and 2, respectively.

3 Testing Methodology and Experimental Program

3.1 Physical Properties of Soil Material

The disturbed samples were subjected to various soil tests like gradation, specific gravity, Consistency limits, light compaction tests, etc. Consistency limits were

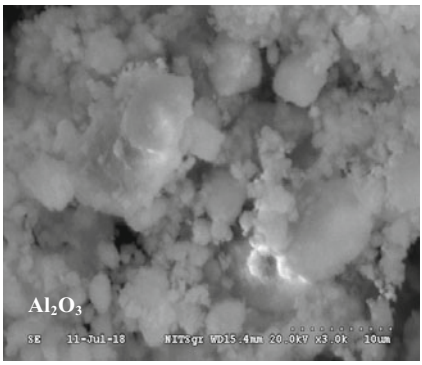

Fig. 1 SEM image for nano-alumina

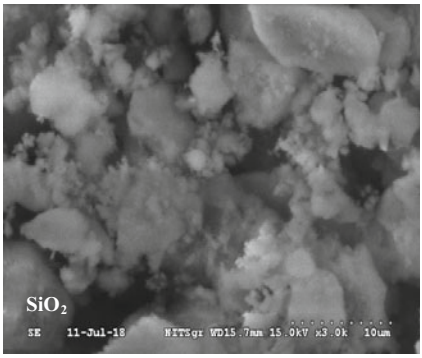

Fig. 2 SEM image for nano-silica

performed on air dried and oven dried samples to check for the organic content. Unconfined compressive strength tests were also conducted on insitu samples to determine shear strength parameters. All the tests were conducted as per the Standard Codal procedures [23–28]. The physical properties of these soil samples are given in Table 2.

3.2 Experimental Program

The experimental program included standard proctor compaction test and unconfined compression tests on soil samples admixed with different percentages of Nano-Alumina and Nano-Silica (0.5, 1.0, 1.5, and 2.0%) with 0.5% increment by dry weight of the soil, respectively. The soil samples were prepared by compacting at $0.90\gamma_{\text{dmax}}$ and corresponding water content on the dry side of optimum (OMC and MDU by standard Proctor test) in a pre-fabricated set-up for conducting unconfined compression tests [28]. After UCS test, soil samples taken near failure plane for the SEM analysis.

Table 2 Physical properties of soil

Property	Site-1	Site-2
Specific gravity, G	2.67	2.61
Natural water content, w_n	28	34
In-situ dry unit weight (kN/m^3)	15.02	12.23
Sand (%)	1	4
Silt (%)	89	91
Clay (%)	10	5
% Finer than 75 μm	99	96
Classification	ML	ML
In situ UCS, q_u (kN/m^2)	57	48.6
In situ UCS, C_u (kN/m^2)	27	24
Optimum moisture content, OMC (%)	19	22
Maximum dry unit weight, MDU (kN/m^3)	17	15.4
Liquid limit, LL (%)	37	42.8
Plastic limit, PL (%)	26	26.3
Plasticity Index, PI = (LL-PL) (%)	11	16.5

4 Results and Discussions

4.1 Physical Index and Compaction Characteristics of Untreated Soil Samples

The soil samples collected from two locations were analyzed as per ASTMD [23]. The specific gravity of these soil samples was determined in accordance with ASTMD [24]. A series of trials were taken on the two samples and the average values of specific gravity are 2.67 for site 1 and 2.61 for site 2, respectively. The particle size distribution analysis for these soil samples was carried out as per relevant codal procedures ASTMD [25] and the particle size distributions curves are shown in Fig. 3. Particle size distribution analysis revealed that the soil is fine grained mainly silt dominated material. Consistency limits such as liquid limit, plastic limit, and shrinkage limits for the Campus soils were determined in accordance with ASTMD [26]. From the test results, the soil is classified as clayey silt with low plasticity (Fig. 4).

The optimum moisture content (OMC) and the maximum dry unit weight (MDU) for soil samples (Site 1 & Site 2) were determined using the Standard compaction test ASTMD [27]. Figure 5 shows the compaction curves for these soil samples. The values of OMC and MDU obtained are 19, 22%, and 17, 15.4 kN/m^3, respectively. Since the dry unit weight for site-2 is relatively less as expected for a stable soil deposits (generally > 17.5 kN/m^3), the soil needs to be improved for sustainable construction of infrastructures.

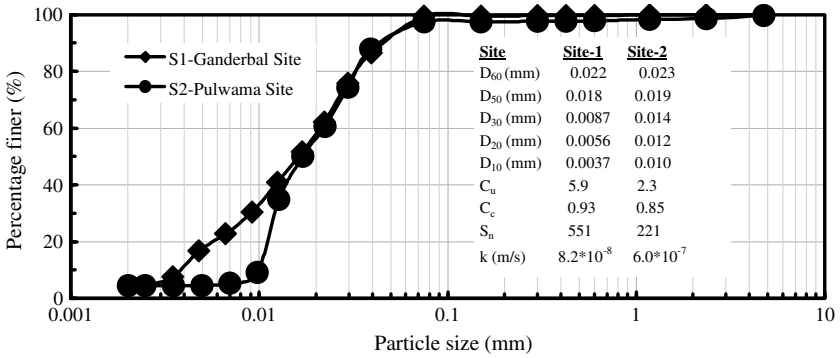

Fig. 3 Particle size distribution curves for soil

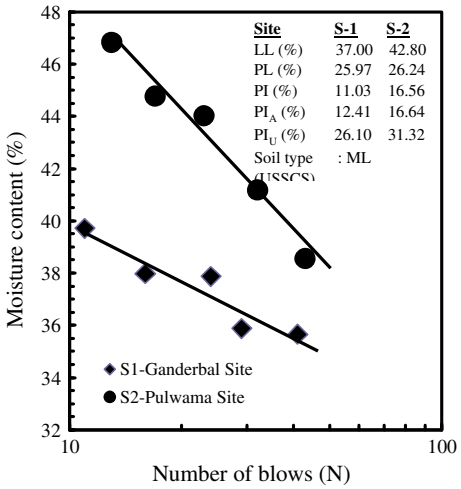

Fig. 4 Flow curves for untreated soils

4.2 Effect of Nanomaterials on Strength Characteristics of Soil

Essentially, the unconfined compression test is a special case of the triaxial compression test of soils where the compression and shear strengths of a soil prism, or cylinder, are measured under zero lateral stress ($\sigma_2 = \sigma_3 = 0$) for short-term stability analysis. In this present research, unconfined compression test was conducted on the soil specimens admixed with different percentages (0.5, 1.0, 1.5, and 2.0%) of Nano-Alumina and Nano-Silica as additives. In both cases, the composite test specimens of height 7.6 cm and diameter 3.8 cm were prepared by statically compacting the mixtures in a pre-fabricated set-up at 0.90 γ_{dmax} and corresponding water content dry side of optimum. The soil samples were tested in an unconfined compression testing machine for "Immediate" test series under a constant strain rate of 0.625 mm/min

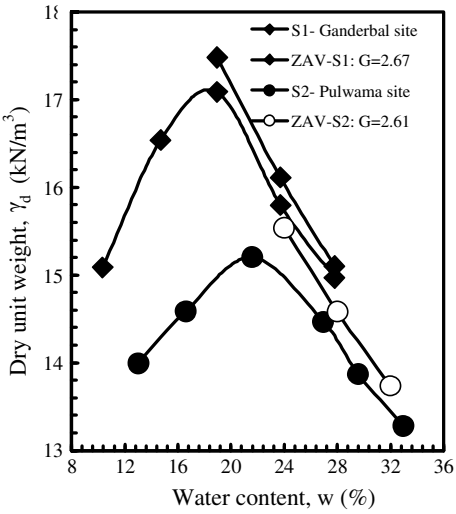

Fig. 5 Compaction curve for untreated soil

[28]. The variation of unconfined compression strength values with increasing nanomaterial content (Al_2O_3 and SiO_2) for site-1 and site-2 are shown in Figs. 6 and 7, respectively.

From Figs. 6 and 7, it is seen that the unconfined compressive strength increases with addition of nanomaterial content. The test results showed that maximum value of UCS is obtained for 1.5% nanomaterial content for both sites. On increasing nanomaterial content beyond 1.5%, the UCS values decrease. It is seen that 1.5% of nanomaterial content is the optimum amount required to maximize the shear strength

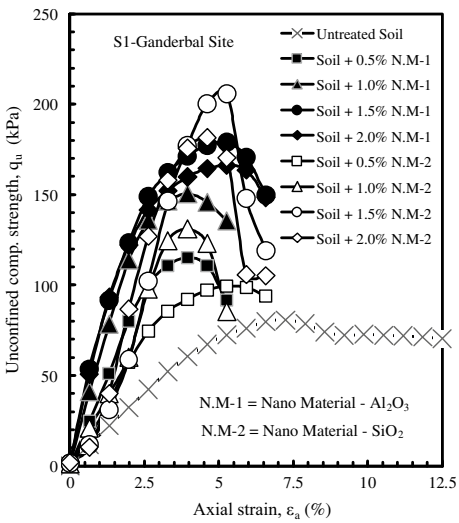

Fig. 6 Effect of nanomaterials on stress–strain behavior of soil for site-1

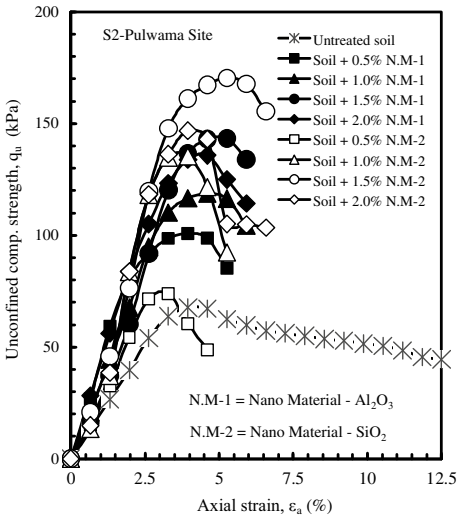

Fig. 7 Effect of nanomaterials on stress–strain behavior of soil for site-2

of the soil for both sites. The UCS values of the both soil samples (site-1 & site-2) at OMC and MDU were 75 kN/m^2 and 67 kN/m^2, respectively. It increased by a great extent with increasing nanomaterial content upto 1.5%. The maximum unconfined compressive strength values of 179 and 206 kN/m^2 were achieved at 1.5% optimum content of Nano-Alumina and Nano-Silica for site-1. Similarly, maximum unconfined compressive strength values of 144 and 170 kN/m^2 were achieved at 1.5% optimum content of Nano-Alumina and Nano-Silica for site-2, which accounts for a 138 and 175% increase in the unconfined compression strength for site-1 and 115 and 154% increase in the unconfined compression strength for site-2, respectively. Similar results have been reported by many researchers that the addition of nanomaterials significantly increase bearing capacity of soils, which results in stiffer soil skeleton matrix [29, 30] and increased compaction and engineering characteristics of weak/marginal soils [9, 31, 32].

The variation of maximum strength with increasing percentages of nanomaterials for both sites is shown in Fig. 8. The variation of failure strain with increasing percentages of nanomaterials for both sites is shown in Fig. 9. From Fig. 8, it is seen that there is significant increase in the unconfined compressive strength and 1.5% nanomaterial content is the optimum content for improvement of soil samples at both locations (e.g., Ganderbal and Pulwama). Beyond 1.5% nanomaterial content, there is a marginal decrease in the unconfined compressive strength, which may be attributed to the fact that the cohesion component of the shear strength ceases to contribute beyond optimum content as the material becomes stiffer. Also, from Fig. 9, it is seen that the composite material becomes too stiffer at 0.5% nanomaterial content, however, the values are very much scattered. It is further seen that failure strain stabilizes at 1.5% nanomaterial content and attains constant value for both samples, which indicates that 1.5% nanomaterial is the optimum content for stabilization of

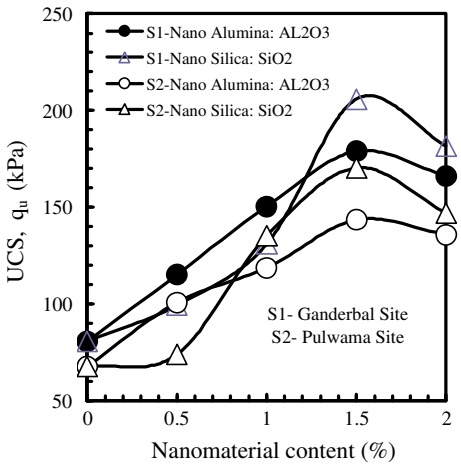

Fig. 8 Variation of UCS with increasing nanomaterial content for both sites

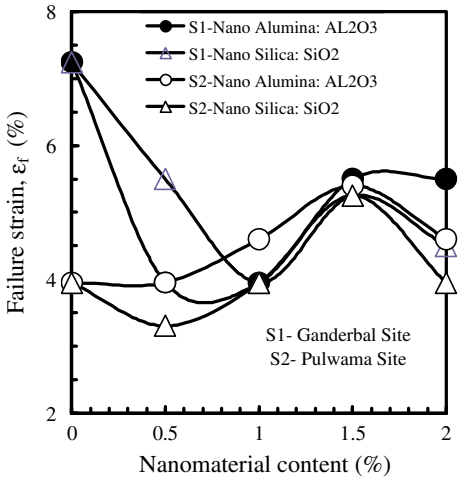

Fig. 9 Variation of failure strain with increasing nanomaterial content for both sites

soils at both locations (e.g., Ganderbal and Pulwama). Similar results have also been reported by many researchers that addition of nanomaterials significantly reduce the water holding capacity of soils, which results in stiffer soil skeleton matrix [33–35].

4.3 Microstructural Analysis Using Scanning Electron Microscope

Microstructural analysis of untreated and treated soil samples was conducted by scanning electron microscopy (SEM), Model: HITACHI S- 3600 N. Scanning Electron

Microscope (SEM) tests were conducted on post unconfined compression tests. After UCS tests, 7.5 mm × 7.5 mm × 7.5 mm air-dried samples were prepared at room temperature for SEM images as shown in Fig. 10. The SEM tests were conducted in both directions on horizontal and vertical surfaces of the sample. SEM images for the untreated soil samples for two sites are shown in Figs. 11 and 12, respectively.

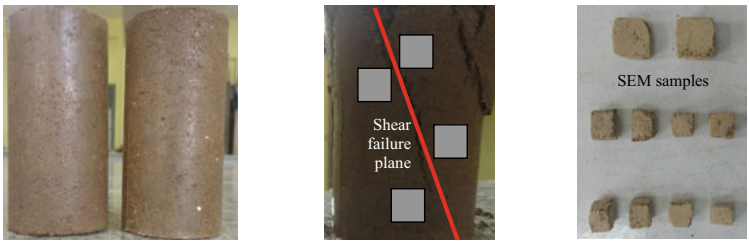

(a). Before UCS test (b). Post UCS test sample (c). SEM samples

Fig. 10 Soil samples prepared with nanomaterials for UCS tests and SEM analysis

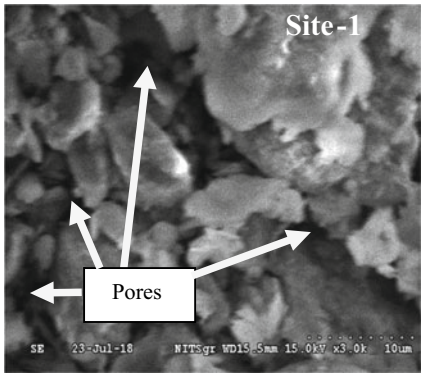

Fig. 11 SEM image for site-1 soil

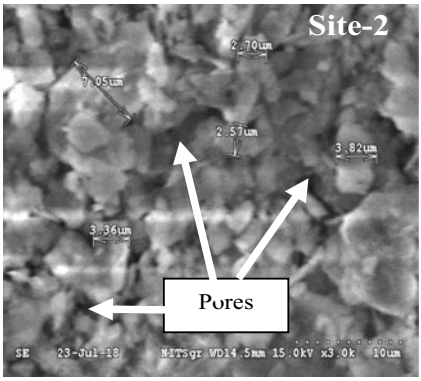

Fig. 12 SEM image for site-2 soil

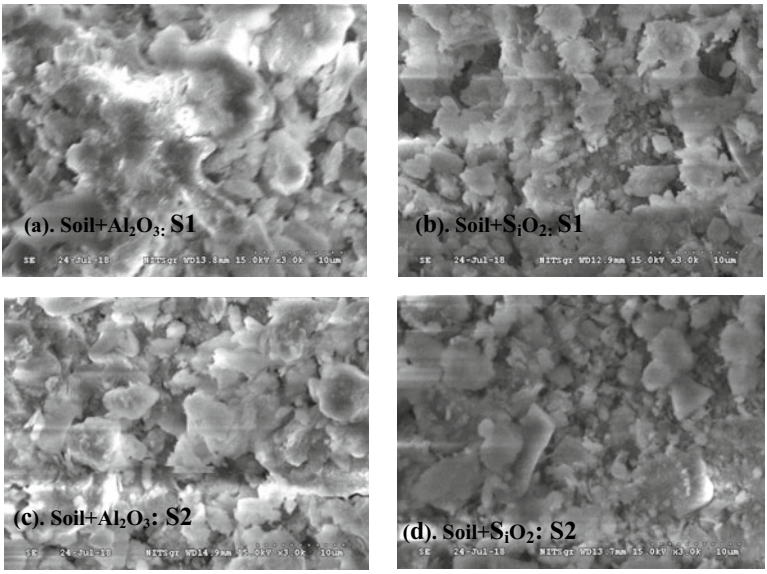

Fig. 13 SEM images of soil samples taken from site 1 (a & b) and site 2 (c & d) treated with different nanomaterials: **a** Soil + Al2O3, **b** Soil + SiO2, **c** Soil + Al2O3, **d** Soil + SiO2

From Figs. 11 and 2, it is seen that the untreated soil samples exhibits a blocky arrangement of clay particles and possess large pore void space. However, when the nanomaterials were added, the treated soil exhibits compact and dense microstructure (Fig. 13), which enhances the mechanical properties of the treated soils. It is seen that SEM images taken on post shear tests indicate a distinct division between smaller voids interpreted as constituting the intra-aggregate pore spaces and the larger inter-aggregate voids and treated soil samples showed closely packed crystals with reduced pore space. Similar studies have also been reported by many researchers in the past [36–39].

5 Conclusions

This present research provides an overview of the applications of nanometric (Nano-Alumina, Nano-Silica) as additives for the stabilization of marginal soils for their bulk utilization in geotechnical engineering applications. The test results showed that the unconfined compression strength of the soil increased significantly at an optimum content of 1.5% nanomaterials. The unconfined compression increased by about more than 2.5–3 times than the untreated soil site-1 and site-2. The SEM analysis showed that the addition of different percentages of nanomaterial to the soil changes the structural arrangement of the clay particles. SEM images clearly indicated a distinct division between smaller voids interpreted as constituting the intra-aggregate

pore spaces and the larger inter-aggregate voids and treated soil samples showed closely packed crystals with reduced pore space. Thus, it is seen that the shear strength characteristics of the marginal soils can be improved on addition of nano-alumina and nano-silica for sustainable development of environment and engineering infrastructures.

Acknowledgments The investigation reported in this paper forms part of research work at, National Institute of Technology, Srinagar. Thanks are due to the institute administration for providing the necessary facilities for carrying out this work and Nano Research Lab, Jharkhand for providing the nanomaterials in time for our research work.

References

1. Roco MC, Williams RS, Alivisatos P (1999) Nanotechnology research directions: IWGN workshop report vision for nanotechnology R&D in the next decade. National Science and Technology Council (NSTC), International Technology Research Institute, World Technology (WTEC) Division, Loyola College USA, 262p. https://itri.loyola.edu/nano/IWGN.Research.Directions
2. Chong KP (2004) Nanoscience and engineering in mechanics and materials. J Phys Chem Solids 65(8–9):1501–1506
3. Roco MC, Bainbridge WS (2005) Societal implications of nanoscience and nanotechnology: Maximizing human benefit. J Nanopart Res 7(1):1–13
4. Jahangir S, Kazemi S (2014) Effect of nano-alumina (N-Al) and nanosilica (NS) as admixtures on concrete behavior. In: International conference on advances in agricultural, biological & environmental sciences (AABES-2014), Dubai (UAE), pp 37–41
5. Pokropivny V, Lohmus R, Hussainova I, Pokropivny A, Vlassov S (2007) Introduction in nanomaterials and nanotechnology. Special lecture course for bachelors, MSc, post-graduates and specialists in nanotechnology. University of Tartu, Ukraine, 225p
6. Metaxa ZS, Konsta-Gdoutos MS, Shah SP (2010) Mechanical properties and nanostructure of cement-based materials reinforced with carbon nanofibers and polyvinyl alcohol (PVA) microfibers. In: ACI spring 2010 convention, pp 115–126
7. Alsharef Jamal MA, Taha MR, Firoozi AA, Govindasamy P (2016) Potential of using nanocarbons to stabilize weak soils. Appl Environ Soil Sci 2016: 1–9. Article ID 5060531. https://dx.doi.org/10.1155/2016/5060531
8. Taha MR, Taha OME (2012) Influence of nano-material on the expansive and shrinkage soil behavior. J Nanopart Res 14(10):1190
9. Parveen S, Rana S, Fangueiro R (2013) A review on nano-material dispersion, microstructure, and mechanical properties of carbon nanotube and nanofiber reinforced cementitious composites. J Nanomater 2013:1–19. Article ID 710175. https://dx.doi.org/10.1155/2013/710175
10. Zaid HM, Taha MR (2012) Effect of nanomaterial treatment on geotechnical properties of a Penang soft soil. J Asian Sci Res 587–592
11. Zhang G (2007) Soil nanoparticles and their influence on engineering properties of soils. In: Conference proceedings: geo-denver 2007-measurement and modeling of soil behavior, Colorado, United States, GSP 173. https://doi.org/10.1061/40917(236)37
12. Ghazi H, Baziar MH, Mirkazemi SM (2011) The effects of nano-material additives on the basic properties of soil. In: 14th Asian regional conference of geotechnic, Hong-Kong
13. Alireza SGS, Mirkazemi SM, Baziar MH (2013) Application of nanomaterial to stabilize a weak soil. In: International conference on case histories in geotechnical engineering, paper 5, pp 1–8. https://scholarsmine.mst.edu/icchge/7icchge/session_06/5

14. Bahmani SH, Bujang BKH, Asadi A, Farzadnia N (2014) Stabilization of residual soil using SiO_2 Nanoparticles and cement. Constr Build Mater 64(14):350–359
15. Zaid HM, Taha MR, Taha JI (2014) Stabilization of soft soil using nanomaterials. Res J Appl Sci Eng Technol 8(4):503–509
16. Norazlan K, Arshad MF, Mukri M, Kamaruzzaman M, Kamarudin F (2014) The Properties of nano-kaolin mixed with kaolin. Electron J Geotech Eng (EJGE) 19(Q):4247–4255
17. Neethu SV, Remya S (2013) Engineering behavior of nanoclay stabilized soil. In: Proceedings of Indian geotechnical conference-2013, theme-4, paper no. 124, pp 1–4
18. Shahin SS, Laila Abd El-Meguid F, Hebaturahman A (2015) Review of nano additives in stabilization of soil. In: Proceedings of 7th international conference on nano technology in construction (NTC-2015), pp 1–11
19. Changizi F, Haddad A (2016) Effect of nano-silica on the geotechnical properties of cohesive soil. Geotech Geol Eng 34:725–753
20. Arya A, Jain A (2017) A review of geotechnical characteristics of nano additives treated soils. In: International conference on recent development in engineering science (ICRDES), Chandigarh, India, p 121
21. García S, Paulina T, Ramírez O, López-Molina J, Nidia H (2017) Influence of nanosilica on compressive strength of lacustrine soft clays. In: Proceedings of 19th international conference on soil mechanics and geotechnical engineering, Coex, Seoul, Republic of Korea, pp 369–372
22. Iswarya R, Satheeskumar V (2018) Influence of nano silica on the geotechnical properties of clayey soil stabilized with lime. Asian J Eng Appl Technol (Special Issue) 7(1):28–32
23. ASTM D 2487 – 06 (2006) Standard practice for classification of soils for engineering purposes (USCS). In: Annual book of ASTM standards, American society for testing and materials, Philadelphia, United States. www.astm.org
24. ASTM D 854-06 (2006) Standard test method for specific gravity of soil solids by water pycnometer. In: Annual book of ASTM standards, Philadelphia, United States. www.astm.org
25. ASTM D 422–63(07e2) (1963) Standard test method for particle size analysis of soils (Sect. 4). In: Annual book of ASTM standards, Philadelphia, vol. 04-08. www.astm.org
26. ASTM D4318-10 (2010) Standard test methods for liquid limit, plastic limit, and plasticity index of soils. In: Annual book of ASTM standards, American society for testing and materials, Philadelphia, United States. www.astm.org
27. ASTM D698-12e2 (2012) Standard test methods for laboratory compaction characteristics of soil using standard effort (12 400 ft-lbf/ft^3 (600 kN-m/m^3)). In: ASTM international, West Conshohocken, PA. www.astm.org
28. ASTM D2166/D2166M-13 (2013) Standard test method for unconfined compressive strength of cohesive soil. In: ASTM international, West Conshohocken, PA. www.astm.org
29. Jarrahzade F, Bajestan MS (2010) Changing clay structure by nanotechnology due to soil stabilization. In: International congress on nanoscience and nanotechnology, Iran, pp 1 2
30. Norazlan K, Fadzil MA, Mukri M, Kamaruzzaman M, Kamarudin F (2015) Influence of nano-soil particles in soft soil stabilization. Electron J Geotech Eng 20(2):731–737
31. Gelsefidi SSA, Mirkazemi SM, Hasan BM (2013) Application of nano-material to stabilize a weak soil. In: Proceedings of 7th international conference on case histories in geotechnical engineering, paper no. 6.10a, pp 1–8
32. Suresh R, Murugaiyan V (2018) Improvement of clay soil using natural fibers and nano silica: a review. Indian J Sci Res 17(2):252–256
33. Mir BA, Sridharan A (2019) Mechanical behaviour of fly-ash-treated expansive soil. Proc Inst Civ Eng-Ground Improv J 72(1):12–24
34. Zhu W, Bartos PJM, Porro A (2004) Application of nanotechnology in construction. Summary of a state-of-the-art report. J Mater Struct 37(9):649–658
35. Gutierrez MS (2005) Potential applications of nano-mechanics in geotechnical engineering. In: Proceedings of the international workshop on misco-geomechanics across multiple strain scales, Cambridge, UK, pp 29–30
36. Gillott JE (1969) Study of the fabric of fine-grained sediments with the scanning electron microscope. J Sediment Petrol 39(1):90–105

37. McKyes E, Yong RN (1971) Three techniques for fabric viewing as applied to shear distortion of a clay. Clays Clay Miner 19(5):289–293
38. Juneja A, Mir BA (2012) Behavior of clay reinforced by sand compaction pile with smear. Proc Inst Civ Eng-Ground Improv J 165(GI2):111–124
39. Mir BA, Juneja A (2016) Model studies on shear behavior of reinforced reconstituted clay. Int J Civ Environ Struct Constr Archit Eng 10(1):87–94

Building Derived Materials—Sand Mixture as a Backfill Material

M. Jayatheja, Anasua Guharay, Arkamitra Kar, and Ashok Kumar Suluguru

Abstract The growing interest in utilizing waste materials in civil engineering applications has opened up the possibility of constructing reinforced soil structures with unconventional backfills. According to World Bank reports (2012), generation of Construction and Demolition Waste (CDW) will reach 5 billion tons by 2025 globally, out of which major generators are Asia-pacific and North America regions. Improper handling and disposal of this inert waste create environmental hazards and also occupy land space. Recycling and reuse of CDW may help to attain a sustainable ecosystem. CDW comprises wood, concrete, and brick, glass, tiles, out of which concrete and brick forms a major part and is termed as Building Derived Materials (BDM). A series of triaxial tests are conducted to investigate the stress–strain relationship and strength of BDM and a mixture of sand and BDM. The laboratory test results are used to establish the parameters required for the hyperbolic modeling of these materials. Hyperbolic parameters are varying with an increase in confining pressures and with percentage addition of BDM. Plastic properties of sand–BDM are computed with this model and well matching with experimental data. The analysis indicates that the performance of sand–BDM mixture, being both lightweight and reasonably strong, compared well with that of sandy gravel, as a backfill material.

Keywords Building derived material (BDM) · Triaxial tests · Hyperbolic model

1 Introduction

Construction and Demolition Waste (CDW) is generated when any infrastructure is rebuilt or repaired. Developing countries like India produce more CDW as part of expansion and construction of new infrastructures like flyovers, buildings, etc. Production of CDW creates storage issues. According to Ganesan [1], 1750 acres of land space is needed for storing CDW annually in India. Stringent laws should be

M. Jayatheja · A. Guharay (✉) · A. Kar · A. K. Suluguru
BITS Pilani, Hyderabad Campus, Hyderabad, India
e-mail: guharay@hyderabad.bits-pilani.ac.in

K. R. Reddy et al. (eds.), *Sustainable Environment and Infrastructure*, Lecture Notes in Civil Engineering 90, https://doi.org/10.1007/978-3-030-51354-2_40

enforced by regulatory authorities for storage, recycling reusing of CDW in engineering applications. Singapore and Japan achieved the highest recycling rate of 99.9% and 99.5% followed by Australia as 90% [2–4]. Natural resources are fast depleting and management of natural resources is an important aspect for the present society. Hence, there is a need to reutilize the generated inert materials like CDW, flyash, slag, plastic into construction activities. CDW is a good alternative to aggregates in road construction [5]. This material is suitable for subbase and base applications as it provides resistance and possesses non-expansive behavior [6–12]. CDW suitability is strongly dependent on mineralogical aspect and parent mineral [13]. Addition of construction waste to bentonite clay increased the specimen strength up to 90% [14]. Cohesion and drained friction angle increased with addition of CDW up to optimum of 30% replacement [15].

The mathematical formulations relating strength, stress–strain, and deformation of any material are significant for practical application in engineering. These are required for predicting the failure in soils when subjected to different types of external loads. This procedure may involve measurable physical parameters that cannot be measured directly. Hence, it is difficult to establish simple formulations of strength criterion and stress–strain relations that can adequately address the mechanical behaviors of soils over a wide range of values of strain [16]. Many models are available to analyze the critical behavior of soils like Cam–clay, hardening soil, Mohr–Coulomb, and Drucker–Prager. Bulk Modulus of soil increased with increase in relative density and confining pressures [16]. Failure pattern and shear bands formation varied with confining pressures; these phenomena can be described by strain rate variation [17]. The hardening soil model (Duncan–Chang Hyperbolic model) predicts the plastic behavior of soils and is applicable to both cohesive and cohesionless soils [18]. A significant advantage of the hyperbolic model is that the values of the required parameters can be determined from the results of conventional triaxial compression tests. Summarizing the existing studies, it can be seen that researchers reported results on the usage of recycled solid waste and their usage in ground improvement. Limited studies are reported on the usage of CDW in ground improvement. The purpose of the present study is to explore the suitability of recycled materials in geotechnical applications. One possible application consists of using Building Derived Material (BDM), the primary subset of CDW in geotechnical applications. This requires thorough analysis of the mechanical properties of such materials and their response under realistic loadings. For this purpose, a series of triaxial compression tests are conducted at different confining pressures to evaluate the strength and stress–strain behavior of soil and soil–BDM blends. The properties are then used to develop a hyperbolic model to be used for numerical analysis.

2 Materials and Methodology

2.1 Materials Used

The BDM is composed of material collected from local construction and demolition sites near Hyderabad campus of BITS-Pilani in Telangana, India. The CDW consists of concrete, brick, ceramic tiles, glass, wood, and plastic; concrete and brick. The concrete and brick component of this CDW is used as BDM for this study. The collected BDM is crushed to sizes less than 10 mm with the help of a jaw crusher.

The sand is collected from Godavari river basin near Telangana state of India. The sand is classified as poorly graded sand (SP) according to Unified Soil Classification System. Physical and mechanical properties are evaluated by grain size analysis (ASTM D6913), specific gravity, compaction tests which are conducted on sand and sand–BDM mixture. BDM is added to sand in different percentages of 0, 5, 10, 20, and 30.

2.2 Test Program

A series of CU triaxial tests are conducted to evaluate the strength properties of sand and sand–BDM mix. The AIMIL triaxial test apparatus consists of a universal cell, an oil-based constant pressure system and a Data Acquisition (DAQ) system. The constant pressure system is connected to universal cell and oil–water interface creates the required confining pressures. Samples of 38 mm diameter and 76 mm height are placed in rubber membrane by pluviatation technique [12]. The samples are placed over pedestal, and glass cap is kept on top of sample with drainage inlet. Drainage outlet from the bottom pedestal is connected to pore pressure panel. Back pressures, axial loading, and displacements are displayed in the DAQ system. Confining pressures of 100, 150, and 200 kPa are maintained in cell and operated at strain rates of 1.25 and 2.00 mm/min. Table 1 describes the test program carried out on samples of sand, sand with varying percentages of BDM (5, 10, 20, and 30%).

Table 1 Test program

Confining pressures (kPa)	Test ID	Test configuration
100	S0 – I, II	Sand + 0% BDM
	S5 – I, II	Sand + 5% BDM
150	S10 – I, II	Sand + 10% BDM
	S20 – I, II	Sand + 20% BDM
200	S30 – I, II	Sand + 30% BDM

I—1.25 mm/min, II—2.00 mm/min

2.3 Numerical Model

Constitutive models give an idea about material behavior in non-linear state. Hyperbolic Model (also known as Hardening Soil Model (HSM)) is one of the most popular plasticity models used by geotechnical engineers. This model is an extension of Mohr–Coulomb model which allows computing at K_0 state and can input pre-consolidation pressure. Model formulation developed [18] provides a constitutive stress–strain relation, which assumes stress–strain relation to be hyperbolic given by Eq. (1).

$$\sigma_1 - \sigma_3 = \frac{\varepsilon}{\frac{1}{E_i} + \frac{\varepsilon}{\sigma_1 - \sigma_3}} \tag{1}$$

where σ_1 and σ_3 are major and minor principal stresses, ε is axial strain, and E_i is initial elastic modulus

Based upon loading conditions, total strains are evaluated using stress–dependent stiffness. Inputs for hyperbolic model are obtained from standard triaxial tests, and initial material stiffness is dependent on confining pressure applied. The summary of the procedure followed in the generation of hyperbolic curve is provided below.

Step 1: Collection of deviatoric stress and axial strain values from CU Triaxial test
Step 2: Transforming curve by dividing axial strain with experimental deviatoric stress values and plotting ($\varepsilon_a/(\sigma_1-\sigma_3)$ vs ε_a)
Step 3: Calculation of 'b' and 'a' values which are slope and intercept of ($\varepsilon_a/(\sigma_1-\sigma_3)$ vs ε_a), respectively
Step 4: Calculation of $(\sigma_1-\sigma_3)_{\text{ultimate}}$ which is inverse of 'b'
Step 5: Calculation of failure ratio (R_f) which is ratio of $(\sigma_1-\sigma_3)_{\text{failure}}$ & $(\sigma_1-\sigma_3)_{\text{ultimate}}$
Step 6: plotting log (E_i/P_a) and log (σ_3/P_a) where P_a is atmospheric pressure of 100 kPa.

3 Results and Discussions

BDM added to poorly graded sand (SP) resulted in the improvement of gradation of soil particles. Figure 1 shows the grain size distrubution of sand and BDM used in this study. 40% relative density is maintained throughout experimentation as per ASTM D698, Table 2 describes the index properties of sand. Sand attains maximum dry unit weight of 18.43 kN/m^3 in vibration test and minimum dry unit weight is recorded as 17.24 kN/m^3.

Consolidated Undrained (CU) tests are performed on specimens of sands, sand–BDM blend in strain-controlled triaxial compression test apparatus. Material hardening behavior is observed among samples. There are different stages in application

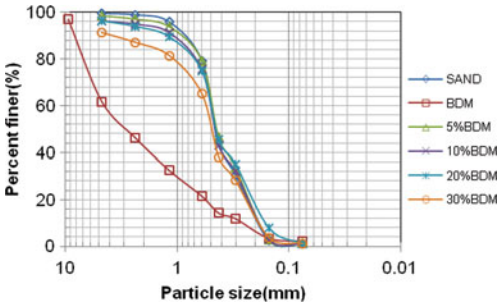

Fig. 1 Grain Size Distrubution of sand–BDM mixtures

Table 2 Properties of sand

Property	Value
Specific Gravity (G)	2.65
Effective size (D_{10}) (mm)	0.3
Coefficient of Uniformity (C_u)	2.5
Coefficient of Curvature (C_c)	0.9
Internal Angle of Friction (φ)	28°
USCS Classification	SP

of load for the sample, in first stage resistance is possessed by soil specimen and applied cell pressure. In stage two, resistance is shown by particle density and pore water present in void spaces where stress–strain curve will follow linearity. In stage three, soil sample reaches yield point and stress–strain curve is perfectly plastic state. Sands exhibit more shear strength when confined. Sand samples posses more deviatoric stress due to angularity in shape of particles. As BDM content increases, the gradation of sand changes from poorly graded to well-graded soil. Shape of BDM particles dominates more than sand particles, void spaces varied proportionally with BDM. Deviatoric stress varies inversely with increase with BDM particles (coarser) is observed. It is also observed that increase in confining pressure is also leading sample to exhibit more deviatoric stress. When strain rates are varied, specimen possesses more hardening nature with increase of BDM. In every case, sample exhibits its peak stress difference value at axial strain of 8–15%. Inclusion of BDM to sand sample increases its drainage characteristics which are suitable for lightweight backfill condition. Specimens tested at 2.00 mm/min [II] (Fig. 3a, b give quick response as time for particles to get rearranged is less compared to strain value of 1.25 mm/min [I] (Figs. 2a, b). From results presented in Table 3, it can be observed that the frictional angle increases in all combinations, the highest is exhibited by S20 due to more interlocking among particles at both strain rates. Addition of more BDM to sand creates more void spaces which in turn reduces interlocking and hence is susceptible to failure under action of load [19]. As sand–20% BDM exhibits more frictional angle and greater resistance to load, it can be considered as optimum value for backfill applications. Hyperbolic stress–strain curves are plotted from obtained CU triaxial

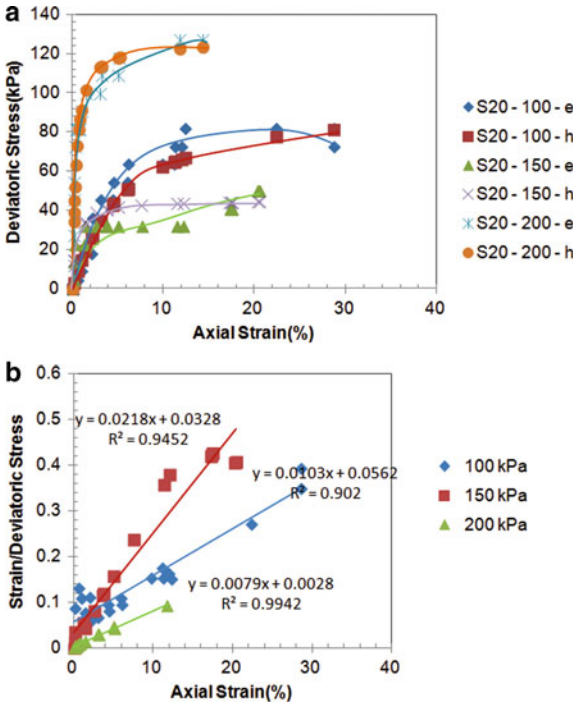

Fig. 2 **a** Stress–Strain curves of Sand–20% BDM (S20) blend at strain rate I (1.25 mm/min). **b** Transformed Stress–Strain curves of Sand–20% BDM (S20) blend at strain rate I (1.25 mm/min)

test data. From Figs. 2 and 3, it can be noticed hyperbolic curves are in agreement with that of experimental data points. Initial elastic modulus (E_i) and ultimate stress difference $(\sigma_1–\sigma_3)_{ult}$ can be generated from hyperbolic curves. From Fig. 2, it can be observed that S20-II possesses more E_i value compared to all other combinations as that curve has major portion in elastic zone. Higher E_i values resemble higher strength and stiffness. It is also observed that E_i and $(\sigma_1–\sigma_3)_{ult}$ vary inversely with strain rate.

Figures 2 and 3 indicate that stress–strain curves take rectangular hyperbola shape; they are replotted into strain vs strain/stress into linear form. In every plot, inverse of intercept gives E_i and inverse of slope gives $(\sigma_1–\sigma_3)_{ult}$ values. Figure 3 shows that S20–II possess less slope in comparison with S20–I; these combinations exhibit more $(\sigma_1–\sigma_3)_{ult}$ than other samples of varying BDM. Angle of internal friction increases proportionally with addition of BDM content till 20% of weight. S20 exhibits greater frictional angle than other combinations, this can be identified as optimum percentage for replacing soil. Increase in strain rates results in slight increase of frictional angle value (Fig. 4). The optimum percentage of BDM is found to be 20% for both the train rates. Initial elastic modulus (E_i) which is a measure of specimen stiffness is calculated from transformed stress–strain plots and is presented in Table 3. It is also observed that initial elastic modulus (E_i) varies proportionally with confining pressures and inversely with strain rates. Samples tested strain rate I (1.25 mm/min) shows relatively more E_i value than other strain rates. This is because at strain rate

Table 3 Variation of E_i with strain rates and confining pressures

Sample ID	Confining pressures		
	100 kPa	150 kPa	200 kPa
S0 – I	46.72	212.7	4.95
S0 – II	93.44	21.69	50
S5 – I	46.72	212.7	4.95
S5 – II	32.46	175.4	32.46
S10 – I	136.9	19.23	66.66
S10 – II	109.8	7.14	55.86
S20 – I	17.79	105.2	357.1
S20 – II	23.92	196	86.02
S30 – I	102	476.1	26.04
S30 – II	12.03	9.165	126.5

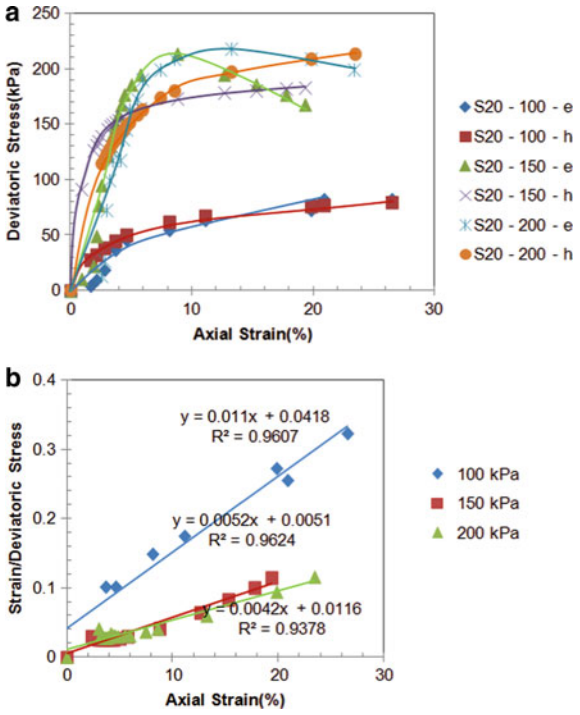

Fig. 3 **a** Stress–Strain curves of Sand–20%BDM (S20) blend at strain rate II (2.00 mm/min). **b** Transformed Stress–Strain curves of Sand–20% BDM (S20) blend at strain rate II (2.00 mm/min)

I particles in soil sample have time to rearrange; in strain rate II soil particles get relatively less time for rearrangement and sample fails quickly.

R_f which is the ratio deviatoric stress at failure to deviatoric stress at ultimate point, is obtained by multiplying slope of transformed graph with peak value of deviatoric stress at failure. Figure 5 shows the variation of R_f with different percentages of BDM

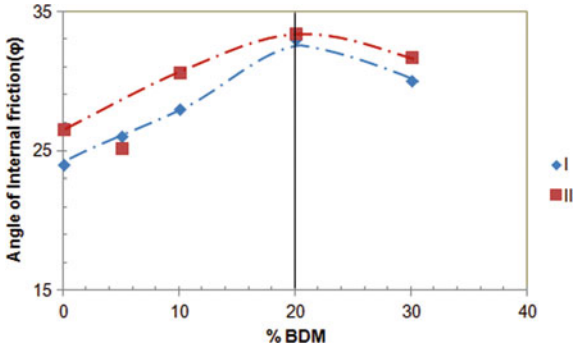

Fig. 4 Variation of frictional angle with BDM

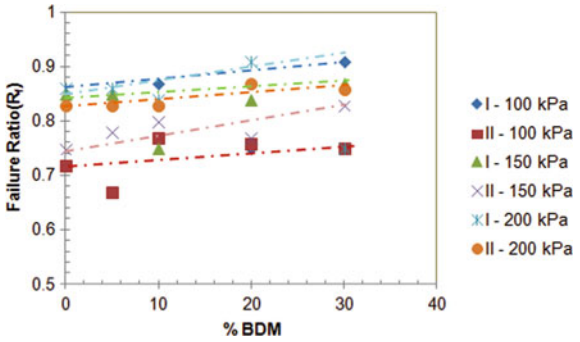

Fig. 5 Variation of Failure ratio (R_f) with BDM

and for defining confining pressures. It is observed that R_f value is in the range of 0.65–0.9, average being 0.8. Sand–BDM samples tested at low confining pressures (100 kPa) exhibits less R_f value and samples tested at high confining pressures (200 kPa) possess more R_f value. Figure 6 which is plot between log (E_i/P_a) and log (σ_3/P_a) is used to determine Modulus number (K) and Modulus exponent (n) values in the form of slope and intercept. Every specific point indicates particular confining pressures and K and n values can be calculated at every confining pressure.

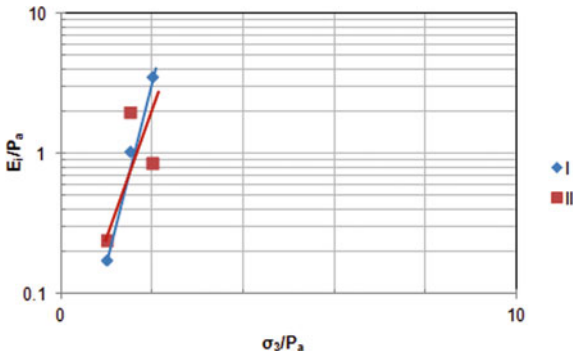

Fig. 6 Variation of elastic modulus with confining pressures

From Fig. 6, it is observed that for S20 blend, K lies in the range of 0.17–2.05 with an average value of 0.76 and n varies between 0.8 and 2.32. No significant changes are observed with variation of strain rate. This study shows that hyperbolic model results are in good agreement with experimental to capture soil–BDM response. The hyperbolic model results can be used to develop a finite element program, which can predict the optimum percentage of BDM at different strain rates.

4 Conclusions

Results from Consolidated Undrained (CU) triaxial test highlight the strength of soil specimen with inclusions of varying percentages of BDM by weight. Impact of variation of strain rate is also presented. Following conclusions can be drawn based on analysis of experimental investigations:

- Experimental results indicate that deviatoric stress increases with increase in confining pressures. Internal angle of friction are functions of confining pressures and increases with BDM content and strain rates. S20 is the optimum proportion for backfill applications; Stress difference values at yield point vary proportionally with BDM content.
- Hyperbolic model which is an extension of Mohr–Coulomb model specifies that confining pressures influences hyperbolic parameters. S10 and S20 show higher initial elastic modulus (E_i) compared to other samples.
- The hyperbolic model results are in good agreement with experimental to capture soil–BDM response. However, it is to be noted that hyperbolic model cannot predict soil behavior beyond peak point accurately.

Results presented and discussed in this paper indicate that BDM can be used as an alternative material for improving the strength of soils. BDM can be a substitute for aggregates and utilized as lightweight backfill material and in turn, can reduce carbon footprint.

References

1. TERI (The Energy and Resources Institute), India at 70: Opportunities in Waste recycling in India, https://www.teriin.org/article/india-70-concerns-and-opportunities-waste-recycling-india. Accessed 24 Jan 2019
2. CCANZ (Cement & Concrete Assoc. of New Zealand), 2011, Best practice guide for the use of recycled aggregates in new concrete, CCANZ Technical Report, New Zealand. www.ccanz.org.nz/files/documents/ad659c71-06cb-44b1-95dd-7b7350fdcd54/TR_14_Recycled_Aggregates_in_New_Concrete_2013.pdf. Accessed 24 Jan 2019
3. NEA (National Environment Agency) (2016) Waste statistics and overall recycling, National environment agency, Singapore, www.nea.gov.sg/energy-waste/waste-management/waste-statistics-and-overall-recycling. Accessed 24 Jan 2019

4. MLIT (Ministry of Land, Infrastructure, Transport and Tourism) (2014) White Paper on Land, Infrastructure, Transport and Tourism in Japan 2014, Ministry of Land Infrastructure Transport and Tourism, Japan. www.mlit.go.jp/common/001063075.pdf. Accessed 24 Jan 2019
5. Leite FC, Motta RS, Vasconcelos KL, Bernucci LLB (2011) Laboratory evaluation of recycled construction and demolition waste for pavements. Constr Build Mater 25(6):2972–2979. https://doi.org/10.1016/j.conbuildmat.2010.11.105
6. O'Mahony MM (1997) An analysis of the shear strength of recycled aggregates. Mater Struct 30(10):599–606
7. Bennert T., Papp Jr. W.J., Maher A., Gucunski N.: Utilization of construction and demolition debris under traffic-type loading in base and subbase applications. Transportation Research Record, J. Transp. Res. Board 1714, 33–39 (2000)
8. Kryckyj PR, Trichês G (200) Use of civil construction waste in urban pavements: a feasibility study. In: Proceedings of the 5th international symposium on environmental geotechnology and global sustainable development. Belo Horizonte (2000)
9. Motta RS (2005) Laboratory study of recycled aggregate from construction and demolition waste to be used as a pavement material in a low volume road. MSc Thesis, University of São Paulo. (in Portuguese) (2005)
10. Poon CS, Chan D (2006) Feasible use of recycled concrete aggregates and crushed clay brick as unbound road sub-base. Constr Build Mater 20(8):578–585
11. Melbouci B (2009) Compaction and shearing behavior study of recycled aggregates. Constr Build Mater 23(8):2723–2730
12. Dave T, Dasaka M (2013) Transistion of earth pressure on rigid retaining walls subjected to surcharge loading. Int J Geotech Eng 6(4):427–436
13. Rodrigues F, Carvalho MT, Evangelista L, de Brito J (2013) Physical chemical and mineralogical characterization of fine aggregates from construction and demolition waste recycling plants. J Clean Prod 52438–445 (2013)
14. Hasan U, Budihardjo ACMA, Nikraz H (2016) Experimental evaluation of construction waste and ground granulated blast furnace slag as alternative soil stabilizers. Geotech Geol Eng (2016)
15. Silva J, de Brito J, Veiga R (2010) Recycled red-clay ceramic construction and demolition waste for mortars production. J Mater Civ Eng 22, 236–244
16. Latini C, Zania V (2016) Triaxial tests in Fontainebleau sand. Report, Technical University of Denmark (2016)
17. Yamamuro Jerry A, Abrantes Antonio E, Lade Poul V (2011) Effect of strain rate on the stress-strain behavior of sand. J Geotech Geoenviron Eng 137(12):1169–1178
18. Duncan JM, Chang CY (1970) Nonlinear analysis of stress and strain in soils. J Soil Mech FoundDiv ASCE 96(SM5):1629–1653
19. Mamo GB, Dey A (2014) Critical overview of the effect of strain rate on d irect shears test results.NES—Congress 2014, Guwahati

Erosion–Filtration Analysis for Assessing Hydraulic Instability of Dams in Morocco and Global Warming Effect

Ahmed Jalil, Ahmed Benamar, and Mohamed Ebn Touhami

Abstract The climate change including very long dry seasons can threaten vulnerability of dams and dikes by reducing their resistance to internal erosion. It is, therefore, questionable how long degradation of soil properties can affect the operating life of hydraulic structures. This research is devoted to investigate the susceptibility to internal erosion of many earth dams in Morocco. For this purpose, many erosion–filtration tests have been conducted on samples collected from core soil or downstream filter of three dams (embankment dam and zoned earth dams). Materials have been analyzed with respect to the particle size distribution, plasticity index, permeability, and their suitability for dam construction. This has been deduced from usual engineering guidelines. The investigation involves combined Hole Erosion–Filtration experiments for modeling internal erosion of a base soil and the filtration through a downward granular filter. The results of experimental hole erosion tests conducted on base soils show a high resistance of the soils against erosion, and a linear enlargement of the hole was recorded. Moreover, usual guidelines indicate a slow to extremely slow erosion of tested core soils and classified as being highly resistant to erosion. The results from combined erosion–filtration tests provide a method on quantitative measurement of the filtration efficiency and particle size selection. Experiments involving previously dried core soils reveal that the desiccation step makes the soil more susceptible to erosion, indicating that drought phase may affect strongly the core resistance against erosion in dams.

Keywords Internal erosion · Filtration · Soil · Desiccation · Earthen dam

A. Jalil (✉) · A. Benamar
Department of Civil Engineering, LOMC UMR 6294, CNRS-University of Le Havre Normandie, 53 rue de Prony, 76600 Le Havre, France
e-mail: ahmed.jalil87@gmail.com

A. Jalil · M. Ebn Touhami
Laboratory of Materials and Environment Engineering, Ibn Tofail University, B.P 242, Kenitra, Morocco

K. R. Reddy et al. (eds.), *Sustainable Environment and Infrastructure*, Lecture Notes in Civil Engineering 90, https://doi.org/10.1007/978-3-030-51354-2_41

1 Introduction

Internal erosion is the primary cause of breaks and incidents of levees, dykes, and dams around the world. Water flowing through a hydraulic embankment structure (dam, dyke) or its foundation may erode fine particles and wash them out. It may even drain exceptionally by overtopping above the structure during a flood.

The two ultimate forms of an embankment failure resulting from water action are the breach (regressive erosion) and the sliding (after the crest settlement). A break is often the result of successive situations and a combination of phenomena that are accelerating the erosion process. Solid particles may detach and be carried away by the flow: it is the internal erosion. It may be just the fine fraction of the soil that is concerned (suffusion), or the whole of a solid matrix (suffusion). In hydraulic structures, internal erosion occurs according to four phases: Initiation, continuation, progression, and initiation of a breach. Concerning pipe erosion, some authors have studied the role of compaction conditions on erosion characteristics and process kinetics. Christensen and Das [1] find a decrease in the rate of soil erosion during the test with increasing initial water content of compaction. Wan and Fell [2, 3, 4] and Lim [5] have shown that the increase in initial water content leads to an increase in the erosion index leading to a better resistance to erosion. However, the magnitude of this increase is related to the soil nature. Wan and Fell [2, 3, 4] and Lim [5] observed an increase of erosion index when initial density increases. To measure the effectiveness of the filter material used in Mazer dam many engineering criteria dealing with the filtration have been used in this study. It has been demonstrate from Terzaghi (cited by Haghighi et al. [6] criterion that the retention and permeability criteria are checked, and according to Istomina (cited by Foster and Fell [7], Fell and Fry [8]) the obtained uniformity coefficient ($10 < Cu = 10.27 < 20$) indicated that filter soil falls in the transition material category.

This research investigates the vulnerability to internal erosion of earthen dams in Morocco suffering desiccation resulting from long drought seasons and lack of rain. Because of climate change, long heat seasons occured this last decade in northern Africa. So, many hydraulic structures (dams and levees) may suffer desiccation which may affect the stability of dams against internal erosion. In the area of studied Mazer

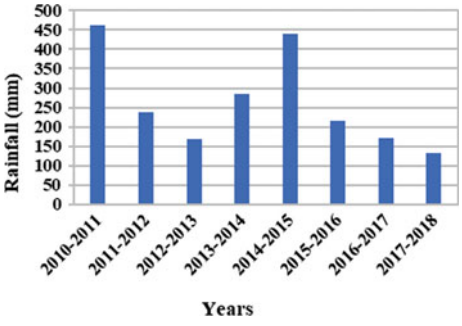

Fig. 1 Evolution of the rainfall in the area of dam location during last decade

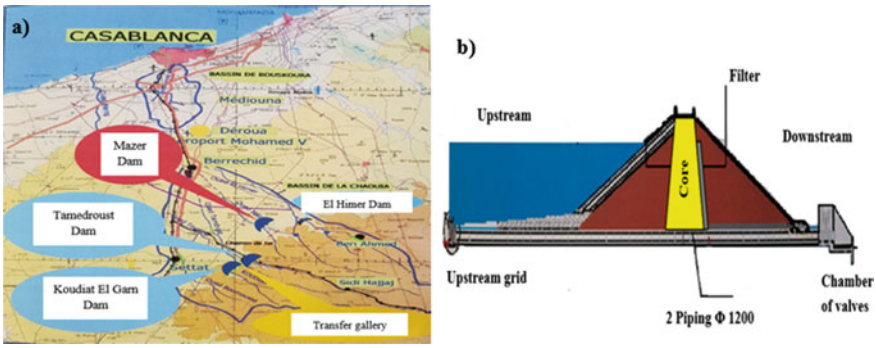

Fig. 2 A map depicting the location of Mazer Dam (**a**) Cut in the axis of the bottom drain (**b**)

dam, the precipitation survey (Fig. 1) from the last decade [9, 10] indicates that the dam region suffered a long drought which could lead to empting the dam reservoir and drying deeply the earth dike and involving cracks within the dam core. So, a new filling of the reservoir may lead to more core susceptibility to internal erosion. This effect was investigated in this study through hole erosion tests of core soil before and after desiccation. After the identification of the dam structures, soil samples have been collected from different zones (core, filter, shoulder) in order to investigate their susceptibility to internal erosion and how long material desiccation may affect their resistance.

2 Materials and Methods

2.1 Dams and Materials Description

After the flooding events on 2002 in Settat-Berrechid region and their effects on industrial and agricultural fields, the arrangement program of Mazer's Dam and the warning system against floods were designed for the preservation of floodplains. Besides the flood prevention, the aim is rather to ensure irrigation of the lands located downstream covering an area of 2500 ha (250.000 Ares), and groundwater recharge whose table suffers a 1 m-per-year drop. In 2011, the Mazer dam was put into operation (Fig. 2).

The core and filter materials tested come from borrowings located in the areas of the reservoir of Mazer dam. The preparation and the homogenization of the materials according to water content and compaction have been achieved following the same conditions as those of the dam currently in operation. Table 1 below summarizes the geotechnical parameters of tested materials from the dam.

Table 1 Soils (core and filter) characteristics

Soil material	Core
Optimum Water content (%)	20
WL (%)	53
IP (%)	25
γ_{max} (t/m^3)	1.70
Soil material	Filter
Optimum Water content (%)	20
% particles < 0.08 mm	3.50
Cu	5.27
γ_{max} (t/m^3)	2.00

2.2 Experimental Setup and Erosion Tests

2.2.1 Test Apparatus

Test apparatus involves a cylindrical plexiglass cell of 140 mm inner diameter and 300 mm of length, a glass graduated tank, a pump, and a turbidimeter. The cell is equipped with pressure transducer controlling the inlet pressure during test, and used in both configurations: hole erosion test (Fig. 3b) and erosion–filtration test (Fig. 3a, Table 2).

The soils were compacted within the column at the fixed density and water content (Table 2) according to the real dam conditions. Tests are aimed at both evaluating the soil erodibility from hole erosion test, and filtration ability from erosion–filtration test at different pressure values, before and after desiccation.

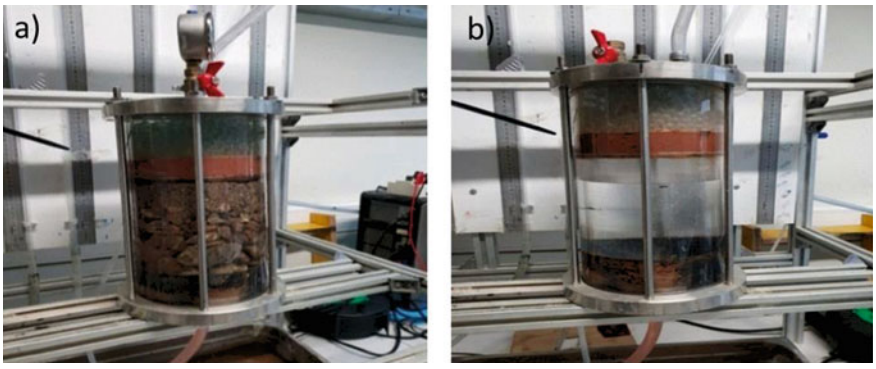

Fig. 3 View of test cell used for erosion–filtration test (**a**) and hole erosion test (**b**)

Table 2 Soils (core and filter) characteristics during tests

Performed test	Hole erosion test	Filtration
Density (kN/m^3)	Base soil: 17	Filter: 20
Water content (%)	20 and 4 (desiccation)	20 and 6 (desiccation)
Initial hole diameter (mm)	15	15
Applied pressures (kPa)	100-150-200-250	100-150-200-250

2.2.2 Test Procedure: Erosion and Filtration Experiments

This experimental work aims to investigate the behavior of soils with respect to the initiation and progression of internal erosion (suffusion), by identifying the influence of hydraulic (load), geometric (nature and proportion of fines, shape), and geotechnical (density, water content) parameters. In this part, we have carried out the Hole Erosion Test (HET) on core material with and without downward filter, by using different values of water content. Sample desiccation was obtained by drying the material, simulating drought periods, and reservoir empting. This is likely to happen, knowing the risk of drought in some areas. In addition, Morocco is very much recognized by its heat returns, especially with the climate change that the world has undergone. However, during periods of floods, when the reservoir water level tends to rise quickly and abruptly, cracks induced by drought period may lead dam embankment suffering internal erosion. Therefore, through these tests, we will be able to estimate the state of dam soil and its behavior following the increase or decrease of water content (until desiccation); something that will allow to measure the vulnerability and efficiency of our soil and conclude on the sustainability of our dam.

3 Effect of Desiccation on Base Soil Erodibility

3.1 Base Soil Erodibility from Hole Erosion Test

Hole Erosion Test (HET) was carried out on the core material under several pressures in order to assess the soil behavior and its resistance to internal erosion.

The specimen was prepared with different water contents ranging from optimum one (20%) to desiccation (4%). The curves below (Fig. 4) show the evolution of erosion kinetics as regards to resulted shear stress from applied pressure, obtained before and after desiccation. Figure 4 depicts how the erosion kinetics of particles detached from the specimen hole evolved over time, which indeed shows a linear relationship between erosion rate ε and shear stress τ. It clearly illustrates how the flowing water under a pressure of 1 bar causes the detachment of particles from the hole surface. As shown on the curves, the erosion kinetics before desiccation

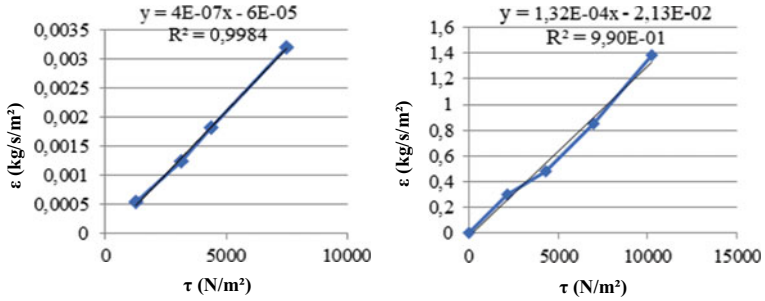

Fig. 4 Evolution of erosion rate with applied pressure before and after desiccation

remains low during the first second of test initiation; however, the erosion rate after desiccation increases considerably. This result indicates the effect of desiccation on internal erosion (a quick particle erosion was observed in the saturation phase at desiccation). Therefore, it proves that lower is the water content of the specimen, more sensitive to the erosion becomes the core soil, promoting the detachment of particles more quickly.

Presented results from Fig. 4 using linear erosion model [11] provide critical shear stress τc and erosion coefficient Ce. Instead of the critical shear stress of core soil before desiccation which was obtained by the extrapolation of the linear relation, the value of soil after desiccation has been deduced from experience (owing to the low value involved) performed at the lowest hydraulic load (0.06 m) when a first erosion occurs.

These parameters allowing the characterization of the soil resistance to erosion are summarized on Table 3 below where $Ie = -\log Ce$ is the erosion index.

In order to address the vulnerability of tested soil as regards to internal erosion, above results (Table 3) were used for soil classification based on Wan and Fell [2] criterion, indicating how long the soil resists to erosion before and after desiccation. Results (Fig. 5) indicated that before desiccation the core soil shows an extremely slow erosion, while after desiccation a moderately rapid erosion was provided. So, the core soil is stable (low vulnerability to erosion) at optimum water content, but after the desiccation the soil becomes highly sensitive to erosion. However, it was observed that even though soil erodibility has been extremely slow, it grows moderately fast after desiccation.

Table 3 Erosion parameters of tested soil in the two configurations

Designation	Before desiccation	After desiccation
τ_c(Pa)	150	8
C_e(s/m)	$4.00\ 10^{-7}$	$1.32\ 10^{-4}$
I_e	6.39	3.87
ρ_d(kg/m^3)	1700	1700

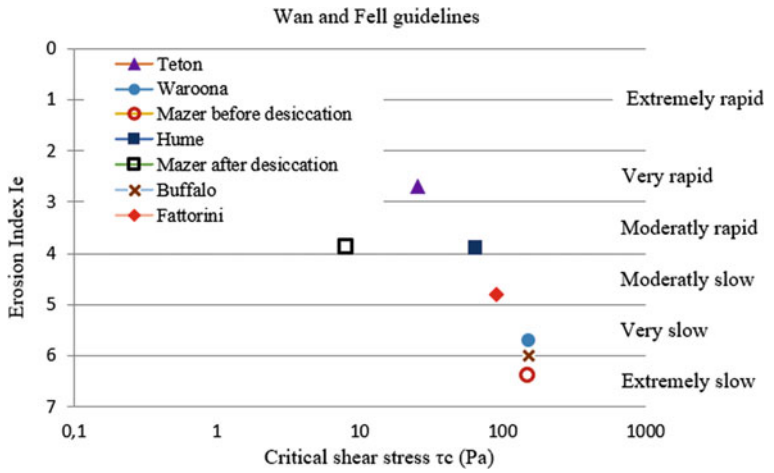

Fig. 5 Soil resistance classification guidelines [2]

From the analysis of the curves describing the hole diameter evolution as well as the eroded solid mass over time, before and after desiccation at different pressures, findings before desiccation indicate that our soil has undergone extremely slow erosion. So, there is a slight enlargement of the hole (Fig. 6a). Nevertheless, the soil of the Mazer dam is much more sensitive to erosion as water content decreases (from 20% up to 4% after desiccation), taking into account the important quantity of cumulated solid mass eroded during the test start, leading to the evolution (enlargement) of hole diameter over time showed on (Fig. 6c).

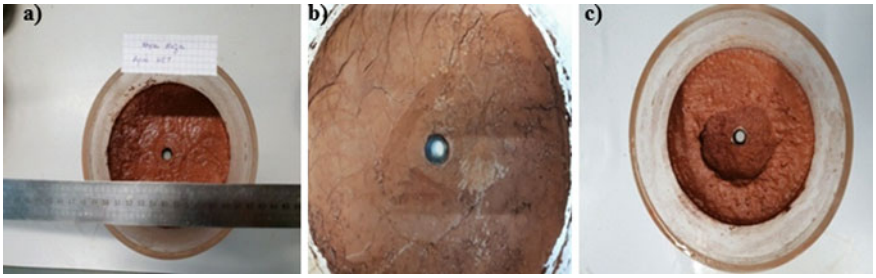

Fig. 6 Pictures of the hole after test without desiccation. (**a**) before test with desiccation, (**b**) after test with desiccation (**c**)

4 Concluding Remarks

Hole erosion tests carried out on the core soil aimed to assess its vulnerability to erosion. It has been showed through the identification of the effectiveness of the tested soil that dam soil is resistant to erosion at the optimum water content. So, the dam will be stable and resistant; thanks to the materials used in its construction. Nonetheless, it has been observed through low water content (after desiccation) that core soil becomes extremely susceptible to erosion because once the drying stage has been reached, the rise of cracks lead to a brutal impact on the efficiency of the soils against erosion. The water content reduction has been achieved to simulate the behavior of dams during the drought, showing the effect of desiccation on dam hydraulic stability which causes cracks within the dam core.

Thus, a new reservoir filling may lead to more core susceptibility to internal erosion. Then may cause the collapse of the structure owing to severe internal erosion process.

So, if the rainfall rate continues to decrease in that area, the risk of drought increases and can threaten the dam stability.

References

1. Christensen RW, Das BM (1973) Hydraulic erosion of remoulded cohesive soils. Soil erosion: Causes and mechanisms; prevention and control, Special Rep. 135, Highway Research Board, Washington, DC, 8–19
2. Wan CF, Fell R (2002) Investigation of internal erosion and piping of soils in embankment dams by the slot erosion test and the hole erosion test. UNICIV Rep R-412, July 2002, The University of New South Wales, Sydney, Australia
3. Wan CF, Fell R (2004) Investigation of rate of erosion of soils in embankment dams. J Geotech Geoenvironmental Eng 130(4):373–380
4. Wan CF, Fell R (2004a). Experimental investigation of internal instability of soils in embankment dams and their foundations. UNICIV Rep. No. R 429, The Univ. of New South Wales, Sydney, Australia
5. Lim S (2006) Experimental investigations of erosion in variably saturated clays Ph-D thesis report. University of New South Wales, Australia, p 197
6. Haghighi I 1, Martin T 1, Chevalier C 1, Reiffsteck P 1 (2010) A Simple and rapid test for studying the influence of water on the microstructure of soils
7. Foster M, Fell R (2001) Assessing embankment dam filters that do not satisfy design criteria. J Geotech Geoenvironmental Eng 127(5):398–407
8. Fell R, Fry JJ (eds) (2007) Internal erosion of dams and their foundations selected and reviewed papers from the workshop on internal erosion, rencontres d'Aussois, France, 25–27 April 2005, Taylor and Francis, 2007, pp. 245
9. https://www.maroc-meteo.net
10. https://www.abhbc.com/index.php/services/situation-des-barrages
11. Reddi LN, Lee I-M, Bonala MVS (2000) Comparison of internal and surface erosion using flow pump tests on a sand-kaolinite mixture. Geotechnical Test J GTJODJ 23(l):116–122

Rainfall Thresholds Triggering Landslides: A Review

Kanwarpreet Singh and Virender Kumar

Abstract In different physiographic and climatic regions worldwide, rainfall is recognized as one of the most common triggering factor for landslides causing severe damage to property and lives of large number of people every year. Urbanization in case of hilly areas has led to the need of detailed study and research in the field of landslides triggered by rainfall. Rainfall thresholds are statistical approximation of minimum rainfall conditions that trigger landslides for a particular mix of geologic, hydrologic, and topographic variables in a particular area. In the hazard-prone areas, the assessment of landslide-triggering rainfall thresholds is useful for development of early warning system. A lot many studies are available on this topic, which determine and estimate the amount of rainfall causing landslides. This paper aims at presenting a current state-of-the-art on the application of rainfall thresholds concepts, techniques, and methods for landslide occurrence with a focus on recent papers (after 2000) published in peer-reviewed journals.

Keywords Landslides · Rainfall thresholds · Physical rainfall threshold models · Empirical rainfall threshold models

1 Introduction

With the phenomenal advances in science and technology in the twentieth century, the world has become global village. The impact of natural and anthropogenic calamities in one part of the world affects the other part of the world. Hence, it becomes imperative to collaborate and share the reasons and the better management of these calamities; safety, relief, and rehabilitation activities through scientific techniques; human capabilities; state-of-the-art machinery and equipment; and experiences to mitigate their effect so that loss of life and property can be minimized. The disastrous phenomena of slippage of slope-forming materials like rock, debris, and earth down a slope under the influence of gravitational force are known as landslides [1], which

K. Singh (✉) · V. Kumar
Civil Engineering Department, National Institute of Technology, Hamirpur 177005, HP, India
e-mail: singhkanwarpreetnit@gmail.com

K. R. Reddy et al. (eds.), *Sustainable Environment and Infrastructure*, Lecture Notes in Civil Engineering 90, https://doi.org/10.1007/978-3-030-51354-2_42

are affecting economy of the countries worldwide by disturbing highways, buildings, bridges, dams, and other engineering structures as well as flora and fauna. The inauspicious geological conditions, drainage patterns eroding hydraulic regime, rainfall, groundwater conditions, deforestation, melting of glaciers and volcanic eruptions, seismicity, and other anthropogenic activities initiate landslides [2, 3]. The rainfall is worldwide well known for initiating slope instability every year, which can be analyzed in the form of threshold value based on its duration. The term threshold is known as a minimum or maximum level of some quantity required for a process or a change to take place in a state [4]; hence, the rainfall amount which when reached or exceeded is likely to cause slope failure activity is called as Rainfall Thresholds (RT). The RT conceptualized by researcher [5] is statistical approximation of critical rainfall conditions for causing landslides, based on the Intensity (I) and Duration (D) of rainfall or cumulative rainfall along with geology, hydrology, and topography-based variables. The reduction in the shear strength of slope-forming soil often takes place due to the increase in the pore water pressure because of infiltration due to excessive rainfall, which initiates landslide [5]. The macropores created by the borrowing animals allow abundant water into the pores which further cause dramatic increase in the pore water pressure [6]. The focus of the current study is to present a current state-of-the-art on the application of rainfall thresholds concepts, techniques, and methods for the possible occurrence of landslide by considering recent publications (after 2000) from peer-reviewed journals.

2 Mechanism of Rainfall-Induced Landslides

The process of triggering of shallow landslides by intense rainfall has been widely explained [7]. The rainfall mechanism for inducing landslides has been shown in Fig. 1. The process of infiltration causes loss in the matric suction which leads to decrease in the shear strength which further causes reduction in the safety factor of the slope resulting in landslide [8, 9]. The unsaturated soil exists at upper layer at 1–3 m height from the ground surface called seasonal unsteady zone because of very sensitive nature of the matric suction at this level toward the boundary conditions. Moreover, this zone is influential in the failure mechanism of shallow structures [10, 11]. The zone below the 3 m ground water table is called steady zone where the distribution of the metric suction is consistent. The seasonal unsteady zone is also important to evaluate the hydraulic conductivity (seepage velocity, soil water characteristic curve (SWCC) of unsaturated soil to the rainfall infiltration) [10, 12].

3 Rainfall Thresholds for Landslides

Rainfall thresholds are helpful for calculating the probability of occurrence of landslides [13]. There are two types of rainfall thresholds known as empirical and physical based [14]. Empirical-based rainfall thresholds depend upon the historical analysis

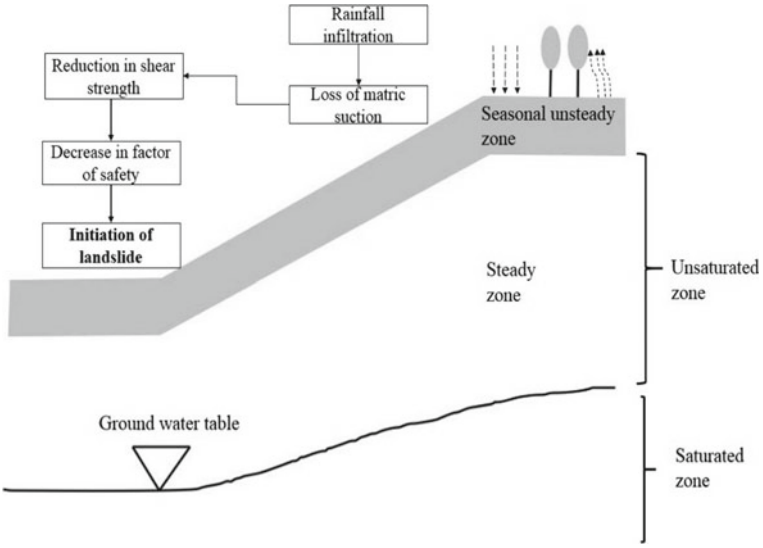

Fig. 1 Overview of mechanism of rainfall-induced landslide

of rainfall with the landslide events [14–19], while the physical thresholds are the numeric models based on the coupling of rainfall and slope stabilizing [7, 20–25]. The collection of accurate and dependable rainfall data and landslides information to define reliable thresholds for triggering of landslides is important but a difficult task [26].

3.1 Physical Model Based Rainfall Thresholds

The general aim of physical rainfall threshold models is to simulate the physical phenomena related to the movement of water that proceeds in the ground, as a result of the meteorological inputs [27]. Physical-based rainfall thresholds inducing landslides can be developed by considering topography, geology, and geotechnical parameters along with the rainfall causing destabilization of slopes [28]. Both time-invariant and time-dependent information are required in this approach [29]. Rainfall can be connected with the slope stabilization conditions through the infiltration models [30, 31]. Location and timing of the forecasted landslides can be determined by physical-based models; because of this, they can be successfully applied in the early warning systems for landslide prediction [32]. The performance of the physical-based models depends upon their coupling with hydrological models for stabilizing the slopes [33].

The hydrological models like steady-state model, transient piston-flow wetting front model, and transient diffusive model can be applied for evaluating rainfall effect on slope stabilization [20]. A researcher [34] developed a hydro-geomorphological

model considering both rainfall intensity and duration effect with slope stability controlling aspects. With the help of some soil-related key parameters in case of slope stability, a hydrology-based model was developed in Mettman Ridge area, Oregon, United States [35]. The time, depth, and movement of the rainfall-induced landslide can be predicted on the basis of pore pressure distribution model [7]. A physical-based SHALSTAB model was applied in Colombian Andes which revealed that about 208 mm of precipitation fell within the three hours which induced 800 landslides events [36]. The changes in the drawdown of water were observed at different durations of the rainfall which reduced the factor of safety [28]. Though physical models can predict the slope failure accurately as they consider the site-specific geotechnical parameters and the dynamic factors like rainfall and soil characteristics, a detailed information related to the hydrology, morphology, lithology, and soil characteristics, etc., is needful for the initiation of slope instability which is very difficult to collect over wide range because few parameters are based on the laboratory and in situ testing [37]. Hence, these models can be effectively applied only over the small sites and in restricted areas [38]. The other limitation is that the application of these models over large areas is not compatible with real-time applications [39].

3.2 Empirical Model Based Rainfall Thresholds

Empirical rainfall thresholds can be developed to analyze a relationship between rainfall and landslides of different regions on the basis of the available database regarding date, time, and amount of rainfall (hourly, daily, and antecedent) related to one particular occurred landslide [40]. Empirical thresholds have been developed at global [41–43], regional [44–48], and local [14–18]) scale. Different empirical-based rainfall thresholds have been developed in the previous literature, namely Intensity–Duration (ID) thresholds, Total Event rainfall thresholds (E), Rainfall Event–Duration thresholds (ED), Rainfall Event–Intensity thresholds (IE), and antecedent rainfall methods as explained below:

Intensity–Duration (ID) thresholds
Various researchers [14, 21, 40, 41, 47, 49–52, 54, 55] have utilized Intensity–Duration (ID) based threshold models as proposed by researcher [56] as given in Eq. 1.

$$I = C + \alpha D^{-\beta} \tag{1}$$

The intensity I can be calculated from the duration D of the rainfall on the basis of the parameters α and β. The value of C may be greater than or equal to zero as in the majority of the study; its value has been taken as zero. An accuracy of such kind of threshold development can be improved by limiting them at local scale for the prediction of slope failure activities.

Total Event rainfall thresholds (E)
The cumulative event rainfall (E) approach has been utilized by number of investigators [18, 57–59] to represent threshold. The researchers [57] used normalized cumulative event rainfall (EMAP) for the Kwa Zulu Natal province in South Africa. The researchers [18] have proposed a hydrogeologic conceptual model using Geo Studio and accumulated rainfall to define the threshold triggering for Taipingshan landslide in Taiwan.

Rainfall Event–Duration thresholds (ED)
The rainfall ED thresholds for inducing mass movements have been utilized by many researchers like [15, 21, 53, 60–63] to evaluate the precipitation amount during the event, based on the Eq. 2.

$$E = \alpha D^{\gamma} \tag{2}$$

Hourly based duration of an event and (α, γ) parameters were used to obtain cumulative event rainfall E amount in millimeters. The (α, γ) are equivalent of (α, β) parameters of the ID thresholds ($\gamma = 1 - \beta$). It has been observed in Sikkim, India at Lanta Khola place that debris flows become active when a 15-day continuous rainfall of 250 mm occurred because of the increase in the soil saturation [64]. A researcher [60] has analyzed 4000 rainfall events for initiating slope failure activities in Italy in the part of Emilia-Romagna region by studying event and duration of rainfall along with the average intensity. Thereafter, the researchers [61] have explored the link between 177 shallow mass movements with a total of 156 rainfall events between years 2002 and 2012 in Sicily. The researchers [62] have determined the relationship between hundred landslides by comparing different E and D values in Italy. Moreover, 2408 shallow landslides have been analyzed along with the 1981 rainfall events recorded from the regional and national rain gauge stations from year 1996 to 2012 [63].

Rainfall event–intensity thresholds (EI)
The threshold models based on event rainfall–intensity (EI) have been documented by some of the researchers [58, 65, 66] based on the Eq. 3.

$$I = \alpha E^{-\beta} \tag{3}$$

Here, α and β are parameters of the IE rainfall thresholds. A researcher [65] performed a study in Yogyakarta and Central Java to determine regional rainfall thresholds using EI equation to draw intensity-accumulated rainfall curve on the basis of the evaluated equation as $I = 331485R^{-2.0653}$ where R is the accumulated rainfall.

Antecedent rainfall methods
Antecedent rainfall can play significant role to cause slope destabilization [67]. There are few models based on antecedent rainfall thresholds for describing rainfall landslide relationship. A minimum rainfall amount of 20 mm was evaluated as a minimum

threshold value which was required to trigger debris flows in Wudu, China on the basis of quantitative Antecedent Soil Water Status (ASWS) model [68]. Thereafter, analysis of the antecedent and peak rainfall amount has been carried out from years 2006–2012, and it was observed that from the 263 mass movements in the Taiwan region, the debris flows were more related to the peak rainfall amount than the antecedent rainfall [69].

It can be noted from the above discussion that the methods based on the empirical models are more useful to develop rainfall thresholds at regional, national, or global scale [70]; however, their application is site specific and cannot be applied to other areas, and temporal accuracy of these types of thresholds remains largely untested [71, 72]. The poor quality of accessible data further can add the degree of uncertainty that can affect the required value of rainfall threshold linked with the landslide activity [73].

4 Conclusion

In this paper, results of research in progress after 2000 in the area of rainfall threshold for triggering landslides have been classified on physical and empirical basis. Physical models have limitations that they require detailed spatial information about the hydrological, morphological, lithological, and soil characteristics that control the initiation of soil slips. This type of information is very difficult to collect precisely over large areas, and is rarely available outside in the field for specifically equipped testing. Empirical rainfall thresholds study needs historical records of landslides and rainfall event records; the authenticity of which is always doubtful in the developing or underdeveloped countries. This study highlighted also the extreme complexity of the phenomena that govern the effects of rainfall upon slope stability. The lack of spatial homogeneity and of time-depending stationary status is the main limitation to a wide use of research results. New efforts are needed to overcome these shortcomings.

References

1. Cruden DM, Varnes DJ (1996) Landslide types and processes, special report. Trans Res Board, Nat Acad Sci 247:36–75
2. Anbalagan R (1992) Landslide hazard evaluation and zonation mapping in mountainous terrain. Eng Geol 32:269–277
3. Ponziani F, Pandolfo C, Stelluti M, Berni N, Brocca L, Moramarco T (2012) Assessment of rainfall thresholds and soil moisture modeling for operational hydrogeological risk prevention in the Umbria region (central Italy). Landslides 9:229–237
4. Reichenbach P, Cardinali M, Vita PD, Guzzetti F (1998) Regional hydrological thresholds for landslides and floods in the Tiber River Basin (central Italy). Environ Geol 35(2–3):146–159

5. Campbell RH (1975) Soil slips, debris flows, and rainstorms in the Santa Monica Mountains and vicinity, southern California. In: US Geological Survey Professional Paper 851. US Government Printing Office, Washington, DC, 51, 1975
6. Pierson TC (1983) Soil pipes and slope stability. Quart J Eng Geol 16:1–11
7. Iverson RM (2000) Landslide triggering by rain infiltration. Water Resour Res 36(7):1897–1910
8. Fredlund DG, Rahardjo H (1993) Soil mechanics for unsaturated soils. Wiley, New York, NY, USA
9. Lu N, Godt J (2008) Infinite slope stability under steady unsaturated seepage conditions. Water Resour Res 44(11):w11404. https://doi.org/10.1029/2008wr006976
10. Leong EC, Rahardjo H (1997) Permeability functions for unsaturated soils. J Geotech Geoenviron Eng ASCE 1118–1126
11. Fredlund DG, Hung VQ (2001) Prediction of volume change in an expansive soil as a result of vegetation and environmental changes. Geotechnical Special Publication No. 115, ASCE, Reston, 24–43, 2001
12. Fredlund DG, Xing A (1994) Equations for the soil-water characteristic curve. Can Geotech J 31(3):521–532
13. Mandal S, Maiti R (2013) Assessing the triggering rainfall-induced landslip events in the Shivkhola watershed of Darjiling Himalaya. West Bengal Eur J Geogr 4(3):21–37
14. Kanungo DP, Sharma S (2014) Rainfall thresholds for prediction of shallow landslides around Chamoli-Joshimath region, Garhwal Himalayas. India. Landslides 11:629–638
15. Marchi L, Arattano M, Deganutti AM (2002) Ten years of debris- flow monitoring in the Moscardo Torrent (Italian Alps). Geomorphology 46:1–17
16. Floris M, Mari M, Romeo RW, Gori U (2004) Modelling of landslide-triggering factors - A case study in the northern Apen- nines, Italy. Lect Notes Earth Sci 104:745–753
17. Giannecchini R (2005) Rainfall triggering soil slips in the southern Apuan Alps (Tuscany, Italy). Adv Geosci 2:21–24. http://www.adv-geosci.net/2/21/2005/
18. Chung MC, Tan CH, Chen CH (2016) Local rainfall thresholds for forecasting landslide occurrence: Taipingshan landslide triggered by Typhoon Saola. Landslides https://doi.org/10.1007/s10346-016-0698-2
19. Peres DJ, Cancelliere A, Greco R, Bogaard TA (2018) Influence of uncertain identification of triggering rainfall on the assessment of landslide early warning thresholds. Nat Hazards Earth Syst Sci 18:633–646. https://doi.org/10.5194/nhess-18-633-2018
20. Crosta GB, Frattini P (2003) Distributed modelling of shallow landslides triggered by intense Rainfall. Nat Hazards Earth Syst Sci 81–93
21. Aleotti P (2004) A warning system of rainfall-induced shallow failure. Eng Geol 73:247–265
22. Brooks SM, Crozier MJ, Glade TW, Anderson MG (2004) Towards establishing climatic thresholds for slope instability: use of a physically-based combined soil hydrology-slope stability model. Pure appl Geophys 16:881–905
23. Montrasio L, Valentino R, Losi GL (2012) Shallow landslides triggered by rainfalls: modeling of some case histories in the Reggiano Apennine (Emilia Romagna Region. Northern Italy Nat Hazards 60:1231–1254
24. Ran QH, Su DY, Fu XD, Wang GQ, He ZG (2012) Physically-based approach to analyze rainfall-triggered landslide using hydraulic gradient as slide direction. Appl Phys Eng 13(12):943–957
25. Yao W, Li C, Zhan H, Zeng J (2019) Time-dependent slope stability during intense rainfall with stratified soil water content. Bull Eng Geol Env. https://doi.org/10.1007/s10064-018-01437-3
26. Brunetti MT, Peruccacci S, Rossi M, Luciani S, Valigi D, Guuzzeti F (2010) Rainfall thresholds for the possible occurrence of landslides in Italy. Nat Hazards Earth Syst Sci 10:447–458
27. Picarelli, L., Vinale F.: Analisi della bibliografia. 81, 2007
28. Luo Y, He S, Chen F, Li X, He J (2015) A physical model considered the effect of overland water flow on rainfall-induced shallow landslides. Geoenviron Disasters 2:8
29. Raia S, Alvioli M, Rossi M (2014) Improving predictive power of physically based rainfall-induced shallow landslide models: a probabilistic approach. Geosci Model Dev 7:495–514

30. Green WH, Ampt G, Studies of soil physics. Part I. The flow of air and water through soils. J Agr Sci 4:1–24
31. Philip JR (1954) An infiltration equation with physical significance. Soil Sci 77(1):153–157, 1911
32. Guzzetti F, Peruccacci S, Rossi M, Stark C (2007) Rainfall thresholds for the initiation of landslides in central and southern Europe. Meteorol Atmos Phys 98:239–267. https://doi.org/10.1007/s00703-007-0262-7
33. Chang KT, Chiang SH (2009) An integrated model for predicting rainfall-induced landslides. Geophys J Roy Astron Soc 105:366–373
34. Iida T (2004) Theoretical research on the relationship between return period of rainfall and shallow landslides, Hydrol Process 739–756
35. Rosso R, Rulli MC, Vannucchi G (2006) A physically based model for the hydrologic control on shallow landsliding. Water Resour 42(6):1–16
36. Aristizabal E, Garcia E, Martinez C (2015) Susceptibility assessment of shallow landslides triggered by rainfall in tropical basins and mountainous terrains. Nat Hazards 78:621–634
37. Tablebi A, Nafarzadegan AR, Malekinezbad H (2010) A review on empirical and physically based modelling of rainfall triggered landslides. Phys Geogr Res Q 70
38. Giannecchini R, Galanti Y, Avanzi GDA (2012) Critical rainfall thresholds for triggering shallow landslides in the Serchio River Valley (Tuscany, Italy). Nat Hazards Earth Syst Sci 12:829–842
39. Rossi G, Catani F, Leoni L (2013) HIRESSS: a physically based slope stability simulator for HPC applications. Nat Hazards Earth Syst Sci 13:151–166. https://doi.org/10.5194/nhess-13-151-2013
40. Jamaludin S, Ali F (2011) An overview of some empirical correlations between rainfall and shallow landslides and their applications in Malaysia. EJGE 16
41. Crosta GB, Frattini P (2001) Rainfall thresholds for triggering soil slips and debris flow. In: Mugnai A, Guzzetti F, Roth G (eds) Proceedings 2nd EGS Plinius conference on mediterranean storms. Siena: 463–487
42. Cannon SH, Gartner JE (2005) Wildfire-related debris flow from a hazards perspective. In: Jakob M, Hungr O (eds) Debris flow hazards and related phenomena. Springer, Berlin, Heidelberg, pp 363–385
43. Hong Y, Adler RF (2008) Predicting global landslide spatiotemporal distribution: Integrating landslide susceptibility zoning techniques and real-time satellite rainfall estimates. Int J Sedim Res 23:249–257
44. Calcaterra D, Parise M, Palma B, Pelella L (2000) The influence of meteoric events in triggering shallow landslides in pyroclas- tic deposits of Campania, Italy. In: Bromhead E, Dixon N, Ibsen ML, Balkema A (eds) Proceedings of the 8th international symposium on landslides Cardiff, 1, 209–214
45. Ahmad R (2003) Developing early warning system in Jamaica: rainfall thresholds for hydrological hazards. National Disaster Management Conference, Ocho Rios, St Ann, Jamaica, 9–10, 2003
46. Godt J (2004) Observed and Modeled conditions for shallow landslide in the Seattle, Washington area. PhD dissertation University of Colorado, Boulder, CO, 2004
47. Dahal RK, Hasegawa S (2008) Representative rainfall thresholds for landslides in the Nepal Himalaya. Geomorphology 100:429–443
48. Ascanio R, Samuele S, Filippo C, Nicola C (2012) Statistical and environmental analyses for the definition of a regional rainfall threshold system for landslide triggering in Tuscany (Italy). J Geogr Sci 22(4):617–629
49. Chleborad F, Baum RL, Godt JW (2006) Rainfall Thresholds for Forecasting Landslides in the Seattle, Washington. Area- Exceedance and Probability. U.S. Geological Survey, Reston, Virginia
50. Hasnawir Kubota T (2008) Analysis of critical value of rainfall to induce landslides and debris–flow in Mt. Bawakaraeng Caldera, South Sulawesi, Indonesia. J Fac Agr Kyushu Univ 53(2):523–527, 2008

51. Miller S, Brewer T, Harris N (2009) Rainfall thresholding and susceptibility assessment of rainfall-induced landslides: application to landslide management in St Thomas. Jamaica Bull Eng Geol Environ 68:539–550
52. Akcali E, Arman H, Firat S, Saltabas L, Gunduz Z (2010) Rainfall thresholds for the initiation of landslides in trabzon province of turkey. Int J Eng App Sci (IJEAS) 2(4):14–26
53. Giannecchini R (2006) Relationship between rainfall and shallow landslides in the southern Apuan Alps (Italy). Nat Hazards Earth Syst Sci 6:357–364. https://doi.org/10.5194/nhess-6-357-2006
54. Peres D, Cancelliere A (2014) Derivation and evaluation of landslide-triggering thresholds by a Monte Carlo approach. Hydrol Earth Syst Sci 18:4913–4931
55. Chen CW, Oguchi T, Hayakawa YS, Saito H, Chen H (2016) Relationship between landslide size and rainfall conditions in Taiwan. Landslides. https://doi.org/10.1007/s10346-016-0790-7
56. Caine N (1980) The rainfall intensity duration control of shallow landslides and debris flows. Geogr Ann 62(1–2):23–27
57. Biafiore M, Braca G, De Blasio A, Martone M, Onorati G, Tranfaglia G (2002) Il monitoraggio ambientale dei territori campani a rischio di frane e di alluvioni: lo sviluppo della rete idropluviometrica del Servizio Idrografico e Mareografico Nazionale, Unpublished report
58. Hong Y, Hiura H, Shino K (2005) The influence of intense rainfall on the activity of large-scale crystalline schist landslides in Shikoku Island. Japan. Landslides 2:97–105. https://doi.org/10.1007/s10346-004-0043-z
59. Cardinali M, Galli M, Guzzetti F, Ardizzone F, Reichenbach P, Bartoccini P (2006) Rainfall induced landslides in December 2004 in South-Western Umbria, Central Italy. Nat Hazard Earth Sys Sci 6:237–260
60. Berti M, Martina MLV, Franceschini S, Pignone S, Simoni A, Pizziolo M (2012) Probabilistic rainfall thresholds for landslide occurrence using a Bayesian approach. J Geophys Res 117:f04006. https://doi.org/10.1029/2012jf002367
61. Melillo M, Brunetti MT, Peruccacci S, Gariano SL, Guzzetti F (2013) A new empirical method to reconstruct rainfall events using an automatic objective procedure. Rend Online Soc Geol 24:210–212
62. Vessia G, Parise M, Brunetti MT, Peruccacci S, Rossi M, Vennari C, Guzzetti F (2014) Automated reconstruction of rainfall events responsible for shallow landslides. Nat Hazards Earth Syst Sci 14:2399–2408
63. Brunetti MT, Peruccacci S, Antronico L, Bartolini D, Deganutti AM, Gariano SL, Iovine G, Luciani S, Luino F, Melillo M, Palladino MR, Parise M, Rossi M, Turconi L, Vennari C, Vessia G, Viero A, Guzzetti F (2015) Catalogue of Rainfall Events with Shallow Landslides and New Rainfall Thresholds in Italy. Eng Geol Soc Territ 2:1575–1579
64. Sengupta. A, Gupta S, Anbarasu K (2009) Rainfall thresholds for the initiation of landslide at Lanta Khola in north Sikkim, India. Nat Hazards 52:31–42. doi:10.1007/s11069-009-9352-9 CrossRefGoogle Scholar
65. Aleotti P, Balzelli P, Bellardone G (2002) Soil slips triggered by October 13–16, 2000 flooding event on the Piedmont Region (North West Italy): Criticall analysis of rainfall data. Geol Tec e Ambient Anno X, Ge, 15–25
66. Muntohar AS (2008) Toward regional rainfall threshold for landslide occurrence in yogyakarta and central of java. Jurnal teknik sipil – ucy, Vol. 3 No. 1, 2008
67. Rahardjo H, Li XW, Toll DG, Leong EC (2001) The effect of antecedent rainfall on slope stability. J Geotech Geological Eng 193–4:371–399
68. Bai S, Wang J, Thiebes B, Cheng C, Yang Y (2013) Analysis of the relationship of landslide occurrence with rainfall: a case study of Wudu County, China. Arab J Geosci https://doi.org/10.1007/s12517-013-0939-9
69. Chen CW, Saito H, Oguchi T (2015) Rainfall intensity–duration conditions for mass movements in Taiwan. Prog Earth Planet Sci 1–13
70. Martelloni G, Segoni S, Fanti R, Catani F (2011) Rainfall thresholds for the forecasting of landslide occurrence at regional scale. Landslides 9:485–495. https://doi.org/10.1007/s10346-011-0308-2

71. Crozier, M.J.: The climate-landslide couple: a Southern Hemisphere perspective. Paleoclimate Res 19:329–350
72. Guzzetti F, Peruccacci S, Rossi M (2005) Definition of critical threshold for different scenarios (WP 1.16). 36, 1996., 2005
73. Jaiswal P, Van Westen CJ (2009) Estimating temporal probability for landslide initiation along transportation routes based on rainfall thresholds. Geomorphology 112:96–105. https://doi.org/10.1016/j.geomorph.2009.05.008